REPORT UAG - 61

WORLD DATA CENTER A

Upper Atmosphere Geophysics

COLLECTED DATA REPORTS FOR STIP INTERVAL II

20 March - 5 May 1976

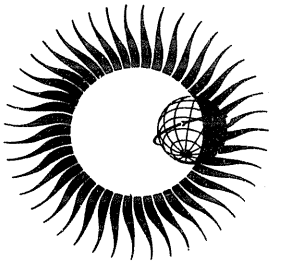

August 1977

WORLD DATA CENTER A

National Academy of Sciences

2101 Constitution Avenue, N.W.

Washington, D. C., U.S.A., 20418

World Data Center A consists of the Coordination Office

and seven Subcenters:

World Data Center A
Coordination Office
National Academy of Sciences
2101 Constitution Avenue, N.W.
Washington, D.C., U.S.A. 20418
[Telephone: (202) 389-6478]

Glaciology:

World Data Center A:
Glaciology
U.S. Geological Survey
1305 Tacoma, Washington, U.S.A. 98402
[Telephone: (206) 593-6506]

Meteorology (and Nuclear Radiation):

World Data Center A:
Meteorology
National Climatic Center
Federal Building
Asheville, North Carolina, U.S.A. 28801
[Telephone: (704) 258-2850]

Oceanography:

World Data Center A:
Oceanography
National Oceanic and Atmospheric Administration
Washington, D. C., U.S.A. 20235
[Telephone: (202) 634-7249]

Rockets and Satellites:

World Data Center A:
Rockets and Satellites
Goddard Space Flight Center
Code 601
Greenbelt, Maryland, U.S.A. 20771
[Telephone: (301) 982-6695]

Rotation of the Earth:

World Data Center A:
Rotation of the Earth
U.S. Naval Observatory
Washington, D.C., U.S.A. 20390
[Telephone: (202) 254-4023]

Solar-Terrestrial Physics (Solar and Interplanetary Phenomena, Ionospheric Phenomena, Flare-Associated Events, Geomagnetic Variations, Magnetospheric and Interplanetary Magnetic Phenomena, Aurora, Cosmic Rays, Airglow):

World Data Center A
for Solar-Terrestrial Physics
Environmental Data Service, NOAA
Boulder, Colorado, U.S.A. 80302
[Telephone: (303) 499-1000, Ext. 6467]

Solid-Earth Geophysics (Seismology, Tsunamis, Gravimetry, Earth Tides, Recent Movements of the Earth's Crust, Magnetic Measurements, Paleomagnetism and Archeomagnetism, Volcanology, Geothermics):

World Data Center A
for Solid-Earth Geophysics
Environmental Data Service, NOAA
Boulder, Colorado, U.S.A. 80302
[Telephone: (303) 499-1000, Ext. 6521]

Notes:

1. World Data Centers conduct international exchange of geophysical observations in accordance with the principles set forth by the International Council of Scientific Unions. WDC-A is established in the United States under the auspices of the National Academy of Sciences.

2. Communications regarding data interchange matters in general and World Data Center A as a whole should be addressed to: World Data Center A, Coordination Office (see address above).

3. Inquiries and communications concerning data in specific disciplines should be addressed to the appropriate subcenter listed above.

WORLD DATA CENTER A
for
Solar-Terrestrial Physics

REPORT UAG - 61

COLLECTED DATA REPORTS FOR STIP INTERVAL II
20 March - 5 May 1976

Helen E. Coffey and John A. McKinnon, Editors
WDC-A for Solar-Terrestrial Physics
Boulder, Colorado USA

August 1977

Published by World Data Center A for
Solar-Terrestrial Physics, NOAA, Boulder, Colorado
and printed by
U.S. DEPARTMENT OF COMMERCE
NATIONAL OCEANIC AND ATMOSPHERIC ADMINISTRATION
ENVIRONMENTAL DATA SERVICE
Asheville, North Carolina, USA 28801

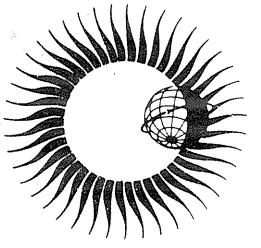

SUBSCRIPTION PRICE: $25.20 a year; $17.30 additional for foreign mailing; single copy price varies.*
Checks and money orders should be made payable to the Department of Commerce, NOAA/NGSDC.
Remittance and correspondence regarding subscriptions should be sent to the National Geophysical and Solar—Terrestrial Data Center, NOAA, Boulder, CO 80302.

PRICE THIS ISSUE $2.95

PALEHUA APRIL 30, 1976 2053 UT

Flare began 2047+1 UT

S08 W46

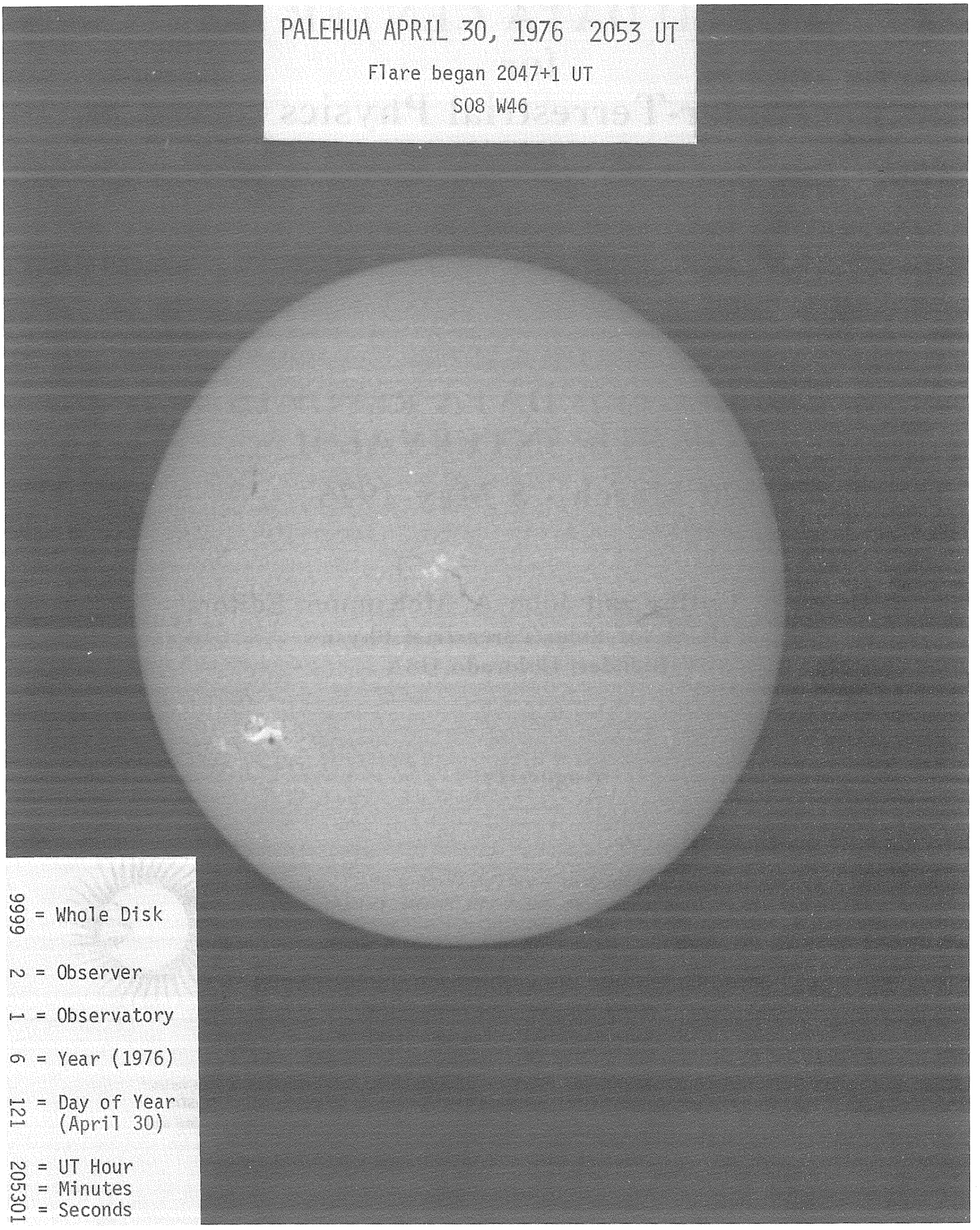

9999 = Whole Disk

2 = Observer

1 = Observatory

6 = Year (1976)

121 = Day of Year (April 30)

2053 = UT Hour
01 = Minutes
= Seconds

FOREWORD

Retrospective World Intervals have generally been "self-declared" because the solar-terrestrial events themselves have identified specific periods for special study. The Retrospective World Interval declared for the period 20 March - 5 May 1976 deviates somewhat from the previous patterns of self-declared intervals inasmuch as the request for this special study was made to the MONSEE Steering Committee by the Study of Traveling Interplanetary Phenomena (STIP) project of SCOSTEP.

The designation of this period as a Retrospective World Interval certainly has merit. This interval occurred within a period of special solar-terrestrial physics studies, as the STIP Project had already designated 15 March - 15 May 1976 as STIP Interval II - a period of concentrated and coordinated studies on traveling interplanetary phenomena. These dates were selected several months in advance primarily because the configuration of several space probes would afford a unique opportunity to study various traveling interplanetary phenomena should the sun cooperate at that time. The sun, indeed, was cooperative, as the period 20 March - 5 May 1976 was very active for a solar minimum period. Solar activity that was associated with several interplanetary and terrestrial disturbances occurred primarily in a region at Carrington Longitude $\sim 45°$.

At a STIP Business Meeting held in Boulder, Colorado, in June 1976, preliminary evaluation of the solar-terrestrial activity that occurred during STIP Interval II, together with the data acquired by various ground-based and satellite detectors, indicated that a significant amount of scientific data had indeed been acquired during this period - perhaps primarily because of the special study in progress at that time. In accordance with established SCOSTEP procedure a request for a Retrospective World Interval went from the STIP Project to the SCOSTEP Monitoring Sun-Earth Environment Committee (MONSEE), as the formal declaration of a Retrospective World Interval is one of the functions of the MONSEE Steering Committee. In conjunction with the formal declaration of this Retrospective World Interval by the MONSEE Steering Committee, World Data Center A for Solar-Terrestrial Physics in Boulder, Colorado, USA generously offered to publish a special UAG report presenting significant solar-terrestrial physics data acquired during the period 20 March - 5 May 1976. Accordingly, a summary of significant preliminary solar-terrestrial physics observations was distributed to the scientific community, and data contributions were solicited with the provision that data to be published should be confined to events believed associated with McMath Plage 14143 (solar rotation 1639) and its return as McMath Plage 14179 (solar rotation 1640).

The response was extremely gratifying, with 67 individual data contributions received from scientists from many countries. It is anticipated that this period of enhanced solar activity, coming as it did during solar minimum, will be studied by many researchers. It is also expected that many scientists will utilize the data contained in this report for various analyses, and that these scientists will acknowledge this UAG report as the source of the data. Acknowledgments such as this are extremely important if similar reports are to be published in the future.

In addition to the special UAG report on this interval, the events during this period, specifically those associated with the solar particle event of 30 April 1976, provided the incentive for another service to be offered by World Data Center A for Solar-Terrestrial Physics - the event oriented data collection. Scientists and organizations with more detailed data than that usually submitted to the World Data Centers are invited to submit these data to World Data Center A for the period 30 April - 2 May 1976 for inclusion in this special event oriented data collection.

The foundation of the monitoring activities is the persistent, routine, high quality data observational programs of solar-terrestrial phenomena conducted in a number of countries by many institutions and individuals. The considerable effort necessary to carry out these observational programs is often not acknowledged; however, these monitoring efforts and the generous sharing of these data are absolutely essential for viable solar-terrestrial physics programs. Although spectacular space missions are usually in the limelight, it would be difficult to utilize these new and exciting observations to their fullest potential without the correlative background measurements. It is therefore with a deep sense of satisfaction that I acknowledge the many responses from the solar-terrestrial physics monitoring community from around the world to this and previous Retrospective World Intervals.

On behalf of the MONSEE Steering Committee and the scientific community I thank Miss Helen E. Coffey, Miss J. Virginia Lincoln, and Mr. John McKinnon for their careful work in organizing and editing the data contributions contained in this data report. In addition I thank the entire staff of World Data Center A for Solar-Terrestrial Physics for their generous offer to undertake the task of publishing this report and for the care given to the final preparation of this document.

M. A. SHEA
Secretary, MONSEE
ICSU Special Committee on Solar-Terrestral Physics

TABLE OF CONTENTS

TABLE OF CONTENTS (continued)

1. SUMMARY OF 20 MARCH-5 MAY 1976 EVENTS

Overview of Solar-Terrestrial Physics Phenomena for the Retrospective World Interval of 20 March - 5 May 1976

by

M. A. Shea
Air Force Geophysics Laboratory
Hanscom Air Force Base
Bedford, Massachusetts 01731

ABSTRACT

A summary of the significant solar-terrestrial events that occurred during the Retrospective World Interval of 20 March - 5 May 1976 has been prepared using data available at the present time. Although this period occurred at solar minimum, it was an active interval - one in which the principal events were associated with solar activity in a region at Carrington Longitude ∿45°. (This active center was designated McMath Plage 14143 during solar rotation 1639 and renumbered McMath Plage 14179 during solar rotation 1640). Among the events summarized are the following:

(1) solar activity during the period 20-23 March 1976 from a region behind the eastern limb of the sun;

(2) a large geomagnetic storm with intense mid-latitude auroral activity on 26 March;

(3) moderate solar particle intensities at the Earth from 26 through 31 March; and

(4) a ground-level solar cosmic ray event on 30 April having a very hard spectrum.

Introduction

During the 18th Plenary Meeting of COSPAR held in Varna, Bulgaria in 1975, members of the Study of Traveling Interplanetary Phenomena (STIP) Project recommended two intervals for special studies. STIP Interval I was scheduled for September and October 1975. STIP Interval II was planned for early 1976 with the final dates of 15 March - 15 May being selected after the successful launch of Helios 2 on 15 January 1976.

Both of these intervals occurred during solar minimum, as illustrated by the graph of observed and "smoothed" sunspot numbers shown in Figure 1. In fact, statistical "sunspot minimum", defined by the minimum in a weighted 13-month average of the Zürich sunspot number, apparently occurred in March 1976, although the observed sunspot number for this particular month was the highest monthly value in a 17-month period (September 1975 - January 1977). To be specific, the period 20 March - 5 May 1976 was very active for solar minimum. Activity took place in a region at Carrington Longitude ∿45° that was associated with several interplanetary and terrestrial disturbances.

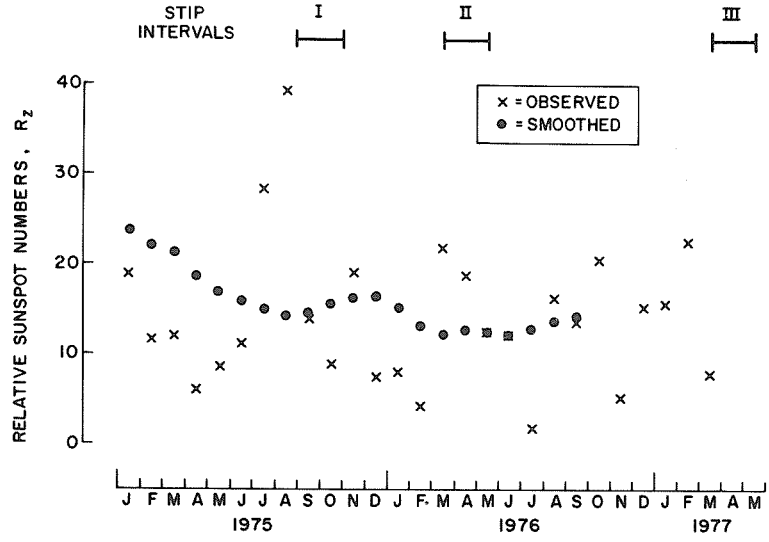

Fig. 1. Observed and smoothed sunspot numbers for the period January 1975 through March 1977. The time periods of the STIP Intervals are indicated by the bars at the top of the figure.

It is anticipated that this period of enhanced solar activity, coming as it did during solar minimum, will be studied by many researchers. Indeed, even while scientists were submitting their data for publication in this report, several of them were analyzing their own results for presentation at the L. D. de Feiter Memorial Symposium on the Study of Traveling Interplanetary Phenomena held in conjunction with the XX COSPAR Meeting in Tel Aviv, Israel, in June 1977. These papers will be published in the conference proceedings.

STIP Interval II - General Observations

The dates for STIP Interval II were selected primarily because of the possibility of obtaining extensive and heretofore unavailable particle, plasma, and magnetic field observations from two space probes close to the sun. These probes, namely, Helios 1 and Helios 2, both underwent perihelion passage during this interval. The orbits of these two probes are shown in Figure 2.

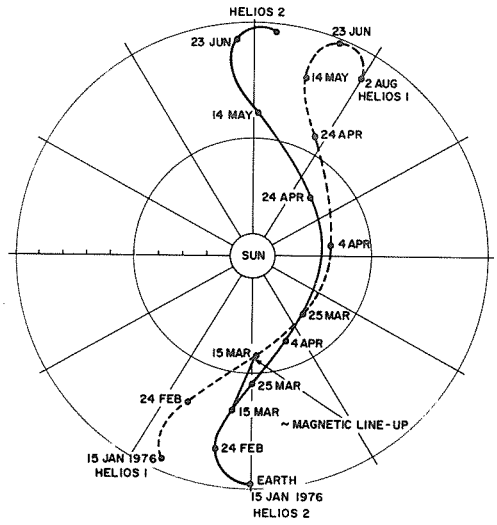

Fig. 2. The orbits of the Helios 1 and 2 space probes with respect to a fixed Sun-Earth line. The time period is from 15 January to August 1976.

In contrast with the typical solar minimum conditions observed during STIP Interval I [Shea *et al.*, 1977], STIP Interval II was a much more active period. Table 1 presents a list of some of the major solar-terrestrial phenomena that occurred between 20 March and 5 May 1976, with emphasis on those believed associated with McMath Plages 14143 and 14179.

An excellent evaluation of major centers of activity on the solar disk for the period 20 March - 5 May 1976 has been prepared by Dodson and Hedeman [page 10 in this volume] who graphically illustrate the daily values of solar and geomagnetic activity in Figure 1 of their paper. Eight solar flares with importance equal to or greater than 1 were reported during the period 20 March - 5 May 1976, and these flares, together with other significant solar activity, are also discussed by Dodson and Hedeman [page 10 in this volume].

Particulate radiation measured on various spacecraft was also enhanced during this period, as shown in several papers including those by Armstrong *et al.*, Richter *et al.*, and Kunow *et al.*, [pages 145, 141, and 134 in this volume]. Since solar wind observations were not included in the data submissions; a plot of these values, taken from issues of *SGD* [1976], is given in Figure 3.

Geomagnetic activity was very disturbed during portions of this interval and very quiet at other times, as illustrated by the planetary magnetic three-hour-range indices, Kp, plotted in Figure 4. Three sudden commencement geomagnetic storms were reported (see Table 1), and each was followed by a period of disturbed geomagnetic activity during which the Kp values reached 8 or greater. Several papers on geomagnetic measurements at particular locations are included in this report as well as papers on various ionospheric effects during this period.

Table 1

List of Significant Solar-Terrestrial Phenomena (20 March - 2 May 1976)

Date 1976	Time (UT)	Event
March 20	0203	Type II radio burst at the east limb (Culgoora)
	2257	Type II radio burst at the east limb (Culgoora)
		Note: Solar wind velocity enhancement on 9 April observed by Pioneer 10 (9.7 AU, 147° east of the Sun-Earth line).
23	0450	X-ray enhancement, east limb (OSO-8)
	0837-0841	Solar flare (S05, E90; McMath Plage 14143; SB)
	0840-1900	X-ray enhancement (GOES-1)
	0841	Type II and Type IV radio bursts (IZMIRAN, Moscow)
	0842	Type IV radio burst (Dürnten)
	0907-0945	Solar flare (S07, E90; McMath Plage 14143; SN)
	1100	Many loops observed in H-alpha, SE limb (Ramey)
26	0233	Sudden commencement geomagnetic storm (Ap=138)
28	1840	Onset of X-ray enhancement, 1-8Å (GOES-1)
	1905-2021	Solar flare (S07, E28; McMath Plage 14143; 1B)
	1915	Onset of 8800 MHz solar noise burst. Maximum at 1934 UT with flux density of 3719 flux units (Sagamore Hill)
	1921-1950	Type II radio burst (Harvard)
	1925-1939	Type IV radio burst (Sagamore Hill)
	1931-2400	Type IV radio burst (Boulder)
31	1108	Onset of X-ray enhancement, 1-8Å (SMA/GOES)
	1138-1350	Solar flare (S07, W09; McMath Plage 14143; 1N)
	1153-1512	Type IV radio burst (Dürnten)
	1356-1407	Solar flare (S08, W09; McMath Plage 14143; SF)
	1437-1442	Solar flare (S10, W03; McMath Plage 14143; SN)
	1445-1508	Solar flare (S11, W08; McMath Plage 14143; SF)
April 1	0255	Sudden commencement geomagnetic storm (Ap=107)
April 30	2043	Onset of X-ray enhancement, 1-8Å (GOES-1)
	2047-2218	Solar flare (S08, W46; McMath Plage 14179; 1B)
	2047	Onset of 2800 MHz solar noise burst at Ottawa. Maximum at 2109 UT with flux density of 1670 flux units.
	2103-2130	Type IV radio burst (Sagamore Hill)
	2107-2129	Type II radio burst (Harvard)
	2120-2125	Onset of GLE (Inuvik, Canada, neutron monitor)
	2125-2130	Onset of PCA (Thule, Greenland; Cape Zhelaniya and Dixon Island, USSR)
	2130	Onset of 6-10 MeV protons observed on SMS/GOES
May 1	0130	Maximum PCA at Thule, Greenland (2.7 dB)
2	1829	Sudden commencement geomagnetic storm (Ap=58 on 2 May; Ap=94 on 3 May)

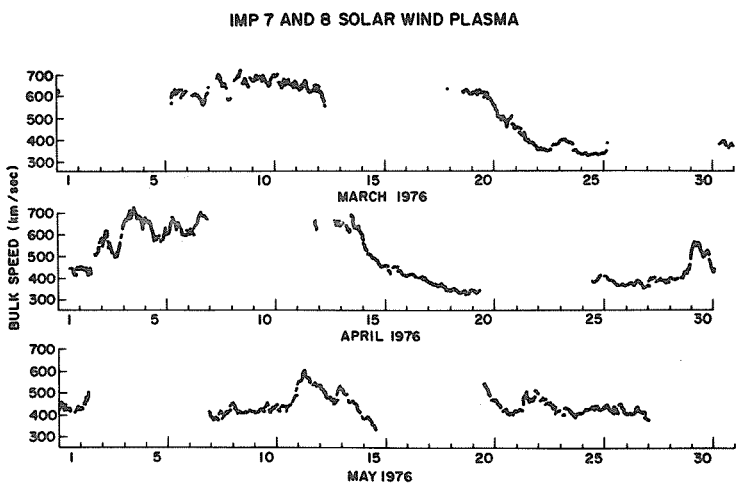

Fig. 3. Solar wind bulk speed measurements observed by the Earth-orbiting spacecraft IMP 7 and IMP 8 for the period 1 March through 31 May 1976. These data, from the MIT plasma probe, were published in *SGD* [1976].

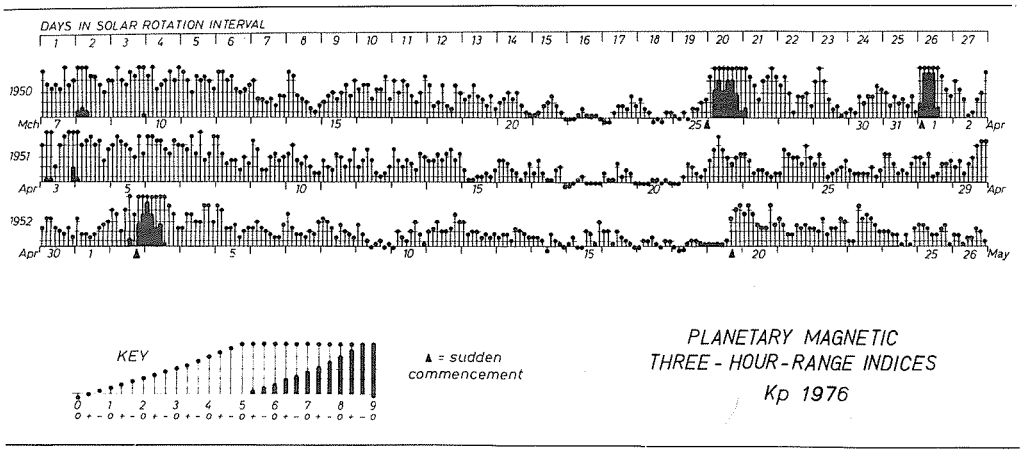

Fig. 4. Planetary magnetic three-hour-range indices, Kp, for the period 7 March through 26 May 1976. The rotation numbers given on the left-hand side of this figure are Bartels rotation numbers and not the solar rotation numbers referred to in the text of this paper.

Cosmic ray measurements are also included, not only because of a ground-level solar cosmic ray event that occurred on 30 April, but also because of neutron monitor data (measurements of ≥ 500 MeV protons) having long been used as an indicator of interplanetary and geomagnetic phenomena. The relative cosmic radiation intensity for this period, as measured by the Deep River neutron monitor, is shown in Figure 5.

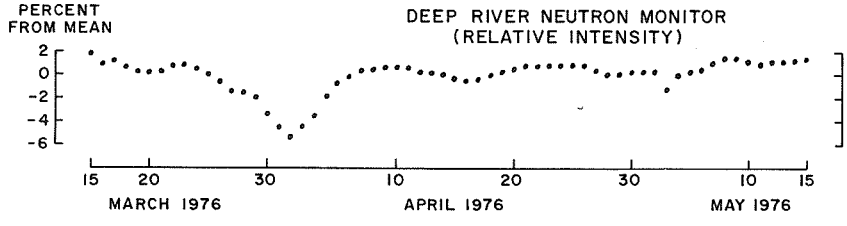

Fig. 5. Graphical display of the relative cosmic ray neutron monitor intensity as measured by the Deep River, Canada, neutron monitor for the period 15 March - 15 May 1976. The daily average intensity was used to determine the points on this figure; the mean is the average value for this entire period.

In addition, other solar-terrestrial physics observations during this interval, such as solar radio data, riometer data, and aeronomy measurements, are included in this report. Although many of the presentations contain data for the entire interval, the majority of these contributions contain data for one or more specific events throughout this period. When studied in their entirety, all of these data should allow researchers to investigate well-separated solar phenomena at sunspot minimum, inasmuch as the number of possible solar sources of the various interplanetary and terrestrial phenomena is drastically reduced from the count occurring near solar maximum.

Significant Events During STIP Interval II

Events of 20 March 1976. Type II radio bursts recorded by the Culgoora, Australia, radioheliograph and radio spectrograph at 0203 and 2255 UT on 20 March 1976 were attributed by Nelson and McLean [page 90 in this volume] to activity 55° and 44° behind the eastern limb of the sun, respectively. These authors concluded that the source of these Type II radio bursts was McMath Plage 14143 (as numbered on solar rotation 1639). Figure 6 illustrates the position of various space probes and the location of McMath Plage 14143 on 20 March 1976. Unfortunately, during this time period, there were no observational data from the Pioneer 9 space probe - measurements that could have confirmed the existence of an interplanetary shock associated with the Type II radio bursts on 20 March.

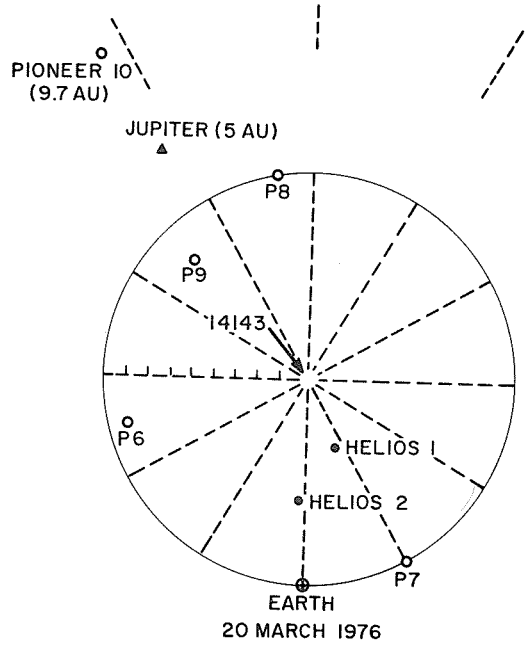

Fig. 6. Positions of important space probes and the planet Jupiter relative to the Sun-Earth line on 20 March 1976. The area within 1 AU is drawn to scale. The radial positions of Jupiter and Pioneer 10 are not drawn to scale, but their angular location is accurate. The Pioneer space probes within 1 AU are designated by the letter P and the appropriate number. The location of McMath Plage 14143 is indicated by the arrow.

The IMP 7 and IMP 8 solar wind observations during March, April, and May 1976, illustrated in Figure 3, show that a high-speed solar wind stream was observed at the earth from 6 to 12 March, returning again from 4 to 7 April. In a preliminary examination of the daily solar wind peak speed samples from the Pioneer 10 spacecraft, located at 9.7 AU, Wolfe [private communication] has confirmed that this same high-speed stream was apparently also observed by the Pioneer 10 space probe.

Events of 23-31 March 1976. McMath Plage 14143 was observed in X-rays by the OSO 8 satellite by 1200 UT on 22 March when this region was still ∿20° behind the eastern limb of the sun. By 0450 UT on 23 March, this region was the major source of X-ray emission on the visible disk, and it continued to be the dominant X-ray source on the sun throughout its transit ["2-30 keV X-ray Data from OSO-8," page 187 in this issue]. At 0837 UT on 23 March, flare activity occurred in McMath Plage 14143 on the eastern limb of the Sun, just as this region was becoming visible from the Earth. This activity is discussed by Dodson and Hedeman [page 10 in this volume]. Akinjan *et al.* [page 48 in this volume] report that an analysis of the radio spectra data obtained by Soviet observatories shows that the radio event, with onset at 0841 UT on 23 March, was a complex set of Type II and Type IV radio bursts.

The positions of the two principal active regions on the visible solar disk on 23 March are shown in Figure 7. Unfortunately, the location of McMath Plage 14143 was not ideally situated for efficient particle detection at the Earth, whereas plage 14127, at W57, was in a good position for efficient particle transport along the interplanetary magnetic field lines to the Earth. Solar particle fluxes at the Earth were enhanced from 23 through 31 March at energies greater than 40 MeV [*SGD*, 1976]. Helios 1 and Helios 2 also observed solar particle flux increases during this time period that Kunow *et al.* [1977] ascribe to the activity in McMath Plage 14143; the >51 MeV proton channel on Helios 2 recorded the highest flux observed during the entire STIP Interval ["MeV Protons, Alpha Particles and Electrons as Observed Aboard Helios 1 and 2 during STIP Interval II," page 134 in this volume]. The Helios space probe data will be a very valuable tool in ascertaining the solar coronal and interplanetary particle propagation conditions during this period.

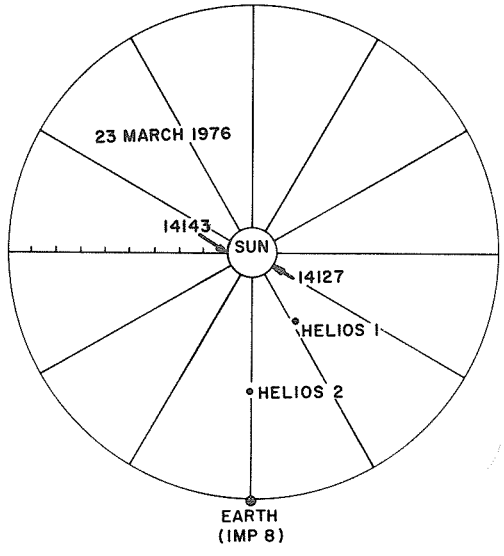

Fig. 7. Positions of the Helios 1 and Helios 2 space probes relative to the Sun-Earth line on 23 March. The locations of McMath Plage 14143 and McMath Plage 14127 are indicated by arrows.

There was a major geomagnetic disturbance on 26 March with a sudden commencement at 0233 UT. The major geomagnetic storm that followed produced an Ap value of 138, making it the fifth highest value of the 20th solar cycle. Intense auroras were observed at a number of mid-latitude locations. Figure 8 is an image of the auroral forms observed at 0925 UT on 26 March. The intense aurora in this figure extends to 58° corrected geomagnetic latitude, indicating a tremendous expansion of the earth's polar cap.

The solar flare that erupted <1905 UT on 28 March was an apparent particle producer, as evidenced by the discrete impulsive increase observed on the IMP 7 and IMP 8 spacecraft at all energies published in *SGD* [1976]. Although Helios 1 did not appear to detect a major particle increase associated with this event, Helios 2 did observe a sudden impulsive increase on all energy channels. Once again the value of the Helios data in aiding our understanding of solar particle propagation conditions in the Sun-Earth region is indicated. Another major sudden commencement geomagnetic storm occurred at 0255 UT on 1 April with an Ap value of 107, and auroras were reported at some mid-latitude locations [*SGD* 1967].

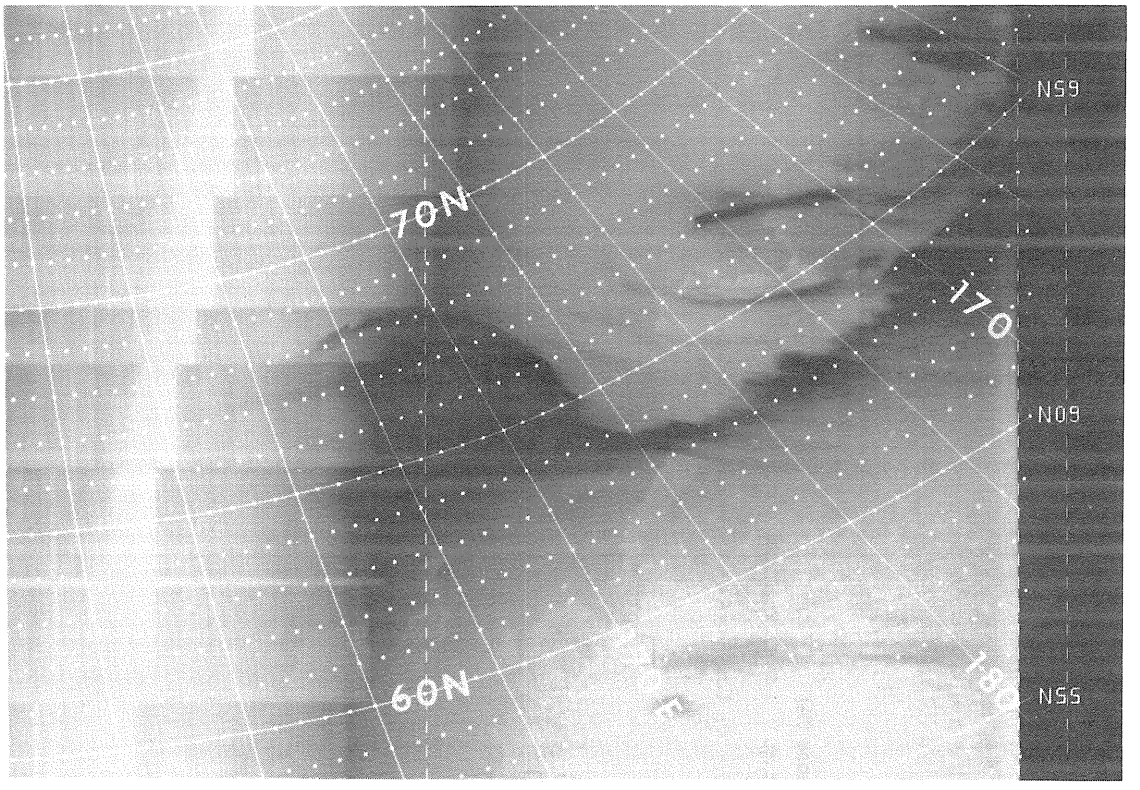

Fig. 8. DMSP satellite image of the moderately bright continuous aurora plus discrete arcs and bands observed on 26 March 1976. In this reverse image the aurora appears black. A background geographic coordinate grid for 100 km altitude has been superposed on the image for reference. The equatorward edge of the bright continuous aurora corresponds to a corrected geomagnetic latitude of 58°. The vertical dashed line designates the satellite subtrack which passes over the equatorward edge of the aurora at 0925 UT. The satellite is in a dawn-dusk orbit; the sunset terminator appears to the left of the image.

Event of 30 April 1976. McMath Plage 14143 returned to the eastern limb of the solar disk on 20 April 1976, at which time it was designated as McMath Plage 14179. On 29 April the frequency of subflares in this region increased markedly ["Overall Evaluation of Major Centers of Activity on the Solar Disk, 20 March - 5 May 1976," page 10 in this volume]. The major flare from this region, at 2047 UT on 30 April (classified as importance 1B), was accompanied by major X-ray and radio emission. This flare is of particular interest because it was the source of a ground-level solar cosmic ray event. From examination of the neutron monitor data from 10 locations, the earliest onset of relativistic protons appears to lie between 2120 and 2125 UT at Inuvik, Canada. Figure 9 shows that its 12% increase was the largest. Comparison of the relative increases at a number of stations having essentially atmospheric cutoff rigidities implied that the relativistic particle flux in this event was quite anisotropic (see Figure 9). In particular, note the relative increases at Inuvik and Goose Bay, Canada. At lower energies an impulsive increase in the electron and proton fluxes was observed on the IMP 8 satellite ["Solar and Interplanetary Particles Observed in the Interval 20 March through 5 May with IMP 8," page 145 in this volume].

In the polar cap a maximum absorption of 2.7 dB was measured by the Thule, Greenland, riometer ["Riometer, Magnetometer, and VLF Ionosonde Data from the Polar Cap, 21 March - 8 May 1976," page in this volume], although "spikes" in the riometer measurements at several Soviet stations indicated maximum absorption values of ∿5.0 dB ["Polar Cap Absorption Event of 30 April - 3 May 1976 by the Riometer Data at the Soviet Arctic and Antarctic Stations," page 248 in this issue]. The relatively modest low-energy particle increase observed by IMP 8, the comparatively small riometer absorption, and the ground-level neutron monitor increase indicate a very hard particle spectrum. Magnetometer records show a sudden commencement geomagnetic storm occurred at 1829 UT on 2 May, followed by major disturbances for the next 24 hours.

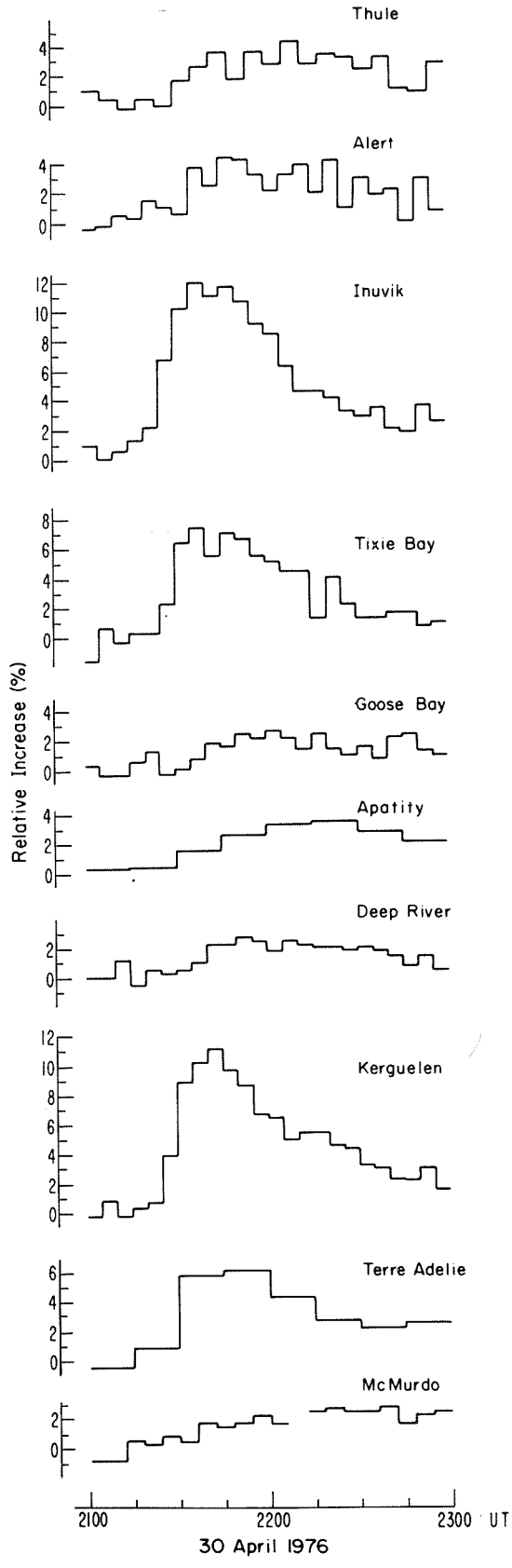

Fig. 9. Relative neutron monitor increases at 10 stations having essentially atmospheric cutoff.

The positions of the Helios space probes on 30 April are shown in Figure 10 together with the position of McMath Plage 14179. Although the flare position was favorably situated for efficient particle propagation from the Sun to the Earth, its location was ∿110° to the east of the Sun-Helios line. This event was observed on both the Helios 1 and Helios 2 space probes, although the time-intensity profile differed markedly between the two satellites ["MeV Protons, Alpha Particles and Electrons as Observed Aboard Helios 1 and 2 during STIP Interval II," page 134 in this volume]. This impulsive, well-isolated, relativistic solar cosmic ray event should also offer a unique opportunity to study solar particle propagation in the solar corona and in the interplanetary medium.

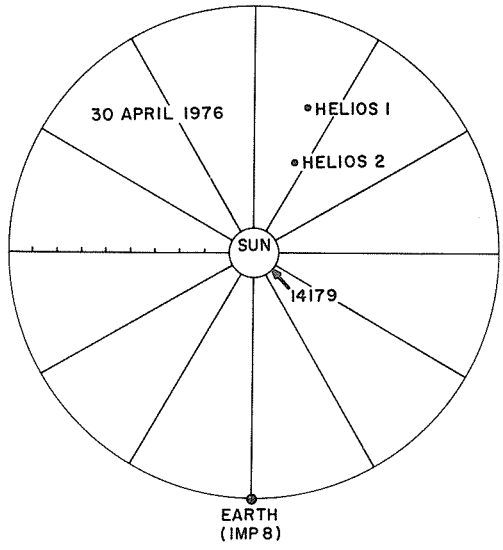

Fig. 10. Positions of the Helios 1 and Helios 2 space probes relative to the Sun-Earth line on 30 April. The location of McMath Plage 14179 is indicated by the arrow.

Summary

STIP Interval II was a coordinated period of observations that coincided with statistical sunspot minimum. Ironically, during this period, there were several exceptional solar events that resulted in the designation of a Retrospective World Interval for the period 20 March - 5 May 1976. The solar activity; the interplanetary particles, fields, and plasmas; and the geomagnetic activity that occurred during this period provide measurements of relatively isolated solar particle and plasma emissions during solar minimum.

REFERENCES

KUNOW, H., G. WIBBERENZ, G. GREEN, R. MÜLLER-MELLIN, M. WITTE, H. HEMPE, and J. FUCKNER (1977) Characteristic Features of Coronal Propagation as Derived from Solar Particle Observations by HELIOS 1 and 2 during STIP Interval II, *Contributed Papers to the Study of Travelling Interplanetary Phenomena/1977*, edited by M. A. Shea, D. F. Smart, and S. T. Wu, Air Force Geophysics Laboratory report, to be published.

SHEA, M. A., D. F. SMART, and H. E. COFFEY (1977) A Summary of Significant Solar-Initiated Events During STIP Intervals I and II, *Study of Travelling Interplanetary Phenomena/1977*, edited by M. A. Shea, D. F. Smart, and S. T. Wu, in the series Astrophysics and Space Science Library, D. Reidel, Dordrecht, Holland, in press.

WOLFE, J. H. (1977) Space Physics Branch, NASA - Ames Research Center, Moffett Field, California.

SGD (1976) *Solar-Geophysical Data*, U.S. Department of Commerce, (Boulder, Colorado, U.S.A. 80302).

2. SOLAR OPTICAL DATA

Overall Evaluation of Major Centers of Activity on the Solar Disk, 20 March - 5 May, 1976

by

Helen W. Dodson and E. Ruth Hedeman
McMath-Hulbert Observatory
of
The University of Michigan
Pontiac, Michigan 48055 USA

1. Introduction

The 47 days from 20 March through 5 May 1976 have been designated by the MONSEE Steering Committee as a "Retrospective World Interval" because of the interesting solar, geophysical, and interplanetary phenomena that occurred during that time span. It is believed that the geophysical effects stemmed primarily from solar events that took place during transits of McMath Plages 14143 and 14179. A request has been made that current studies be centered primarily on phenomena associated with these two regions. These plages represent the second and third transits of a center of activity located at latitude S07 and at Carrington longitude of approximately 44°. This center of activity constituted part of a brief pulse or temporary general increase in solar activity that began early in March and lasted until late June 1976 (see Figure 1).

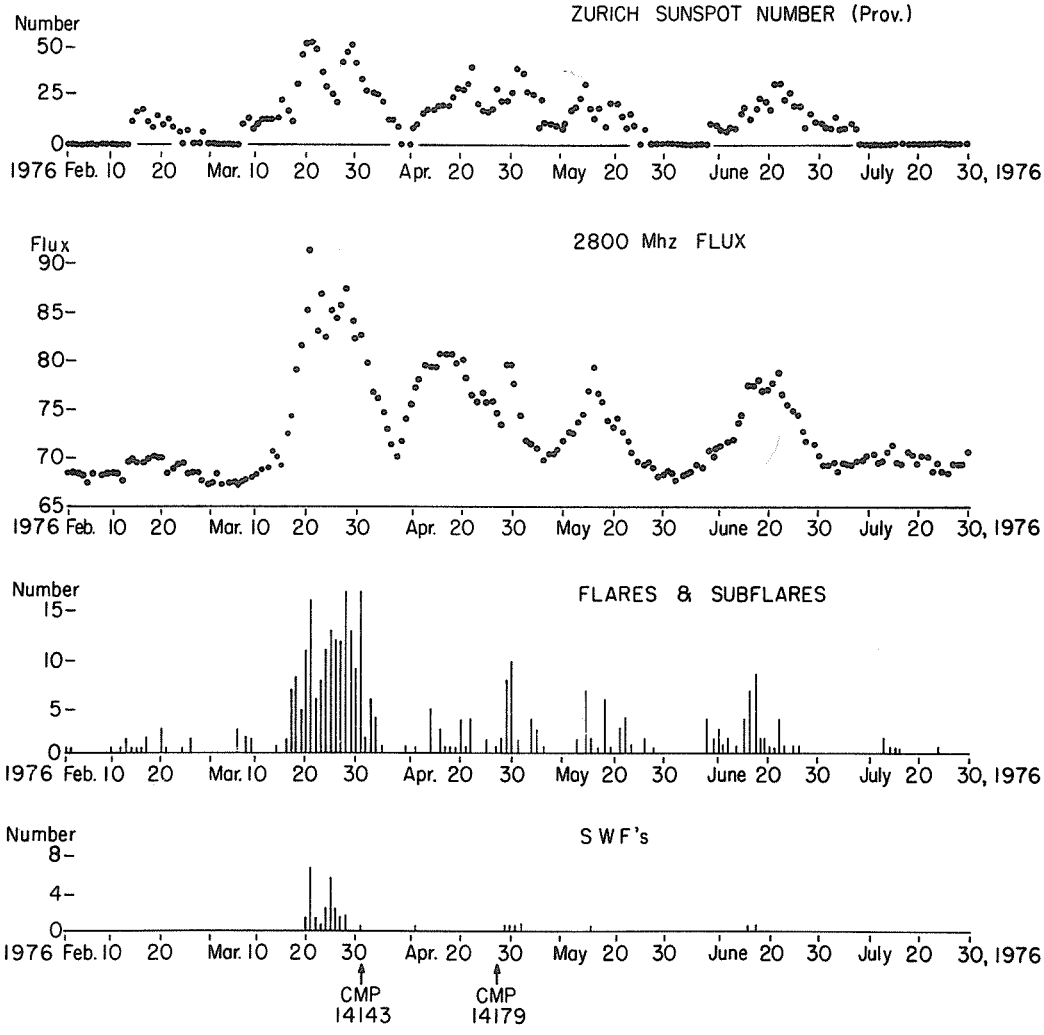

Fig. 1. Various measures of solar activity showing temporary increase from early March to late June 1976.

2. Transit of McMath Plage 14143 (24 March - 9 April, 1976)

McMath Plage 14143 (latitude S07, longitude ~ 44°) crossed the central meridian on 30-31 March 1976. It was in its second rotation having formed on the disk on 5 March when it was 3 days west of the central meridian. During its first appearance as Plage 14118 (see Figure 2), the region exhibited no special signs of enhanced activity and rotated over the west limb on 9 March. The plage and spot returned to the east limb on 24 March as a very bright, well-developed, flaring region. It had grown and developed markedly while on the invisible hemisphere. During the March transit of the solar disk, this region, Plage 14143, dominated the entire hemisphere in which it was located (see Figure 3d).

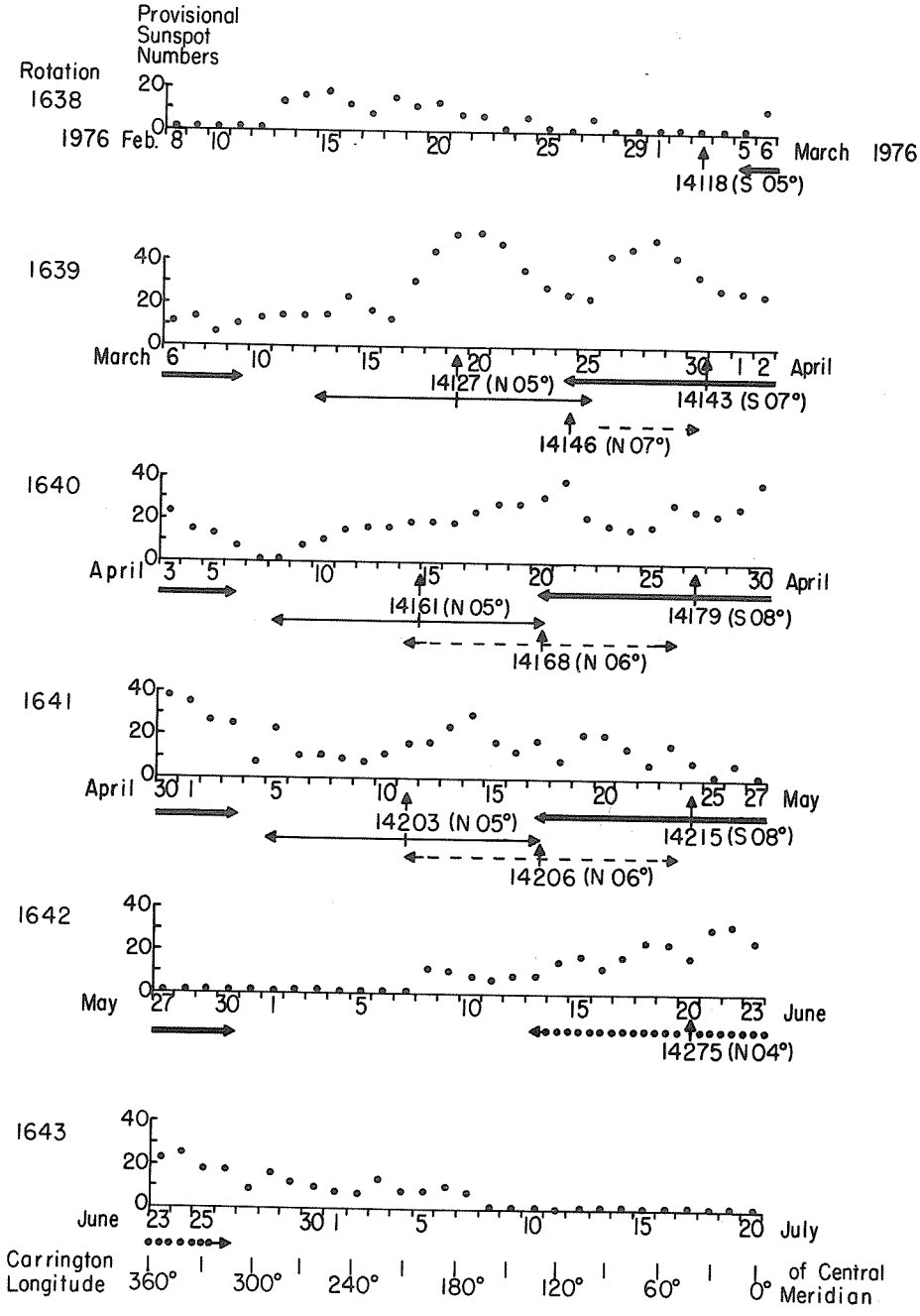

Fig. 2. Summary of information about location and times of disk transit of principal centers of activity, 8 Feb. - 20 July 1976. Provisional Zürich sunspot numbers (heavy dots) are shown for comparison. Vertical arrows indicate date of CMP. Horizontal arrows indicate disk passage of an active region. Returns of same center of activity are represented by repetitions of the same horizontal symbols in successive rotations.

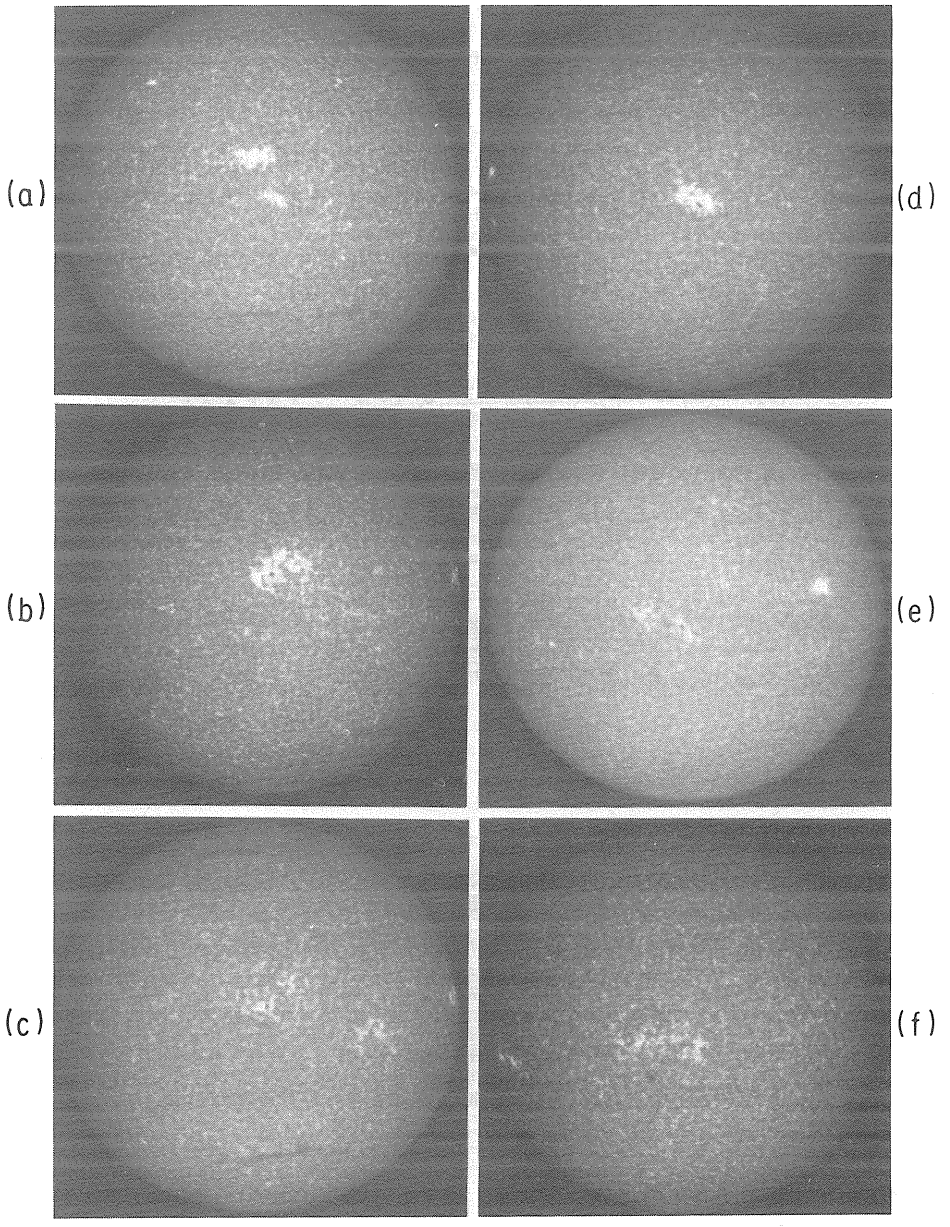

Fig. 3. Calcium spectroheliograms showing two centers of activity near central meridian during each of three solar rotations, March-May 1976.

Center (1), N 05°, L~196°	Center (2), S 07°, L~44°
(a) Plage 14127, March 19	(d) Plage 14143, March 30
(b) Plage 14161, April 14	(e) Plage 14179, April 27
(c) Plage 14203, May 11	(f) Plage 14215, May 24

Plage 14143 contained Mount Wilson Spot Group number 19669, which was classified by Mount Wilson Observatory as a γ spot with δ configuration throughout the entire interval of their observations, 25 March - 3 April. The region apparently reached maximum development and activity during the eastern half of its transit with average spot area $\sim$ 600 millionths and plage area $\sim$ 3000 millionths of the solar hemisphere. Flare activity also was greater in magnitude and frequency from east limb to central meridian passage than during the western transit of the disk (see Figure 4).

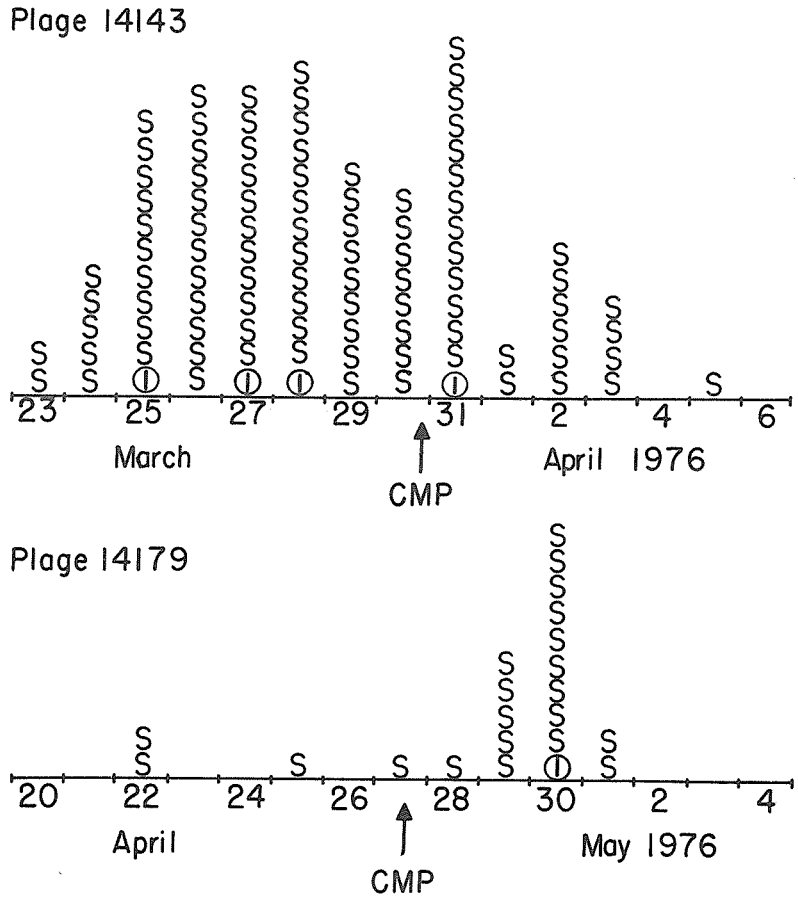

Fig. 4. Numbers of flares and subflares each day in plages 14143 and 14179.

There were eight flares in Plage 14143 that met our criteria for "major" flares (see UAG Reports 14 and 52).† These flares with their Comprehensive Indices are identified by asterisks in Table 1. Although 99 flare brightenings were reported in the region, all but 4 were subflares (see Figure 4). No flare with Hα importance as great as 2 was observed. It is probable, however, that the bright subflare reported at 0837 UT on 23 March at S05 E90 was the elevated aspect of a more important flare in Plage 14143, which, at that time, was still entirely behind the east limb. This event was accompanied by Type IV radio emission, X-ray enhancements, and SWF of importance 3 that lasted for 101 min. Its Comprehensive Index of 12 is the highest for any flare in the Retrospective Interval (see Table 1).

Thirteen flare events in Plage 14143 were associated with reported SWFs. Information about these 13 flares with enhanced ionizing radiation is given in Table 2. This list includes three of the four flares of importance 1 in Plage 14143, but the well observed, two-ribbon flare of importance 1n with Type IV radio emission and X-ray enhancement at 1138 UT on 31 March is not in the list. It is probable that this omission represents some deficiency in the ionospheric data rather than a peculiarity of the flare. This flare apparently was associated with other forms of ionospheric disturbances.

---

† A flare is considered "major" if it satisfies any one of the following criteria:

SWF or SID of importance ≥ 3
Hα flare, importance ≥ 3
10 cm flux ≥ 500 X 10^{-22} $Wm^{-2}Hz^{-1}$
Type II burst
Type IV radio emission, with duration 10 min.

TABLE 1

PROFILES AND COMPREHENSIVE INDICES FOR ALL "IMPORTANT" FLARE-EVENTS, MARCH 1 - APRIL 30, 1976

DATE 1976	FLARE DATA OR OTHER INFORMATION				MCMATH PLAGE	PROFILE	INDEX
March *20	(0205 UT - Type II burst) No flare reported. Culgoora Radioheliograph event P.A. 70°-80°				-	00110	2
20	1356-1408	1400	Sf	N05 W20	14127	00020	2
	1435-1456	1438	Sf	N03 W20			
*20	(2257 UT - Type II burst) No flare reported. Culgoora Radioheliograph event P.A. 40°-70°				-	10020	3
*21	0750-0835	0800	1b	N04 W29	14127	31100	5
21	(1115 UT - SID) No flare reported. No flare patrol 1111-1230 UT.				—	20000	2
21	1306-1323	1310	Sn	N03 W33	14127	20100	3
21	1829-1924	1845	Sb	N03 W34	14127	20101	4
*23	0837-0841	0839	Sb	S05 E90	14143	30234	12
	0907-0945	0915	Sn	S07 E90			
24	0016-0043	0018	1n	N02 W66	14127	11201	5
*25	1154-1229	1201	Sn	S06 E75	14143	10232	8
*25	1305-1430	1325	1n	S05 E69	14143	11232	9
26	1334-1401	1341	Sf	S04 E61	14143	00022	4
26	1439-1455	1441	Sn	S08 E62	14143	10121	5
*26	(1720 UT - Type IV) No flare reported.-					00030	3
27	1156-1230	1206	1n	S10 E49	14143	21122	8
*28	0546-0613	0556	Sb	S07 E37	14143	10113	6
*28	0922-1002	0933	Sn	S08 E31	14143	00032	5
		0946					
*28	1342-1353	1344	Sf	S06 E37			
	1534-1555		Sf	S06 E27	14143	00030	3
	1625-1634		Sf	S06 E25			
*28	1905-2021	1921	1b	S07 E28	14143	11332	10
		1932					
29	1152-1232	1221	Sf	S09 E26	14143	00020	2
*31	1140-1350	1200	1n	S07 W09	14143	11132	8
		1230					
April *5	(2152 UT - Type IV) No flare reported.- No flare patrol 2045-2515 UT.					00031	4
7	(1723 UT - Continuum) No flare reported.				-	00020	2
9	0019-0050	0021	1f	N06 E80	14161	01000	1
*20	1740-1846	1836	Sf	N03 W77	14161	00231	6
*29	1904-1940	1920	Sn	S08 W31	14179	10131	6
*30	1243-1306	1247	Sn	S06 W41	14179	10132	7
*30	2048-2218	2059	1b	S08 W45	14179	21332	11
		2108					

* This event qualifies as a "major" flare according to criteria in UAG Reports 14 and 52.

TABLE 2

REPORTED SHORT WAVE FADES* ASSOCIATED IN TIME WITH FLARE EVENTS IN McMATH PLAGES 14143 AND 14179

DATE	SWF Time	SWF Imp.	Hα FLARES Time	Hα FLARES Imp.	POSITION	X-RAY DATA †	RADIO FREQ. DATA
			Plage 14143 (Mar.23-Apr.6, 1976)				
March 23	0839-1020	3	0837-0841	Sb	S05 E90	X1	IV
			0907-0945	Sn	S07 E90		
24	1836-1916	1-	1900-1913	Sf	S11 E85	-	-
25	0705-0730	1	0704-0714§	Sf	S05 E76	C7	-
25	1152-1350	1	1154-1229	Sn	S06 E75	M1	IV
25	1325-1355	1	1305-1430	1n	S05 E69	-	IV
25	1720-1740	1	1636-1830	Sn	S05 E68	C6	-
26	0837-0845	1-	0830-0858	Sn	S09 E59	-	-
26	1441-1500	1	1439-1455	Sn	S08 E62	C7	Contin.
27	1203-1248	2-	1156-1230	1n	S10 E49	M1	Contin.
27	2044-2123	1-	2043-2108	Sn	S07 E42	-	-
28	0553-0747	1	0546-0613	Sb	S07 E37	M1	II
28	1919-2054	1+	<1905->2021	1b	S07 E28	X1	IV
							G.B. 10cm
31	0453-0640	1-	0453-0527	Sn	S07 W03	C9	-
			Plage 14179 (Apr.20-May 3, 1976)				
April 29	1909-2034	1-	1904-1940	Sn	S08 W31	M0	IV
30	2047-0153	2+	<2049->2218	1b	S08 W46	X2	II & IV
							G.B. 10cm
May 1	2141-0112	1	2140-2154	Sf	S08 W60	M2	II, IV

* Reported in Solar Geophysical Data Bulletin

† From Preliminary Report and Forecast of Solar Geophysical Data

§ Also a subflare in 14127 at 0703-0709, N03 W88

It should be noted that because the latitude of Plage 14143 was S07, it passed through the apparent center of the solar disk on 30-31 March. The heliographic latitude of disk center, B_0, for this date was -6.62°. This circumstance may have had some bearing on the geophysical effects associated with region 14143.

The plage (14143) and spot (No. 19669) traversed the west limb on 6 April, apparently diminishing in size and complexity (see Figure 5).

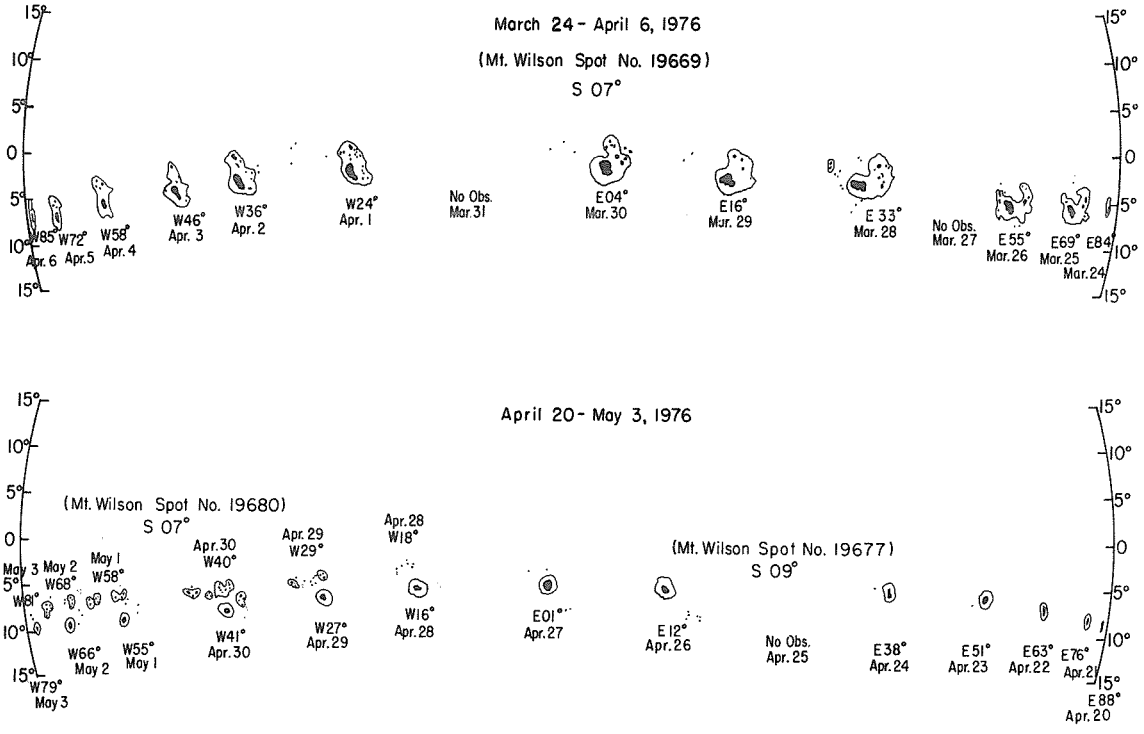

Fig. 5. Daily drawings from the McMath-Hulbert observatory of Mt Wilson spot nos. 19669, 19677, and 19680, March - May 1976.

3. Transit of McMath Plage 14179 (20 April - 3 May, 1976)

The center of activity that in March and early April was known as McMath Plage 14143 apparently continued to diminish in size and complexity as it traversed the invisible solar hemisphere. It returned to the east limb on 20 April and was listed as McMath Plage 14179 (see Figure 2). As is frequently the case, this aging plage had divided into two components (area ~ 1500 millionths of the hemisphere). The intensity had diminished from 3.5 in March to only 2.5 in April (see Figure 3e).

During its entire April transit of the visible hemisphere, the plage contained Mount Wilson spot 19677, latitude S10, longitude ~ 41°. The spot was classified as αf from limb to limb. Flare activity associated with plage 14179 was low during the first 9 days of its passage from east limb to W20 (20-28 April) (see Figure 4). During this interval, only five subflares were reported and none were associated with a Short Wave Fade or a distinctive radio frequency event. However, on 27 April a circumstance of apparent significance began. Small, new spots appeared a few degrees to the north and west of the large stable umbra of Mount Wilson spot group 19677 (see Figure 5). In succeeding days these spots increased in number and area and were catalogued by Mount Wilson as a new spot group, number 19680. Both of the Mount Wilson spot groups occurred in the following part of Plage 14179. For 3 days the new spot was classified as magnetic type β, but from 30 April to 2 May inclusive, it became magnetically complex and was classified as $\beta\gamma$. On 30 April and 1 May it had δ characteristics. The development of this magnetically complex spot in the close neighborhood of a previously existing spot can be seen clearly in the summarized spot drawings of Figure 5.

On 29 April, 3 days after the appearance of this new spot group, the frequency of flaring in Plage 14179 increased markedly and continued high through 1 May (see Figure 4). All of the flare events in the region were reported as subflares with the exception of a flare of importance 1 on 30 April at 2047 UT, S08 W46. This latter event was accompanied by long enduring X-radiation, a great burst at 2800 MHz, as well as Types II and IV at meter wavelengths. The Comprehensive Index for this flare was 11 (see Table 1). The reported SWF lasted for more than 5 hours and neutron monitors recorded a ground level cosmic ray enhancement in time assocation with the flare. Geomagnetic disturbance reached high levels on 2 and 3 May.

This flare on 30 April and the phenomena associated with Plages 14143 and 14179 are good examples of isolated flaring regions and significant flares occurring on the sun even though the sun, as a whole, is apparently very close to "minimum" in the course of successive 11-year cycles. If future observations place solar minimum in 1976, it should be noted that residual activity, as measured by sunspot number, during this minimum was at an unusually high level. It may even prove to be higher than that during the mimimum of 1964 which, itself, was unusually high (*IQSY ANNALS, 4,* 3, 1969).

4. Summary of Important Solar Flare Events in March and April 1976

In the past, for the years 1955 to 1974, we have prepared Experimental Comprehensive Indices and profiles of the electromagnetic radiation for all flares that met at least one of the criteria that we set up for "major" flares (see UAG Reports 14 and 52 and section 2 of this study). For the present study, we have derived the same type of profile and index for flare events in the 2 months of March and April 1976, but we have lowered the limits for inclusion in the survey. In Table 1 we summarize data relating to what might be called "important" solar-flare events for the months of March and April 1976. The table includes data for all flares that met any one of the following criteria:

a. Sudden Ionospheric Disturbance, importance ≥ 2
b. Hα importance ≥ 1
c. 10 cm flux > 100 units
d. Dynamic spectrum showed either Type II or Type IV or continuum

Those events that also satisfied the criteria for "major" flares, as in the earlier compilations, are identified by asterisks.

The list includes 28 events with indices ranging from 1 to 12. For three of the events (0837 or 0907 UT, 23 March; 1905 UT, 28 March; and 2048 UT, 30 April) the indices were ≥ 10 and indicated flare events with outstanding electromagnetic radiation, especially in the radio frequency end of the spectrum. In no case was the Hα importance greater than one. The flare on 23 March may have been the greatest of the three events since its Hα aspect probably was severly limited because Plage 14143, in which it apparently occurred, was still behind the east limb, and only elevated aspects of the flare were observable. During the Retrospective Interval, there were three periods of severe geomagnetic disturbance. They were centered on 26 March, 1 April, and 3 May. Were the three especially significant flares mentioned above associated with these three geomagnetic effects?

5. Other Centers of Activity During the Retrospective Interval

It should be noted that the increase of flaring that began on 17 March (see Figure 1) and the marked onset of ionospheric disturbances, X-ray enhancements, and radio frequency events that began on 20 March 1976 (the first day of the Retrospective Interval) apparently were not associated with Plage 14143 and the center of activity of principal concern in this study. Instead, the phenomena of 20-22 March apparently stemmed from solar events in McMath Plage 14127 (N05, Carrington longitude $\sim 196°$, CMP 19 March), a region that dominated the solar hemisphere on the side of the sun opposite to that which contained the center of activity of major interest (See Figures 2 and 3).

This additional plage, number 14127, was in its first rotation in March 1976. It came over the east limb on 13 March as a very small spotless plage. Spots were first seen in the plage on 16 March. As the region approached the central meridian, the plage and spot grew in area and magnetic complexity. The spot, Mount Wilson 19667, was classified as β except on 20 and 21 March when it was $\beta\gamma$. On 21 March it also displayed a δ configuration.

Sixty-seven flare events were reported in the region; 12 were accompanied by SWFs. Two of the flares, on 21 March and 24 March, were considered to be of Hα importance 1. The remainder were subflares. In April the region returned as Plage 14161 and had a small number of flares. This center of activity had diminished greatly by its third and last rotation in May (see Figures 2 and 3).

The only other plage of some significance to cross the disk during the Retrospective Interval was McMath 14168 (N06, Carrington longitude $\sim 130°$, CMP 20 April) (see Figure 2). This region in its second rotation contained a small α spot and was the site of only a few flares. Type II and Type IV radio bursts on 20 April appear to have been time-associated with a subflare in this plage.

Finally, in the interest of things not understood in the development of solar activity, it can be pointed out that the pulse of activity that commenced in early March and ended in late June 1976, both began and ended with the formation of significant centers of activity in Carrington longitude $\sim 45° - 50°$ (see Figure 2). However, the relevant center of activity at the beginning of the pulse (Plages 14118, 14143, 14179) was in southern latitude of $\sim 05°$ while the closing center of activity (Plage 14275), with its newly formed spot, was at north 04°. These circumstances provide yet another example of the observation that for relatively long intervals of time a single longitude zone may dominate the development of solar activity and that the formation of individual centers of activity may not always be independent phenomena.

Acknowledgments:

The authors acknowledge with gratitude support from NASA grant NGL-23-005-275 and from contract NOAA 03-4-022-94 in the preparation of this report.

Large Scale Observations in the Hα Line of McMath Regions 14143 and 14179

by

V. Gaizauskas and J.-René Roy
Herzberg Institute of Astrophysics
National Research Council of Canada
Ottawa, Canada K1A OR6

The solar events of March and April 1976 arouse considerable interest because they occurred during an unusually extended period of quiescence in the solar cycle.

I. General Development of the Active Regions

The plage McMath 14118 first appeared near latitude S05 on the Sun on 5 March and passed over the west limb on 9 March 1976. This active center returned to the east limb as a complex sunspot group, McMath 14143, on 24 March and again as McMath 14179 on 20 April 1976. It was photographed at the Ottawa River Solar Observatory (ORSO) on 11 days during two successive disk passages on a scale of 15 arcseconds per mm through a Zeiss 0.25Å birefringent filter mounted within the 25-cm photoheliograph of the ORSO [Gaizauskas, 1976]. Filtergrams were obtained at 3 second intervals in the core of Hα and, on seven days, at 14 other wavelengths distributed across the Hα profile. The mean distance between two parallel lines formed by the reticle wires in each of the Figures 1-5 corresponds to 150 000 km.

Figures 1 a, b (bottom sequence) display the sunspot group viewed 1.3Å off-band in the blue or the red wings of Hα. In the same figure, corresponding filtergrams are shown in the core of Hα (except the frame for 4 April which is at Hα + 0.4Å). The spot group was classified as a complex γ magnetic configuration. The boundary between opposite polarities was aligned roughly NS (cf. Mt. Wilson sunspot drawings); the active region filament extended EW through the active center (see the Hα sequence). The most conspicuous features of the sunspot configuration were a slight reduction of the sunspot area and a pronounced westward drift of the (-) spot marked by an arrow on 26, 28, 29 March and on 2 April 1976. During cycle 20, (+) polarities were normally leading in the Southern Hemisphere. The total displacement between 26 March and 2 April amounted to 40 000 km, half of which took place between 26 and 28 March. On 28 March (the day of a large flare), an opposite (+) polarity had emerged so close to the drifting (-) sunspot as to be contained within the same penumbra (Figure 1a, 28 March 1948 UT). The apparent rotation of the sunspot group is probably spurious and can be attributed to perspective effects as the group was carried across the tilted surface of the rotating sun ($P \sim -26°$, $B \sim -6°$).

The Hα filtergrams show the evolution of the large active region filament during disk passage. Note that on most days the filament did not pass continuously through the active center; it was interrupted by a network of fibrils near the region of highest magnetic field intensity. The fibril orientation was more or less parallel to the direction of the filament on 29 March but was transverse to the filament on 2 April. The Hα emission visible in the umbra of the larger spot and the light plage extending as a ribbon to the north of the filament may have been residues of the 28 March flare of 1920 UT.

Figure 2 shows the return of the active center as McMath 14179 on 29, 30 April and 2 May 1976. The activity on 30 April was related to a chain of small sunspots (Mt. Wilson 19680 classified as βf on 29 April and βγ on 30 April and 2 May) north of a more stable and larger sunspot (Mt. Wilson 19677, classified αf). The most important change of sunspot configuration and emergence took place between 29 and 30 April. The Mt. Wilson drawings reveal mixed (-) polarities within the common penumbra surrounding the (+) sunspot marked by an arrow on 30 April, 1243 UT.

The Hα filtergrams indicate considerable rearrangement of chromospheric features between 29 and 30 April. For example, on 29 April, giant fibril structures interconnected three spots (Figure 2; 1453 UT). On the 30th the fibril structures had disintegrated, presumably owing to the emergence of opposite magnetic polarities within the middle spot of this trio. The dominant Hα feature was the group of twisted fibril strands (April 30, 1234 UT) spreading along the boundary between opposing magnetic fields. The short filament trailing the active center was still visible on 2 May.

II. Flares in McMath 14143 and 14179

Figure 1a shows a subflare near maximum on 26 March (1444 UT) which apparently coincided with a small X-ray burst recorded by the satellite GOES-1. A 1B flare took place in McMath 14143 on 28 March 1976 starting 1905 UT and reaching maximum around 1932 UT. Our observations began near flare maximum at 1937 UT and continued until 2150 UT when the flare was still fading. Throughout these observations, the Hα profile was scanned between -1.3 and +1.3Å.

Figure 3 depicts the two-ribbon character of the flare at maximum brightness and the formation of bright loops interconnecting the flare ribbons during the postmaximum phase. The negative images, prepared from reversals at unity gamma of the original photographs, were printed to emphasize the fine struc-

ture within the brightest parts of the flare. The positive prints are an attempt to reveal the same over-exposed details without losing the structure in the fainter chromospheric background. They were prepared from internegatives in which the density scale was compressed photographically to lie within a range compatible with the latitude of normal printing paper.

Throughout our observations the brightest parts of the flare lay over the umbra of the large southern sunspot and a small area marked by an arrow in the off-band frame 19:48:08 UT (Figure 4). We did not detect any change in the position of these bright emitting centers. The fine structure of the ribbons in the off-band pictures (Figure 4) differed markedly from the bright amorphous blobs seen in Hα (Figure 3). The brightness at the outer edges of both flare ribbons dropped off very sharply. During our observations, the ribbons did not spread apart as sometimes reported for flares of this type. Instead, the ribbons shrank mostly from their inner edges as the flare faded. The reasons for this absence of lateral expansion can be sought in the fact that both ribbons were rooted in regions of large magnetic flux.

The short connecting bridge at 19:48:19 UT (see arrow in Figure 3) was the first sign of the loop prominence system shown at later times in Figure 3 (20:07:28 and 20:21:56 UT). The loop system was most clearly seen at 0.74Å in the red wing of Hα (Figure 4, 20:07:50 UT) and, although subdued, was still visible in the red wing when observations ended near 2150 UT.

A curious absorption feature extending westward from the umbra of the large spot was conspicuous near maximum (see arrow on Figure 3 at 19:37:58 UT). This feature and the adjacent bright emission underwent drastic modifications as the flare faded. The filament at the neutral line in the active region did not evolve much during the flare, except at the extreme west end (Figure 3, 20:07:28 and 20:21:56 UT). Dark arched structures became activated northwest of the flare during the late phase (Figure 4, 20:07:08 and 20:21:53 UT). This activity was accompanied by the the appearance of a surge-like feature, visible in the blue wing images, which was apparently falling back towards the bright kernel marked by the arrow in the frame at 19:48:08 UT, Figure 4.

On 30 April 1976, a subflare (-N) occurred in McMath 14179 at S06 W44, starting at about 1242 UT, reaching maximum around 1248 UT and ending around 1306 UT (Figure 5). The brightest knots of the flare were located 30 arcsec northwest from the chain of sunspots (see arrow in frames at 12:48:49 and 12:50:11 UT), and appeared to be associated with the small filament on the leading side of the active center. The event was accompained by a simple type 2800 MHz burst which reached 42 solar flux units at 1244.3 UT. We were unable to scan the profile of Hα automatically during this event, but had to rely on manual adjustment of the Hα filter to record off-band images. We terminated our observations before the large event starting at 2047 UT.

An energetic subflare, previously unreported, was observed through thin clouds on 2 May 1976 to be in progress at 1939 UT. It was located at a site of mixed magnetic polarities, the westernmost group of small sunspots seen in the frame of Figure 2 for 1956 UT, 2 May. The maximum phase, judged from emission in the wings of Hα, occurred at 1943 UT. Emission in the core of the line had subsided by 1953 UT, but associated filament eruptions that were detected in the wings of Hα continued for at least another ten minutes.

Summary of Observing Periods at the Ottawa River Solar Observatory for McMath Regions 14143 and 14179

DATE 1976	START OF OBSERVATIONS (UT)	APPROX. DURATION (HOURS)	WAVELENGTH MODE (BANDPASS 0.25Å)
March 26	1433	1.3	Automatic. 14 steps between ±1.3Å
28	1937	2.2	"
29	1522	3.2	"
30	1551	3.9	Hα only
April 2	2010	1.5	Automatic. 14 steps between ±1.3Å
3	1748	0.7	"
4	1756	0.87	
	2007	1.3	"
5	1930	2.1	"
29	1443	0.7	Manual. Hα and several wavelengths in red and blue wings
30	1234	0.5	"
May 2	1856	2.5	Automatic. 16 steps between ±1.4Å

The data consist of monochromatic images on 35 mm film of an area 4x5 arcmin^2 on the Sun. The typical interval between exposures was 3 seconds.

REFERENCE

GAIZAUSKAS, V. 1976 The Ottawa River Solar Observatory, *J. Roy. Astron. Soc. Canada, 70*, p. 1.

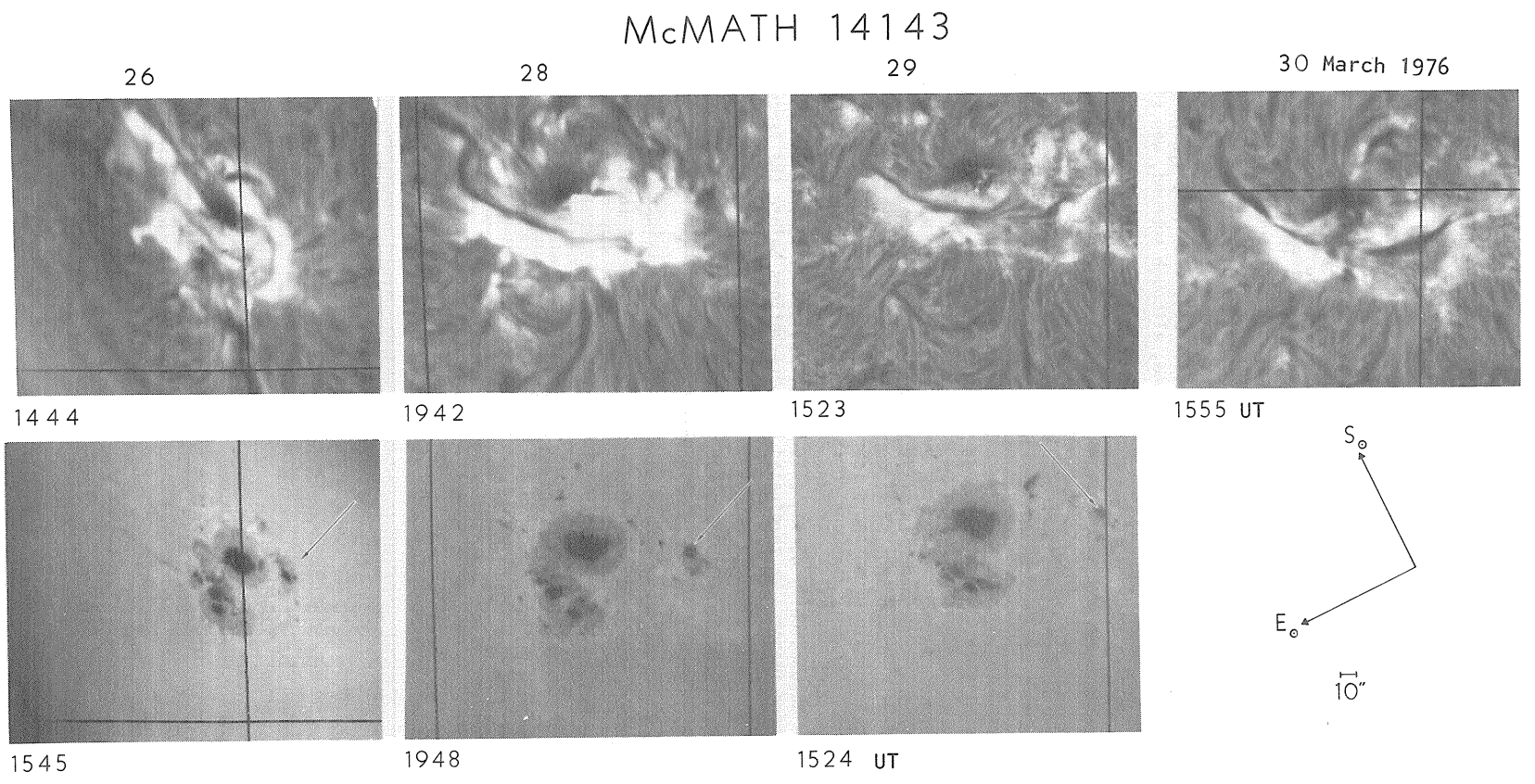

Figure 1a

Fig. 1. Disk passage of active center McMath 14143. In the top sequence, the Hα filtergrams display the evolution of the surrounding chromospheric structure. The frames for 26 and 28 March were taken while flares were in progress. The sequence at the bottom shows frames taken far enough (∿± 1.3 Å) in the wings of Hα to display the sunspot structure. The sunspot marked by by an arrow is drifting westward. The mean distance between two parallel lines formed by the reticle wires in each of the Figures 1-5 corresponds to 150 000 km.
(A) Sequence for 26, 28, 29 and 30 March 1976.
(B) Sequence for 2, 3, 4 and 5 April 1976.

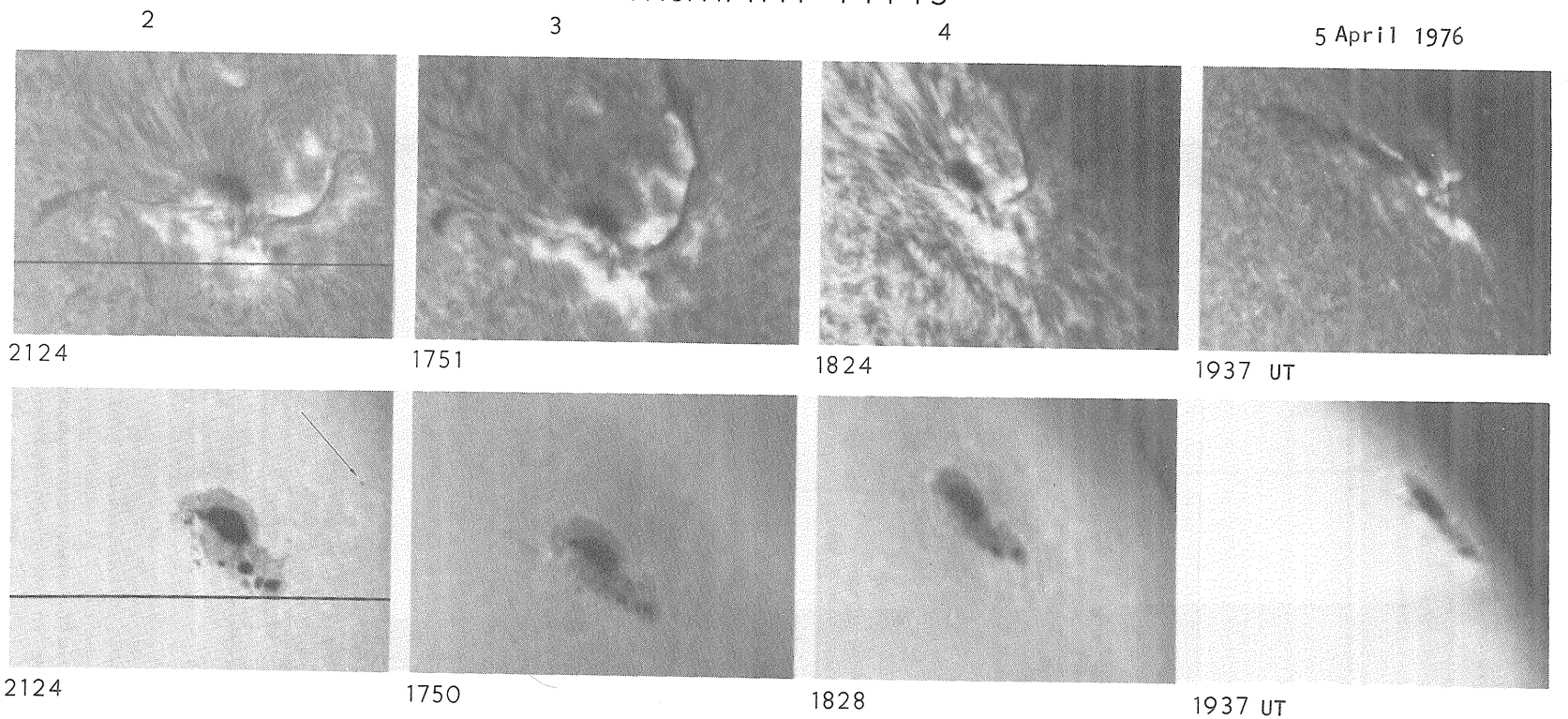
McMATH 14143
2
3
4
5 April 1976
2124
1751
1824
1937 UT
2124
1750
1828
1937 UT
10"

Figure 1b

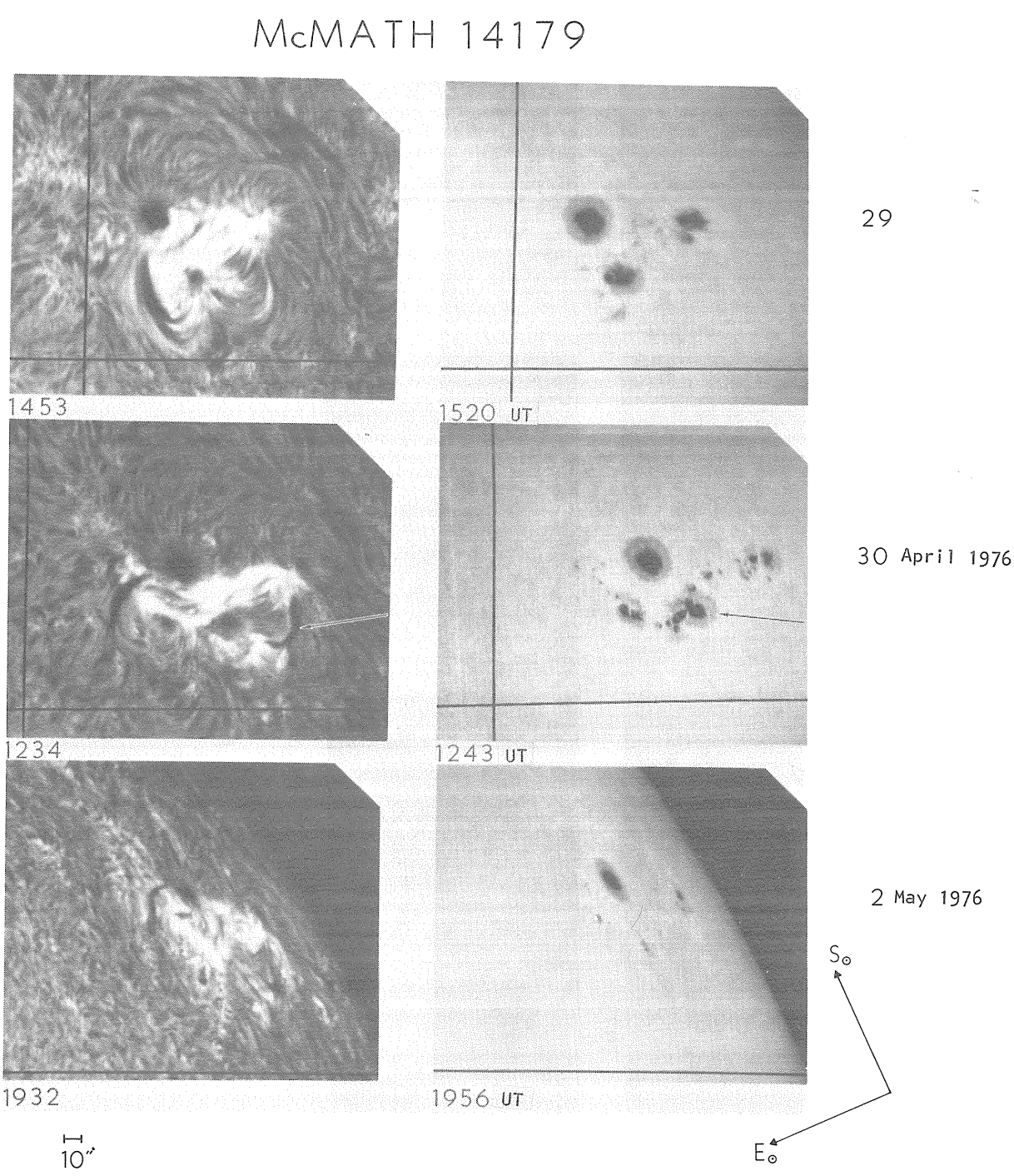

Fig. 2. Active center McMath 14179. The left column corresponds to Hα filtergrams taken in the core of the line, while the filtergrams in the right column were taken in the wing of the line (∿± 1.3 Å). The Hα filtergram at 1234 UT was taken shortly before the eruption of the subflare displayed in Figure 5.

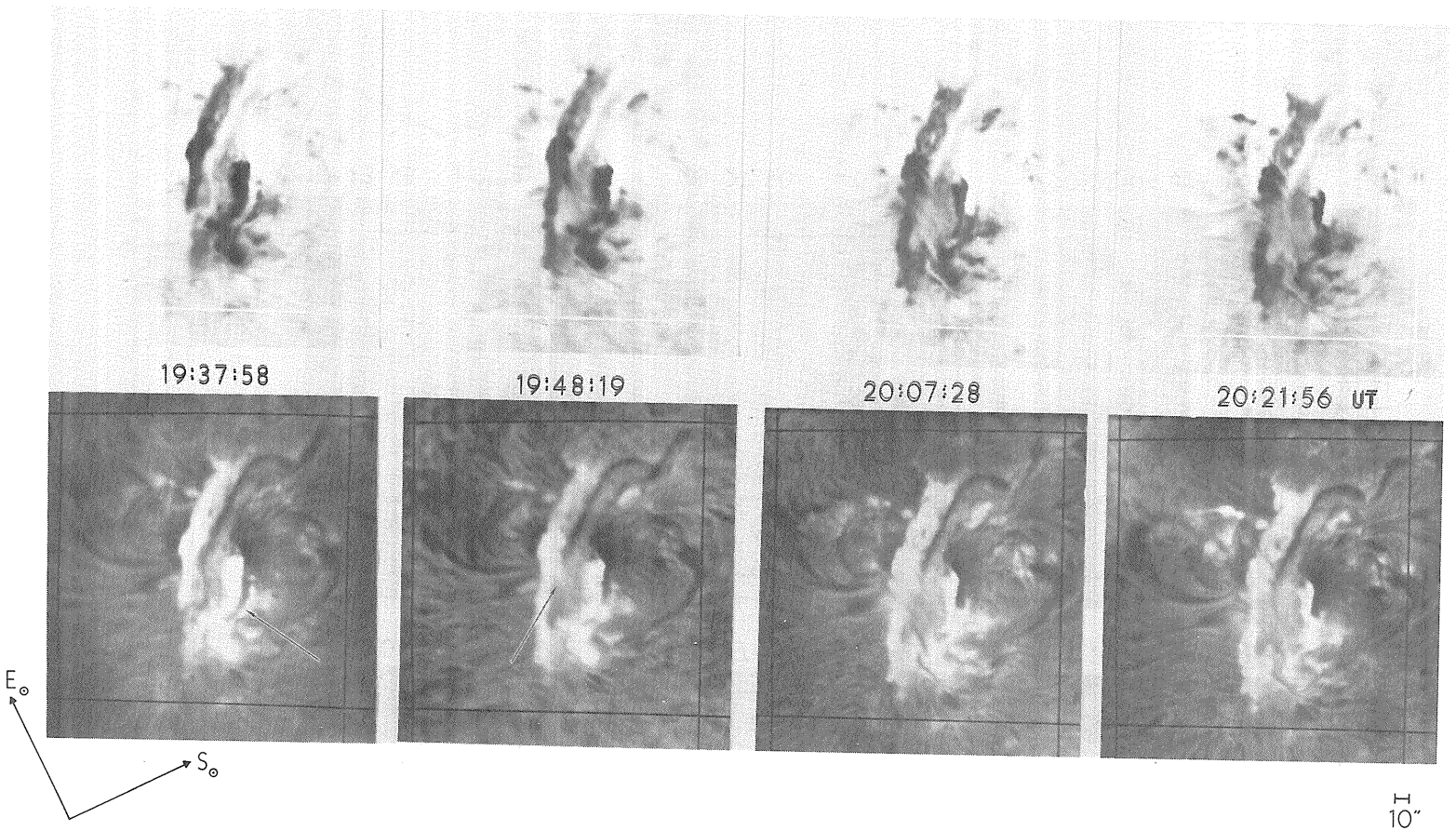

Fig. 3. Negative (top row) and positive (bottom row) prints of filtergrams taken in the core of Hα during and after the maximum phase of the 1B flare in McMath 14143 on 28 March 1976. Notice the loop prominence system bridging the two bright ribbons of the flare after 19:48:19 UT.

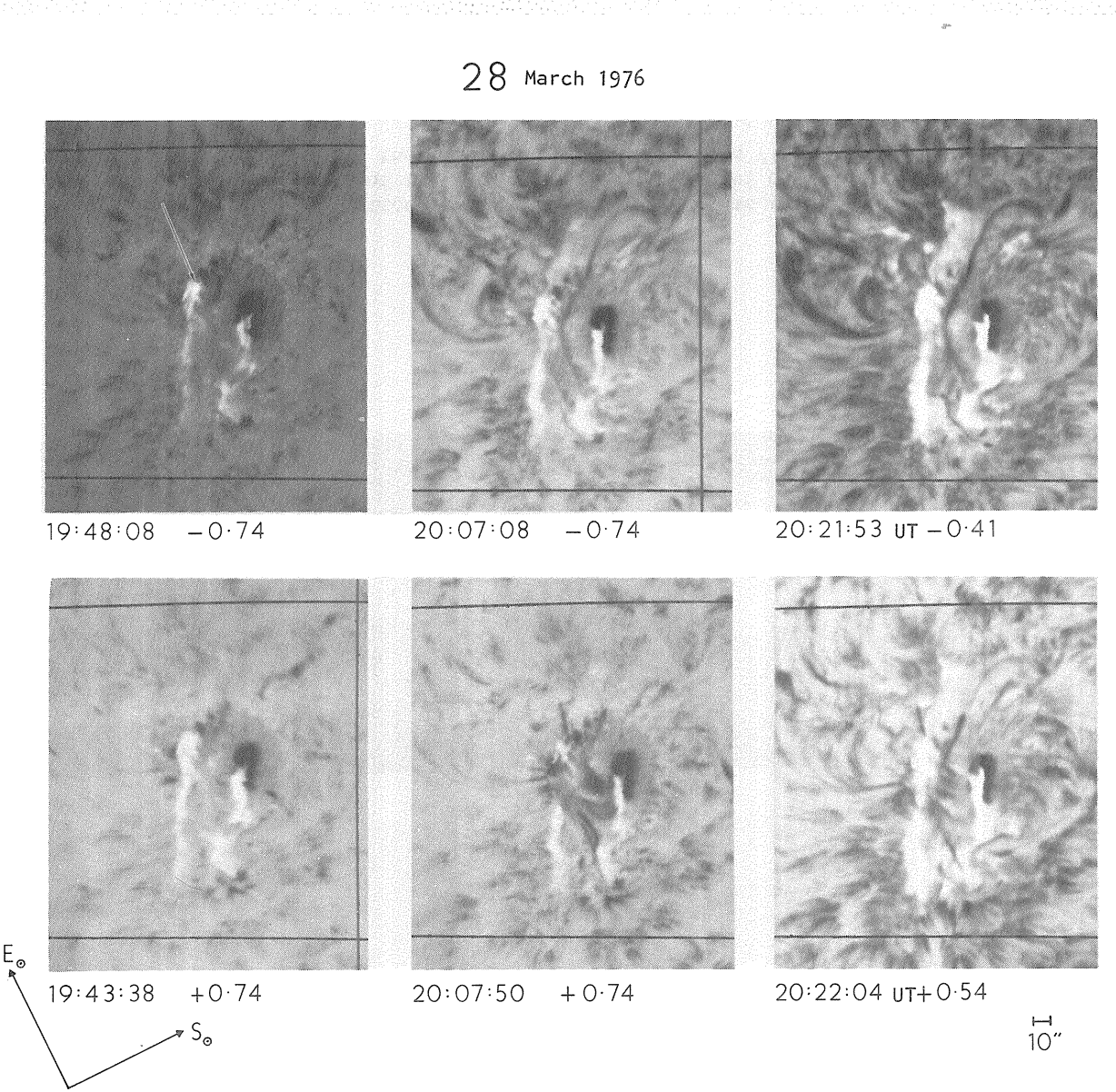

Fig. 4. Hα filtergrams taken off-band during the 1B flare in McMath 14143 on 28 March 1976. Notice the fine structure of the flare ribbon at 19:48:08 UT (-0.74) and the strong absorption (20:07:50 UT and 20:22:04 UT) indicative of the mass motion associated with the loops seen in Figure 3.

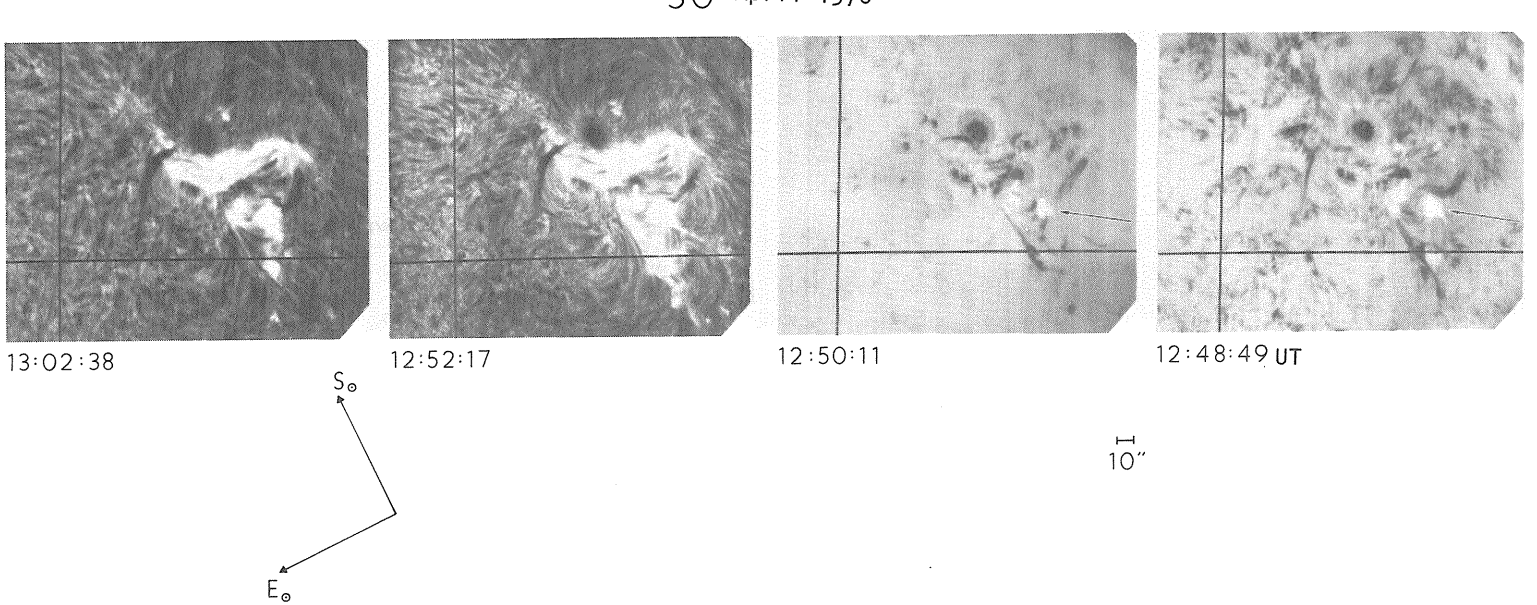

Fig. 5. Off-band and on-band Hα filtergrams of a subflare in McMath 14149. The bright compact flare center was displaced from the chain of sunspots seen in Figure 2 (30 April at 1243 UT) and appeared to be associated with the filament shown with an arrow in Figure 2 (30 April, 1234 UT).

In chronological order, the wavelengths of the frames are: Hα-0.5Å; Hα+1.0Å; Hα center; Hα center.

Observations of the Satellite - Type Sunspot Complex Region of 26 April - 3 May, 1976 at Mt. Sayan Observatory

by

V.V. Kasinskii, V.I. Polyakov, V.G. Zandanov
Siberian Institute of Terrestrial Magnetism, Ionosphere and Radio Wave Propagation of the Academy of Sciences, Siberian Division, Irkutsk, USSR

At the Mt. Sayan Observatory of the SibIZMIR, using the solar optical and radio astronomy equipment, daily observations of the McMath region 14179 (N24 according to *Solar Data* bulletin, USSR) were performed during the active period 26 April - 3 May 1976.

The following data on solar activity have been obtained:

1) The visual magnetic field strength measurements at the separate sunspot points
2) Large-scale (the sun disk diameters of about 550 mm) drawings of sunspot configuration
3) Selected Hα pictures of the region ($\Delta\lambda = \pm 0.5$Å, $\lambda = \pm 0.5$Å)
4) The radio microbursts at the wavelength of 3.5 cm

Figure 1 represents the drawings of the complex McMath Region No. 14179 with magnetic field strength measurements in the separate sunspots added. In Figure 2 three successive phases of development of the region in Hα are given. The summary data of the radio events in the region are presented in Table 1.

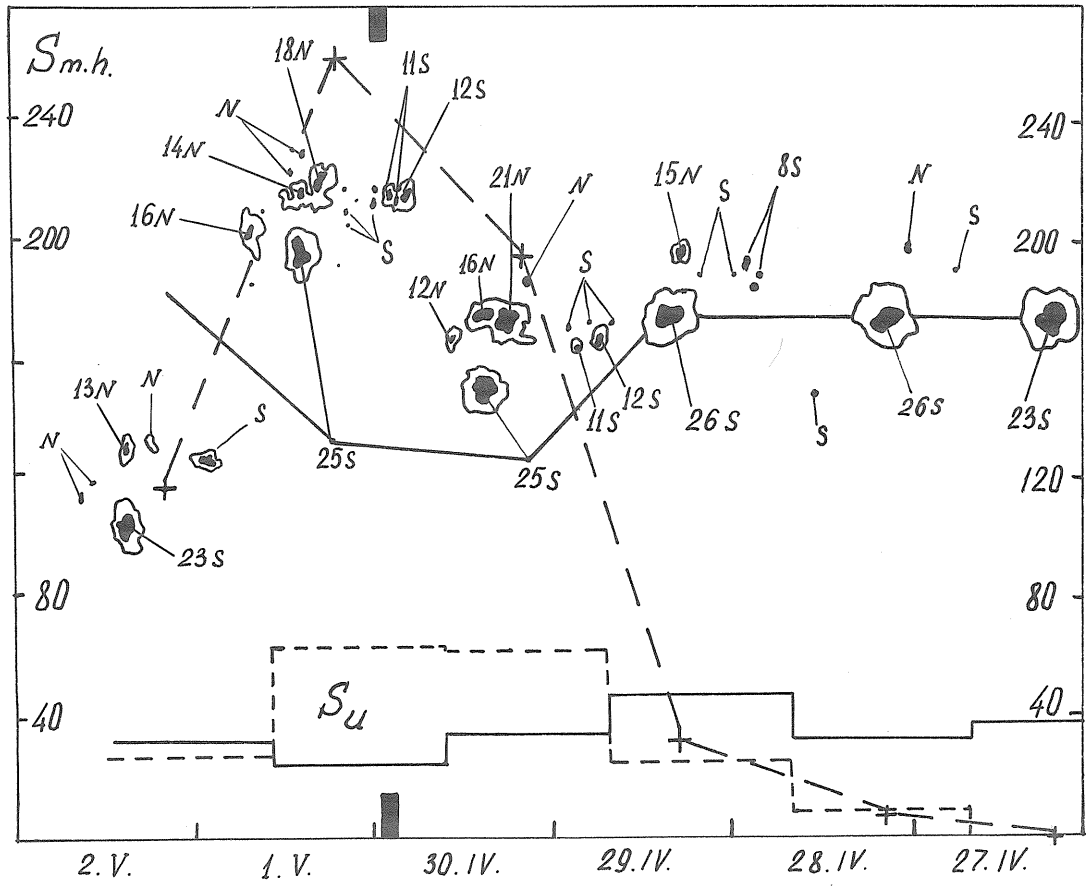

Fig. 1. The top half of the figure shows the development of the unipolar spot and its satellite group; the dashed line represents the satellite area in millionths of the solar hemipshere (m.h.). Magnetic field strengths are given in units of 100 gauss. The nuclear components of the spot area (S_u) are presented below.

The main picture of general development of the region is given in Figure 1. The preliminary results of detailed area development together with analysis of supplementary information (Figure 2, Table 1) lead us to the following conclusions:

The McMath region 14179 represents an interacting complex of two neighboring sunspot groups, one of which was unipolar and stable, the other one a typical satellite group with a rapid development [Kasinskii, 1972]. The first appearance of this satellite was recorded at 0017 UT, 28 April in the form of two small bipolar spots (Figure 1). Because the flare took place on 30 April (2130 UT) the role of satellite spot groups as flare precursors gains support [Kasinskii, 1973].

During the first three days, 27-29 April, when the satellite's area in millionths of solar hemisphere (28 m.s.h.) remained lower than that of unipolar component (160 m.s.h.), the latter was stable in area and in magnetic field strength (H = 2600 gauss). Between 29-30 April, the process of interaction of the two components began. A decrease of 60 m.s.h. in the area S of the unipolar component and a sharp increase of 160 m.s.h. in the satellite area occurred. The rate of change of the area (dS/dt) was -3 m.s.h. per hour and +8 m.s.h. per hour, respectively. Therefore, the rate of satellite area growth was 8/3 times higher than the decay rate of the unipolar spot. Taking into account the further growth of the satellite spot group on 1 May (dS/dt = 2.5 m.s.h./h), we concluded that after 0448 UT on 29 April a strong emergence of new magnetic flux occurred. According to Rust's [1974] observations, this seems to be the necessary condition for a flare.

According to the hypothesis proposed by Kasinskii and Krat [1973], the rapid development of a newborn magnetic feature should lead to the generation of a disturbance--one which may adopt the form of tsunami waves in the vicinity of the active complex. As a result of dissipation of the hydraulic energy of this wave, a flare process may occur as suggested by Kasinskii [1967]. In analyzing the phenomena: "new magnetic flux emergence- subsequent flare", we proceed from the phenomenological hypothesis: the larger the newborn magnetic flux in an active complex, the more probable the appearance of a strong disturbance and flare therein. This hypothesis necessarily has a probable character because a chain of processes influencing each other lies between the new satellite appearance and the flare itself as the final state.

Note in Figure 1 that the new magnetic field eruption occurs on the background of diminishing (Figure 1) or sinking of the old field (unipolar sunspot). After the end of the process of interaction, the area of the unipolar component returns nearly to its previous value: S(2 May) $\cong$ 0.968 S(28 April). This is an indication of the partly elastic character of the interaction.

In connection with the flare generation in McMath 14179 we noted that the compactness index of the unipolar component equaled 1.0, while that of the satellite group was 0.7 - 0.8 [Kasinskii *et al.*, 1976].

Chromosphere (Hα)

The observations were made on the large solar coronograph (F = 7 m, sun disk diameter of about 130 mm) using the Hale Hα-filter. Satisfactory pictures were made for three times: 0806 UT on 27 April, 0320 UT 28 April and 1045 UT on 29 April, capturing three different development stages of the active region (Figure 2). In Figure 2a radial filaments are visible near the unipolar spot which manifests the open and stable magnetic structure. On 28 April the radial filaments disappear; to the west of the spot a new broad filament occurs; and the brightness of the flocculi increases. At 1045 UT on 29 April the magnetic field emergence into the chromosphere is completed, and both the satellite spot group and the large flocculi, which are three times larger in area than the unipolar sunspot, become visible.

Radio Bursts in the 3.5 cm Bandwidth

On the small baseline radio interferometer of the SibIZMIR the daily observations of the local radio sources were measured for 28 and 29 April. For a detailed description of the instrument see Zandanov and Treskov [1973]. This instrument registers only the flux from the local sources from the Sun by excluding the full solar flux. The visibility function of an extended source in the case of a two-antenna interferometer:

$$F(d,w) = \frac{J_1(k,d,w)}{k\, d\, (w/2)}$$

where $k = 2\pi/\lambda$ = the wave number
d = the base length,
λ = wavelength,
J_1 = the Bessel function of the first order
w = the angular dimension of the Sun.

The results of the observations of the radio bursts are summarized in Table 1.

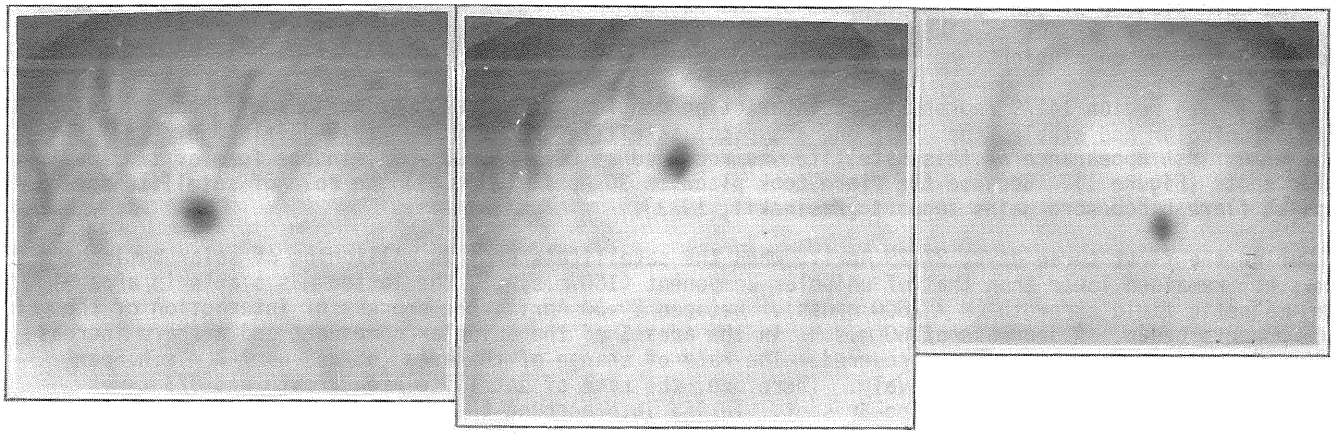

27 April 0806 UT 28 April 0320 UT 29 April 1045 UT

Fig. 2. Development of McMath active region No. 14179 over three sucsessive days in the Hα line.

Table 1

Summary Data of the Radio Events in McMath Region 14179

Date 1976	Time UT	Power (%) of the total flux	Duration (seconds)	Notes
28 April	0715-0716	1.8	10	impulsive
	0738	4.7	30	"
	0756-0806	4.3	10-50	6 burst groups
	0813-0829	4.0	10-30	5 "
	0840-0844	2.9	10; 3.2 min	3 "
	0856	4.0	15	impulsive
	0910	1.9	20	"
	0913	5.0	90	"
	0919	5.0	120	complex
	0925	5.0		
29 April				
	0747-0750	2.7	20	impulsive
	0815	2.9	10	"
	0821	1.2	5	"
	0823	3.0	-	complex
	0825	2.7	10	impulsive
	0841-0844	3.0	-	"
	0849	2.5	10	"
	0900	4.0	90	"
	0903	2.0	5	"
	0909	1.7	10	"
	0915	1.0	60	"
	0925	1.3	25	"

The regular interval of the observations in each day is from 0100 to 0900 UT. The real nature of the microbursts listed in Table 1 is not well understood. These bursts may be related to some instability conditions in the chromosphere over the active region. According to *Solar-Geophysical Data* [1976], from 0813 to 0847 UT and from 0835 to 0843 UT on 29 April subflares were recorded and from 0825 to 0910 UT impulsive bursts of Type I were observed.

The main parameters of the interferometer are listed below.

a)	bandwidth; wavelength	8750 MHz; λ = 3.5 cm
b)	length of the base	d = 136 λ
c)	antenna temperature with one mirror	T = 2500 K
d)	fluctuation sensitivity with the time constant t = 1 s	$\Delta T \cong 1$ K

REFERENCES

KASINSKII, V.V. 1967 Granulation, waves and the non-stationary processes in the solar atmosphere, *Res., Observ., Investig., I.Q.S.Y., 4,* p. 44.

KASINSKII, V. V. 1972 On the large scale interrelation between the chromospheric flare generated sunspots and the satellite groups, *Solar-Terrestrial Physics, 3,* Moscow, p. 296.

KASINSKII, V. V. 1973 On the role of the satellite groups as the proton flares predecessors, *Res. Geom. Aeron. Solar Phys., 26,* p. 118.

KASINSKII, V. V. and V. A. KRAT 1973 On the solar tsunami, *Solar Physics, 31,* 219.

KASINSKII, V. V., E. V. IVANOV and V. N. OBRIDKO 1976 The compactness index of the solar active regions and the proton events characteristics, *Symp. KAPG on Solar-Terrestrial Physics, Tbilisi-Moscow, 1,* 3.

RUST, DAVID M. 1974 Observation of flare associated magnetic field changes, in *Flare Related Magnetic Field Dynamics, NSAR, Boulder, Colorado,* 243.

ZANDANOV, V. G. and T. A. TRESKOV 1973 Application of the interferometer for the investigation of the solar radio wave fluctuations, *Res. Geom. Aeron. Solar Phys., 26,* 118.

SGD 1976 *Solar-Geophysical Data, 381-382 Part 1,* May-June 1976, U.S. Department of Commerce (Boulder, Colorado, U.S.A. 80302)

24 Flares Recorded Between 25 March 1976 and 1 May 1976 in Manila Observatory Region No. 162 (McMath 14143 and 14149 or SESC 690 and 700)

by

Alfredo Tejones and Francis Heyden, S.J.
Manila Observatory
Republic of the Philippines

DATE 1976	FLARE #	START/STOP (UT)	POSITION	AREA	IMP	Δt (hours)	ΔI (hours)
Mar. 25	01	0614/0619	S08 E78	0.30	Sn	0.08	----
	02	0704/0714	S05 E76	0.41	Sf	0.12	0.75
	03	2310/2318	S07 E67	0.41	Sf	0.13	----*
26	04	0001/0011	S05 E64	0.30	Sf	0.17	0.72
	05	0715/0720	S08 E59	0.21	Sf	0.21	7.07
	06	0721/0735	S06 E64	1.01	Sb	0.24	0.02
	07	0833/0858	S08 E58	0.30	Sf	0.42	0.96
	08	2300/2311	S07 E51	0.82	Sf	0.18	----*
27	09	0201/0213	S08 E58	0.82	Sn	0.20	2.84
	10	0318/0333	S07 E48	1.01	Sn	0.25	1.08
	11	0518/0526	S07 E56	0.82	Sf	0.13	1.75
	12	0550/0610	S10 E48	0.21	Sf	0.34	0.49
	13	0628/0640	S08 E62	0.62	Sn	0.21	0.29
	14	0726/0730	S06 E53	0.82	Sf	0.07	0.76
	15	2333/2339	S10 E42	0.82	Sf	0.10	----*
	16	2353/0000	S08 E43	0.52	Sf	0.12	0.23
28	17	0555/0608	S07 E34	1.24	Sb	0.24	5.92
29	18	0523/0524	S07 E19	0.82	Sn	0.02	----*
30	19	0531/0539	S07 E06	0.62	Sf	0.13	----*
31	20	0156/0207	S09 E02	0.41	Sf	0.19	----*
Apr. 30	21	0424/0429	S11 W04	0.52	Sf	0.08	----*
	22	0605/0607	S08 W40	0.62	Sn	0.01	2.28
	23	2205/2235	S09 W49	1.13	Sn	0.51	----*
May 01	24	2155/2210	S08 W61	0.92	Sn	0.25	----*

NOTES: AREA is in square degrees of hemisphere.
ΔI = interval between recurrences of flares.
* = observation made locally on following day.
Observations on 29, 30 and 31 March were based on visual data because of camera failure.
Data for 28, 29, 30 and 31 March were sporadic because of intermittent clouds.
The same was true for the return of Region 162 on 30 April.

The radio frequency data for the 24 flares listed in the table above is not significant. The Δt (duration of the flare) is quite close to the time predicted by the importance the observers assigned, but the interval, ΔI, between successive flares in the same region has no significance. This is partially but not necessarily due to passing clouds, except at the end of April.

Photographic prints of the 16 flares that were easily visible on 35 mm film taken through an H-alpha filter are available from the WDC-A for Solar-Terrestrial Physics. Unfortunately, prints could not be made of each of the 24 flares because of faintness, haze and instrumental problems. The following pages contain the daily spectroheliograms taken in H-alpha and in the K line of ionized calcium. None of these prints shows a flare, but they do present a detailed picture of the region on the Sun in which the flare activity took place. Moreoever, they illustrate the quality of the observations we are making available to the scientific community.

SPECTROHELIOGRAM OF HYDROGEN (H-Alpha)

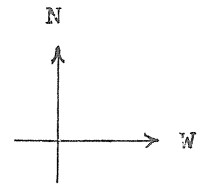

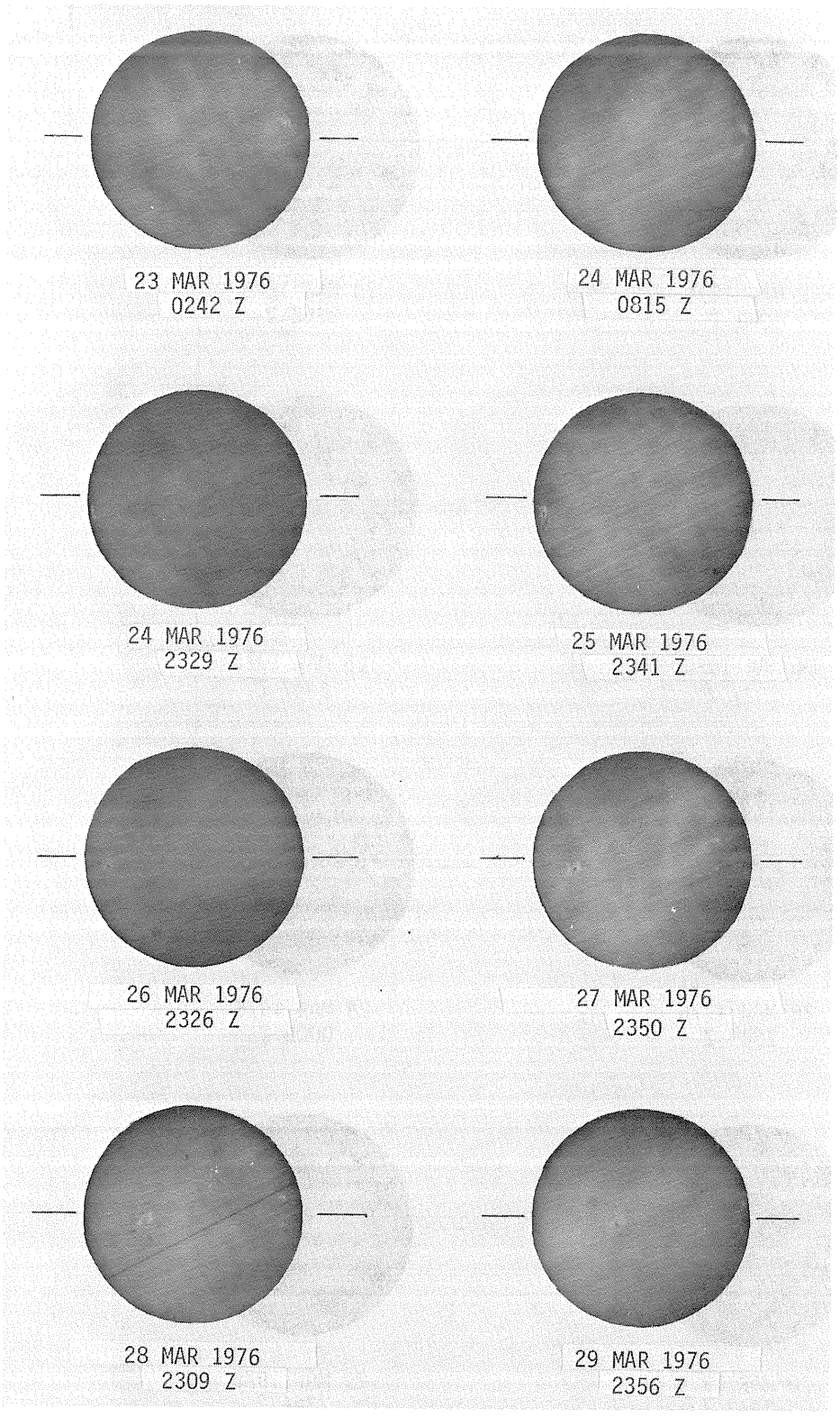

SPECTROHELIOGRAM OF CALCIUM II (K)

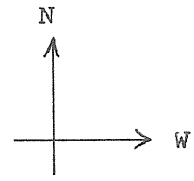

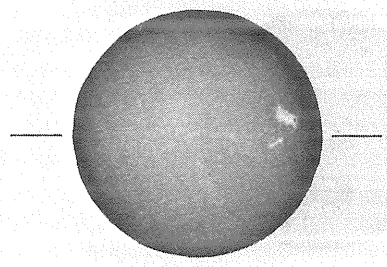

22 MAR 1976
2341 Z

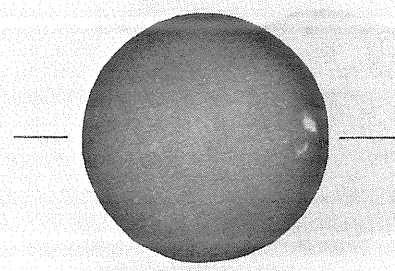

23 MAR 1976
2352 Z

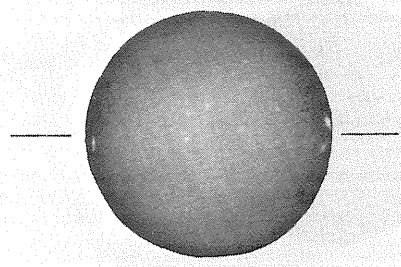

24 MAR 1976
2327 Z

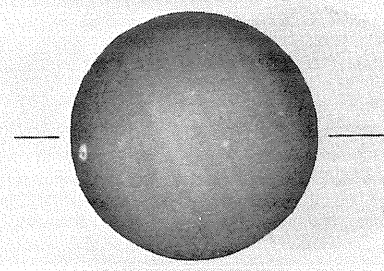

25 MAR 1976
2347 Z

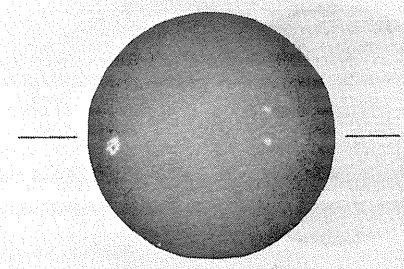

26 MAR 1976
2340 Z

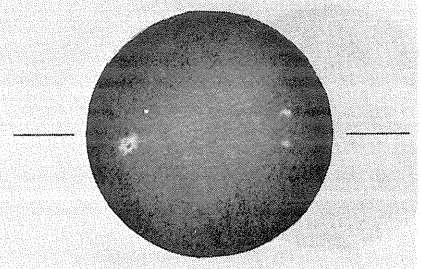

28 MAR 1976
0006 Z

28 MAR 1976
2333 Z

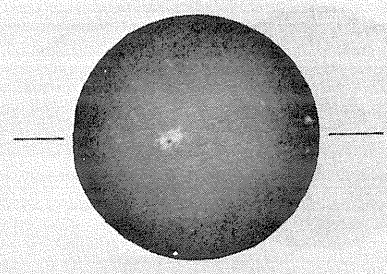

29 MAR 1976
2344 Z

SPECTROHELIOGRAM OF HYDROGEN (H-Alpha)

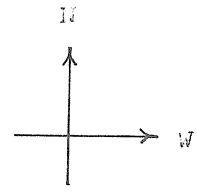

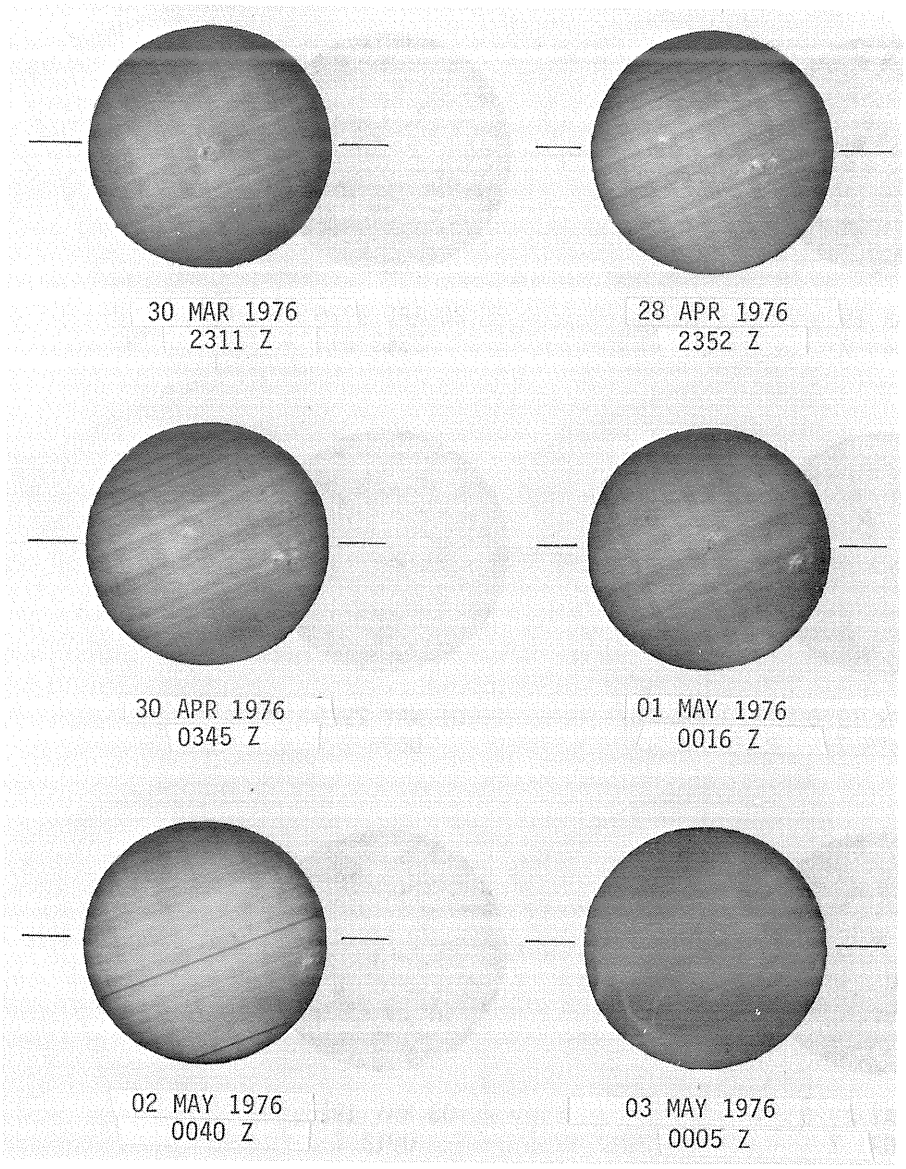

SPECTROHELIOGRAM OF CALCIUM II (K)

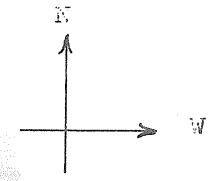

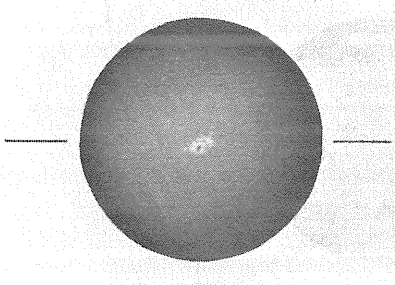

30 MAR 1976
2345 Z

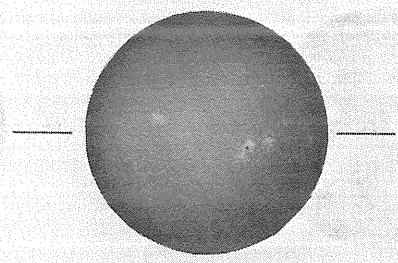

28 APR 1976
2343 Z

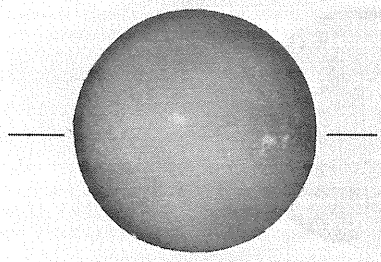

30 APR 1976
0325 Z

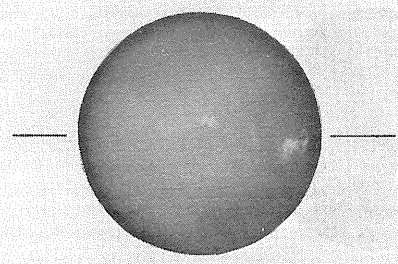

01 MAY 2976
0008 Z

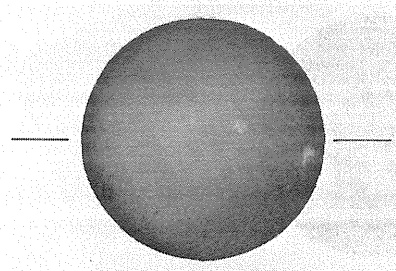

02 MAY 1976
0031 Z

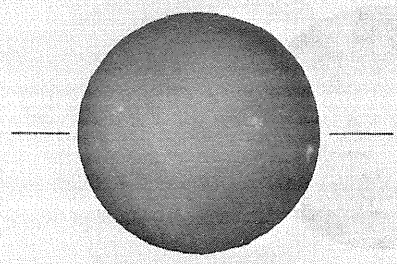

03 MAY 1976
0012 Z

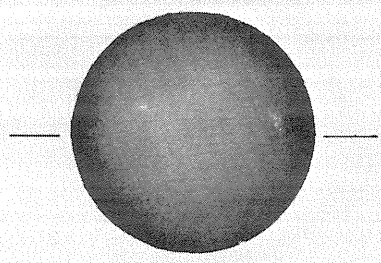

04 MAY 1976
0030 Z

Energy Content of Flares in McMath Regions 14143 and 14179 (March 1976)

by

Eva Marková
Observatory Úpice
542 32 Czechoslovakia

Rising activity occurred in McMath Region 14143 (14179) before solar minimum appeared. This region developed into a large magnetically complex group and produced several energetic events. At Upice Observatory the first subflare beginning before 1022 UT at N03 W33 was observed in the region on 21 March 1976; an importance 1B flare was observed on the same day before 0917 UT at a S09 E90 position. On 27 March a 1N flare at S17 E48 occurred, and still in the same region, a fourth flare was observed on 31 March, beginning at 1140 UT and ending at 1545 UT. At Upice this last event was observed only after 1400 UT.

Preliminary Calculation of the Amount of the Energy in Hα Flares

After Obashev [1968] the energy in Hα is directly proportional to the total flare duration and may be expressed in the following form:

$$E_{H\alpha} = 2.5\times10^{23}\ \alpha\ U\ T^{2.5}\ \text{ergs},$$

where U is the energy radiated from the region of the flare per unit volume and unit time in Hα; T is the flare duration time in seconds; and α is the transformation coefficient which lies in the range $0.75 < \alpha < 1$. When the mean energy $U = 0.02$ ergs/cm^3 s and $\alpha = 0.8$, the energy radiated in Hα emission may be expressed as

$$E_{H\alpha} = 4\times10^{21}\ T^{2.5}.$$

Table 1 introduces the energies radiated in Hα emission from several flares in McMath Regions 14143 and 14179. These flares were chosen on the basis of instructions from the Special Committee on Solar-Terrestrial Physics.

Table 1. Energies Radiated in Hα Emission.

Date 1976	Start UT	Max UT	End UT	Dur (s)	Imp	Position	Energy (ergs)
March 23	0837	0839	0841	240	SB	S05 E90	3.6×10^{27}
28	1834	1843	1855	1260	SN	S07 E26	2.3×10^{29}
31	1138	1200	1350	7920	1N	S07 W09	2.2×10^{31}
April 30	2047	2059	2118	1860	1B	S08 W46	6.0×10^{29}

Energy of the Flares Radiated in the X-ray Region

Thomas and Teske [1971] found that the value of the total energy radiated in the soft X-ray range between 8-12 Å was almost equivalent to the total flare energy radiated in the Hα line. Despite non-reliable information about the size and brightness of flares behind the limb, it is very important to determine the total energy radiated in the soft X-ray portion of the spectrum and in the other spectral regions. The total energy radiated during the X-ray outburst is determined from the following time integral [Van Allen, 1967]:

$$W = 2\pi R^2 \int_{t_1}^{t_2} F'_\lambda\, dt,$$

where F'_λ is the difference between the total energy flux and the flux level of the "quiet Sun"; t_1 is the beginning of the event; t_2 is the end of the event; and R is the Sun-Earth distance.

The emitted X-ray energy flux was measured by the GOES 1 satellite in the wavelength ranges 0.5-4Å and 1-8Å [*SGD*, 1976]. The published curves measured by satellite were divided into two equal parts; the dividing line was transferred from the logarithmic paper; and the value F'_λ was directly measured. Values of the total energy radiated during the X-ray outbursts are shown in Table 2.

Table 2. Total Energies Radiated During the X-ray Outbursts.

Date 1976	Wavelength Range (Å)	Start UT	Dur (s)	F'_λ (ergs/cm^{2}s)	Energy (ergs)
March 23	0.5-4	0837	8580	9×10^{-5}	1.08×10^{27}
	1-8	0837	10980	9×10^{-4}	1.45×10^{28}
28	0.5-4	1837	48180	4×10^{-5}	2.70×10^{27}
	1-8	1837	48180	1×10^{-3}	6.75×10^{28}
April 30	0.5-4	2043	10800	1.1×10^{-4}	1.66×10^{27}
	1-8	2043	13600	9×10^{-4}	1.71×10^{28}

Energy of the Flares Radiated in the Radio Range

The energy of the radio outburst is almost negligible in comparison to the total energy released during the flare over all wavelengths. Consider, for example, the energies of many impulsive bursts and those of the more slowly varying radio events. These energies lie in the ranges 10^{22}-10^{23} and 10^{23}-10^{24} ergs, respectively [Krüger, 1969; 1972].

We can determine the total radiated energy in the radio outburst from the relation

$$E = \pi R^2 F_T \Delta f,$$

where F_T is the total flux in the given frequency range Δf. For F_T we took the values of the mean flux density from *SGD* [1976]. For every frequency interval typically three wavelengths were taken from *SGD*. These three cases were used in calculating the mean durations and the mean total fluxes. The latter were used in the calculation of the energy over the considered frequency range. Table 3 lists three computed energies for the chosen flares.

Table 3. Energies of Selected Flares.

Date 1976	Freq (MHz)	Start UT	Max UT	Dur (min)	Mean Dur (min)	Flux Density (s.f.u.)	Mean Flux Density (s.f.u.)	Δf (MHz)	Energy (ergs)
March 23	113	0841.3	0842.9	59		900			
	228	0841.3	0842	8.7	34.6	380	593.3	270	4.8×10^{22}
	245	0840	0842	36		500			
	410	0840	0854.4	26		180			
	606	0840.7	0843.3	13.6	21.9	178	176.3	2700	8.8×10^{22}
	808	0840.6	0843.7	26		171			
	1415	0840.6	0842.9	28.9		86			
	2695	0840.3	0843	29.2	32.5	150	131.3	2700	4.7×10^{23}
	2950	0840.2	0849.6	39.4		158			
	4995	0840.3	0845.6	29.2		300			
	8800	0840.8	0845.3	28.7	24.1	520	346	27000	1.4×10^{24}
	9100	0840.5	0847	14.5		218			

Table 3. (Continued)

Date 1976	Freq (MHz)	Start UT	Max UT	Dur (min)	Mean Dur (min)	Flux Density (s.f.u.)	Mean Flux Density (s.f.u.)	Δf (MHz)	Energy (ergs)
March 28	100	2136	2136.5	1.8		600			
	245	1914.9	1932.4	107.4	54.6	180	390	270	4.8×10^{23}
	410	1915	1921.4	118.3		310			
	606	1914.5	1917	146.8	132.6	730	520	2700	1.8×10^{24}
	1415	1914.2	1927.3	50.8		2500			
	2695	1914.6	1929	47.4	52.4	570	1180	2700	1.4×10^{24}
	2800	1914	1936	59		470			
	4995	1914.7	1929	45.3		950			
	8800	1915.4	1927.5	44.6	39.8	1100	1085.6	27000	9.8×10^{24}
	9400	1916.2	1934.3	29.5		1206.8			
March 31	127	1153	1235	140		350			
	234	1223	1224.3	1.8	86.5	10	151.6	270	3.0×10^{22}
	245	1149	1314.5	117.7		94.9			
	410	1140	1155.3	30.7		143.3			
	606	1152	1156.2	18	21.9	367.8	198	2700	9.8×10^{22}
	808	1153.2	1155	17		83			
	1030	1152	1158	18		90			
	1415	1152	1155.1	52	28.2	16.2	38.1	2700	2.4×10^{22}
	2695	1153.6	1159.3	14.7		8.2			
	4995	1152.2	1157.4	16.4		4.5			
	7000	1153.7	1157.4	81.4	34.2	15	7.2	27000	5.6×10^{22}
	9100	1156.5	1157.5	5		2			
April 30	100	2102	2103.6	94		130			
	227	2103	2107	29	74	90	163	270	2.7×10^{22}
	245	2101.7	2103.4	99.1		269			
	410	2100	2104.4	103.1		900			
	500	2101	2103	106	93.8	150	651.7	2700	1.4×10^{24}
	606	2055.6	2107	72.3		905			
	1415	2050	2107.1	37.8		815			
	2695	2055.3	2108.7	24.7	28.8	234	524.7	2700	3.4×10^{23}
	2800	2101	2109	24		525			
	4995	2050.2	2108.7	30.8		614			
	8800	2054.7	2107.7	29.9	26.4	789	824.8	27000	4.9×10^{24}
	9400	2102.1	2108.6	18.5		1071.3			

Magnetic Energy in the Volume of the Flare

We can determine the value of the magnetic energy from the equation

$$E = (B^2/8\pi)V,$$

where V is the volume of the flare, determined as the product of the area of the flare and the thickness of the chromosphere and B is the magnetic intensity of the active region, the mean values of which were taken from *SGD* [1976]. In Table 4 the magnetic energies of the chosen flares are introduced. The energy for the flare on 23 March could not be determined because it occurred on the east limb and thus prevented the area from being measured.

Table 4. Magnetic Energies of Selected Flares

Date 1976	Start UT	Max UT	Position	Energy (ergs)
March 28	1834	1843	S07 E26	2.2×10^{30}
31	1138	1200	S07 W09	1.1×10^{31}
April 30	2047	2059	S08 W46	1.7×10^{31}

Conclusion

The quantity of the calculated energy radiated in the individual parts of the electromagnetic spectrum is given in Table 5 for selected flares from the period March - May 1976. In the radio range the energies were calculated for the m, dm and cm wavelengths; the dm range has been divided into the intervals 3-10 and 1-3 dm. In comparison with other energies quoted these values for emission at tens of meters are substantially lower.

Table 5. Energies Radiated in the Individual Parts of the Electromagnetic Spectrum.

Wavelength Interval	23 March	28 March	31 March	4 April
Hα (6563Å)	3.6×10^{27}	2.3×10^{29}	2.3×10^{31} ergs	6.0×10^{29}
X-ray (0.5-4Å)	1.08×10^{27} ergs	2.7×10^{27} ergs	-	1.66×10^{27} ergs
X-ray (1-8Å)	1.45×10^{28}	6.75×10^{28}	-	1.71×10^{28}
Radio burst (m)	4.8×10^{22}	4.8×10^{23}	3.0×10^{22}	2.7×10^{22}
Radio burst (3-10 dm)	8.8×10^{22}	1.8×10^{24}	9.8×10^{22}	1.4×10^{24}
Radio burst (1-3 dm)	4.7×10^{23}	1.4×10^{24}	2.4×10^{22}	3.4×10^{23}
Radio burst (cm)	1.4×10^{24}	9.8×10^{24}	5.6×10^{22}	4.9×10^{24}
Magnetic energy in volume of flare	-	2.2×10^{30}	1.1×10^{31}	1.7×10^{31}

REFERENCES

KRIVSKÝ, L., A. TLAMICHA, J. HALENKA, J. LAŠTOVICKA, P. TRÍSKA, S. PINTÉR and J. ILENCÍK. 1972. Development and Spatial Structure of Proton Flares Near the Limb and Coronal Phenomena, *Bull. Astron. Inst. Czech.*, *23*, 94-104.

KRÜGER, A. 1972. Physics of Solar Continuum Radio Burst, *Akademie Verlag*, Berlin.

KRÜGER, A. 1969. Fifth Consultation on Solar Physics and Hydromagnetics, Potsdam, *Geod. Geopf. Veroff. R. H.*, *13*, 27.

OBASHEV, S. O. 1968. *Solar Activity.*

PINTÉR, S. 1972. Energy Content of Solar Flares, *4th Inter. Sem.*, Leningrad.

THOMAS, R. J. and R.G. TESKE. 1971. Solar Soft X-rays and Solar Activity II. Soft X-ray Emission during Solar Flares, *Solar Phys.*, *16*, 431-453.

VAN ALLEN, J. A. 1967. Solar X-ray Flare of July 7, 1966, *J. Geophys. Res.*, *72*, 5903-5911.

1976. *Solar-Geophysical Data, 380-382 Part I*, April - June 1976, U. S. Department of Commerce, (Boulder, Colorado, U.S.A. 80302).

1976. *Solar-Geophysical Data, 385-386 Part II*, September - October 1976, U. S. Department of Commerce, (Boulder, Colorado, U.S.A. 80302).

3. SOLAR RADIO DATA

Highlights of Solar Radio Data, 20 March - 5 May 1976

by

John P. Castelli and William R. Barron
Air Force Geophysics Laboratory (AFSC)
Hanscom AFB, Massachusetts 01731

and

Victor L. Badillo, S.J.
Manila Observatory
Manila, Republic of the Philippines

ABSTRACT

Principal solar radio data for this UAG report on the Retrospective World Interval, 20 March - 5 May 1976, are presented. Three very important radio outbursts occurred on 23 and 28 March and on 30 April. Since the data are drawn from patrols dedicated to warning and prediction of geophysical phenomena, applicable prediction signatures of the data are discussed.

Introduction

Observations for this report were made at the USAF solar radio facility, Sagamore Hill, Hamilton, Massachusetts (N42.632, W70.821) and at the Manila Observatory, Quezon City, Philippines (N14.663, E121.083). The Sagamore Hill Observatory is maintained by the Air Force Geophysics Laboratory and is staffed by personnel of the Air Weather Service; the Manila Observatory solar radio observations are made under Air Force contracts. Both observatories are stations of the USAF/AWS world-wide solar network that report data in real time to the AWS Global Weather Center.

The great variety of activity between 20 March and 5 May 1976 is important historically, since it occurred during sunspot minimum. This ill-defined minimum period may be several years long, and its relation to the old or new sunspot cycle remains imprecise. Indicators that cycle 20 was changing came as early as mid-1971 when the polarity of the solar north pole reversed. The following year, 1972, the solar south pole reversed its polarity [Gillespie *et al.*, 1973]. The first sunspot of cycle 21 was then reported to have been sighted at high latitudes in the solar southern hemisphere on 22 August 1975. Subsequently, various observatories reported high latitude spots, indicative of new cycle activity even as old cycle spots remained. Based on the radio viewpoint that minimum values of flux density in the centimeter wavelength range represent the crossover between sunspot cycles, sunspot minimum may have been reached sometime between June 1975 and June 1976.

The activity in March-May 1976 was not the only period of importance during the recent period of sunspot minimum. For example, on 21 August 1975, a major solar radio outburst accompanied by proton activity and a PCA event occurred. However, this event, in which the flare originated at N26 W71, may indeed have been from a new cycle sunspot region. Somewhat earlier, between 1972 and 1974 as sunspot minimum approached, some of the most spectacular events of sunspot cycle 20 occurred in old cycle regions at low latitudes.

In contrast to the 21 August 1975 event, the activity in March-May 1976 seems to have originated from an old sunspot cycle region at low latitude. Though the period of this report starts with 20 March, for the dramatic activity it can only start on 23 March with McMath Region No. 14143. Nevertheless, the extreme quiet of the whole Sun radio emission found in February 1976 first started to change as early as 12 or 13 March when McMath Region No. 14127 at about N02 came around the east limb. Figures 1 and 2 show the variation of the "quiet" Sun radio emission for the months of March and April 1976.

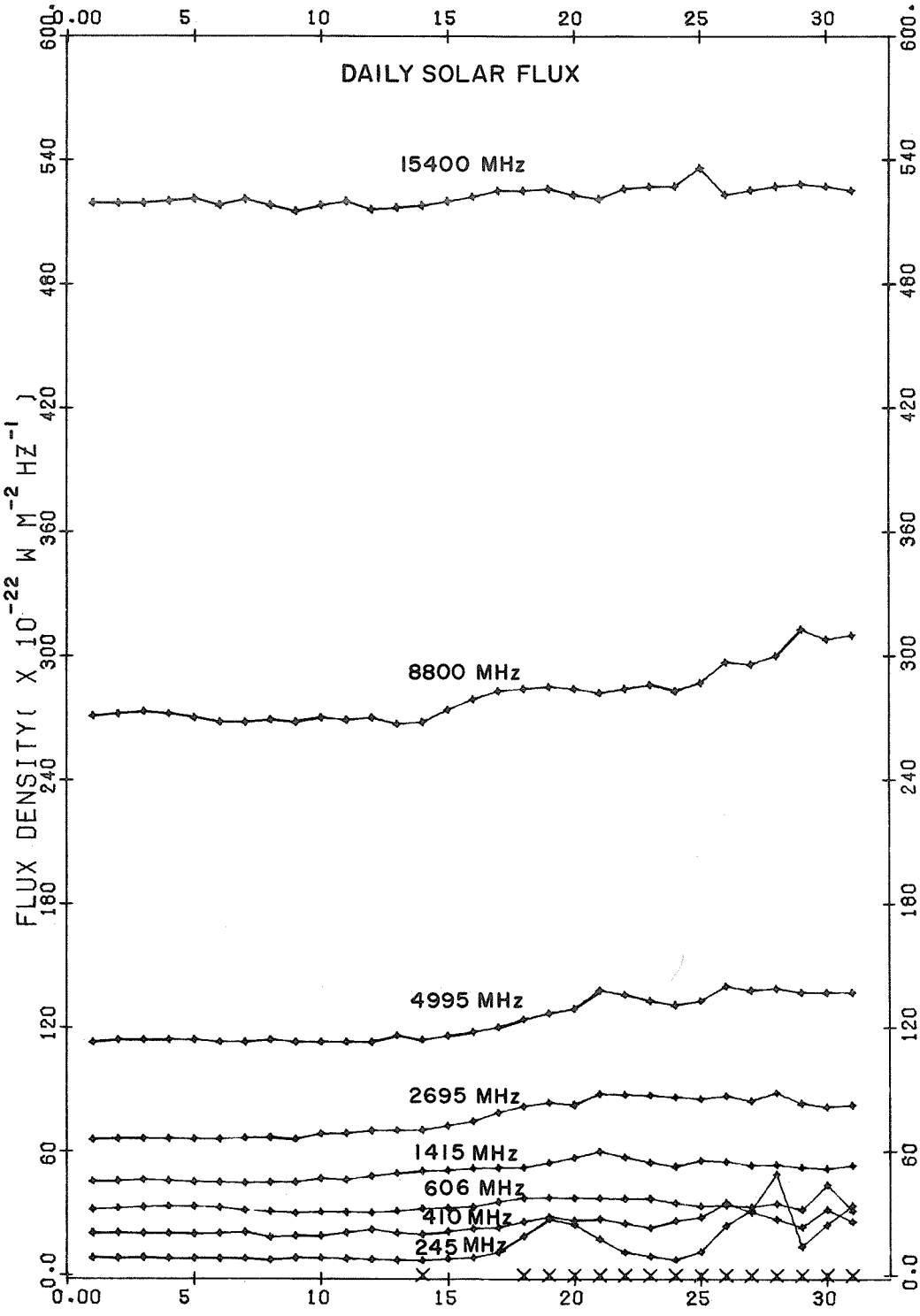

Fig. 1. Variation of the "quiet" sun radio emission for March 1976. The Xs along the bottom of the figure mark days on which distinctive events occurred.

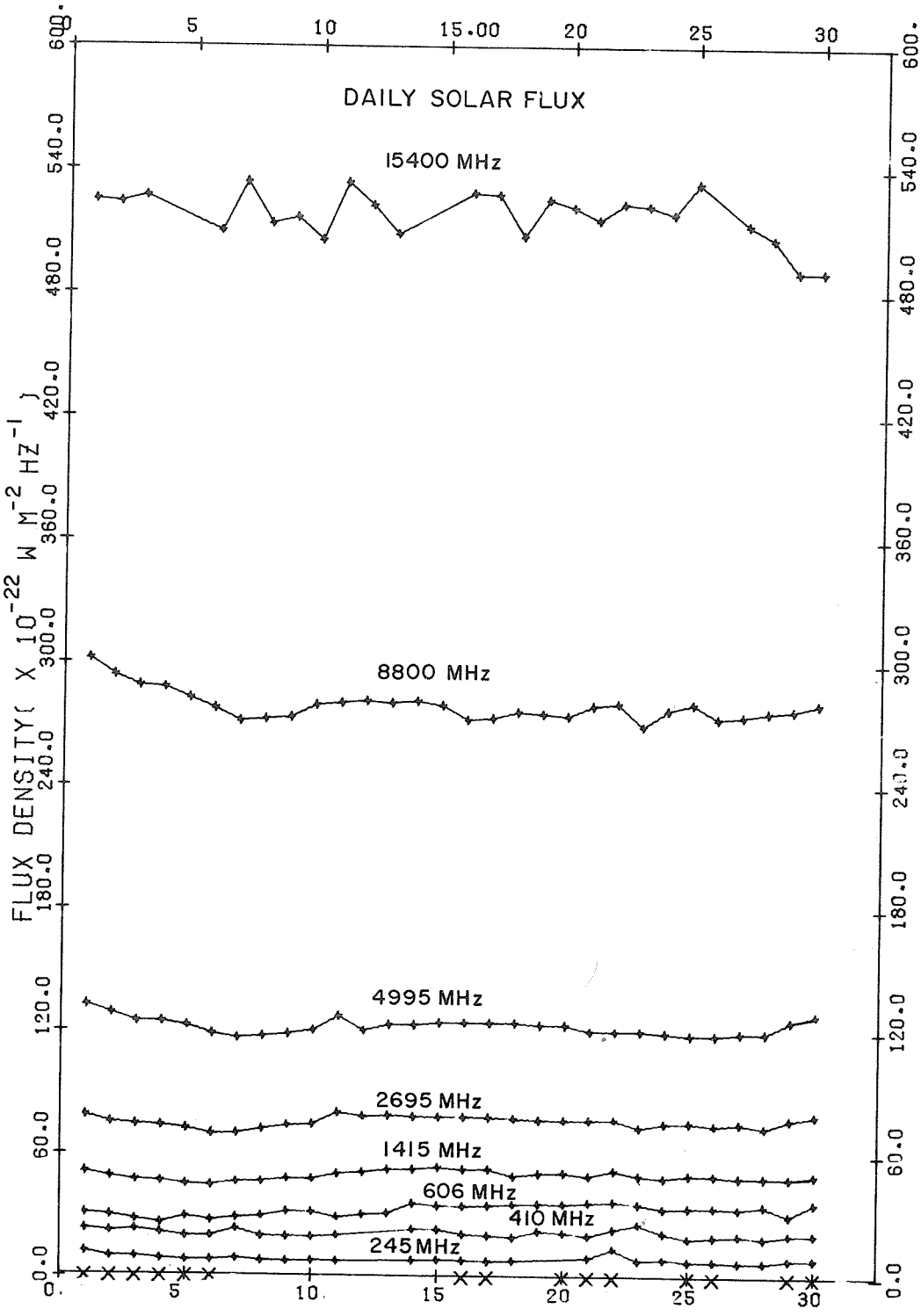

Fig. 2. Variation of the "quiet" sun radio emission for April 1976. The Xs along the bottom of the figure mark days on which distinctive events occurred.

23 March 1976

The leadoff event of the period was the radio burst recorded at Manila on 23 March 1976, which started at about 0845 UT. Because of poor weather conditions at numerous optical observatories, the location of the associated flare was much in doubt. Ultimately the outburst was identified with a subflare at about S06 E90 (Carrington longitude 044°) in what came to be known as McMath Region No. 14143. In view of the intensity of activity, however, we are suspicious of the low flare classification. Burst statistics are given below in Table 1.

Table 1. The 23 March 1976 Solar Radio Burst.

FREQ (MHz)	TIME UT START	TIME UT MAX	DUR (MIN)	TYPE EVENT	FLUX DENSITY $X10^{-22} W m^{-2} Hz^{-1}$ PEAK	FLUX DENSITY $X10^{-22} W m^{-2} Hz^{-1}$ MEAN	INTEGRATED FLUX DENSITY $J m^{-2} Hz^{-1}$
8800	0840.8	0845.3	28.7	47	1350.0	520.0	$8.7X10^{-17}$
8800		0847.1	-0.0	47	1400.0	-0.0	
4995	0840.3	0845.6	29.2	47	760.0	300.0	$5.2X10^{-17}$
4995		0847.1	-0.0	47	950.0	-0.0	
2695	0840.3	0843.0	29.2	47	550.0	150.0	$2.6X10^{-17}$
2695		0844.9	-0.0	47	350.0	-0.0	
1415	0840.6	0842.9	28.9	46	370.0	86.0	$1.4X10^{-17}$
1415		0845.0	-0.0	46	293.0	-0.0	
606	0840.8	0843.3	13.6	47	580.0	178.0	$1.3X10^{-17}$
606		0844.8	-0.0	47	430.0	-0.0	
8800	0909.5	0909.5	-0.0	29	156.0	-0.0	
4995	0909.5	0909.5	-0.0	29	72.0	-0.0	
2695	0909.5	0909.5	-0.0	29	54.0	-0.0	
1415	0909.5	0909.5	-0.0	29	20.4	-0.0	
606	0854.4	0854.4	-0.0	29	24.2	-0.0	

Also observed were (1) a dekametric sweep frequency continuum of intensity 3 at 24 to 48 MHz from 0842.2 to 0856.8 UT, (2) a Type III, intensity 2 burst from 0904.1 to 0905.4 UT at 32 to 48 MHz, and (3) Type IV in the meter wavelength range recorded at observatories other than Sagamore Hill and Manila. The radio burst profiles as recorded at Manila are shown in Figure 3. Though the Manila data are insufficient to test rigorously for conformity to the U-shaped spectrum of peak flux density used in a yes or no prediction of proton activity [Castelli and Guidice, 1976], meter wavelength data from other observatories confirmed the presence of the "U" signature [Castelli and Barron, 1977]. It still remains unclear whether or not proton activity of any great importance occurred, but the 20-40 and 40-80 MeV proton channels aboard IMP 7 and 8 recorded the onset of a particle increase on 23 March [*SGD*, 1976a]. A PCA of about 1 dB would have been expected by techniques reviewed in Castelli and Guidice [1976]. No provision, however, was made in the prediction scheme for the unfavorable east limb position of the flare/burst. Note in Table 1 that the integrated flux density exceeded 10^{-17} Joules m^{-2} Hz^{-1}--a threshold that seems statistically valid for detectable proton emission.

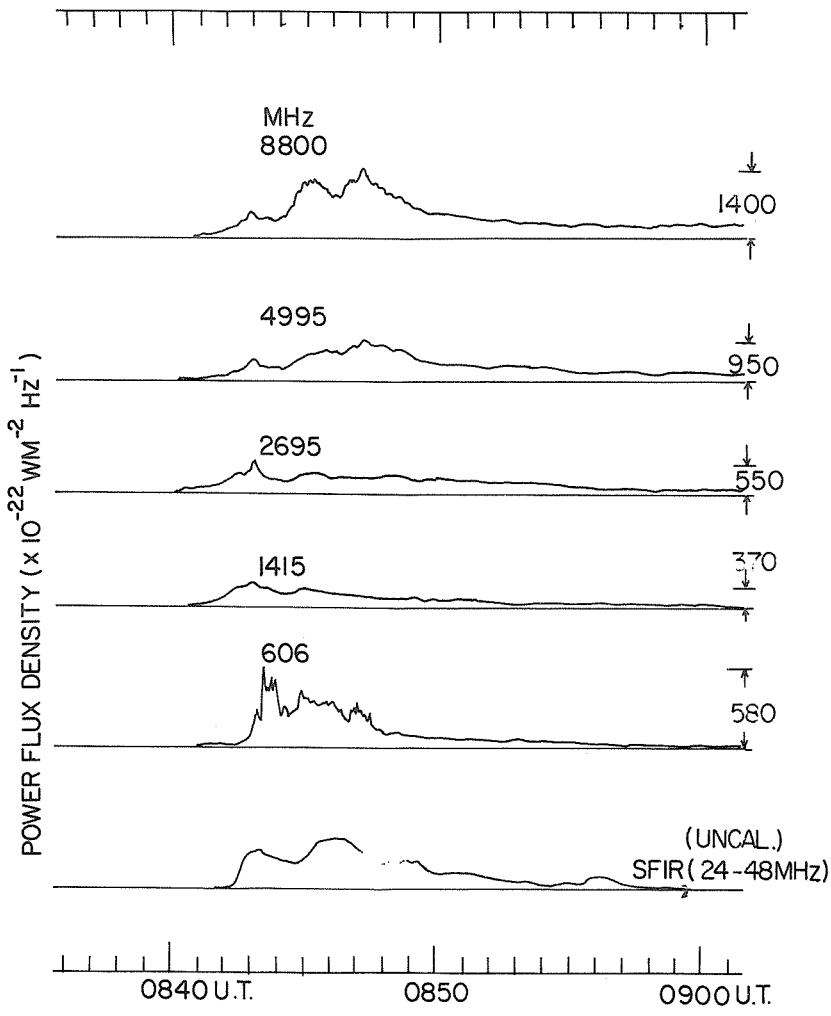

Fig. 3. The great radio burst observed on 23 March 1976 at Manila Observatory, Republic of the Philippines.

28 March 1976

As McMath Region No. 14143 advanced from the east limb, centimeter wavelength activity with associated X-ray and SID events increased. The region grew rapidly in area and developed magnetically a delta configuration on 26 March. After a period of relatively low geomagnetic activity on 23-25 March, the A_p reached an unusually high value of 138 on 26 March. Only eight or nine times in the previous 15 years had such a level been exceeded. Most probably this severe geomagnetic activity is to be associated with region 14143, yet it is difficult to locate an accompanying radio event other than that of the 0843 UT burst on 23 March--a connection that seems somewhat far removed.

The second important radio outburst of the period started on 28 March at about 1900 UT and was associated with a 1B flare at S07 E28 (Max 1935 UT). Though the radio peak flux spectrum resembled that of the 23 March event, especially in the centimeter range, it was, however, weaker in the meter range. A small proton increase was expected, but it was not predicted on the basis of a rigorous analysis of the spectrum. The data recorded at Sagamore Hill are shown in Table 2 below; Figure 4 shows the burst profiles.

Table 2. 28 March 1976 Solar Radio Burst.

FREQ (MHz)	TIME UT START	MAX	DUR (min)	TYPE EVENT	FLUX DENSITY $X10^{-22}Wm^{-2}Hz^{-1}$ PEAK	MEAN	INTEGRATED FLUX DENSITY ($J\ m^{-2}Hz^{-1}$)
35000	1927.0E	1934.2	48.2D	47	995.0	300.0U	$8.64x10^{-17}$
15400	1927.0E	1934.2	31.0D	47	2384.0	710.0U	$13.2\ x10^{-17}$
8800	1915.4	1927.5	44.6	47	3236.0	1100.0	$29.0\ x10^{-17}$
8800		1934.1	-0.0	47	3719.0	-0.0	
4995	1914.7	1929.0	45.3	47	1856.0	950.0	$24.8\ x10^{-17}$
4995		1934.6	-0.0	47	3155.0	-0.0	
2695	1914.6	1929.0	47.4	47	718.0	570.0	$15.1\ x10^{-17}$
2695		1936.0	-0.0	47	1890.0	-0.0	
1415	1914.2	1927.3	50.8	47	8174.0	250.0	$7.7\ x10^{-17}$
1415		1938.4	-0.0	47	554.0	-0.0	
1415		1958.0	-0.0	47	284.0	-0.0	
606	1914.5	1917.0	146.8	47	363.0	730.0	$7.7\ x10^{-17}$
606		1939.0	-0.0	47	2448.0	-0.0	
606		1958.2	-0.0	47	331.0	-0.0	
606		2050.5	-0.0	47	791.0	-0.0	
410	1915.0	1921.4	118.3	49	351.0	310.0	$10.6\ x10^{-17}$
410		1940.2	-0.0	49	1024.0	-0.0	
410		1958.6	-0.0	49	765.0	-0.0	
410		2050.9	-0.0	49	784.0	-0.0	
245	1914.9	1932.4	107.4	49	587.0	180.0U	$11.6\ x10^{-17}$
245		1951.0U	-0.0	49	609.0D	-0.0	
245		2008.0	-0.0	49	609.0	-0.0	
245		2052.6	-0.0	49	32.0	-0.0	
8800	2000.0	2000.0	47.0	29	59.8	29.9	
4995	2000.0	2000.0	30.0	29	29.1	14.6	
2695	2002.0	2002.0	23.0	30	14.8	7.4	
1415	2005.0	2005.0	131.0	30	10.4	5.2	
606	2141.3	2141.3	34.7	29	31.8	15.9	
410	2113.3	2113.3	62.7	29	51.5	25.8	
245	2102.3	2102.3	81.7	29	23.3	11.7	

Sweep frequency dekametric activity at Sagamore Hill was as follows:

Time of Burst	Type	Int	Freq
1922.9 - 1925.1	IIIG	I	25 - 40
1925.2 - 1939.3	IV	III	25 - 68
1939.3 - 2301.0	CONT	II	25 - 75
2136.5 - 2137.1	V	II	25 - 65

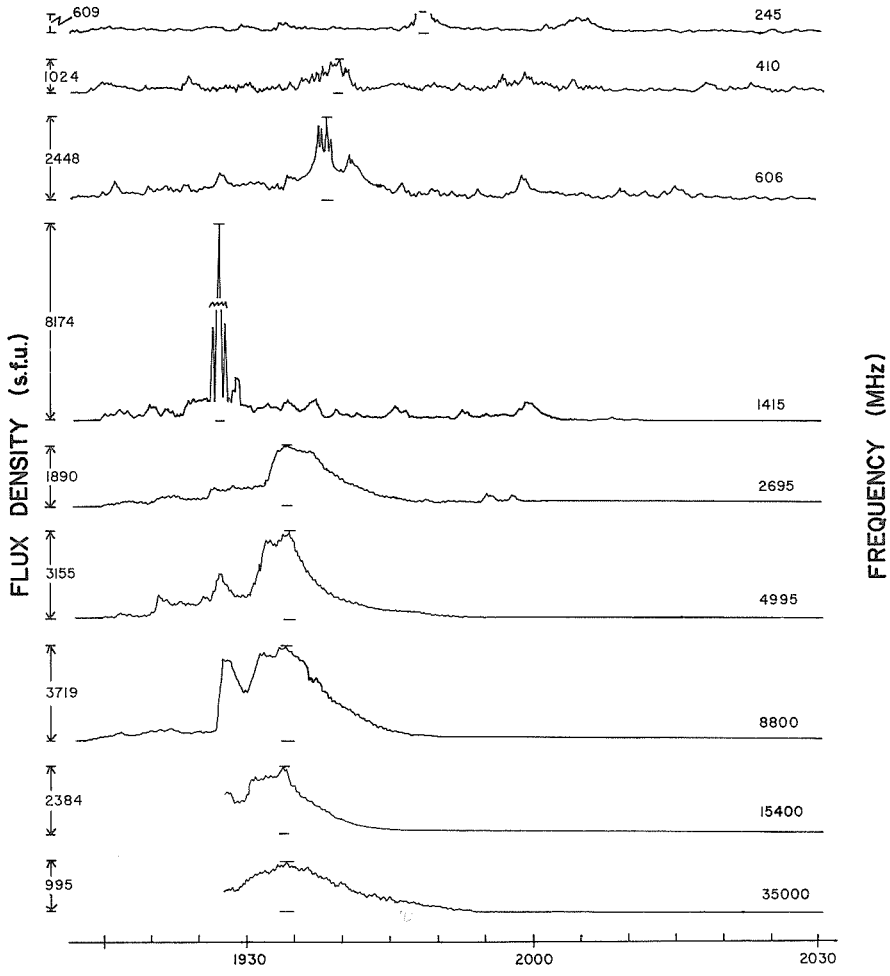

Fig. 4. The great burst observed on 28 March 1976 at Sagamore Hill Radio Observatory, Hamilton, Massachusetts.

30 April 1976

From the time of the 28 March outburst until west limb passage of region No. 14143 on about 6 or 7 April, burst activity decreased to only an occasional centimeter burst. Long-duration noise storm activity, which reached its greatest bandwidth on 26 March when 245, 410, and 606 MHz were all affected, receded to only 245 MHz. (Actually on 26 March noise storm activity at 410 MHz reached its highest level for the entire period). Region 14143 returned to the east limb about 20 April as McMath Region No. 14179, and it continued to be extremely quiet until 29 April when a few microwave bursts with associated SIDs occurred. As expected, these events displayed a spectral maximum in the vicinity of 10 000 MHz.

On 30 April at about 0845 UT, Manila observed a significant burst at 8800 MHz without associated dekametric continuum. The most important event of the day - indeed of the whole lifetime of the region - started at about 2050 UT on 30 April. The associated importance 2B flare located at S08 W46 probably started at about 2047 UT, reached a maximum near 2059 UT, and ended at about 2218 UT. Ultimately, there was a PCA event and even a Ground Level Event (GLE). The radio data from Sagamore Hill are listed below in Table 3. In the 25-75 MHz range, a Type IV, intensity 2 burst was observed between 2103.2 and 2130 UT; a continuum event was observed from 2130 to 2338 UT.

Table 3. 30 April 1976 Solar Radio Burst

FREQ (MHz)	TIME UT START	TIME UT MAX	DUR (min)	TYPE EVENT	FLUX DENSITY $X10^{-22}Wm^{-2}Hz^{-1}$ PEAK	FLUX DENSITY MEAN
35000	2102.3	2108.9	18.2	47	1176.0	353.0
15400	2054.3	2108.7	31.1	47	2540.0U	762.0U
8800	2054.7	2107.7	29.9	47	2630.0	789.0
4995	2050.2	2108.7	30.8	47	2046.0	614.0
2695	2055.3	2108.7	24.7	47	1500.0E	500.0E
1415	2050.0	2107.1	37.8	47	2717.0	815.0
1415		2117.8	-0.0	47	1830.0	-0.0
606	2055.6	2107.0	72.3	47	3018.0	905.0
606		2118.3	-0.0	47	745.5	-0.0
410	2100.9	2104.4	103.1	49	3000.0	900.0
410		2120.5	-0.0	49	825.0	-0.0
245	2101.7	2103.4	99.1	49	897.0	269.0
245		2124.2	-0.0	49	161.6	-0.0
35000	2120.5	2120.5	51.2	29	175.0	69.9
15400	2125.4	2125.4	46.8	29	81.5U	32.6U
8800	2124.6	2124.6	36.4	29	72.0	28.8
4995	2121.0	2121.0	40.0	29	51.6	20.6
2695	2120.0	2120.0	41.0	29	10.2	4.0
1415	2127.8	2127.8	83.4	29	9.1	3.6
606	2207.9	2207.9	44.6	29	21.1	8.4

The plot of the peak flux density yields the characteristic U-shape spectrum predictive of subsequent proton emission. The spectrum of this burst reveals several other significant features: (1) the centimeter f_{max} is near 13 000 MHz (perhaps higher than average), a position that has been statistically identified with a high magnetic field in the flare region; (2) the slope of the spectrum above f_{max} is rather gentle (not steep), predictive of a moderately hard energy distribution of the radiating electrons; (3) the broad spectral U (relative flatness), sometimes expected for the occurrence of a relatively hard proton spectrum according to Bakshi and Barron [1975], is not well confirmed; and (4) the spectral U null point is shallow, implying that a strong, uniform radiation occurred throughout most of the microwave region.

A hard proton spectrum is indicated by particle data given in [*SGD*, 1976b]. Moreover, the occurrence of a Ground Level Event is the ultimate proof of the hardness of the proton energy spectrum. The burst integrated flux densities (mean flux density times duration in min) derived from Table 3 are shown below in Table 4.

Table 4. Burst Integrated Flux Densities.

Frequency (MHz)	Integrated Flux Density x 10^{-17} (Joules m^{-2} Hz^{-1})
35000	3.8
15400	17.0
8800	14.8
4995	11.6
2695	7.2
1415	18.1
606	39.1
410	55.6
245	37.4

By using the 8800 MHz integrated flux density, one might have predicted a >10 MeV proton flux of about 50 particles $cm^{-2}s^{-1}sr^{-1}$ [Straka and Barron, 1970; Castelli and Guidice, 1976 (see Figure 19)]. We calculated an absorption of about 2.3 dB from the occasionally used relation

$$P = 10\ A^2,$$

where P = the number of >10 MeV protons and A = the 30 MHz riometer absorption in dB. The estimated value of 2.3 dB lies close to the 2.7 dB actually measured. Note too that the predicted proton flux is in reasonable agreement with data published in [*SGD*, 1976b].

REFERENCES

BAKSHI, P. and W. R. BARRON 1975 Spectral Correlations between Solar Flare Radio Bursts and Associated Proton Fluxes II, *AFCRL Rpt. #TR-75-0579.*

CASTELLI, J. P. and D. A. GUIDICE 1976 Impact of Current Solar Radio Patrol Observations, in *Vistas in Astronomy, 19,* pp. 355-384 Pergamon Press, New York.

CASTELLI, J. P. and W. R. BARRON 1977 A Catalog of Solar Radio Bursts 1966-1976 Having Spectral Characterisitics Predictive of Proton Activity, *J. Geophys. Res.,* to be published.

GILLESPIE, B., J. HARVEY, W. LIVINGSTON and K. HARVEY 1973 Polar Magnetic Fields and the New Solar Cycle, *Ap. J., 186,* L85-L86.

STRAKA, R. M. and W. R. BARRON 1970 Multifrequency Solar Radio Bursts as Predictors for Proton Events, *Agard Conf. Proc., 49,* 10-1 to 10-10.

SGD 1976a *Solar-Geophysical Data, 385 Part II,* p. 45, March 1976, U.S. Department of Commerce, (Boulder, Colorado, U.S.A. 80302).

SGD 1976b *Solar-Geophysical Data, 387 Part II,* November 1976, U.S. Department of Commerce, (Boulder, Colorado, U.S.A. 80302).

The Outburst of 23 March 1976

by

S. T. Akinjan, L. M. Bakunin, G. P. Chernov, I. M. Chertok, V. A. Kovalev and O. S. Korolev
Solar Radio Laboratory, IZMIRAN, Moscow, U.S.S.R.

The outburst of 23 March 1976 starting at about 0841 UT was one of the most intensive radio bursts observed in 1976. At the Solar Radio Laboratory, IZMIRAN, the burst was recorded by radiometers at 207 and 3000 MHz and by spectrographs in the ranges 45-90 MHz [Markeev, 1961], 93-186 MHz [Korolev, 1975], and 180-236 MHz [Markeev and Chernov, 1971].

At the fixed frequencies 207 and 3000 MHz the burst had a complicated form (Figure 1). One can see the sharp onset of the emission in the burst at 3000 MHz which began about 1 min before (~0840.5 UT) the burst at 207 MHz. The moments of the maximum intensity (~0842.6 UT) do not differ by more than 0.3 min.

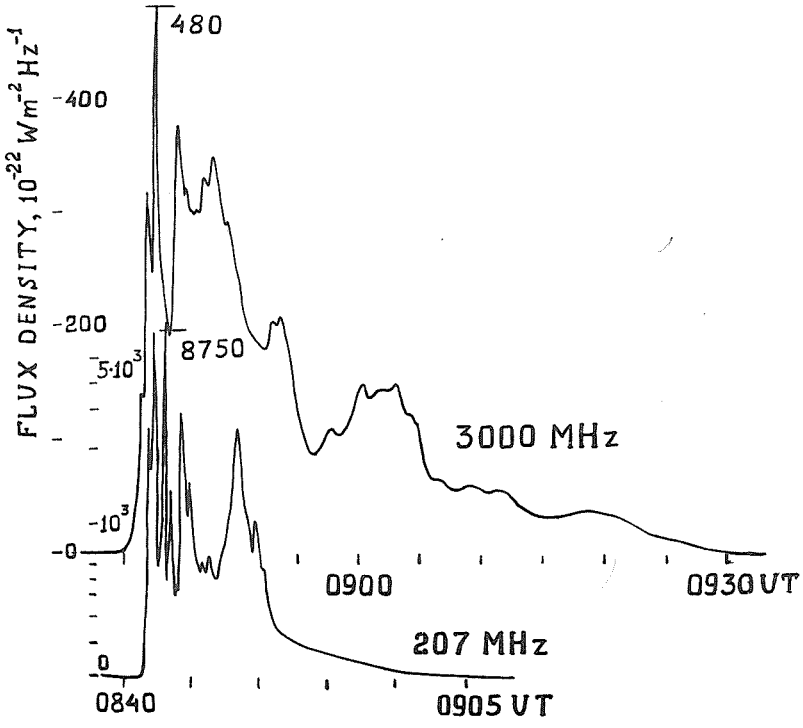

Fig. 1. Single frequency flux records of the outburst on 23 March 1976 at 207 and 3000 MHz.

The dynamic spectra of the outburst at meter wavelengths are shown in Figure 2. The spectrum in the range 93-186 MHz has been obtained by a spectrograph with a lower sensitivity. The analysis of the spectra shows that the given event is a complex set of Type II and IV bursts.

The Type IV burst consists of two intensive continuum components which may be classified either as flare continua [Robinson and Smerd, 1975] or as broadband continua [Böhme, 1972]. The first one, lasting ~1.7 min, coincides in time with the rise phase of the microwave burst and is characterized by a rapid drift of a sharp initial boundary of the emission. In the range 186-45 MHz the frequency drift velocity of the boundary is characteristic of Type III bursts. In the range 186-93 MHz the drift velocity is equal to several tens of MHz sec^{-1}. In the range 90-45 MHz the drift may be measured more exactly. Here $df/dt \sim 18.5$ MHz sec^{-1} at the frequencies up to 53 MHz; at $f < 53$ MHz a sharp decline in the drift takes place; and in the band 53-45 MHz the drift velocity decreases to about 2.1 MHz sec^{-1}.

The second intensive continuum component starts at 0843.6 UT and has the lifetime of 1-2 min. In this component a sharp initial boundary with drift velocity about 50 MHz sec^{-1} is seen in a range of 180-236 MHz. In all other ranges the boundary is diffuse.

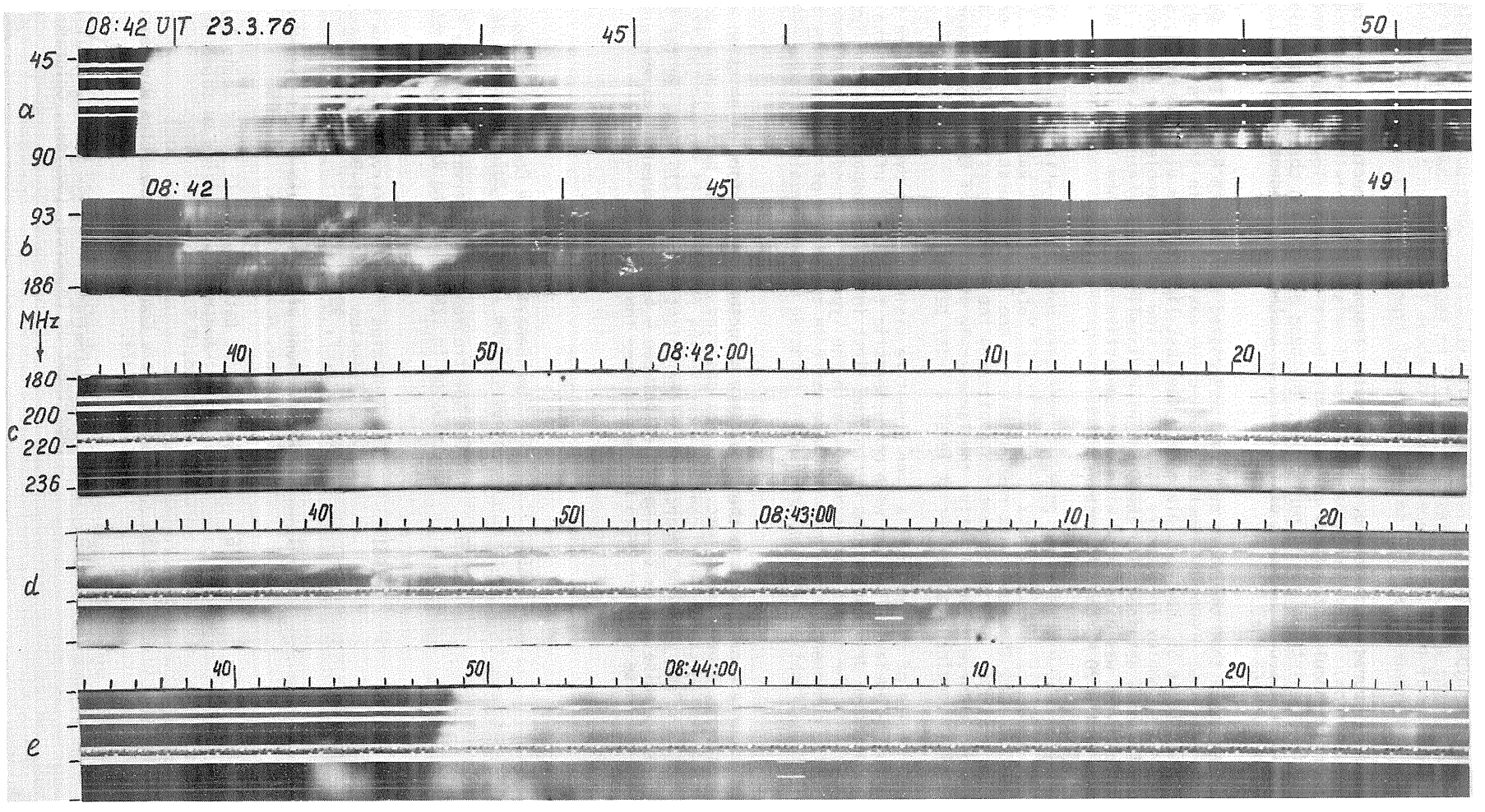

Fig. 2. Dynamic spectra of the outburst on 23 March 1976 in the ranges: (a) 90-45 MHz; (b) 93-186 MHz (low sensitivity); and (c-e) 180-236 MHz (high time and frequency resolution).

In terms of the plasma hypothesis, the indicated drift velocities correspond to a certain disturbance propagating through the corona with velocities 7×10^9 - 10^{10} km sec^{-1}. For example, in the first component at $f < 53$ MHz, the velocity of the disturbance is equal to about 2×10^9 km sec^{-1}. Most probably electron streams generate such disturbances, as they do in the case of Type III bursts.

As far as the Type II burst is concerned, the irregular fragmentary structure is characteristic of the event under consideration. The separate bands of Type II emission are visible beginning near 215 MHz (Figure 2). The important peculiarity of the given Type II burst is a very slow frequency drift of the emission during certain time intervals. In particular, the band of emission observed beginning at 0847.5 UT, which is either a second harmonic of the burst or another independent one, has almost a zero drift at frequencies below ~65 MHz.

There is strong evidence that the above event was associated with McMath Region 14143, even though at the time of the burst this spot group lay about 10° behind the east limb. In the first place, *SGD* [1976] includes a flare of importance SB that took place near the east limb at 0839 UT on 23 March; secondly, the associated Type II burst's complex fragmentary structure and slow drift resembled the 20 March 1976 event at 0205 UT; and finally, data obtained with the Culgoora radioheliograph [McLean and Nelson, 1976], indicated that the 23 March event was associated with the same active region - one localized ~56° behind the east limb at the time of the 20 March 1976 outburst.

The association of the events of 20 and 23 March 1976 with McMath Region 14143 gives a clue to the interpretation of the unusually slow frequency drift of the 23 March Type II burst. Indeed, the radioheliograph's data testify that the shock wave responsible for the Type II burst of 20 March propagated in the corona along a curved path. The shock wave that initiated the Type II burst of 23 March also appears to have propagated along a curve. Consequently, the large-scale structure of the coronal magnetic field above McMath Region 14143 remained stable over at least a 3-day period.

Certain characteristics of the outburst's fine structure visible in the dynamic spectra illustrated in Figure 2 are (1) quasi-regular pulsations with characteristic time scales of 5-10 s in the 45-90 MHz frequency range, (2) negative drift pulsations during the first intensive component of the Type IV burst, and (3) drift variations in the pulsations associated with the Type IV's second intensive component. During the second intensive component, a tendency to phase shift in the middle of the frequency range is evident: moments of intensifications at high frequencies coincide with the minima in radio emission at low frequencies.

Due to the radio source's proximity to the limb, fine structure in the form of emission and absorption stripes (zebra pattern, fiber bursts, etc.) was not observed against the background of the outburst up to 0858 UT. A number of pulsations have continuations in the ranges 93-186 MHz and 180-236 MHz. Within the latter interval, one can see some demarcation of the pulsations near 215 MHz. In the high resolution spectrum the numerous pulsations with time scales between 0.5-1 s are apparent as well. During the burst's initial part, the phase shift at ~215 MHz may be seen too.

REFERENCES

BÖHME, A. 1972 The Time Behaviour of the Continua During the Initial Stage of Type IV Bursts, *Solar Physics, 24*, 457.

KOROLEV, O. S. 1975 The Spectrographical Observations of the Sun's Radio Emission in IZMIRAN in the Range 93-186 MHz, *Astron. Zh., 52*, 1247.

MARKEEV, A. K. 1961 The Apparatus for the Observations of the Enhanced Solar Emission in Range 45-90 MHz, *Geomagnetism and Aeronomy, 1*, 999.

MARKEEV, A. K. and G. P. CHERNOV 1971 Observations of Solar Radio Bursts With High Spectral Resolution, *Soviet Astron., 14*, 835.

MCLEAN, D. J. and D. J. NELSON 1976 Some Recent Data on Type II Solar Radio Bursts, *Report at Soviet-Australian Symposium on Solar Radio Astronomy*, Leningrad, U.S.S.R.

ROBINSON, R. D. and S. F. SMERD 1975 Solar Flare Continua at the Metre Wavelengths, *Proc. ASA, 2*, 374.

1976 *Solar-Geophysical Data, 380 Part I*, April 1976, U. S. Department of Commerce, (Boulder, Colorado 80302).

Some Characteristics of the Noise Storm of 26-31 March 1976

by

S. T. Akinjan, I. M. Chertok, V. V. Fomichev, A. A. Gnezdilov and O. S. Korolev
Solar Radio Laboratory IZMIRAN
Moscow, U.S.S.R.

The disk passage of McMath active Region 14143 in the period 26-31 March 1976 was accompanied by an intensive noise storm. Using data from a 207 MHz radiometer and a 74 MHz polarimeter, we shall discuss two events of 28 and 31 March in which sharp intensifications of radio emission took place. Moreover, we shall describe some properties of the quasi-regular variations of the burst and continuum noise storm components.

The Event of 28 March

One can judge this event by data shown in Figure 1. Its most interesting peculiarity is a sharp intensification of the radio emission starting at approximately 0930 UT at 207 MHz. For about 40 min at this frequency the continuum intensity increased by a factor of 4-4.5 despite a practically invariable burst intensity. Thereafter, the continuum level remained enhanced for several hours.

An analogous intensification of the radio emission took place at 74 MHz as well. It is very important, however, to emphasize that at this frequency the start of the intensification and the decline of the burst activity superposed on the enhanced continuum lagged the 207 MHz response by 25-35 min. Moreover, the intensification of the radio emission was accompanied by a gradual increase in the degree of average polarization - from $p \sim 0\%$ at the beginning of the event to $p \sim 50\%$ near 1200 UT.

The continuum radio emission component was right-hand circularly polarized. As far as the bursts were concerned, during the initial stage of the event, those with different signs and polarization degree were present, testifying to the complex structure of the source. During the last half hour of the observation, the bursts with right-hand polarization and p up to 50% predominated.

The Event of 31 March

This event (Figure 2) was analogous in many respects to that of 28 March. Here the sharp intensification of the radio emission took place; the intensity of the continuum component at 207 MHz rose by approximately a factor of 10 within about 25 min; the number and intensity of the bursts essentially increased; and a 40-min delay occurred between the increases at 207 and 74 MHz.

The polarization, however, was more complicated because its sense changed at 1305 UT. The moderate right-hand polarization ($p \sim 20\%$) during the initial stage of the event shifted to a left-hand polarization of approximately the same value by the end of the observation period.

The main characteristics of the two events described above allow us to classify them as either sharp intensification of the noise storms or stationary Type IV bursts even though it is known that quite small differences exist between these two kinds of meter wavelength activity. An analysis of these events' dynamic spectra [Bakunin *et al.*, 1977] shows that fine-structure elements usually observed in Type IV bursts were present together with the Type I bursts characteristic of noise storms.

Both events seem to be associated with importance 1N flares that occurred in McMath Region 14143 at a time near the onset of the radio emission intensification at 207 MHz [*SGD*, 1976]. Outwardly propagating disturbances in the corona most probably caused the two radio events described here. Variations in the radio emission intensity and polarization suggest that these disturbances were accompanied by a successive intensification of the magnetic field at the corresponding coronal levels and by a rebuilding of the radio source structure. From the time delay between the events at 207 and 74 MHz we estimated the velocity of the magnetic field enhancement in the corona. Assuming that the generation of the radio emission at 207 and 74 MHz takes place at altitudes $0.15R_\odot$ and $0.7R_\odot$, respectively, we found velocities from 150 to 250 km sec^{-1}.

It should be noted that according to Kai and Sekiguchi [1973] magnetic field movements in the solar atmosphere occur during active region development. Furthermore, these field fluctuations and spot group growth are accompanied by a successive intensification of the radio emission of the S-component and noise storm. The authors found, however, that in these cases the velocity of the corresponding disturbance was much smaller, being about 1-2 km sec^{-1}.

Quasi-Periodic Variations

Below we describe some properties of the variations of radio emission at 207 MHz in the noise storm with time scales from several minutes to several tens of minutes. In Figure 3 the daily variations of

the number (N) of Type I bursts with an amplitude of 1-1.5 times the quiet-Sun level every 10 min are shown. Here the variations of the minimum flux density (I) during the same time interval are shown as well. A number of interesting peculiarities of the radio emission variations may be noted. First of all one can see the large quasi-regular variations of the burst number (up to a few hundreds of percent) on a time scale from about half an hour to 1-1.5 hours. Secondly, note the presence of variations in the continuum intensity on a time scale similar to N but with smaller amplitude (about 10-50 percent). Sometimes the variations in the burst number occur independently of those in the continuum (see the data for 25, 26 and 28 March). At other times, and in particular on 27, 30, and 31 March, a strong correlation between the continuum and burst variations can exist. See 30 March, for example, when almost synchronous variations of N and I occurred on about a 1-hour time scale and with a relative amplitude of 50-90 percent.

Quasi-regular variations with a time scale of 3-5 min (characteristic of the majority of the noise storms) have been observed also in the storm under consideration. Figure 4 illustrates an example of such variations. Occasionally these fluctuations have an amplitude as large as 90% of the quiet-Sun level. One can see such variations during the enhanced phase of radio emission in the 28 March event (see Figure 1 between 0940-1000 UT) and again superposed on the background of the hours of fluctuations on 30 March.

It is likely that some part of the continuum variations with different time scales is due to the overlap of a large number of bursts because (1) the burst variations with a time scale of 1-1.5 hours were most visible the day before the noise storm intensified on 28 and 31 March, (2) spectrographic observations [Bakunin *et al.*, 1977] indicate that the large burst variations on 27 March appear to be connected with a decline in the number of different bursts at frequencies near 207 MHz, and (3) the same data suggest that the burst variations on 26 March took place over a wider frequency range.

REFERENCES

BAKUNIN, L. M., G. P. CHERNOV, and I. M. CHERTOK 1977 The Fine Structure of Meter Radio Emission Associated With McMath Active Region 14143, *this issue*, p. 106.

KAI, K, and H. SEKIGUCHI 1973 Evolutionary Relation Between Type I Storm Activity and the S-Component at Centimetre Wavelength, *Proc. ASA, 2*, 217.

SGD 1976 *Solar-Geophysical Data, 380 Part I*, April 1976. U. S. Department of Commerce, (Boulder, Colorado, U.S.A. 80302).

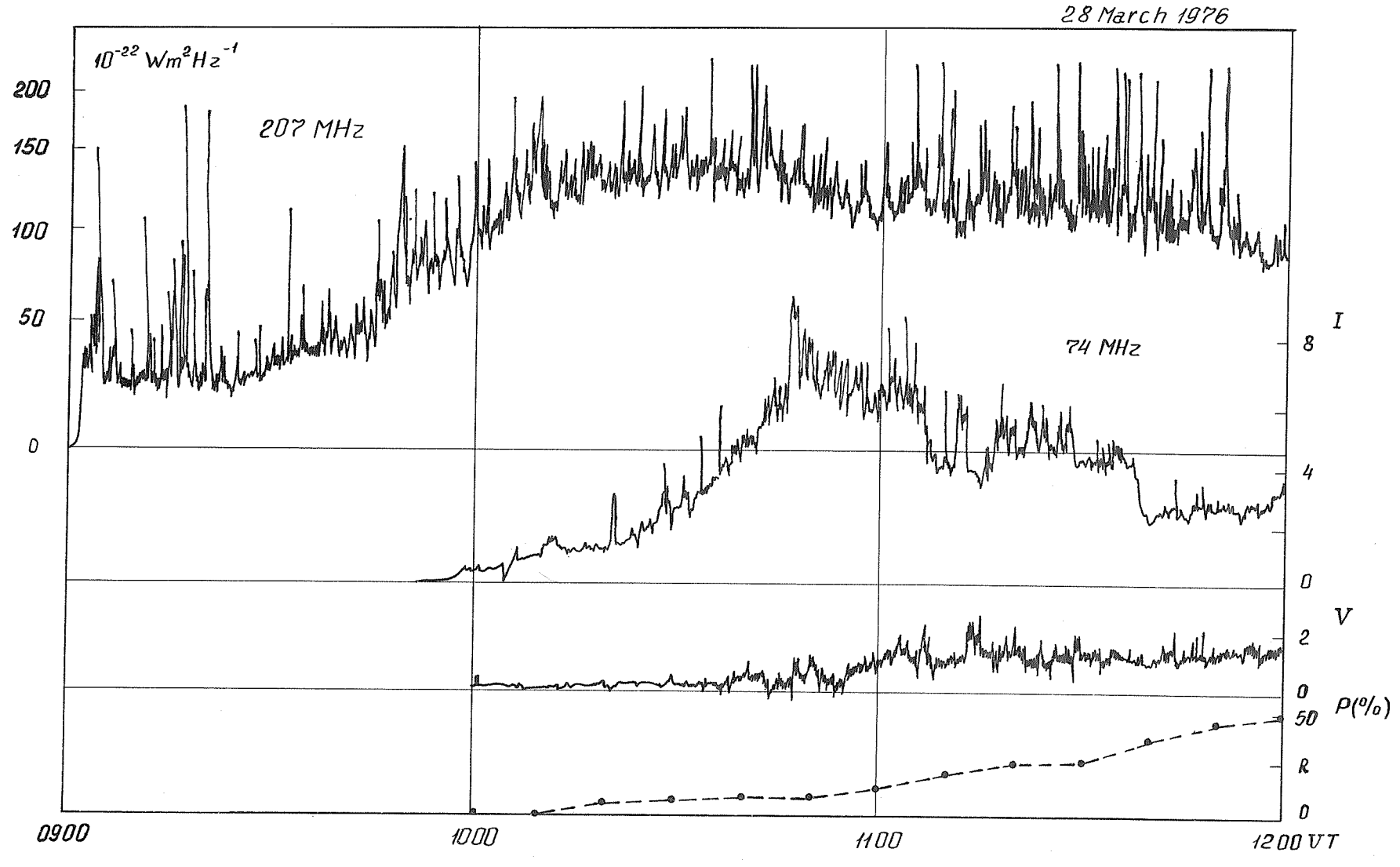

Fig. 1. The record of flux density at 207 MHz, and the total intensity (I), the intensity of the circularly polarized component ($V=I_R-I_L$) in arbitrary units, and the average degree of polarization (p) at 74 MHz are shown for the event on 28 March 1976.

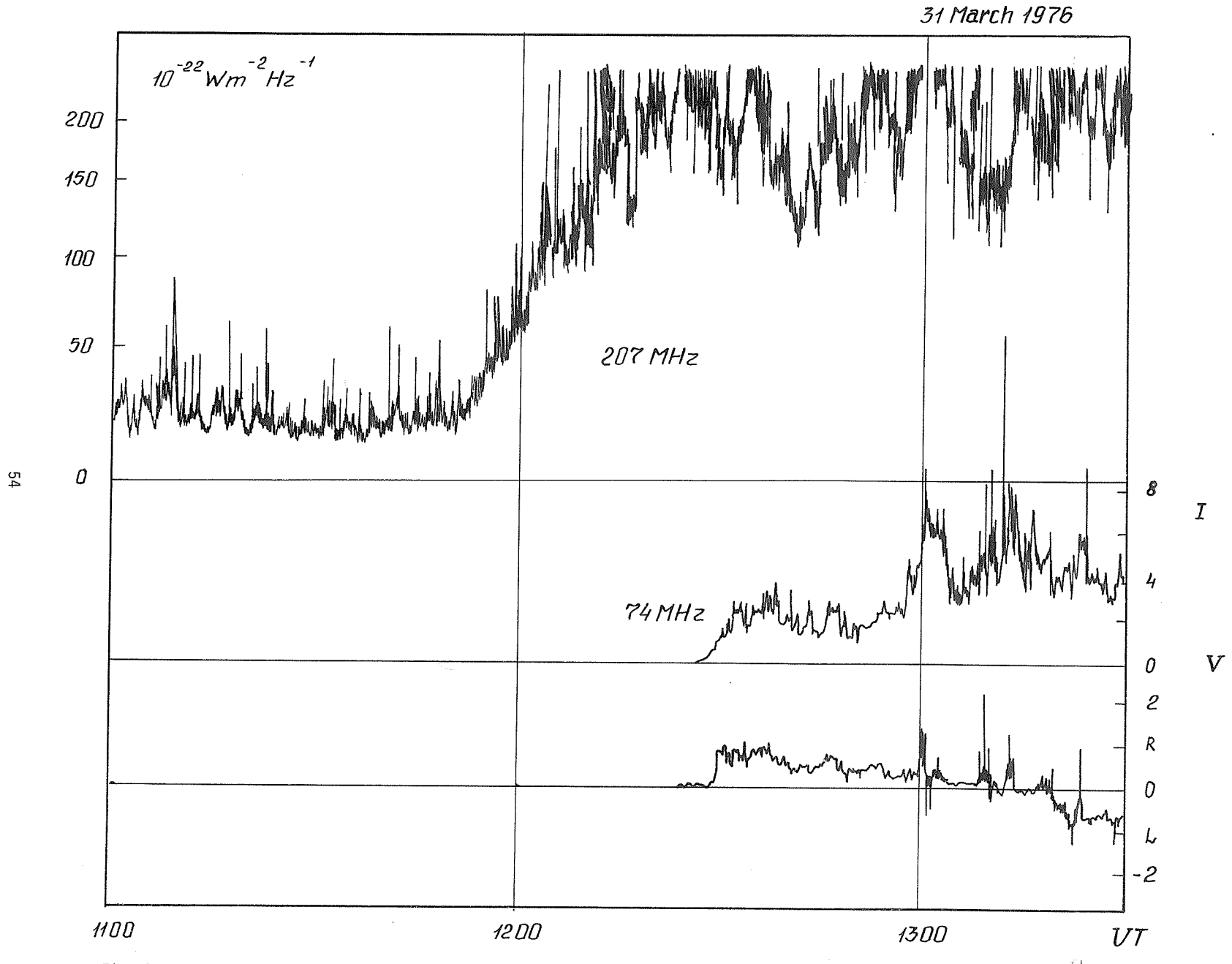

Fig. 2. The record of flux density at 207 MHz, and the total intensity (I) and the intensity of the circularly polarized component ($V=I_R-I_L$) in arbitrary units at 74 MHz are shown for the event on 31 March 1976.

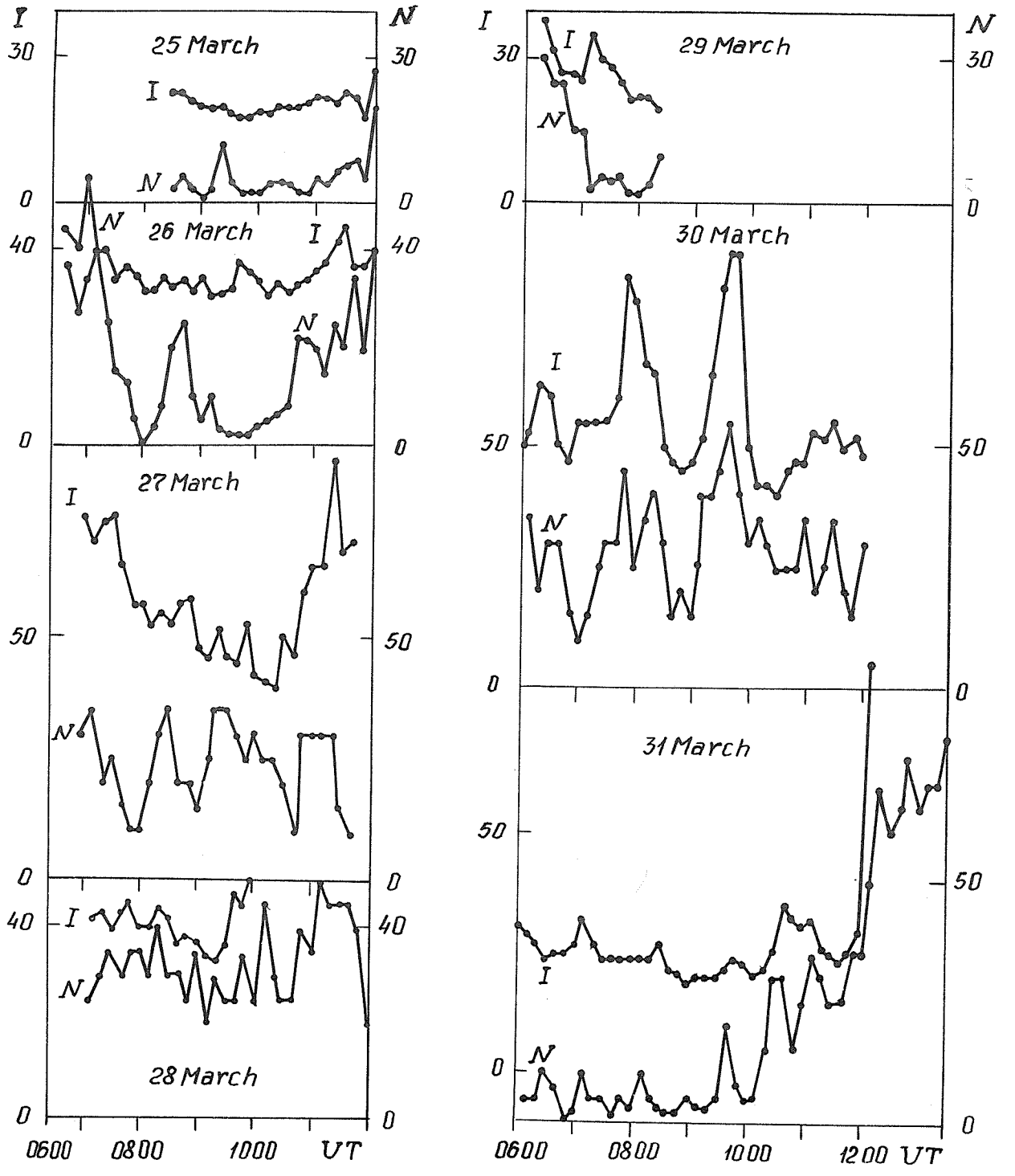

Fig. 3. Variations in the number of Type I bursts (N) and in the minimum flux density (I) every 10 min at 207 MHz during the noise storm of 26-31 March 1976. The minimum flux density is expressed in arbitrary units.

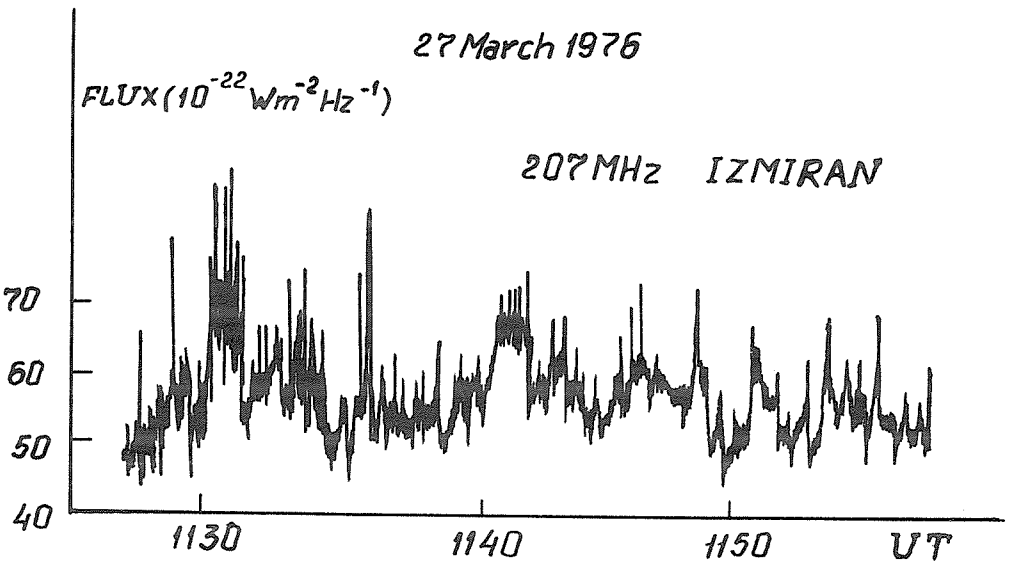

Fig. 4. Fragment of record of the 27 March 1976 noise storm at 207 MHz.

Solar Radio Emission at Hoeven March - May 1976

by

M. A. Klaassen
Public Astronomical Observatory
"Simon Stevin"
Hoeven, The Netherlands

TOTAL FLUX OBSERVATIONS AT 242 MHz, MARCH 1976 .

Flux density in solar units ($.10^{-22}.\ ^{W}/_{m^2}.Hz$).

DATE: 1976	Obs. Period (UT) Start	End	Flux density (solar units) 08^h-11^hUT	11^h-14^hUT	Daily mean	Outstanding Occurrences.
March 1	05.00	16.00	8.5	8	8.2	
2	05.00	16.00	8.5	8.5	8.5	
3	05.00	16.00	9	8	8.5	
4	05.00	16.00	9	8.5	8.7	
5	05.00	16.00	9	9	9	
6	05.00	16.00	10	9	9.5	
7	05.00	16.00	9	9	9	
8	05.00	16.00	9	9	9	
9	05.00	16.00	9	9	9	
10	11.00	16.00	-	8.5	8.5	
11	05.00	16.00	9	8.5	8.7	
12	05.00	16.00	8.5	8.5	8.5	
13	05.00	16.00	8	7.5	7.7	
14	05.00	16.00	8	7.5	7.7	
15	05.00	16.00	7	7	7	
16	05.00	16.00	8	8.5	8.7	
17	05.00	16.00	12	14	13	D
18	05.00	16.00	18	19	19	D
19	05.00	16.00	26	20	23	D
20	05.00	16.00	50	36	43	D
21	11.00	16.00	-	30	30	D
22	-	----	-	-	-	
23	05.00	16.00	20	13	17	D
24	05.00	16.00	17	10	14	D
25	05.00	16.00	13	23	18	D
26	05.00	16.00	21	34	28	D
27	05.00	16.00	40	35	37	D
28	13.00	16.00	-	45	45	D
29	05.00	16.00	12	14	13	D
30	05.00	16.00	40	30	35	D
31	05.00	16.00	17	60	39	D
				Monthly mean:	17	

TOTAL FLUX OBSERVATIONS AT 242 MHz, APRIL 1976 .

Flux density in solar units ($.10^{-22}$. $W/_{m^2}$. Hz).

DATE: 1976	Obs. Period (UT) Start	End	Flux density (solar units) 08^h-11^hUT	11^h-14^hUT	Daily mean	Outstanding Occurrences.
April 1	06.00	17.00	16	9	13	D
2	06.00	17.00	11	9	10	D
3	06.00	17.00	8	7	7.5	D
4	10.00	17.00	-	8	8	
5	06.00	17.00	6	7	7.5	
6	06.00	17.00	6	6	6	
7	06.00	17.00	6	6	6	
8	06.00	17.00	6	6	6	
9	06.00	17.00	7	6	6.5	
10	06.00	17.00	7	7	7	
11	06.00	17.00	7	7	7	
12	06.00	17.00	7	8	7.5	
13	06.00	17.00	8	8	8	
14	06.00	17.00	8	8	8	
15	06.00	17.00	8	8	8	
16	06.00	17.00	9	8	8.5	
17	06.00	17.00	8	9	8.5	
18	06.00	17.00	9	8	8.5	
19	06.00	17.00	8	8	8	
20	06.00	17.00	9	9	9	D
21	06.00	17.00	9	10	9.5	D
22	06.00	17.00	10	15	13	D
23	06.00	17.00	9	9	9	
24	06.00	17.00	11	9	10	
25	06.00	17.00	9	9	9	
26	06.00	17.00	9	9	9	
27	06.00	17.00	8	8	8	
28	06.00	17.00	9	9	9	
29	06.00	17.00	8	9	8.5	D
30	06.00	17.00	10	12	11	D
31						

Monthly mean: 8.5

TOTAL FLUX OBSERVATIONS AT 242 MHz, MAY 1976 .

Flux density in solar units ($.10^{-22}$. W/m^2 . Hz).

DATE: 1976	Obs. Period (UT) Start	End	Flux density (solar units) 08^h-11^hUT	11^h-14^hUT	Daily mean	Outstanding Occurrences.
May 1	05.00	18.00	8	7	7.5	
2	05.00	18.00	8	9	8.5	
3	05.00	18.00	9	9	9	
4	05.00	18.00	8	8	8	
5	05.00	18.00	9	9	9	
6	05.00	18.00	7	6	6.5	
7	05.00	18.00	6	6	6	
8	05.00	18.00	7	8	7.5	
9	05.00	18.00	8	7	7.5	
10	05.00	18.00	9	9	9	
11	05.00	18.00	9	9	9	
12	05.00	18.00	9	9	9	
13	05.00	18.00	9	9	9	
14	05.00	18.00	9	9	9	
15	05.00	18.00	9	9	9	
16	05.00	18.00	9	8	8.5	
17	05.00	18.00	8	7	7.5	
18	05.00	18.00	7	7	7	
19	05.00	18.00	8	8	8	
20	05.00	18.00	8	8	8	
21	05.00	18.00	8	7	7.5	
22	05.00	18.00	7	8	7.5	
23	05.00	18.00	7	7	7	
24	05.00	18.00	7	8	7.5	
25	05.00	18.00	8	7	7.5	
26	05.00	18.00	8	8	8	
27	05.00	18.00	8	8	8	
28	05.00	18.00	7	7	7	
29	05.00	18.00	8	7	7.5	
30	05.00	18.00	8	8	8	
31	05.00	18.00	8	8	8	

Monthly mean: 7.9

OUTSTANDING OCCURRENCES, MARCH 1976.

Flux density in solar units (. 10^{-22} . W/m^2 . Hz).

DATE 1976.	FREQ	STATION	TYPE	START TIME UT	TIME OF MAX. UT	DUR MIN	FLUX DENSITY PEAK	FLUX DENSITY MEAN	REMARKS
March 17	242	HOVN	44NS	06.00 E	--	660D	--	--	
18	242	HOVN	44NS	06.00 E	--	660D	--	--	
19	242	HOVN	44NS	06.00 E	--	660D	--	--	
20	242	HOVN	44NS	06.00 E	--	660D	--	--	
21	242	HOVN	44NS	11.00 E	--	300D	--	--	
23	242	HOVN	44NS	06.00 E	--	660D	--	--	
23	242	HOVN	49GB	08.40.5	--	1.5	450D	--	
23	242	HOVN				25	450D	--	
24	242	HOVN	44NS	06.00 E	--	180	--	--	
24	242	HOVN	27RF	06.30 E	08.00	120	17	14	
24	242	HOVN	27RF	08.30	09.30	90	22	14	
25	242	HOVN	27RF	11.43	12.29	60U	100	50	
25	242	HOVN	27RF	13.07 U	13.15	54	100	36	
25	242	HOVN	44NS	06.00 E	--	660D	--	--	
26	242	HOVN	44NS	06.00 E	--	660D	--	--	
27	242	HOVN	44NS	06.00 E	--	660D	--	--	
28	242	HOVN	44NS	13.00	--	180D	--	--	
29	242	HOVN	44NS	06.00 E	--	660D	--	--	
29	242	HOVN	6 M	09.14	09.16	8	30	15	
29	242	HOVN	7 M	10.44.5	10.46.5	4	70	17	
29	242	HOVN		10.52	11.00	13	20	15	
29	242	HOVN	U46M	15.50	16.06	20	20	15	
30	242	HOVN	44NS	06.00 E	--	660D	--	--	
30	242	HOVN	27RF	07.12	07.47	70	100	50	
30	242	HOVN	27RF	09.00	09.20	5	70	45	
31	242	HOVN	44NS	06.00 E	--	660D	--	--	
31	242	HOVN	24R	11.54	--	160	--	75	

OUTSTANDING OCCURRENCES, April 1976.

Flux density in solar units (. 10^{-22} . $W/_{m^2}$. Hz).

DATE 1976	FREQ	STATION	TYPE	START TIME UT	TIME OF MAX. UT	DUR MIN	FLUX DENSITY PEAK	FLUX DENSITY MEAN	REMARKS
April 1	242	HOVN	44NS	05.30E	-	720	-	-	
2	242	HOVN	44NS	05.30E	-	720	-	-	
3	242	HOVN	6 S	08.46	08.48.5	3	170D	22	
20	242	HOVN	44NS	05.30E	-	720	-	-	
21	242	HOVN	7 C	15.20.5	15.21	1	110	11	
21	242	HOVN		15.21.5	15.26	4	45	18	
21	242	HOVN		15.40	1553	35	14	12	
22	242	HOVN	43NS	08.03	-	180	-	13	
22	242	HOVN	43NS	15.18E	-	-	-	20	
29	242	HOVN	43NS	16.10	-	180D	-	11	
30	242	HOVN	44NS	05.00E	-	780D	-	-	
30	242	HOVN	49GB	12.42	12.44U	6	150D	150D	
30	242	HOVN			12.58	33	40D	14	
30	242	HOVN	41F	08.12	-	7	-	-	
30	242	HOVN	6S	08.23	08.23.2	0.5	100D	-	
30	242	HOVN	6S	08.44	08.44.5	3	33	16	

OUTSTANDING OCCURRENCES, MAY 1976.

Flux density in solar units (. 10^{-22} . $W/_{m^2}$. Hz).

DATE 1976.	FREQ	STATION	TYPE	START TIME UT	TIME OF MAX. UT	DUR MIN	FLUX DENSITY PEAK	FLUX DENSITY MEAN	REMARKS
May	No outstanding Occurrences								

Interferometric Observations at 408 MHz of the Radio Sources Associated With the McMath Region 14143

by

A. Abrami and U. Koren
Trieste Astronomical Observatory
I 34131 Trieste, Italy

The solar radio emission at 408 MHz associated with the activity center in the McMath Region 14143 was observed by means of the radio interferometer of the Trieste Astronomical Observatory during the whole time of its presence on the solar disk. The instrument used is a simple correlation interferometer formed by two antennas 100 wavelengths apart in the East-West direction. Such an instrument can give only a low resolving power in the observation of the continuum sources because the fringe distance at the meridian is just 34.4 minutes of arc. However, a better resolution can be performed for fast impulsive emissions by using the "amplitude ratio method" between the interferometric and radiometric amplitude of each burst [Abrami, 1974].

Because of the rare presence of noise storm activity at 408 MHz, the number and density of such events are very low. Therefore, the presence of this kind of activity, which began on 23 March and lasted for more than 10 days, is, by itself, an outstanding peculiarity of this active center. In fact, two additional days of observation were rejected because of the small number of bursts.

The daily distributions of burst positions are reported in Figure 1. These are representative of the rotational motion of the radio center projected on the solar disk. In the reference frame used for these diagrams the abscissa is the interferometric distance from the hour circle passing through the center of the disk, and the ordinate is the density (in percent) of burst positions per prime of arc normalized to the total number of bursts (N) considered. For each day N is also given in Figure 1. The daily distributions, which have been cleaned up from noise contributions inherent in the reduction method, differ greatly in the widths and details of their profiles from day to day. These details, however, are not correlated with the number of observed bursts.

From the diagrams shown in Figure 1, the mean position for each day and the width of the distribution were evaluated. These data were then used to construct Figure 2, which points out the correlation between the position of the radio source and the sunspot group's location (obviously reduced to the same frame). Because the points split into two, well defined, straight-line segments, this diagram shows definitely the distribution in height of the emitting regions. It gives an independent confirmation of the complexity of the radio source implied from details in the profiles of Figure 1. In fact, the mean positions for days near the meridian transit show an evident double alignment, indicative of two emitting centers in which the western part was predominant during the first days and the eastern one stronger during the last days of transit. It is noticeable that in the days during which we observed an interchange of the emission between the two sources, the distributions in Figure 1 displayed the greatest width and the most complicated structure. The two-folded structure of the center was also independently confirmed by the interferometric observations at Nançay at 169 MHz [*SGD*, 1976].

We can use the slope of the two straight lines passing through the points in Figure 2 to evaluate the mean height of the emitting sources over the photosphere. The values thus obtained are $0.24R_\odot$ for the preceding source (equivalent to 165 000 km) and $0.14R_\odot$ for the following one (equivalent to 97 000 km). The distance between the two sources at the transit was 2.7 minutes of arc.

Source positions for the first 2 days are not satisfactorily included in these alignments. Because these observations were made near the limb and because strong refraction effects exist in the solar corona, these radio emitters correspond to sources at much higher altitudes. This situation, however, allows an evaluation of the height in the radial direction. With this aim in mind we computed the position of the sunspot group in the interferometric reference frame for these days to be equal to 13.1 and 13.3 primes of arc, respectively; the ratio between the radio positions and these values gives us a height of about 250 000 km.

The values thus obtained for the heights of the sources both on the disk and at the limb agree satisfactorily with a case previously observed by one of us [Abrami, 1974] at the same frequency and with the same instrument.

The positions obtained for 25 March deserve particular consideration because they strongly disagree with the other measured locations. The two positions represented in Figure 2 for this day are related to two successive periods of emission separated by a lack of activity. We have no satisfactory explanation for these peculiar positions. Moreover, they are confirmed in our observations of the continuum emission [*Oss. Solari*, 1976]. It is noticeable that the observed separation of these two emission centers (equal to 2.1 minutes of arc) does not disagree with the separation estimated during transit. It would be interesting to compare this anomalous result with other independent measures at the same or at nearby frequencies.

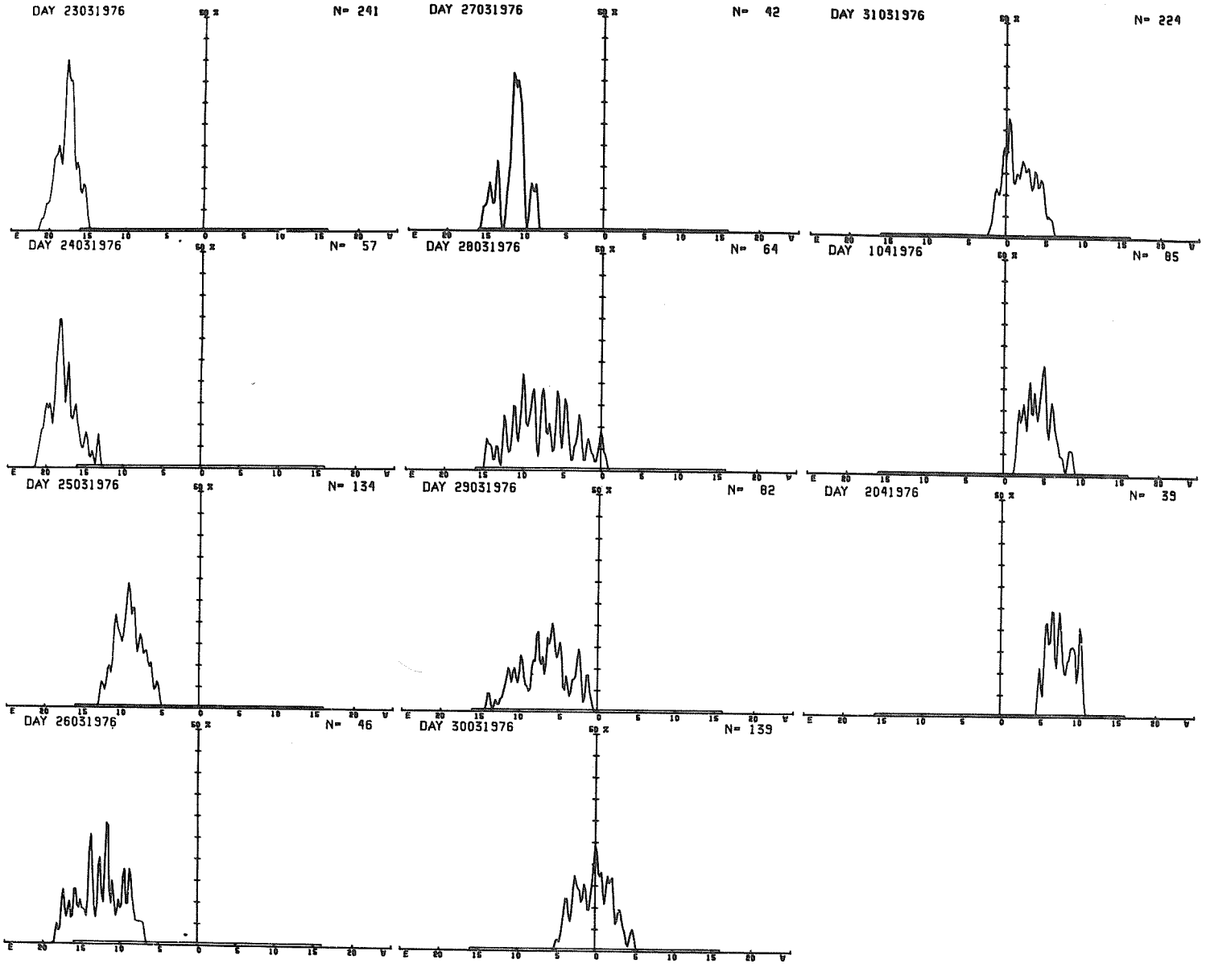

Fig. 1. Distributions of the burst positions related to the McMath Region 14143. The abscissa is the interferometric distance from the hour circle passing through the center of the disk. The ordinate is the density (in percent) of burst positions per prime of arc referred to the total number N of bursts considered. N is given for each day.

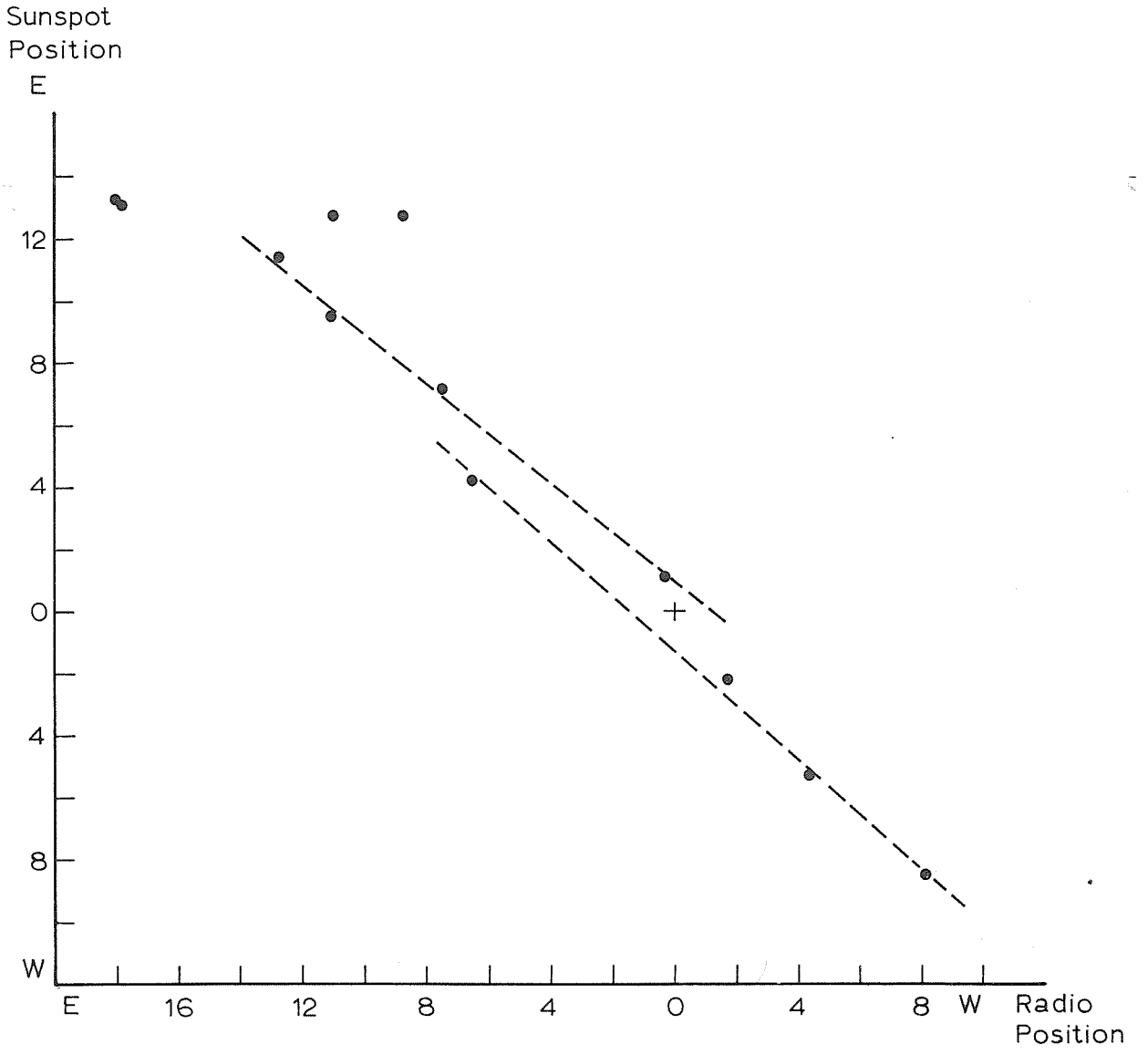

Fig. 2. Sunspot versus radio positions during the period 23 March - 2 April 1976.

REFERENCES

ABRAMI, A. 1974 Some Preliminary Results on the Distribution of Type I Bursts at 408 MHz, *Proc. 4th CESRA Meetings*, 123.

1976 *Osserv. Astron di Trieste, Osservazioni Solari No. 41*, 8, Trieste, Italy.

SGD 1976 *Solar-Geophysical Data, 380 Part I*, 15, April 1976, U. S. Department of Commerce, (Boulder, Colorado, U.S.A. 80302).

Solar Activity Associated with McMath Regions 14143 and 14179: Observations on 600 MHz, 408 MHz and 27 kHz

by

C. Gonze
Département de Radioastronomie et Physique Solaire
Observatoire Royal de Belgique
Uccle, Belgique

Introduction

The total solar radio flux at 600 MHz is measured regularly with a 7.5 m reflector at the radio astronomical station of Humain-Rochefort. East-west drift scans of the Sun on 408 MHz are obtained with the east-west base of the Humain interferometer (Maximum resolving power: 3.5'). Sudden Enhancements of Atmospherics (SEA) are recorded at Humain and Uccle on 27 kHz.

Outstanding Occurrences on 600 MHz

Date 1976	Type		Start Time (UT)	Time of Max (UT)	Duration (min)	Flux Density ($10^{-22}Wm^{-2}Hz^{-1}$) Peak	Mean	Remarks
March 20	41	SER	0750	0750.8	5	81	-	
	1	S	1004.3	1004.5	0.6	18	9	
	2	S	1014.6	1015.2	1.2	28	10	
	2	S	1433	1433.5	1	45	20	
21	27	RF	0757	--	33	--	-	
	2	S	0757	0758	1.5	38	20	
	2	S	0759.8	--	0.4D	--	-	(h)
	45	C	0807.7	0809	5	107	25	
	27	RF	1249	1253	25	5	3	
22	4	C	0808	0808.2	2.5	44	10	
23	4	S	0614	0614.1	0.6	18	9	
	48	C	0841.3	0844	58	560	57	
	4	S	0951.5	0952.5	1.2	50	8	
	41	SER	1023.5	1024.2	8.5	118	-	
25	41	F	0611.2	0613	3	122	10	
	41	F	0704.8	0706.5	2.5	18	4	
	49	GB	1128	1317	304	700	34	
26	40	F	0836	0847.5	24	10	4	
	41	SER	1038.8	1039	1.3	27	4	
	46	C	1441	1444	3.8	50	20	
	1	S	1519.5	1520	1	7	4	
27	45	C	1202U	1204.5U	-	--	-	
	1	S	1225.2	1225.4	0.3	6	3	
28	45	C	0531.5	--	1	--	-	(1)
	4	C	0534.5	0535	1	--	-	(1)
	41	SER	0555.5	0603	14	260	-	(1)
	40	F	0933	1017.5	60	16	6	
	3	S	1235.2	1235.3	0.4	12	6	
29	4	C	1042	1043.8	1.2	20	6	
	27	RF	1453	1456.5	13	8	5	
30	--	-	0528.4	0528.6	2.2	--	-	(1)
	44	NS	0600E	0915U	660D	--	-	
	8	S	1020.5	--	0.2	120	60	

Outstanding Occurrences on 600 MHz (continued)

Date 1976	Type		Start Time (UT)	Time of Max (UT)	Duration (min)	Flux Density ($10^{-22}Wm^{-2}Hz^{-1}$) Peak	Mean	Remarks
March 31	44	NS	0600E	1012U	630D	--	-	
	4	S	0703	0704	2	22	12	
	47	GB	1153U	1158U	17	945	-	
	47	GB	1349U	1357.5U	45U	360	140	
April 6	1	S	1038	1038.5	1	8	3	
	21	GRF	1209	1210	3.5	5	3	
	1	S	1411	1411.2	0.4	4	2	
April 20	45	C	1751	--	43D	--	-	(c)
21	4	C	1523	1528	5	12	4	
30	45	C	0843	0843.8	3.2	72	25	
	47	GB	1243	1245.5	13	1100	52	
May 3	2	S	0747.5	0748	1.2	7	4	

Remarks: (h): Occurrence recording perturbed by a time mark
(1): Occurrence during sunrise
(c): Occurrence during sunset

Days of no observations: 2 May

EAST-WEST SOLAR SCANS

HUMAIN, BELGIUM

408 MHz - 73 cm

Half-power beamwidth : 3'.5

MARCH 1976

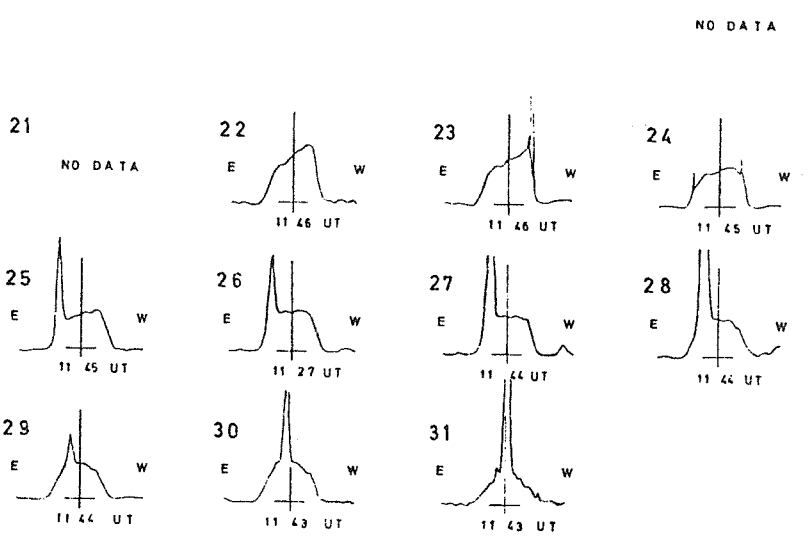

EAST-WEST SOLAR SCANS

HUMAIN, BELGIUM

408 MHz - 73 cm

Half-power beamwidth : 3.5

APRIL 1976

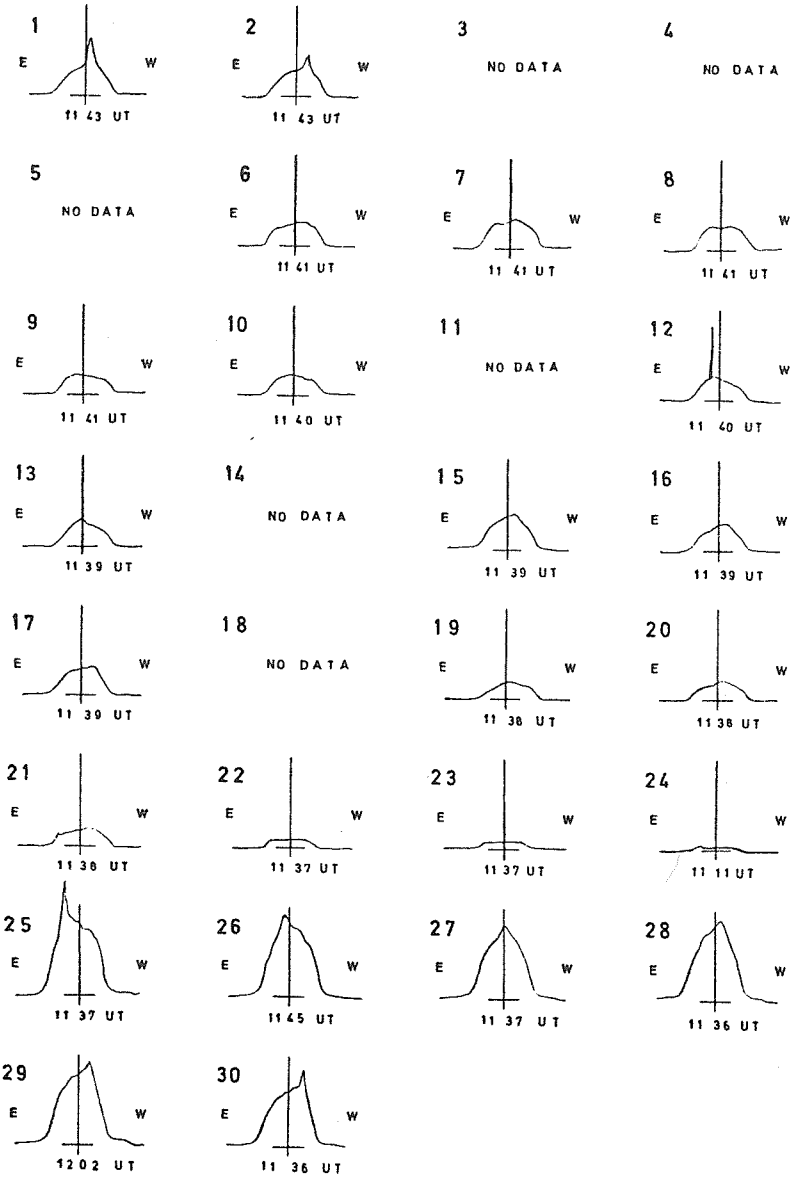

MAY 1976

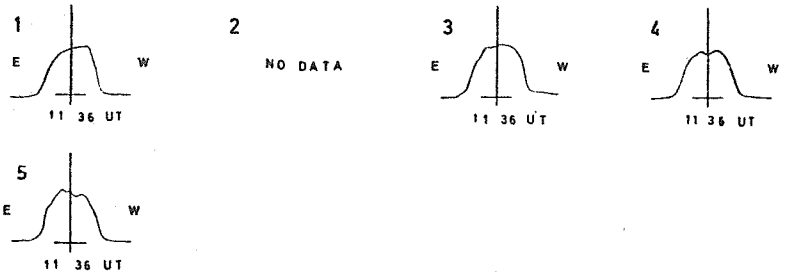

Solar Activity on 408 MHz Associated with McMath Plages 14143 and 14179

The Sun was observed from 0730 to 1500 UT so that 43 drift curves were obtained each day. When a source becomes visible on a drift curve, the corresponding transit time of the center of the solar disk is given ("first observation" column) with the importance of the source activity according to the following scale:

1 :			LR ≤ 0.1	x Q.S.
2 :	0.1 x Q.S.	≤	LR ≤ 1	x Q.S.
3 :	1 x Q.S.	≤	LR ≤ 2	x Q.S.
3^+:	2 x Q.S.	≤	LR	

where Q.S. denotes the estimated Quiet Sun level, and LR represents the level rise corresponding to the source in the McMath plages 14143 and 14179. When a time indication appears in the "last observation" column, it means that the activity of the observed source has the same importance on all drift curves recorded during the "first - last observation" period.

Date 1976	First Obs. (UT)	Last Obs. (UT)	Imp	Remarks
March 22	--	--	-	No activity
23	0738	0810	1	
	0849		3^+	Outstanding
	0900		1	
	0922		1	
	1245		1	
24	0810		2	
	0900	0932	2	
	1145	1153	2	East of 143
	1236	1245	2	East of 143
	1302		2	East of 143
	1320	1330	2	East of 143
25	0836	0900	1	
	0911	0932	2	
	0942	0951	3	
	1001	1019	2	
	1028	1037	3	
	1045	1103	2	
	1111	1120	3	
	1128	1136	2	
	1145	1153	3	
	1202	1339	3^+	Outstanding at
	1349	1419	2	1311 and 1320
26	0737	1102	2	
	1111	1136	3	
	1302	1442	3^+	
27	0736	0754	3D	Off scale
	0808	1018	2	
	1027	1102	3	
	1111	1419	3^+	Off scale; max at 1210
	1429	1453	2	
28	0808	0822	3D	Off scale
	0835	0847	2	
	0948		3	
	0909	0930	2	
	0940	1419	3^+	Off scale; max at 1018
	1430	1454	2	
March 29	0736	1441	2	
30	0735	0949	3D	Off scale; max at 0929
	0958	1453	3^+	Off scale
31	0735	1440	3^+	Off scale; max at 1418
April 01	0820	0958	2	
	1007		3	
	1016	1043	2	
	1052		3	
	1100	1208	2	
	1217		3^+	
	1225		2	
	1234	1243	3^+	
	1251	1319	2	
	1329		3^+	
	1338	1441	2	
02	0734	1453	2	
21	0755	0823	2	
	0859		3	
	0921		2	
	0931		3	
	0941		2	
	0951	1000	3	
	1009	1019	2	
	1028	1054	3^+	
	1120	1138	2	
	1203		2	
	1221		2	
	1239	1248	2	
	1334	1355	2	
	1452		2	
22	1054		3	
	1120		2	
	1416	1440	2	
23	0846	0858	2	
	0950		3	
	1027		2	

Date 1976	First Obs. (UT)	Last Obs. (UT)	Imp	Remarks
April 24	0834		2	
	0949	1120	2	
	1212		2	
	1324		2	
25	0806	0833	2	
	0857		2	
	0919	0929	2	
	1008	1220	2	
	1229		3	
	1238	1506	2	
26	0857	1500	2	
27	0833	0948	2	
	1110	1220	2	
	1229		3	
	1238	1345	2	
	1355	1406	3+	
	1417	1428	2	
April 28	0832	1228	2	
	1246	1539	2	
29	0832	0844	2	Eclipse from
	1202	1523	2	0845 to 1157 UT
30	0818	0831	2	
	0844		3+	
	0855	1238	2	
May 01	0748	1315	2	
03	0830		1	
	0947	1136	2	
	1202	1406	2	
04	0926	1006	1	
	1015	1356	2	
05	0904	1442	1	

Remarks: 1. When D appears under the column heading "Importance (Imp)", the importance is equal to or greater than the indicated value.

2. Days of no observation were 20 and 21 March; 3, 4, 5, 11, 14, and 18 April; and 2 May 1976.

Sudden Enhancements of Atmospherics (27 kHz)

Date 1976	Start (UT)	Max (UT)	End (UT)	Importance	Remarks
March 21	0755	0815	0850	3+	
	1114	1120	1128	1	
	1250	1307	1352	2	
23	0845	0849	0918U	2	
25	1125	1159U	--	-	
26	0720	0724	0745U	3	
	1440	1448	1556	2	
27	1202	1210	1237	2	
28	0555	0601	0610	2	
April 07 *	0537	0553	0611	2	Uncertain
30	0821	0846	0923	1	
	0948	0958	1018	1	
	1244	1259	1334	1	
	1449	1507	1513U	1	
May 02	1241	1328	1350	2	Uncertain
	1536	1544	1620	1	Uncertain

* : Day of no observation at Humain.

Flux and Circular Polarization from Microwave Solar Activity and Some Related Low Ionosphere Effects (24 March - 30 April 1976)

by

Pierre Kaufmann, L. Rizzo Piazza and J. C. Raffaelli
Centro de Radio Astronomia e Astrofisica (CRAAM)
Universidade Mackenzie
Sao Paulo, SP, Brasil

ABSTRACT

We describe 7 GHz flux and circular polarization due to the activity associated with McMath Regions 14143 and 14179, which produced bursts in the period 24 March - 30 April 1976. Low terrestrial ionosphere response to solar activity was investigated through VLF propagation phenomena.

1. General Activity

In Table 1 we relate all events recorded at Itapetinga Radio Observatory, Atibaia, SP, Brasil, within the selected period. On the left we list the 7 GHz events with the usual notation for the data description. Here we indicate only the mean polarization degree (in percent) because the polarization can show significant changes with time that are uncorrelated with the temporal flux changes [Wassenberg, 1971; Kaufmann and Marques dos Santos, 1974]. On the right side of the table we indicate the sudden ionospheric disturbances (SIDs) observed over the very low frequency (VLF) propagation paths of Liberia-Atibaia (SP), at 10.2 kHz and 13.6 kHz, in a 5.20 Mm distance; and Argentina-Atibaia (SP), at 10.2 kHz, in a 3.14 Mm distance.

In Figure 1 we show daily measurements of flux and polarization at 7 GHz. These correspond to the contribution from the slowly varying component associated with the selected McMath Regions 14143 and 14179. Note region 14161's contributions between 10 and 20 April 1976. McMath Region 14143 is clearly the most important active center observed in March. The daily flux shows the well-known cos ϕ dependence, where ϕ is the heliographic longitude of the active center as well as the polarization degree direction. The polarization remained left-handed, with a possible exception on 23 March 1976. Although the CMP of McMath Region 14143 was 31 March, its maximum polarization occurred on 26-28 March. Moreover, since the slowly varying component and the burst activity displayed no right-hand polarization, we concluded that the effect of magneto-ionic coupling was nil [Takakura, 1961]. The left-hand polarization of the emission from the dominant preceding spot in McMath Region 14143 implied a polarity reversed from that of the preceding solar cycle and solar hemisphere [Paes de Barros and Kaufmann, 1972].

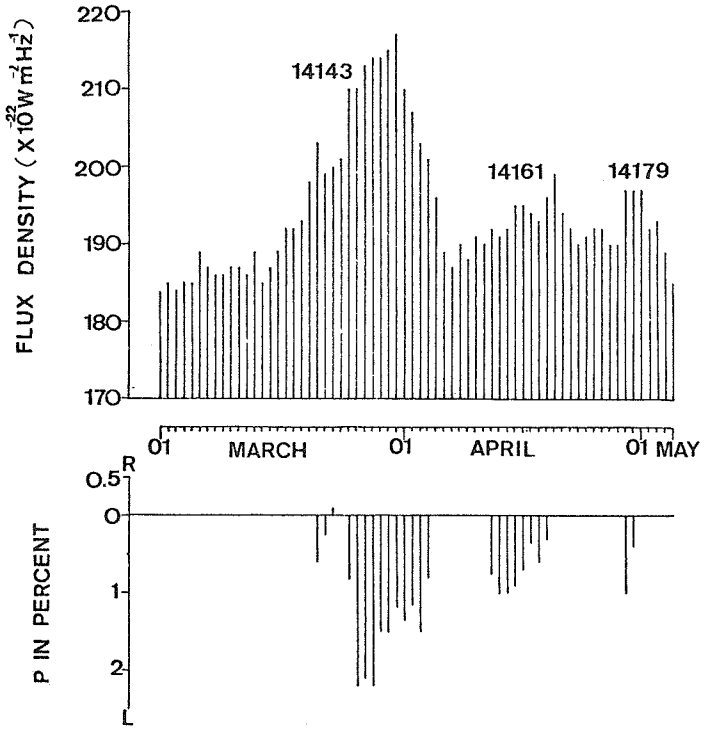

Fig. 1. Daily flux and percent of circular polarization of the quiescent Sun at 7 GHz for the period 1 March - 5 May 1976. The numbers indicate the McMath Regions contributing to increase the background data.

Table 1. 7 GHz Burst Data and SIDs Observed at VLF in the Period 24 March - 30 April 1976.

	7 GHz SOLAR BURSTS								VLF PATH: LIBERIA - ATIBAIA, S.P. f=13.6kHz; d=5.2Mm			VLF PATH: LIBERIA - ATIBAIA, S.P. f=10.2kHz; d=5.2Mm			VLF PATH: ARGENTINA - ATIBAIA, S.P. f=10.2kHz; d=3.14Mm		
Date 1976	Start Time (UT)	Time of Max (UT)	Duration (Min)	Flux Density 10^{-22}W/m^{2}Hz Peak	Flux Density 10^{-22}W/m^{2}Hz Mean	NOAA Type	McMath Plage Region	Mean Polarization	Start Time (UT)	Time of Max (UT)	ΔΦ/d (°/Mm)	Start Time (UT)	Time of Max (UT)	ΔΦ/d (°/Mm)	Start Time (UT)	Time of Max (UT)	ΔΦ/d (°/Mm)
Mar.																	
24	1835.1	1835.8	1.0	6	3	1	14143	32% L									
25	1109.2	1109.6	1.1	4	2	1	14143	59% L									
	1132.7	1220.4	170.6	134	-	21	"	-	1135	1215	11.3	1137	1215	14.1	1137	1215	11.1
	1137.2	1138.1	3.6	12	6	2	"	25% L									
	1158.9	1159.9	2.6	7	3	1	"	8% L									
	1209.0	1220.4	115.2	131	-	21	"	-									
	1214.8	-	20.4	84	45	1	"	2% L									
	1217.2	1220.4	5.5	43	26	3	"	11% L									
	1310.1	1310.7	3.2	26	17	4	"	6% L									
	1313.3	-	29.5	80	44	20	"	7% L									
26									1311	1317	1	1313	1318	1.8	1320	1334	1.5
	1439.2	-	1.5	7	7	28	"	0	1442	1453	6.1	1442	1455	6.0	1442	1456	5.9
	1440.7	1443.5	5.5	219	87	46	"	10% L									
	1446.2	-	12.2	-	10	29	"	12% L									
27	1202.7	1204.4	5.6	63	-	46	"	-	1204	1217	7.1	1204	1219	9.5	1204	1227	11.1
	1325.2	1325.9	2.1	8	2	1	"	4% L									
	1437.7	1438.8	12.3	13	7	21	"	38% L	1417	1430	2.4	1410	1427	2.1	1412	1430	1.2
	1438.4	1438.8	0.9	9	4	1	"	29% L									
	1439.3	1439.9	1.0	5	3	2	"	21% L									
28	1211.3	-	2.5	7	4	1	"	16% L				1230	1239	1.1	1230	1243	1.2
	1339.0	-	1.2	-	4	28	"	14% L									
	1340.2	1340.5	0.9	19	9	4	"	23% L									
	1341.1	-	25.8	-	-	29	"	-									
	1737.2	1738.0	1.8	27	13	4	"	0									
	1821.1	-	7.0	-	-	40	"	-									
	1836.7	1914.9	38.2	52	26	28	"	9% L									
	1914.9	1933.9	18.1	2939	1338	47	"	17% L	1902	1936	5.2	1902	1938	4.9	1900	1938	17.6
	1952.0	1952.0	47.3	103	57	29	"	1% L									
29	1203.8	-	489.2	17	-	25	"	-									
	1203.8	-	-	-	-	40	"	-									
30	1901.1	1901.6	13.0	18	9	4	"	6% L									
31												1137	1157	2.2	1137	1150	1.5
	1153.7	1157.4	81.4	24	15	23	"	7% L	1155	1222	6.1	1200	1215	3.5	1200	1225	3.5
	1154.9	1155.5	1.2	8	4	1	"	26% L									
	1156.4	1157.4	1.7	14	7	2	"	25% L									
	1159.2	1200.0	1.9	7	3	1	"	24% L									
												1225	1230				
	1330.8	1330.9	1.3	12	6	2	"	23% L	1250	1316	4.2	1300	1315	1.8	1245	1325	4.1
Apr.																	
01	1047.5	1121.0	97.6	18	9	23	"	23% L									
	1120.8	1121.0	0.6	8	4	2	"	51% L									
03	1632.3	1632.7	0.8	23	11	8	"	10% R									
29	1124.0	1124.4	0.4	5	3	28	14179	0	1115	1132	2.4						
	1124.4	1124.6	0.6	50	25	4	"	6% L									
	1125.0	1125.0	9.3	17	0	29	"	0									
	1907.9	1909.8	1.9	14	4	28	"	0									
	1909.8	1910.6	3.9	141	63	4	"	7% L									
	1913.7	1913.7	21.5	17	9	29	"	0									
30	1133.7	1134.3	1.0	9	4	1	"	0									
	1241.9	1242.6	0.7	4	2	28	"	0	1242	1255	2.8	1242	1303	3.2			
	1242.6	1244.3	3.8	43	22	4	"	11% R									
	1246.5	1246.5	290.6	9	0	29	"	0									
	1737.1	1737.1	192.9	9	4	26	"	0									
	1839.2	1839.6	0.9	12	6	2	"	0									

Finally, the daily variation of VLF phase is indicative of particle precipitation in the terrestrial lower ionosphere [Westerlund *et al.*, 1969]. We received VLF signals from Liberia in a nearly W-E propagation path, and from Argentina in a nearly S-N path. Both paths partially cross the South Atlantic Geomagnetic Anomaly where the effect of precipitating particles can be particularly important [Mendes *et al.*, 1970]. Clear changes in daily phase variation were noted on the Liberia-Atibaia path from 28-31 March 1976 (i.e., an overall phase advance of nearly 10 μs); the effect was much weaker on the Argentina-Atibaia transmissions during the same days (i.e., less than about 5 μs).

2. The Events of 26 March (1439 UT) and of 31 March (1154 UT)

The event of 26 March, starting about 1439 UT, occurred in McMath Region 14143; its flux and polarization development as a function of time at 7 GHz is shown in Figure 2. This event was studied in detail by Kaufmann [1976]. The most striking feature is the quasi-periodic structure evident between 1443 and 1445 UT. It has a period of 17 s and is similar to the kind of events described by Janssens *et al.* [1973]. This structure has no periodicity in polarization degree, contrary to what would be expected if the oscillations were due to trapped electrons [Janssens *et al.*, 1973]. Perhaps the burst emission source lay deep in the active center, allowing the polarizing propagation media to remain unaffected by the burst pulsations.

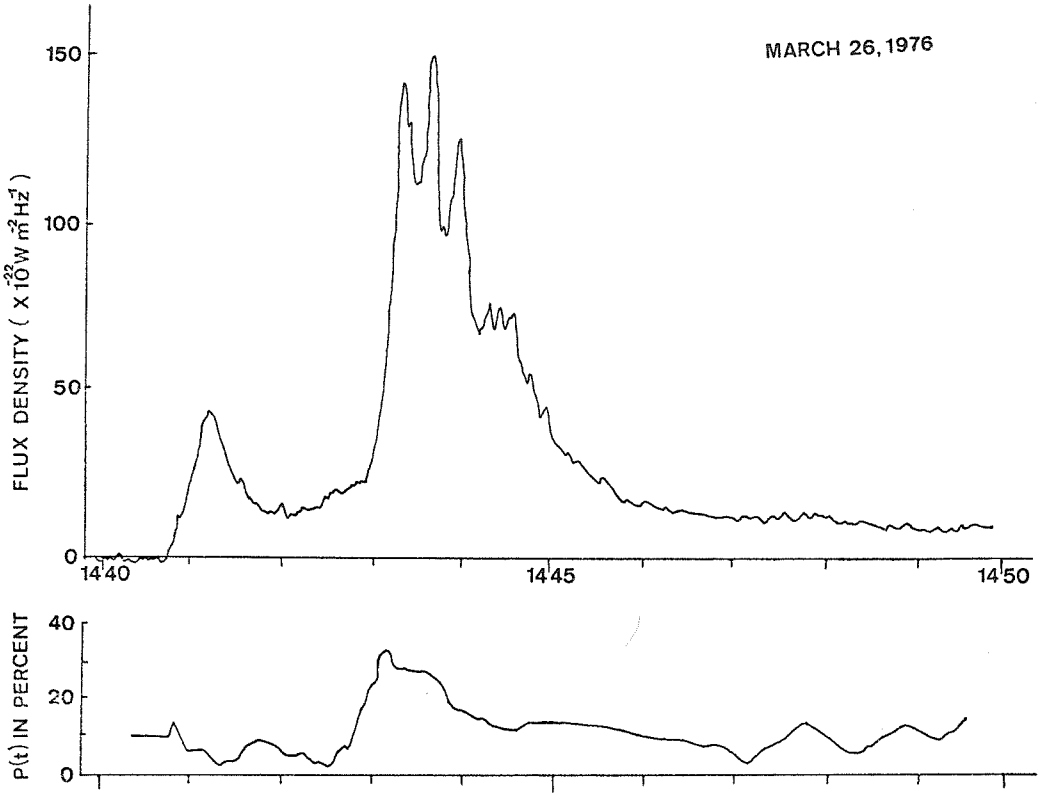

Fig. 2. 7 GHz flux and polarization development with time of the event of 26 March 1976.

The VLF SID associated with this event was of long duration starting at 1442 UT with a maximum at about 1455 UT; however, these VLF measurements were taken with a recording time constant of 50 seconds.

In Figure 3 we show another weak event recorded on 31 March with start time at about 1154 UT. It corresponded to quite a long period of activity, more than one hour. The polarization degree vs. time development is quite uncorrelated with the flux vs. time development. Some known basic features [Wassenberg, 1971; Kaufmann and Marques dos Santos, 1974] are again confirmed, for both events, i.e., peaks in polarization degree tend to occur previous to the peaks in flux, and events with larger intensity have smaller polarization degrees.

For the event in Figure 3, a corresponding SID displays a smooth phase advance with time, confirming in this example (as well as in the other events of the period) that the SIDs usually do not show any structure with time, irrespective of the complexity of time structures observed at microwaves [Kaufmann and Mendes, 1970].

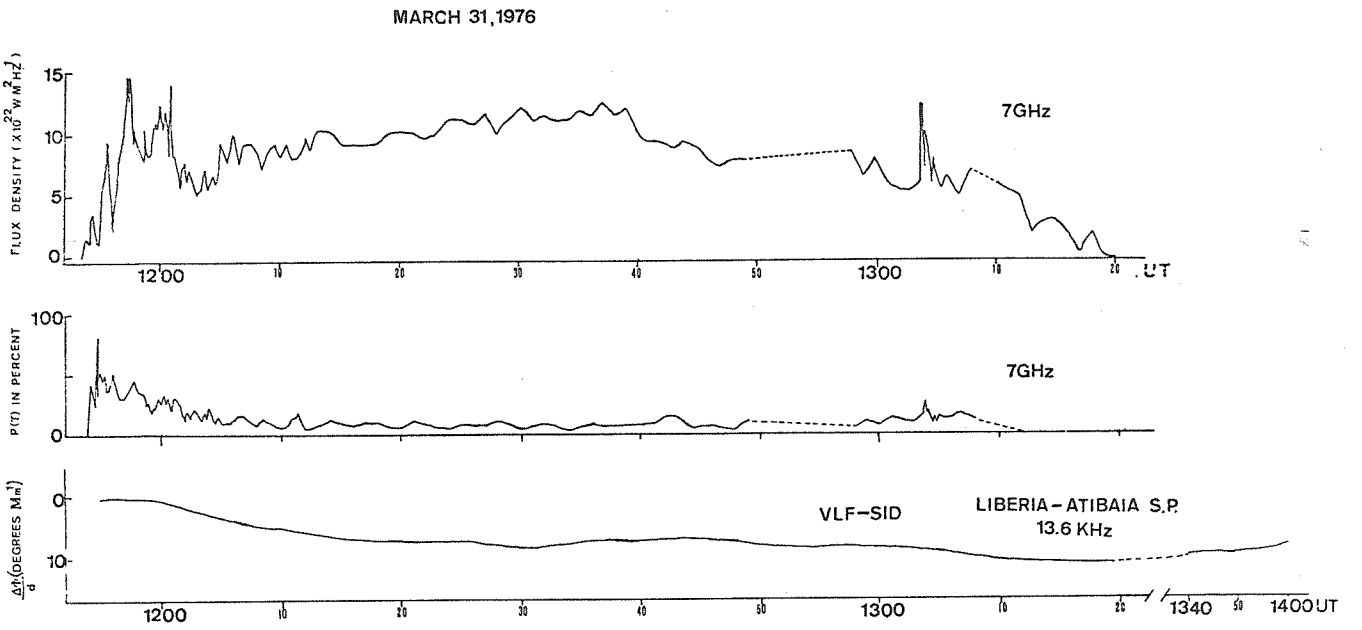

Fig. 3. The weak event of 31 March 1976.

3. The Great Burst at 1837 UT on 28 March 1976

(a) General Features

This was the largest event that we recorded in the period. At 7 GHz the burst began about 1837 UT; reached a maximum flux of 2940 x 10^{-22}Wm^{-2}Hz^{-1} at 1934 UT; and ended sometime after 2030 UT when our observation period ended. In Figure 4 we show the general development of the event in flux, in polarization degree (left-handed), and in terms of an associated large, smoothly developed SID observed at VLF.

The errors in estimating the polarization degree (i.e., the ratio $[(S_R - S_L)/(S_R + S_L)]$, where S_R and S_L are the flux densities for right- and left-hand circular polarization, respectively) become much smaller for larger fluxes.

In the scale of Figure 4 we can see again the basic features of polarization degree development with time. We could tentatively associate the slow overall change in polarization from 1902 to 1940 UT (i.e., of about 0.2) to the velocity of a magnetohydrodynamic shock wave produced by the flare detonation [Kaufmann and Marques dos Santos, 1974]. Assuming a characteristic scale of the magnetic field of $L_H \sim 10^9$m, a magnetic field of $H \sim 10^2$ gauss, and a frequency $f = 7 \times 10^9$ Hz, we obtain a velocity of about 1000 km s^{-1}, which is comparable to a Type II associated shock wave.

(b) Fast Pulsations

We found a very unusual modulation in flux density superposed on the main time structure shown in Figure 4 -- one that began with the event and remained present to the burst's end. We defined too a period of 4.7 ± 0.9 s by counting the number of pulses per min over a 75-minute interval. This modulation, however, lacked the same quasi-periodic oscillations described by Janssens *et al.* [1973] and displayed in the 26 March event of Figure 2. Moreover, in the 28 March burst these 4.7-second fluctuations cannot be confused with the much larger time structures that they modulate (see Figure 4).

The pulsations were more clearly defined whenever the flux density was high. Two high time resolution examples are shown in Figures 5 and 6 at 1931-1932 UT and 1933-1935 UT, respectively. These same figures also show that the polarization degree remained nearly stable, as in the larger oscillations seen in the event of 26 March (Figure 2). Another pecularity of this phenomenon is that the relative change in flux density (ΔS) remained about the same in comparison to the mean flux density ($\bar{S}$) defined for any given min. Using the time interval in which the burst was more intense and the effect was therefore more accurately defined (1916 - 1956 UT), we plotted the ratio $\Delta S/\bar{S}$. This appeared nearly constant for $50 \lesssim \bar{S} \lesssim 3000 \times 10^{-22}$Wm^{-2}Hz^{-1}, i.e., for $\Delta S/\bar{S} \simeq 10\%$ and implied that the flux density development with time could be described by a function of the form

$$S = \bar{S}\,(1 + a \cos \omega t),$$

where $\bar{S}$ is defined at every min, and $a = \Delta S/\bar{S}$, $\omega = 2\pi/T$, and $T \sim 4.7$ s. The lack of oscillation in the polarization degree and the approximately constant ratio may suggest that the observed pulsation could be associated with the burst source emitting mechanism.

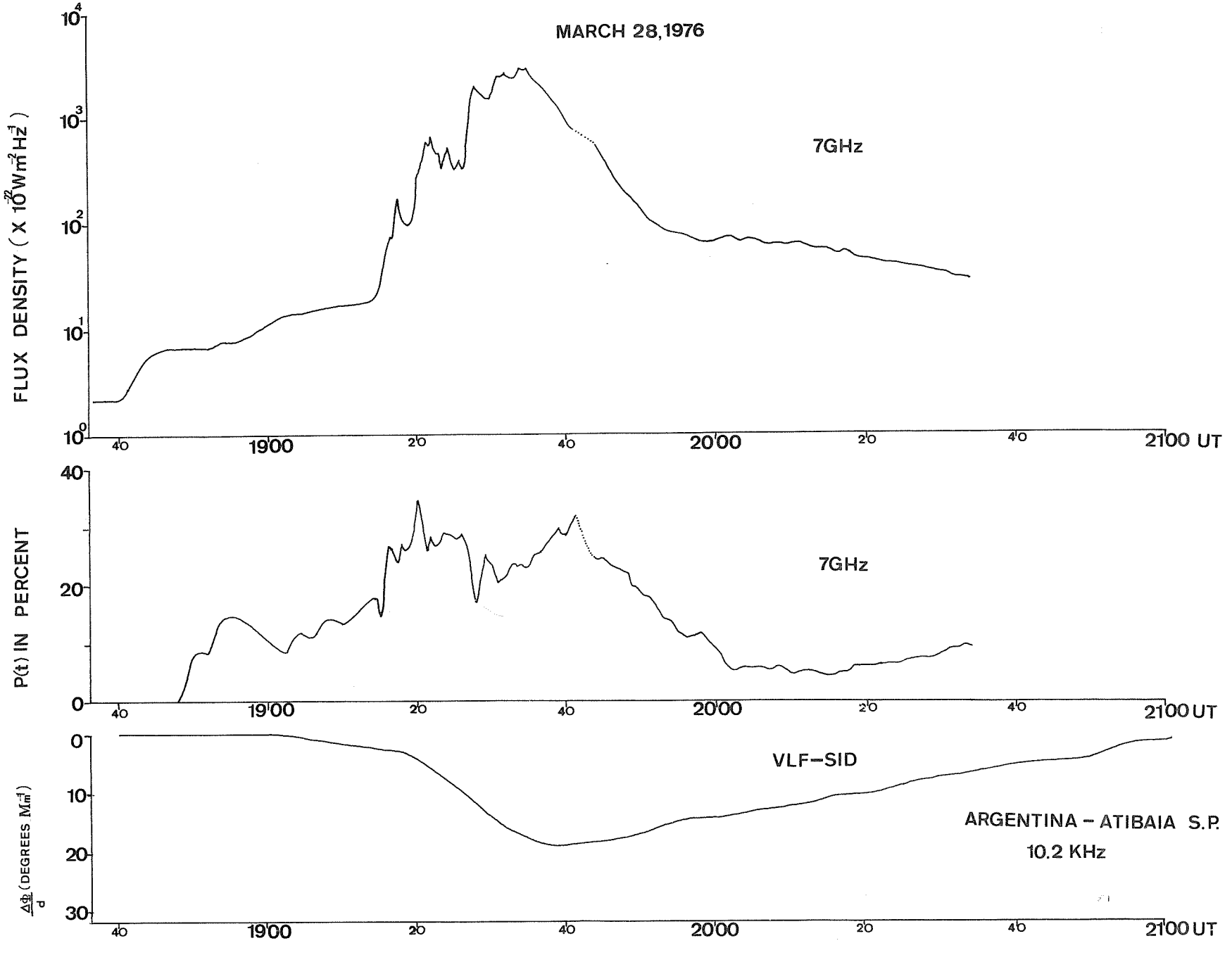

Fig. 4. Overall development with time of the great burst of 28 March 1976, in a compressed time scale.

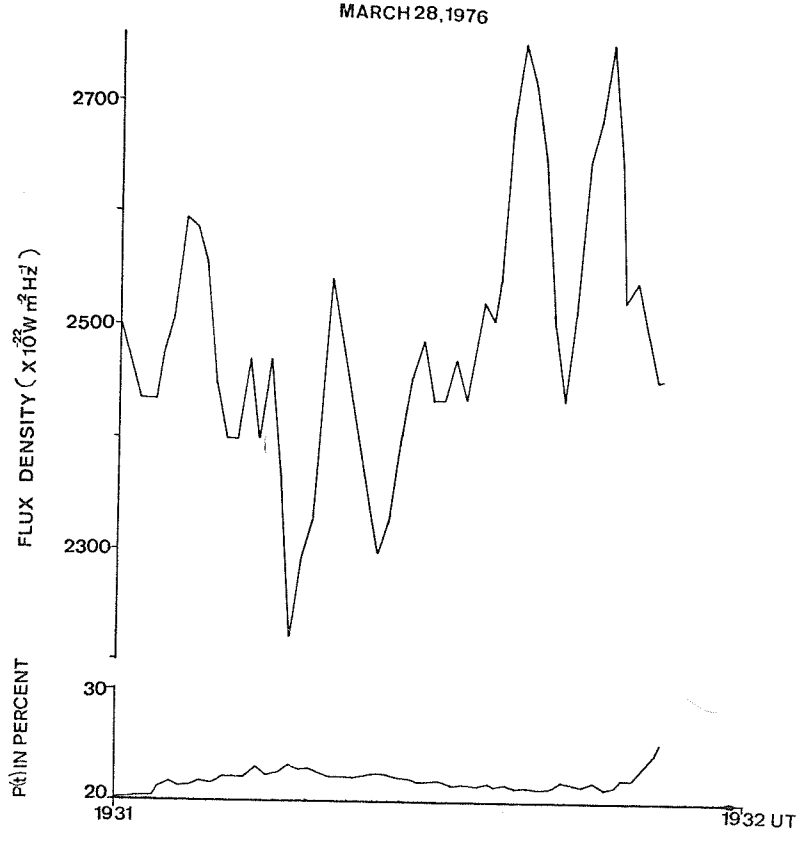

Fig. 5. High time resolution record sample showing the fast modulation in flux that does not affect polarization.

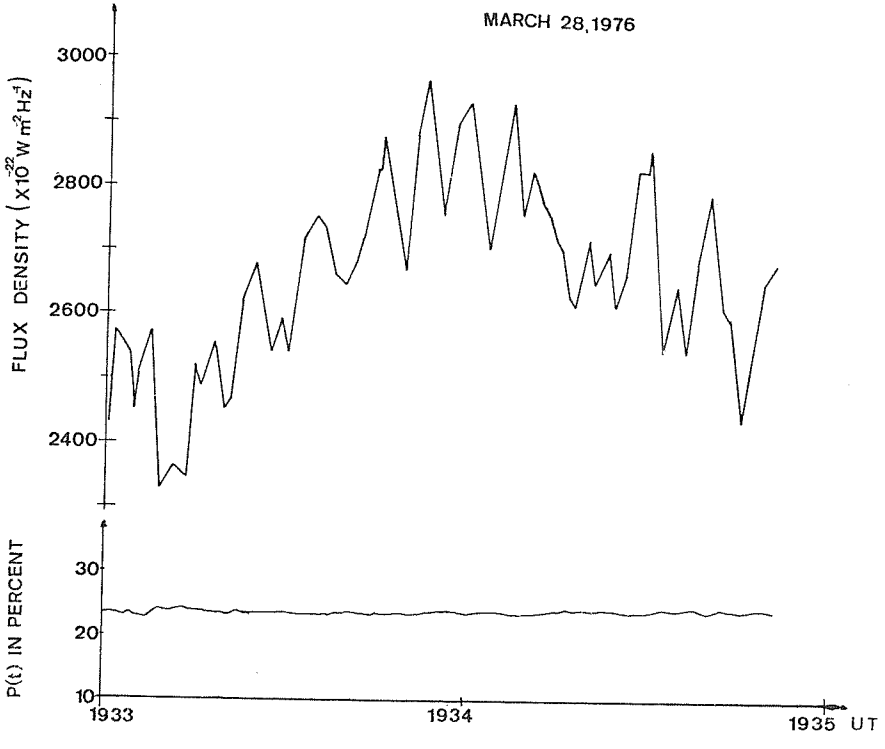

Fig. 6. High time resolution record sample showing the fast modulation in flux that does not affect polarization.

Acknowledgments

We acknowledge the data reduction and the illustrations performed by N. Pires, P. Iacomo, Jr., M. I. D. R. Prado and V. N. D. Borges, and the typing performed by F. A. C. Fonseca. This research was partially supported by the Brazilian Research Agencies CNPq, FAPESP and CAPES, and partially by US AFOSR.

Summary

The most important activity was associated with McMath Region 14143 in March 1976. A great burst was observed on the 28th followed by a PCA-like anomaly of small importance on VLF propagation paths between 28 and 31 March.

A new feature was discovered in the larger burst recorded at 7 GHz on 28 March. It contained a fast, nearly cyclical structure in time superposed on the burst profile with a period of about 4.7 s. The modulation persisted throughout the entire event, i.e., for more than about 80 min, and the relative flux oscillations remained nearly constant for all levels of flux intensity. The polarization degree was left-handed and failed to correlate with the oscillations. This may indicate the variations were associated with the emission mechanism rather than with the oscillations of the magnetic field, or with the mirroring of electrons in magnetic loops, or with other propagation phenomena.

REFERENCES

JANSSENS, T. J., K. P. WHITE III and R. M. BROUSSARD 1973 Quasi-Periodic Structure in Solar Microwave Bursts, *Solar Phys.*, *31*, 207-217.

KAUFMANN, P. and A. M. MENDES 1970 The Correlation Between Sudden Phase Anomalies and Solar Microwave Radio Bursts, *J. Atmosph. Terr. Phys.* *32*, 427-432.

KAUFMANN, P. and P. MARQUES DOS SANTOS 1974 Time Development of Circular Polarization Solar Microwave Bursts, *Astron. & Astrophys.*, *34*, 197-201.

KAUFMANN, P. 1976 *Solar Phys.*, in press.

MENDES, A. M., S. ANANTHAKRISHNAN, and M. H. PAES DE BARROS 1970 Phase and Amplitude Changes of VLF Signals Associated with PCA Events, with Reference to the South Atlantic Geomagnetic Anomaly, *Ann. Géophys.*, *26*, 483-492.

PAES DE BARROS, M. H. and P. KAUFMANN 1972 On the Long-Term Behaviour of the Circular Polarization From Coronal Condensation Radio Emission at 4.3 cm Wavelength, *Solar Phys.*, *27*, 203-207.

TAKAKURA, T. 1961 Limiting Polarization of Solar Microwave Emission, *Publ. Astron. Soc. Japan*, *13*, 312-320.

WASSENBERG, W. 1971 On the Polarization of Solar Microwave Bursts Observed at 17 GHz, *Solar Phys.*, *20*, 130-135.

WESTERLUND, S., F. H. REDER and C. ABOM 1969 Effects of Polar Cap Absorption Events on VLF Transmissions, *Planet. Space Sci.*, *17*, 1329-1374.

Multichannel Spectrometer Observations With 0.005 s Time Resolution in the Range 0.2 - 1.4 GHz During the Events of March 1976

by

F. Dröge
Radiosternwarte der Universität Kiel
D 2300 Kiel 1, German Federal Republic

The fine structures (FS) observed during the events of 23 March 1976 at 0840 UT and 31 March 1976 at 1150 UT are presented diagramatically, and characteristic FS are shown in sections of recordings with high time resolution.

The Spectrometer

The technical data of the digital multichannel spectrometer are as follows:

Frequency range	0.2 - 1.4 GHz
Frequency resolution	1 MHz
Time resolution	0.002 s
Dynamic range	40 - 50 dB
Sensitivity	0.2 dB
Number of channels	30
Reproduction (scale)	up to 40 cm/s

The intensity scales are logarithmic.

During the observations from March to April 1976, 26 channels were in operation at the following frequencies:

MHz	MHz	MHz	MHz	MHz	MHz
239	400	597	795	1025	1415
240	404	601	800	1029	1419
241	406	602	801	1030	1420
-	410	603	805	1031	1425
-	405	607	-	1035	-

The time resolution was reduced to 0.005 s.

The Fine-Structures (FS) Diagram

The FS diagram illustrating the spectrometer-observed fine structures resembles a dynamic spectrum, i.e., intensity plotted in a time-frequency plane. Symbols subdividing regions into the various kinds of FS activity and continuum are listed below Figure 2 along with the FS classification scheme. In each number pair shown the upper one indicates the FS's intensity (Δi) in dB; the lower one indicates its duration (Δt) in seconds between half-power points. Approximate absolute intensities of the FS can be obtained by defining the underlying continuum (i_C) in the slow recording profiles (LR) and by using the dB values given in the FS diagram.

The Event of 23 March 1976 at 0840 UT

Although Figure 2 contains detailed information on this event, several of its characteristics are evident in the slow recording traces shown in the left panel of Figure 1. It is a short Type IV burst in the meter and decimeter ranges with 20 min duration; its intensity is strongest and increases most rapidly in the meter range; its 100 flux unit level nearly coincides with the limits of the Type IV continuum; and its maximum intensity occurs shortly after the onset of the burst. In Figure 2, A', B', C' and D' denote regions of homogeneous FS; outside these regions FS activity is insignificant.

Region A'. We found strong Type III activity up to 9 dB at 0.2 GHz; several excursions of lesser intensity occurred up to 0.4 GHz. Panel a_1 in Figure 3 represents a section of the spectrometer observations and shows a Type III group with typical smooth structures and a one-to-one correspondence over a 2 MHz frequency distance.

Section a_2 shows the recording of the maximum (21 000 flux units) at 239 and 241 MHz with high time and frequency resolution. In the slow recording profiles of Figure 1 this maximum appears only as a sharp peak. Note the steep decline within 1 s (by 14 dB); this pulsation is probably a short Type V burst.

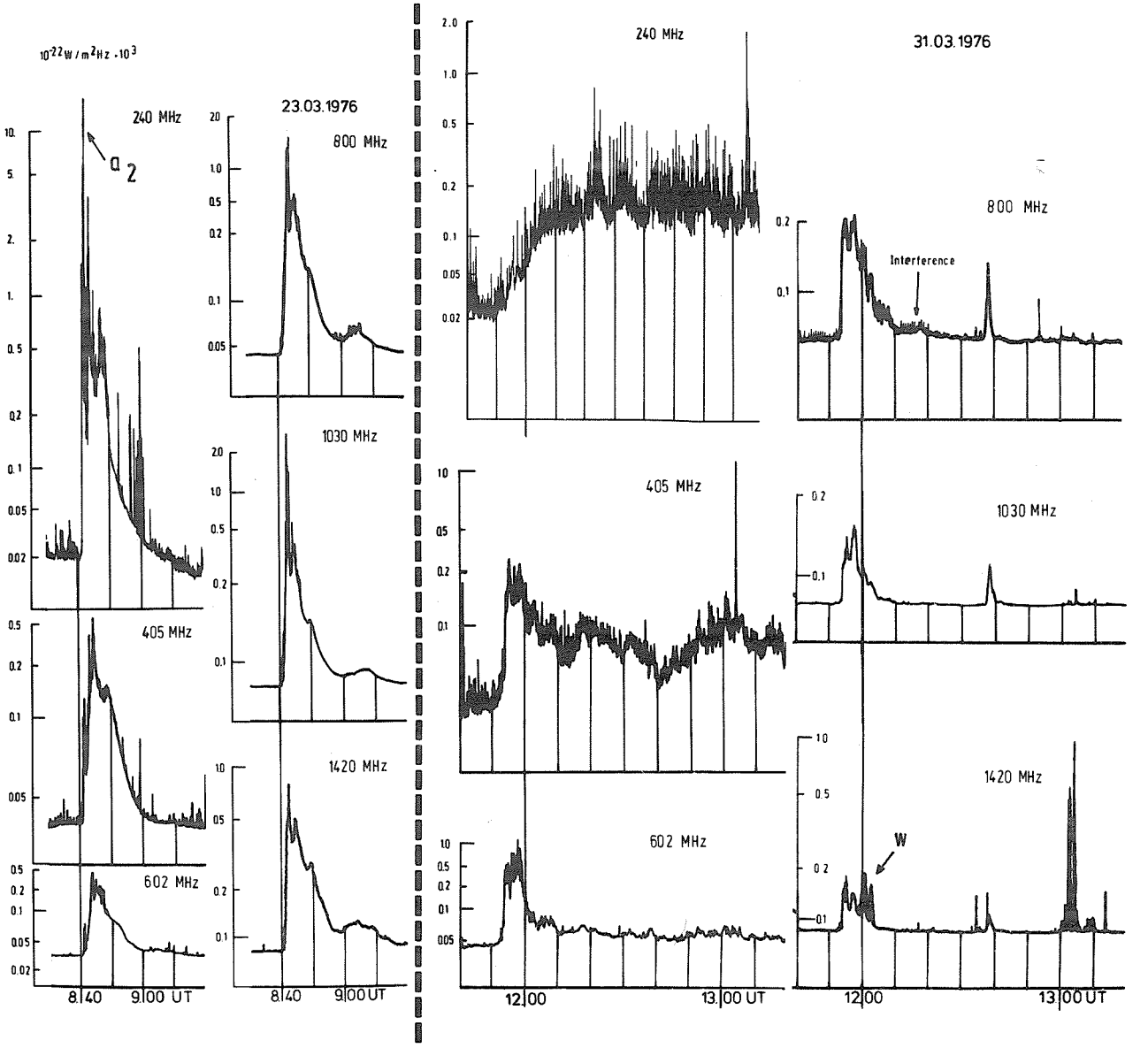

Fig. 1. Slow recordings with about 0.5 s time constant.

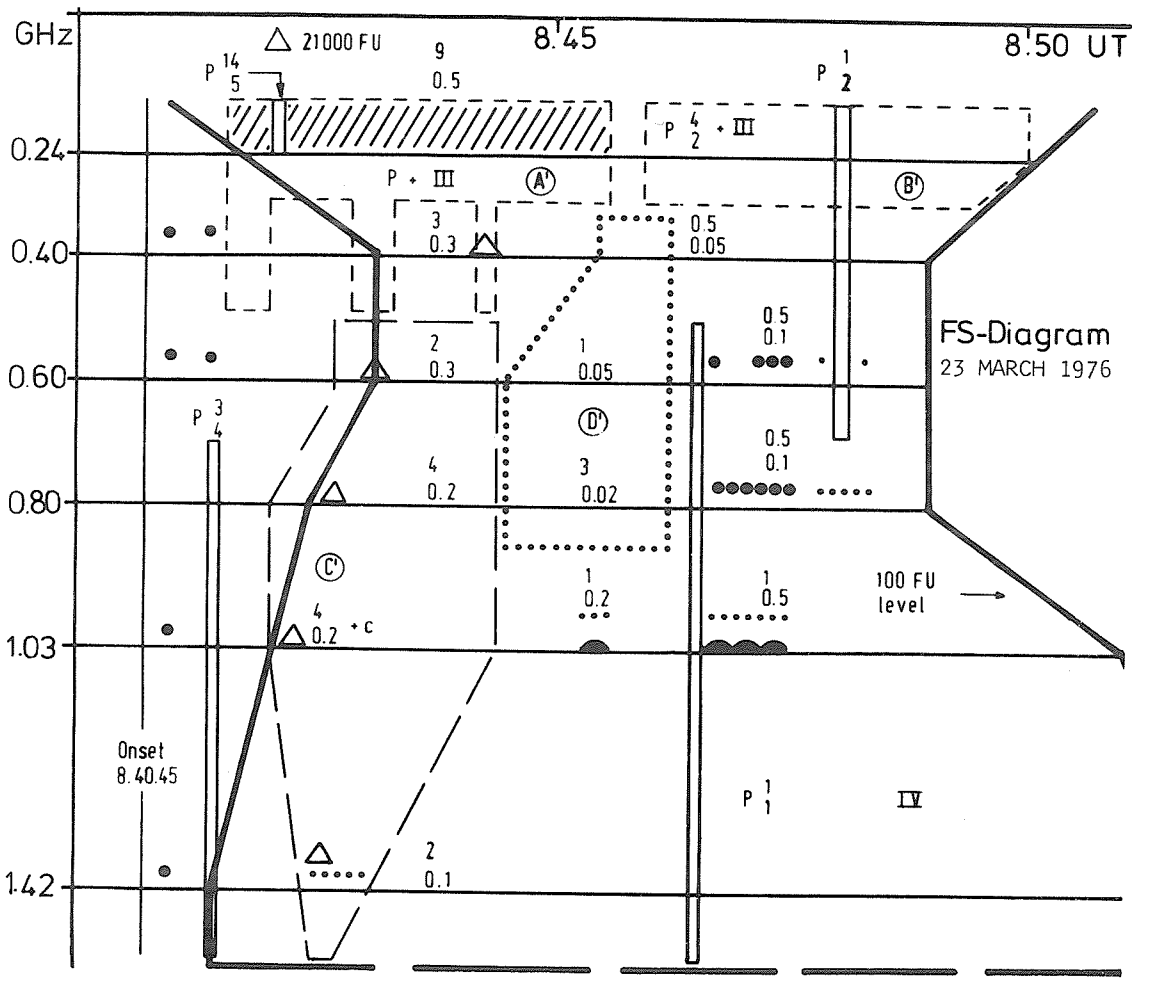

Symbols

Ranges

I continuum
IV "
V "

stronger intens. of FS or cont.
maximum
FS-range

Profiles

weak
isolated
complex = c
periodic or regular

pulsation = P
absorption = A

3 means
0.1

Δi = 3 dB (int.)
Δt = 0.1 s (dur.)

Fig. 2. Fine-structures diagram of the 23 March 1976 event at 0840 UT and key to symbols.
The same definitions apply to the symbols used in Figure 4.

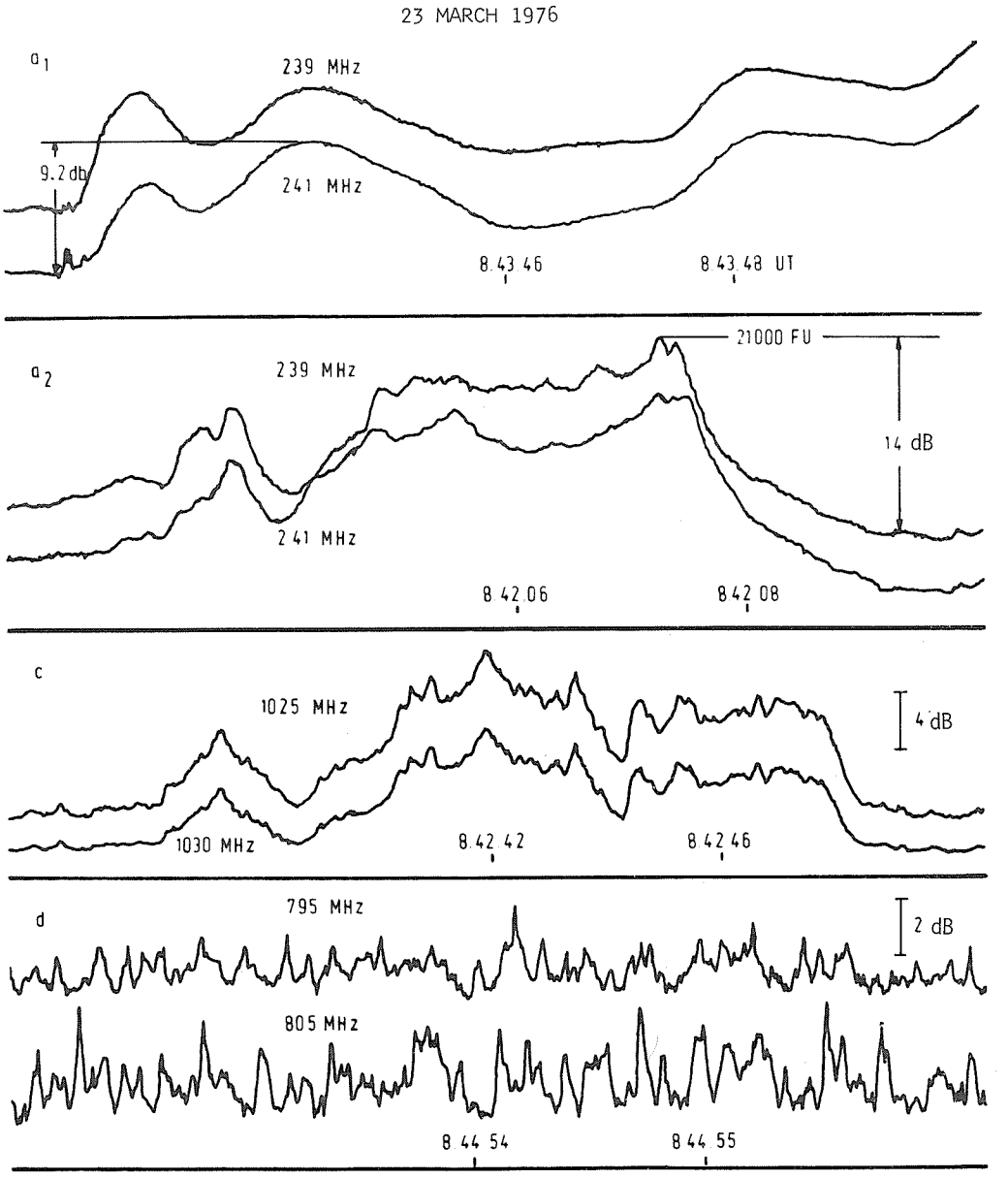

Fig. 3. Sections of the recordings with high time resolution for the 23 March 1976 event. Type III bursts are shown in section a_1, impulsive Type V in a_2, complex fine-structures and impulsive continuum in c, and spikes in d. Compare each panel with its corresponding region in Figure 2.

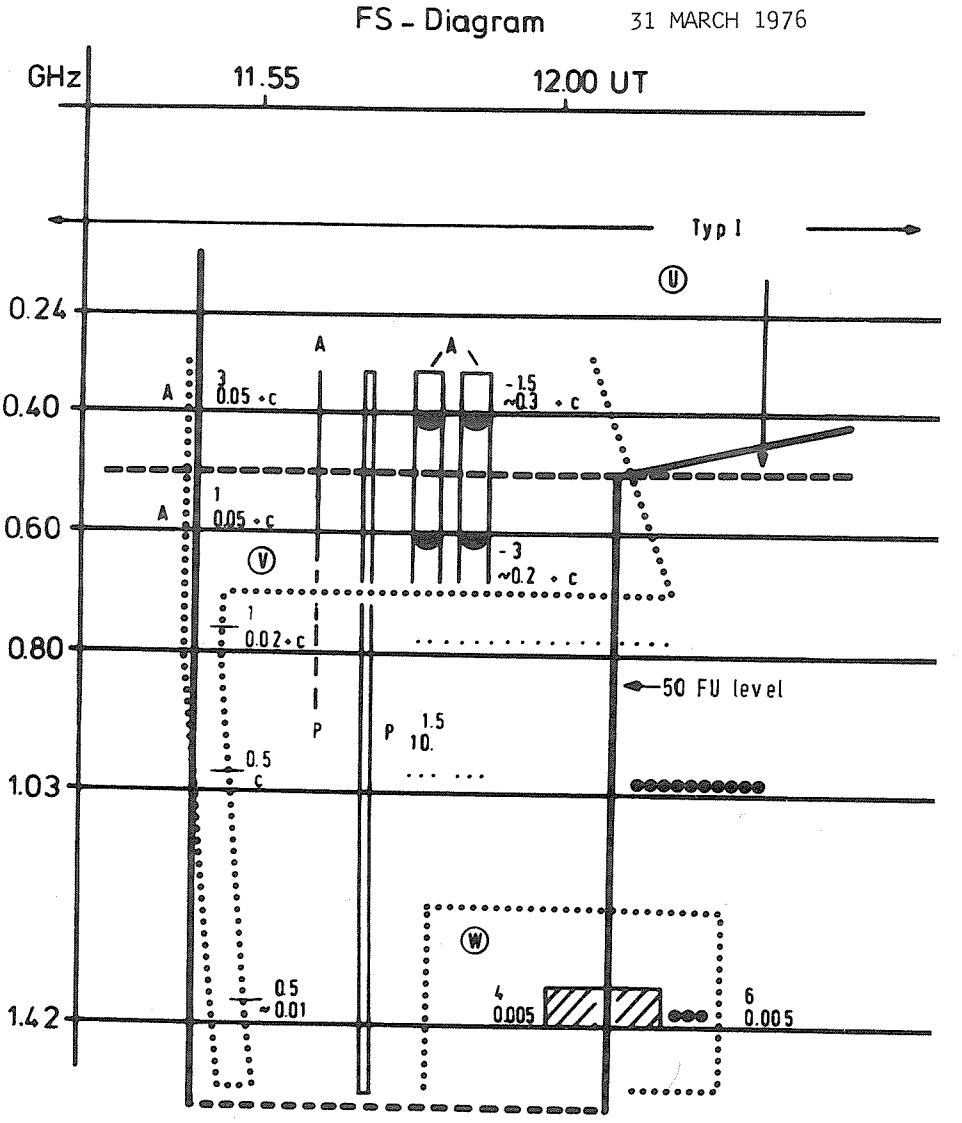

Fig. 4. Fine-structures diagram of the 31 March 1976 event at 1150 UT.

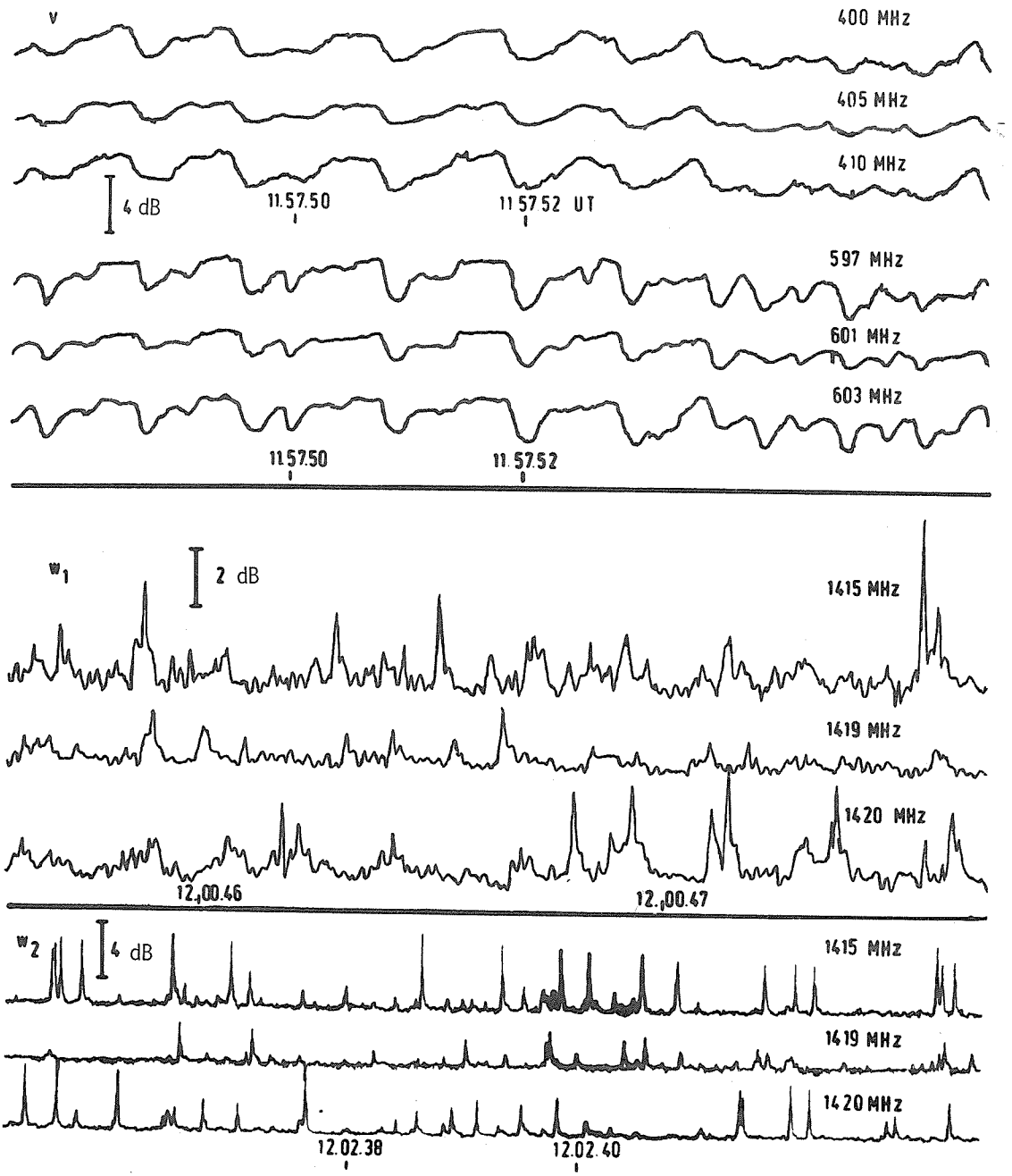

Fig. 5. Sections of the recordings with high time resolution for the 31 March 1976 event. Absorptions are shown in section v, spikes in w_1, and isolated spikes in w_2. Compare each panel with its corresponding region in Figure 4.

Region B'. This area is characterized by decreasing Type III activity and pulsations with 2 s durations.

Region C'. Complex FS of 0.1 s duration, and similar to those in section c of Figure 3, often appear in the decimeter range together with an impulsive continuum. Their bandwidth is generally about 40 MHz, and at a 5 MHz distance, as in section c, they are identical.

Region D'. FS with durations as short as those appearing in this region are usually called "spikes". Because the bandwidths of these structures span only a few MHz, little correlation is evident between the 795 and 805 MHz profiles shown in section d of Figure 3. A detailed survey of "spikes" is given by Tarnstrom [1971] and Dröge [1977].

Broadband Pulsations. Narrow, unshaded, vertical rectangles in the FS diagram signify broadband pulsations with durations of a few seconds and intensities of a few dB.

The Event of 31 March 1976 at 1150 UT

Observations were disturbed by a strong noise storm up to 0.4 GHz which had begun several days earlier. The event in question is a weak Type IV burst in the decimeter range with 15 min duration (see right half of Figure 1). In the FS diagram of Figure 4 the 50 flux unit level almost corresponds to the extension of the Type IV continuum. Regions U, V, W in Figure 4 indicate the areas of homogeneous FS.

Region U. Before the event the Type I bursts reached an intensity of about 100 flux units; during the event they increased to 300 flux units.

Region V. Throughout the region we found weak, complex FS with durations from 0.1 to 0.01 s. Of interest are the numerous absorptions at 0.4 and 0.6 GHz which appear in isolation, in groups, and in a nearly periodic pattern. Typically, their bandwidths are about 200 MHz (see Figure 5v), yet sometimes they can reach 400 MHz. Moreover, they drift toward higher frequencies at a rate of about 3 000 MHz/s. In the two strong groups near 1157:30 and 1158:20 UT the distances between absorptions are 0.2 - 3 s (see Figure 4). In the meter wavelength range Benz [1976] has called these absorptions "sudden reductions".

Region W. The shortest spikes in this area have durations of 5 ms. In the first part of the activity they number about 20 per second (see Figure $5w_1$). At the end, however, they appear as isolated profiles with 6 dB intensity (see Figure $5w_2$). The correlation between channels 1419 and 1420 MHz is very weak, implying that the bandwidths of these spikes are smaller than 1 MHz.

Weak, slow pulsations with durations of about 10 s were observed only at the onset of the burst and at 1156:55 UT (see Figure 4).

As the two FS diagrams illustrate, fine-structures activity during the bursts nearly covered the whole time-frequency range. Such a signature has emerged before [Dröge, 1976].

REFERENCES

BENZ, A. O. and JAN KUIJPERS — 1976 — Type IV dm Bursts: Onset and Sudden Reductions, *Solar Physics, 46,* 275.

DRÖGE, F. — 1976 — Sind die weltweiten Beobachtungen und Beobachtungsmethoden der solaren Radiostrahlung bei Bursts ausreichend?, *Kleinheubacher Berichte, 19,* 351.

DRÖGE, F. — 1977 — Millisecond Fine-Structures of Solar Burst Radiation in the Range 0.2 - 1.4 GHz, *Astron. Astrophys.*, in press.

TARNSTROM, G. L. and K. W. PHILIP — 1971 — Solar Radio Spike Bursts, *Scientific Report,* University of Alaska.

The Evolution and the Structure at Wavelength 1.35 cm of the Local Source Related to the McMath Proton Region 14179

by

V. A. Efanov, I. G. Moiseev, and N. S. Nesterov
The Crimean Astrophysical Observatory, USSR

Observations of the Sun during passage of McMath Region 14179 were carried out at the Crimean Astrophysical Observatory on wavelength 1.35 cm with a 22-meter radio telescope. The resolution of the instrument's beam was 2.5 by 2.6 arc minutes, and the sensitivity of the radio polarimeter in each channel was about 1 K with a 1-second time constant. Parameters I and V of Stokes were simultaneously recorded [Domnin *et al.*, in press].

Since the methods of observation and data processing were described by Efanov and Moiseev [1971], they will not be discussed here. Radio source characteristics related to McMath Region 14179 are listed in Table 1 in the following sequence: date of observation, flux density in unpolarized (F_I) and in circularly polarized (F_V) emission, and the degree of polarization (P_V). The brightness temperature of the quiet Sun was assumed to be 9700 K [Efanov *et al.*, 1971] for calibration of the unpolarized component.

Table 1. Characteristics of 1.35 cm Radio Source Associated With McMath Region 14179

Date of Observations April 1976	F_I (s.f.u.)*	F_V (s.f.u.)*	P_V (%)
23.51	1.40	0.056	4.1
24.47	1.39	0.110	7.9
26.34	0.93		
27.47	0.55	0.077	14.0
28.43	0.42	0.046	10.9
28.54	0.93		
29.28	3.80	0.21	5.6
30.39	10.70	0.58	5.4

* s.f.u. = one solar flux unit = 10^{-22}Wm^{-2}Hz^{-1}

The data from Table 1 are plotted in Figure 1 together with the area of the sunspot group (S) in millionths of the solar hemisphere. It can be seen that variations of the source flux in polarized as well as in unpolarized emission correlate with those of the area of the spot group. While the sunspot area increased by only a factor of 2 between 28 and 30 April, the unpolarized and circularly polarized fluxes increased by factors of 25 and 12, respectively. Such an increase in radio emission flux was probably due to the appearance of new spots within the group, for the degree of source polarization did exhibit a slight dependence on group evolution. The main variations in source polarization, however, stemmed from its directivity [Efanov *et al.* 1973; Moiseev, in press].

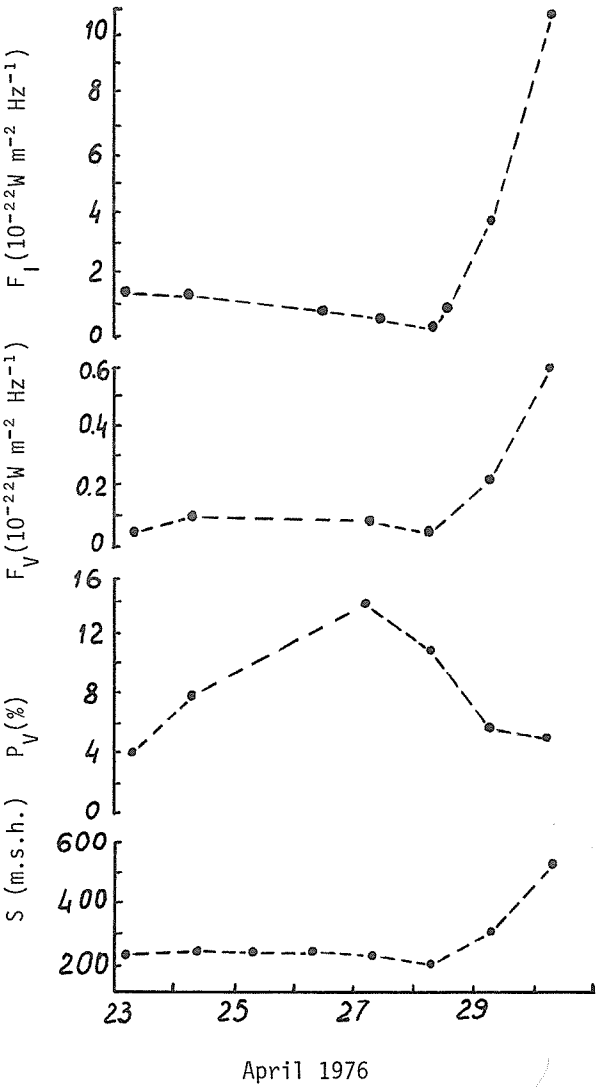

Fig. 1. Time dependence of the unpolarized flux density (F_I), of the circular polarized flux density (F_V), and of the degree of polarization (P_V) of the radio emission source at 1.35 cm associated with McMath Region 14179. The sunspot area (S) in millionths of the hemisphere is also given.

Structure of the source at wavelength 1.35 cm was determined during the solar eclipse on 29 April 1976. This observation method and its attendant data processing techniques have been described by Domnin [in press]. Figure 2 contains a solar radio map obtained shortly before the eclipse, and it includes the trajectory of the Moon's limb center. The isophotes are in units of the quiet Sun antenna temperature.

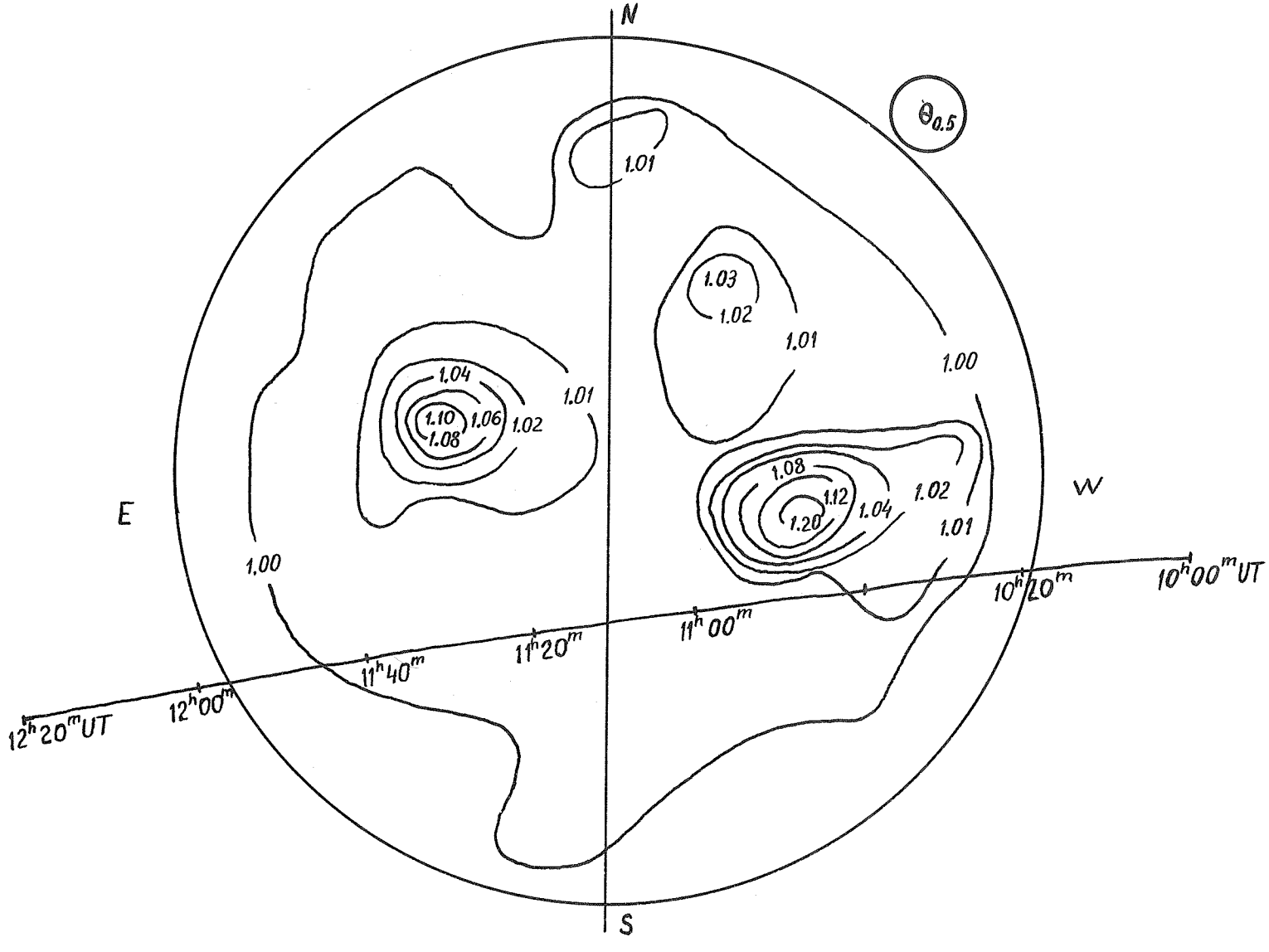

Fig. 2. Radio map of the Sun at 1.35 cm of 0810 UT on 29 April 1976. Isophotes are expressed in units of the quiet Sun antenna temperature. The trajectory of the Moon's limb center is also shown.

By the time of the eclipse, the radio source under study had assumed a S08 W28 position. Figure 3 shows the brightness distribution across the source together with the sunspot group in white light. Plates of the Sun used in the figure were obtained during the eclipse. Intervals of 0.5 - 2 min separated these photographs which were taken through the optical telescope, AFR-2, located near the radio telescope. Spot umbras are shaded, and the polarities and the strengths in hundreds of gauss of their associated magnetic fields are given according to *Solnechnie Dannie*, N. 4 [1976]. Arcs indicate start and end times of the disappearance and reappearance of source details.

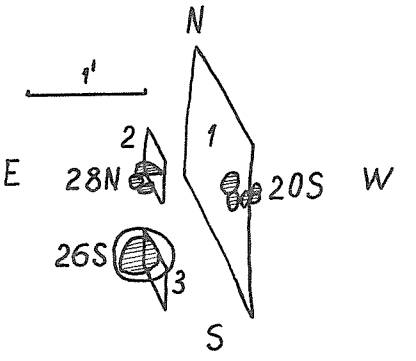

Fig. 3. Positions of source details relative to sunspots in McMath Region 14179. Spot umbras are shaded, and polarities and strengths in hundreds of gauss are indicated for associated magnetic fields.

The source consisted of three components that are numbered 1, 2 and 3 in Figure 3. Their positions and dimensions in polarized and unpolarized emission were about the same; they tended to be displaced with respect to the spot group center; and all three components were left-hand circularly polarized. Component 2's emission should have been right-hand circularly polarized and should have corresponded to the extraordinary wave [Zheleznyakov, 1964] because of its proximity to spots with north polarities. Its left-handed polarization emphasized the complexity of the local magnetic field. During the entire observation period, region 14179's radio source was left-hand circularly polarized.

The dimension, brightness temperature, flux density in polarized and unpolarized emission, and the degree of polarization are listed in Table 2 for each radio component. Each entry represents the mean value of the parameter measured during the occultation and reemergence of the source. Brightness distributions across the components were assumed to be uniform. Comparison of the data given in Tables 1 and 2 for 29 April indicate that nearly all the source emission at 1.35 cm was concentrated in three components: before the eclipse the region's flux density equaled 3.8 x 10^{-22}Wm^{-2}Hz^{-1}; the total flux density from the three components isolated by the eclipse equaled 3.2 x 10^{-22}Wm^{-2}Hz^{-1}; and the diffuse component's emission equaled not more than 20% of the source's total flux density.

Table 2. Component Radio Source Characteristics at 1.35 cm.

Component No.	Dimension (arc seconds)	T_I (10^3 K)	F_I (s.f.u.)	T_V (10^3 K)	F_V (s.f.u.)	P_V (%)
1	32	59	1.75	3.5	0.103	5.9
2	12	314	1.20	10.2	0.043	3.6
3	8	128	0.25	19.2	0.038	15.0
		Total	3.20	Total	0.284	

About 2 days before the proton outburst in McMath Region 14179, the emission of its related radio source began to rise rapidly at wavelength 1.35 cm. This increase was mainly due to the appearance of new spots. At that time the source consisted of three components with dimensions of 8-30 arc seconds. Their brightness temperatures in unpolarized and circularly polarized emission lay in the ranges (60-300)x10^3K and (3-20)x10^3K, respectively. Brightness distributions across the source in polarized emission testified to the region's complex magnetic field configuration.

REFERENCES

DOMNIN, S. L., V. A. EFANOV E. S. KORSENSKAYA, V. A. KORSENSKY I. G. MOISEEV, N. S. NESTEROV, and I. D. STREPKA — The System of Recording and Processing of Radio Astronomical Data in Real Time, *Izvestiya Krimskoy Astroph. Obs., 57,* in press.

DOMIN, S. L., V. A. EFANOV, V. A. KORSENSKY, I. G. MOISEEV, and N. S. NESTEROV — Structure of a Local Source on the Sun Obtained From the Eclipse Observations With the 22-meter Radio Telescope in the Integral and Polarized Light at 1.35 cm, *Izvestiya Krimskoy Astroph. Obs., 58*, in press.

EFANOV, V. A. and I. G. MOISEEV — 1971 — Observations of the Solar Radio Emission at 8, 13 and 16 mm, *Izvestiya Krimskoy Astroph. Obs., 43,* 21.

EFANOV, V. A. and I. G. MEISEEV — 1973 — On the Circular Polarized Emission Over the Bipolar Group of Sunspots at 8 mm Wavelength, *Izvestiya Krimskoy Astroph. Obs., 47,* 58.

MOISEEV, I. G. — On the Circular Polarized Emission Over the Bipolar Groups of Sunspots at 1.35 cm, *Izvestiya Krimskoy Astroph. Obs., 56*, in press.

ZHELEZNYAKOV, V. V. — 1964 — *Radio Emission of the Sun and Planets,* "Nauka", Moscow.

1976 — *Solnechnie Dannie,* N 4.

Type II Radio Bursts of 20 March 1976 Originating From Well Behind the Solar Limb

by

G. J. Nelson and D. J. McLean
Division of Radiophysics
CSIRO
Sydney, Australia

Introduction

On 20 March 1976 the Culgoora radioheliograph [Wild, 1967; Sheridan *et al.*, 1973] and radio spectrograph [Sheridan, 1967] recorded two Type II bursts above the Sun's east limb. These events occurred at 0203 and 2255 UT; the first event has already been discussed by McLean and Nelson [1977]. No H-alpha activity was visible near the east limb until about 4 days later when McMath Region 14143 rotated into view. Since there is little doubt that this region was the source of the bursts on 20 March, these events were caused by flares located about 55° and 44° behind the limb, respectively. Events of this type have been observed before [e.g., Smerd, 1970], but not from such great distances behind the limb.

The Type II Burst at 0203 UT on 20 March 1976

The dynamic spectrum of this burst is shown in the upper half of Figure 1. Important features to note include the following:

(a) The three main emission bands in the Type II burst. With the possible exception of some small features near 0216 UT, these emission bands are not harmonically related.

(b) During the first 5 min of the burst, the emission cuts off abruptly at low frequencies. The cutoff frequency drifts to lower frequencies much more rapidly than do the individual bands.

(c) The irregularity of the burst (a feature common among Type II limb events).

(d) The initial Type III bursts at 80 MHz (e.g. at 0203:38 and 0203:42 UT). These appear stunted compared to normal Type III bursts. Presumably they also come from 55° behind the limb.

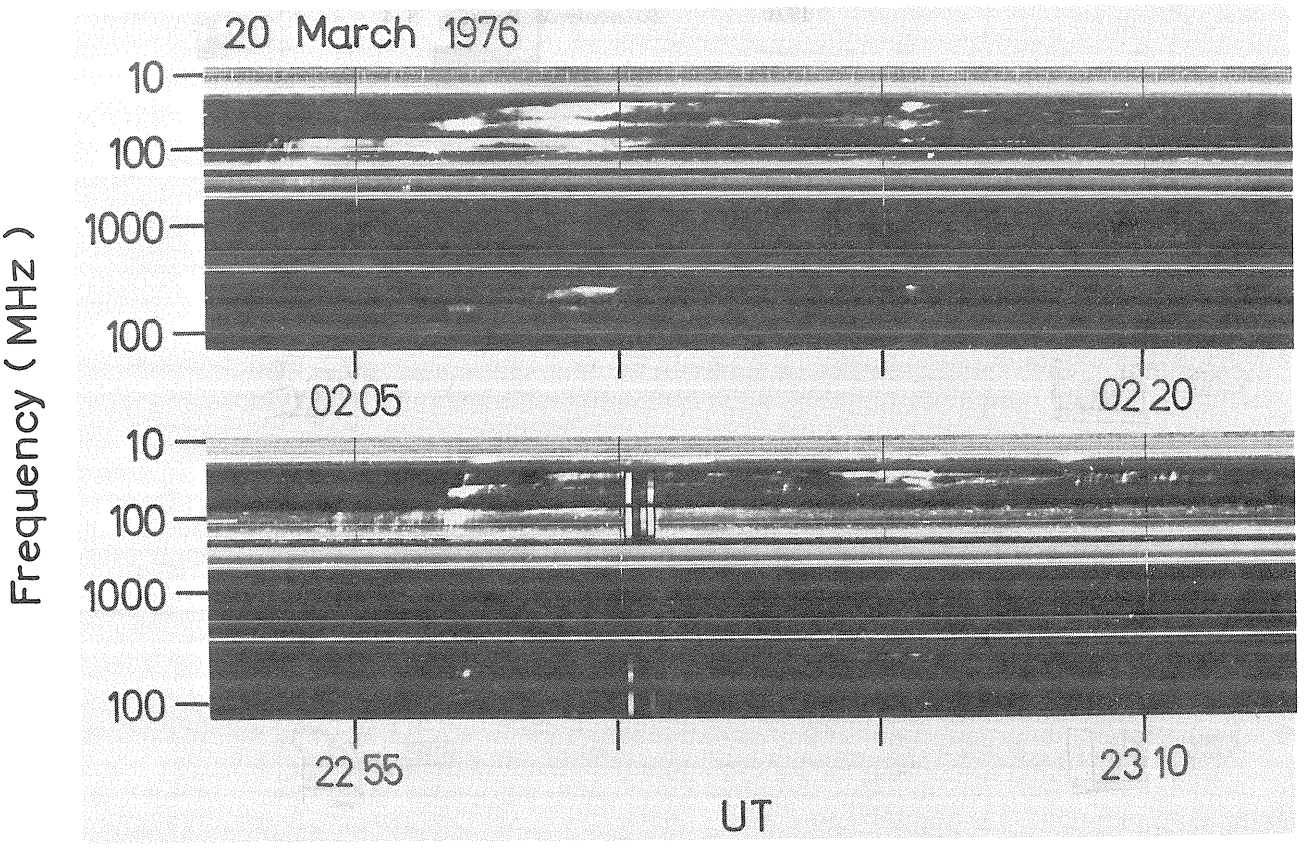

Fig. 1. Dynamic spectra of the two Type II bursts recorded 20 March 1976. For each frequency and time the intensity is shown by the whiteness of the record. Horizontal straight lines are due to interference. Below each spectrum the range from 25 to 200 MHz is repeated at lower sensitivity.

Figure 2 gives the radial positions of the Type II and Type III bursts at 80 and 43 MHz and of an unrelated noise storm at 160 MHz. The Type II sources (particularly at 43 MHz), after moving slightly outward, thereafter move inward. This implies that the intersection of the shock front with the relevant plasma level moves from slightly behind the limb to possibly 40° in front of the limb [McLean and Nelson, 1977].

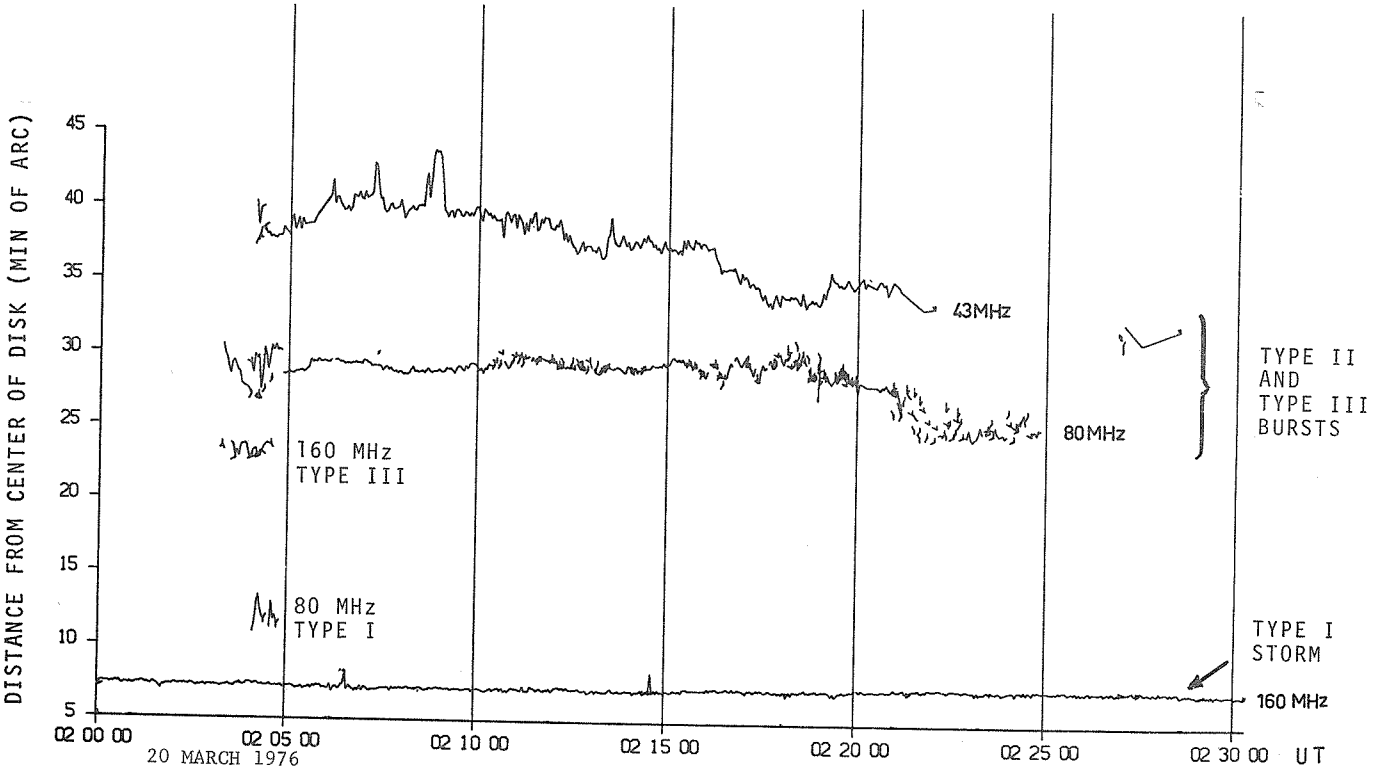

Fig. 2. A plot showing the distances of the centroids of the different souces from the center of the solar disk as a function of time.

The centroids of all the observed sources are plotted in Figure 3. For Type II bursts behind and at the limb emission at the second harmonic of the plasma frequency is expected because fundamental emission is severely attenuated [Riddle, private communication quoted by Dulk *et al.*, 1976]. The highest Type II sources at 43 and 80 MHz in Figure 3 would therefore originate above the limb at the 21.5 and 40 MHz plasma levels, respectively. Refraction and scattering, however, cause harmonic sources to appear nearer the Sun than their true positions. Thus, the observed heights of 2.5 and 1.85$R_\odot$ are lower limits to the real heights of the 21.5 and 40 MHz plasma levels, respectively. If the emission were fundamental, the sources would appear further out than their true positions, and the observed source heights would then be lower limits to the 43 and 80 MHz plasma levels.

Although they are not shown separately in Figures 2 and 3, the Type III bursts at the beginning of the event are observed at 80 MHz in positions scattered among the Type II burst positions. Generally the Type III electrons travel along magnetic field lines, and in this case the Type II shock waves are also guided along the magnetic field. This agrees with observations of the 30 March 1969 "behind the limb" event [Dulk *et al.*, 1971] in which the shock waves traveled along coronal field lines deduced from observed photospheric fields.

Note the large transverse extent of the shock front at 80 MHz and the apparently much smaller extent at 43 MHz. This is illustrated further in Figure 4 which shows typical individual sources at each frequency. This observation suggests that the lateral extent of the particular shock front producing this Type II burst decreases with height. However, while the transverse source size decreases with height, the radial size increases as in previous observations [Nelson and Robinson, 1975]. This probably occurs because the scattering from irregularities in the corona increases as the frequency decreases. The sources typically cover a range of heights corresponding to a 2:1 range in plasma frequency.

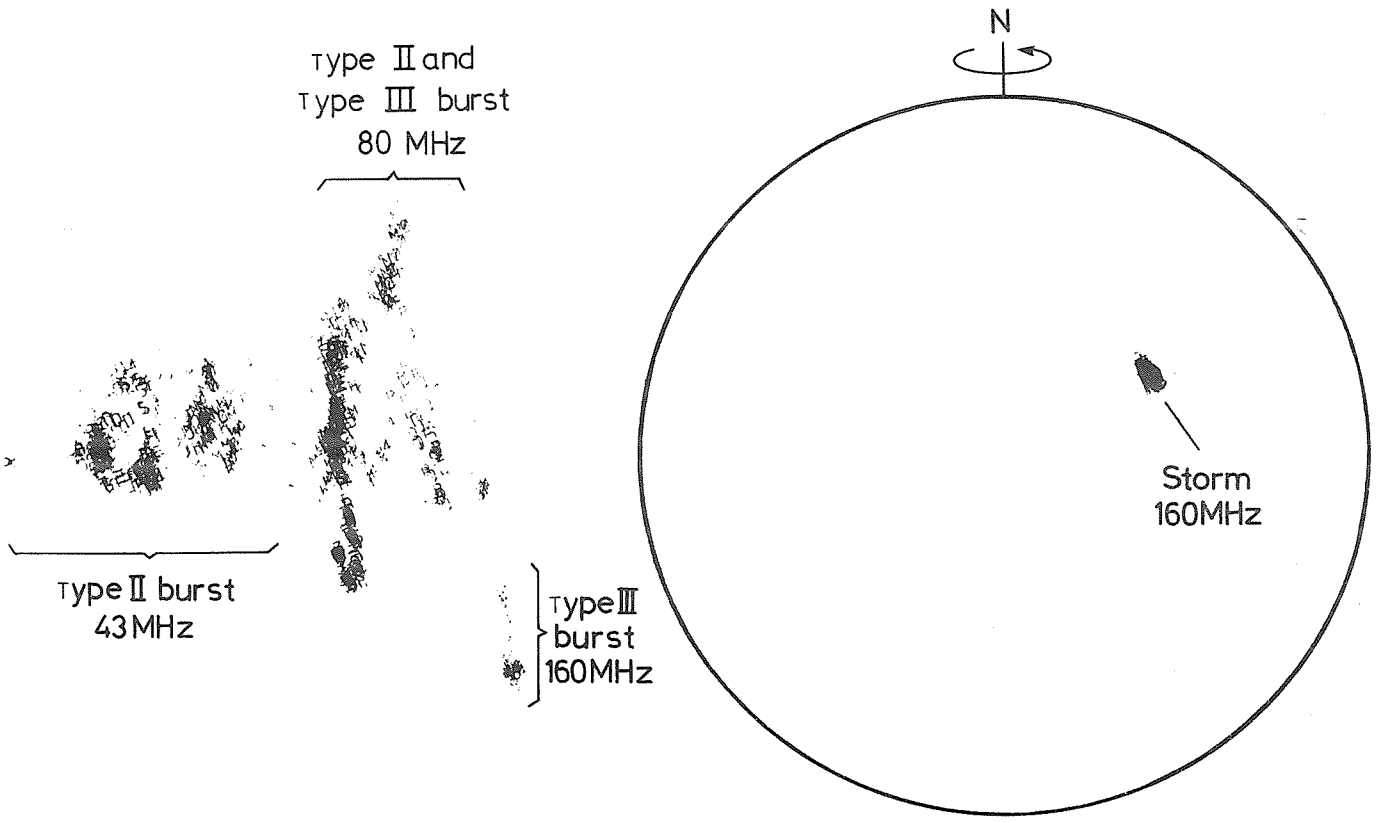

Fig. 3. Map of centroid positions observed with the Culgoora radioheliograph from 0200 to 0230 UT on 20 March 1976. On this figure the position of the centroid of each source observed during a half-hour period is marked by a small symbol. The individual symbols cannot be distinguished, but the superposition of many symbols marks clearly the positions of the important sources.

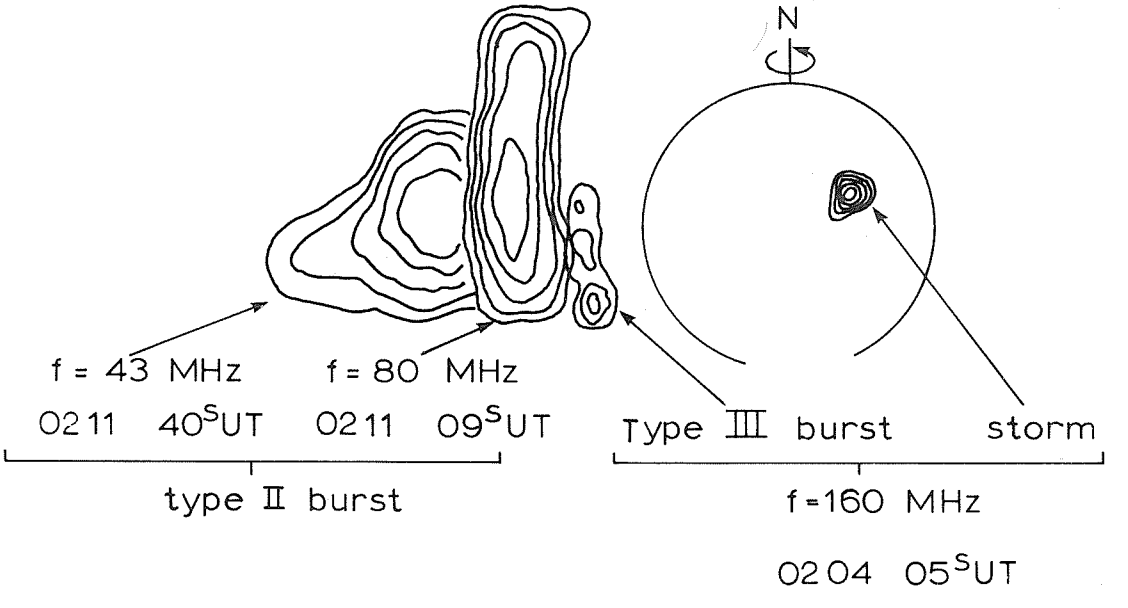

Fig. 4. Composite contour diagram showing typical sizes and positions of sources observed at the three observing frequencies of the Culgoora radioheliograph during the first Type II event on 20 March 1976.

Figure 5 shows two possible models of the shock paths which may explain the observations. The first of these assumes rectilinear outward paths for the disturbances and explains the source positions but not the slow drift rates of the individual Type II bands and the fast drift rate of the low-frequency cutoff at the start of the burst. To explain these as well, the second model with curved propagation paths is required. Thus, the shock wave was refracted along a curved path, as in the 30 March 1969 event described by Smerd [1970].

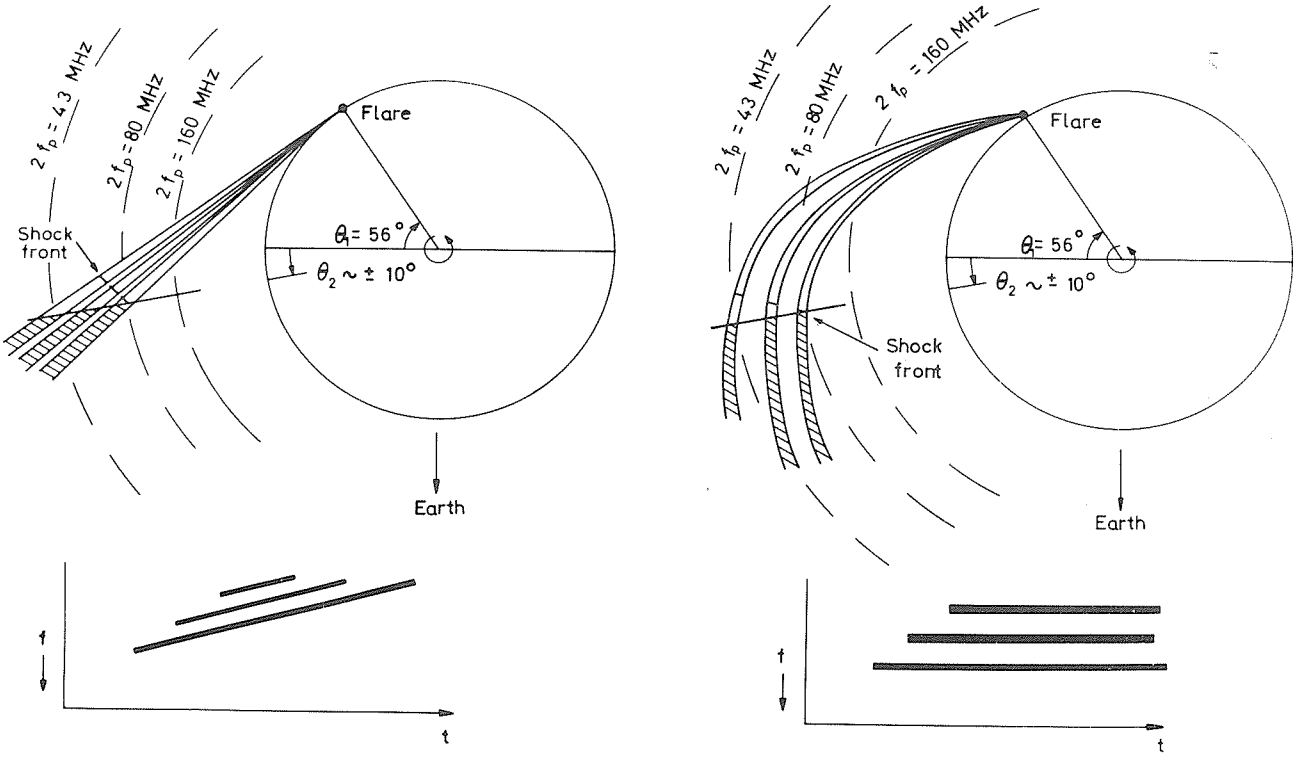

Fig. 5. Two stages in the development of a model to explain the low-frequency cutoff observed in the spectrum of the Type II shown at the top of Figure 1. At left a shock front, broken into about three fragments, propagates away from the flare along straight paths. Due to scattering and refraction, only part of the shock front's path is visible from Earth-that portion beyond some surface near the front limb (cross-hatching in figure). The dynamic spectrum of the Type II burst predicted by this model is indicated below the diagram. At right we assume that the shock disturbance traveled along curved paths, as in the 30 March 1969 event. The predicted spectrum is in better agreement with the observations.

The Type II Burst at 2255 UT on 20 March 1976

The spectrum of this Type II burst, which is shown in the lower half of Figure 1, is somewhat similar to the earlier event. The structure is very irregular with little evidence of related harmonic bands. There is some suggestion of a steeply-sloped, low-frequency cutoff early in the burst. A very interesting feature is the reverse slope of one of the Type II bands just after 2305 UT is probably caused by downward refraction of the shock wave.

Figure 6 shows the radial positions of all observed sources. The close-in sources at 80 and 160 MHz are from an unrelated Type I storm. The Type II source positions initially decrease in height, then rise and later fall again. The two falls are possibly caused by two successive shock fronts each in turn intersecting the 40 and 21.5 MHz plasma levels forward of the limb. The rise in between is due to the second shock front approaching the limb from behind and again emitting at the relevant plasma levels as it moves.

The spread in transverse source positions shown in Figure 7 again indicates a large extent for the shock wave at the 40 MHz plasma level (80 MHz harmonic emission) and a smaller but still quite large extent at the 21.5 MHz level as well. The sources appear slightly lower than in the previous event (1.83 and 2.27$R_\odot$ at 40 and 21.5 MHz, respectively). As was the case for the previous event, the Type II and Type III positions are indistinguishable. This again suggests that the Type II shock waves propagated along magnetic field lines.

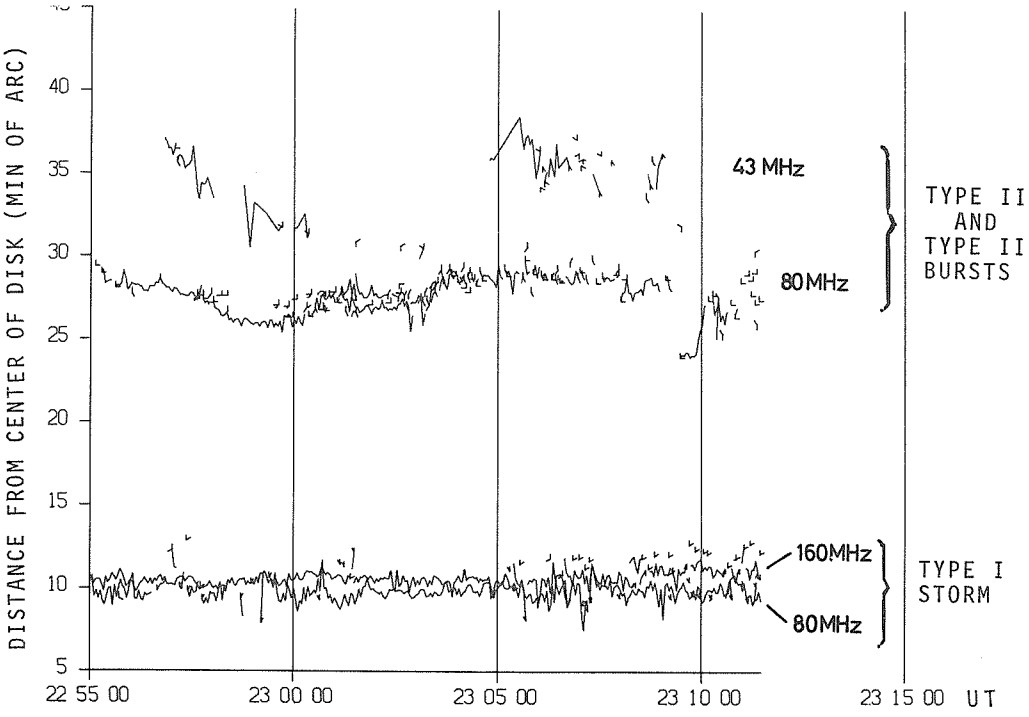

Fig. 6. A plot showing the distances of the centroids of the different sources from the center of the solar disk as a function of time on 20 March 1976.

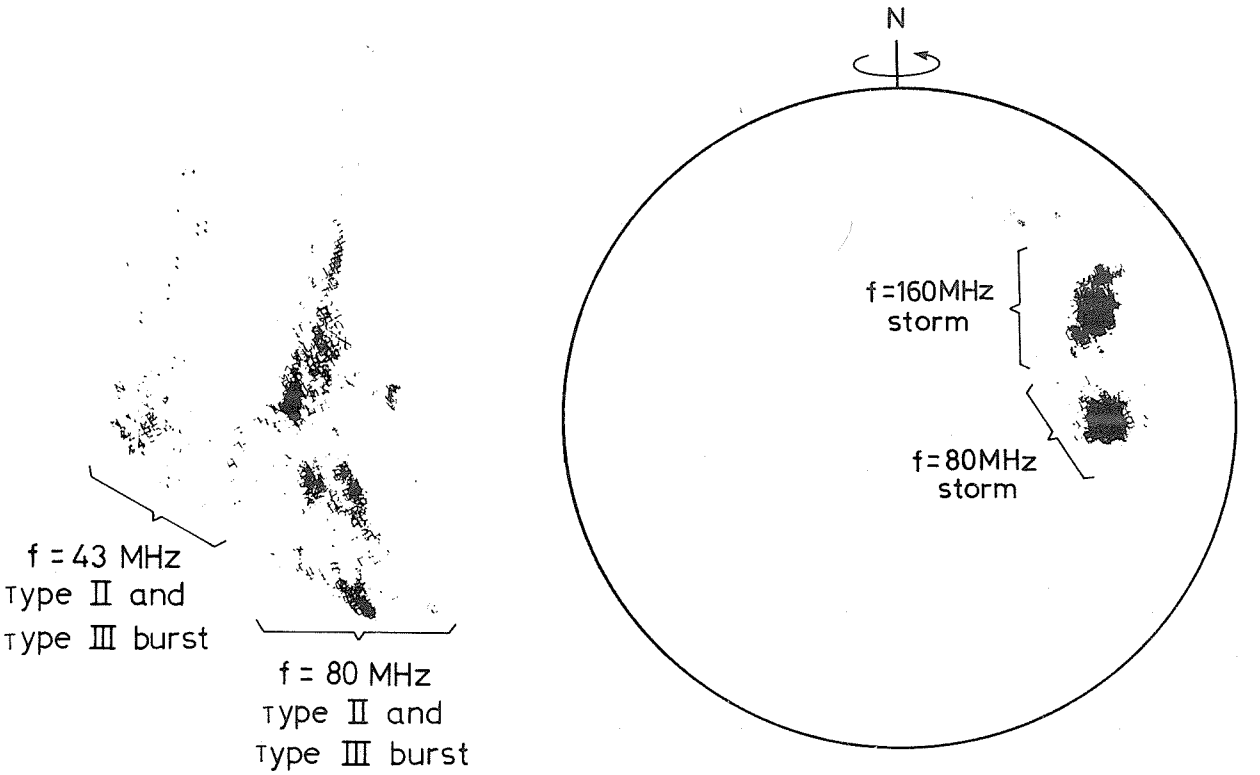

Fig. 7. Map of centroid positions (corrected for ionospheric refraction) observed with the Culgoora radioheliograph from 2255 to 2311 UT on 20 March 1976. On this figure the position of the centroid of each source observed during a half-hour period is marked by a small symbol. The individual symbols cannot be distinguished, but the superposition of many symbols marks clearly the positions of the important sources.

Typical countours for the different sources are shown in Figure 8. Of particular interest is the very large radial size of the 43 MHz source, which extends over heights corresponding to well over an octave range of plasma frequency.

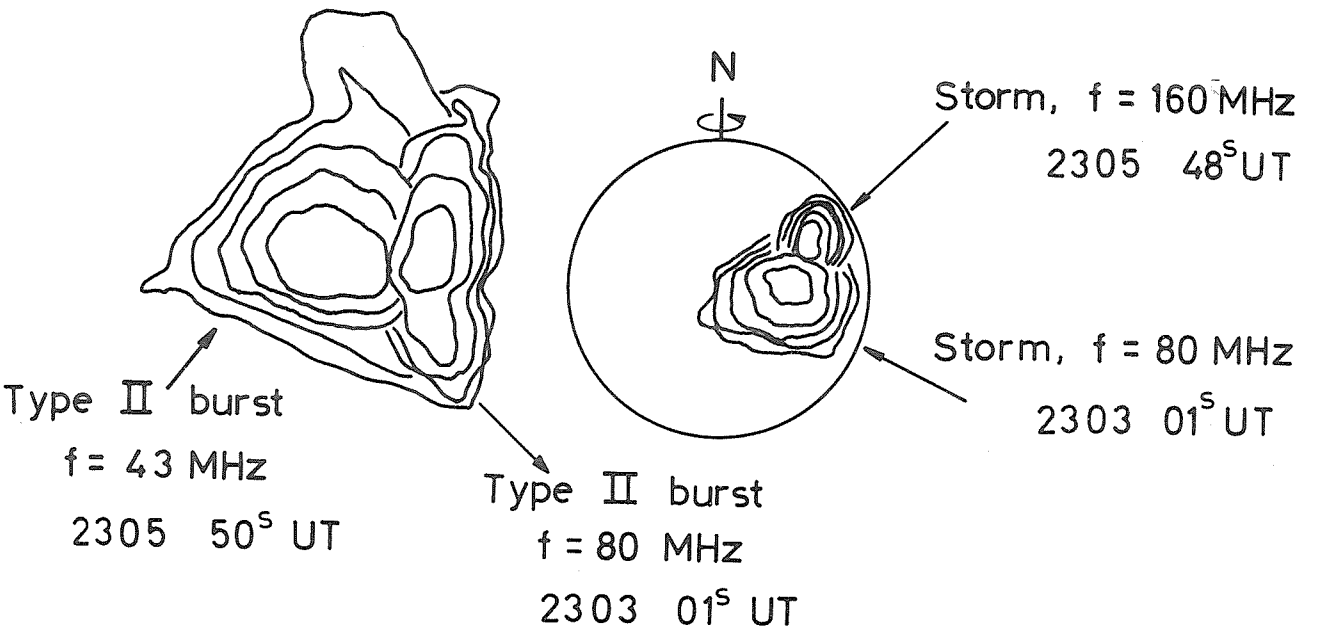

Fig. 8. Composite contour diagram showing typical sizes and positions of sources observed at the three observing frequencies of the Culgoora radioheliograph during the second Type II event on 20 March 1976.

Summary

Observations have been made of two Type II radio bursts originating from well behind the solar limb. The results support the previous conclusions that Type-II-producing shock waves can be refracted along curved paths and can move along magnetic field lines. An interesting new observation is that although the radial source size increases with height, its transverse dimension may decrease. The latter is ascribed to a decrease in lateral extent of the shock wave with height; the former to increased scattering from coronal irregularities at greater heights (lower frequencies). The 40 and 21.5 MHz plasma levels were at heights of at least 1.85 and 2.4$R_\odot$, respectively.

REFERENCES

DULK, G. A., M. D. ALTSCHULER, and S. F. SMERD — 1971 — *Astrophys. Lett.*, *8*, 235.

DULK, G. A., S. F. SMERD, R. M. McQUEEN, J. T. GOSLING, A. MAGUN, R. T. STEWART, K. V. SHERIDAN, R. D. ROBINSON, and S. JACQUES — 1976 — White Light and Radio Studies of the Coronal Transient of 14-15 September 1973. I. Material Motions and Magnetic Field, *Solar Phys.*, to be published.

McLEAN, D. J. and G. J. NELSON — 1977 — Recent Data on Type II Radio Bursts, *IVUZ Radiofizika.*, to be published.

NELSON, G. J. and R. D. ROBINSON	1975	*Proc. Astron. Soc. Aust.*, *2*, 370.
SHERIDAN, K. V.	1967	*Proc. Astron. Soc. Aust.*, *1*, 58.
SHERIDAN, K. V., N. R. LABRUM, and W. J. PAYTEN	1973	*Nature*, *238*, 115.
SMERD, S. F.	1970	*Proc. Astron. Soc. Aust.*, *1*, 305.
WILD, J. P. (Ed.)	1967	The Culgoora Radioheliograph, *Proc. IREE Aust.*, *28*, No. 9.

Solar Radio Burst of Spectral Type II Recorded at Fort Davis, Texas, During the Period 20 March - 2 May 1976

by

Alan Maxwell
Harvard Radio Astronomy Station
Fort Davis, Texas 79734

Observing hours at the Harvard Radio Astronomy Station, Fort Davis, Texas during the period March through May 1976, were from 1315 - 2345 UT. At this time the station was operating four sweep-frequency receivers covering the band 25 to 580 MHz. Summaries of the spectral characteristics of solar radio bursts recorded during the period under consideration have been published in *Solar-Geophysical Data*. This report provides more detailed information on four Type II bursts recorded over that period.

Figure 1 shows a solar radio outburst that commenced on 28 March 1976 at 1919 UT. The outburst begins with a sequence of Type III bursts which are followed by a somewhat confused Type II burst that commences at 1921. (Some stations reported this latter burst as having characteristics mainly of Type IV emission).

Figure 2, for 5 April 1976, shows a Type II burst beginning at 2158 UT. The burst is faint, but emission at the fundamental and second harmonic are clearly visible.

Figure 3, for 20 April 1976, shows a Type II burst commencing at approximately 1803 UT.

Figure 4, for 30 April 1976, shows Type III bursts commencing at 2103 UT. Type II emission seems to commence at 2107 with evidence of emission at a fundamental of 50 MHz and a second harmonic at 100 MHz. There is also some evidence of "herringbone" bursts. The Type IV emission that begins at 580 MHz at 2103 seems to have an envelope which connects in a general way with the Type II burst that is first seen at frequencies of about 100 MHz at 2107. Thus, the Type IV emission might be interpreted in terms of radiation from a "piston" pushing the shock that gave rise to the type II emission in the meter band.

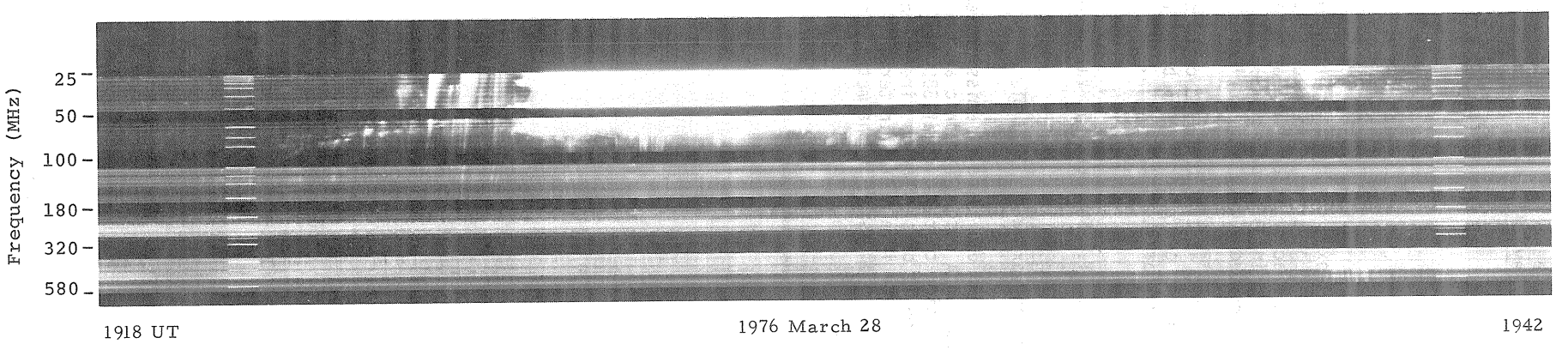

Fig. 1. Solar radio spectral record between 1918 and 1942 UT on 28 March 1976.

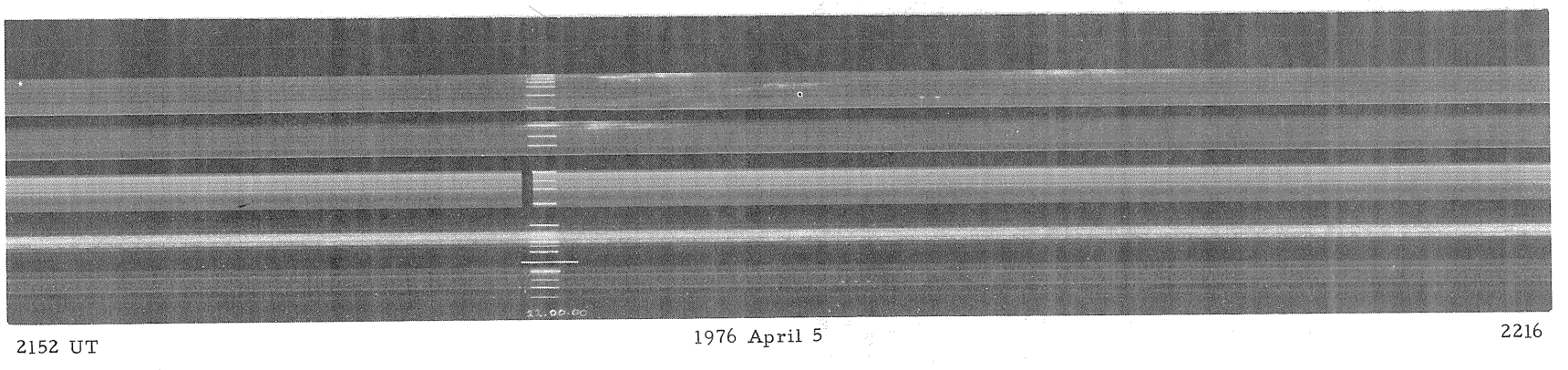

Fig. 2. Solar radio spectral record between 2152 and 2216 UT on 5 April 1976.

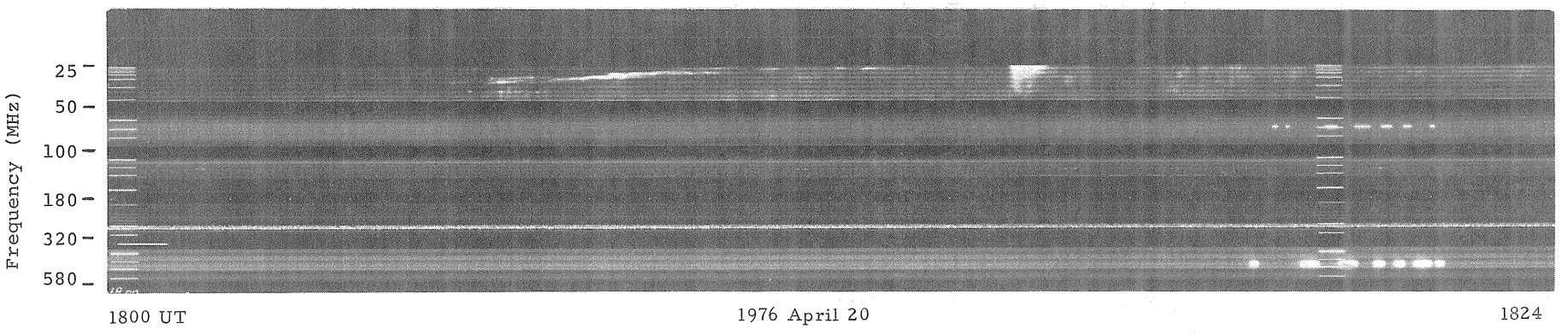

Fig. 3. Solar radio spectral record between 1800 and 1824 UT on 20 April 1976.

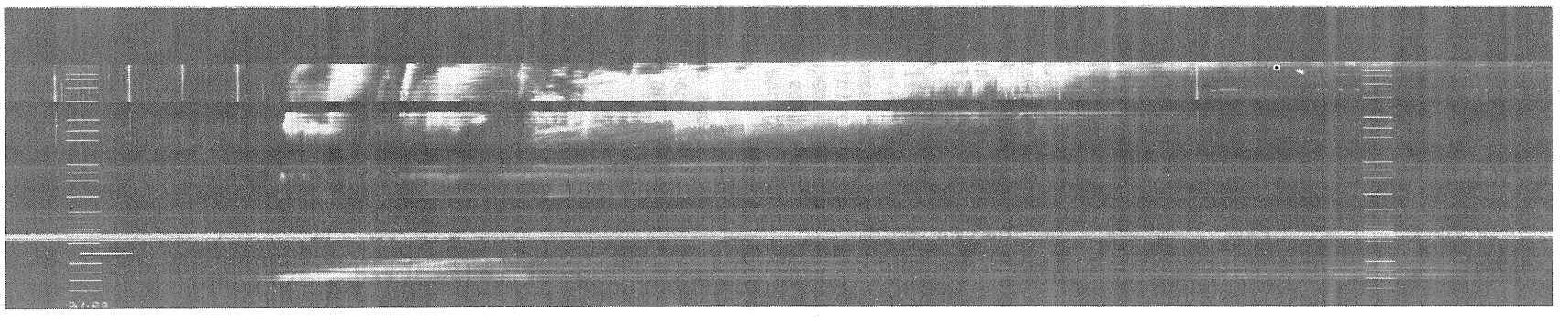

Fig. 4. Solar radio spectral record between 2059 and 2123 UT on 30 April 1976.

The Type III Burst Activity at the End of March 1976

by

H. W. Urbarz
Astronomical Institute of Tübingen University
Weissenau Station, 7980 Rasthalde, GFR

From 25 March to 1 April 1976 the Type III burst activity increased considerably as shown by "Spectral Observations of Solar Radio Emission," *Solar-Geophysical Data* (*SGD*). From these data a revised list was extracted to avoid multiple reporting of the same events by several observatories. Based upon a number of criteria not mentioned here, classes of events were distinguished but counted as one: (1) III = IIIb, (2) IIIg, (3) IIIGG, and (4) IIIG + x, IIIGG + x, where x = V, DP, RS, U. Type IIS,N bursts were not considered because of their similarity to radio noise storms.

Figure 2 shows a plot of the number of events per hour vs time and the number of events per 12 hours vs time for the period of time in question. On the average there are two events per hour separated by random intervals. The rate per hour shows three double maxima whose distinct peaks are separated by 2, 1, and 6 hours, respectively, while the intervals between the double-maxima groupings are 24 and 48 hours, respectively. From the rate-per-12-hours plot an increase is found on 26, 27, and 29 March. There is a total of 209 events, 43 of which are associated with flares (standardized *Solar-Geophysical Data*). It is remarkable that 40 of the events stemmed from the same region, McMath No. 14143. Since at that time there were only two other small regions on the disk, the majority of the other events may be assumed to have originated within region 14143. McMath Region 14143's Type III burst activity correlates with the group's increase in plage area, spot area, and spot number (*SGD*). Moreover, before 29 March a decrease in these three parameters occurred; after 29 March the rate rose again.

According to Figure 2 the Type III burst activity occurred within a short time interval compared with the lifetime of the region. In most of the Type III active regions of 1970 - 1971 earlier investigations found that the event rate peaked within 1 or 2 days. Region 14143's events were observed between 57° and 18° east of the central meridian -- a time during which the spot group bore the magnetically complex δ configuration. The time sequence of the energy releases, called the flare-burst pattern, indicates directly when instabilities extending to coronal heights take place in the magnetic structure. The physical mechanisms generating one event of the burst sequence should be investigated in context with the physics of the whole pattern.

The histogram of Figure 1 shows a predominance of Type IIIG events (over 50%). Dynamic spectra of the burst groups recorded at Weissenau show very high fluxes, and spectral observation data also give intensities of 2 or 3 for most of the events.

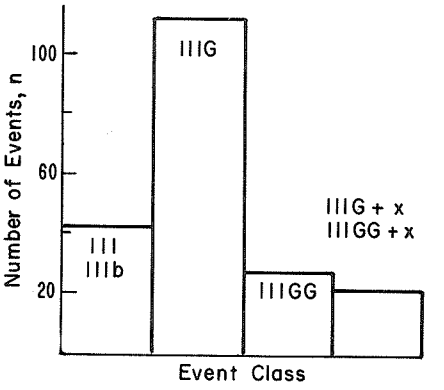

Fig. 1. Frequency of occurrence of Type III event classes.

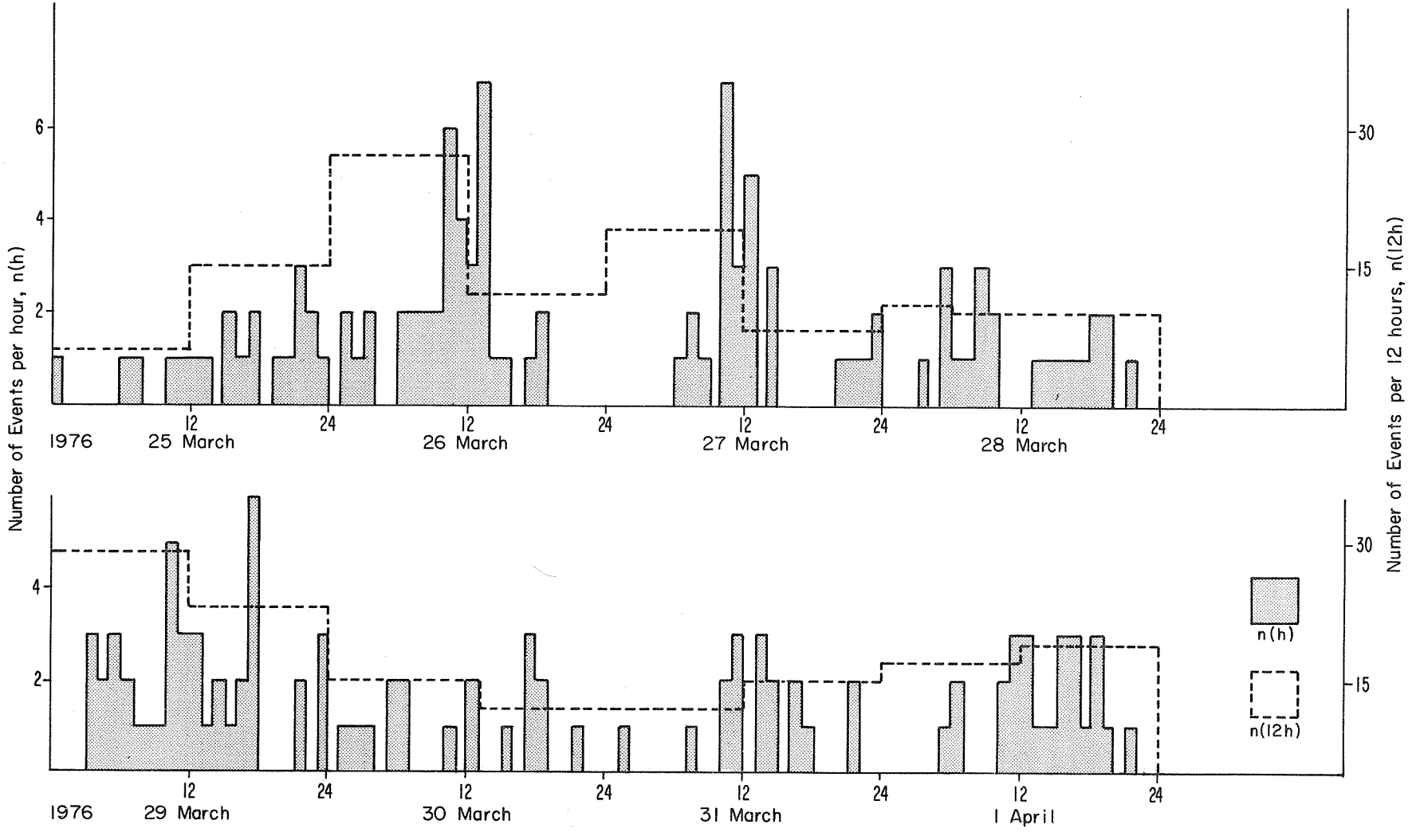

Fig. 2. The shaded histogram depicts the number of Type III events recorded per hour and should be read with scale at left; the dashed line outlines the event frequency per 12 hours and should be read with scale at right.

The Type III/IV Compound Burst of 30 April 1976

by

H. W. Urbarz
Astronomical Institute of Tübingen University
Weissenau Station, 7980 Rasthalde, Ravensburg, GFR

The active region McMath No. 14179 produced a number of flares and bursts during its third rotation. When the magnetic configuration changed from αf on 30 April to δ on 1 May, three large flare-burst events occurred, including a proton event which occurred most likely on 30 April at 2047 UT. This report, however, briefly summarizes only the 1242 UT event as recorded at Weissenau.

Figure 1 shows a Type IIIGG from 500 to 30 MHz and a continuum-like feature from 1000 to 300 MHz. In channels 1 and 6, however, the event appears too weak on film due to misadjustments in the display device. In channel 5 the Type IV continuum, which shows some grained structure, overlaps the start frequencies of the Type III bursts. The latter also show strong flux variations toward lower frequencies.

The spectrum plotted in Figure 2 from absolute fluxes (*Solar-Geophysical Data*, Outstanding Occurrences) shows two maxima. By comparison with the film event one may distinguish between the Type III and Type IV portions of the spectrum. The former shows large scatter of the flux in both maxima as expected from the discontinuous Type III features on film. The Type IV spectrum at the higher frequencies may be identified as the maximum and the high-frequency slope of synchrotron emissivity curves, while toward lower frequencies a cutoff below 500 MHz is implied - a result in agreement with Figure 1.

Events very similar in their time and frequency structure to the compound burst described above have been recorded at Weissenau Station. They include one at 0822 UT on 3 Mar 1969; the second part of an event on 17 Sept 1969; the first half of events at 0936 and 1530 UT on 1 Mar 1970; and an event on 11 Dec 1970.

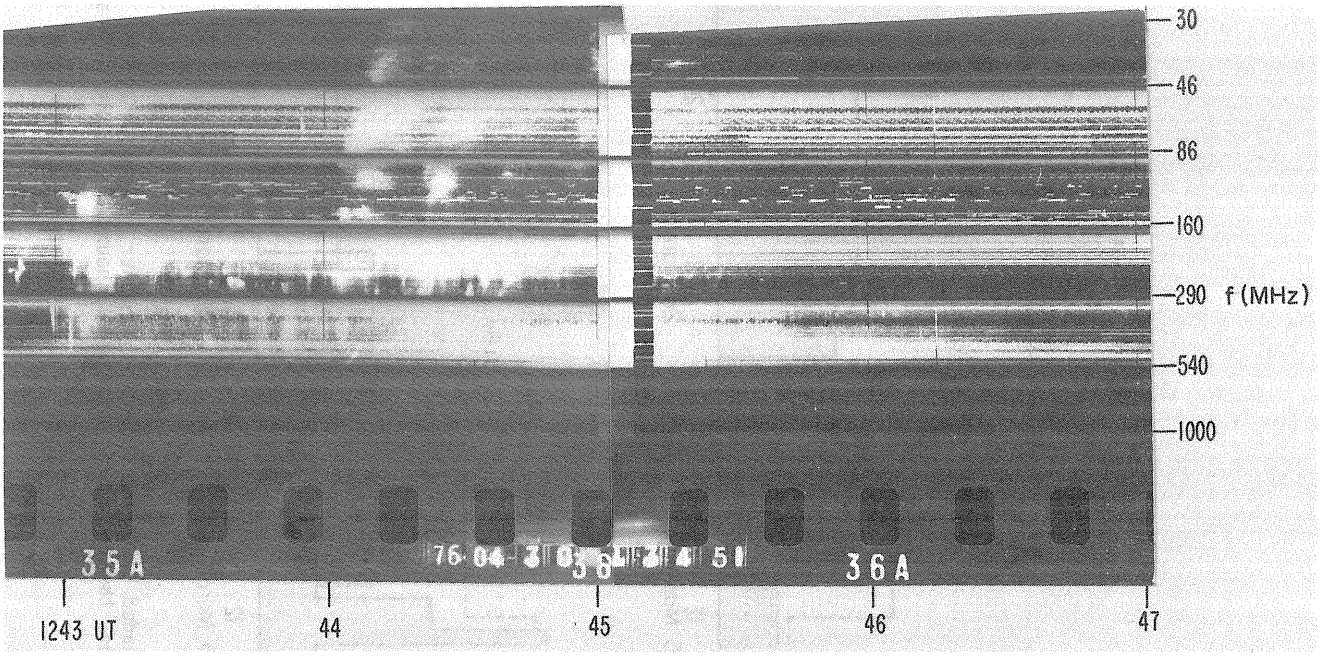

Fig. 1. Six-channel dynamic spectrum of Type III/IV compound burst at 1242 UT on 30 April 1976.

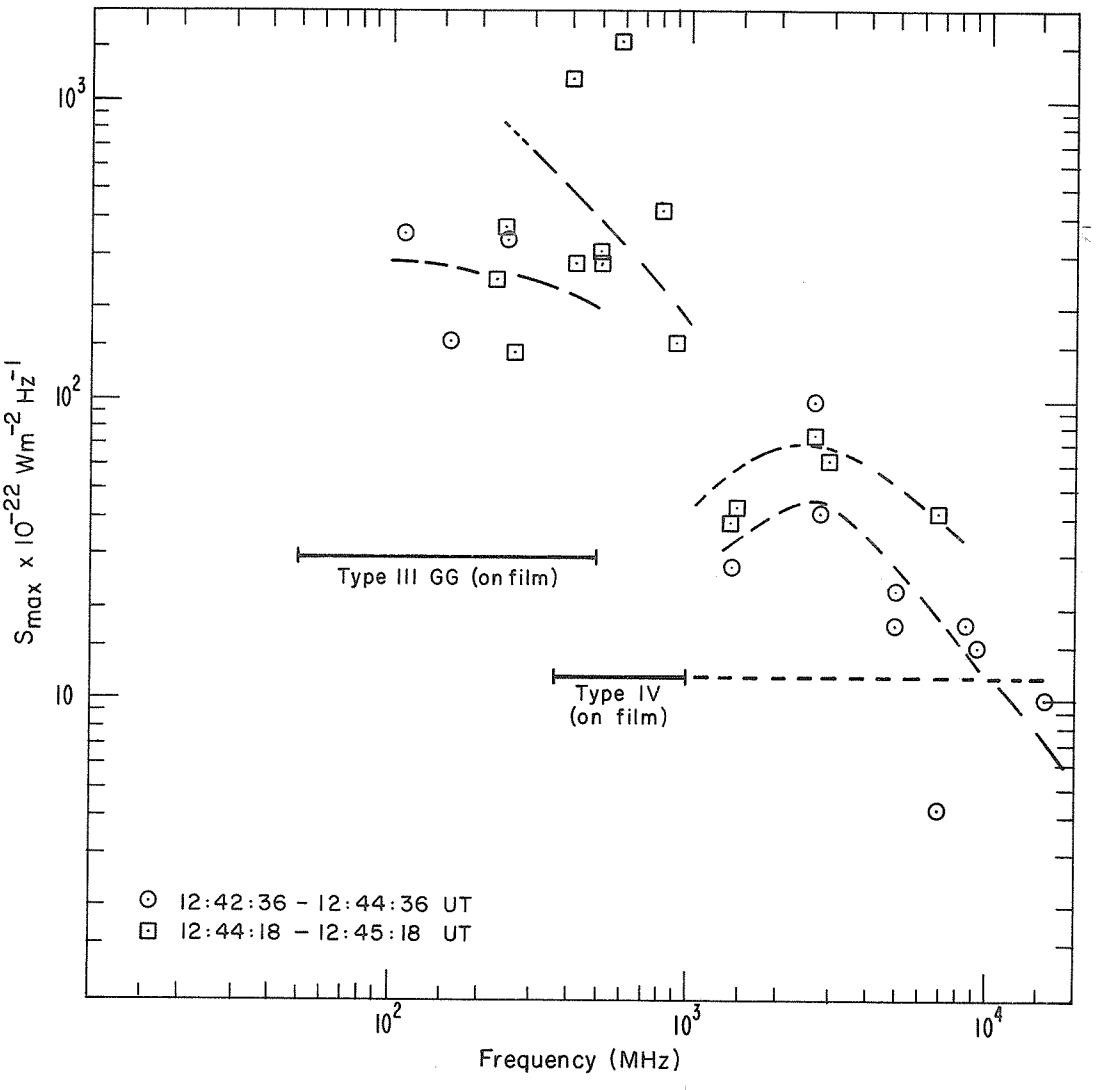

Fig. 2. Absolute flux spectrum of the Type III/IV compound burst at 1242 on 30 April 1976.

Metric Radio Continuum Activity During 11 March to 10 May 1976

by

Kunitomo Sakurai
Institute of Physics
Kanagawa University, Rokkakubashi
Yokohama 221, Japan

During the period from 16 March to 2 April 1976, the activity on the metric radio continuum observed at 200 MHz increased twice as shown in Figure 1. These increases seemed to be related to the passage of two active sunspot groups across the solar disk: McMath Regions 14127 and 14143. The increased level of these continuum activities is of the same order as that observed in early August 1972, during which time a large sunspot group produced four proton flares as it traversed the solar disk [Sakurai, 1973].

After 5 April 1976, the 200 MHz metric continuum activity declined to a flux intensity closely approaching the background level usually observed during quiet periods. This activity never increased again to the level observed between 16 March and 2 April, indicating that the active coronal regions which produced the continuum increase during the above period disappeared during their passage over the invisible disk.

Although these active regions never recurred, it seems very useful to investigate the growth of radio continuum sources in the solar corona [Sakurai, 1976].

I wish to thank Mr. Fujio Yamashita of the Hiraiso Branch, Radio Research Laboratories for supplying the radio records.

REFERENCES

SAKURAI, K. 1973 Metric Radio Continuum Activity Associated with the Active Region McMath No. 11976 in August 1972, *in Rep. UAG-28, Part I*, p. 227, World Data Center A for Solar-Terrestrial Physics, NOAA, Boulder, Colorado.

SAKURAI, K. 1976 Solar Radio Continuum Storms, *Astrophys. Space Sci.*, *42*, 349.

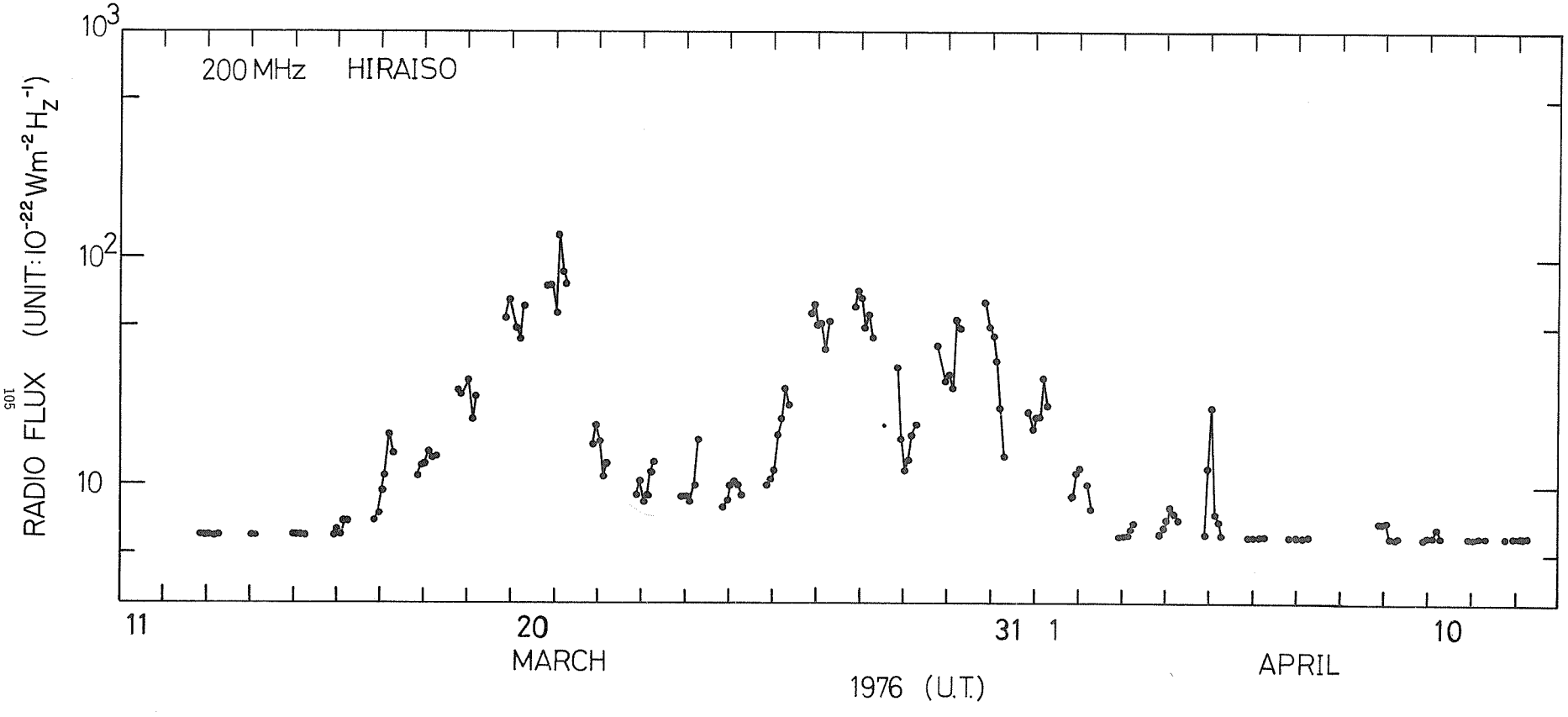

Fig. 1. Metric continuum activity at 200 MHz from 11 March to 12 April 1976.

The Fine Structure of Meter Radio Emission Associated With McMath Active Region 14143

by

L. M. Bakunin, G. P. Chernov, I. M. Chertok
Solar Radio Laboratory IZMIRAN
Moscow, U.S.S.R.

This report describes the fine structure of several types of meter solar radio bursts observed at IZMIRAN in the period from 25 March to 2 April 1976. The Type III bursts were recorded with a spectrograph in the range 45-90 MHz and with a polarimeter at 74 MHz [Amiantov *et al.*, 1970]. The observations of the noise storm were made with our high time resolution spectrograph in the range 180-236 MHz. The latter works on the principle of the magnetic variometer in the swept-frequency heterodyne. The time and frequency resolution of this spectrograph is equal to 0.02 s and 0.25 MHz, respectively. In combination with a 10-meter diameter parabolic antenna, the instrument has a sensitivity of about one quiet Sun level. The working regime of the spectrograph was changed depending on radio and TV interference.

Noise Storm

25 - 26 March. The noise storm associated with McMath active region 14143 started before 24 March. On 25 March the more frequent Type I bursts occurred followed by complex groups and chains of Type I emission the next day. Both the single bursts and the compound groups and chains, however, were devoid of fine structure. The intensity of burst and continuum components of the noise storm began increasing as the active region approached the central meridian.

27 March. On this day the radio spectrograph operated from 0847 to 1141 UT. A further development of the noise storm took place. The number and intensity of Type I bursts at frequencies below 200 MHz increased, and simultaneously weak drifting bursts with a fine structure at frequencies above 220 MHz appeared. Often for 5 - 10 min no bursts at intermediate frequencies occurred. Figures 1a and 1b illustrate this effect most clearly within the periods 0855-0935, 0950-1000, 1011-1027 UT, etc. When the variations of the noise storm intensity over time scales of the order of minutes are considered, these gaps ought to be taken into account.

Fine structure, taking the form of Type I bursts with short lifetimes and various frequency drifts, appeared at the high frequency edge of the spectrograph's range. A weak, miniature U-burst at 0952:23 UT is shown in Figure 1a. (In this and in following figures the bursts mentioned in the text are marked by arrows.) Spike-bursts with durations about or shorter than 0.05 s were observed together with drifting Type I bursts beginning from 0953 UT (see Figure 1b). In Figure 1c unusual short duration bursts are illustrated: the one at 1049:49 may be considered a low frequency extension of a rapidly drifting decimeter burst; the event at 1125:30 UT appears to be the low frequency part of a miniature Type III burst.

28 March. The McMath active region 14143 approached within 30° of the central meridian. The number of spike-bursts increased perhaps because of the strong directivity of the emission. Sometimes spike-bursts compose the fine structure in Type I bursts, as in the right spectrum of Figure 2c. Here the second Type I burst in this chain consists of a number of small elements (spike-bursts). The solar origin of Type I burst fine structure has been confirmed by observations from distant observatories and by polarization data obtained with another receiver [Chernov, 1974; 1976].

The left spectrum in Figure 2c contains a spike-burst with an unusual V-like form over the frequency range 206-214 MHz. The duration of each branch of the burst does not exceed about 0.06 s.

In the noise storm under consideration the emission terminates in a sharp, high frequency cutoff boundary. This phenomenon is rather rare. In Figure 2b one can see that the boundary displays a negative frequency drift of about 0.2 MHz/s.

An intensification of the continuum starting at approximately 0930 UT marked another peculiarity of the 28 March noise storm. For several hours thereafter the flux density remained at the high level of about 120 s.f.u. (1 s.f.u. = 10^{-22} W m^{-2} Hz^{-1}). Distinguishing this noise storm continuum from stationary Type IV emission presents difficulties because the fine structure characteristic of Type IV continua has been observed against its background.

The given noise storm contains broadband, short lifetime, fast drift or "instantaneous" bursts (see Figure 2a). Each represents a broadband enhancement of the continuum emission and may be considered as a 0.1 to 0.5 -second brightening or as a spike-brightening. For approximately an hour after 0945 UT about 20 such events took place. Unlike the well-known pulsations in the decimeter range [Gotwols, 1972], these continuum brightenings are irregular and occur as single bursts or in groups. Analogous Type IV burst events that occurred on 4 August 1972 have been described by Akinjan *et al.* [1973].

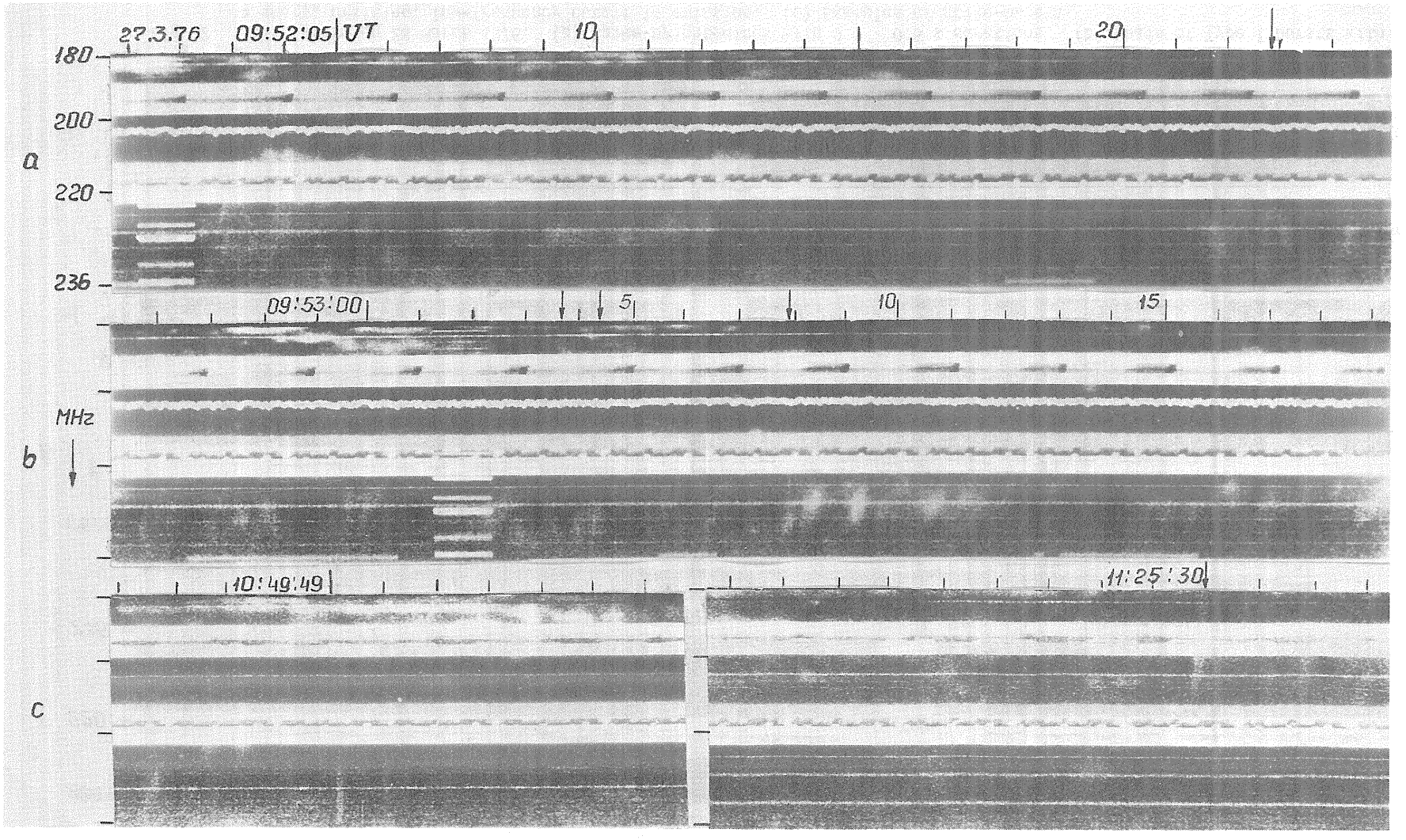

Fig. 1. High resolution dynamic spectra over the frequency range 180 -236 MHz of the noise storm on 27 March 1976. Constant-frequency stripes indicate TV interference. The bursts mentioned in the text are marked by arrows.

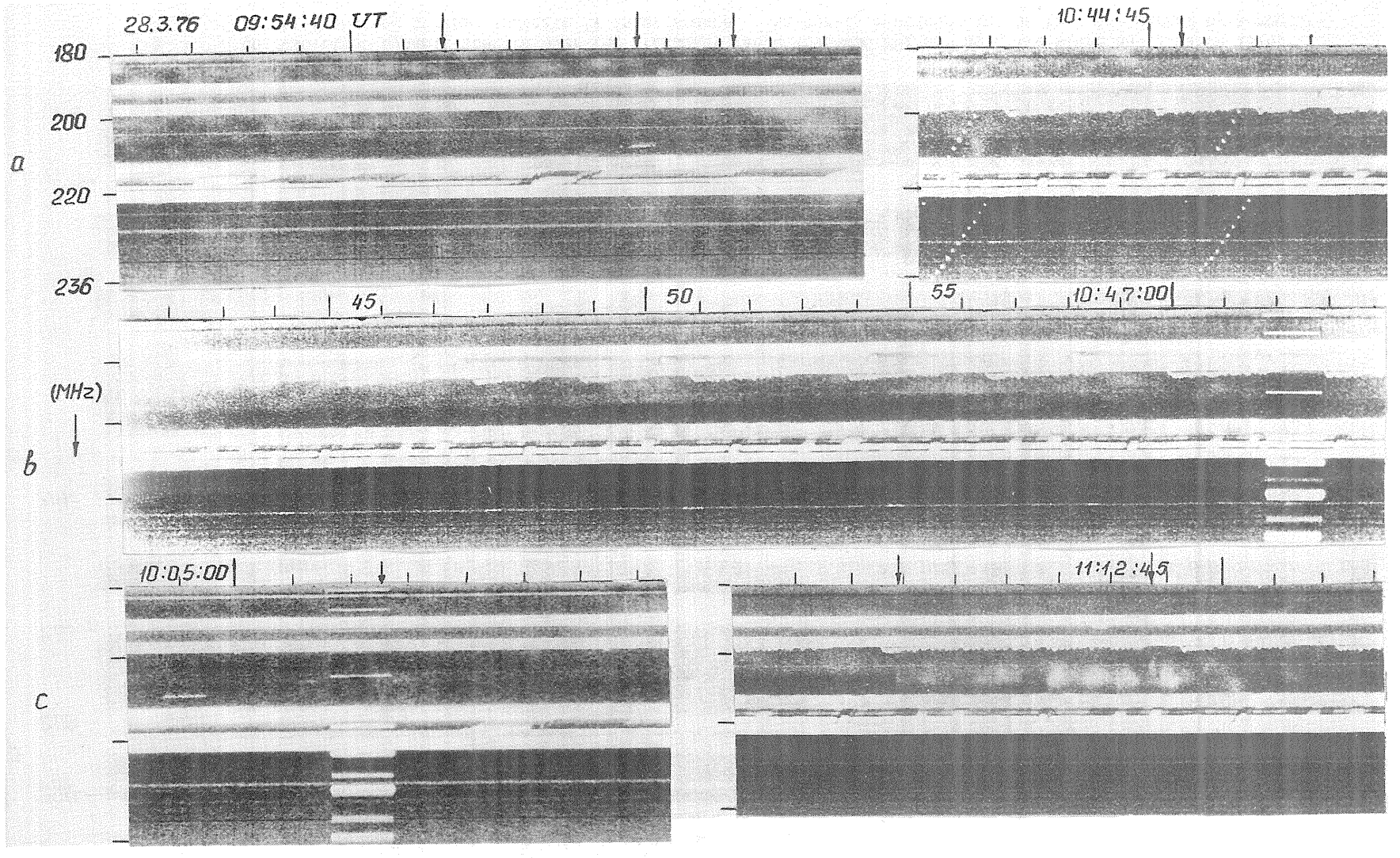

Fig. 2. Noise storm on 28 March 1976. (a) Spike-brightenings with 0.1 - 0.5 s durations. (b) Chain of Type I bursts with a sharp, drifting, low-frequency cutoff in emission. (c) Examples of spike-bursts.

29 - 30 March. Though the active region approached the central meridian, the area and magnetic field strength of the spot group remained unchanged [*SGD*, 1976]. A slowly changing active region may explain the weak noise storm observed on these 2 days.

31 March. Weak noise storm continued to 1130 UT followed by an intensification of the continuum up to 150 s.f.u. in which the number of bursts increased and the fine structure typical of Type IV continuum emission appeared. Figure 3a shows too that the number of different spike-bursts increased sharply and concentrated at the low frequency edge of the drift bursts. Signatures of the latter resemble Type III bursts, but they have a sharp cutoff in emission at frequencies where spike-bursts appear (see interval 1341:52 - 1341:54 UT). Broadband spike-bursts, only characteristic of Type IV emission, were observed as well. The burst of 1339:58 UT shown in Figure 3b may represent an example of the spike-brightening mentioned above. In the left spectrum of Figure 3b the arrow marks a U-shaped spike-burst with turning frequency near 214 MHz and a poorly developed descending branch.

During the period 1350-1355 UT, a remarkable increase in the number of fast drift, spike-bursts ("rain" type event) took place. Note the low frequency boundary of this structure near 195 MHz.

It should be pointed out that an emission and absorption stripe, fine structure pattern (zebra pattern; fiber bursts) failed to materialize against the background of the Type IV continuum on 31 March. Its absence appears to reflect the open magnetic field configuration above the active region: such a simple magnetic field geometry agrees with the growth in the group's major spot during 30 and 31 March [*SGD*, 1976].

1 - 2 April. During the period a weak noise storm prevailed, apparently due to a gradual decline in the spot group's area. Observations included rare groups of Type I bursts.

Type III Bursts

Although few in number, the groups of Type III bursts observed with the high resolution spectrograph show a fine structure. In particular, the complex group of Type III bursts of 27 March shown in Figure 4a consists of a number of short duration (0.3-0.5 s) bursts drifting through the whole frequency range and of a much longer lasting continuum. The latter is especially intensive at the edges of the ranges and may represent Type V emission. On the contrary, the group of Type III bursts of 28 March shown in Figure 4b consists of longer duration bursts. In this event the end of the emission's frequency drift below 195 MHz is evident.

Interest has increased recently in the polarization structure of Type III bursts [Slottje, 1974; Santin, 1976]. Polarimeter observations at 74 MHz, which have been performed in the period under consideration, with a time resolution of about 0.05 s allowed us to investigate variations in the polarization degree during the course of Type III bursts. In Figure 5 the dynamic spectra in the range 45-90 MHz together with time profiles of the total intensity I, the circular polarization component $V = I_R - I_L$, and the polarization degree $p = V/I$ for two Type III bursts are shown. The magnitudes of the polarization degree at the start and the end of the bursts are not indicated because p is measured inaccurately during these phases of the time profile.

One can see that in the initial burst (Figure 5a), during the rise phase of the intensity, the polarization degree decreases from p about 40% to an approximately constant 20% level characteristic of the intensity decay phase. In this burst the maximum in the circular polarization V occurs about 0.3 s before it does in the total intensity channel. Small variations in p observed during the final part of the event appear to be due to an overlapping of other independent bursts not visible in the dynamic spectrum.

The polarization of the second Type III burst (Figure 5b) differs somewhat from the first. Here the polarization degree exhibits small variations while decreasing with time from $p \sim 50\%$ to 40%. It is important to note that the two bursts mentioned above differ in other respects as well. In particular, the first event rises to a maximum within about 1 s (to half-flux level) and lasts about 1.9 s; the second burst rises in about 2 s and terminates after 3.2 s. Moreover, burst number one drifts about 12.5 MHz/s, stopping near ~ 52 MHz; burst number two drifts 36 MHz/s as it reaches maximum intensity. Properties of the intensity time profile suggest that the second Type III burst represents radio emission at the second harmonic of the plasma frequency. This may explain the absence of remarkable variations along the burst's course.

Establishing a connection between Type III bursts and polarization structure demands an analysis of a large number of events. At present we are undertaking such a study from polarization measurements at 74 MHz.

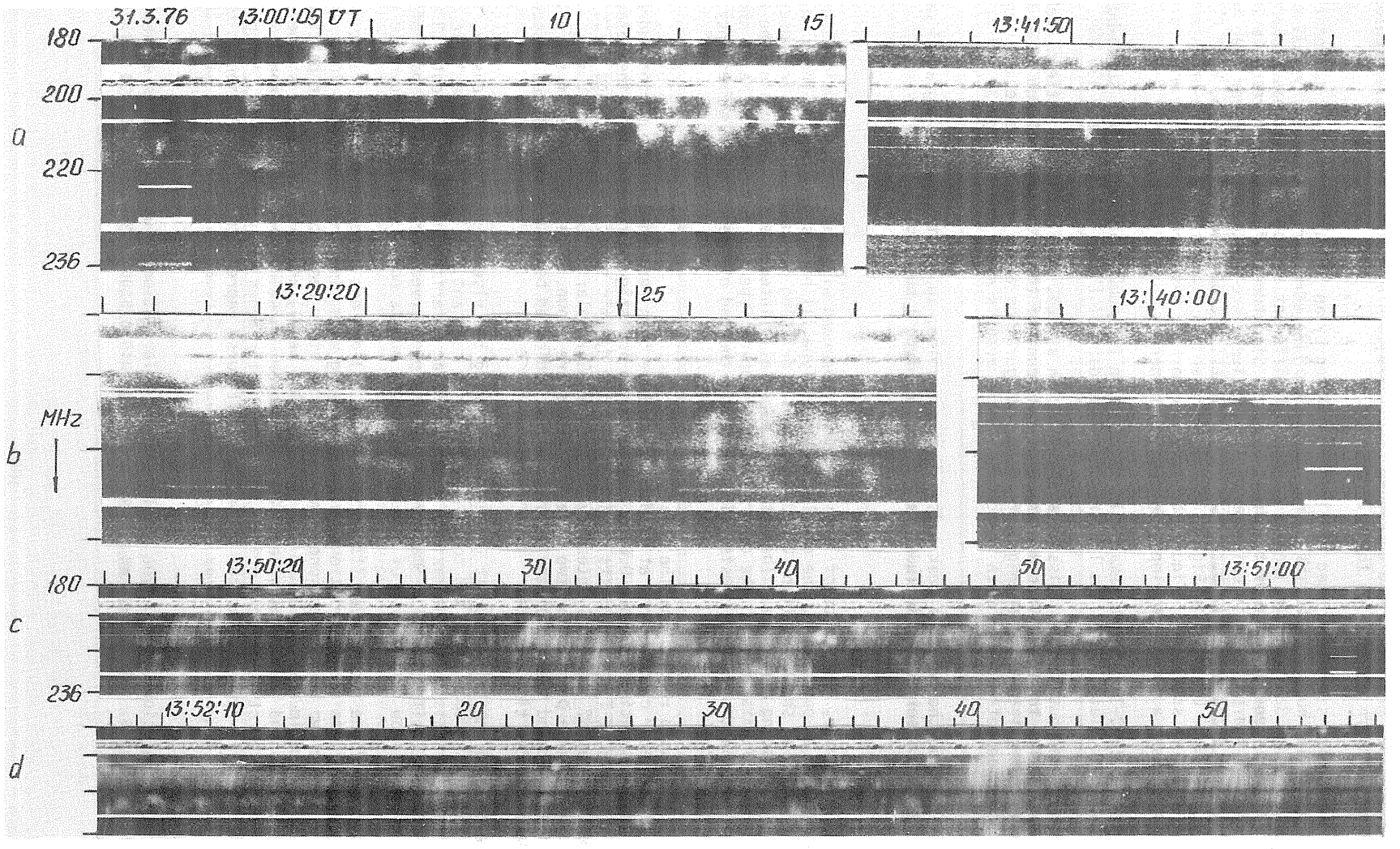

Fig. 3. Spike-bursts observed against the background of Type IV continuum emission on 31 March 1976.

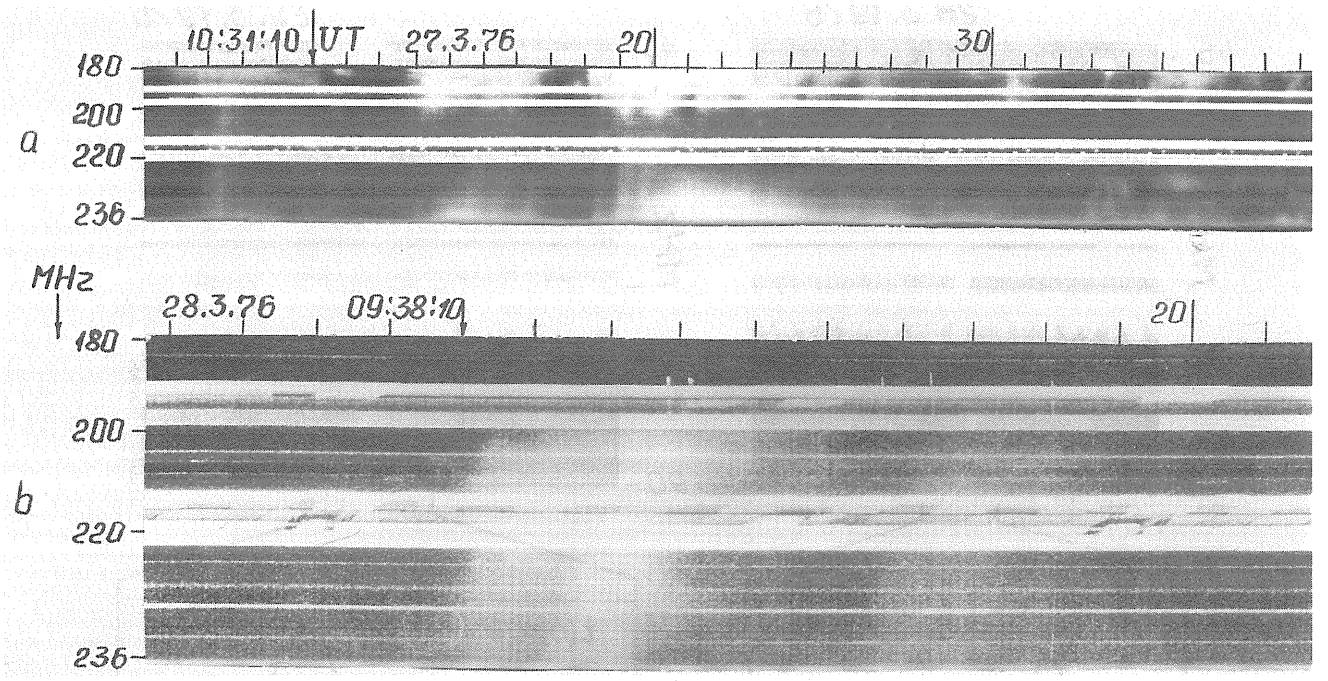

Fig. 4. Type III bursts with fine structure in the frequency range 180 - 236 MHz recorded on 27 and 28 March 1976.

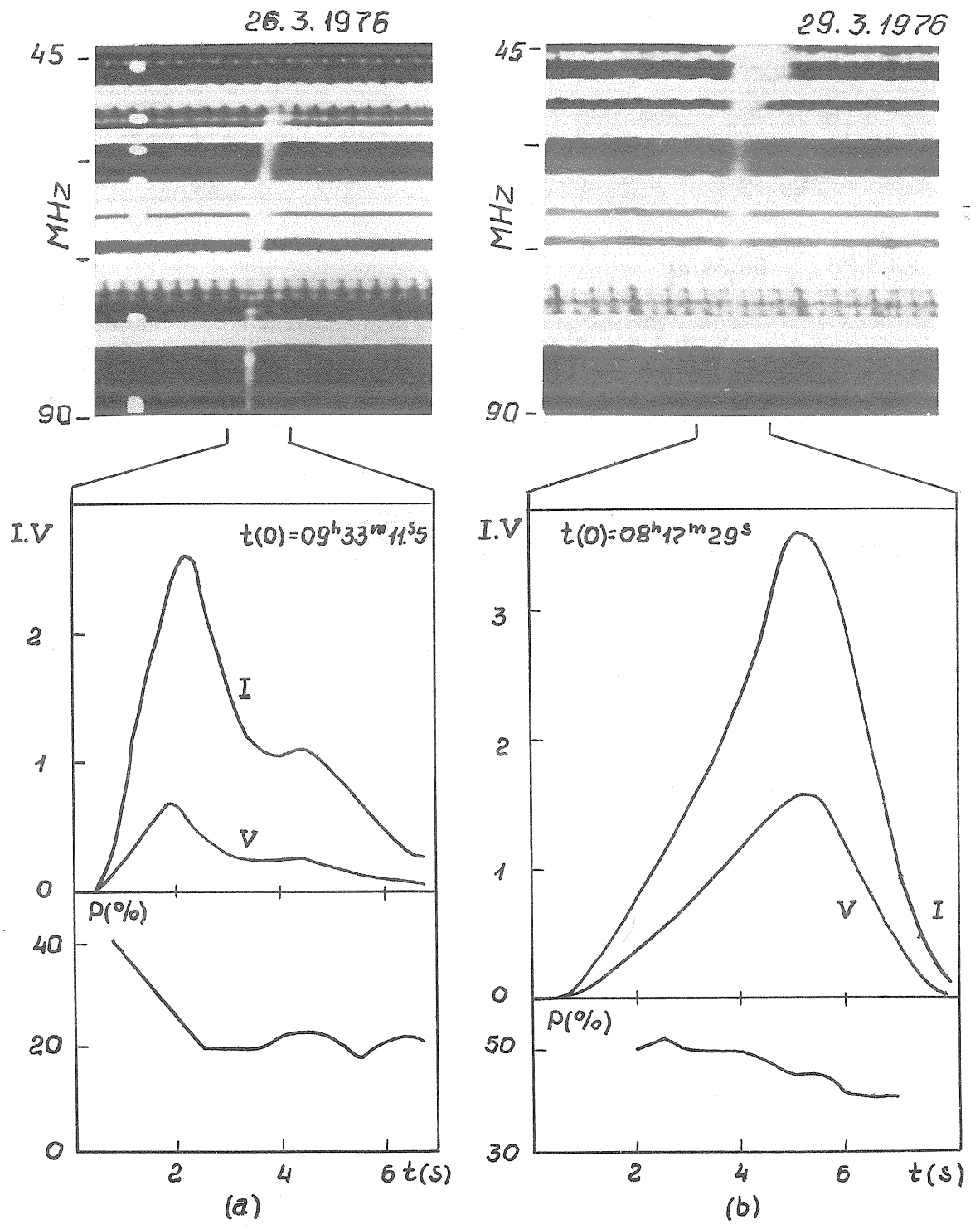

Fig. 5. Dynamic spectrum and time profiles of intensity (I), circular polarization component ($V = I_R - I_L$) in arbitrary units, and degree of polarization (p) at 74 MHz for two Type III bursts on 26 and 29 March 1976.

REFERENCES

AKINJAN, S. T., A. M. KARACHUN, V. A. KOVALEV, A. K. MARKEEV, V. V. FOMICHEV, G. P. CHERNOV, and I. M. CHERTOK — 1973 — Observations of the Solar Radio Emission at IZMIRAN During the Proton Flare on August 4, 1972, *Solar Data, Soln. Dannye, No. 7*, 108.

AMIANTOV, S. A., A. M. KARACHUN and A. K. MARKEEV — 1970 — Radio Astronomic Equipment of IZMIRAN, *Collection of Proceedings of the Session of Scientific Council of the USSR Academy of Science on Complex Radio Astronomy*, IZMIRAN, p. 40 (in Russian).

CHERNOV, G. P. — 1974 — The Search of the Diffraction Structure in Meter Solar Radio Bursts, *Solar Data, Soln. Dannye, No. 12*, 75.

CHERNOV, G. P. — 1976 — On the Association of Spike-Bursts With Type I and III Bursts, *Physics of Solar Activity*, IZMIRAN, p. 112 (in Russian).

GOTWOLS, B. L. — 1972 — Quasi-Periodic Solar Radio Pulsations at Decimetric Wavelengths, *Solar Phys.*, *25*, 232.

SANTIN, P. — 1976 — The Time and Polarization Profile of Type III Solar Radio Bursts at Meter Wavelengths, *Astron. Astrophys.*, *49*, 193.

SLOTTJE, C. — 1974 — Polarization Fine Structure in Solar Radio Bursts of Type III on Short Meter Wavelengths, *Astron. Astrophys.*, *32*, 107.

1976 — *Solar Data, Soln. Dannye, No. 3*, Nauka, Leningrad.

SGD — 1976 — *Solar-Geophysical Data, 380 - 381 Part I*, April - May 1976, U. S. Department of Commerce, (Boulder, Colorado, U.S.A. 80302).

Spectral Evolution of March/April 1976 Decimetric Type IV Radio Events

by

A. O. Benz, M. Berney and M. R. Perrenoud
Radio Astronomy Group
Microwave Laboratory ETH
Zürich, Switzerland

Introduction

The activity of McMath Regions 14143 and 14179 was observed by the two Zürich radio spectrographs. The *analog* instrument [Tarnstrom, 1973] in Dürnten, which is reasonably sensitive from about 150 MHz, sweeped continuously 4 times per second from 100 to 1000 MHz. The *digital* equipment [Asper and Benz, 1975] swept from 204 to 450 MHz in 1 MHz steps and measured each frequency at a rate of 8 Hz. The latter spectrograph made at least partial recordings on magnetic tape of most of the activity during the period. Frequency calibration was done on-line. Although receiver calibration (but not antenna calibration) for the period was possible, the difference between calibrated and uncalibrated data in temperature was small, and the aspect of the curves remained the same. In the resulting frequency profiles narrowband dips and humps were due to the antenna characteristic or to weak interference.

Here we present the observed Type IV and the DCIM activity. The Type IVs consist of 4 events (termed "class A") with broad bandwidth, smooth appearance, slow pulsations (periods 10s and longer), and fine structure. They are all preceded by Type III activity and (except for the last event) by 20-50 min of strong strong Type I activity. Three other events called "class C" contain large and dense decimetric Type III groups and/or DCIM ("fast drift" pulsations) with apparently no continuum. Their duration is typically 1-5 min, as compared to 10 min to several hours for "class A" events. An intermediate class occurs in the 23 March event that combines the features of both A and C classes. It is thus termed "B". The similar appearances of events within one class is striking in the analog records.

For clearness evident terrestrial interference (e.g., TV emission) is omitted, and the values are interpreted between the two nearest unperturbed measurement points. On the time profiles (Figures 1, 4, 5 and 8) the first time written on the abscissa corresponds to the first tick mark. The longer tick marks show the rounded values of time. For the lowest curve the value of the logarithm of the temperature at the tick mark where the profile ends is given in all plots in uncalibrated arbitrary units (ar.u.) for comparison.

"Class A" Events

25 March. The 25 March event starts around 1145 UT with strongly enhanced Type I-like activity at about 300 MHz. This activity slowly spreads to a lower frequency. At the same time an underlying continuum gains in intensity. From 1223 to 1240 UT this continuum has relatively little structure, and its spectrum remains remarkably constant (see Figure 2a). At 1308:35 UT a second phase starts abruptly with maximum intensity at higher frequencies (about 600 MHz). During the next 10 min the spectrum undergoes considerable change (Figure 2b). Broadband pulsations without measurable drift occur throughout the event. A zebra pattern is clearly visible from 1310 until 1311 UT (Figure 3). The maximum at 1317 UT is preceded by a group of Type III bursts. The details of this rise are shown in Figure 4. During this maximum phase quasi-regular broadband pulsations with periods of 11 seconds predominate at 300 ± 50 MHz.

28 March. Starting around 0940 UT with groups of Type III bursts, a smooth continuum predominantly located in the metric band rises slowly to considerable intensity. This event is preceded by strong Type I activity near 250 MHz, similar to the 25 March event.

31 March. This longest and strongest burst observed during the period shows broadband pulsations in the first 15 min. Starting at 1158 UT the pulsations are strongest at the highest frequency and fade out near 200 MHz (Figure 5). The spectrum (Figures 6 and 7) shows that the initial maximum intensity is beyond 450 MHz. After about 1200 UT considerable activity with fine structure (cf., Figure 6) develops at metric frequencies. The overall slope of the spectrum then remains constant for the next hour and flattens out afterward. The high frequency (450 MHz) intensities remain nearly constant from 1210 to 1356 UT, whereas the low frequencies show large fluctuations and fine structure.

30 April (b). This Type IV event, which occurred between 1242.7 and 1253 UT, is by far the shortest event of "class A". It extends from the lower limit of our frequency range (100 MHz) to about 900 MHz. The event started with small Type III-like features at low frequency (see Figure 10b). At about 1243:00 UT several broadband spikes (probably Type III) of 1 to 5-second duration coincide with the beginning of the Type IV continuum (see Figure 8b). Its maximum intensity is initially around 280 MHz (Figure 9), but it moves to lower frequencies until strong Type III-like activity occurs near 370 MHz and below at 1244:21 UT (see also Figure 10b). The latter initiates a continuum with a maximum at a frequency above 450 MHz at 1245:06 UT (Figure 8b) and a small subsidiary peak at 1253 UT.

"Class B" Event

23 March. The complex event of 23 March, which occurred between 0841 and 0858 UT, was recorded only by the analog spectrograph (see Figure 11). It is composed of at least the following elements:

(1) Weak Type III bursts during the initial stage at low frequencies between 0841.2 and 0841.6 UT.

(2) Two strong features at metric wavelengths drifting to lower frequencies at rates comparable to Type II bursts.

(3) A Type IV continuum that is probably composed of two parts separated at about 400 MHz. The low frequency part seems to extend below 100 MHz and follows the Type II-like features; the weaker high frequency part is shorter in duration and has maximum intensity around 700 MHz.

(4) DCIM-like pulsations starting at 0842.4 UT from 500-1000 MHz. They fade out after 0844 UT and become part of the continuum.

"Class C" Events

27 March. The total duration of this activity was 5.3 min: from 1203.2 until 1208.5 UT. Figure 12 shows some details at the low frequency part of the event. The maximum intensity occurred near 700 MHz. According to the analog observations, the spectrum reached a minimum near 500 MHz. Whereas the drifts of single bursts were not measurable in the high frequency analog record, they could be calculated from the the low frequency digital spectrogram shown in Figure 12. The measured drift rates of -73 and -500 MHz/s reflected the Type III character of this "class C" event. Sagamore Hill data indicated that this "class C" event was associated with dekametric continuum.

28 March (a). The 28 March event, which occurred between 0601.2 and 0608.6 UT, and the one on 27 March have homologous spectra. Type III and DCIM activity are clearly separable in time.

30 April (a). This event - preceded by Type III activity at 0840 UT - only lasted from 0843.2 til 0845.3 UT, and thus represents the shortest "class C" event recorded. At its low frequency boundary some time structures show Type III-like appearance (see Figure 8a). Reversed drift rates are evident in Figures 10a.

Acknowledgments: We thank A. Paschke for his help with data handling and observing. The development of the ETH spectrographs is financed in part by the Swiss National Science Foundation.

REFERENCES

ASPER, H. K. and A. O. BENZ 1975 Der Computer gesteuerte Radiospektrograph der ETH Zürich, *Verhandl. der Schweizerischen Naturforschenden Gesellschaft, 19,* 119.

TARNSTROM, G. L. 1973 Preliminary Results of the Zürich Radio-Spectrograph, *Astron. Mitteil. Eidg. Sternwarte Zürich,* Nr. 317.

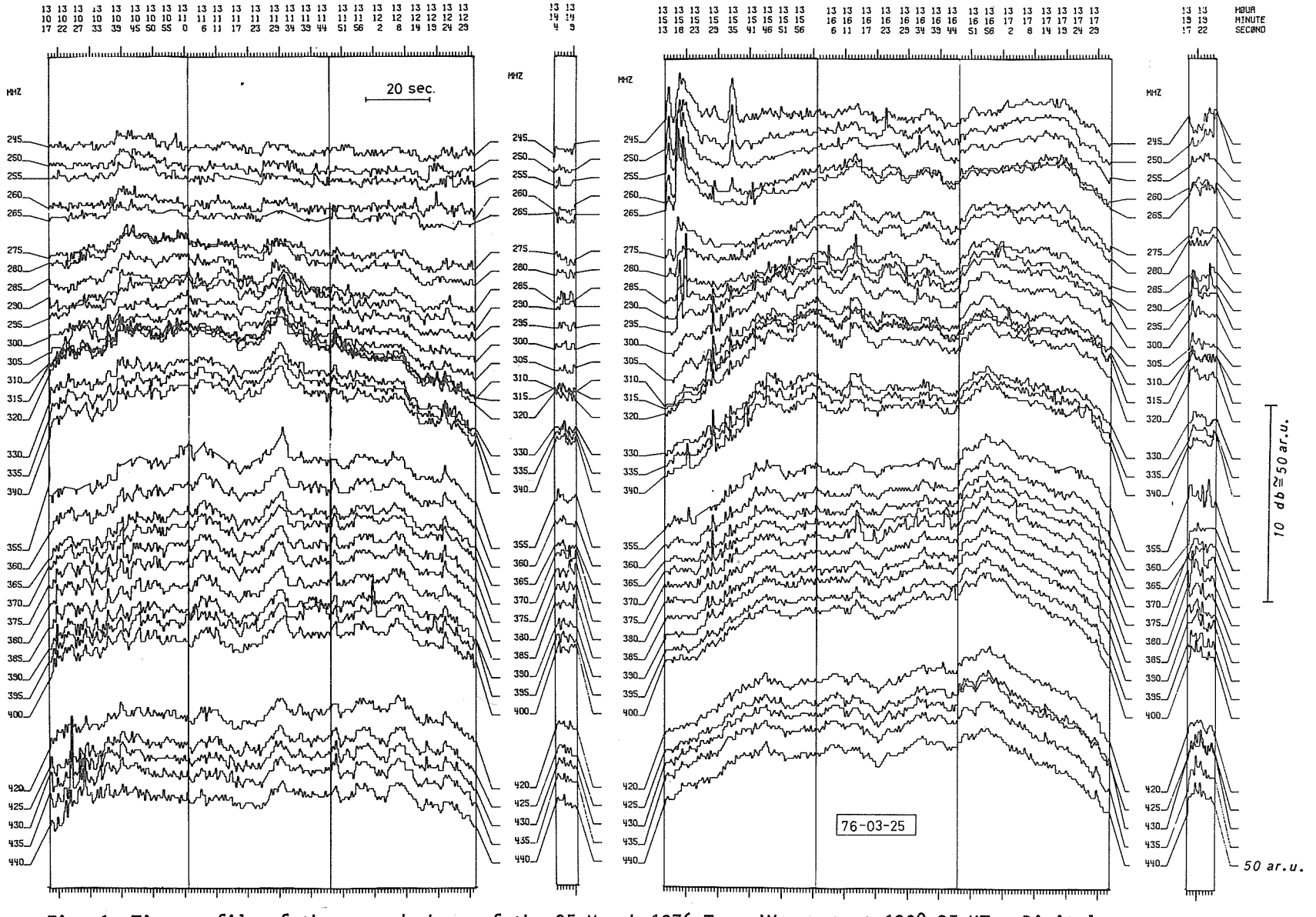

Fig. 1. Time profile of the second phase of the 25 March 1976 Type IV event at 1308:35 UT. Digital measurements have been registered between 1310:17 and 1319:25 UT with three interruptions. The abscissa is time, and the ordinate is the logarithm of the calibrated temperature in dB. Lines are plotted at 5 MHz steps (omitting disturbed frequencies) between 245 and 440 MHz. The values are averaged for 5 MHz and 0.5-second intervals (4 sweeps). The most disturbed frequencies remaining are 255, 265, and 355 MHz.

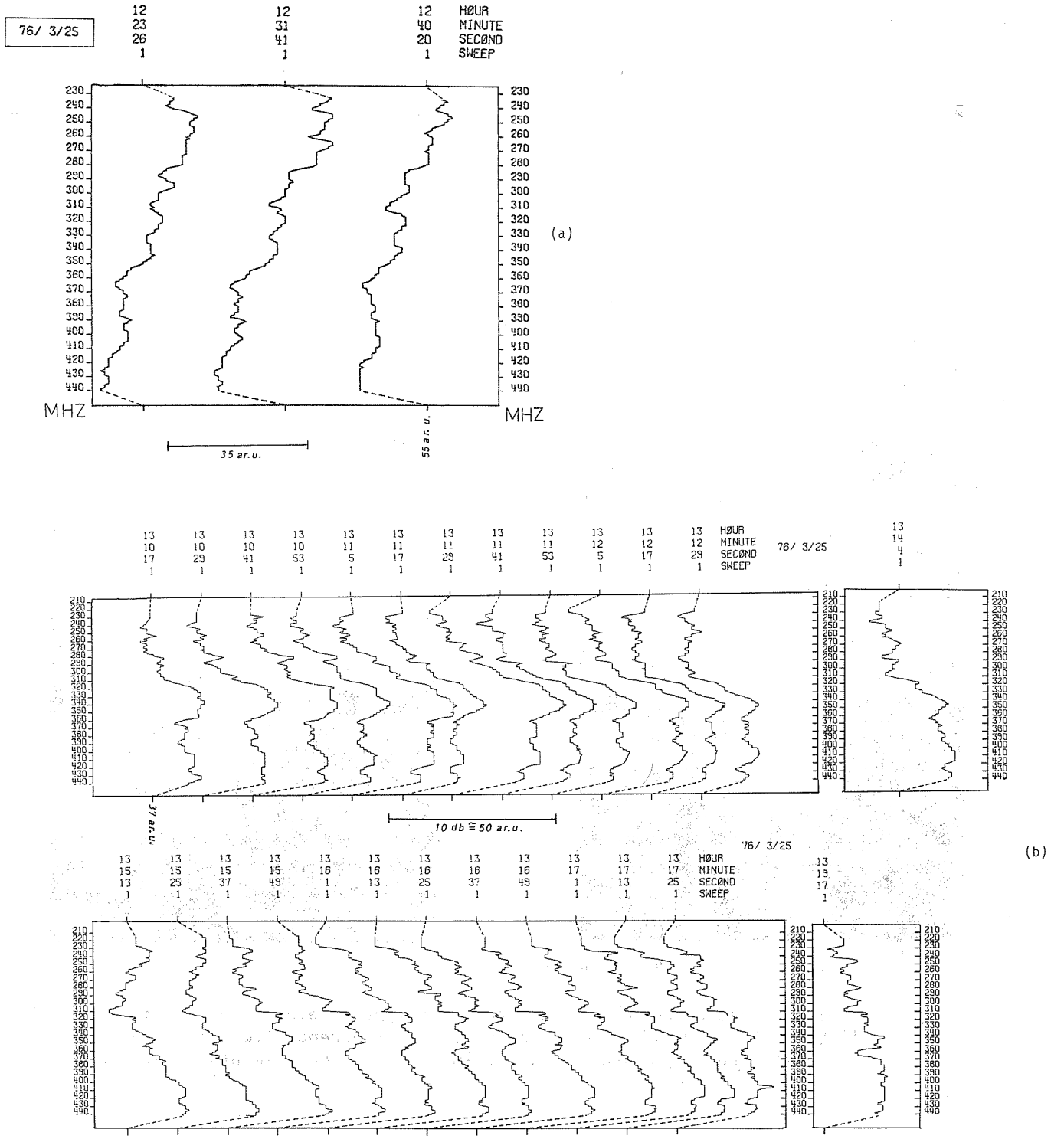

Fig. 2. Frequency profile (spectrum) of the 25 March 1976 Type IV event. Three curves representative of the first phase are plotted in Figure 2a. For the second phase, curves are plotted every 12 s in Figure 2b. The frequency is given in MHz along the ordinate. The logarithm of the temperature is given along the abscissa in arbitrary units in Figure 2a, as calibrated values in dB in Figure 2b. The plotted values are averaged in time at 0.5-second intervals. A gliding average of 5 MHz width has been applied in frequency.

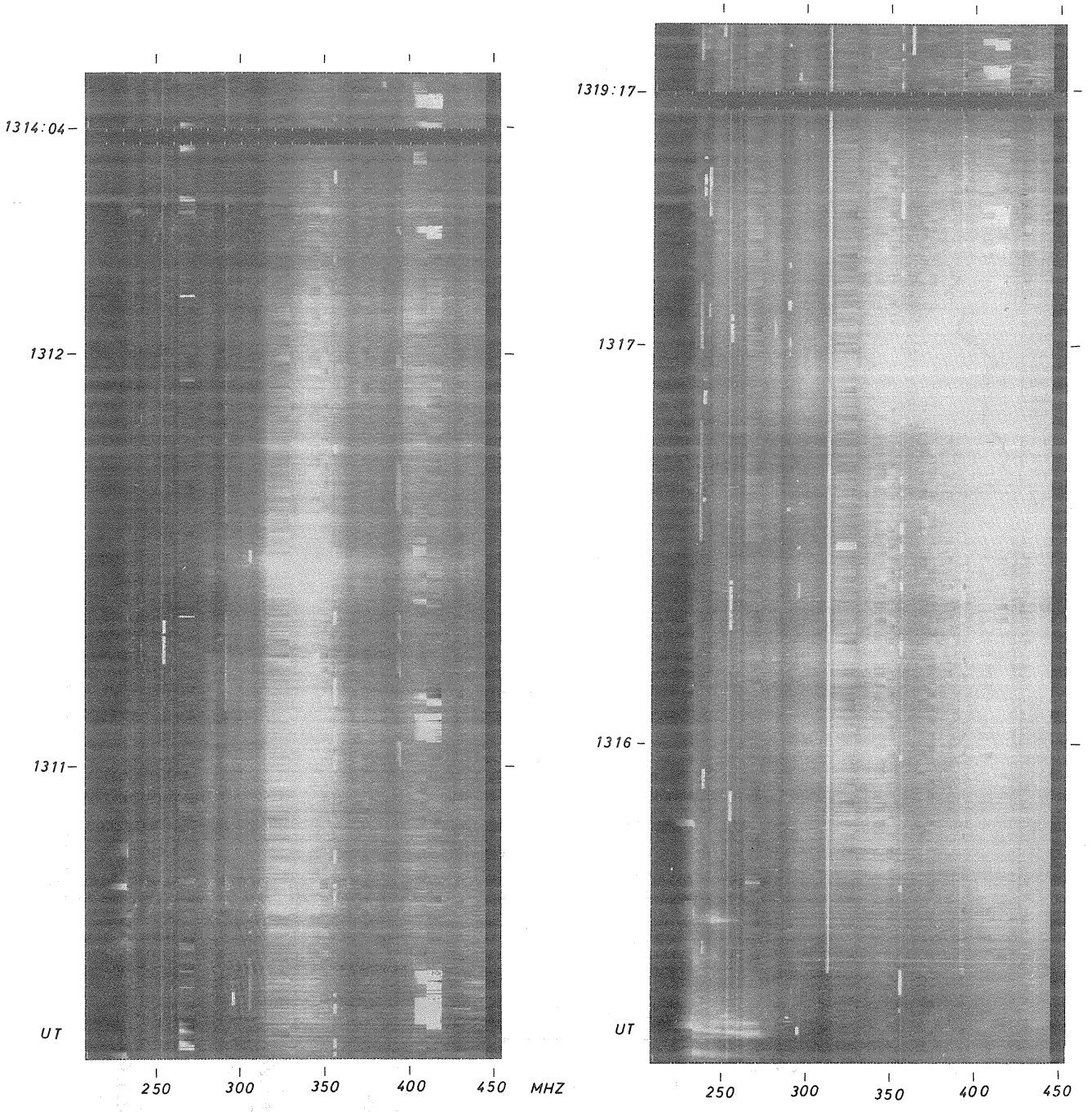

Fig. 3. Digital spectrogram of the 25 March 1976 Type IV event from 1310:17 to 1319:25 UT. Time lies along the ordinate; frequency lies along the abscissa; and brightness indicates intensity. One elementary rectangle is 1 MHz high and 1/8 s wide.

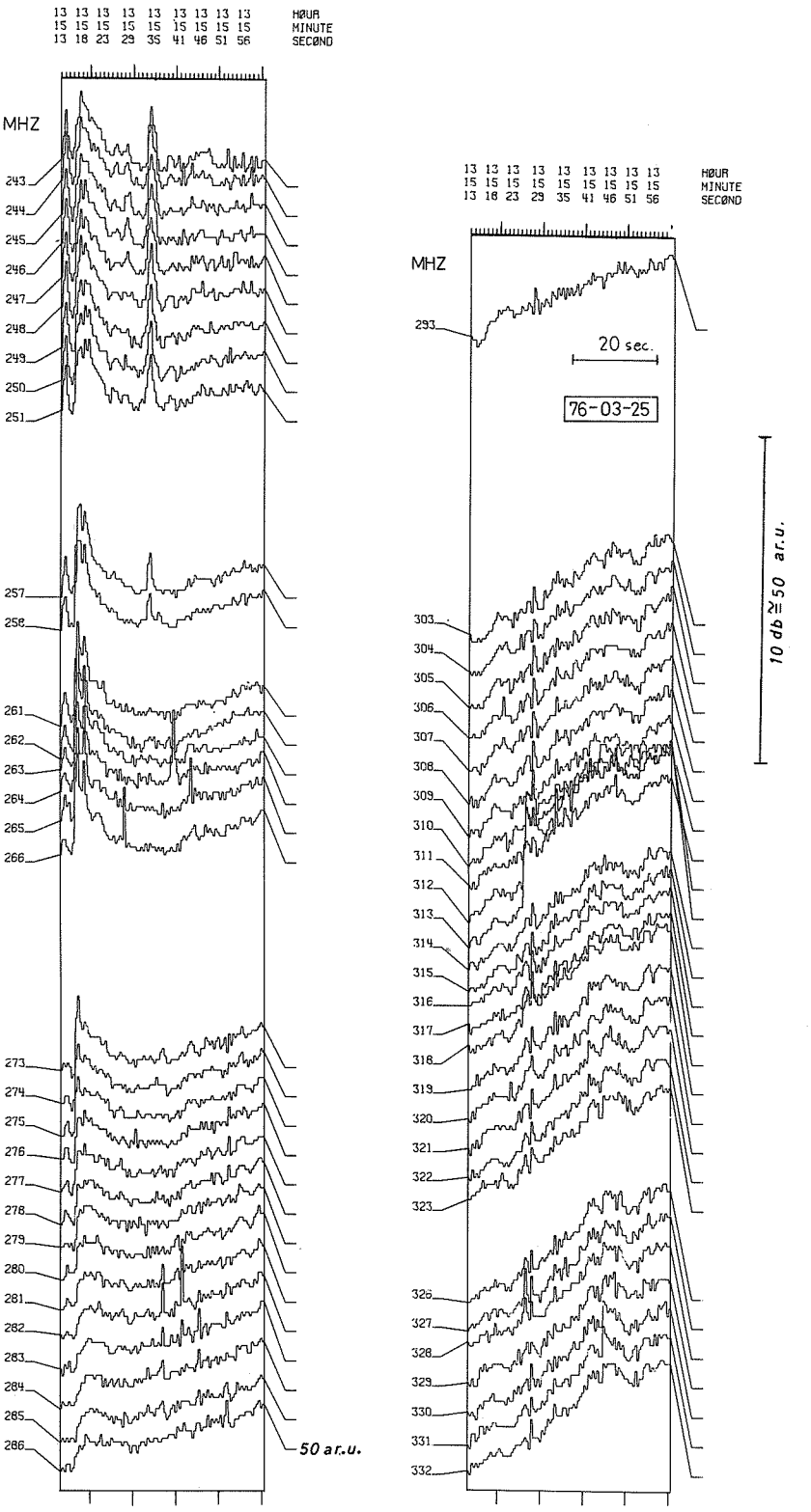

Fig. 4. Time profile details between 1315:13 and 1316:00 UT of the 1308 UT Type IV burst of 25 March 1976. Lines are plotted for every unperturbed MHz between 243 and 332 MHz. The axes are the same as in Figure 1. The 312 and 313 MHz lines are enhanced by a terrestrial emitter from 1315:25 UT. The values are averaged for 0.5-second intervals.

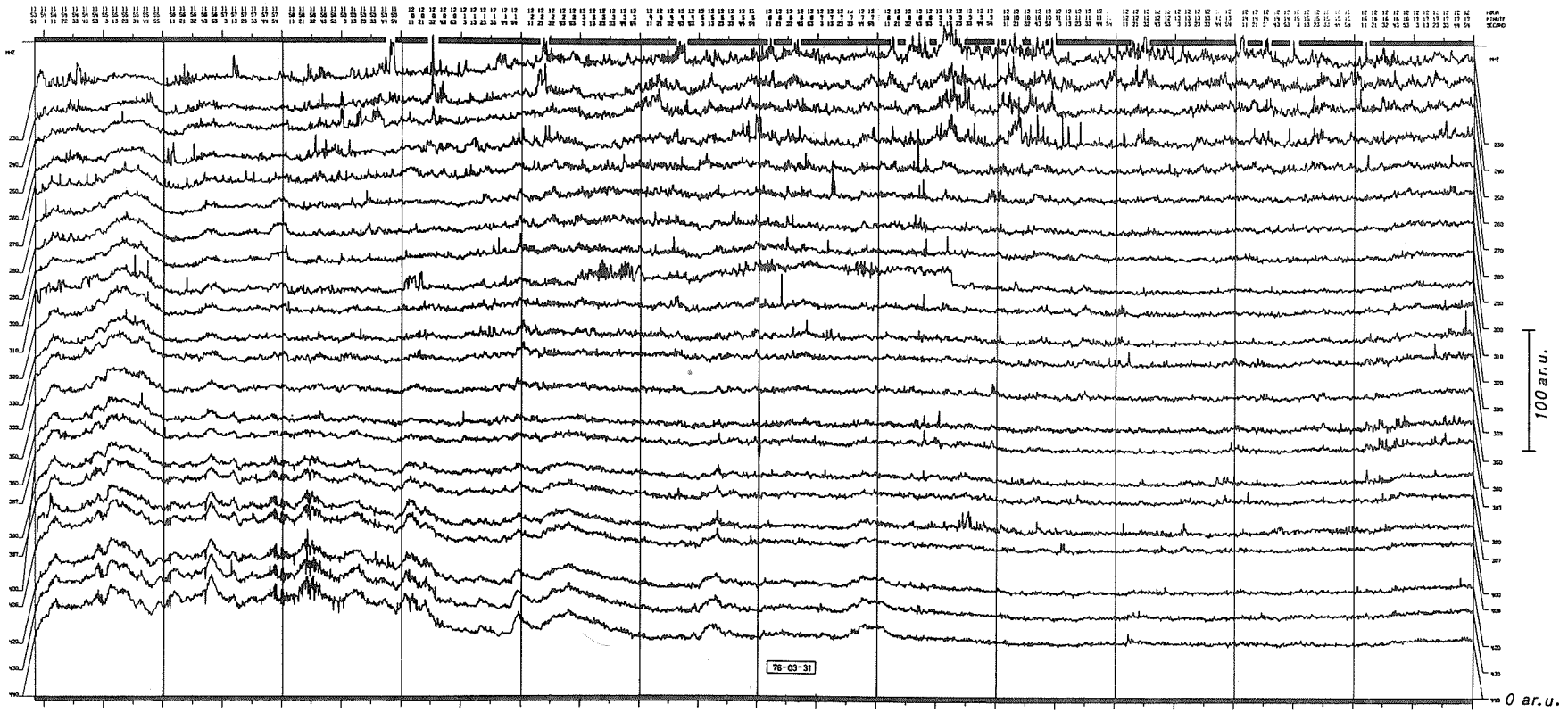

Fig. 5. Time profile from 1153:51 to 1218:00 UT of the 1152 UT Type IV event of 31 March 1976. The coordinate axes are similar to those of Figure 1, but the logarithm of the temperature is given in arbitrary units. Lines are plotted in about 10 MHz steps for least disturbed frequencies between 230 and 440 MHz. The values are averaged for 0.5-second intervals. The most disturbed frequencies remaining are 260, 310 and 400 MHz.

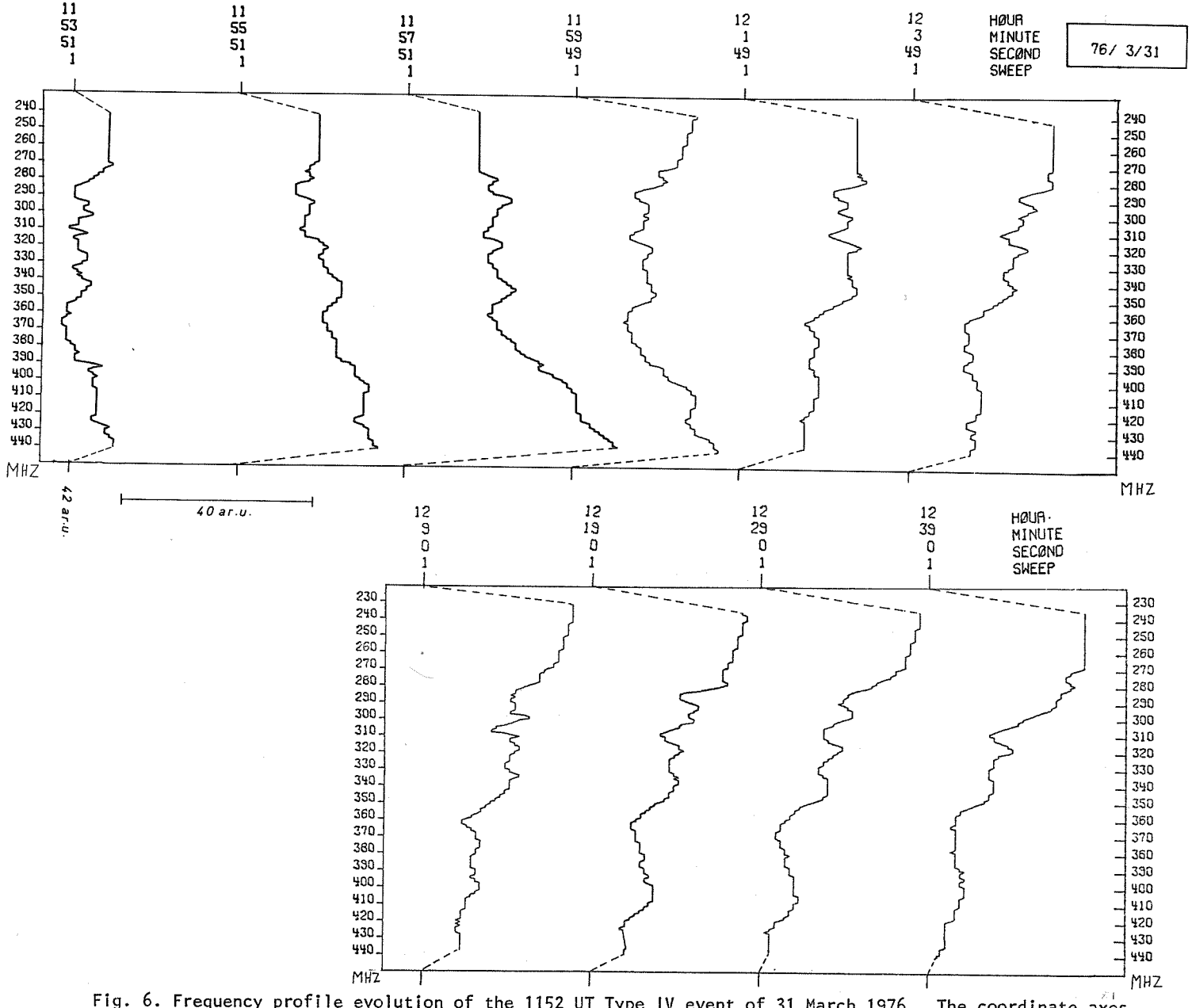

Fig. 6. Frequency profile evolution of the 1152 UT Type IV event of 31 March 1976. The coordinate axes are the same as those of Figure 2a, and the logarithm of the temperature is also plotted in arbitrary units. The values are averaged as in Figure 2a. The rising phase of the burst is shown above; a spectrum is plotted about every 2 min between 1153:51 and 1203:49 UT. The continuous phase of the burst is shown below with a spectrum plotted every 10 min.

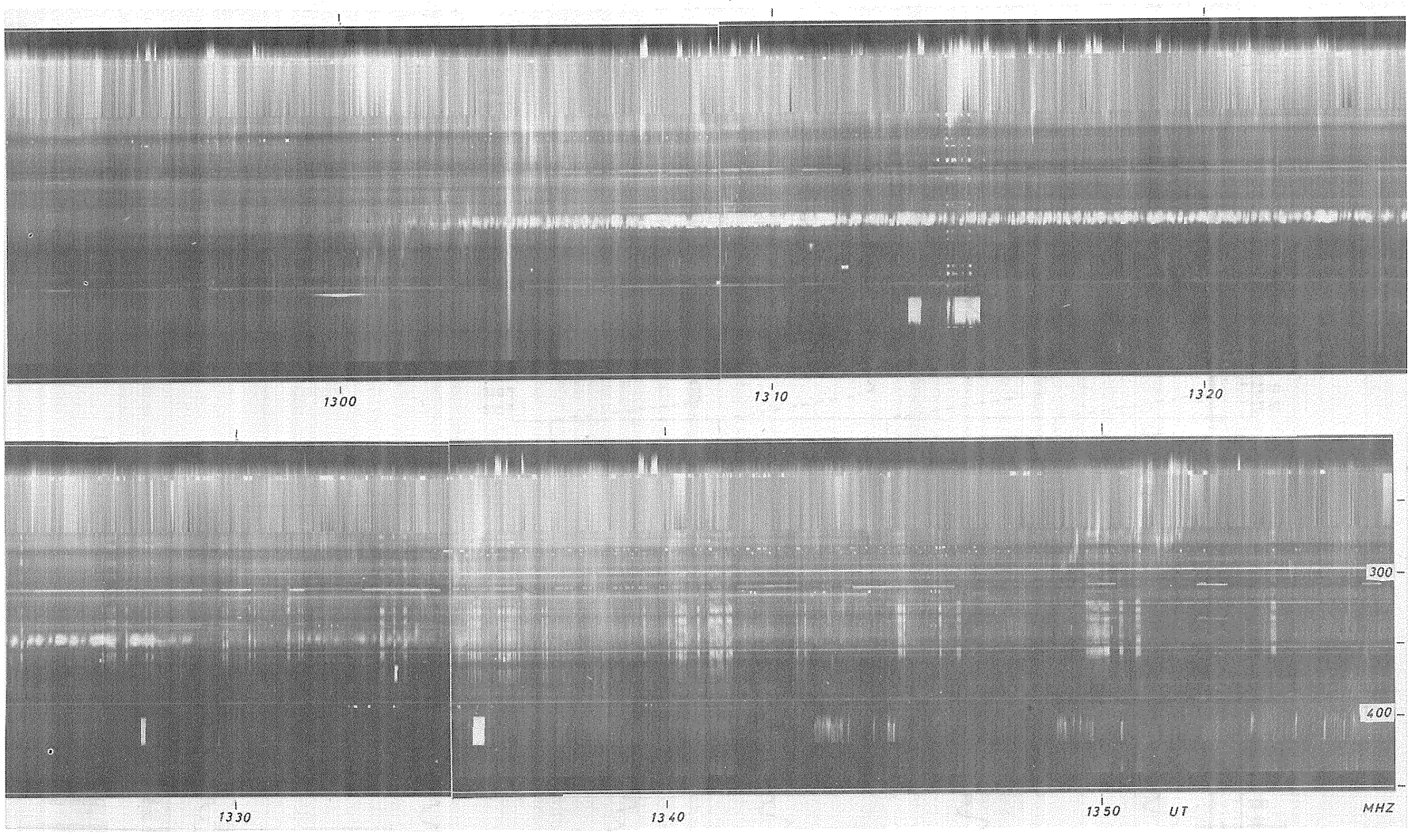

Fig. 7. Digital spectrogram of the 1152 UT Type IV event of 31 March 1976. The representation is the same as Figure 3. Until 1243:47 UT the elementary rectangles represent values averaged for 0.5 s in time and smoothed over 5 MHz intervals in frequency (gliding average). From 1243:48 to 1356:47 UT the values are not averaged: one elementary rectangle is 1 MHz high and 1/8 s wide.

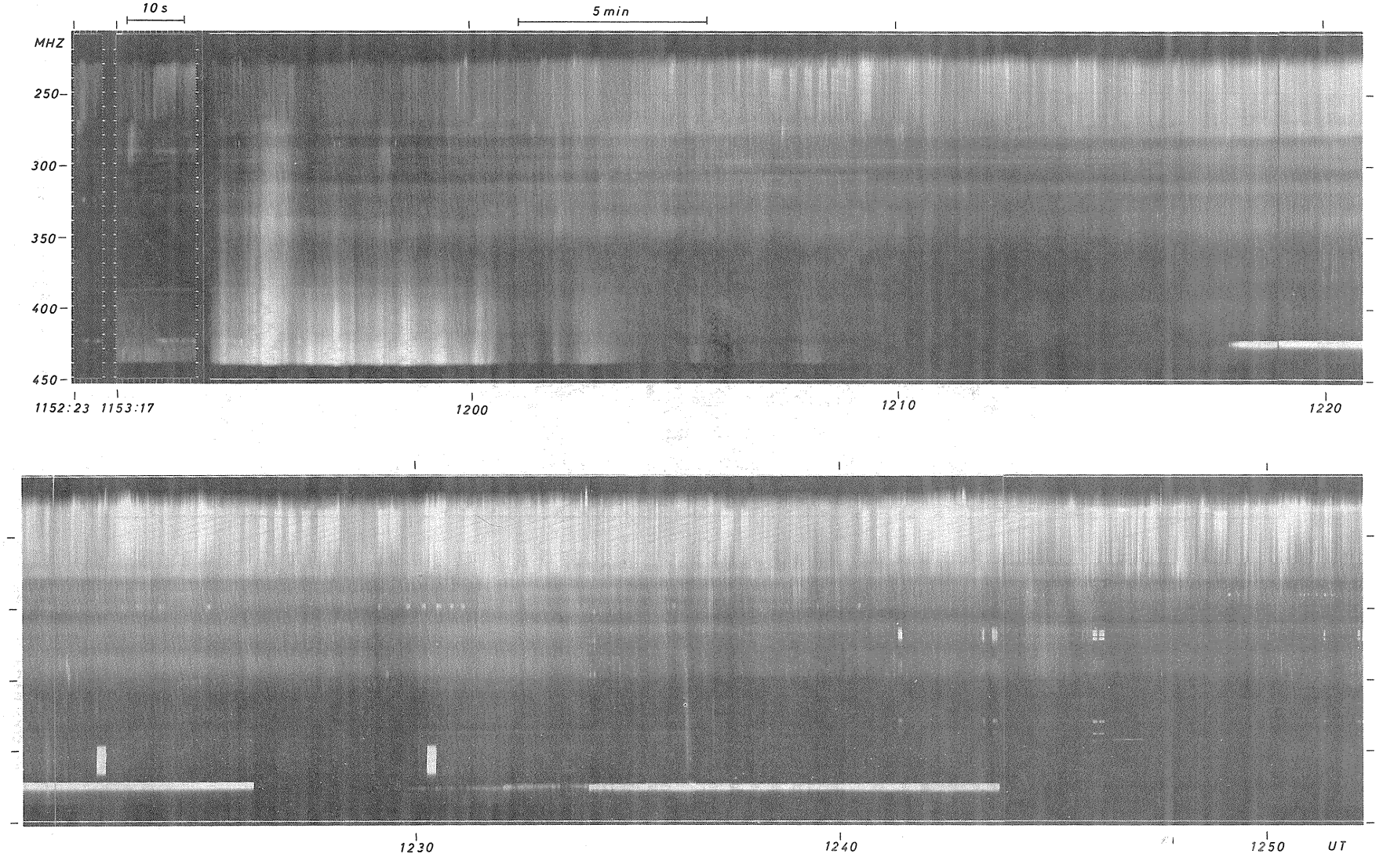

Fig. 7. (continued) 76-03-31

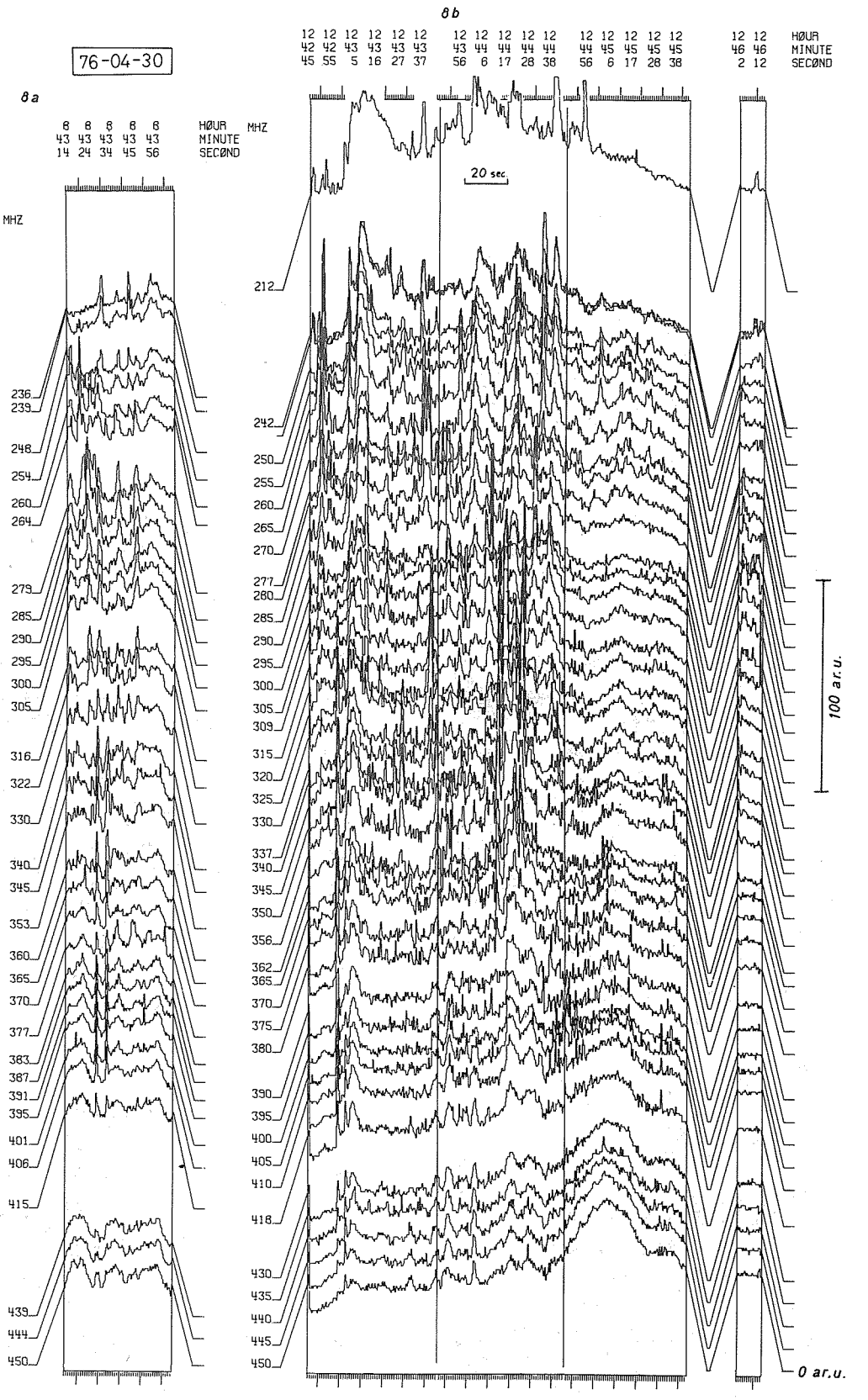

Fig. 8. Time profile of the 30 April 1976 bursts at 0839 UT (8a) and 1242 UT (8b). The coordinate axes are the same as in Figure 5. Lines are plotted every 5 MHz for undisturbed frequencies. The values are averaged for 0.5 second intervals.

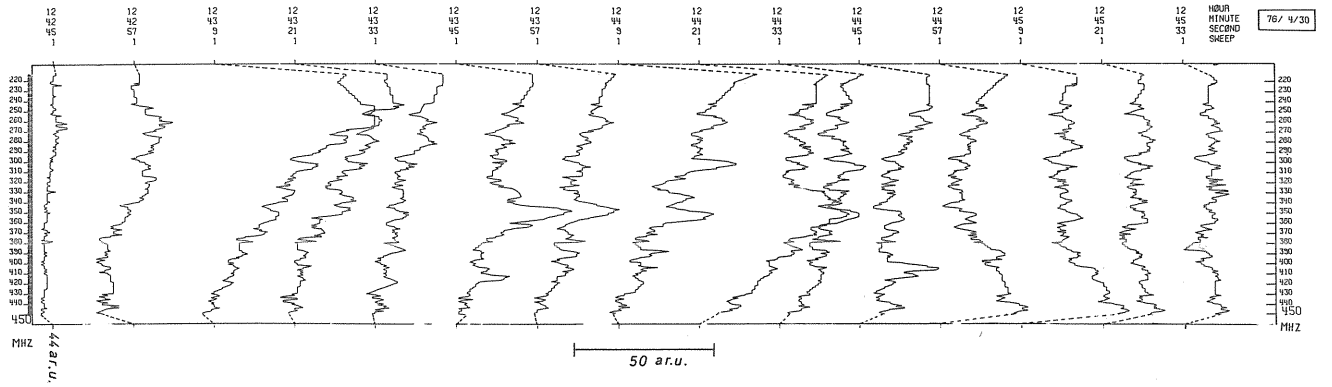

Fig. 9. Frequency profile evolution of the 1242 UT Type IV burst of 30 April 1976. The coordinate axes are the same as in Figure 2b (logarithmic temperature in arbitrary units). The values are only time averaged over 0.5-second intervals. Lines are plotted every 12 s between 1242:45 and 1245:33 UT.

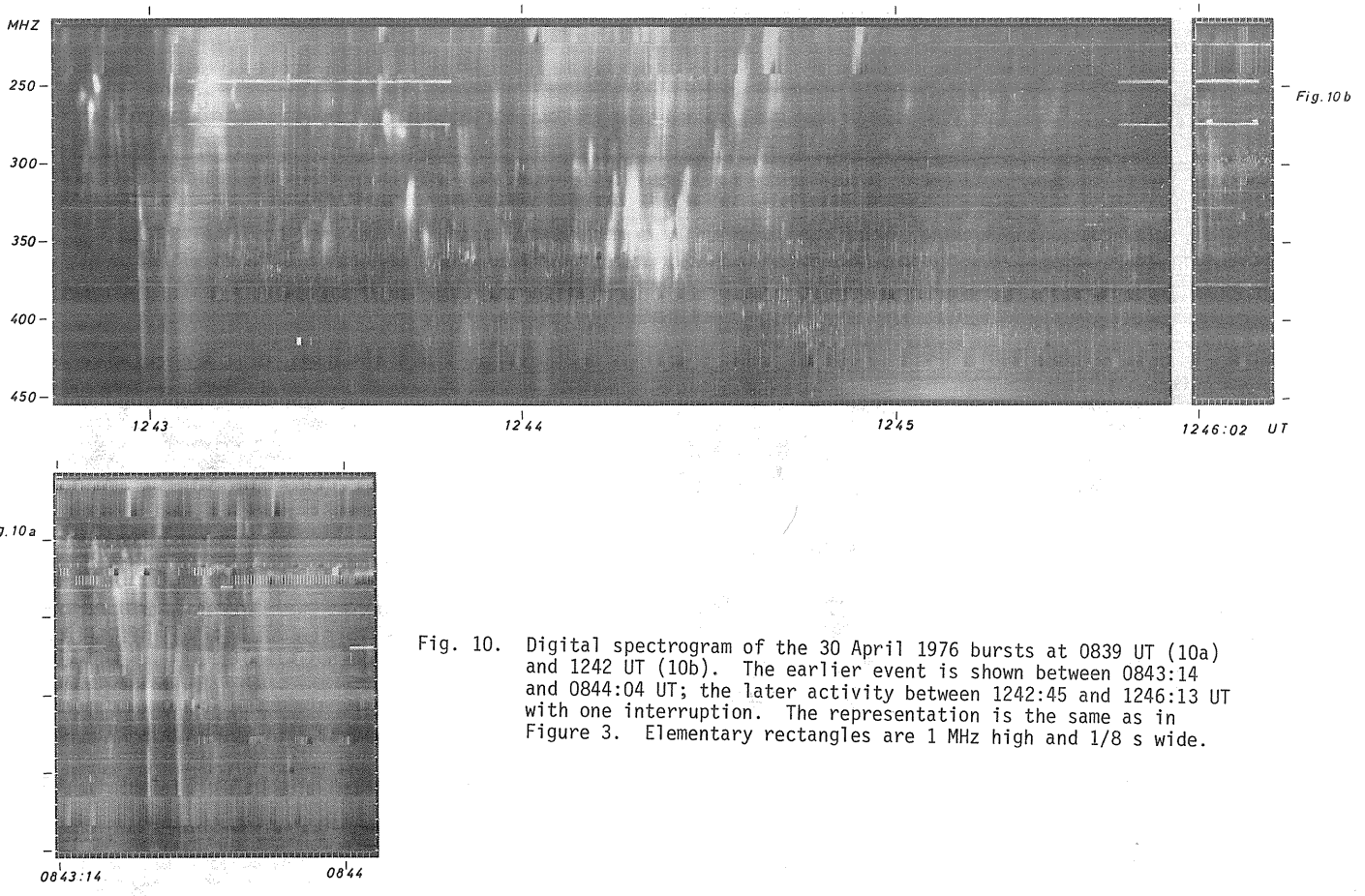

Fig. 10. Digital spectrogram of the 30 April 1976 bursts at 0839 UT (10a) and 1242 UT (10b). The earlier event is shown between 0843:14 and 0844:04 UT; the later activity between 1242:45 and 1246:13 UT with one interruption. The representation is the same as in Figure 3. Elementary rectangles are 1 MHz high and 1/8 s wide.

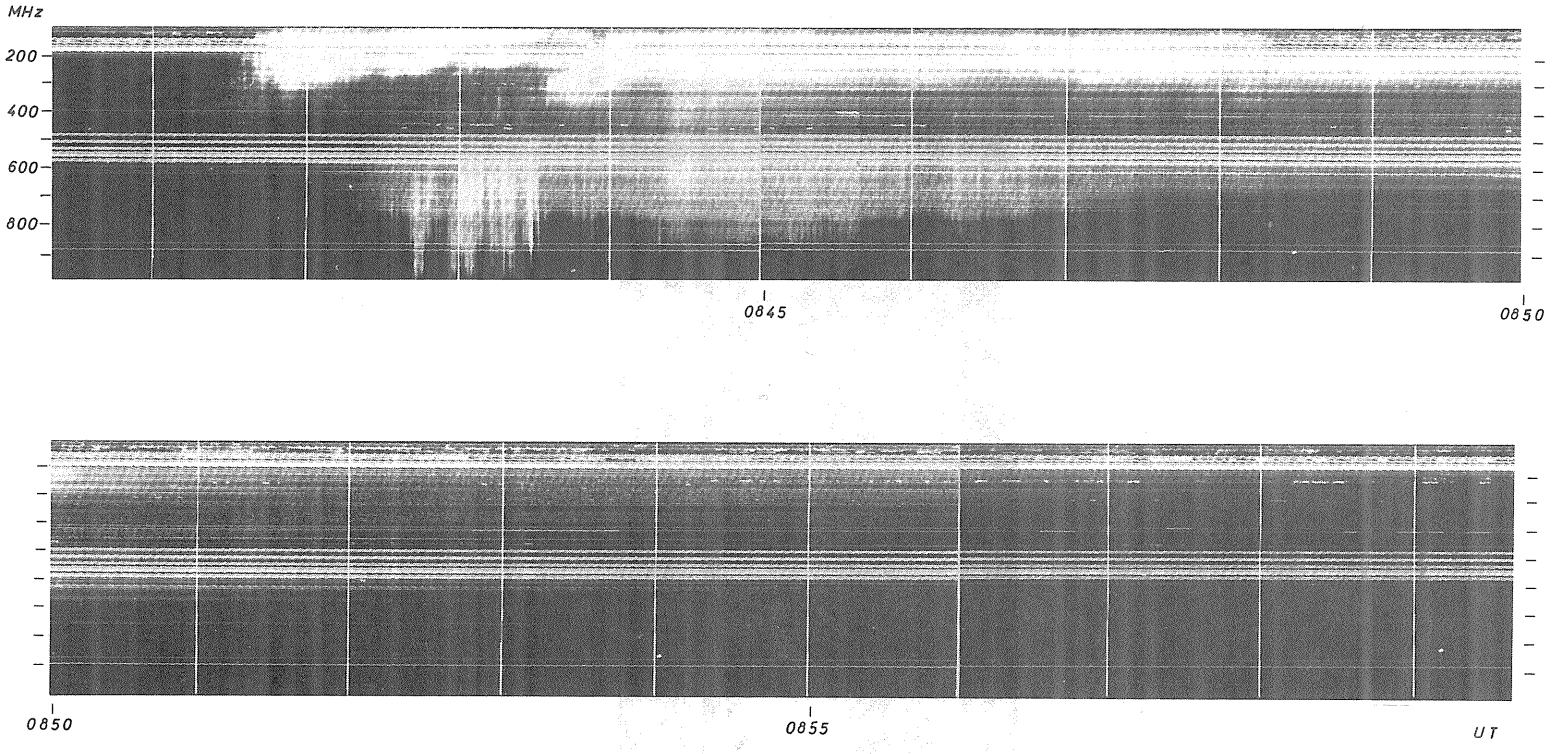

Fig. 11. Analog spectrogram of the 0841-0858 UT Type IV DCIM burst of 23 March 1976. Time is on the abscissa; frequency is on the ordinate; and brightness indicates intensity. Lines at constant frequency are terrestrial interferences.

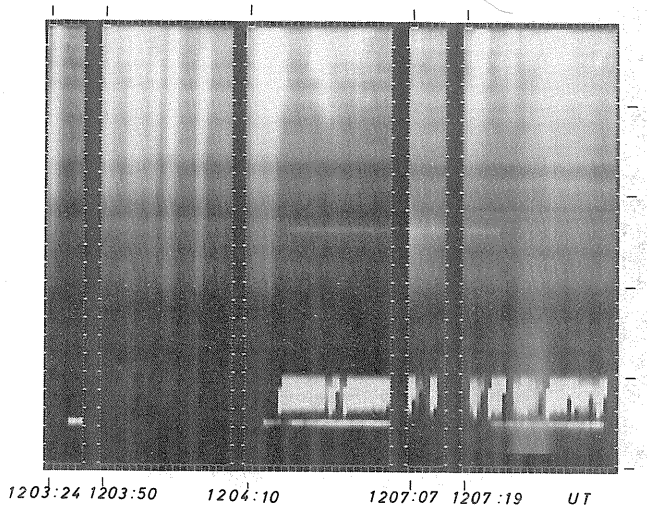

Fig. 12. Digital spectrogram of the 1203.2 UT event of 27 March 1976 between 1203:24 UT and 1207:39 UT with four interruptions. The representation is like the one in Figure 3. The elementary rectangles represent values averaged over 0.5-second intervals and smoothed over 5 MHz (gliding average).

Velocities of Propagation of March/April 1976 Coronal and Interplanetary Shock Waves

by

Stephen Pintér
Geophysical Institute
Slovak Academy of Sciences
947 01 Hurbanovo Czechoslovakia

The search for relationships between specific solar events and various interplanetary and geophysical phenomena remains one of the fundamental problems of solar physics and physics of the interplanetary medium. Investigating these relationships can contribute to understanding flare processes, to determining the origin of the ejected plasma cloud with its attendant shock waves, and to clarifying the evolution of these waves as they propagate through interplanetary space.

Velocity is a key parameter in explaining flare-generated, solar coronal and interplanetary shock waves. In an earlier paper [Pintér, 1973] I showed that the velocities of solar coronal shock waves computed from the frequency drifts of Type II radio bursts are, on a case-by-case basis, extremely close to the computed initial velocities of interplanetary shock waves. In fact, the two speeds are linearly correlated.

Using densities from the Baumbach-Allen coronal model multiplied by 10, the coronal shock wave velocities observed during STIP Interval II, 20 March - 5 May 1976, were computed from the frequency drift of Type II radio bursts. The relationship between the coronal shock wave velocities, i.e., the initial velocities of interplanetary disturbances ($V_r \equiv V_o$), and the mean velocities of the interplanetary shock waves is discussed below.

Table 1 contains data on the observed solar flares, Type II bursts, and interplanetary shock waves from the period of interest. The interplanetary shock waves were identified by sudden commencements of geomagnetic storms. Table 1 also includes three computed quantities: the Type II shock velocity (V_r) generated from the observed frequency drift; the mean propagation velocity ($\bar{V}_{ob}=R/\Delta t$) of the assumed flare-generated interplanetary shock waves; and the shock wave average velocity ($\bar{V}_{cal}=V_o-d\Delta t/2$). Delta t represents the travel time of each disturbance and was taken as the difference between the onset times of the Type II burst and the geomagnetic SSC; V_o equals the initial velocity of the interplanetary shock wave derived from the Type II frequency drifts; and d represents the degree of shock wave deceleration. The expression $2.8\times10^{-9}V_o^2$ was used for d [Pintér, 1973].

Comparing radial velocities of the coronal shock waves with the mean velocities of the associated interplanetary shock waves (see Table 1) clearly indicates deceleration because $V_r>V_{ob}$. Note too, the agreement between the computed and observed average velocities of each interplanetary shock wave. For those cases investigated the interplanetary disturbance represents a continuation of the coronal shock wave, and during its propagation into interplanetary space, it decelerates.

TABLE 1

SOLAR FLARE				TYPE II SOLAR RADIO BURST						INTERPLANETARY SHOCK WAVES			
DATE 1976	START UT	LOCATION	IMP	START UT	END UT	FREQUENCY (MHz)	IMP	STATION	TYPE II SHOCK Vel(V_r) (km/s)	DATE	SHOCK UT	$\bar{V}_{ob}$ (km/s)	$\bar{V}_{cal}$ (km/s)
March 20	-	E144	-	0203	0216	100-25	3	Culgoora	1480	March 20	2200 (IPS of 3C48)	1305	1260
20	-	E133	-	2255	2310	100-25	1	Culgoora	1390	-	-	-	-
23	0837	S08 E90	SB	0842	0858	300-100	2	Durnten	2590	March 26	0233	731	675
28	1905	S07 E28	1B	1925	1948	80-30	3	Harvard	705	April 1	0255	522	506
April 30	2047	S07 W47	2B	2107	2129	80-30	3	Harvard	1250	May 2	1829	915	893

The author wishes to thank Dr. A. Maxwell of the Harvard Radio Physics Station, Fort Davis, Texas, U.S.A.; Dr. G. J. Nelson of CSIRO Division of Radio Physics, Australia; Dr. H. Urbarz of the Aussenstelle des Astronomischen Institutes der Thuriner, FRG; and Dr. A. O. Benz of the Radio Astronomy Group, Zurich, Switzerland, for providing the radiospectrograms.

REFERENCES

Pintér, Stephen 1973 Close Connection Between Flare-Generated Coronal and Interplanetary Shock Waves, *Nature Physical Science, 243*, 96.

Positions of Satellites 20 March through 5 May 1976

by

R. H. Hilberg, M. J. Teague, and J. I. Vette
IMS/Satellite Situation Center
Code 601, Goddard Space Flight Center
Greenbelt, Maryland 20771 U.S.A.

Introduction

The International Magnetospheric Study/Satellite Situation Center (IMS/SSC) is involved with the display and dissemination of the positions of satellites of interest to magnetospheric physics. This involves both predicted and achieved positions of many geocentric satellites, as well as heliocentric satellites orbiting within 1 AU. With the extension of these techniques to include other heliocentric satellites and planets around which artificial satellites are orbiting, the Study of Traveling Interplanetary Phenomena (STIP) program can be serviced in a manner similar to the IMS program. We demonstrate here some of the techniques used and provide information on a broad range of satellites during the Retrospective World Interval. The SSC and its services to the IMS community have been outlined recently by Sugiura and Vette [1977].

High-Altitude Satellites

The positions of the high-atlitude (apogee above 12 R_E) geocentric satellites have been displayed in a number of coordinate systems relevant to the study of the magnetosphere. The most interesting factors for these satellites are the times when they cross the magnetopause, the Earth's bow shock, or the geomagnetic tail near the neutral sheet. The most concise representation is a daily bar chart that provides a semiquantitative three-dimensional picture of these boundary crossings and traversals through the magnetosheath and magnetotail, as well as through the region of near-Earth space in the interplanetary medium. The predicted orbits for seven such satellites, including the Moon, have recently been provided for the first half of 1977 in IMS/SSC Report No. 7 [1976]. A report will be issued in the future in the same format for the first half of 1976 using the achieved or refined orbits for such satellites and will include the data acquisition times for each one. In addition, it is hoped that the actual boundary crossing times (as opposed to model boundaries) based on the plasma and magnetic field experiments aboard the satellites can be included. An example of this type of display is given in Figure 1. Here the data acquisition periods are shown, but the boundary crossings are based on models instead of actual data.

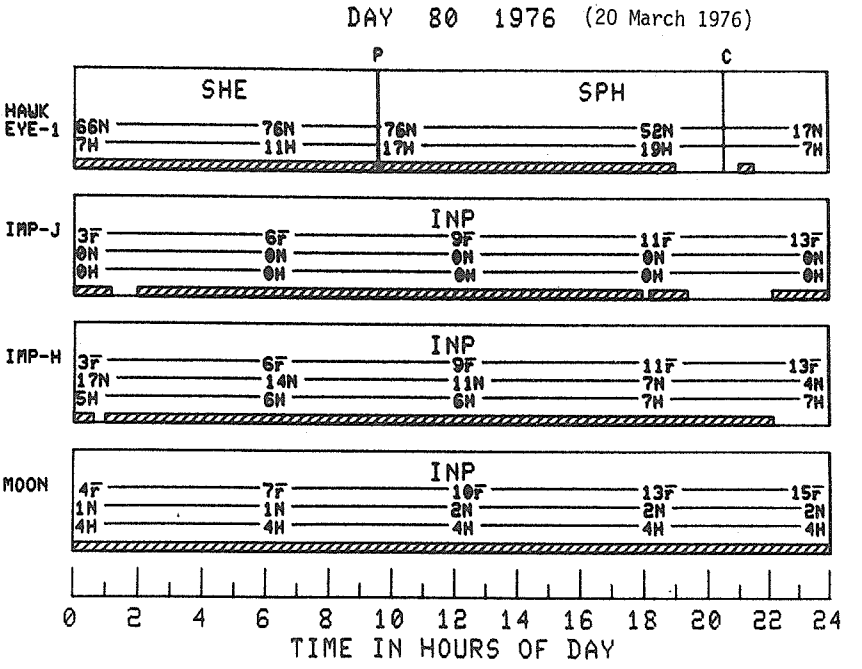

Fig. 1. Bar chart giving positions of four satellites for day 80, 1976 (20 March 1976). This chart indicates the region of space for each satellite and denotes when the satellites cross the magnetopause (P) or enter the cusp (C). Local time and latitude are given for each satellite. When a satellite is interplanetary, the distance from the bow shock in Earth radii is also given. For full details see IMS/SSC Report No. 7.

The bar charts shown in Figures 2 and 3 provide the most pertinent information in a concise manner over the period of 47 days covering the Retrospective World Interval in question. In these charts, the bow shock is denoted by an S and the magnetopause by a P for 11 satellites. The numbers above the symbols give the hour of the day to two decimal places for the model magnetopause crossing times. The numbers below the symbols provide the model bow shock crossing times. On this scale, it is not possible to label each region or to provide the other parameters given in Figure 1. The interplanetary region, denoted by INP, can be labeled in most cases, and the solid line in the center of each row, depicting a specific satellite, indicates this region of space. The magnetosheath region is denoted by a series of dots, and the magnetosphere is denoted by the dashes. When the complete period between two magnetopause crossings is in the magnetotail, this is indicated by the TAL symbol. During certain passes, the satellite comes within 2 R_E of the nominal position of the neutral sheet. These periods are shown by asterisks, where the positions of these symbols indicate the approximate time of day such occurrences appear. The actual times for neutral sheet passes are given in Table 1.

Table 1. Neutral Sheet Passes, Days 80-126 1976 (20 March - 5 May 1976).

Satellite	Date	Entry Time (DOY/h)	Exit Time (DOY/h)
Moon	Apr 13	104/6.48	104/10.91
Moon	13	104/16.34	105/8.66
IMP-H	24	115/17.37	116/1.93
Solrad 11B	29	120/9.52	121/8.66
Solrad 11A	30	121/ 7.24	121/12.82
Solrad 11B	May 4	125/8.86	126/8.34
Vela 5B	4	125/18.30	125/19.00
Solrad 11A	5	126/7.60	126/13.68

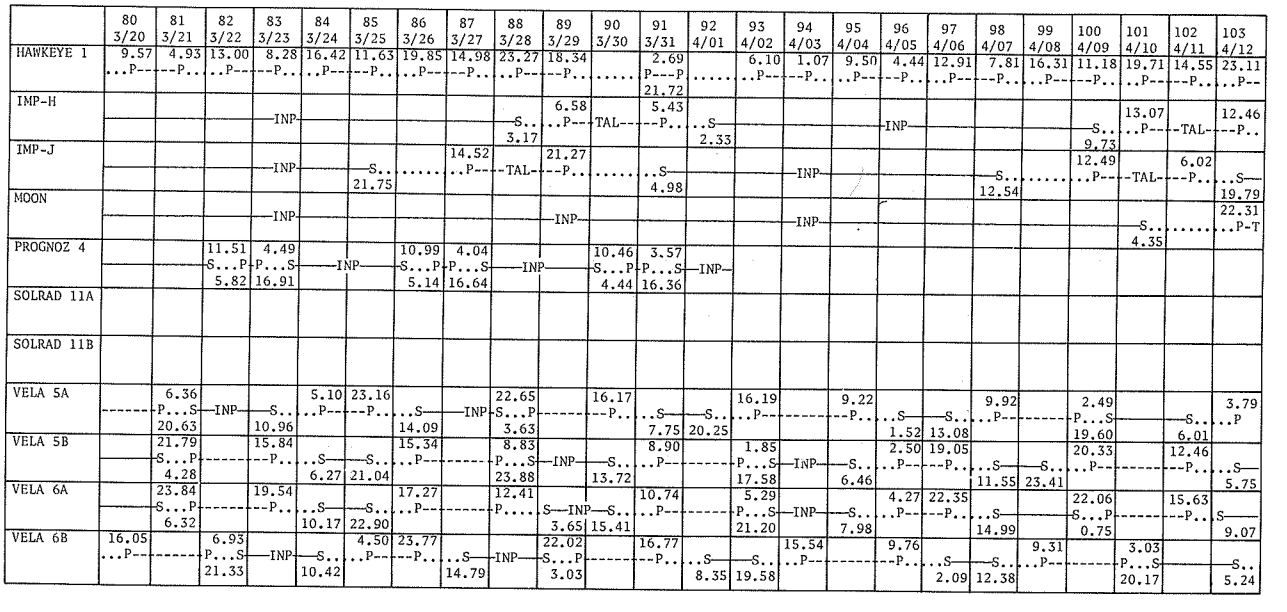

Fig. 2. Bar chart showing locations of 11 satellites during days 80 through 103, 1976 (20 March - 12 April 1976). Solid, dashed, and dotted lines represent the interplanetary medium, the magnetosphere, and the magnetosheath regions, respectively. Numbers above these lines give time of day of magnetopause crossings, those below bow shock crossings. Day of year and calendar dates are given on top row.

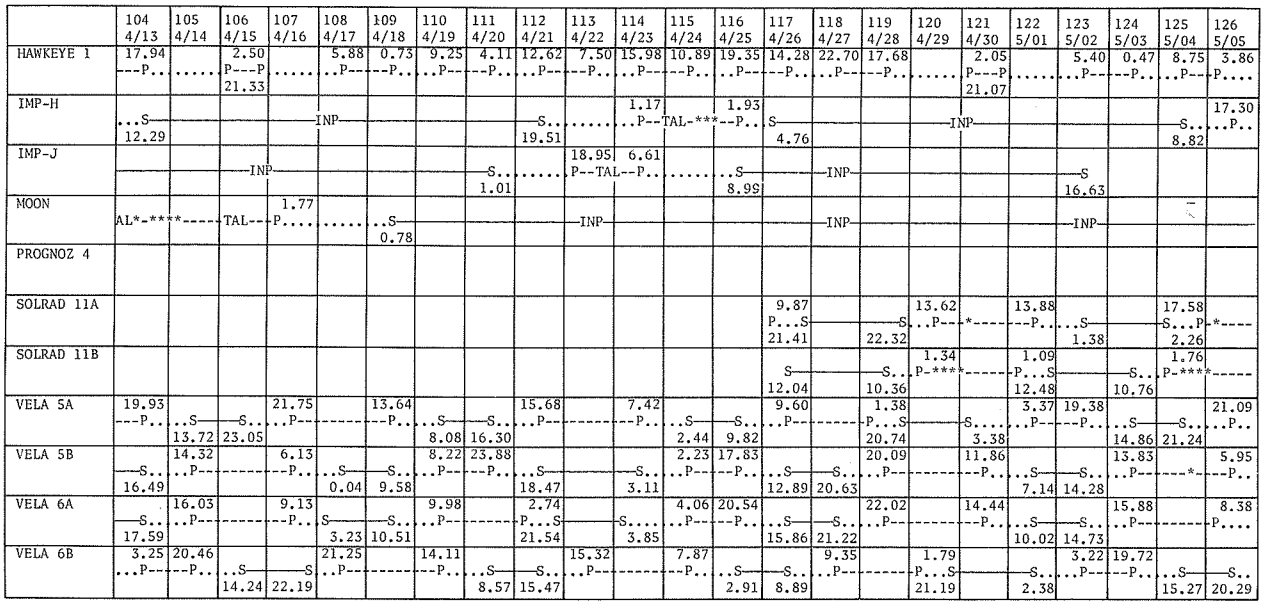

Fig. 3. Bar chart showing locations of 11 satellites during days 104 through 126, 1976 (13 April - 5 May 1976). Solid, dashed, and dotted lines represent the interplanetary medium, the magnetosphere, and the magnetosheath regions, respectively. Numbers above these lines give time of day of magnetopause crossings, those below bow shock crossings. Day of year and calendar dates are given on top row.

The Moon has been included in Figures 2 and 3 because the ALSEP 12 and 15 suprathermal ion detectors were still operating. The ALSEP 12 detector was commanded off on 3 May 1976. Prognoz 4 stopped operating sometime in early spring, but because the exact date is not known, Prognoz 4 is shown through 31 March. Although Solrad 11A and 11B were launched on 15 March, they did not reach their high-altitude orbits until later, and the experiments were not turned on until approximately 22 April. The SSC had orbit elements with the first epoch on 26 April; earlier epoch elements have just been obtained, but not in time to include positions in this paper.

Low- and Medium-Altitude Satellites

There are 17 low- and medium-altitude satellites that carry some experiments useful for obtaining magnetospheric data. The orbit characteristics listed in Table 2 are the only form succinct enough to indicate the satellite positions in this paper. For the geostationary satellites, longitude and drift rate appear instead of perigee and apogee. The experiments that are of interest are included in IMS/SSC Report No. 9 [1977].

Heliocentric Satellites

The positions of the heliocentric satellites are presented in Figure 4 as projected onto the ecliptic plane in a coordinate system that rotates with the Earth. Pioneer 7 does not appear because it was turned off on 10 February 1976, and Pioneer 10 was too far away from the Sun to be shown conveniently on the chosen scale. The planet Venus is shown because Venera 9 and 10 were operable during this period.

Concluding Remarks

The approximate positions of 35 satellites during the period 20 March through 5 May 1976 have been presented to aid those interested in studying traveling interplanetary phenomena during the Retrospective World Interval. Those desiring more details may contact the IMS/Satellite Situation Center.

Table 2. Orbital Characteristics of Low- and Medium-Altitude Satellites

Satellite Name	Epoch (D/M/Y)	Period (min)	Incl.	Perigee (km alt)	Apogee (km alt)	Longitude	Drift/Day
AE-C	30/6/76	90.2	67.9°	283	294	--	--
AE-E	30/6/76	102.4	19.6°	151	1589	--	--
ATS 5	30/6/76	1436.2	3.4°	--	--	105.26°W	0.006°W
ATS 6	30/6/76	1436.2	0.1°	--	--	33.63°E	0.0104°E
DMSP Series	--	~101.0	~99°	~800	~875	--	--
GOES 1	30/6/76	1436.0	0.4°	--	--	75°W	0.031°W
INTERCOSMOS 14	11/12/75	105.2	74°	345	1707	--	--
ISIS 1	30/6/76	128.2	88.4°	579	3516	--	--
ISIS 2	30/6/76	113.6	88.1°	1358	1428	--	--
NOAA 3	30/6/76	116.1	101.9°	1504	1512	--	--
NOAA 4	30/6/76	114.9	101.6°	1447	1461	--	--
SMS 1	30/6/76	1436.2	2.0°	--	--	104°W	0.0054°E
SMS 2	30/6/76	1436.3	0.2°	--	--	135°W	0.014°W
Solrad 10	30/6/76	94.6	51°	425	577	--	--
SRATS	30/6/76	117.7	31.5°	247	2907	--	--
S3-2	Planned	96.0	97°	230	900	(actually orbited in late 1975)	
TIP 1	30/6/76	100.6	90.0°	737	841		

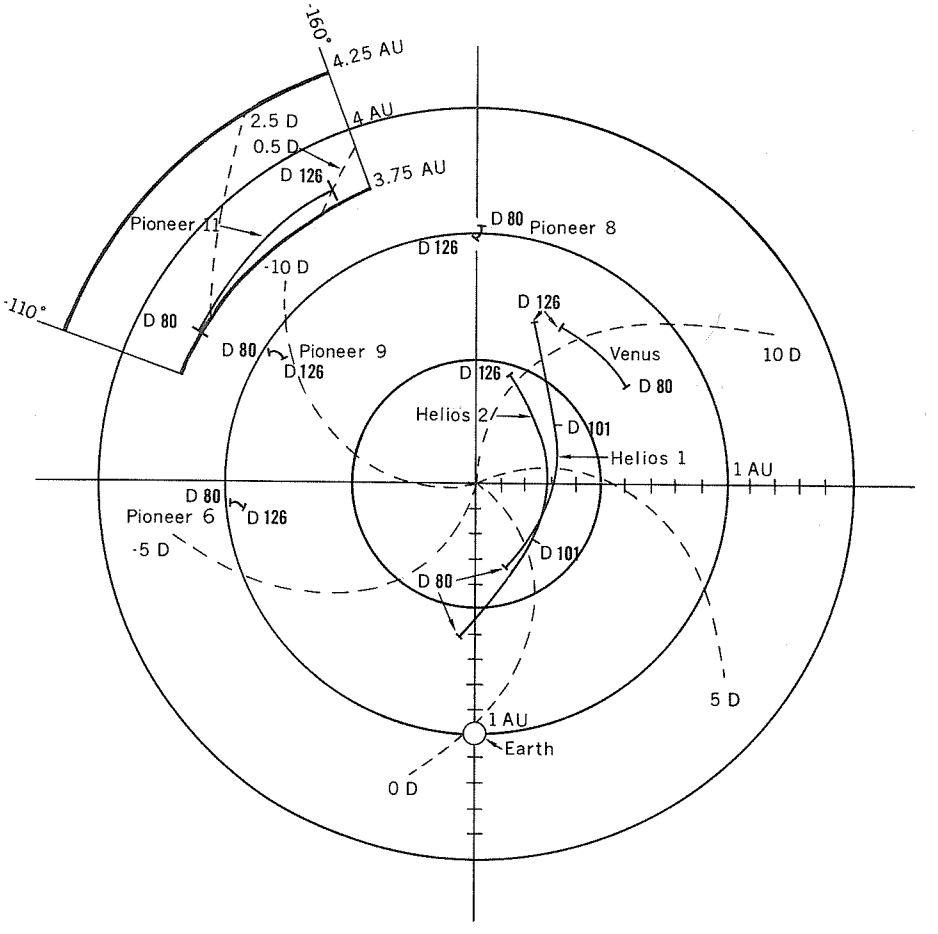

Fig. 4. Heliocentric orbits projected onto the ecliptic plane. Radial distance (in AU) is plotted as a function of right ascension relative to the Earth. The dashed curves give corotation delay times in days.

REFERENCES

SUGIURA, M., and J. I. VETTE	1977	"The IMS Satellite Situation Center", *Trans. AGU, 58,* 70-74.
IMS/SSC Report No. 7	1976	Daily Summary for IMS High-Altitude Satellites, Days 1-181 1977 (October 1976), WDC-A, National Space Science Data Center, (GSFC, Greenbelt, MD 20771 U.S.A.).
IMS/SSC Report No. 9	1977	IMS Directory of Spacecraft and Experiment Scientific Contacts (January 1977), WDC-A National Space Science Data Center, (GSFC, Greenbelt, MD 20771 U.S.A.).

MeV Protons, Alpha Particles and Electrons as Observed Aboard HELIOS 1 and 2 During STIP Interval II

by

H. Kunow, R. Müller-Mellin, B. Iwers, M. Witte, H. Hempe
G. Wibberenz, G. Green, J. Fuckner
Institut für Kernphysik, Universität Kiel, 2300 Kiel, Fed. Rep. Germany

The HELIOS 1 and 2 spacecraft, which were launched on 10 December 1974 and 15 January 1976 respectively, are spin stabilized space probes with highly excentric orbits around the sun in the ecliptic plane. The trajectories of both spacecraft, starting with the launch day of HELIOS 2 through the end of 1976, are shown in Figure 1. The STIP Interval II includes the perihelion passages of HELIOS 1 at 0.31 AU and HELIOS 2 at 0.29 AU with HELIOS 1 preceding HELIOS 2. The open and solid circles mark the positions of HELIOS 1 and 2 at the time of the solar particle events during this period as observed by the University of Kiel Cosmic Ray Experiment.

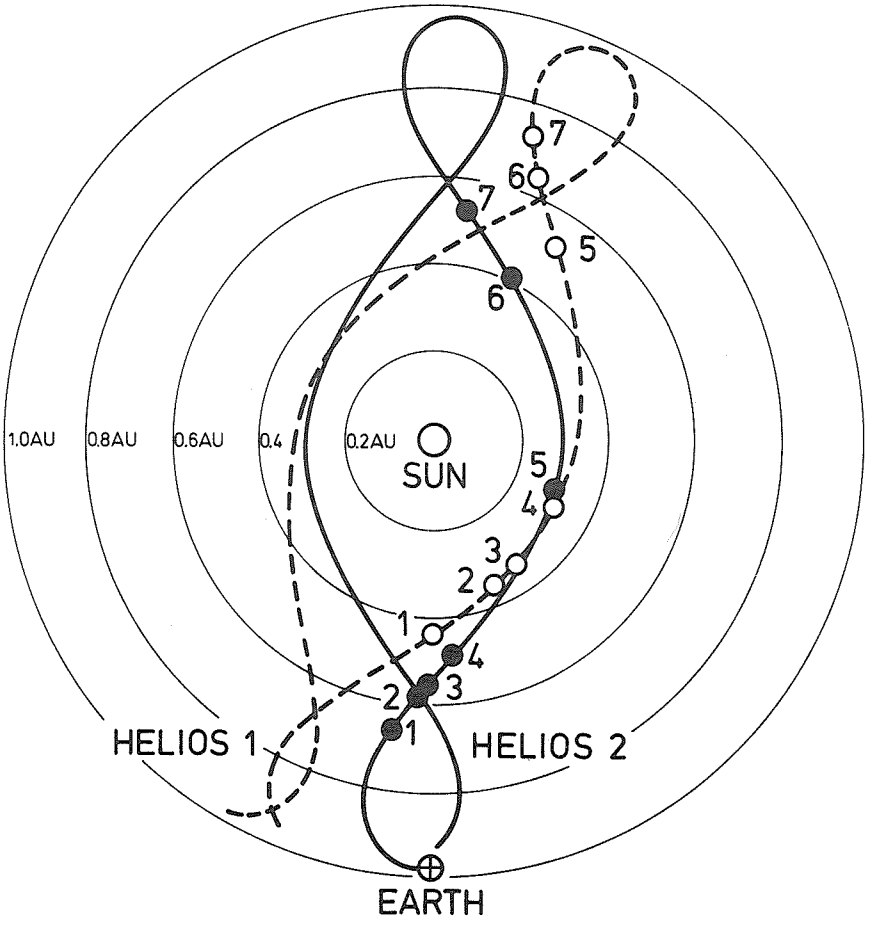

Fig. 1. HELIOS 1 and 2 orbits with respect to a fixed earth-sun line. The open and solid circles mark the positions of HELIOS 1 and 2 at the time of the solar particle events during STIP Interval II.

The detector telescope, described in detail by Kunow *et al.* [1975], is shown schematically in Figure 2. It consists basically of five solid state detectors 1...5 surrounded by an anticoincidence scintillator A. Penetrating particles are further analyzed by a sapphire Cerenkov detector C. The 100-micron thick, surface barrier, silicon detector 1 is used to discriminate between electrons and nucleons.

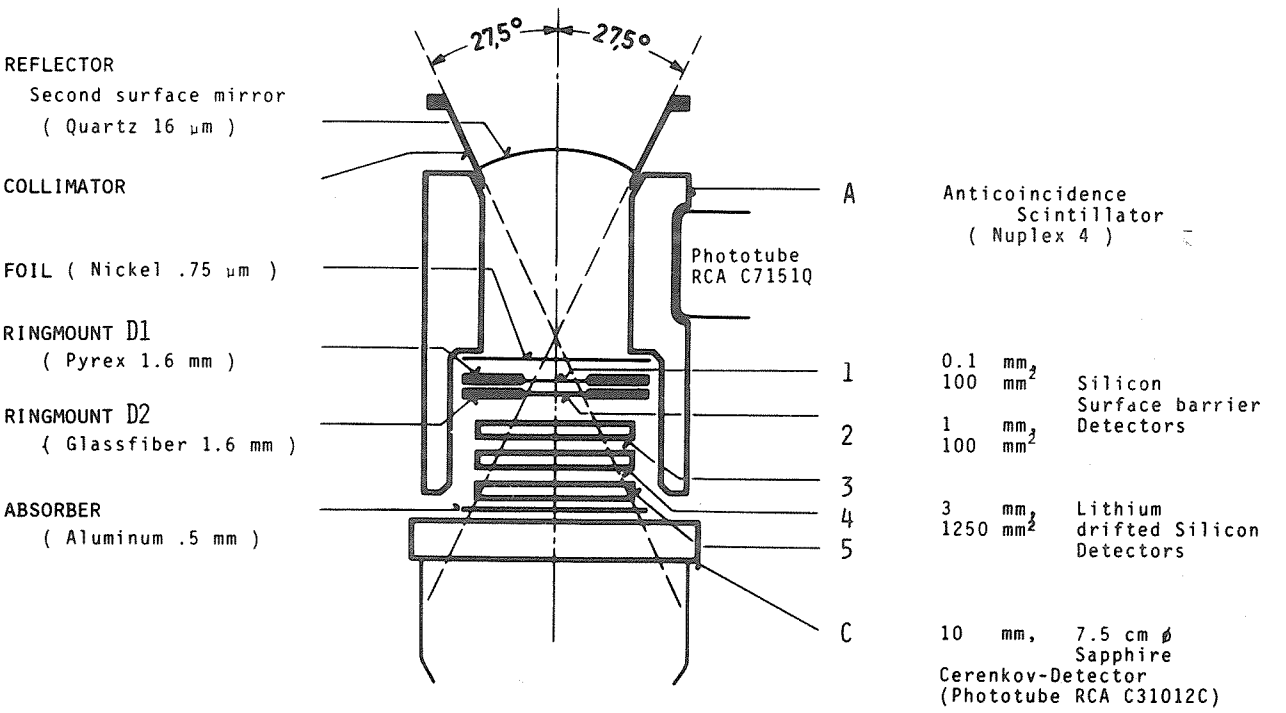

Fig. 2. Schematic cross section of the detector telescope of the University of Kiel Cosmic Ray Experiment on board HELIOS 1 and 2.

Table 1 summarizes some of the experiment characteristics. In column 1 "Acronym" identifies particle species: P for protons, A for nucleons with $Z \geq 2$, and E for electrons. The numbers indicate roughly the lower energy thresholds (in MeV/N) of that counting rate channel. If a second number appears, it indicates the upper energy threshold of that channel. For each particle species the precise values of the energy thresholds are given in columns 2 and 3 for HELIOS 1 and 2 respectively; the geometric factors are given in columns 4 and 5; and those detectors that are pulse height analyzed (PHA) and indicated in column 6. Whether or not the direction of incidence in eight, 45°-wide sectors is determined is given in column 7. Note that the energy thresholds for electrons are only rough estimates due to scattering in the detector system. The time resolution of the counting rates for the above energy channels depends on telemetry bit rate and varies between 13.5 s and 43.2 min.

Table 1. Experiment Characteristics of HELIOS 1 and 2.

Acronym	Energy Window (MeV/N) HELIOS 1	HELIOS 2	Geometric Factor (cm^2sr) HELIOS 1	/ HELIOS 2	Detectors with PHA	No. of Sectors
P1	1.3 - 3.8	1.7 - 3.7	0.48	0.43	-	8
P4	3.8 - 12.8	3.7 - 12.7	0.48	0.43	1,2	8
P13	12.8 - 26.8	12.7 - 27.4	0.48	0.43	1,2,3	8
P27	26.8 - 36.6	27.4 - 37.3	0.48	0.43	2,3,4	8
P37	36.6 - 50.7	37.3 - 51.0	0.48	0.43	3,4,5	1
P51	> 50.7	> 51.0	2.23	2.23	4,5,C	8
A2	1.7 - 3.7	2.0 - 3.6	0.48	0.43	-	8
A4	3.7 - 12.7	3.6 - 12.6	0.48	0.43	1,2	8
A13	12.7 - 26.6	12.6 - 27.2	0.48	0.43	1,2,3	8
A27	26.6 - 36.5	27.2 - 37.2	0.48	0.43	2,3,4	1
A37	36.5 - 48.1	37.2 - 48.3	0.48	0.43	3,4,5	1
A48	> 48.1	> 48.3	2.23	2.23	4,5,C	1
E0.3	$\gtrsim$ 0.3	$\gtrsim$ 0.3	0.49	0.46	-	8
E0.8	$\gtrsim\gtrsim$ 0.8	$\gtrsim\gtrsim$ 0.8	0.49	0.46	2,3	8
E2	$\gtrsim\gtrsim$ 2.0	$\gtrsim\gtrsim$ 2.0	0.49	0.46	2,3,4	1
E3	$\gtrsim$ 3.0	$\gtrsim$ 3.0	0.49	0.46	3,4,5*	1

* only HELIOS 1

Very close to solar minimum a period of increased solar activity occurred between March and May 1976. Figure 3 shows the hourly averages of selected HELIOS 1 counting rates. There are at least six well-defined intensity increases, numbered 1 through 7 with number 4 left out for reasons to be explained later. The individual events, some of them with a complex structure, are most clearly resolved in the 4-13 MeV proton range.

Event 1 has a steep energy spectrum for proton and alpha particles, but it contains no electrons. Event 2 shows the presence of electrons, and in channel A2 it displays a remarkably high helium content - one amounting in channel A4-13 (not shown in Figure 3) to 50% of the proton intensity. Note also the very short rise time and fast decay of this event.

Event 3 is complex, consisting of at least three clearly separable peaks and exhibiting the highest proton flux observed by HELIOS 1 in the period under discussion. The first peak of this event with its short rise and decay times is detectable even in the high energy proton channel P>51. Note also the subsequent Forbush decrease in this channel, which lasts for several days, indicating disturbances in the interplanetary medium.

Event 5 closely resembles event 1, having a similar time profile, energy spectrum, proton to alpha ratio, and absence of electrons. Events 1 and 5 are classified as recurrent because they can be associated with the same corotating interplanetary structure.

Event 6 shows high proton intensities with a flat energy spectrum, but it contains few alpha particles. Electrons are present with a similar time behavior as the protons. Event 7 rides on the decay phase of event 6 and is characterized by short rise and decay times for electrons and for low energy protons and alpha particles.

Figure 4 shows the corresponding counting rates as observed by HELIOS 2 on the same time scale as in Figure 3. Most of the events are also seen by HELIOS 1, but there are characteristic differences which can be used to study coronal and interplanetary propagation effects. The numbering of the events in Figure 4 is equivalent to Figure 3; this time, however, event 4 is marked but event 5 is missing.

Event 4 is detected in all channels with a marked increase also evident in the high energy proton channel P>51. The peak in the P>51 channel is followed by a sharp Forbush decrease. To explain why HELIOS 1 failed to observe the event requires additional information. A comparison of the coronal longitude for both space probes with the Hα synoptic chart suggests that HELIOS 2 is inside the fast propagation cone for McMath flare region 14143, whereas HELIOS 1 is connected to a source region which is separated from the flare region by a neutral line.

Why the recurrent event 5 is detected by HELIOS 1 but not by HELIOS 2 may be due to the latitudinal separation of the two space probes. By the time HELIOS 2 is connected to the Carrington longitude of event 5, it is only at 0.8° above the equator, whereas HELIOS 1 at the time of event 5 is 7° north.

Event 6 is displayed on an expanded time scale in Figures 5 and 6 as seen by HELIOS 1 and 2. These particles might have been released from region 14179 (14143 and 14118 in previous rotations). On 30 April Earth observations include a flare in this region, the first 2B flare in more than a year. Although the two space probes are connected via magnetic field lines to solar longitudes separated from the flare regions by 160° and 140°, there is a remarkable intensity increase in the proton channels for both spacecraft. A noticeable difference exists, however, in the onset characteristics between HELIOS 1 and HELIOS 2.

See Kunow *et al.* [1976] for the more detailed report presented at the annual fall meeting of the AGU.

REFERENCES

KUNOW, H., G. WIBBERENZ, G. GREEN, R. MÜLLER-MELLIN M. WITTE, H. HEMPE 1975 Das Kieler Experiment zur Messung der Kosmischen Strahlung zwischen 1.0 und 0.3 AE, *Raumfahrtforschung, 19,* 253-257.

KUNOW, H. G. WIBBERENZ, G. GREEN R. MÜLLER-MELLIN, M. WITTE, H. HEMPE 1976 Solar Cosmic Ray Particle Events Detected with HELIOS Between 0.3 and 1.0 AU, *Transactions, American Geophysical Union, 57,* 978.

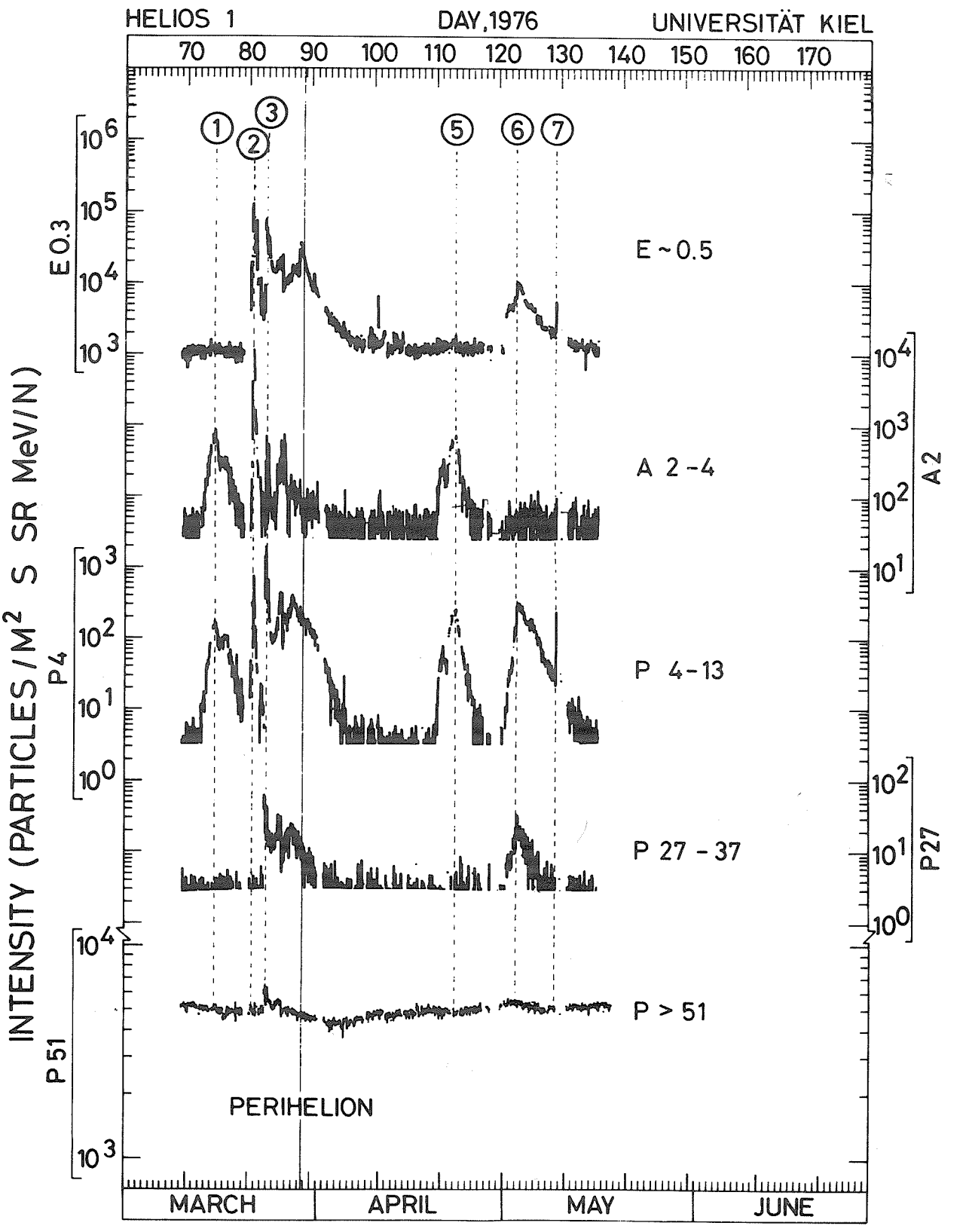

Fig. 3. Hourly mean intensities as measured by HELIOS 1 during STIP Interval II.

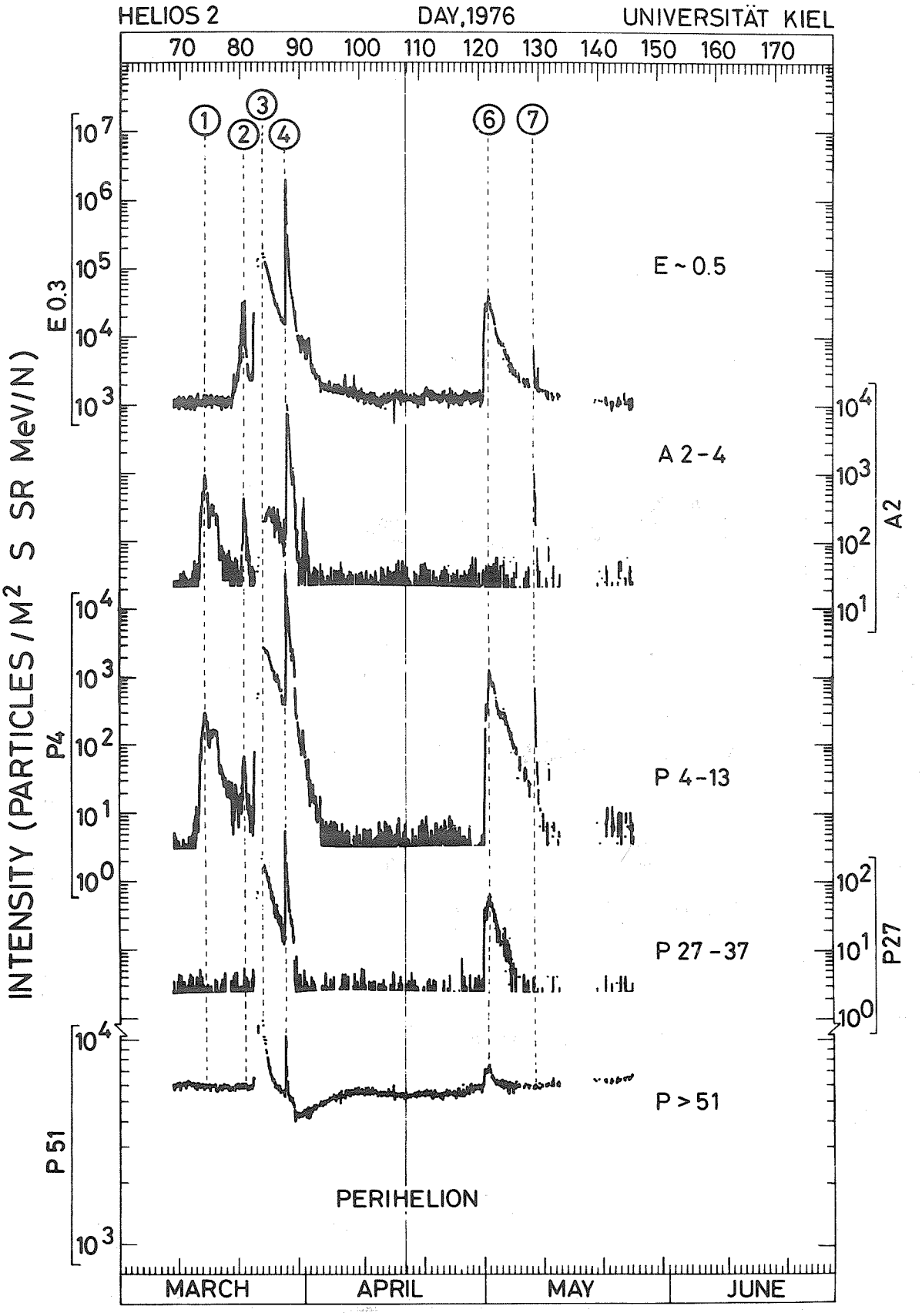

Fig. 4. Hourly mean intensities as measured by HELIOS 2 during STIP Interval II.

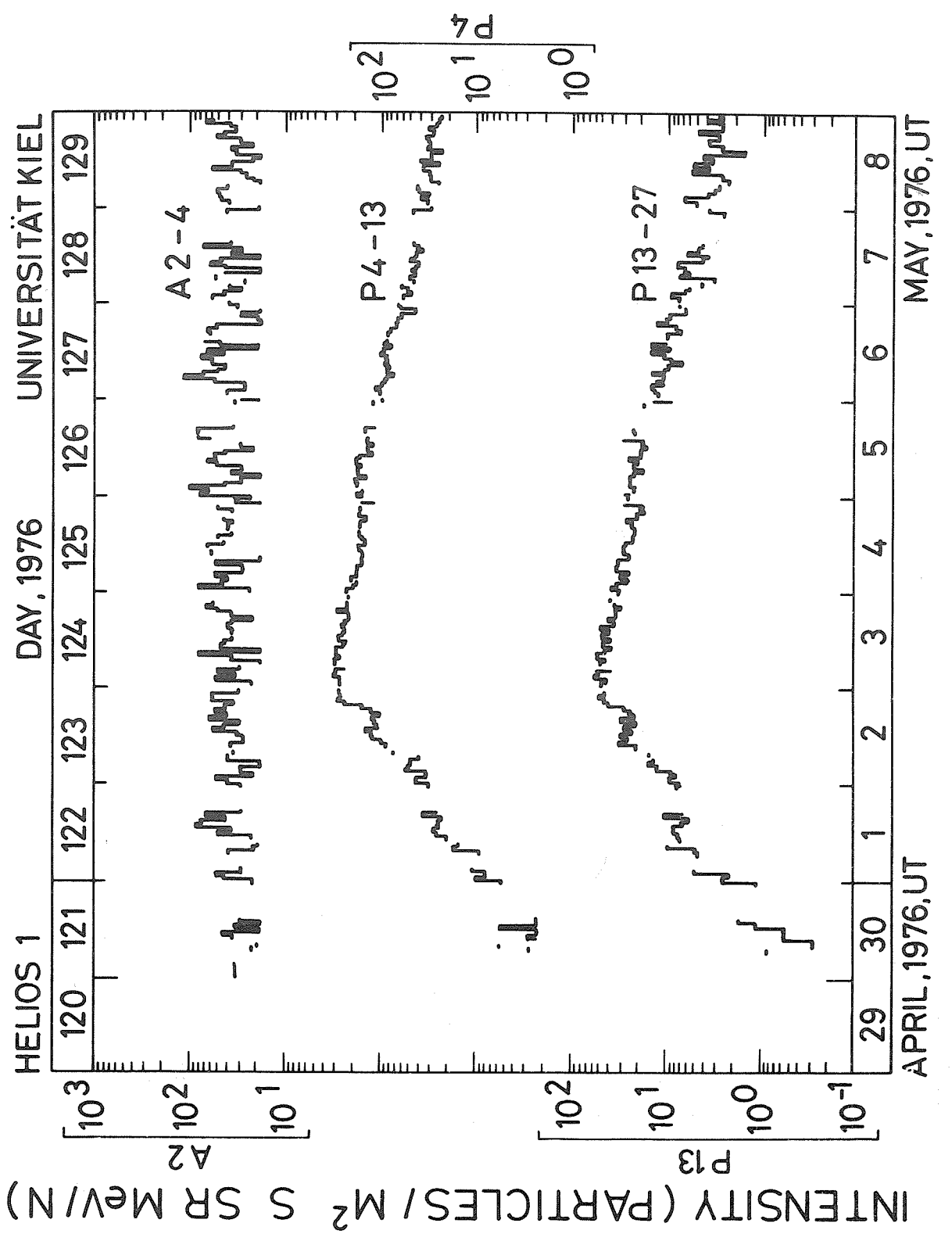

Fig. 5. Hourly mean intensities for the time period of even 6 as measured by HELIOS 1.

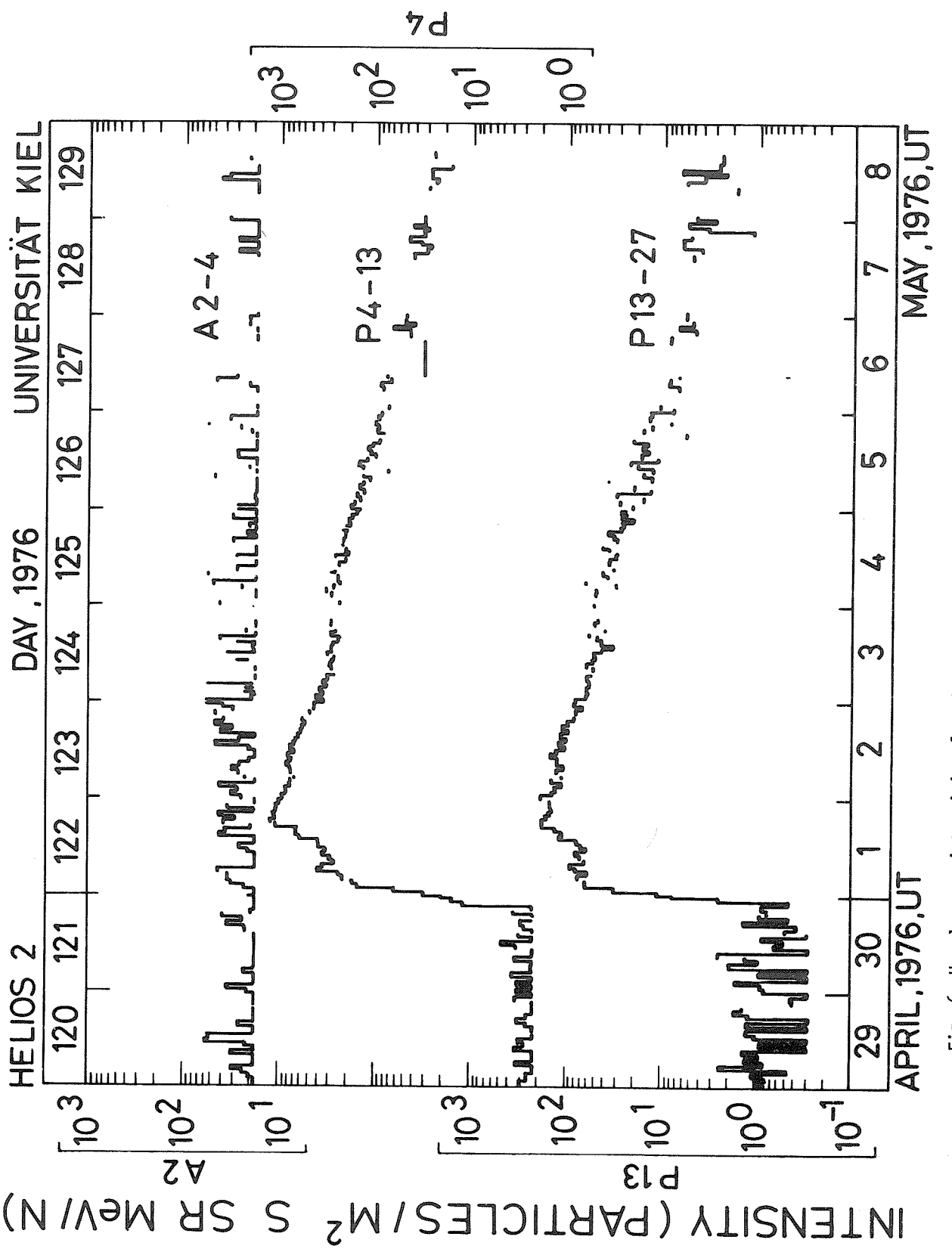

Fig. 6. Hourly mean intensities for the time period of event as measured by HELIOS 2.

Low-Energy Electron (> 20 keV) and Proton (> 80 keV) Observations on Board Helios-1 and -2 During March - May 1976

by

A. K. Richter, E. Keppler and K. Richter
Max-Planck-Institut für Aeronomie
3411 Katlenburg-Lindau 3, Germany

The German-US space probes HELIOS-1 and -2 were launched on 10 December 1974 and 15 January 1976 into heliocentric orbits with aphelions of about 1 AU and perihelions of 0.31 and 0.29 AU, respectively. The spacecrafts are spinning at a rate of about one revolution per second with their spin axis normal to the ecliptic plane. The antenna of HELIOS-1 is pointing to the north, of HELIOS-2 to the south. HELIOS-1 spins counterclockwise when viewed from the north. The two space probes are tracked by the Deep Space Network (DSN) and by the German stations Effelsberg and Weilheim. HELIOS also has the capability to store data on board in a 500 kbit memory. Thus, if the spacecrafts are not tracked directly, scientific data from both satellites are available for nearly 24 hours per day. Only when the space probes are behind the sun (blackout phase) are data not obtained continuously.

To measure low-energy, keV electrons, protons, and positrons deep in interplanetary space, both HELIOS-1 and -2 carry on board a low-energy charged particle spectrometer from the Max-Planck-Institut für Aeronomie (MPAE). The apertures of these instruments have an acceptance cone of 20° full angle, and they are pointing out at an angle of 7° relative to the normal of the spin axis. The spectrometer is thus scanning approximately in the ecliptic plane. As shown in Figure 1, the measurements are performed first by separating the electrons, protons, and positrons in an inhomogeneous magnetic field of $\sim$ 800 gauss maximum, and then by detecting these particles with separate semiconductor detectors. Electrons are deflected according to their rigidity onto four different detectors (electron detectors), while the protons traverse the magnetic field almost unaffected and enter a two-detector telescope arrangement (proton telescope). The signals from the electron detectors and from the front detector of the proton telescope in anticoincidence with its back detector are subsequently amplified and passed into one 16-channel pulse height analyzer. Thus, protons and electrons are measured separately in 16 energy channels, ranging from 80 - 6200 keV for protons and 16 - 2000 keV for electrons on HELIOS-1. These proton and electron energy limits on HELIOS-2 are 87 - 6200 keV and 20 - 2000 keV. At the same time, while the space probe is spinning, these measurements are divided into 16 sectors. Therefore two different sets of proton and electron measurements are available: spectral measurements in 16 energy channels for certain directions and energy-integral measurements in all 16 directions simultaneously. In addition, observations of protons > 6200 keV, of positrons in the energy range 150 - 550 keV, and of the background due to high-energy cosmic rays are obtained. The time resolution of the instrument depends on the bit rate of the space probes, which varies from 8 - 4096 bps. At the highest bit rate energy-integral, angular distributions for electrons or protons are obtained every 13.5 s; a full set of spectral measurements in all 16 directions takes 108 s. At low bit rate a reduced format is used; at the lowest bit rate of 8 bps, a full set of information from 8 directions instead of 16 requires 19 min. Finally, we emphasize that this spectrometer measures for the first time low-energy electrons and protons deep in interplanetary space with high resolution in time, energy, and direction.

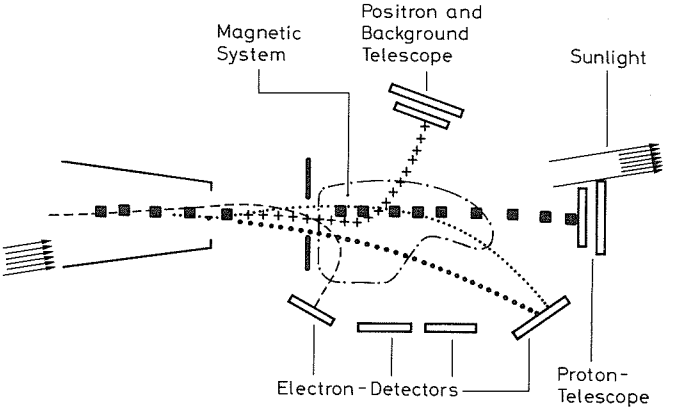

Fig. 1. Principle of detection of low-energy electrons, protons, and positions by the MPAE charged particle spectrometer.

In Figure 2 we plot the heliocentric trajectories of Earth, HELIOS-1, HELIOS-2, and Mercury from the beginning of March to the end of May 1976. The distances between the various dots represent the fraction of the orbit traversed in 5 days. A number of interesting configurations - radial and/or magnetic field line ups - occur between HELIOS-1 and -2 and Earth during this special time interval (STIP II interval).

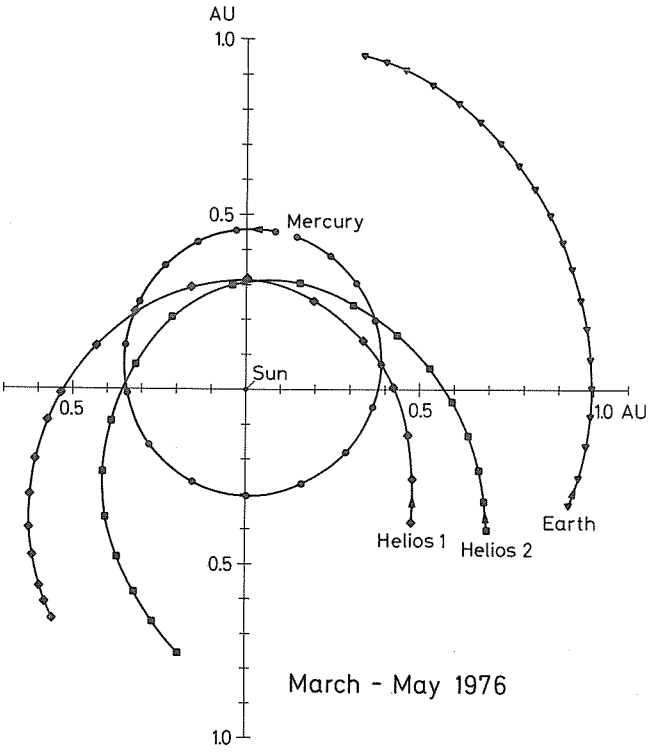

Fig. 2. Positions of HELIOS-1, HELIOS-2, Earth, and Mercury from 1 March to 31 May 1976 in heliocentric coordinates. Distance between the dots corresponds to 5 days.

In Figures 3 and 4 the intensity(counts/seconds)-time profiles of the low-energy electrons and protons and of the cosmic ray background are shown, as observed by HELIOS-1 and -2 during March - May 1976. For these plots we used energy-integral data of the finest time scale, averaged over the 16 angular directions. The dead layers in front of the first electron and proton detectors determine the energy ranges $E_e > 16$ keV and $E_p > 80$ keV, for HELIOS-1 and for HELIOS-2 these two lower limits are 20 keV and 87 keV. Despite a thicker dead layer, the first electron detector on HELIOS-2 encounters an increasing amount of scattered sunlight during perihelion because it approaches the sun closer than its counterpart on HELIOS-1. Thus, at the end of March 1976, the electron intensity increases continuously, as can be seen from Figure 4. During April and May this detector was switched off, increasing the lowest electron energy threshold of the experiment to ~100 keV. Except for this incident all other detectors and the entire electronic system behaved very well on both HELIOS-1 and -2. It should be noted that in Figures 3 and 4 we have subtracted the entire background from the electron and proton channels. Because the data coverage of HELIOS-1 during May 1976 was still too poor at the time this report was written, we omitted these electron and proton intensity-time histories from Figure 3.

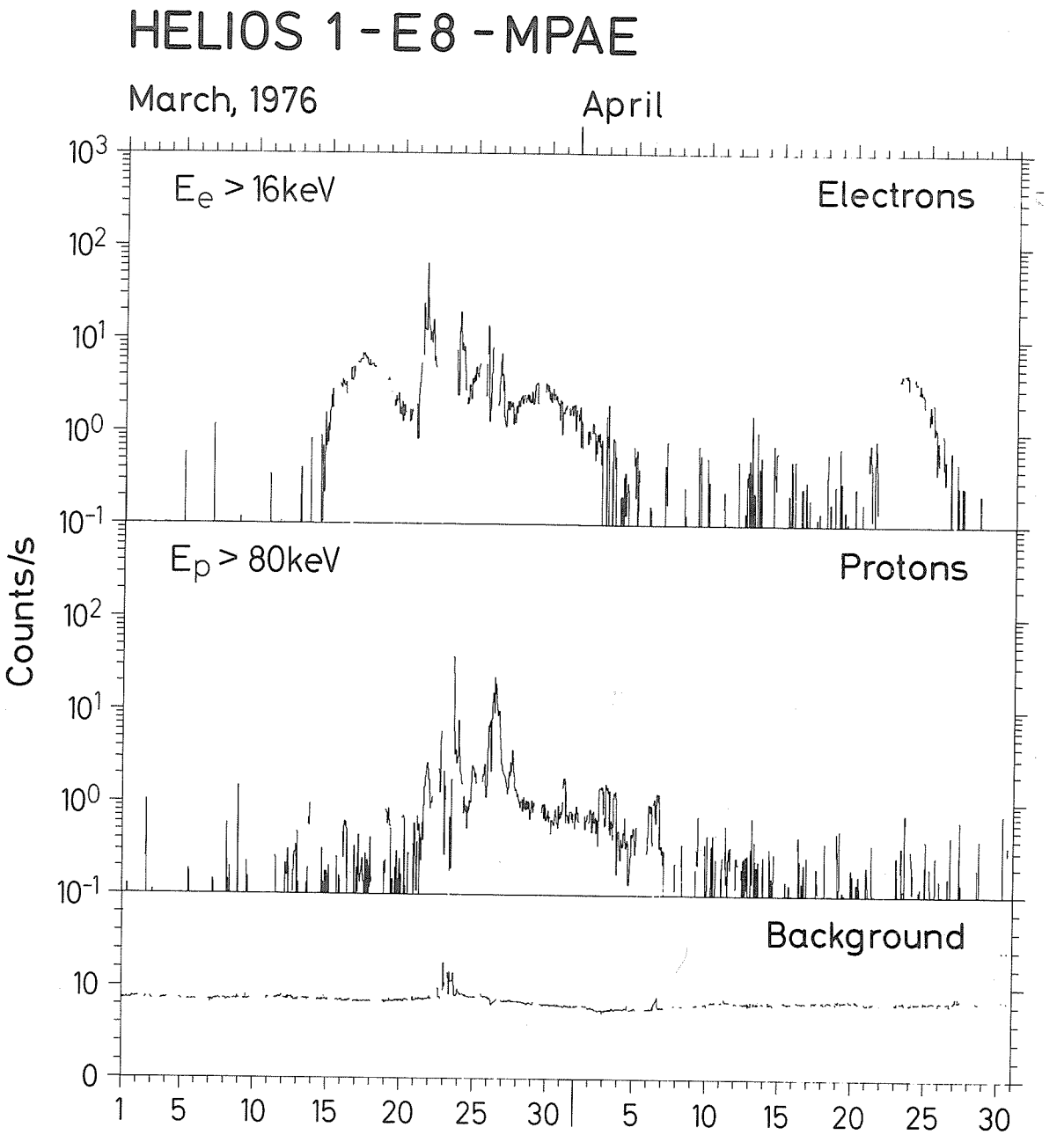

Fig. 3. Time profiles of the energy-integral, of the omnidirectional electron and proton counting rates, and of the background intensities as observed by HELIOS-1 during March - April 1976. In the electron and proton plots the background is subtracted.

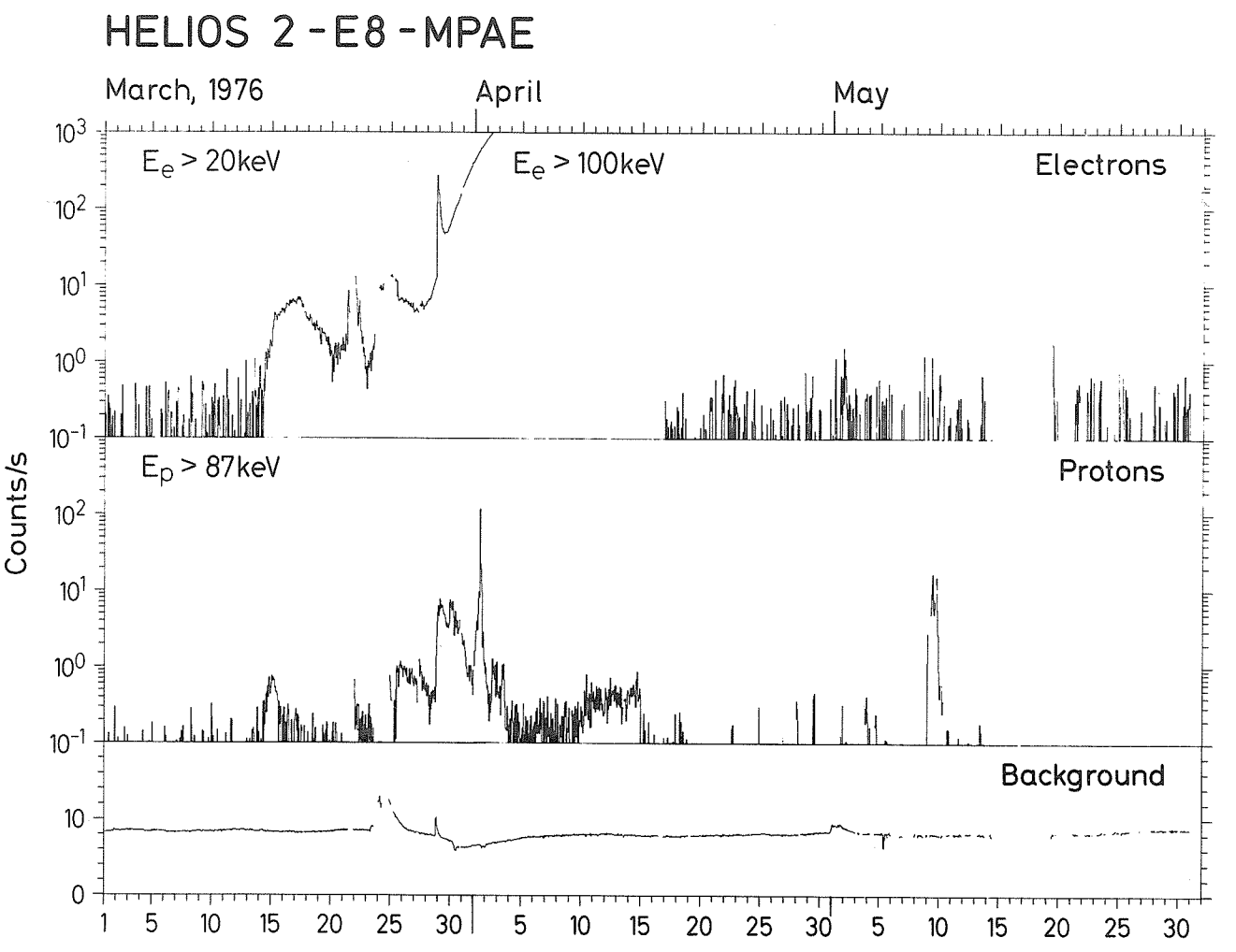

Fig. 4. Time profiles of the energy-integral, of the omindirectional electron and proton counting rates, and of the background intensities as observed by HELIOS-2 during March - May 1976. In the electron and proton plots the background is subtracted.

Solar and Interplanetary Particles Observed in the Interval 20 March Through 5 May with IMP 8

by

T. P. Armstrong and R. B. Decker
University of Kansas
Lawrence, Kansas 66045 U.S.A.

and

S. M. Krimigis and J. W. Kohl
Applied Physics Laboratory
The Johns Hopkins University
Laurel, Maryland 20810 U.S.A.

Introduction

These data are derived from the Charged Particle Measurement Experiment (CPME) instrument aboard IMP 8. This instrument is a solid state detector telescope that measures electrons, protons, alpha particles, medium nuclei, and heavy ($Z \geq 20$) nuclei fluxes. These detectors are described elsewhere [Sarris *et al.*, 1976; Armstrong and Krimigis, 1976; Armstrong *et al.*, 1977].

To characterize the solar particle fluxes for this time period we selected representative data channels and made 3-hour averages of the spin-averaged count rates. The channels we use are P4, protons; A3, alpha particles; Z1, medium nuclei; Z3, iron group nuclei; and E4, electrons. The passbands are given in Table 1. The geometric factor of all channels is 1.51 cm^2 sr.

Table 1. Selected Passbands From the Charged Particle Measurements Experiment.

Channel	Ion Species	Passband
P4	Protons	$2.0 \leq E_p \leq 4.6$ MeV
A3	Alpha Particles	$1.8 \leq E_\alpha \leq 4.2$ MeV/nucleon
Z1	Carbon, Nitrogen, Oxygen	$0.7 \leq E \leq 3.3$ MeV/nucleon
Z3	$Z \geq 20$	$3.1 \leq E \leq 8.8$ MeV/nucleon
E4	Electrons	$E > 0.22$ MeV

To average the data we divided the day into uniform 3-hour segments beginning with hour 0. In the tabulations and plots we used day of the year (DOY) in which day 1, e.g., is 1 January, etc. For the sake of brevity in this presentation, we included only IMP 8 data, however, in preparing the annotations on the plots and in the event summary of Table 2, we referred to the entire IMP 7 and 8 data set at 5-minute average time resolution.

The location of the spacecraft was considered in the identification of some of the electron responses as magnetospheric bursts. For the general identification of solar particle fluxes, however, and at the particle energies we present here, the location of the spacecraft in its nominal 35 R_E orbit is only of minor importance and we have not included it. Orbital information for IMP 8 (J) is available elsewhere [WDC-A/NSSDC, 1975].

The next section gives a brief description of the main features of the intensity versus time profiles shown in Figures 1-5. A chronology of all the major particle increases is given in Table 2, and tabulation of the 3-hour average rates is given in the Appendix.

Description of the Plots

The graphs of 3-hour average count rate versus time are presented in histogram style with the ± one standard deviation of the count rates shown. Tick marks are given at one-day intervals on the time axis. Figure 1 shows a plot of the count rate of the >0.22 MeV electron channel (E4) in which a variety of phenomena are shown. Flare events are probably present on 21 (DOY 81), 26 (DOY 86), and 28 (DOY 88) March and on 21 (DOY 112) and 30 (DOY 121) April. We have attributed those on 26 and 28 March to McMath Region 14143 and on 21 April to 14179. Those on other days appear to have onset times more closely following flares in other regions as determined from the grouped Hα flare data in the Comprehensive Reports [SGD, 1976]. The electron increases identified with flares in region 14143 are denoted by open circles and those in 14179 by filled circles. The most prominent magnetospheric electron bursts are also denoted in Figure 1. The background rate of the E4 channel is about 0.22 counts/s due to omnidirectionally penetrating cosmic rays.

Table 2. Chronology of Major Solar and Interplanetary Energetic Particle Effects, 20 March through 5 May 1976.

Day of Year	Date 1976	Time (UT)	Comments
81	Mar 21	0820	Onset of >0.22 MeV electrons. Probable source was 1B (N04 W29) flare having onset at 0750 UT in McMath Region 14127.
		≈1200	Onset of protons, alphas, and mediums from above flare.
		1320	Onset of >0.22 MeV electrons. Probable source was -N (N03 W33) flare having onset at 1306 UT in McMath Region 14127.
		1910	Onset of >0.22 MeV electrons. Probable source was -B (N03 W34) flare having onset at 1829 UT in McMath Region 14127.
		2300	Onset of >0.22 MeV electrons. Probable source was -N (N03 W37) flare having onset at 2228 UT in McMath Region 14127.
83-86	23-26	0900 1200	Probable Jovian >0.22 MeV electron fluxes at Earth.
85	25	≈0900	Alpha particle onset probably from activity in McMath Region 14143; -F (S06 E74) flare having onset at 0914 UT possible source.
86	26	0300-1000	Large, irregular modulation of interplanetary ion and electron intensities. This may be associated with the SSC disturbance of 0233 UT.
		1100-1200	Electron and ion onset from uncertain but probable eastern hemisphere flare. McMath Region 14143; -B (S06 E65) flare with onset at 0715 or -N (S09 E59) flare with onset at 0830 UT are likely sources.
88	28	1935	Onset of >0.22 MeV electrons from 1B (S07 E28) flare in McMath Region 14143 having onset of 1905 UT.
		2200	Ion onset from above flare. This epoch is comparatively poor in $Z \geq 20$ nuclei.
92	Apr 01	0255	SSC-associated spike in interplanetary ions and electrons.
101-106	10-15	----	Slow increase to several peaks of interplanetary ion intensities. These fluxes were comparatively rich in alpha particles and medium heavy nuclei. There were no discernible electrons in this particle increase.
112	21	0415	Probable ion and electron onset from uncertain flare in McMath Region 14161; 1F (N03 W77) with onset at 1740 UT on 20 April is the closest possibility.
116-120	25-29	----	Interplanetary particle increase. Flare association is uncertain. These fluxes were comparatively rich in alpha particles and medium heavy nuclei but lacked electrons.
121	30	0600	Very small onset of >0.22 MeV electrons. Possible source was a -F (S08 W38) flare with onset at 0557 UT in McMath Region 14179.
		1250	Onset of >0.22 MeV electrons from flare in McMath Region 14179; -N (S06 W41) having onset at 1242 UT is the closest possibility. This was a small electron event. No associated ions were identified.
		2115	Onset of >0.22 MeV electrons from flare in McMath Region 14179; 1B (S08 W46) having onset at 2047 UT.

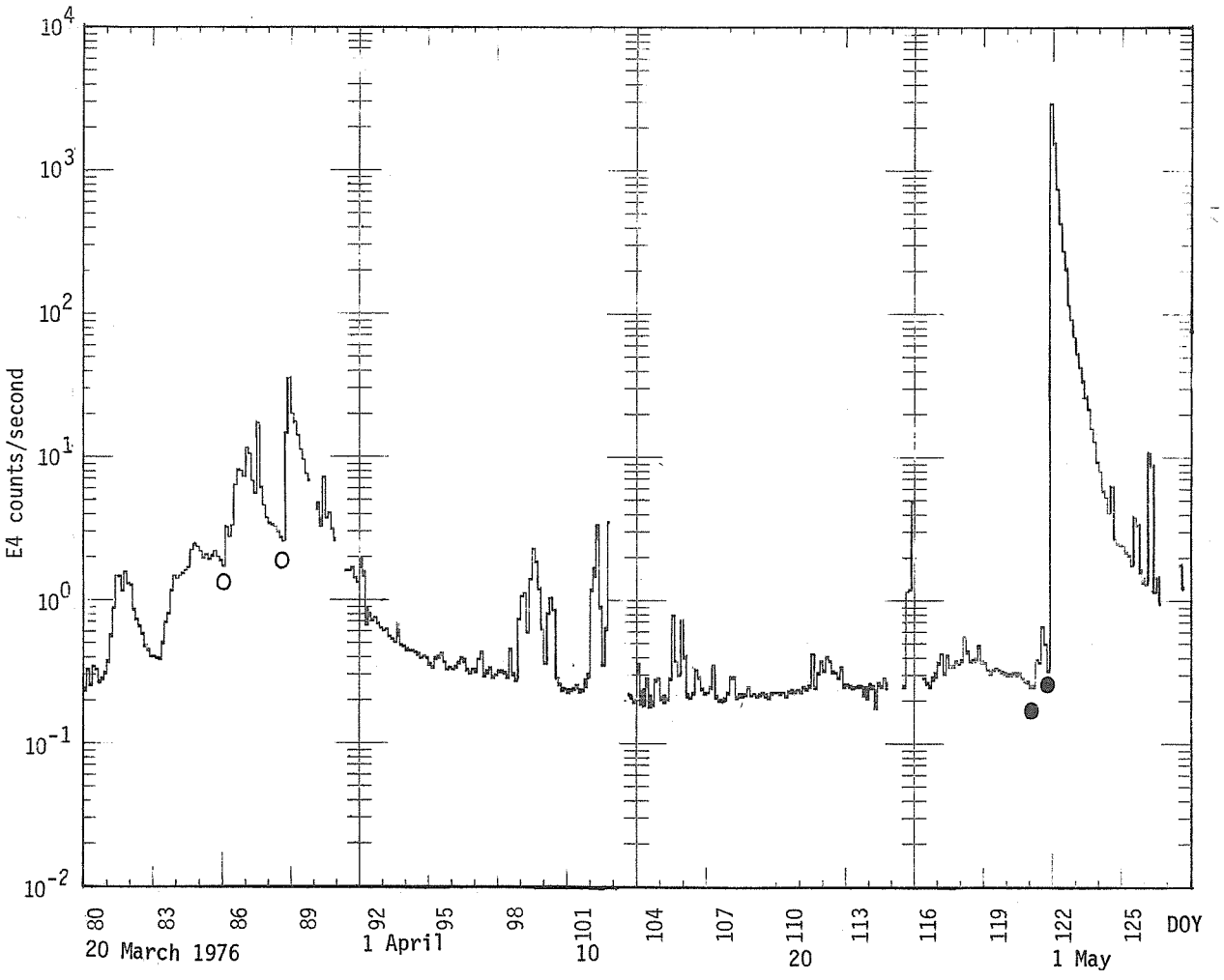

Fig. 1. Three-hour averaged count rate of the >0.22 MeV electron channel (E4) for the period 20 March - 5 May 1976 (DOY 80-126). The electron increases identified with flares in region 14143 are noted by open circles and those in 14179 by filled circles.

Figure 2 shows 3-hour averaged count rates of 2.0 to 4.6 MeV protons. Several common features of low energy interplanetary ion intensities not obviously associated with flares are present on days 101-106 and 116-120. These gradual intensity increases show no identifiable velocity dispersive onsets and may represent spatial structures of the interplanetary medium. The lowest rates measured by the P4 channel were $\sim 2 \times 10^{-3}$ counts/s which we believe were due to foreground particles; the lowest rate observed with the CPME instrument due to the "quiet-time interplanetary" particles in the 2.0 to 4.6 MeV passband was $\sim 8 \times 10^{-4}$ counts/s [Krimigis *et al.*, 1975]. The 100% duty cycle of the instrument yields a sensitivity of $\sim 10^{-4}$ counts/s for one count/3 hours.

Figure 3 shows the 3-hour averaged count rates of 1.8 to 4.2 MeV/nucleon alpha particles. This plot suggests the possible occurrence of another flare-associated ion intensity increase at ~0900 UT on 25 March (DOY 85) not evident in Figures 1 and 2. Flare activity was present in McMath Region 14143 during the preceding 6 hours with a -F (S06 E74) flare onset at 0914 UT and another -F (S06 E83) flare at 0612 UT. Even though the association of the ion increase with such extreme eastern subflares is uncertain, we cannot exclude this possibility.

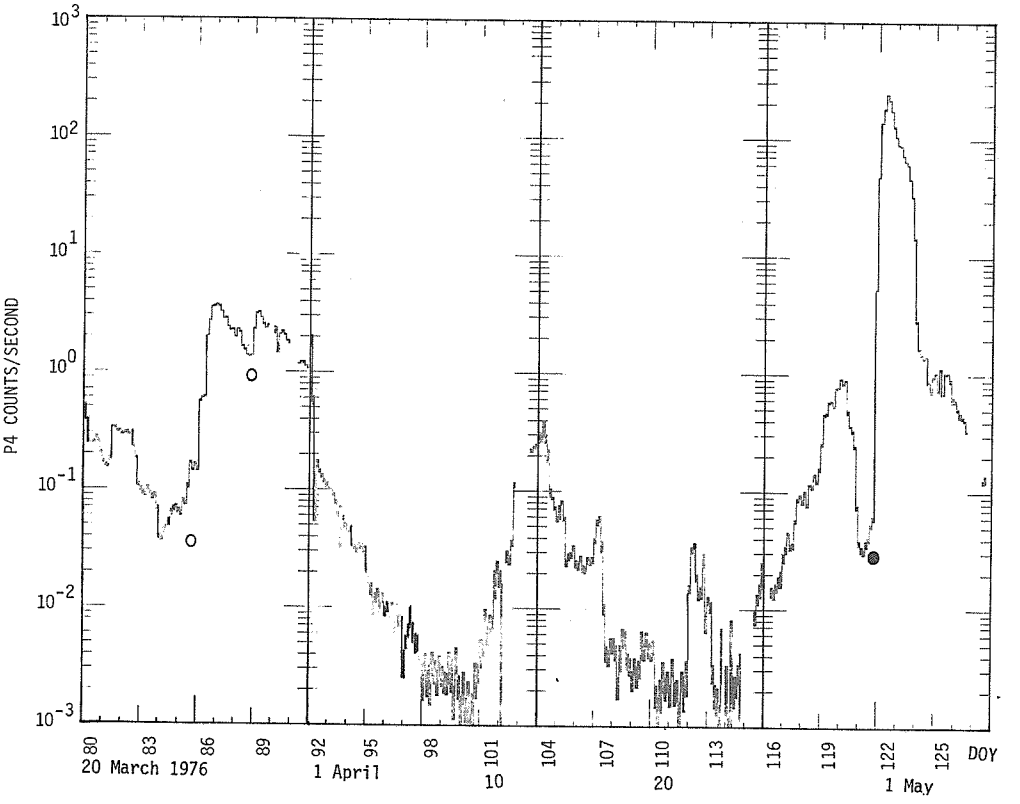

Fig. 2. Three-hour averaged count rate of the 2.0 to 4.6 MeV proton channel (P4) for the period 20 March - 5 May 1976 (DOY 80-126). The proton increases identified with flares in region 14143 are noted by open circles and those in 14179 by filled circles.

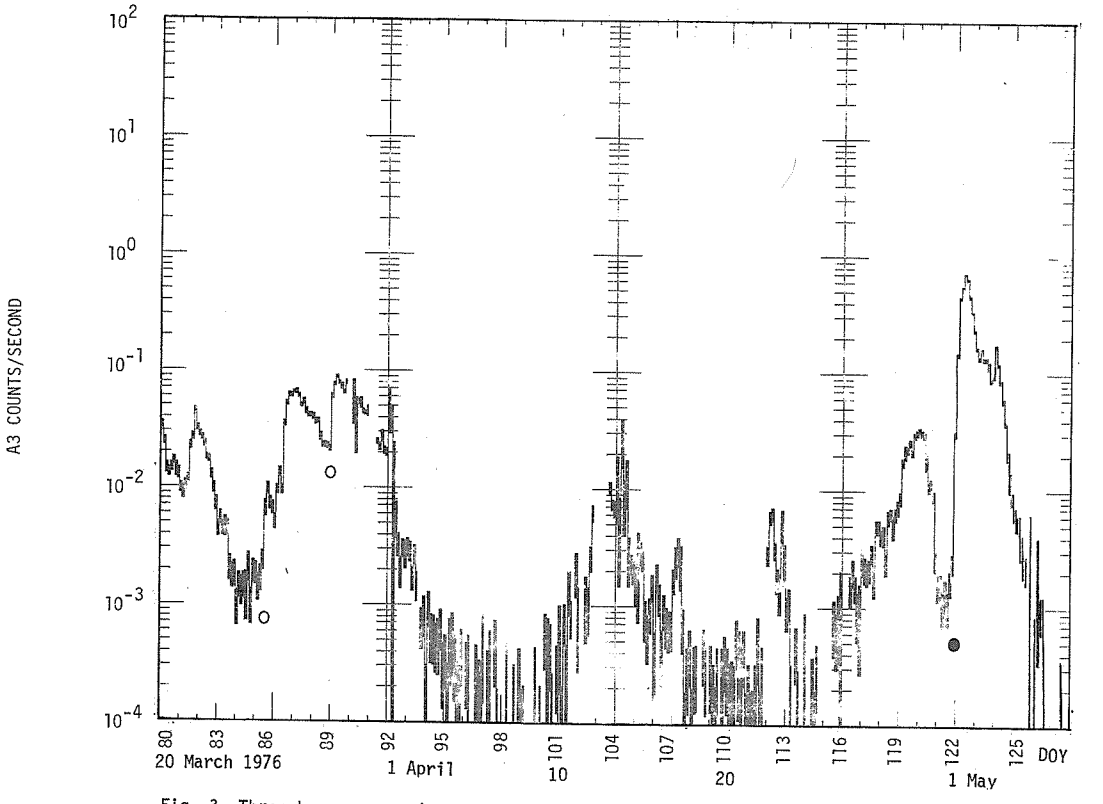

Fig. 3. Three-hour averaged count rate of the 1.8 to 4.2 MeV/nucleon alpha particle channel (A3) for the period 20 March - 5 May 1976 (DOY 80-126). The alpha particle increases identified with flares in Region 14143 are noted by open circles and those in 14179 by filled circles.

Figure 4 shows the 3-hour averaged count rates of the Z1 channel, sensitive primarily to C, N and O nuclei in the passband 0.7 to 3.3 MeV/nucleon. The fluxes attributed to McMath Region 14143 are again denoted by open circles and to McMath Region 14179 by closed circles.

Figure 5 shows the 3-hour averaged count rates of the Z3 channel, sensitive to nuclei with $Z \geq 20$ in the passband 3.1 to 8.8 MeV/nucleon. This channel responds principally to iron nuclei in flare events [Armstrong *et al.*, 1977]. The most remarkable feature of Figure 5 is the difference in Z3 response following the flares of 25 and 28 March. The second flare was followed by ion intensities that were depleted in $Z \geq 20$ ions. It is tempting to speculate that the flare of 25 March in McMath Region 14143 had available iron-enriched material for injection into the flare acceleration process and that the flare of 28 March did not.

Acknowledgments

This research has been supported in part by NASA under Task I of contract #N00017-72-C-014 with the Department of the Navy.

REFERENCES

ARMSTRONG, T. P. and S. M. KRIMIGIS 1976 Interplanetary Acceleration of Relativistic Electrons Observed With IMP 7, *J. Geophys. Res.*, *81*, 677-682.

ARMSTRONG, T. P., S. M. KRIMIGIS, D. HOVESTADT, B. KLECKER and G. GLOECKLER 1977 Observation of Temporal and Spatial Variations in the Fe/O Charge Composition of the Solar Particle Event of 4 July 1974, *Solar Physics*, in press.

KRIMIGIS, S. M., J. W. KOHL and T. P. ARMSTRONG 1975 The Magnetospheric Contribution to the Quiet-Time Low Energy Nucleon Spectrum in the Vicinity of Earth, *Geophys. Res. Letters 2*, 457-460.

SARRIS, E. T., S. M. KRIMIGIS and T. P. ARMSTRONG 1976 Observations of Magnetospheric Bursts of High Energy Protons and Electrons at ~35 R_E with IMP 7, *J. Geophys. Res.*, *81*, 2341-2355.

SGD 1976 *Solar-Geophysical Data*, 385, 386, 387 Part II, September, October, November 1976, U.S. Department of Commerce, (Boulder, Colorado, U.S.A. 80302).

WDC-A/NSSDC 1975 IMS/Satellite Situation Center Report, Predicted Orbit Plots for IMP-J-1976, Report No. 4, December 1975, WDC-A/ National Space Science Data Center.

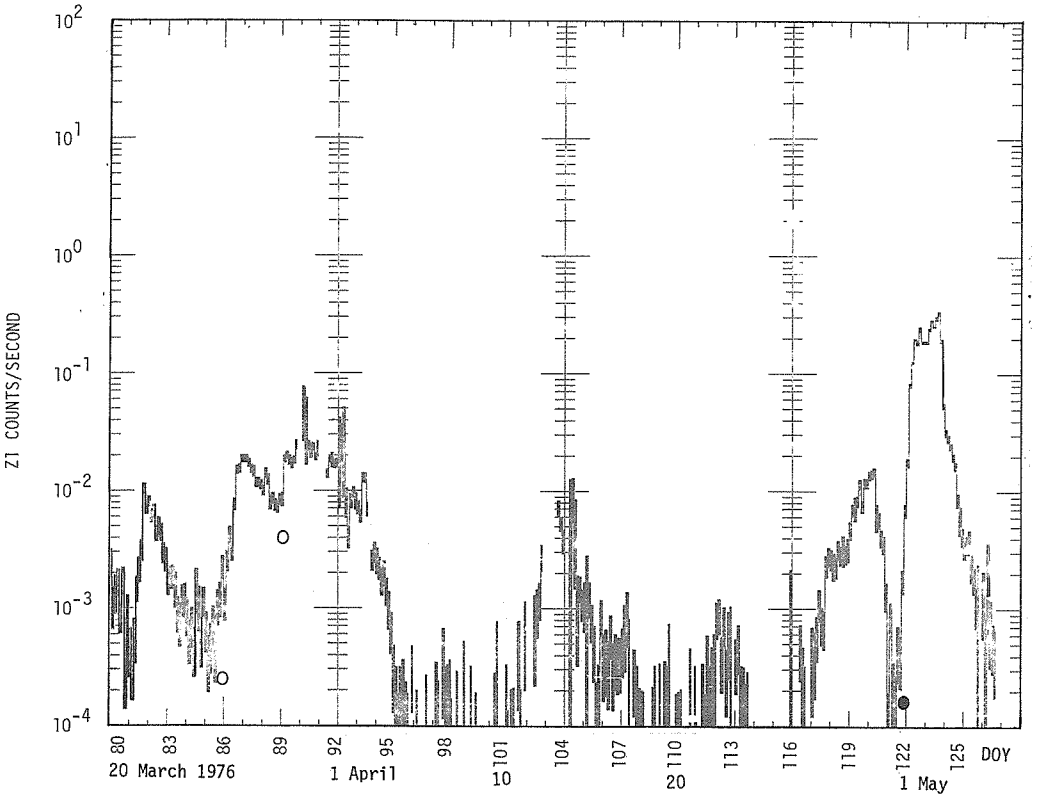

Fig. 4. Three-hour averaged count rate of the Z1 channel, sensitive to carbon, nitrogen and oxygen nuclei in the passband 0.7 to 3.3 MeV/nucleon, for the period 20 March - 5 May 1976 (DOY 80-126). The flux increases identified with flares in region 14143 are noted by open circles and those in 14179 by filled circles.

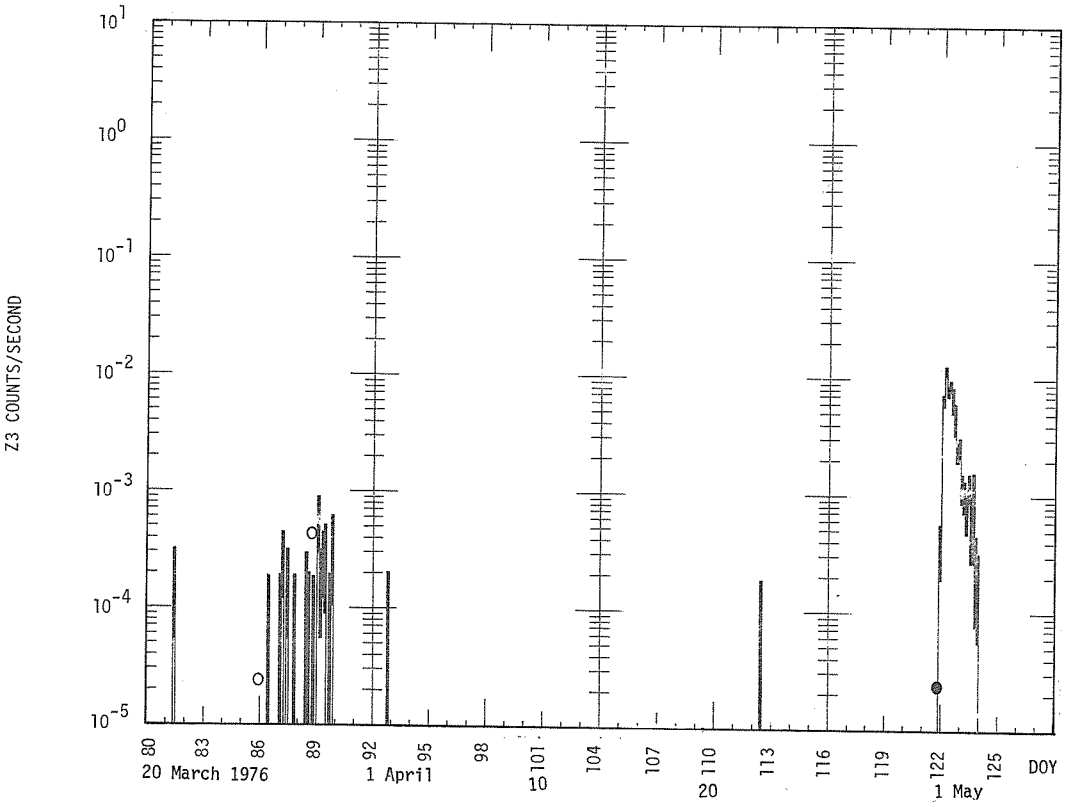

Fig. 5. Three-hour averaged count rate of the Z3 channel, sensitive to nuclei with $Z \geq 20$ in the passband 3.1 to 8.8 MeV/nucleon, for the period 20 March - 5 May 1976 (DOY 80-126). The flux increases identified with flares in region 14143 are noted by open circles and those in 14179 by filled circles.

APPENDIX

Tabulation of 3-hour Averaged Count Rates from IMP 8, 20 March - 5 May 1976 (DOY 80-126)

The units of the following table are counts/second. Day is day of the year, e.g., day 1 is 1 January, etc. Hour is universal time of the start of the averaging interval. Count rates of E4 that are dominated by magnetospheric particles are shown by M. See Table 1 for an explanation of the passbands of the P4, A3, Z1, Z3, and E4 channels.

DATE 1976	DOY	HR	P4 RATE	P4 UNC	A3 RATE	A3 UNC	Z1 RATE	Z1 UNC	Z3 RATE	Z3 UNC	E4 RATE	E4 UNC
Mar 20	80	0	0.51468	0.00905	0.03435	0.00237	0.00250	0.00065	0.00000	0.00000	0.23656	0.00631
	80	3	0.38080	0.00771	0.02506	0.00195	0.00187	0.00041	0.00000	0.00000	0.32588	0.00711
	80	6	0.25146	0.00662	0.01473	0.00159	0.00138	0.00049	0.00000	0.00000	0.25702	0.00667
	80	9	0.24092	0.00526	0.01350	0.00123	0.00170	0.00044	0.00000	0.00000	0.34196	0.00614
	80	12	0.25122	0.00551	0.01482	0.00132	0.00096	0.00034	0.00000	0.00000	0.32623	0.00623
	80	15	0.27380	0.00561	0.01696	0.00139	0.00173	0.00045	0.00000	0.00000	0.26918	0.00555
	80	18	0.25916	0.00780	0.01425	0.00182	0.00047	0.00033	0.00000	0.00000	0.28225	0.00811
	80	21	0.20294	0.00556	0.01330	0.00143	0.00092	0.00038	0.00000	0.00000	0.30912	0.00686
21	81	0	0.17026	0.00400	0.00988	0.00096	0.00047	0.00021	0.00000	0.00000	0.37136	0.00591
	81	3	0.15888	0.00448	0.00910	0.00107	0.00038	0.00022	0.00000	0.00000	0.56422	0.00846
	81	6	0.15438	0.00382	0.01043	0.00100	0.00057	0.00023	0.00000	0.00000	0.88043	0.00915
	81	9	0.18208	0.00411	0.01195	0.00105	0.00148	0.00037	0.00018	0.00013	1.47955	0.01170
	81	12	0.33436	0.00618	0.02270	0.00161	0.00218	0.00050	0.00000	0.00000	1.46908	0.01297
	81	15	0.33012	0.00616	0.02676	0.00176	0.00314	0.00060	0.00000	0.00000	1.16129	0.01156
	81	18	0.30794	0.00564	0.04605	0.00218	0.01043	0.00104	0.00000	0.00000	1.57432	0.01272
	81	21	0.31407	0.00570	0.03173	0.00181	0.00713	0.00086	0.00000	0.00000	1.30373	0.01159
22	82	0	0.29632	0.00525	0.02863	0.00163	0.00802	0.00086	0.00000	0.00000	1.26357	0.01085
	82	3	0.30304	0.00534	0.02676	0.00159	0.00612	0.00076	0.00000	0.00000	0.85663	0.00897
	82	6	0.30313	0.00595	0.02335	0.00164	0.00677	0.00088	0.00000	0.00000	0.73817	0.00926
	82	9	0.29212	0.00524	0.01822	0.00132	0.00435	0.00064	0.00000	0.00000	0.65288	0.00788
	82	12	0.29977	0.00639	0.01782	0.00154	0.00503	0.00083	0.00000	0.00000	0.58217	0.00886
	82	15	0.22849	0.00518	0.01287	0.00123	0.00448	0.00073	0.00000	0.00000	0.47894	0.00752
	82	18	0.18143	0.00424	0.00991	0.00099	0.00298	0.00054	0.00000	0.00000	0.44708	0.00665
	82	21	0.10747	0.00378	0.00735	0.00097	0.00262	0.00059	0.00000	0.00000	0.40362	0.00721
23	83	0	0.09952	0.00304	0.00445	0.00064	0.00167	0.00039	0.00000	0.00000	0.40419	0.00613
	83	3	0.09184	0.00294	0.00552	0.00072	0.00187	0.00042	0.00000	0.00000	0.39409	0.00608
	83	6	0.08985	0.00291	0.00451	0.00065	0.00188	0.00042	0.00000	0.00000	0.39053	0.00606
	83	9	0.09951	0.00410	0.00470	0.00089	0.00151	0.00050	0.00000	0.00000	0.50055	0.00917
	83	12	0.09313	0.00310	0.00454	0.00068	0.00093	0.00031	0.00000	0.00000	0.70201	0.00850
	83	15	0.08532	0.00333	0.00210	0.00053	0.00078	0.00032	0.00000	0.00000	0.80016	0.01018
	83	18	0.08826	0.00309	0.00182	0.00044	0.00118	0.00036	0.00000	0.00000	1.15452	0.01116
	83	21	0.06885	0.00274	0.00187	0.00045	0.00120	0.00036	0.00000	0.00000	1.47884	0.01277
24	84	0	0.03886	0.00209	0.00099	0.00033	0.00099	0.00031	0.00000	0.00000	1.41585	0.01250
	84	3	0.03860	0.00189	0.00148	0.00037	0.00056	0.00023	0.00000	0.00000	1.47439	0.01169
	84	6	0.04370	0.00214	0.00136	0.00038	0.00073	0.00028	0.00000	0.00000	1.54190	0.01270
	84	9	0.04529	0.00205	0.00149	0.00037	0.00047	0.00021	0.00000	0.00000	1.59458	0.01220
	84	12	0.05144	0.00366	0.00130	0.00058	0.00151	0.00062	0.00000	0.00000	1.69380	0.02070
	84	15	0.06256	0.00337	0.00215	0.00062	0.00107	0.00044	0.00000	0.00000	2.24044	0.01989
	84	18	0.06771	0.00277	0.00101	0.00034	0.00056	0.00025	0.00000	0.00000	2.41169	0.01644
	84	21	0.06963	0.00259	0.00194	0.00043	0.00116	0.00033	0.00000	0.00000	2.33533	0.01503
25	85	0	0.06447	0.00248	0.00189	0.00042	0.00066	0.00025	0.00000	0.00000	2.19632	0.01439
	85	3	0.06172	0.00243	0.00143	0.00037	0.00038	0.00019	0.00000	0.00000	1.98587	0.01379
	85	6	0.07879	0.00281	0.00171	0.00041	0.00050	0.00022	0.00000	0.00000	2.06273	0.01440
	85	9	0.07465	0.00264	0.00243	0.00048	0.00077	0.00026	0.00000	0.00000	1.93826	0.01346
	85	12	0.10437	0.00429	0.00664	0.00108	0.00054	0.00031	0.00000	0.00000	2.03429	0.01920
	85	15	0.16524	0.00431	0.00985	0.00107	0.00105	0.00035	0.00000	0.00000	2.18664	0.01568
	85	18	0.14512	0.00425	0.00735	0.00095	0.00122	0.00039	0.00000	0.00000	1.98798	0.01554
	85	21	0.16039	0.00398	0.00676	0.00081	0.00226	0.00047	0.00000	0.00000	1.87624	0.01359
26	86	0	0.14583	0.00384	0.00513	0.00072	0.00111	0.00033	0.00000	0.00000	1.72076	0.01316
	86	3	0.55705	0.00724	0.00957	0.00095	0.00254	0.00049	0.00000	0.00000	3.21721	0.01737
	86	6	0.59354	0.00781	0.01357	0.00118	0.00421	0.00066	0.00000	0.00000	2.74178	0.01680
	86	9	0.61051	0.00752	0.00962	0.00094	0.00306	0.00053	0.00009	0.00009	3.32179	0.01753
	86	12	1.99867	0.01442	0.03494	0.00190	0.00767	0.00089	0.00000	0.00000	6.35491	0.02571
	86	15	2.69211	0.01689	0.05303	0.00237	0.01493	0.00126	0.00000	0.00000	8.00765	0.02928
	86	18	3.54355	0.01974	0.06208	0.00262	0.01527	0.00130	0.00000	0.00000	7.98180	0.02962
	86	21	3.59793	0.01875	0.06185	0.00246	0.01863	0.00136	0.00000	0.00000	7.28109	0.02680

DATE 1976	DOY	HR	P4 RATE	P4 UNC	A3 RATE	A3 UNC	Z1 RATE	Z1 UNC	Z3 RATE	Z3 UNC	E4 RATE	E4 UNC
Mar 27	87	0	3.68789	0.01870	0.06561	0.00249	0.01868	0.00133	0.00009	0.00009	11.50755 M	0.03334
	87	3	3.58376	0.01844	0.06614	0.00250	0.01858	0.00133	0.00029	0.00016	10.43632 M	0.03164
	87	6	3.24554	0.01817	0.06082	0.00249	0.01721	0.00132	0.00000	0.00000	6.74988	0.02625
	87	9	2.83231	0.01618	0.05059	0.00216	0.01536	0.00119	0.00018	0.00013	5.55660	0.02268
	87	12	2.84639	0.02119	0.05418	0.00292	0.01467	0.00152	0.00000	0.00000	17.16712 M	0.05484
	87	15	2.39674	0.01642	0.04524	0.00225	0.01182	0.00115	0.00000	0.00000	6.08547	0.02622
	87	18	2.27547	0.01464	0.04204	0.00200	0.01183	0.00106	0.00009	0.00009	4.55669	0.02084
	87	21	2.26224	0.01457	0.04201	0.00199	0.01121	0.00103	0.00000	0.00000	3.71940	0.01871
28	88	0	1.96355	0.01358	0.04027	0.00195	0.01006	0.00097	0.00000	0.00000	3.41278	0.01794
	88	3	2.29620	0.01476	0.03668	0.00186	0.01418	0.00116	0.00000	0.00000	3.35391	0.01784
	88	6	2.17650	0.01569	0.03724	0.00205	0.01252	0.00119	0.00000	0.00000	3.24788	0.01913
	88	9	1.62721	0.01544	0.02719	0.00199	0.00902	0.00108	0.00015	0.00015	2.97844	0.02085
	88	12	1.52605	0.01240	0.02326	0.00153	0.00872	0.00094	0.00010	0.00010	2.71781	0.01652
	88	15	1.37981	0.01140	0.02312	0.00147	0.00763	0.00085	0.00000	0.00000	2.57773	0.01557
	88	18	1.34980	0.01123	0.02275	0.00146	0.00728	0.00082	0.00009	0.00009	14.63468	0.03747
	88	21	1.37867	0.01179	0.02168	0.00148	0.00842	0.00092	0.00000	0.00000	35.58643	0.06072
29	89	0	2.32151	0.01819	0.05996	0.00293	0.00852	0.00111	0.00059	0.00029	20.10912	0.05477
	89	3	3.12387	0.01709	0.07698	0.00268	0.01865	0.00132	0.00019	0.00013	17.53474	0.04075
	89	6	3.20124	0.01746	0.08849	0.00289	0.02016	0.00138	0.00028	0.00016	14.05249	0.03663
	89	9	2.89427	0.02125	0.07870	0.00344	0.01848	0.00169	0.00030	0.00021	11.24043	0.04132
	89	12	2.52728	0.02191	0.07319	0.00377	0.01723	0.00186	0.00000	0.00000	9.55299	0.04304
	89	15	2.34385	0.01514	0.06569	0.00253	0.01833	0.00134	0.00010	0.00010	7.57935	0.02719
	89	18	2.49213	0.02121	0.07892	0.00377	0.02453	0.00210	0.00036	0.00025	6.80981	0.03508
30	90	3	2.23389	0.16513	0.05859	0.02392	0.05208	0.02604	0.00000	0.00000	4.51660	0.23481
	90	6	1.59040	0.14895	0.03906	0.01953	0.03906	0.02255	0.00000	0.00000	3.47900	0.20608
	90	9	2.09200	0.02007	0.05494	0.00327	0.02417	0.00215	0.00000	0.00000	7.12813M	0.03725
	90	12	2.19087	0.03347	0.05341	0.00521	0.02256	0.00340	0.00000	0.00000	3.71860	0.04361
	90	15	2.07441	0.01429	0.04509	0.00211	0.02353	0.00152	0.00000	0.00000	4.01926	0.01990
	90	18	1.83650	0.01313	0.04326	0.00201	0.01948	0.00135	0.00000	0.00000	3.13245	0.01720
	90	21	1.78322	0.02981	0.04521	0.00452	0.02275	0.00328	0.00000	0.00000	2.63169	0.03466
31	91	9	1.17683	0.01069	0.02478	0.00155	0.01399	0.00117	0.00000	0.00000	1.61503	0.01255
	91	12	1.20980	0.01071	0.02243	0.00145	0.01878	0.00137	0.00000	0.00000	1.60182	0.01228
	91	15	1.19949	0.01986	0.02776	0.00301	0.01844	0.00246	0.00000	0.00000	1.66114	0.02333
	91	18	1.12361	0.01070	0.02114	0.00147	0.01697	0.00131	0.00000	0.00000	1.42350	0.01204
	91	21	1.06657	0.01166	0.02032	0.00161	0.01721	0.00149	0.00000	0.00000	1.33259	0.01304
Apr 1	92	0	1.83105	0.21143	0.04883	0.01993	0.02441	0.01726	0.00000	0.00000	1.85547	0.15050
	92	3	0.57114	0.04111	0.03906	0.01044	0.02741	0.00969	0.00000	0.00000	1.51840	0.06916
	92	6	0.09766	0.04367	0.01221	0.01221	0.03005	0.02125	0.00000	0.00000	0.76730	0.10346
	92	9	0.16694	0.01050	0.00563	0.00188	0.00819	0.00227	0.00000	0.00000	0.78856	0.02289
	92	12	0.14214	0.00507	0.00331	0.00076	0.00411	0.00086	0.00000	0.00000	0.72645	0.01146
	92	15	0.13062	0.00479	0.00196	0.00059	0.00823	0.00120	0.00000	0.00000	0.74595	0.01145
	92	18	0.11865	0.00347	0.00304	0.00056	0.00963	0.00099	0.00010	0.00010	0.68430	0.00833
	92	21	0.11082	0.00493	0.00280	0.00078	0.00823	0.00133	0.00000	0.00000	0.64034	0.01183
2	93	0	0.10238	0.00339	0.00315	0.00059	0.00728	0.00091	0.00000	0.00000	0.60902	0.00830
	93	3	0.10243	0.00326	0.00290	0.00055	0.00615	0.00080	0.00000	0.00000	0.62566	0.00807
	93	6	0.09119	0.00294	0.00171	0.00040	0.01298	0.00111	0.00000	0.00000	0.56129	0.00729
	93	9	0.07792	0.00280	0.00271	0.00052	0.01300	0.00114	0.00000	0.00000	0.52861	0.00729
	93	12	0.06186	0.00263	0.00148	0.00041	0.00697	0.00089	0.00000	0.00000	0.51034	0.00762
	93	15	0.05258	0.01987	0.00000	0.00000	0.00000	0.00000	0.00000	0.00000	0.62081	0.06581
	93	18	0.05751	0.00236	0.00068	0.00026	0.00261	0.00050	0.00000	0.00000	0.48356	0.00683
	93	21	0.04986	0.00246	0.00084	0.00032	0.00305	0.00061	0.00000	0.00000	0.47271	0.00758
3	94	0	0.04883	0.00274	0.00015	0.00015	0.00260	0.00063	0.00000	0.00000	0.44569	0.00823
	94	3	0.04553	0.00220	0.00096	0.00032	0.00223	0.00049	0.00000	0.00000	0.43956	0.00683
	94	6	0.03529	0.00202	0.00058	0.00026	0.00173	0.00045	0.00000	0.00000	0.44372	0.00716
	94	9	0.03334	0.00194	0.00057	0.00025	0.00203	0.00048	0.00000	0.00000	0.43036	0.00698
	94	12	0.03098	0.00171	0.00047	0.00021	0.00142	0.00037	0.00000	0.00000	0.41824	0.00630
	94	15	0.03352	0.00206	0.00051	0.00025	0.00101	0.00036	0.00000	0.00000	0.39290	0.00705
	94	18	0.03427	0.00179	0.00065	0.00025	0.00066	0.00025	0.00000	0.00000	0.40346	0.00615
	94	21	0.03107	0.00177	0.00030	0.00017	0.00030	0.00017	0.00000	0.00000	0.39506	0.00631
4	95	0	0.02205	0.00143	0.00037	0.00019	0.00019	0.00013	0.00000	0.00000	0.35428	0.00572
	95	3	0.01707	0.00126	0.00019	0.00013	0.00039	0.00009	0.00000	0.00000	0.34003	0.00562
	95	6	0.01455	0.00153	0.00048	0.00028	0.00016	0.00016	0.00000	0.00000	0.38767	0.00776
	95	9	0.00996	0.00134	0.00054	0.00031	0.00018	0.00018	0.00000	0.00000	0.39755	0.00851
	95	12	0.01212	0.00119	0.00035	0.00020	0.00012	0.00012	0.00000	0.00000	0.41571	0.00695
	95	15	0.01330	0.00112	0.00019	0.00013	0.00009	0.00009	0.00000	0.00000	0.36856	0.00588
	95	18	0.01002	0.00097	0.00019	0.00013	0.00000	0.00000	0.00000	0.00000	0.32876	0.00554
	95	21	0.01217	0.00111	0.00041	0.00020	0.00030	0.00018	0.00000	0.00000	0.33515	0.00583

DATE 1976	DOY	HR	P4 RATE	P4 UNC	A3 RATE	A3 UNC	Z1 RATE	Z1 UNC	Z3 RATE	Z3 UNC	E4 RATE	E4 UNC
Apr 5	96	0	0.00917	0.00095	0.00000	0.00000	0.00000	0.00000	0.00000	0.00000	0.32835	0.00570
	96	3	0.01016	0.00101	0.00030	0.00017	0.00010	0.00010	0.00000	0.00000	0.33888	0.00584
	96	6	0.00864	0.00118	0.00032	0.00023	0.00000	0.00000	0.00000	0.00000	0.36396	0.00765
	96	9	0.00957	0.00143	0.00000	0.00000	0.00000	0.00000	0.00000	0.00000	0.38649	0.00917
	96	12	0.00766	0.00145	0.00000	0.00000	0.00000	0.00000	0.00000	0.00000	0.37495	0.01024
	96	15	0.00966	0.00112	0.00027	0.00019	0.00013	0.00013	0.00000	0.00000	0.32502	0.00663
	96	18	0.00786	0.00088	0.00020	0.00014	0.00000	0.00000	0.00000	0.00000	0.30736	0.00554
	96	21	0.00738	0.00085	0.00020	0.00014	0.00000	0.00000	0.00000	0.00000	0.32695	0.00565
6	97	0	0.00344	0.00092	0.00049	0.00035	0.00000	0.00000	0.00000	0.00000	0.31867	0.00883
	97	3	0.00505	0.00071	0.00000	0.00000	0.00020	0.00014	0.00000	0.00000	0.38406	0.00623
	97	6	0.00632	0.00087	0.00024	0.00017	0.00012	0.00012	0.00000	0.00000	0.42568	0.00712
	97	9	0.00809	0.00159	0.00030	0.00030	0.00000	0.00000	0.00000	0.00000	0.30888	0.00957
	97	12	0.00598	0.00109	0.00000	0.00000	0.00040	0.00028	0.00000	0.00000	0.31218	0.00786
	97	15	0.00495	0.00089	0.00047	0.00027	0.00016	0.00016	0.00000	0.00000	0.33395	0.00724
	97	18	0.00490	0.00069	0.00010	0.00010	0.00019	0.00014	0.00000	0.00000	0.28921	0.00528
	97	21	0.00423	0.00067	0.00000	0.00000	0.00021	0.00015	0.00000	0.00000	0.29874	0.00560
7	98	0	0.00242	0.00081	0.00000	0.00000	0.00000	0.00000	0.00000	0.00000	0.31698	0.00920
	98	3	0.00348	0.00059	0.00000	0.00000	0.00000	0.00000	0.00000	0.00000	0.31432	0.00560
	98	6	0.00231	0.00058	0.00029	0.00020	0.00014	0.00014	0.00000	0.00000	0.30651	0.00664
	98	9	0.00236	0.00089	0.00000	0.00000	0.00000	0.00000	0.00000	0.00000	0.29162	0.00991
	98	12	0.00342	0.00079	0.00000	0.00000	0.00000	0.00000	0.00000	0.00000	0.44864	0.00899
	98	15	0.00291	0.00067	0.00015	0.00015	0.00031	0.00022	0.00000	0.00000	0.29970	0.00677
	98	18	0.00237	0.00061	0.00000	0.00000	0.00000	0.00000	0.00000	0.00000	0.27574	0.00660
	98	21	0.00327	0.00064	0.00025	0.00018	0.00000	0.00000	0.00000	0.00000	0.73630M	0.00963
8	99	0	0.00263	0.00050	0.00009	0.00009	0.00019	0.00013	0.00000	0.00000	1.05626M	0.01000
	99	3	0.00236	0.00049	0.00010	0.00010	0.00000	0.00000	0.00000	0.00000	1.12141M	0.01072
	99	6	0.00228	0.00047	0.00000	0.00000	0.00009	0.00009	0.00000	0.00000	0.59495M	0.00751
	99	9	0.00323	0.00097	0.00000	0.00000	0.00000	0.00000	0.00000	0.00000	1.40778M	0.02035
	99	12	0.00277	0.00088	0.00000	0.00000	0.00000	0.00000	0.00000	0.00000	2.28427M	0.02515
	99	15	0.00164	0.00052	0.00000	0.00000	0.00000	0.00000	0.00000	0.00000	1.83662M	0.01728
	99	18	0.00364	0.00088	0.00022	0.00022	0.00000	0.00000	0.00000	0.00000	1.18639M	0.01616
	99	21	0.00216	0.00048	0.00000	0.00000	0.00000	0.00000	0.00000	0.00000	0.61939M	0.00820
9	100	0	0.00141	0.00038	0.00010	0.00010	0.00000	0.00000	0.00000	0.00000	0.36285M	0.00605
	100	3	0.00219	0.00066	0.00000	0.00000	0.00000	0.00000	0.00000	0.00000	0.80094M	0.01269
	100	6	0.00128	0.00043	0.00056	0.00028	0.00014	0.00014	0.00000	0.00000	1.00330M	0.01188
	100	9	0.00156	0.00078	0.00039	0.00039	0.00039	0.00039	0.00000	0.00000	0.85682M	0.01822
	100	12	0.00088	0.00036	0.00044	0.00025	0.00000	0.00000	0.00000	0.00000	0.28960	0.00651
	100	15	0.00143	0.00043	0.00013	0.00013	0.00000	0.00000	0.00000	0.00000	0.25623	0.00579
	100	18	0.00253	0.00084	0.00000	0.00000	0.00000	0.00000	0.00000	0.00000	0.23960	0.00825
	100	21	0.00281	0.00052	0.00029	0.00017	0.00019	0.00014	0.00000	0.00000	0.23658	0.00474
10	101	0	0.00421	0.00112	0.00059	0.00042	0.00000	0.00000	0.00000	0.00000	0.23283	0.00833
	101	3	0.00462	0.00069	0.00010	0.00010	0.00010	0.00010	0.00000	0.00000	0.23499	0.00490
	101	6	0.00875	0.00096	0.00074	0.00028	0.00010	0.00010	0.00000	0.00000	0.24124	0.00504
	101	9	0.00609	0.00119	0.00024	0.00024	0.00000	0.00000	0.00000	0.00000	0.24744	0.00764
	101	12	0.00743	0.00129	0.00137	0.00056	0.00046	0.00032	0.00000	0.00000	0.23185	0.00723
	101	15	0.00762	0.00088	0.00081	0.00029	0.00010	0.00010	0.00000	0.00000	0.23535	0.00489
	101	18	0.01649	0.00457	0.00000	0.00000	0.00000	0.00000	0.00000	0.00000	0.26292	0.01814
	101	21	0.02246	0.00276	0.00200	0.00082	0.00068	0.00048	0.00000	0.00000	0.29601	0.01000
11	102	0	0.01812	0.00283	0.00091	0.00065	0.00000	0.00000	0.00000	0.00000	1.17306M	0.02360
	102	3	0.00814	0.00814	0.00000	0.00000	0.00000	0.00000	0.00000	0.00000	1.57335M	0.13066
	102	6	0.00000	0.00000	0.00000	0.00000	0.00000	0.00000	0.00000	0.00000	3.02734M	0.38447
	102	9	0.02763	0.00323	0.00113	0.00065	0.00075	0.00053	0.00000	0.00000	0.88492M	0.01823
	102	12	0.02583	0.00228	0.00101	0.00045	0.00101	0.00045	0.00000	0.00000	0.35136M	0.00841
	102	15	0.03586	0.00234	0.00259	0.00063	0.00122	0.00043	0.00000	0.00000	0.63065M	0.00981
	102	18	0.11224	0.00429	0.00623	0.00101	0.00276	0.00067	0.00000	0.00000	3.50621M	0.02392
12	103	15	0.22180	0.00578	0.01019	0.00125	0.00723	0.00104	0.00000	0.00000	0.21935	0.00576
	103	18	0.23392	0.00462	0.00737	0.00082	0.00521	0.00069	0.00000	0.00000	0.20443	0.00432
	103	21	0.24208	0.00690	0.00685	0.00116	0.00379	0.00087	0.00000	0.00000	0.19886	0.00626
13	104	0	0.28646	0.03054	0.01221	0.00705	0.00000	0.00000	0.00000	0.00000	0.33264	0.03186
	104	3	0.29059	0.02631	0.00501	0.00354	0.00000	0.00000	0.00000	0.00000	0.20851	0.02346
	104	6	0.34624	0.05544	0.02713	0.01213	0.00630	0.00630	0.00000	0.00000	0.21230	0.03002
	104	9	0.27626	0.01884	0.00797	0.00399	0.00908	0.00371	0.00000	0.00000	0.26456	0.02167
	104	12	0.20074	0.02334	0.01221	0.00546	0.00501	0.00354	0.00000	0.00000	0.19769	0.02170
	104	15	0.09714	0.00705	0.00267	0.00119	0.00111	0.00079	0.00000	0.00000	0.19149	0.01022
	104	18	0.08711	0.00284	0.00231	0.00046	0.00148	0.00037	0.00000	0.00000	0.27438	0.00504
	104	21	0.07161	0.00268	0.00201	0.00045	0.00110	0.00033	0.00000	0.00000	0.28243	0.00532

DATE 1976	DOY	HR	P4 RATE	P4 UNC	A3 RATE	A3 UNC	Z1 RATE	Z1 UNC	Z3 RATE	Z3 UNC	E4 RATE	E4 UNC
Apr 14	105	0	0.05809	0.00364	0.00160	0.00060	0.00115	0.00051	0.00000	0.00000	0.20490	0.00684
	105	3	0.06646	0.00949	0.00247	0.00175	0.00142	0.00142	0.00000	0.00000	0.20450	0.01533
	105	6	0.08043	0.00334	0.00290	0.00063	0.00126	0.00042	0.00000	0.00000	0.20346	0.00530
	105	9	0.05832	0.00241	0.00248	0.00050	0.00080	0.00028	0.00000	0.00000	0.28290	0.00531
	105	12	0.02479	0.00170	0.00081	0.00031	0.00047	0.00024	0.00000	0.00000	0.78829	0.00966
	105	15	0.02753	0.00181	0.00059	0.00016	0.00012	0.00012	0.00000	0.00000	0.37654	0.00665
	105	18	0.02871	0.00167	0.00088	0.00023	0.00020	0.00014	0.00000	0.00000	0.30294	0.00544
	105	21	0.03275	0.00179	0.00147	0.00038	0.00089	0.00030	0.00000	0.00000	0.71506	0.00839
15	106	0	0.02391	0.00173	0.00038	0.00022	0.00038	0.00022	0.00000	0.00000	0.39721	0.00709
	106	3	0.02315	0.00180	0.00181	0.00050	0.00042	0.00024	0.00000	0.00000	0.21666	0.00550
	106	6	0.02668	0.00172	0.00119	0.00036	0.00033	0.00019	0.00000	0.00000	0.20731	0.00478
	106	9	0.02172	0.00151	0.00042	0.00021	0.00062	0.00025	0.00000	0.00000	0.22299	0.00483
	106	12	0.02154	0.00151	0.00095	0.00032	0.00032	0.00018	0.00000	0.00000	0.32503	0.00584
	106	15	0.02577	0.00161	0.00070	0.00027	0.00040	0.00020	0.00000	0.00000	0.28997	0.00538
	106	18	0.02495	0.00153	0.00066	0.00025	0.00038	0.00019	0.00000	0.00000	0.23805	0.00472
	106	21	0.02624	0.00158	0.00066	0.00025	0.00038	0.00019	0.00000	0.00000	0.22439	0.00461
16	107	0	0.03801	0.00189	0.00168	0.00040	0.00047	0.00021	0.00000	0.00000	0.22699	0.00461
	107	3	0.05423	0.00349	0.00248	0.00075	0.00068	0.00039	0.00000	0.00000	0.24516	0.00744
	107	6	0.05808	0.00367	0.00304	0.00084	0.00093	0.00046	0.00000	0.00000	0.34894	0.00912
	107	9	0.03418	0.00373	0.00233	0.00095	0.00040	0.00040	0.00000	0.00000	0.21126	0.00918
	107	12	0.00993	0.00106	0.00068	0.00028	0.00000	0.00000	0.00000	0.00000	0.19990	0.00479
	107	15	0.00414	0.00062	0.00089	0.00009	0.00028	0.00016	0.00000	0.00000	0.20875	0.00434
	107	18	0.00385	0.00060	0.00028	0.00016	0.00019	0.00013	0.00000	0.00000	0.20425	0.00438
	107	21	0.00486	0.00072	0.00042	0.00021	0.00010	0.00010	0.00000	0.00000	0.22513	0.00486
17	108	0	0.00487	0.00070	0.00010	0.00010	0.00010	0.00010	0.00000	0.00000	0.28880	0.00535
	108	3	0.00426	0.00064	0.00029	0.00017	0.00010	0.00010	0.00000	0.00000	0.28852	0.00528
	108	6	0.00217	0.00046	0.00030	0.00017	0.00000	0.00000	0.00000	0.00000	0.20725	0.00452
	108	9	0.00391	0.00095	0.00000	0.00000	0.00000	0.00000	0.00000	0.00000	0.21529	0.00691
	108	12	0.00570	0.00104	0.00000	0.00000	0.00000	0.00000	0.00000	0.00000	0.21519	0.00644
	108	15	0.00564	0.00078	0.00043	0.00022	0.00011	0.00011	0.00000	0.00000	0.21981	0.00489
	108	18	0.00357	0.00058	0.00028	0.00016	0.00019	0.00013	0.00000	0.00000	0.24681	0.00480
	108	21	0.00326	0.00056	0.00000	0.00000	0.00000	0.00000	0.00000	0.00000	0.21614	0.00453
18	109	0	0.00249	0.00050	0.00030	0.00017	0.00020	0.00014	0.00000	0.00000	0.22118	0.00467
	109	3	0.00328	0.00055	0.00019	0.00013	0.00000	0.00000	0.00000	0.00000	0.21278	0.00448
	109	6	0.00269	0.00053	0.00010	0.00010	0.00021	0.00015	0.00000	0.00000	0.22022	0.00477
	109	9	0.00310	0.00054	0.00028	0.00016	0.00019	0.00013	0.00000	0.00000	0.22311	0.00458
	109	12	0.00504	0.00135	0.00000	0.00000	0.00037	0.00037	0.00000	0.00000	0.21578	0.00880
	109	15	0.00438	0.00077	0.00026	0.00019	0.00000	0.00000	0.00000	0.00000	0.21059	0.00529
	109	18	0.00553	0.00073	0.00038	0.00019	0.00000	0.00000	0.00000	0.00000	0.22499	0.00462
	109	21	0.00443	0.00065	0.00028	0.00016	0.00009	0.00009	0.00000	0.00000	0.22639	0.00462
19	110	0	0.00430	0.00065	0.00020	0.00014	0.00010	0.00010	0.00000	0.00000	0.22702	0.00470
	110	3	0.00481	0.00070	0.00020	0.00014	0.00010	0.00010	0.00000	0.00000	0.22235	0.00476
	110	6	0.00185	0.00041	0.00018	0.00013	0.00000	0.00000	0.00000	0.00000	0.22620	0.00457
	110	9	0.00139	0.00038	0.00053	0.00024	0.00000	0.00000	0.00000	0.00000	0.21552	0.00479
	110	12	0.00191	0.00060	0.00037	0.00026	0.00000	0.00000	0.00000	0.00000	0.22957	0.00659
	110	15	0.00273	0.00079	0.00023	0.00023	0.00023	0.00023	0.00000	0.00000	0.23049	0.00710
	110	18	0.00213	0.00048	0.00042	0.00021	0.00000	0.00000	0.00000	0.00000	0.23063	0.00492
	110	21	0.00244	0.00048	0.00009	0.00009	0.00019	0.00013	0.00000	0.00000	0.23786	0.00472
20	111	0	0.00189	0.00042	0.00019	0.00013	0.00000	0.00000	0.00000	0.00000	0.22903	0.00465
	111	3	0.00322	0.00055	0.00010	0.00010	0.00000	0.00000	0.00000	0.00000	0.24414	0.00482
	111	6	0.00197	0.00044	0.00010	0.00010	0.00020	0.00014	0.00000	0.00000	0.23882	0.00485
	111	9	0.00207	0.00044	0.00019	0.00013	0.00009	0.00009	0.00000	0.00000	0.25172	0.00487
	111	12	0.00121	0.00046	0.00052	0.00030	0.00034	0.00024	0.00000	0.00000	0.42152M	0.00851
	111	15	0.00248	0.00049	0.00010	0.00010	0.00019	0.00014	0.00000	0.00000	0.24500	0.00483
	111	18	0.00203	0.00068	0.00023	0.00023	0.00024	0.00024	0.00000	0.00000	0.30924	0.00842
	111	21	0.00272	0.00091	0.00000	0.00000	0.00030	0.00030	0.00000	0.00000	0.37109	0.01064
21	112	0	0.01498	0.00118	0.00278	0.00051	0.00083	0.00028	0.00000	0.00000	0.32194	0.00546
	112	3	0.03208	0.00180	0.00585	0.00077	0.00091	0.00030	0.00000	0.00000	0.39708	0.00633
	112	6	0.03498	0.00182	0.00632	0.00077	0.00038	0.00019	0.00000	0.00000	0.37503	0.00595
	112	9	0.01880	0.00133	0.00308	0.00054	0.00075	0.00026	0.00009	0.00009	0.31491	0.00542
	112	12	0.01326	0.00112	0.00171	0.00040	0.00029	0.00017	0.00000	0.00000	0.31258	0.00545
	112	15	0.01395	0.00167	0.00140	0.00053	0.00060	0.00034	0.00000	0.00000	0.28939	0.00759
	112	18	0.02663	0.00373	0.00511	0.00162	0.00053	0.00053	0.00000	0.00000	0.33475	0.01322
	112	21	0.00793	0.00169	0.00251	0.00095	0.00000	0.00000	0.00000	0.00000	0.25599	0.00959
22	113	0	0.01193	0.00105	0.00092	0.00029	0.00037	0.00019	0.00000	0.00000	0.25631	0.00487
	113	3	0.01045	0.00102	0.00111	0.00033	0.00050	0.00022	0.00000	0.00000	0.25117	0.00502
	113	6	0.00287	0.00052	0.00019	0.00013	0.00019	0.00013	0.00000	0.00000	0.24562	0.00484
	113	9	0.00185	0.00041	0.00000	0.00000	0.00019	0.00013	0.00000	0.00000	0.24789	0.00479
	113	12	0.00169	0.00044	0.00045	0.00023	0.00011	0.00011	0.00000	0.00000	0.25236	0.00535
	113	15	0.00114	0.00040	0.00014	0.00014	0.00014	0.00014	0.00000	0.00000	0.25063	0.00598
	113	18	0.00465	0.00233	0.00000	0.00000	0.00000	0.00000	0.00000	0.00000	0.23107	0.01783
	113	21	0.00000	0.00000	0.00000	0.00000	0.00000	0.00000	0.00000	0.00000	0.22716	0.02196

DATE 1976	DOY	HR	P4 RATE	P4 UNC	A3 RATE	A3 UNC	Z1 RATE	Z1 UNC	Z3 RATE	Z3 UNC	E4 RATE	E4 UNC
Apr 23	114	0	0.00229	0.00103	0.00045	0.00045	0.00000	0.00000	0.00000	0.00000	0.25005	0.01046
	114	3	0.00076	0.00044	0.00000	0.00000	0.00000	0.00000	0.00000	0.00000	0.24786	0.00759
	114	6	0.00407	0.00407	0.00000	0.00000	0.00000	0.00000	0.00000	0.00000	0.20559	0.03251
	114	9	0.00209	0.00063	0.00019	0.00019	0.00000	0.00000	0.00000	0.00000	0.25914	0.00704
	114	12	0.00225	0.00047	0.00010	0.00010	0.00000	0.00000	0.00000	0.00000	0.25042	0.00496
	114	15	0.00283	0.00054	0.00030	0.00018	0.00000	0.00000	0.00000	0.00000	0.28269	0.00536
	114	18	0.00271	0.00157	0.00000	0.00000	0.00000	0.00000	0.00000	0.00000	0.25479	0.01504
24	115	12	0.00877	0.00131	0.00077	0.00038	0.00000	0.00000	0.00000	0.00000	0.25851	0.00695
	115	15	0.01230	0.00134	0.00059	0.00029	0.00000	0.00000	0.00000	0.00000	1.14834M	0.01296
	115	18	0.01460	0.00197	0.00081	0.00047	0.00000	0.00000	0.00000	0.00000	1.19622M	0.01798
	115	21	0.02000	0.00485	0.00102	0.00102	0.00106	0.00106	0.00000	0.00000	4.85025M	0.07189
25	116	9	0.01428	0.00131	0.00145	0.00042	0.00048	0.00024	0.00000	0.00000	0.28451	0.00586
	116	12	0.01375	0.00138	0.00205	0.00053	0.00027	0.00019	0.00000	0.00000	0.26522	0.00601
	116	15	0.01540	0.00120	0.00151	0.00038	0.00019	0.00013	0.00000	0.00000	0.25144	0.00487
	116	18	0.01734	0.00183	0.00094	0.00042	0.00000	0.00000	0.00000	0.00000	0.28461	0.00727
	116	21	0.01825	0.00289	0.00093	0.00065	0.00000	0.00000	0.00000	0.00000	0.30248	0.01231
26	117	0	0.02758	0.00237	0.00260	0.00072	0.00041	0.00029	0.00000	0.00000	0.36331	0.00861
	117	3	0.03251	0.00209	0.00216	0.00054	0.00040	0.00023	0.00000	0.00000	0.42255	0.00754
	117	6	0.04332	0.00209	0.00202	0.00045	0.00061	0.00025	0.00000	0.00000	0.30871	0.00558
	117	9	0.03420	0.00186	0.00213	0.00046	0.00111	0.00033	0.00000	0.00000	0.40715	0.00639
	117	12	0.03519	0.00182	0.00292	0.00052	0.00075	0.00027	0.00000	0.00000	0.34536	0.00569
	117	15	0.05701	0.00242	0.00164	0.00041	0.00072	0.00027	0.00000	0.00000	0.34786	0.00598
	117	18	0.08543	0.00282	0.00494	0.00068	0.00233	0.00047	0.00000	0.00000	0.37290	0.00590
	117	21	0.09209	0.00295	0.00499	0.00069	0.00283	0.00052	0.00000	0.00000	0.36052	0.00582
27	118	0	0.08320	0.00291	0.00408	0.00064	0.00264	0.00052	0.00000	0.00000	0.38207	0.00624
	118	3	0.09766	0.00387	0.00419	0.00081	0.00232	0.00060	0.00000	0.00000	0.55759	0.00932
	118	6	0.07805	0.00275	0.00240	0.00048	0.00231	0.00047	0.00000	0.00000	0.43792	0.00648
	118	9	0.11511	0.00341	0.00595	0.00077	0.00323	0.00057	0.00000	0.00000	0.37742	0.00617
	118	12	0.11162	0.00326	0.00635	0.00078	0.00285	0.00052	0.00000	0.00000	0.38533	0.00604
	118	15	0.13970	0.00610	0.00500	0.00115	0.00321	0.00093	0.00000	0.00000	0.38480	0.01009
	118	18	0.12281	0.00366	0.00629	0.00083	0.00294	0.00057	0.00000	0.00000	0.47716	0.00721
	118	21	0.15618	0.00505	0.00728	0.00108	0.00326	0.00073	0.00000	0.00000	0.36951	0.00781
28	119	0	0.25891	0.00579	0.00862	0.00105	0.00467	0.00078	0.00000	0.00000	0.36887	0.00691
	119	3	0.45746	0.00651	0.01768	0.00128	0.00703	0.00081	0.00000	0.00000	0.32811	0.00551
	119	6	0.46782	0.01344	0.02158	0.00286	0.00723	0.00166	0.00000	0.00000	0.31488	0.01100
	119	9	0.58127	0.00744	0.02244	0.00146	0.00826	0.00089	0.00000	0.00000	0.32799	0.00558
	119	12	0.59052	0.00751	0.02581	0.00157	0.01149	0.00105	0.00000	0.00000	0.33515	0.00566
	119	15	0.54366	0.00713	0.02116	0.00141	0.00749	0.00084	0.00000	0.00000	0.32932	0.00555
	119	18	0.76126	0.00875	0.02982	0.00173	0.01183	0.00109	0.00000	0.00000	0.31510	0.00562
	119	21	0.78830	0.00867	0.03106	0.00172	0.01178	0.00106	0.00000	0.00000	0.31006	0.00544
29	120	0	0.92727	0.00929	0.03314	0.00176	0.01377	0.00113	0.00000	0.00000	0.30134	0.00529
	120	3	0.84492	0.00889	0.03124	0.00171	0.01406	0.00115	0.00000	0.00000	0.30180	0.00532
	120	6	0.90812	0.00963	0.02993	0.00175	0.01460	0.00122	0.00000	0.00000	0.30715	0.00560
	120	9	0.48365	0.01366	0.01762	0.00260	0.00616	0.00154	0.00000	0.00000	0.30315	0.01069
	120	12	0.36795	0.00659	0.01092	0.00114	0.00577	0.00082	0.00000	0.00000	0.31135	0.00604
	120	15	0.33005	0.00556	0.01161	0.00104	0.00403	0.00061	0.00000	0.00000	0.28547	0.00517
	120	18	0.24736	0.00503	0.00909	0.00096	0.00357	0.00060	0.00000	0.00000	0.26705	0.00522
	120	21	0.07448	0.00264	0.00252	0.00048	0.00131	0.00035	0.00000	0.00000	0.26900	0.00501
30	121	0	0.03703	0.00188	0.00153	0.00038	0.00010	0.00010	0.00000	0.00000	0.25216	0.00492
	121	3	0.03299	0.00175	0.00158	0.00038	0.00084	0.00028	0.00000	0.00000	0.25070	0.00483
	121	6	0.03129	0.00179	0.00102	0.00032	0.00020	0.00014	0.00000	0.00000	0.38286	0.00625
	121	9	0.03634	0.00220	0.00133	0.00042	0.00013	0.00013	0.00000	0.00000	0.36801	0.00700
	121	12	0.03976	0.00215	0.00103	0.00034	0.00047	0.00023	0.00000	0.00000	0.65735	0.00874
	121	15	0.05180	0.00225	0.00166	0.00040	0.00039	0.00020	0.00000	0.00000	0.49692	0.00695
	121	18	0.06024	0.00236	0.00240	0.00047	0.00175	0.00040	0.00000	0.00000	0.32475	0.00548
	121	21	5.38517	0.02297	0.03055	0.00172	0.00689	0.00082	0.00039	0.00019	2966.31934	1.31562
May 1	122	0	49.12889	0.07209	0.14620	0.00371	0.01767	0.00129	0.00670	0.00080	1561.76074	0.71086
	122	3	141.38422	0.12852	0.44661	0.00669	0.08017	0.00283	0.01189	0.00109	738.45532	0.39378
	122	6	184.14960	0.14792	0.55627	0.00719	0.12618	0.00343	0.00800	0.00086	427.32825	0.25784
	122	9	244.29950	0.18563	0.71187	0.00848	0.19723	0.00446	0.00879	0.00094	274.39893	0.19364
	122	12	217.09973	0.36462	0.64062	0.01667	0.18800	0.00899	0.00679	0.00170	206.34625	0.35330
	122	15	177.88892	0.29610	0.45869	0.01393	0.23915	0.01019	0.00477	0.00144	115.87512	0.24592
	122	18	130.31641	0.11902	0.33595	0.00558	0.18453	0.00414	0.00241	0.00047	90.48248	0.09665
	122	21	106.58179	0.10891	0.23328	0.00469	0.18691	0.00420	0.00265	0.00050	69.75546	0.08434
2	123	0	90.43509	0.09513	0.16724	0.00394	0.18603	0.00416	0.00121	0.00033	52.56541	0.07251
	123	3	89.89478	0.09554	0.13664	0.00360	0.23953	0.00476	0.00104	0.00031	42.91345	0.06468
	123	6	74.62445	0.08612	0.16295	0.00388	0.28140	0.00510	0.00074	0.00026	34.26791	0.05730
	123	9	66.56027	0.08539	0.13344	0.00367	0.25391	0.00507	0.00121	0.00035	25.84743	0.05192
	123	12	61.45522	0.11863	0.13280	0.00529	0.29865	0.00793	0.00063	0.00036	21.66368	0.06794
	123	15	46.85208	0.14725	0.11764	0.00731	0.32552	0.01201	0.00093	0.00065	15.91541	0.08642
	123	18	33.21437	0.06671	0.08828	0.00334	0.19244	0.00502	0.00027	0.00019	12.96299	0.04180
	123	21	14.61260	0.03760	0.09669	0.00306	0.05350	0.00227	0.00019	0.00014	9.21484	0.02974

DATE 1976	DOY	HR	P4 RATE	UNC	A3 RATE	UNC	Z1 RATE	UNC	Z3 RATE	UNC	E4 RATE	UNC
May 3	124	0	2.85759	0.02091	0.17294	0.00517	0.03156	0.00217	0.00000	0.00000	7.96886M	0.03521
	124	3	1.67904	0.01505	0.12204	0.00408	0.02842	0.00193	0.00000	0.00000	5.80202M	0.02838
	124	6	1.50047	0.01189	0.08634	0.00285	0.02425	0.00151	0.00000	0.00000	5.26423M	0.02233
	124	9	1.39447	0.01136	0.05891	0.00233	0.01961	0.00135	0.00000	0.00000	4.10045M	0.01948
	124	12	1.44354	0.01228	0.03791	0.00199	0.01652	0.00131	0.00000	0.00000	6.25256M	0.02700
	124	15	0.87652	0.01110	0.02007	0.00168	0.00849	0.00110	0.00000	0.00000	2.69329	0.01957
	124	18	0.72131	0.01739	0.01210	0.00225	0.00587	0.00157	0.00000	0.00000	2.48898	0.03223
	124	21	0.95806	0.01073	0.00867	0.00102	0.00422	0.00071	0.00000	0.00000	2.43697	0.01709
4	125	0	1.02808	0.00977	0.00639	0.00077	0.00325	0.00055	0.00000	0.00000	2.40761	0.01495
	125	3	0.75512	0.00873	0.00527	0.00073	0.00354	0.00060	0.00000	0.00000	2.15390	0.01476
	125	6	1.14252	0.01481	0.00520	0.00100	0.00384	0.00006	0.00000	0.00000	2.07931	0.01995
	125	9	0.70424	0.01182	0.00337	0.00082	0.00238	0.00069	0.00000	0.00000	1.76317	0.01871
	125	12	1.03515	0.01045	0.00232	0.00049	0.00179	0.00044	0.00000	0.00000	3.79447M	0.02001
	125	15	1.02726	0.01264	0.00217	0.00058	0.00111	0.00042	0.00000	0.00000	3.34862M	0.02278
	125	18	0.89997	0.02935	0.00000	0.00000	0.00121	0.00121	0.00000	0.00000	1.59848	0.04532
	125	21	0.63476	0.04150	0.00315	0.00315	0.00000	0.00000	0.00000	0.00000	1.39465	0.06524
5	126	0	0.60253	0.01690	0.00000	0.00000	0.00132	0.00076	0.00000	0.00000	1.30447	0.02499
	126	3	0.51007	0.01435	0.00042	0.00042	0.00042	0.00042	0.00000	0.00000	10.55973M	0.06649
	126	6	0.46191	0.02124	0.00233	0.00164	0.00213	0.00151	0.00000	0.00000	8.56857M	0.09359
	126	9	0.43265	0.01016	0.00078	0.00045	0.00075	0.00043	0.00000	0.00000	1.16365	0.01729
	126	12	0.41293	0.00647	0.00091	0.00030	0.00051	0.00023	0.00000	0.00000	1.41277	0.01198
	126	15	0.33578	0.00685	0.00028	0.00020	0.00042	0.00024	0.00000	0.00000	0.93943	0.01147

Observations of Solar Cosmic Rays by "Meteor" Satellite in March - May 1976

by

S.I. Avdyushin, N.K. Pereyaslova,
Yu.M. Kulagin, M.N. Nazarova, I.E. Petrenko

Institute of Applied Geophysics
Hydrometeorological Service
Moscow, USSR

ABSTRACT

Solar cosmic ray fluxes measured experimentally by the "Meteor" Satellite during the periods 22-30 March and 29 April - 4 May 1976 are presented. Included too are comparison of fluxes with accompanying geophysical phenomena and a brief interpretation of the results obtained.

Observations of solar cosmic ray fluxes were carried out by the "Meteor" Satellite, which was launched on 11 July 1975 into a nearly circular orbit of 900 km height and 81.2° inclination. The satellite's orbital period around the Earth was ~102 min.

The equipment installed on board included the following: (1) a set of charged particle detectors with a memory device for storing roughly 18 hours of acquired data, (2) a scintillation counter, consisting of a photomultiplier tube and plastic scintillator (PF), to record protons with energies E_p>90 MeV, and (3) a Geiger counter with hemispheric absorbers (screens) of various thicknesses to record protons with energies <90 Mev. Specifics of each detector are given in Table 1. The view angle of the detectors for the soft electron component is $\sim 2\pi$; for energetic protons the detectors are practically isotropic. The time for impulse reception is 12 s.

Table 1. Detector Characteristics

Detector Type	Screen Thickness (g/cm^2)	Sensitivity: Electrons (MeV)	Sensitivity: Protons (MeV)	Detector Effective Area (cm^2)	Interval Between Counts (s)
SBM - 10 No. 1	0.04 steel	>0.15	>5	0.14	48
" No. 2	0.3	>0.7	>15	0.14	48
" No. 3	0.8	>1.7	>25	0.29	48
" No. 4	1.6	>3.2	>40	0.29	48
PF	1 Al	>0.5	>90	20	24
	8 brass				

Proton intensities of solar and galactic cosmic rays were obtained from particle flux measurements in polar zones within a range of invariant latitudes (>67-72°) that corresponds to the spread in detector threshold energy. Depending on the satellite trajectory, observations represent coverage over 5 - 15 min.

In the period 26 - 30 March 1976, "Meteor" recorded proton fluxes within the energy range 5-40 MeV in the Earth's high-latitude magnetosphere. Table 2 lists proton fluxes measured in the northern and southern polar zones of the Earth's magnetosphere during 22 - 30 March 1976. Figure 1 shows a graph of these integral intensities for energies >5, >15, >25, >40 and >90 MeV.

Solar cosmic ray events in March 1976 originated from proton flares in McMath Region No. 14143. Unipolar group No. 19669 had been observed near this region's position since 24 March. Thereafter the spot group's area grew rapidly; the number of individual spots increased; the magnetic field became more complicated; and the radio emission at 3 and 8 cm intensified. In fact, the flux density ratio (F_{3cm}/F_{8cm}) exceeded unity, implying that the evolving region would eventually emit protons.

Three severe flares of 1B importance occurred in this spot group on 25, 27 and 28 March, and the first two of these events obviously served as the source of solar cosmic ray fluxes recorded near Earth. All three flares were accompanied by X-ray bursts: Types II, III, and IV radio bursts; and ionospheric disturbances [*SGD*, 1976].

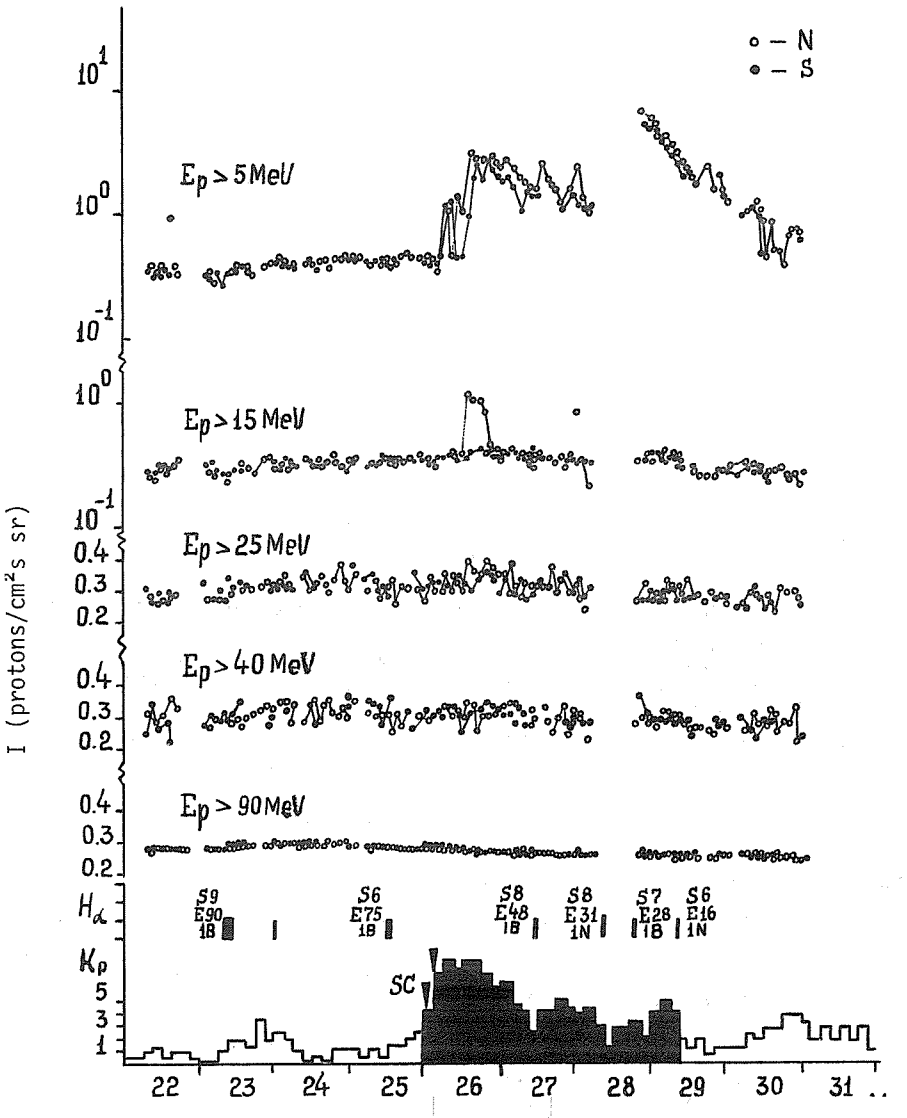

Fig. 1. Proton fluxes with energies above 5, 15, 25, 40 and 90 MeV and the Kp index with flares and geomagnetic storm sudden commencements superposed for the period 22 - 31 March 1976.

Table 2. Proton Fluxes Measured by the "Meteor" Satellite from 29 March - 30 April 1976.

Data	TUT	Hemi-sphere	J proton cm^{-2}sec^{-1}ster^{-1}				
			E_p>5MeV	>15MeV	>25MeV	>40MeV	>90MeV
22.III 1976	0808	S	0,85	0,28	0,81	0,26	0,28
	0858	N	0,88	0,26	0,29	0,82	0,27
	0952	S	0,81	0,28	0,27	0,85	0,28
	1042	N	0,84	0,25	0,27	0,29	0,28
	1136	S	0,83	0,82	0,80	0,28	0,28
	1225	N	0,88	0,81	0,28	0,81	0,28
	1319	S	0,85	0,80	0,80	0,29	0,28
	1408	S	0,84	0,28	0,82	0,29	0,28
	1500	S	0,99	0,29	0,28	0,28	0,28
	1549	N	0,86	0,81	0,29	0,87	0,28
	1781	N	0,83	0,84	0,29	0,84	0,28
23.III 1976	0251	S	0,83	0,80	0,83	0,28	0,28
	0342	N	0,84	0,27	0,27	0,28	0,28
	0481	S	0,82	0,82	0,27	0,81	0,28
	0526	N	0,29	0,26	0,28	0,80	0,28
	0619	S	0,83	0,27	0,81	0,80	0,28
	0854	S	0,26	0,27	0,27	0,82	0,29
	0948	S	0,82	0,28	0,85	0,80	0,29
	1036	N	0,83	0,28	0,29	0,29	0,28
	1181	S	0,83	0,28	0,81	0,81	0,29
	1218	N	0,89	0,27	0,83	0,80	0,29
	1315	S	0,88	0,29	0,83	0,86	0,80
	1400	N	0,87	0,82	0,80	0,28	0,29
	1543	N	0,84	0,29	0,82	0,80	0,29
	1725	N	0,82	0,27	0,81	0,82	0,29
	2048	N	0,89	0,82	0,82	0,88	0,29
	2231	N	0,40	0,82	0,83	0,84	0,29
	2320	S	0,40	0,83	0,81	0,28	0,80
24.III 1976	0012	N	0,48	0,28	0,82	0,88	0,80
	0104	S	0,88	0,28	0,81	0,81	0,80
	0155	N	0,40	0,83	0,82	0,84	0,80
	0246	S	0,89	0,82	0,82	0,85	0,80
	0336	N	0,48	0,29	0,85	0,85	0,80
	0429	S	0,88	0,84	0,81	0,83	0,80
	0520	N	0,86	0,80	0,82	0,29	0,29
	0614	S	0,87	0,81	0,82	0,85	0,80
	1032	N	0,40	0,85	0,85	0,29	0,29
	1126	S	0,48	0,84	0,86	0,85	0,80
	1215	N	0,89	0,82	0,81	0,86	0,29
	1807	S	0,87	0,81	0,81	0,28	0,80
	1857	N	0,42	0,85	0,83	0,28	0,29
	1588	N	0,48	0,80	0,85	0,84	0,29
	1719	N	0,86	0,83	0,82	0,85	0,80
	1902	N	0,44	0,89	0,80	0,82	0,29
	2048	N	0,44	0,82	0,84	0,81	0,80
	2225	N	0,47	0,81	0,89	0,83	0,80
	2314	S	0,48	0,28	0,83	0,84	0,29
25.III 1976	0008	N	0,45	0,85	0,81	0,81	0,29
	0057	S	0,42	0,83	0,89	0,87	0,29
	0147	N	0,44	0,84	0,86	0,86	0,29
	0608	S	0,41	0,80	0,84	0,86	0,29
	0658	N	0,40	0,83	0,80	0,82	0,28
	0752	S	0,42	0,81	0,85	0,85	0,29
	0842	N	0,41	0,83	0,84	0,81	0,29
	0937	S	0,48	0,87	0,80	0,84	0,29
	1025	N	0,43	0,85	0,28	0,81	0,29
	1120	S	0,40	0,85	0,82	0,28	0,29
	1209	N	0,88	0,83	0,82	0,81	0,29
	1302	S	0,44	0,84	0,28	0,87	0,29
	1349	N	0,40	0,84	0,84	0,26	0,29
	1533	N	0,46	0,85	0,26	0,81	0,28
	1715	N	0,48	0,83	0,82	0,28	0,28
	1857	N	0,46	0,85	0,81	0,82	0,28
26.III 1976	0002	N	0,84	0,84	0,27	0,66	0,28
	0052	S	0,41	0,82	0,82	0,82	0,28
	0142	N	0,88	0,85	0,85	0,80	0,28
	0236	S	0,42	0,86	0,83	0,81	0,29
	0327	N	0,85	0,29	0,80	-	0,28
	0419	S	0,45	0,86	0,88	0,83	0,29
	0605	S	1,17	0,86	0,80	0,81	0,28
	0654	N	1,06	0,84	0,86	0,84	0,28
	0746	S	1,20	0,86	0,82	0,84	0,28
	0837	N	0,45	0,82	0,81	0,81	0,27
	0931	S	0,46	0,81	0,85	0,84	0,28
	1021	N	1,89	0,88	0,83	0,82	0,28
	1115	S	0,45	0,82	0,85	0,81	0,28
	1205	N	1,02	0,87	0,81	0,80	0,27
	1259	S	0,96	0,84	0,82	0,26	0,27
	1846	N	3,86	1,29	0,40	0,85	0,27
	1439	S	1,84	0,88	0,81	0,82	0,27
	1428	N	2,92	1,08	0,86	0,84	0,27
	1707	N	2,64	1,08	0,85	0,27	0,27
	1800	S	1,75	0,42	0,85	0,83	0,27
	1851	N	2,56	0,85	0,87	0,81	0,27
	1948	S	2,56	0,41	0,87	0,85	0,27
	2034	N	2,59	0,43	0,89	0,81	0,27
	2128	S	2,16	0,45	0,86	0,84	0,27
	2215	N	2,48	0,42	0,86	0,82	0,27
	2304	S	1,94	0,89	0,84	0,83	0,27
	2355	N	2,28	0,86	0,85	0,84	0,27
27.III 1976	0045	S	1,77	0,88	0,29	0,81	0,27

Table 2 (Continued)

Data	TUT	Hemisphere	J proton cm^{-2}sec^{-1}ster^{-1} Ep>5MeV	>15MeV	>25MeV	>40MeV	>90MeV
	0188	N	2,98	1,89	0,86	0,85	0,27
	0230	S	1,84	0,89	0,84	0,81	0,27
	0822	N	2,41	0,40	0,29	0,85	0,26
	0411	S	1,55	0,42	0,88	0,28	0,27
	0558	S	1,94	0,86	0,29	0,84	0,26
	0644	N	1,87	0,88	0,80	0,82	0,27
	0742	S	1,01	0,85	0,54	0,28	0,26
	0881	N	1,76	0,87	0,58	0,28	0,26
	0927	S	1,49	0,40	0,28	0,88	0,27
	1014	N	1,59	0,88	0,82	0,82	0,27
	1111	S	1,44	0,85	0,80	0,80	0,27
	1157	N	1,58	0,89	0,82	0,82	0,27
	1258	S	1,45	0,87	0,84	0,81	0,27
	1848	N	2,65	0,91	0,82	0,88	0,27
	1523	N	1,81	0,84	0,81	0,80	0,26
	1702	N	1,52	0,82	0,88	0,26	0,26
	1848	N	1,55	0,87	0,29	0,80	0,26
	2026	N	1,24	0,81	0,84	0,84	0,26
	2117	N	1,17	0,85	0,55	0,29	0,26
	2208	N	1,62	0,89	0,28	0,25	0,26
	2258	S	1,44	0,86	0,80	0,27	0,26
	2350	N	2,40	0,87	0,81	0,88	0,26
28.II 1976	0041	S	1,15	0,88	0,88	0,80	0,27
	0182	N	1,81	0,82	0,28	0,81	0,26
	0224	S	1,05	0,84	0,28	0,29	0,26
	0315	N	1,01	0,25	0,24	0,28	0,26
	0408	S	1,07	0,88	0,80	0,29	0,26
	2022	N	6,68	0,84	0,28	0,28	0,26
	2111	S	5,05	0,84	0,28	0,87	0,27
	2209	N	5,77	0,88	0,88	0,80	0,26
	2258	S	5,07	0,88	0,27	0,81	0,26
	2345	N	5,29	0,82	0,27	0,29	0,26
29.II 1976	0035	S	4,80	0,89	0,80	0,29	0,26
	0127	N	4,24	0,89	0,29	0,27	0,26
	0220	S	4,19	0,84	0,27	0,29	0,26
	0310	N	4,05	0,41	0,27	0,82	0,26
	0402	S	3,89	0,88	0,29	0,29	0,26
	0452	N	4,84	1,61	0,88	0,82	0,26
	0547	S	3,27	0,86	0,81	0,80	0,26
	0637	N	3,25	0,88	0,82	0,80	0,25
	0731	S	3,01	0,86	0,81	0,29	0,26
	0821	N	3,02	0,87	0,81	0,81	0,25
	0916	S	2,85	0,81	0,27	0,29	0,26
	1004	N	2,52	0,88	0,29	0,28	0,26
	1059	S	1,98	0,81	0,28	0,29	0,26
	1147	N	2,38	0,81	0,84	0,26	0,26
	1242	S	2,17	0,81	0,28	0,24	0,25
	1331	N	1,91	0,28	0,28	0,27	0,27
30.II 1976	0541	S	0,95	0,26	0,25	0,80	0,26
	0638	N	1,05	0,88	0,26	0,26	0,26
	0727	S	1,09	0,29	0,25	0,26	0,25
	0815	N	1,19	0,80	0,29	0,81	0,26
	0911	S	0,92	0,27	0,81	0,24	0,25
	0959	N	1,05	0,80	0,29	0,28	0,26
	1053	S	0,46	0,29	0,28	0,29	0,25
	1142	N	0,88	0,26	0,27	0,28	0,25
	1257	S	0,45	0,25	0,24	0,28	0,26
	1326	N	0,88	0,28	0,29	0,82	0,25
	1507	N	0,50	0,28	0,27	0,81	0,26
	1647	N	0,48	0,80	0,28	0,26	0,25
	1852	N	0,89	0,27	0,81	0,28	0,25
	2012	N	0,69	0,25	0,80	0,28	0,25
	2154	N	0,75	0,26	0,80	0,82	0,24
	2337	N	0,76	0,22	0,28	0,28	0,24
	0025	S	0,67	0,28	0,25	0,24	0,24

N = Northern Polar Zone

S = Southern Polar Zone

Proton fluxes from the 25 March flare (1154 UT; S07 E75) arrived at Earth after the shock wave from the flare on the 23rd. At 1346 UT on the 26th the fluxes for E_p>5 MeV peaked near 40 particles/cm^{2}s. Proton intensities at energies $\gtrsim$5 MeV varied considerably because the K_p index rose as high as 8 several times.

Throughout the initial, the arrival, and the flux enhancement periods, a considerable asymmetry in proton penetration into the polar caps emerged: the flux over the southern cap was 1.6 times greater than that over the northern zone. During times of maximum and decline in the proton flux, the asymmetry reversed itself; the flux intensity over the northern cap exceeded that over the southern cap by more than a factor of three. The sense of the asymmetrical proton intensities failed to exhibit a dependence on the dominant direction of the interplanetary magnetic field, because the sector field sign remained negative over the $\gtrsim$10 hours of observed nonsymmetrical fluxes. Moreover, according to the regularity established by Pereyaslova *et al.* [1976] and Mikirova *et al.*[1976], proton fluxes penetrating the southern polar cap should predominate whenever the interplanetary field points toward the sun. It is therefore difficult to explain the north-south asymmetry. Perhaps severely disturbed geomagnetic conditions and sign variations in the interplanetary magnetic field over a 24-hour period affect particle penetration into high-latitude zones.

A second enhancement of solar protons was recorded on 28 March - a particle injection due to the flare on the 27th at 1204 UT at S08 E48. This event generated protons with energies in the range 5-15 MeV. For protons with E_p>5 MeV the maximum intensity registered was $\sim$100 particles/cm^{2}s. Again, the sign of the observed polar flux asymmetry did not coincide with the direction of the interplanetary magnetic field sector: north polar zone fluxes exceeded south polar zone fluxes during a 5 to 6-hour period of negative (toward the sun) interplanetary field. The flare on 28 March at 1905 UT at S07 E28 failed to generate a significant proton flux.

McMath Region No. 14143 returned to the east limb on 19 April and was renumbered as plage 14179 during its third rotation; it contained Mt. Wilson spot group No. 19677. At 2048 UT on 30 April 1976, an importance 2B chromospheric flare, resembling the letter "Y" in its Hα structure, erupted at S09 W47. An X-ray burst with peak intensity of 0.18 ergs/cm^{2}s in the 1 - 8Å passband, Type I - IV meter wavelength radio bursts, SIDs, and PCA accompanied the flare [*SGD*, 1976].

Figure 2 shows detector data for E_p above 5, 15, 25, 40 and 90 MeV and K_p index values for the period 29 April - 4 May 1976. Since the flare occurred 47° west of the central meridian, the interplanetary lines of force provided the accelerated protons a direct path to Earth. Thirty min after the event began enhanced particle fluxes were recorded near Earth; they reached a maximum value about 2.5 hours after the flare itself maximized. South polar cap proton intensities exceeded those over the northern cap and peaked near 500 protons/cm^{2}s sr at E_p>5 MeV. For E_p>90 MeV the particle flux maximized at 15 protons/cm^{2}s sr.

Data on proton fluxes recorded by the "Meteor" Satellite from 29 April to 4 May 1976 are presented in Table 3, and integral spectra of the protons are given in Figure 3. On 30 April the Apatity, Alert and Deep River neutron monitors recorded the 2B flare's associated ground level event. The integral spectrum may be expressed in power form as

$$I(E>E_0) = I_0 E^{-\gamma}.$$

The spectral index (γ) assumed the value 1.5 initially. Gradually the spectrum softened and γ equaled 3.5 by 2 May. A short-term asymmetry in solar cosmic ray penetration into the Earth's magnetosphere was evident. In this case the sense of the flux imbalance agreed with the sign of the interplanetary magnetic field. For example, on 30 April the interplanetary magnetic field was directed toward the sun, and solar cosmic ray protons penetrated mainly into the southern polar cap. By 0200 UT on 1 May, the ratio between the southern and northern polar cap intensities was $\simeq$ 1.5.

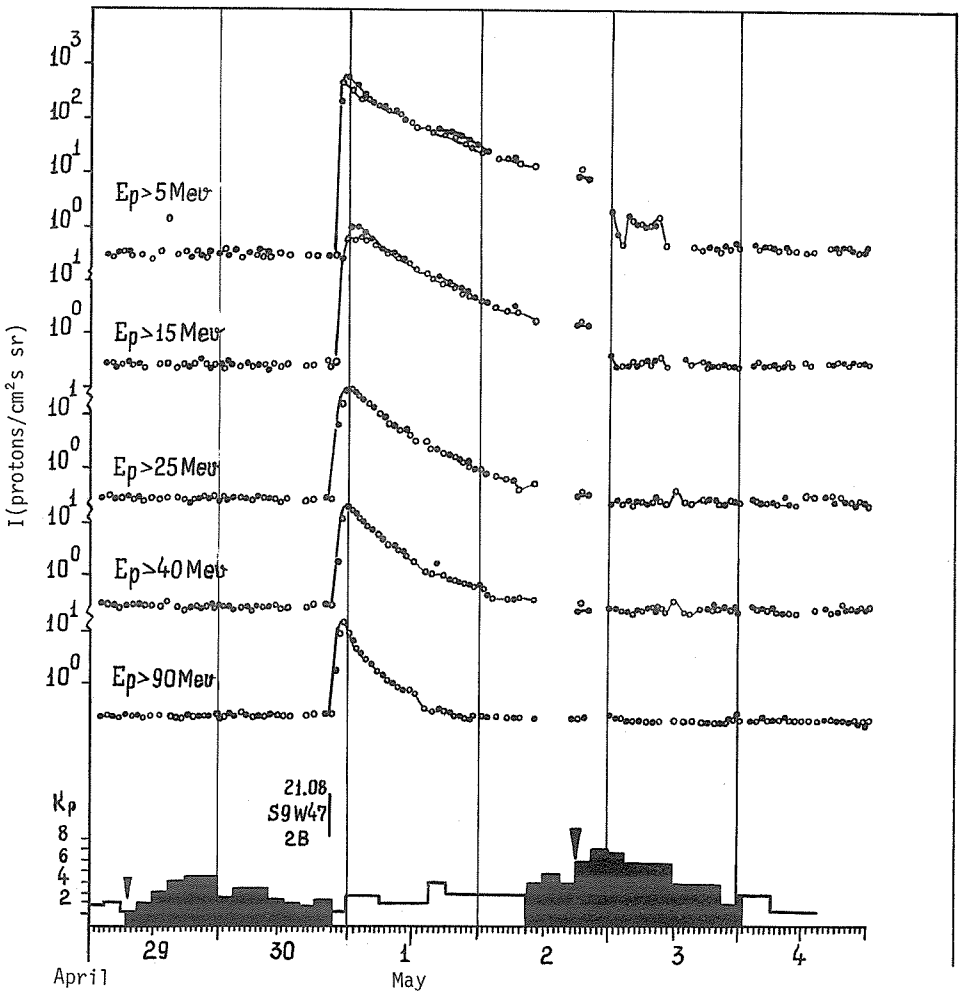

Fig. 2. Proton fluxes with energies above 5, 15, 25, 40 and 90 MeV and the Kp index with flare and geomagnetic storm sudden commencements superposed for the period 29 April - 4 May 1976.

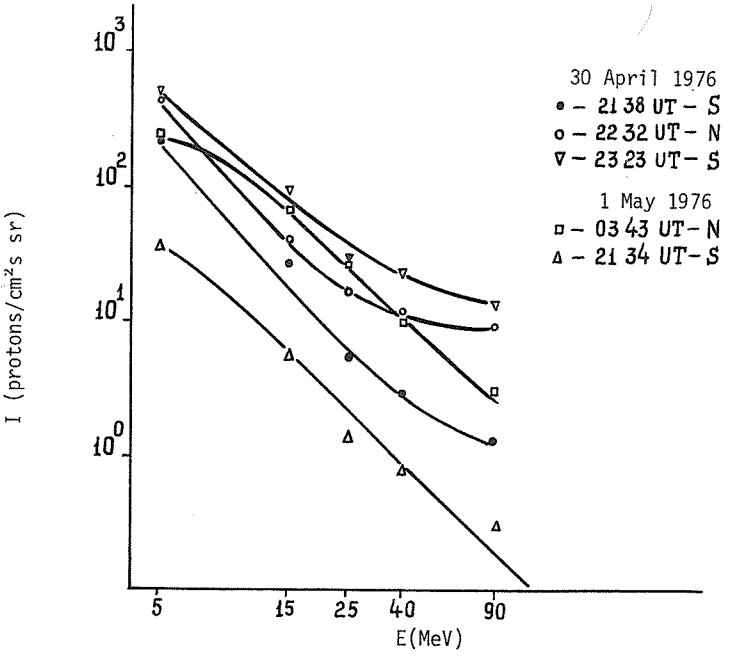

Fig. 3. Integral spectra for the 30 April 1976 event.

Table 3. Proton Fluxes Measured by the "Meteor" Satellite from 29 April - 4 May 1976.

Data	TUT	Hemi-sphere	J proton cm^{-2} sec^{-1} ster^{-1} Ep>5MeV	>15MeV	>25MeV	>40MeV	>90MeV
29.IV 1976	0300	S	0,297	0,275	0,288	0,3I2	0,266
	0354	N	0,279	0,279	0,295	0,287	0,258
	0447	S	0,3I4	0,250	0,242	0,295	0,270
	0538	N	0,34I	0,267	0,287	0,245	0,263
	0629	S	0,334	0,283	0,299	0,288	0,27I
	072I	N	0,29I	0,267	0,284	0,3I2	0,260
	08I2	S	-	0,277	0,298	0,3I2	0,260
	0903	N	0,295	0,259	0,259	0,277	0,256
	I044	N	0,249	0,257	0,287	0,296	0,258
	I228	N	0,344	0,284	0,259	0,275	0,257
	I407	N	I,530	0,233	0,259	0,325	0,260
	I55I	N	0,297	0,289	0,296	0,277	0,268
	I729	N	0,344	0,262	0,267	0,26I	0,26I
	I8I9	S	0,267	0,28I	0,242	0,275	0,263
	I9I4	N	0,3I5	0,334	0,278	0,293	0,264
	2003	S	0,302	0,265	0,309	0,259	0,265
	2055	N	0,279	0,238	0,30I	0,285	0,265
	2I46	S	0,3I4	0,270	0,284	0,309	0,266
	2238	N	0,357	0,293	0,320	0,284	0,262
	2329	S	0,303	0,275	0,262	0,287	0,268
30.IV 1976	0022	N	0,348	0,249	0,30I	0,285	0,264
	0II2	S	0,275	0,253	0,283	0,287	0,268
	0257	S	0,346	0,252	0,287	0,27I	0,266
	0348	N	0,28I	0,262	0,295	0,277	0,259
	044I	S	0,307	0,282	0,283	0,288	0,267
	0532	N	0,308	0,275	0,293	0,232	0,262
	0624	S	0,326	0,27I	0,3II	0,30I	0,27I
	07I6	N	0,277	0,28I	0,3I6	0,277	0,265
	0807	S	0,303	0,259	0,2II	0,280	0,267
	0852	N	0,297	0,286	0,3II	0,3I5	0,265
	I040	N	0,323	0,260	0,253	0,267	0,266
	I22I	N	0,300	0,259	0,282	0,262	0,263
	I544	N	0,300	0,294	0,256	0,284	0,267
	I727	N	0,287	0,27I	0,294	0,303	0,26I
	I8I8	S	-	0,334	0,283	0,30I	0,267
	I956	S	0,298	0,244	0,826	0,290	0,268
1.V 1976	00I5	N	372	94,5	30,5	I9,5	8,89
	0I08	S	408	I08	29,I	I7,9	6,79
	0I57	N	229	73,3	2I,3	I3,4	4,87
	0254	S	287	78,6	2I,I	II,6	4,07
	0343	N	24I	68,2	I6,8	9,97	3,07
	0437	S	238	60,5	I4,0	7,68	2,40
	0527	N	I74	46,5	II,3	6,30	I,85
	06I9	S	I67	4I,0	9,66	5,32	I,58
	0709	N	I84	33,5	7,84	4,I7	I,28
	0802	S	I37	33,8	7,20	4,26	I,2I
	0852	N	III	25,4	5,90	3,2I	0,982
	0946	S	98,3	27,3	6,2I	3,34	0,986
	I034	N	9I,7	20,7	4,46	2,42	0,795
	I2I4	N	73,7	I6,7	3,7I	I,9I	0,676
	I358	N	7I,I	I3,57	3,I6	I,55	0,38
	I538	N	60,2	II,5	2,49	I,35	0,35
	I629	S	74,8	I2,9	2,64	I,99	0,36
	I722	N	54,3	9,6I	2,I5	I,I0	0,33
	I8I0	S	62,6	9,95	2,II	I,24	0,34
	I903	N	42,4	8,II	I,69	0,9I	0,3I
	I952	S	45,4	7,58	I,70	0,92	0,3I
	2045	N	36,I	6,54	I,40	0,78	0,30
	2I34	S	35,9	5,4I	I,39	0,78	0,30
	2227	N	29,I	5,04	I,I4	0,69	0,29
	23I8	S	32,I	5,07	I,02	0,69	-
2.V 1976	00II	N	27,8	4,65	I,09	0,59	0,29
	0I03	S	27,2	4,20	0,88	0,4I	0,29
	0338	N	I9,0	3,45	0,76	0,37	0,28
	05I8	N	I8,9	2,78	0,73	0,40	0,27
	06I5	S	20,2	3,8I	0,68	0,40	0,28
	0704	N	I4,9	2,77	0,40	0,37	0,30
	I0I7	N	I2,8	2,I3	0,63	0,35	0,27
	I805	S	8,69	I,66	0,33	0,23	0,27
	I854	N	I0,4	I,98	0,36	0,35	0,27
	I943	S	7,36	I,44	0,34	0,24	0,26
3.V 1976	0000	S	2,I0	0,38	0,25	0,28	0,25
	0052	S	0,44	0,25	0,28	0,29	0,25
	0I4I	N	0,49	0,29	0,26	0,26	0,25
	0244	S	I,63	0,28	0,28	0,24	0,24
	0332	N	I,37	0,33	0,25	0,23	0,24
	0427	S	I,29	0,30	0,28	0,25	-
	05I4	N	I,I9	0,35	0,27	0,26	0,23
	06I0	S	I,28	0,34	0,27	0,28	0,24
	0659	N	I,28	0,30	0,26	0,30	0,24
	075I	S	I,26	0,33	0,32	0,27	0,25
	083I	N	I,62	0,4I	0,30	0,27	0,24
	I024	N	0,49	0,3I	0,25	0,29	-
	I204	N	-	-	0,42	0,37	0,24
	I347	N	-	0,37	0,28	0,22	0,24
	I529	N	0,48	0,30	0,26	0,22	0,24
	I7II	N	0,48	0,32	0,32	0,27	0,24
	I800	S	0,45	0,3I	0,30	0,28	0,24
	I852	N	0,48	0,27	0,27	0,25	0,24
	I940	S	0,44	0,27	0,28	0,33	0,25
	203I	N	0,39	0,27	0,25	0,26	0,24
	2I24	S	0,45	0,29	0,26	0,29	0,25
	22I7	N	0,4I	0,28	0,28	0,28	0,28
	2308	S	0,48	0,27	0,26	0,30	0,30
	2400	N	0,4I	0,26	0,27	0,25	0,24
4.V 1976	0236	S	0,48	0,30	0,29	0,28	0,25
	0327	N	0,42	0,32	0,30	0,28	0,24
	042I	S	0,44	0,28	0,27	0,28	0,26
	0509	N	0,44	0,29	0,25	0,25	0,25
	0604	S	0,47	0,3I	0,26	0,30	0,25
	0654	N	0,4I	0,28	0,27	0,28	0,25
	0745	S	0,44	0,27	0,32	0,25	0,26
	0836	N	0,40	0,33	0,24	0,26	0,25
	I0I8	N	0,37	0,27	0,25	0,24	0,25
	I20I	N	0,37	0,32	0,32	-	0,25
	I342	N	0,39	0,3I	0,28	0,26	0,26

REFERENCES

MIKIROVA, N. A., N. A. MIKRYUKOVA, W. N. NAZAROVA, N. K. PEREYASLOVA and I. E. PETRENKO — 1976 — O prostranstvennon raspredelenii solnetshnikh kosmitsheskikh lutsheij v magnitosfere Zemli, *Izvestiya AN SSSR, ser. fizitsheskaya, 40,* 471-476.

PEREYSASLOVA, N. K., M. N. Nazarova, S. M. Mansurov and L. G. Mansurova — 1976 — Nekotorie zakonomernosti svyazi solnetshnikh lutsheij v polyarnikh oblastyakh s sektornoij strukturoij mej-planetarnogo magnitnogo polya, *Geomagnetizm i aeronomiya, 16,* 407-412.

SGD — 1976 — *Solar-Geophysical Data, 380, 381, 383, Part I,* April, May, July 1976, U.S. Department of Commerce, (Boulder, Colorado, U.S.A. 80302).

Variations of Electron Fluxes in the Outer Radiation Belt from Observations of the "Meteor" Satellite in March 1976

by

S.I. Avdyushin, F.L. Dlikman, E.A. Ginzburg, V.A. Kuzmina
Yu.M. Kulagin, G.A. Kirdina, A.B. Malyshev and P.M. Svidskii

Institute of Applied Geophysics
Hydrometeorological Service of the USSR
Moscow, USSR

ABSTRACT

Data on the structure of electron fluxes with energies above 0.15 Mev, 0.7 Mev, and 1.7 Mev in the outer radiation belt are presented as observed by the "Meteor" satellite during the period 25 - 29 March. It is shown that spatial and spectral variations can be explained by the local impact of ring current electrons on precipitation and acceleration processes.

Experimental results on variations of electron fluxes within the outer radiation belt during a magnetic storm with sudden commencement are discussed in this paper. The magnetic disturbance used here as an example began about 2400 UT on 25 March 1976 and produced a maximum Dst value of 220γ at 0900 UT on 26 March [*SGD*, 1976].

"Meteor" satellite data have been used to complete this study. These observations consist of flux measurements from a circular orbit ~900 km above the Earth's surface and inclined 81° with respect to the equator. Electrons with energies more than 0.15 Mev, 0.7 Mev, 1.7 Mev, and 3 Mev were recorded. Threshold energy values were measured by placing a hemispheric screen of known thickness around the gas-discharge counters. Detector sensitivity was isotropic within the limits of solid angle 2π.

Figures 1a - 1d show the dependence of elctron fluxes of the above energies on L during different periods of the 25 March 1976 magnetospheric storm. Figure 1a shows electron distributions in the pre-storm period; Figures 1b and 1c illustrate electron distributions during storm development; and Figure 1d displays the electron flux profiles after the storm. One can note the following peculiarities of the period:

a) The energy spectrum of electrons and their spatial distribution changed markedly by 0930 UT on 26 March. The maximum of electron flux at all energies fell between an L value of 3.0 and 3.2. Electron flux values with energy above 0.7 Mev decreased sharply from levels recorded on 25 March.

b) At 1810 UT on 26 March the position of electron flux maximum at each energy shifted to a lower L value and increased in magnitude.

c) After the storm on 29 March, the spatial redistribution of the electrons was completed at each energy. It is clear that energetic particles filled the gap between the inner and outer radiation belts and that electron fluxes with energies above 0.15 Mev and 0.7 Mev exceeded flux values recorded during the pre-storm period on 25 March.

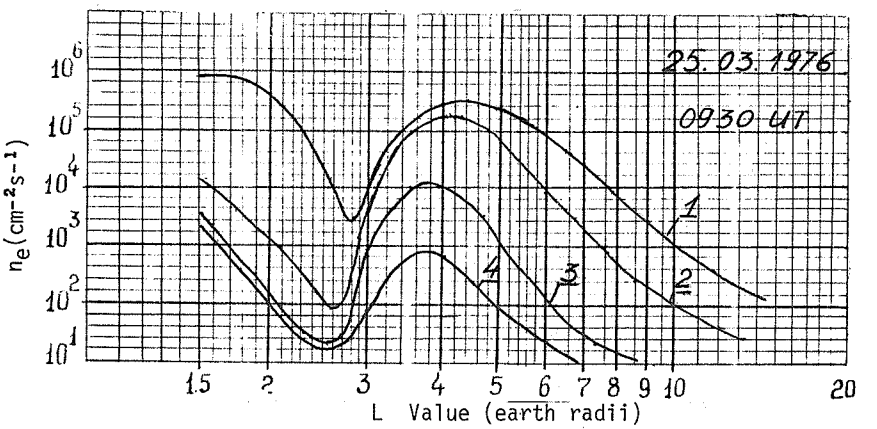

Fig. 1a. Distribution of electron fluxes with energies above 0.15 Mev (1), 0.7 Mev (2), 1.7 Mev (3), and 3 Mev (4) during the pre-storm period at 0930 UT on 25 March 1976.

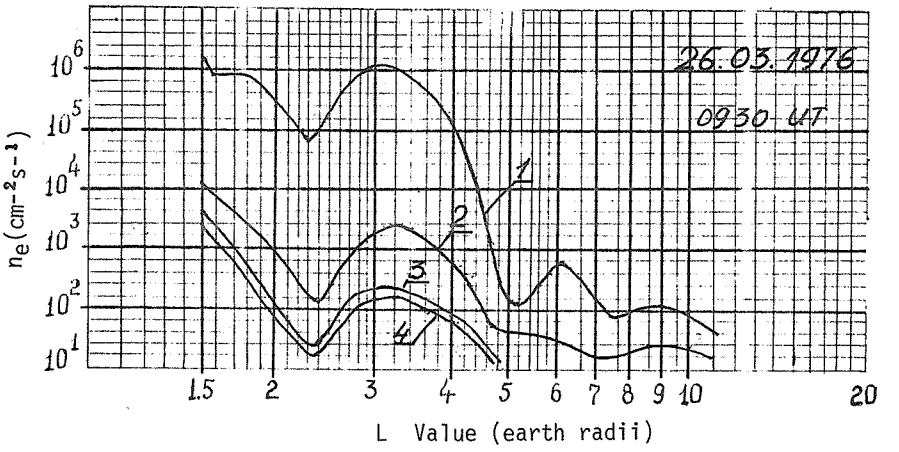

Fig. 1b. Distribution of electron fluxes with energies above 0.15 Mev (1), 0.7 Mev (2), 1.7 Mev (2), and 3 Mev (4) during storm development at 0930 UT on 26 March 1976.

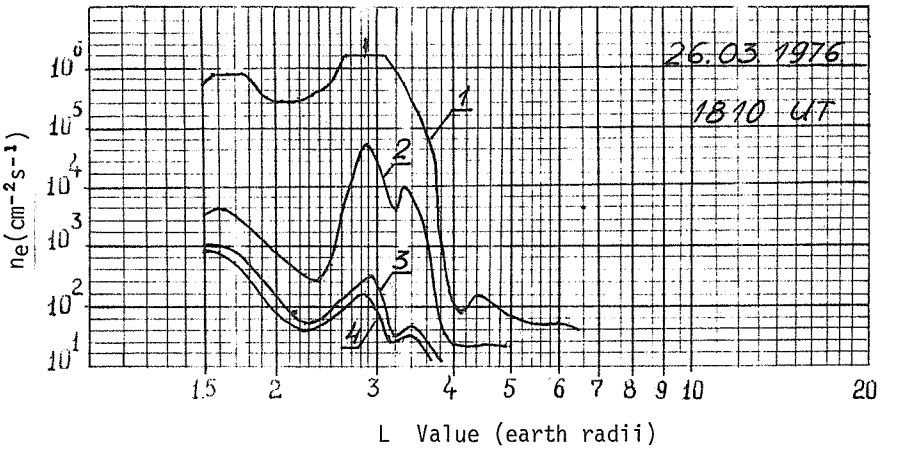

Fig. 1c. Disbribution of electron fluxes with energies above 0.15 Mev (1), 0.7 Mev (2), 1.7 Mev (3), and 3 Mev (4) during storm development at 1810 UT on 26 March 1976.

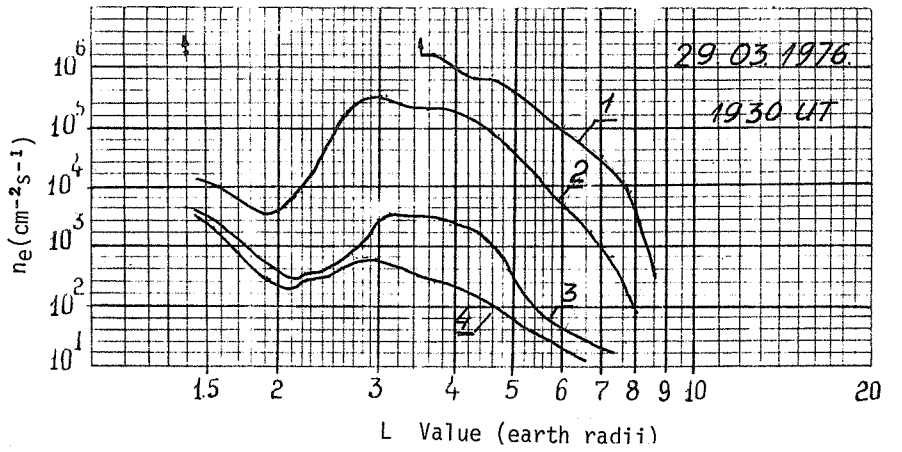

Fig. 1d. Distribution of electron fluxes with energies above 0.15 Mev (1), 0.7 Mev (2), 1.7 Mev (3), and 3 Mev (4) after the storm at 1930 UT on 29 March 1976.

Figures 2a and 2b give detailed observations on electron flux variations with energies more than 0.7 Mev on 26 - 27 March. The data are presented as synoptic maps of particle flux isolines in L; the geomagnetic longitude of the satellite's crossing of the outer radiation belt forms the x coordinate. Individual maps are drawn for the Northern and Southern Hemispheres and for the ascending and descending halves of the satellite orbit. The direction of satellite movement is shown by an arrow. Circled numbers in each quadrant refer to the same orbit. The UT time of crossing the belt's outer boundary during each orbit part and the corresponding magnetic local time (MLT) for Figure 2a are given in Table 1. Table 2 lists similar data for Figure 2b. Such a representation of the data allows us to compare low-altitude fluxes at similar magnetic local times and to isolate longitudinal variations.

Table 1.

UT and Magnetic Local Times (MLT) of Outer Belt Boundary Crossings for Figure 2a.

Date 1976	Orbit No.	Quadrant I UT (MLT)	Quadrant II UT (MLT)	Quadrant III UT (MLT)	Quadrant IV UT (MLT)
March 25	1	2036(0.0)	2044(5.0)	2125(11.0)	2130(15.5)
	2	2217(23.4)	2226(5.7)	2306(10.3)	2320(18.8)
26	3	2357(22.0)	0010(6.4)	0046(9.4)	0100(18.7)
	4	0138(21.0)	0153(7.4)	0230(8.7)	0243(19.8)
	5	0330(20.3)	0335(8.0)	0411(8.1)	0430(20.3)
	6			0556(7.8)	0612(20.4)
	7	0648(19.9)	0703(8.5)	0740(7.8)	0757(20.4)
	8	0831(20.0)	0847(8.4)	0923(8.1)	0940(20.2)
	9	1015(20.3)	1031(7.9)	1108(8.7)	1123(19.8)
	10	1158(20.8)	1214(7.4)	1251(9.6)	1306(19.5)
	11	1340(21.3)	1356(6.9)	1434(10.3)	1447(18.8)
	12	1522(21.7)	1538(6.5)		
	13	1704(22.1)	1718(4.1)	1757(11.3)	1807(17.8)
	14	1846(22.3)	1859(5.3)	1936(10.1)	1947(17.8)

Table 2.

UT and Magnetic Local Times (MLT) of Outer Belt Boundary Crossings for Figure 2b.

Date 1976	Orbit No.	Quadrant I UT (MLT)	Quadrant II UT (MLT)	Quadrant III UT (MLT)	Quadrant IV UT (MLT)
March 26	1	1846(22.3)	1859(5.3)	1936(10.7)	1947(17.8)
	2	2028(22.5)	2041(5.6)	2117(10.2)	2129(17.3)
	3	2209(22.6)	2257(9.7)	2257(9.7)	2312(17.9)
27	4	2350(21.5)	0006(6.7)	0039(9.1)	0055(19.0)
	5	0131(21.2)	0149(7.2)	0222(8.6)	0239(19.6)
	6	0314(20.1)	0331(7.9)	0405(7.9)	0423(20.1)
	7				0607(20.3)
	8	0643(19.6)	0658(8.6)	0735(7.5)	0751(20.3)
	9	0826(19.8)	0841(8.3)	0919(8.0)	0935(20.0)
	10	1009(20.3)	1025(7.8)	1103(8.7)	1118(19.6)
	11	1152(20.8)	1209(7.1)	1246(9.6)	1335(21.7)
	12	1335(21.7)	1351(5.7)	1429(12.1)	1442(17.6)
	13	1517(22.0)	1532(5.7)		
	14	1659(22.6)	1712(4.9)	1751(13.0)	1801(15.8)

Figures 2a and 2b contain the following main peculiarities:

a) The first two orbits given in Figure 2a present measurements before the magnetic storm began. Flux distributions correspond to the quiet magnetosphere.

b) The first crossing of the outer radiation belt after the storm began took place at 0010 UT on 26 March during the third orbit (Quadrant II). The isoline shift to lower L at the inner belt boundary and upward at the outer boundary obviously corresponds to enhanced precipitation, resulting from magnetospheric compression during a sudden impulse.

c) Electron flux variations at the outer boundary of the belt were observed during orbits 4 (Quadrant III) and 5 (Quadrant I). This fact probably reflects the development of substorm activity during the period [Ginzburg and Malyshev, 1974].

d) The shift in the outer boundary of the >0.7 Mev electron fluxes to lower L and the simultaneous decrease in the trapped particle fluxes were caused by a sharp increase in the precipitation rate of trapped electrons. Maximum fluxes were recorded between about 0700 and 0800 UT, just before Dst variations reached their maximum.

Beginning at 1300 UT on 26 March, a gradual increase in electron fluxes with energies above 0.7 Mev occurred. These fluxes peaked near L = 2.9. Figure 2b shows the dynamics of this growth.

The results presented show that during a severe magnetospheric storm one can easily distinguish two phases of energetic electron flux variations: an electron precipitation into the atmosphere and a generation (acceleration) of new particles with energies up to 1 Mev. The processes occur at the background of intensive ring current and enhanced pitch-angle diffusion. The coincidence in the maxima of accelerated electron flux distributions for different energies reflects an accelerating mechanism acting near a given L. The closeness of this maximum L value to the position of the maximum ring current intensity and the occurrence of continuously enhanced precipitation during this period indicate that VLF waves, generated by ring current instabilities, may play a significant role in the acceleration process.

REFERENCES

GINZBURG, E. A. and A. B. MALYSHEV 1974 Povedenie Granitsty Zakhvata vo Vremya Magnitosfernoi Subburi, *Trudy IPG, N29,* 5-8.

1976 *Solar-Geophysical Data, 381 Part I,* U.S. Department of Commerce, (Boulder, Colorado, U.S.A. 80302).

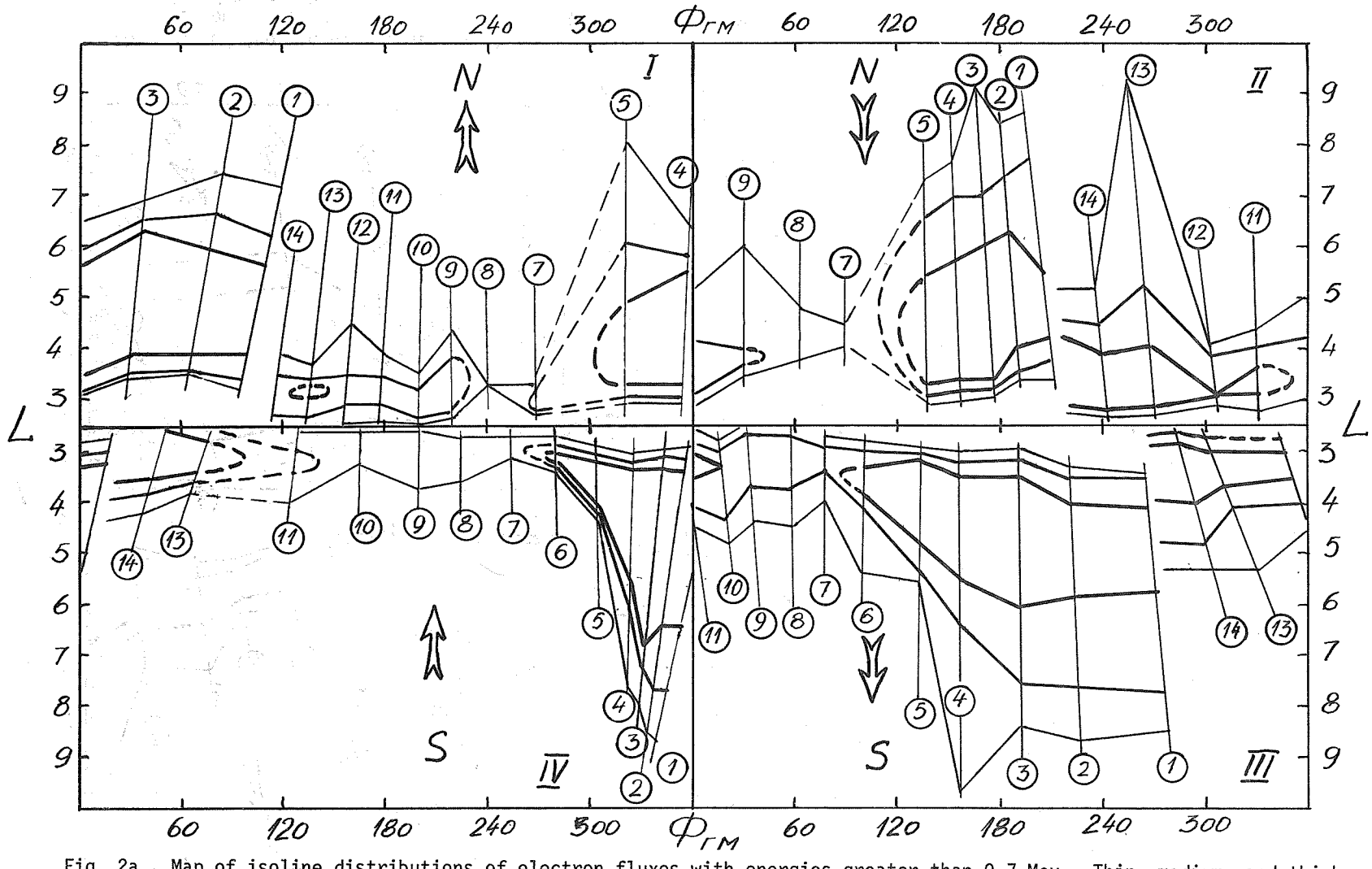

Fig. 2a. Map of isoline distributions of electron fluxes with energies greater than 0.7 Mev. Thin, medium, and thick contour lines denote fluxes of 10^2, 10^3, and 10^4 electrons/cm^{2}s as observed by the "Meteor" satellite during 25 - 26 March 1976.

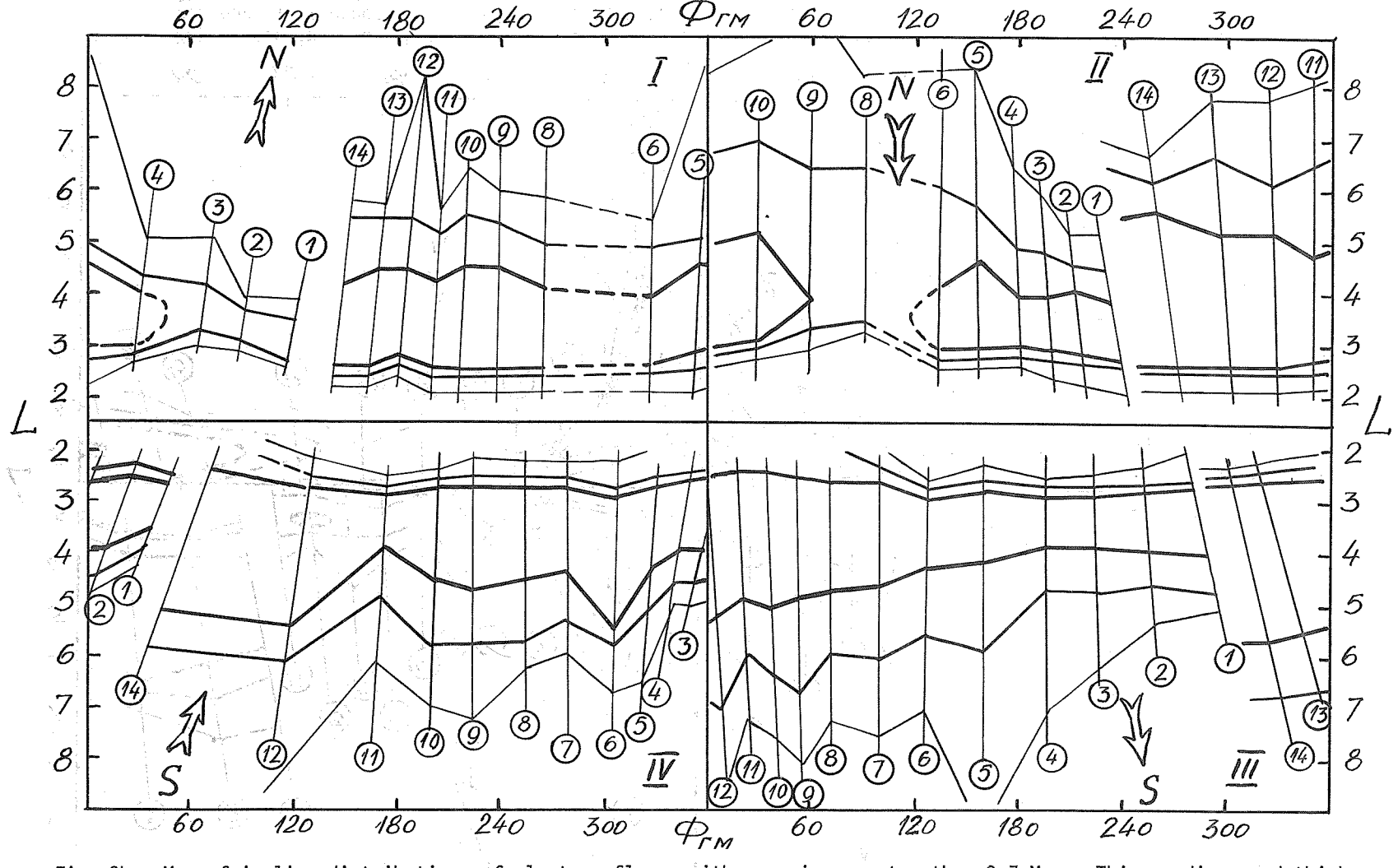

Fig. 2b. Map of isoline distributions of electron fluxes with energies greater than 0.7 Mev. Thin, medium, and thick contour lines denote fluxes of 10^2, 10^3, and 10^4 electrons/cm^{2}s as observed by the "Meteor" satellite during 26-27 March 1976.

Low-Energy Precipitating Electrons Over the Polar Caps Recorded by Instruments on DMSP Satellites

by

H. W. Kroehl and M. A. Henning
National Geophysical and Solar-Terrestrial Data Center
Environmental Data Service
NOAA, Boulder, CO 80302 U.S.A.

and

C. -I. Meng
Space Sciences Laboratory
University of California
Berkeley, CA 94720 U.S.A.

Introduction

Measurements of precipitating low-energy electrons over the polar cap regions have been recorded recently by instruments on the satellites ISIS, IMP and DMSP. Winningham and Heikkila [1974] identified three types of soft particle precipitation which they named polar rain, polar shower, and polar squall. The most common type, polar rain, is a uniform, weak flux of low-energy electrons in which the electron energy flux is enhanced above the quiet-time level. Characteristic features have been described by Fennell *et al.* [1975], Yeager and Frank [1976], Foster and Burrows [1976], and Meng and Kroehl [1977]. Though these investigators disagree on the source of the electrons, none doubts that solar conditions and the interplanetary field orientation affect the electron flux. The purpose of this data report is to present the "polar rain" characteristics over both polar regions during the STIP Interval II period from 20 March to 5 May 1976. Observations consist of average counts of uniform electron precipitation measured in the three lowest energy channels.

The Defense Meteorological Satellite Program (DMSP)

The Air Weather Service's DMSP instrumentation offers an opportunity to study polar cap and auroral phenomena because the dawn/dusk and noon/midnight polar orbiting satellites operate continually near 800 km altitude. Two of the DMSP instruments are of interest to upper atmospheric physicists: a scanning optical telescope and a precipitation electron spectrometer, measuring electron energies between 0.2 and 20 keV. Characteristics of the electron spectrometer have been described by Mizera *et al.* [1975] and Meng [1976].

The National Geophysical and Solar-Terrestrial Data Center receives the DMSP electron data arranged in eight-second blocks. Each block contains the geographic location and universal time of the satellite, the corrected geographic subpoint (CGS) of the satellite transferred along magnetic field lines [Cain, *et al.*, 1965] to 110 km altitude, the geomagnetic coordinates [Gustafsson, 1969] of the CGS, the magnetic local time, and the eight, one-second counts for the six energy channels. The geometric factors for the three channels reported here are 4.92×10^{-5} cm^2 sr for 0.2 keV, 1.23×10^{-4} for 0.5 keV, and 3.10×10^{-4} for 1.3 keV; the accumulation interval is one-tenth second for each second's value.

Selection Criteria

Only those observations made when each satellite's corrected geomagnetic latitude (CGL) exceeded N73 on the nightside or S75 on the dayside defined a polar cap crossing. A count level less than 2 000 (corresponding to a differential energy flux of $\sim 10^8$ particles/cm^2 s sr keV) within an individual sample of the 0.2 keV channel was also used to identify an incursion into the polar cap. The uniform, weak flux was distinguished from auroral precipitation, polar showers, polar squalls, and polar cusp precipitations by selecting only those times when the 0.2 keV channel recorded less than 500 counts. This last constraint caused many polar cap crossings to separate into two or more segments. The most appropriate segment was then chosen, averaged, and reported here, depending upon the number of one-tenth second counts averaged and the corrected geomagnetic latitudes included.

Data

For a variety of reasons, we do not have all the data from every orbit during this 47-day period. Furthermore, because both satellites were in dawn/dusk orbits at 99° inclination sometimes neither the southern nor the northern CGL threshold was exceeded. Thus, data gaps exist in the accompanying table.

In Table 1 under the column heading "Time (UT)" the tabulated value denotes the time of the last eight-second block for the polar cap crossing rounded to the nearest 10 min. The qualifying comments listed by number are defined below.

1. The latitudes crossed by the satellite are less than 75° CGL.
2. Possible contamination in the 1.3 keV channel due to sunlight-related effects (Fennell, private communication).
3. Less than 50, one-second values were used in the average.
4. The average counts may be inflated by polar cusp precipitation along its poleward edge.
5. The average counts may be inflated by poleward edge auroral zone precipitations.
6. (N.D.) - No data are available for this channel during this crossing.

The daily mean counts for the 20 March - 5 May period over each hemisphere are presented in Figure 1. Also identified are the inferred interplanetary sector structures and the times of geomagnetic storm sudden commencements (SSCs). Note the enhancements following the SSCs and, more importantly, the north-south asymmetry in the counts and its dependence upon the sector structure.

REFERENCES

CAIN, J. C., W. E. DANIELS, S. J. HENDRICKS and D. C. JENSEN — 1965 — An Evaluation of the Main Geomagnetic Field, 1940-1962, *J. Geophys. Res., 70,* 3647.

FENNELL, J. F., P. F. MIZERA, and D. R. CROLEY, JR. — 1975 — Low-Energy Polar Cap Electrons During Quiet Times, *Proc. Int. Conf. Cosmic Rays 14th, 4,* 1267.

FOSTER, J. C. and J. R. BURROWS — 1976 — Electron Fluxes Over the Polar Cap, 1. Intense keV Fluxes During Poststorm Quieting, *J. Geophys. Res., 81,* 6016.

GUSTAFSSON, G. — 1969 — A Revised Corrected Geomagnetic Coordinate System, *Kiruna Geophysical Observatory, Report No. 694,* Royal Swedish Academy of Science.

MENG, C. -I. — 1976 — Simultaneous Observations of Low-Energy Electron Precipitation and Optical Auroral Arcs in the Evening Sector by the DMSP 32 Satellite, *J. Geophys. Res., 81,* 2771.

MENG, C. -I. and H. W. KROEHL — 1977 — Enhanced Uniform Precipitation of Low-Energy Electrons Over the Polar Cap, *J. Geophys. Res., 82,* in press.

MIZERA, P. F., D. R. CROLEY, JR., F. A. MORSE, and A. L. VAMPOLA — 1975 — Electron Fluxes and Correlations With Quiet Time Auroral Arcs, *J. Geophys. Res., 80,* 2129.

WINNINGHAM, J. D. and W. J. HEIKKILA — 1974 — Polar Cap Auroral Electron Fluxes Observed With ISIS 1, *J. Geophys. Res., 79,* 949.

YEAGER, D. M. and L. A. FRANK — 1976 — Low-Energy Electron Intensities at Large Distances Over the Earth's Polar Cap, *J. Geophys. Res., 81,* 3966.

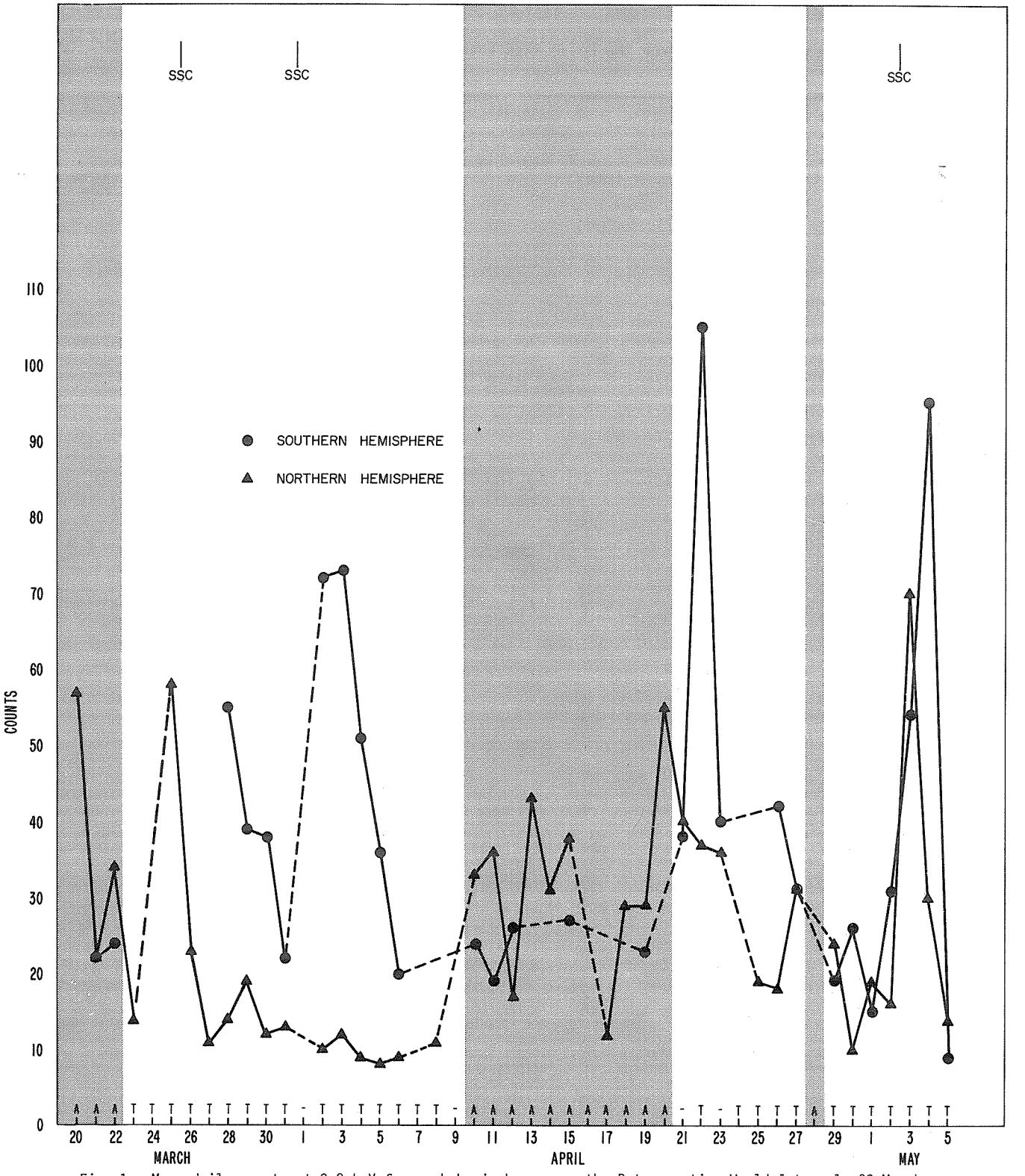

Fig. 1. Mean daily counts at 0.2 keV for each hemisphere over the Retrospective World Interval, 20 March - 5 May 1976. Alternate shaded and unshaded regions denote the dominant direction of the interplanetary magnetic field as either "away" or "toward" the Sun. A = away; T = toward; and dashed lines indicate gaps in the coverage.

Table 1.

Daily Mean Counts Over the Polar Caps Observed by the DMSP Satellites.

		Northern Hemisphere				Southern Hemisphere			
Date 1976	Time (UT)	0.2 keV (cts)	0.5 keV (cts)	1.3 keV (cts)	Comments	0.2 keV (cts)	0.5 keV (cts)	1.3 keV (cts)	Comments
March									
20	0050	45	26	6					
	0210					234	177	90	(3)
	1740	69	70	516	(2)				
	2110	38	8	5					
	2252	102	75	90					
21	0030	37	14	7					
	0210	133	160	428	(1,2)				
	0400	28	11	7					
	0440					60	104	10	
	0540	22	12	8					
	0620					17	7	6	
	0720	23	11	8					
	0800					18	6	6	
	0900	16	9	8					
	0940					22	7	5	
	1040	17	9	8					
	1220	11	8	7					
	1400	15	16	10	(1)				
	1550	22	12	7	(1)				
	1730	21	11	7	(1)				
	1910	46	19	9	(1)				
22	0240					27	15	10	
	0340	28	16	8					
	0430					39	N.D.	9	
	0520	21	10	8					
	0610					22	9	7	
	0700	37	15	9					
	0750					22	9	7	
	0840	43	18	10					
	0930					24	8	7	(3)
	1030	31	13	9					
	1110					59	15	10	(3)
	2220	40	15	10					
23	0000	40	14	9					
	0150	33	13	9					
	0230					87	18	11	(3)
	1700	10	5	6					
	1840	10	6	6					
	2020	13	7	7					
	2200	14	8	7					
	2350	14	8	8					
24	0130	67	20	10					
	0210					248	153	59	(3)
25	0250	215	417	699	(3)				
	1630	34	13	7	(1)				
	1950	96	23	8					
	2130	66	19	7					
	2320	51	16	8					
26	0100	49	18	7					
	0230	50	16	8					
	1430	27	10	5	(1,3)				
	1610	23	9	4	(1,3)				
	1750	13	27	45	(1,3)				
	2120	15	8	6					
	2300	15	9	10					

Table 1. (continued)

Daily Mean Counts Over the Polar Caps Observed by the DMSP Satellites.

Date 1976	Time (UT)	Northern Hemisphere 0.2 keV (cts)	0.5 keV (cts)	1.3 keV (cts)	Comments	Southern Hemisphere 0.2 keV (cts)	0.5 keV (cts)	1.3 keV (cts)	Comments
March									
27	0040	17	9	6					
	2100	10	6	4	(3)				
	2240	11	7	4					
28	0030	13	6	4					
	0250					40	18	12	(3)
	0350	20	8	5					
	0430					57	26	17	
	0530	27	20	4					
	0620					48	31	N.D.	
	0710	17	7	4					
	0750					55	19	6	
	0850	14	7	5					
	0940					38	11	5	
	1030	16	7	4					
	1120					193	37	7	(4)
	1210	11	6	5					
	1400	14	6	5	(3)				
	1720	8	5	3					
	1900	21	6	4					
	2040	51	17	5	(3)				
	2230	20	8	3					
29	0010	14	6	3					
	0240					24	12	5	
	0340	19	6	3					
	0420					41	19	5	
	0520	18	6	3					
	0600					37	17	46	
	0700	18	7	3					
	0840	19	10	7					
	0920					35	14	4	
	1020	35	8	3					
	1100					42	15	4	
	1340	24	7	3	(1,3)				
30	0400					32	14	5	
	0500	40	13	4					
	0550					38	N.D.	5	
	0640	37	10	3					
	0730					36	13	4	
	0820	17	6	3					
	0900					43	15	4	
	1000	1	6	3					
	1050					60	15	4	
	1140	12	5	4					
	1650	9	N.D.	3	(1)				
	1830	11	5	3					
	2010	33	6	3					
	2200	12	5	3					
	2340	10	4	2					
31	0120	13	5	3					
	0210					19	8	4	(3)
	0350					18	7	4	
	0440	13	5	3					
	0530					15	7	4	
	0630	16	5	3					
	0710					22	7	4	
	0810	21	7	3					

Table 1. (continued)

Daily Mean Counts Over the Polar Caps Observed by the DMSP Satellites.

		Northern Hemisphere				Southern Hemisphere			
Date 1976	Time (UT)	0.2 keV (cts)	0.5 keV (cts)	1.3 keV (cts)	Comments	0.2 keV (cts)	0.5 keV (cts)	1.3 keV (cts)	Comments
March									
31	0850					27	9	4	
	0950	20	7	4					
	1030					39	10	4	
	1130	12	5	3					
	1216					86	35	20	(4)
	1310	12	5	3	(1)				
	1450	13	5	3	(1,3)				
	1630	11	5	3	(1,3)				
	2000	10	9	7					
	2140	9	5	3	(3)				
	2320	26	11	4					
April									
1	0100	12	5	3					
2	0320					76	26	7	
	0420	19	6	3					
	0500					68	N.D.	6	
	0556	27	15	3					
	0640					55	27	8	
	0730	29	6	4	(3)				
	0820					177	146	20	
	0920	100	17	3	(3)				
	1000					145	161	148	(3)
	1100	150	211	N.D.	(3)				
	1421	9	3	2	(3)				
	1600	7	3	2	(1)				
	1745	5	4	6	(1)				
	2110	10	3	2	(1)				
	2300	11	4	2					
3	0040	13	4	2					
	0300					65	20	3	
	0400	14	3	2					
	0440					75	30	13	(3)
	0540	12	4	97	(2)				
	0630					71	17	3	
	0720	11	4	2					
	0810					297	164	11	
	0950					75	65	18	
	2050	8	3	2					
	2240	7	3	2					
4	0020	9	4	2					
	0200	117	235	272	(3)				
	0250					71	49	129	
	0340	15	3	2					
	0430					31	11	3	
	0520	19	4	2					
	0610					36	11	2	
	0710	9	3	2					
	0750					69	12	2	
	0850	7	2	1					
	0930					51	N.D.	3	
	1030	19	87	397	(2)				
	1110					102	14	2	(4)
	1350	3	2	1	(3)				
	1530	2	3	6	(1)				
	1710	23	18	36	(1,3)				
	1900	54	9	2	(1,3)				
	2040	14	4	2					
	2220	4	2	2					

Table 1. (continued)

Daily Mean Counts Over the Polar Caps Observed by the DMSP Satellites.

		Northern Hemisphere				Southern Hemisphere			
Date 1976	Time (UT)	0.2 keV (cts)	0.5 keV (cts)	1.3 keV (cts)	Comments	0.2 keV (cts)	0.5 keV (cts)	1.3 keV (cts)	Comments
April									
5	0010	4	3	2					
	0150	11	2	1					
	0320	8	3	1					
	0410					31	11	N.D.	
	0510	18	4	1					
	0550					41	15	2	
	0650	11	N.D.	4					
	0740					36	12	2	
	0830	16	16	17					
	0920					40	9	3	
	1010	7	3	1	(3)				
	1100					31	7	9	
	1150	5	3	2					
	1330	6	2	1	(3)				
	1520	84	151	374	(2,3)				
	1700	3	2	1	(1,3)				
	1840	6	3	1	(1)				
	2020	6	N.D.	1					
	2210	11	4	4					
	2350	29	19	21					
6	0130	8	3	1	(3)				
	0400					22	8	1	
	0450	8	3	1					
	0540					27	N.D.	1	
	0630	15	4	2					
	0720					19	N.D.	N.D.	
	0820	9	3	1					
	0900					38	6	1	
	1000	28	5	1					
	1040					15	4	1	
	1140	64	35	4					
	1220					10	5	5	
	1320	17	6	3	(3)				
	1640	5	2	1	(1)				
	1820	6	3	2	(1)				
	2150	16	90	1					
	2330	4	2	1					
7	0110	4	2	1					
	2320	13	4	6					
8	0100	5	2	2					
	1610	11	4	1	(1)				
	1800	16	5	3	(1)				
9	2250	18	6	1	(3)				
10	0030	19	6	2					
	0200	14	4	1	(3)				
	0300					18	6	N.D.	
	0350	33	10	2					
	0440					23	N.D.	2	
	0530	27	10	2					
	0620					32	9	2	
	0710	31	14	2					
	0800					24	7	1	
	0900	35	23	13					
	0940					25	N.D.	1	
	1040	39	21	4					
	1120					55	11	1	(4)
	1220	45	23	14					

Table 1. (continued)

Daily Mean Counts Over the Polar Caps Observed by the DMSP Satellites.

		Northern Hemisphere				Southern Hemisphere			
Date 1976	Time (UT)	0.2 keV (cts)	0.5 keV (cts)	1.3 keV (cts)	Comments	0.2 keV (cts)	0.5 keV (cts)	1.3 keV (cts)	Comments
April									
10	2050	122	46	3	(1,3)				
	2230	77	44	9					
11	0010	27	12	2					
	0240					37	14	3	(3)
	0340	36	18	3					
	0420					13	5	2	
	0510	30	20	2					
	0600					18	12	2	
	0700	20	25	3					
	0740					20	8	2	(3)
	0840	102	34	10					
	0920					52	18	2	(4)
	1020	204	30	5					
	1110					59	15	2	(4)
	1340	39	23	5	(3)				
	1850	81	54	11	(1,3)				
	2030	17	8	2					
12	0010	27	12	2					
	0140	49	21	5					
	0410					27	14	5	
	0500	17	8	2					
	0550					37	9	2	
	0640	23	7	2					
	0730					10	4	1	
	0820	17	6	1					
	0910					26	19	2	
	1010	7	4	3	(3)				
	1050					26	6	2	
	1830	16	28	17	(1,3)				
	2020	45	39	19	(1,3)				
	2200	19	8	2					
	2340	7	4	2	(3)				
13	0120	45	42	3					
	0300	42	11	2	(3)				
14	1440	11	8	10	(1,3)				
	1800	14	16	11	(1,3)				
	1940	66	23	11	(3)				
	2130	31	11	4	(3)				
	2310	40	77	57					
15	0050	28	33	7					
	0320					36	7	2	(3)
	0410	21	13	3					
	0500					12	5	2	
	0600	38	14	2	(3)				
	0640					27	7	2	
	0740	132	35	4	(3)				
	0820					10	4	2	
	0920	70	11	2	(3)				
	1000					23	7	2	
	1100	116	29	4	(3)				
	1140					39	62	64	(3,4)
	1750	15	10	4	(3)				
	1930	31	56	5					
	2110	17	8	2					
	2300	18	5	1					

Table 1. (continued)

Daily Mean Counts Over the Polar Caps Observed by the DMSP Satellites.

		Northern Hemisphere				Southern Hemisphere			
Date 1976	Time (UT)	0.2 keV (cts)	0.5 keV (cts)	1.3 keV (cts)	Comments	0.2 keV (cts)	0.5 keV (cts)	1.3 keV (cts)	Comments
April									
16	0040	13	4	1					
	0210	48	10	2	(3)				
17	1530	16	6	3	(1)				
	1720	13	3	1	(1)				
	1900	8	3	1					
	2040	9	3	1					
	2230	12	4	1					
18	0010	16	4	2					
	0150	15	4	1					
	0230					183	18	3	(3)
	1700	29	15	12	(1,3)				
	1840	32	9	2	(1,3)				
	2020	25	5	1					
	2200	30	6	1					
	2350	12	3	1					
19	0130	47	8	2					
	0400					22	4	1	
	0450	15	3	1					
	0540					23	N.D.	3	
	0640	24	5	2					
	0720					11	4	1	
	0820	10	3	1					
	0900					28	8	2	
	1000	38	8	1					
	1040					33	7	1	
	1140	35	11	1					
	1320	26	8	1					
	1500	28	7	1	(1,3)				
	1640	33	9	1	(1)				
	1830	28	15	14	(1)				
	2010	30	21	10					
	2150	27	7	2					
	2330	35	8	1					
20	0120	68	14	2					
	1630	50	54	19	(1,3)				
	1810	74	17	2	(1,3)				
	2000	148	44	5	(3)				
	2140	55	18	2					
	2320	35	8	1					
21	0100	70	16	2					
	0330					77	15	3	
	0420	54	11	2					
	0510					29	8	2	(3)
	0600	50	12	3					
	0650					33	9	2	
	0740	39	14	3					
	0830					40	12	2	
	0930	40	18	4					
	1010					37	9	2	
	1110	24	6	2					
	1200					46	8	2	(4)
	1250	39	13	2					

Table 1. (continued)

Daily Mean Counts Over the Polar Caps Observed by the DMSP Satellites.

		Northern Hemisphere				Southern Hemisphere			
Date 1976	Time (UT)	0.2 keV (cts)	0.5 keV (cts)	1.3 keV (cts)	Comments	0.2 keV (cts)	0.5 keV (cts)	1.3 keV (cts)	Comments
April									
22	0310					59	11	1	
	0410	74	28	12					
	0450					59	N.D.	2	
	0550	36	9	1					
	0640					120	N.D.	2	
	0730	40	31	48					
	0820					109	62	43	
	0910	27	9	7					
	1000					100	33	2	
	1050	22	6	1					
	1130					109	24	2	(3)
	1230	9	6	4	(3)				
	1420	9	3	1	(1,3)				
	1600	11	4	1	(1,3)				
	1740	15	4	1					
	1920	40	6	1					
	2100	45	9	2					
	2250	87	14	2	(3)				
23	0030	40	6	1					
	0210	53	36	24	(3)				
	0300					16	7	1	
	0400	30	7	1					
	0440					28	12	1	
	0540	25	7	3					
	0620					67	22	2	
	0720	36	9	1					
	0800					40	14	1	
	0900	24	5	1					
	0940					56	16	2	
	1040	99	110	17	(1,3)				
	1120					52	31	12	(3)
	1220	40	7	1					
25	1700	32	62	160	(1,2)				
	1830	19	20	6					
	2020	18	5	1					
	2200	19	11	1	(3)				
	2350	18	5	1					
26	0130	18	5	1					
	0210					42	13	2	
27	0340					31	10	N.D.	
	0430	42	8	2					
	0520					32	12	1	
	0600	34	8	1					
	0700					31	N.D.	1	
	0750	32	7	1					
	0840					30	9	2	
	0940	42	11	2					
	1020					42	10	2	
	1120	31	8	2					
	1200					109	26	8	(4)
	1300	21	6	1					
	1620	42	10	2	(1,3)				
	1800	22	7	1	(1)				
	1950	14	4	1					
	2130	30	8	2					
	2310	31	8	2					

Table 1. (continued)

Daily Mean Counts Over the Polar Caps Observed by the DMSP Satellites.

		Northern Hemisphere				Southern Hemisphere			
Date 1976	Time (UT)	0.2 keV (cts)	0.5 keV (cts)	1.3 keV (cts)	Comments	0.2 keV (cts)	0.5 keV (cts)	1.3 keV (cts)	Comments
April									
28	0100	24	6	1					
29	0310					18	8	N.D.	
	0400	18	5	2					
	0450					23	8	1	
	0540	28	6	2					
	0630					20	26	2	
	0720	19	6	2	(3)				
	0810					18	7	2	
	0950					74	17	2	(4)
	1050	27	7	2					
	1130					82	19	2	(4)
	1230	64	27	39	(3)				
	1550	25	5	1					
	1730	31	7	1					
	1920	21	6	1	(3)				
	2100	22	5	1					
	2240	24	6	3					
30	0030	15	5	2					
	0340	27	19	2					
	0430					26	13	5	
	0530	11	4	1					
	0610					10	N.D.	1	
	0710	9	8	1					
	0750					28	12	3	
	0850	11	5	1					
	0940					15	5	1	
	1030	6	3	1					
	1110					58	12	2	(4)
	1350	8	3	1	(3)				
	1720	7	3	1	(1)				
	1900	7	3	1	(1)				
	2220	12	47	6	(3)				
May									
1	0010	14	10	8					
	0150	19	15	26					
	0230					14	9	8	(3)
	0420					15	9	7	
	0510	25	9	6					
	0600					15	N.D.	7	
	0650	24	8	5					
	0740					17	7	5	
	0830	10	5	4					
	0920					16	7	4	
	1020	8	4	3					
	1100					32	9	5	(4)
	1200	8	4	3					
	1240					8	5	5	(3)
	1340	28	24	N.D.					
	2030	19	5	3	(3)				
	2210	14	4	2					
	2350	35	8	3					
2	0140	22	5	2					
	0220					14	5	2	(3)
	0310	38	9	3					
	0400					19	5	N.D.	
	0500	20	4	2					
	0540					18	N.D.	3	

Table 1. (continued)

Daily Mean Counts Over the Polar Caps Observed by the DMSP Satellites.

Date 1976	Time (UT)	Northern Hemisphere 0.2 keV (cts)	0.5 keV (cts)	1.3 keV (cts)	Comments	Southern Hemisphere 0.2 keV (cts)	0.5 keV (cts)	1.3 keV (cts)	Comments
May									
2	0720					31	12	4	
	0910					65	18	4	
	1000	12	4	2					
	1050					45	11	3	
	1140	12	5	3					
	1230					105	15	2	(4)
	1320	14	4	2					
	1650	9	3	2	(1,3)				
	2200	25	12	5					
3	0120	55	13	2					
	0340					42	27	29	
	0440	106	33	4					
	0530					56	18	3	
	0620	172	68	5					
	0710					119	60	4	
	0800	144	62	4					
	0850					51	17	3	
	0940	41	23	10					
	1030					63	14	2	
	1210					39	10	2	
	1310	90	33	2					
	1630	37	36	118	(1)				
	1810	68	44	3					
	2000	22	9	5					
	2140	86	208	N.D.					
	2320	33	18	2					
4	0110	21	8	1					
	0330					46	14	N.D.	
	0430	56	21	4					
	0510					150	N.D.	2	
	0610	47	21	4					
	0650					177	36	2	
	0750	46	14	1					
	0830					85	34	2	
	0930	38	11	2	(3)				
	1020					106	41	3	
	1110	46	15	2					
	1150					66	66	74	
	1800	19	27	2					
	1940	6	2	1					
	2120	8	5	6					
	2310	4	2	1					
5	0050	23	4	1					
	0220	10	4	1					
	0310					9	3	1	
	0410	37	10	1					
	0500					9	4	1	
	0550	33	6	1					
	0640					9	3	1	
	0820					8	3	1	
	0910	14	4	1					
	1000					13	4	2	
	1100	28	7	1					
	1140					33	10	1	(4)
	1240	9	3	1					

Variations of Threshold Geomagnetic Rigidities in the Period March - May 1976 and Their Connection with the Ring Current

by

S.I. Avdyushin, Yu.M. Kulagin, F.L. Dlikman, V.A. Kuzmina
G.A. Kirdina, A.V. Malyshev, V.A. Mokhova, P.M. Svidskii

Institute of Applied Geophysics
Hydrometeorological Service of the USSR
Moscow, USSR

Observational results of the position of the knee of latitudinal variation of galactic radiation during the period 20 March - 5 May 1976 are presented. These observations were made by proton detectors with 90 MeV threshold energies installed on the "Meteor" Satellite. Changes in the knee position of the latitudinal variation during magnetospheric storms are compared with Dst variations. From the data presented it follows that changes in the positive knee of latitudinal galactic cosmic ray variation result from the ring current evolution in the magnetosphere and the corresponding decrease it produces in threshold geomagnetic rigidities.

The main information of threshold geomagnetic rigidity variations is contained in comparatively low-energy particles - those with energies from several MeV to several tens of MeV. Observations during intrusions of solar cosmic rays by balloon and satellite [Hakura, 1966; Bingham *et al.*, 1968] and by ground-level recordings [Paulikas *et al.*, 1968; Leinbach *et al.*, 1965] of the absorption of cosmic radio emissions provided the results described here.

Variations in rigidity cutoff within the energy range of 1 GeV were not explored in detail. Nevertheless, many studies exist in which the effects of the ring current [Dorman *et al.*, 1965], of the space restriction of the magnetosphere [Rothwell, 1959], and of the magnetospheric tail on rigidity cutoff distributions have been calculated [Smart *et al.*, 1969]. These calculations show that during magnetospheric disturbances the ring current makes the main contribution to the rigidity cutoff variations at middle latitudes, i.e., for energies ~1 GeV.

In this paper a direct comparison of geomagnetic rigidity cutoff variations with ring current intensities is made. In order to hold the cosmic ray energy constant, we used energies corresponding to the knee of the latitudinal variation of galactic cosmic rays. Dst-variation values were used to indicate the ring current intensity.

Measurements of cosmic ray intensities were made by detectors with 90 MeV threshold energies on the "Meteor" Satellite. The detector is a scintillation counter with a plastic scintillator, a 12.5 cm^2 area, and a threshold energy value specified by a screen 10 g/cm^2 in thickness. Detector pulses were sent to a recording device and stored for 12 seconds. During each 12-second interval, a memory unit preserved the number of accumulated counts.

The position of the knee of galactic radiation was determined as the point at which detector readings decreased by 2σ from the mean number of counts in the polar plateau region. Here σ represents the mean square deviation determined from counting statistics.

Observational results in the period 20 - 30 March (see Figure 1) and during the interval 29 April - 5 May (see Figure 2) are discussed below. The data given in the figures are 3-hour mean values and include (a) cosmic radiation flux density, (b) L value of the knee of galactic cosmic radiation intensity, (c) Dst-value variation [*SGD*, 1976], and (d) K_p index.

During 20 - 30 March, when the magnetosphere was disturbed, the knee position in the variation of galactic radiation with latitude (L_{kcr}) remained practically constant. Only small variations about a mean value of L=3.8 were observed. Secondly, when the ring current began to develop, the position of the knee shifted toward the geomagnetic equator. During the storm on 26 March, L_{kcr} reached a minimum L value of 2.85 at the same time that Dst maximized. A similar time variation is shown in Figure 2. This behavior of the knee position in the latitudinal variation of cosmic ray intensity corresponds to a decrease in threshold geomagnetic rigidities produced by the evolving ring current.

Note the variations observed on 23 - 24 March 1976. As depicted in Figure 1, rapid increases in L_{kcr}, from 3.8 to 4.1, occurred. These positive excursions from the quiet-day level were accompanied by an increase in the cosmic ray intensity. This event together with the evolution of negative, 20-gamma Dst variations occurred simultaneously. Since during these days there was no increase in geomagnetic activity, a decrease in the solar wind dynamic pressure may have caused the effect. The reduced pressure would allow the magnetosphere to expand, leading to both an increase in the threshold geomagnetic rigidities and a decrease in the horizontal component of the equatorial magnetic field.

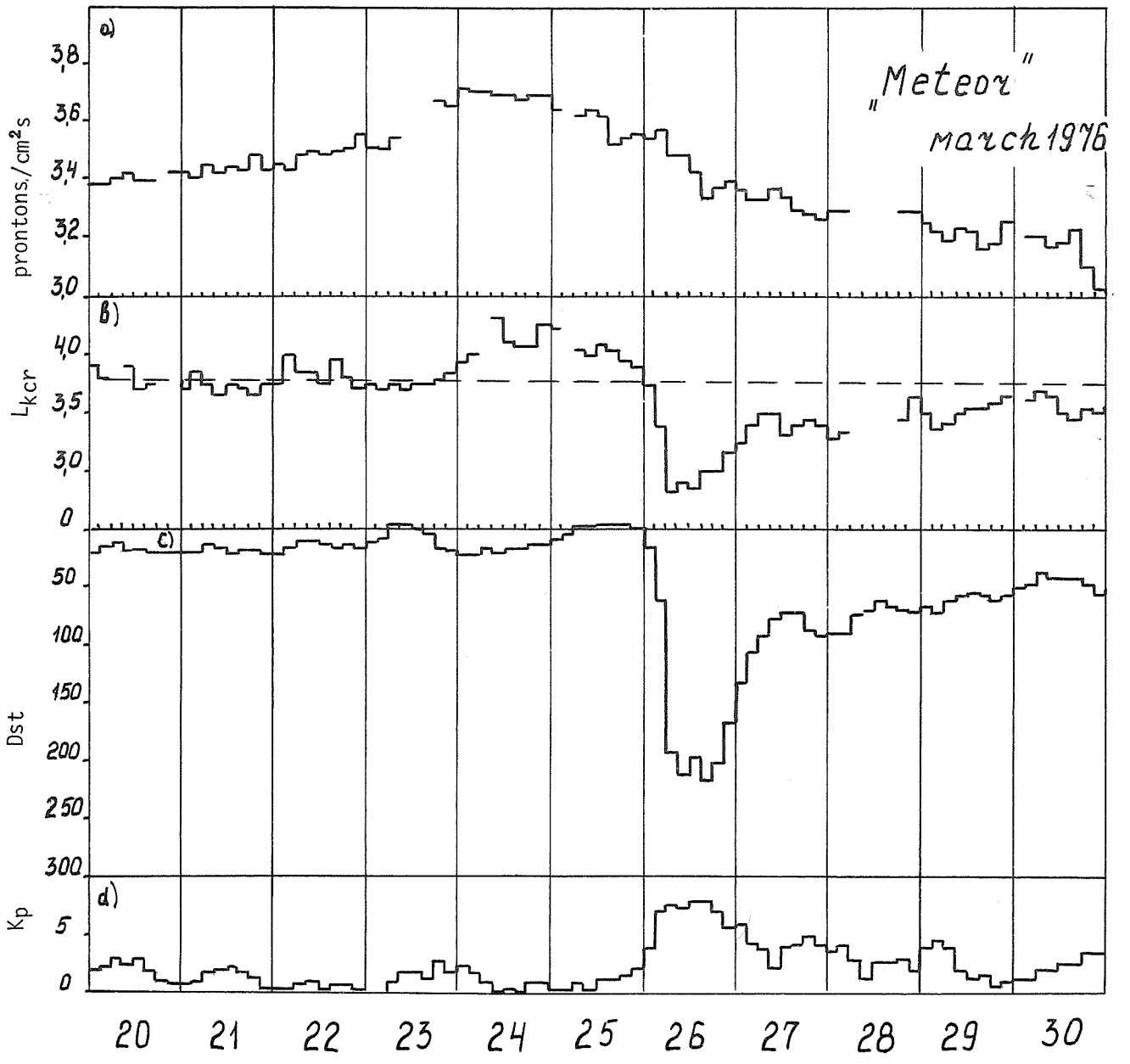

Fig. 1. Three-hour mean values of (a) cosmic ray flux density for protons ≥ 90 MeV as measured by the "Meteor" Satellite, (b) L value of the knee of galactic cosmic radiation intensity (L_{kcr}), (c) Dst-variation value, and (d) K_p index during the period 20 - 30 March 1976.

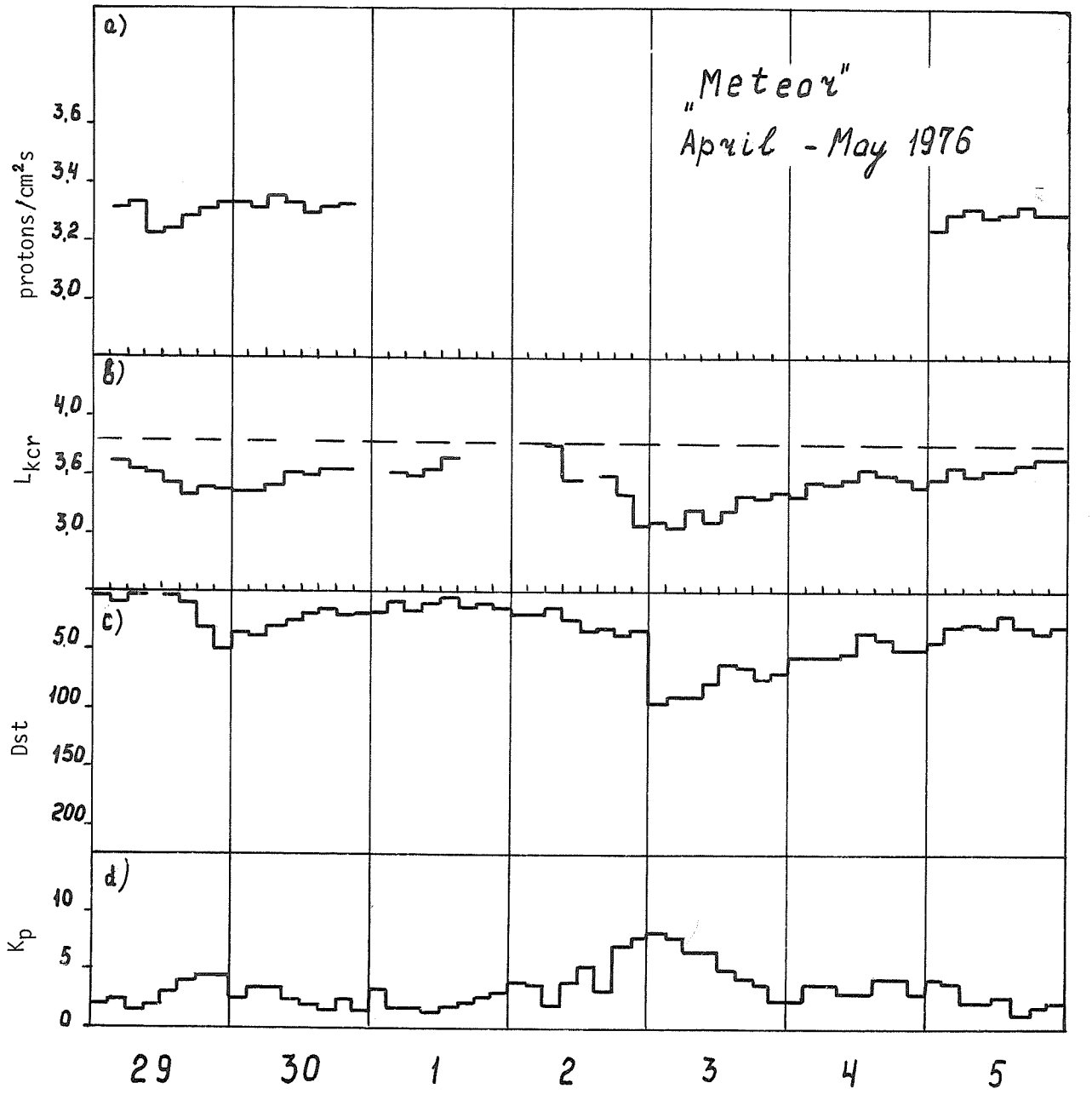

Fig. 2. Three-hour mean values of (a) cosmic ray flux density for protons ≥ 90 MeV as measured by the "Meteor" Satellite, (b) L value of the knee of galactic cosmic radiation intensity (L_{kcr}), (c) Dst-variation value, and (d) K_p index during the period 29 April - 5 May 1976.

REFERENCES

BINGHAM, R. G., D. M. SAWYER, I. F. ORMES and W. R. WEBBER — 1968 — Direct Measurements of Geomagnetic Cutoffs for Cosmic-Ray Particles in the Latitude Range 45° to 70° Using Balloons and Satellites, Tenth International Conference on Cosmic Rays, Calgary, *Canad. J. Phys., 46,* 1078-1081.

DORMAN, L. I., M. I. TYASTO and V. S. SMIRNOV — 1965 — Utshet Vliyaniya Tokov v Radiatcionnikh Poyasakh na Jestkost Otsekaniya Kosmitsheskikh Lutsheij, *Geomagnetizm i Aeronomiya, 5,* 913-918.

HAKURA, Y. — 1966 — Latitude Dependence of Non-Störmer Cutoffs for Charged Particles Invading Quiet Geomagnetic Field, *Rept. Ionosphere and Space Res., Japan, 20,* 60-62.

LEINBACH, H., D. Venkatesan and R. PARTHASARATHY — 1965 — The Influence of Geomagnetic Activity on Polar Cap Absorption, *Planet. Space Sci., 13,* 1075-1095.

PAULIKAS, G. A., I. B. BLAKE and S. C. FREDEN — 1968 — Low-Energy Solar-Cosmic-Ray Cutoffs: Diurnal Variations and Pitch-Angle Distributions, *J. Geophys. Res., 73,* 87-95.

ROTHWELL, P. — 1959 — Magnetic Cutoff Rigidities of Charged Particles in the Earth's Field at Times of Magnetic Storms, *J. Geophys. Res., 64,* 2026-2028.

SMART, D. F., M. A. SHEA and R. GALL — 1969 — The Daily Variation of Trajectory-Derived High-Latitude Cutoff Rigidities in a Model Magnetosphere, *J. Geophys. Res., 74,* 4731-4738.

1976 — *Solar-Geophysical Data,* 381-383 Part I, May-July 1976, U.S. Department of Commerce, (Boulder, Colorado, U.S.A. 80302).

2-30 keV X-Ray Data From OSO-8

by

C. J. Wolfson, L. W. Acton, D. T. Roethig, and K. L. Smith
Lockheed Palo Alto Research Laboratory
Palo Alto, California 94304 U.S.A.

Introduction

This report presents key examples of data obtained during the STIP Interval II from the Lockheed Mapping X-ray Heliometer (MXRH) instrument on the NASA Orbiting Solar Observatory-8 (OSO-8) satellite. The MXRH responds to solar X-rays in the 1.5-30 keV energy range and has a spatial resolution of about 2 min of arc. Investigators are invited to contact the Lockheed group for additional MXRH data for this or other periods. The MXRH became operational 24 June 1975. Daily Daily MXRH maps of the sun have been published in *Solar-Geophysical Data - Prompt Reports* since August 1975.

Instrument Description

The MXRH looks radially outward from the rotating wheel of the OSO-8 satellite. It contains three detection systems, each collimated in one dimension with Oda-type mechanical collimators [Bradt *et al.*, 1968; Oda, 1965]. The collimators have a FWHM of 2.0 arc min, although other instrumental effects broaden the instrument response function to about 4 arc min under some conditions. Each field of view is tilted 120° from the others. These systems are called Vertical, Slant A, and Slant B, with the Vertical system field of view parallel to the satellite spin axis. As the wheel rotation sweeps these fields of view past the sun, one obtains three one-dimensional distributions which can be unfolded to locate and isolate emitting X-ray regions. Each spatial distribution consists of 31 successive strips, or Area Segments, parallel with a system's field of view. Examples of these distributions are shown in Figures 3, 5 and 8. The wheel rotates at approximately 6 revolutions per min and, under normal operation, 4 revolutions are required to form a complete set of three distributions.

The instrument includes different types of proportional counter detectors which combine to provide spectral information from approximately 1.5 to 30 keV. The lower value is established by the thinnest Be window (75μm) and the practical upper value is determined by the solar spectrum - a limit often much lower than 30 keV. Spectral information is obtained by analyzing the proportional counter signals with 15-channel pulse height analyzers.

Medium sensitivity detectors (called Large Detectors) are situated behind each of the three collimated systems along with detectors of other sensitivities: a more sensitive detector is Thin Window Detector-B (TWD-B) in the Slant B system, the most sensitive detector is TWD-A, and the least sensitive detector is Vertical Small. Switching between pairs of these detectors provides a dynamic range of $>10^5$. For example, in Figure 4 there is an automatic switch from Vertical Large to Vertical Small Detector on the rise of the X-ray burst near 2245 UT and a switch back on the decay. Since the Vertical Small Detector has less detection area and a different spectral response than Vertical Large, both the amplitude (by a factor of from 4-12) and profile of the light curve change when the detectors switch.

Effective areas as a function of energy for three of the detectors are shown in Figure 1. The observation time for a point source is about 0.02 s per solar scan because the data are integrated over 27 of the collimator fan beams. Details of the instrument, its subsystems, and its operational modes are given in the Technical Manual for the Mapping X-ray Heliometer instrument on OSO-8 [Wolfson, Acton, and Gilbreth, 1975].

General Observations

The active region selected by the MONSEE Steering Committee for study under STIP Interval II was observed by the MXRH instrument for four solar rotations. X-rays from this region were first detected early on 6 March at approximately S05 W40, and the region continued to emit detectable X-rays until it was significantly behind the west limb on 11 March. The plage was named McMath 14118 during this rotation.

For both rotations 2 and 3, which occurred during the specified STIP interval, the region (first designated McMath 14143 and then 14179) was continuously emitting relatively intense X-radiation. Specific observations during these two rotations will be presented in the next section. Rotation 4 (McMath 14215) began in X-rays on 17 May with the last significant X-ray flux observed on 23 May when the region was near disk center. Calcium plage was reported until the region rotated over the west limb. There was no rotation 5 in X-rays or calcium plage.

It is impractical to present all of the MXRH data for the two disk transits included in STIP Interval II. Instead, a synopsis of the available data is presented in Figure 2 (the gaps principally result from periods when the satellite was behind the earth or in the South Atlantic Anomaly radiation belt). We will be happy to provide data on particular periods to anyone requesting it. Data near the events specifically

listed in MONSEE Bulletin No. 8 are discussed in the following section and are representative of the MXRH data.

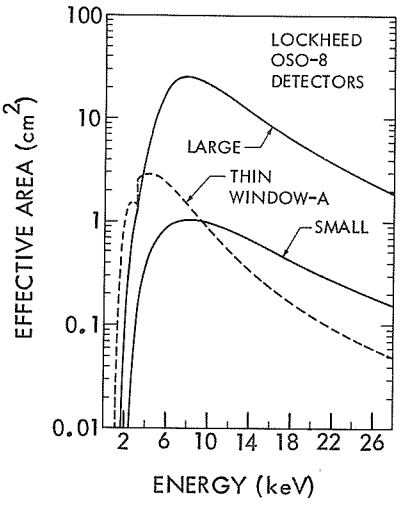

Fig. 1. Calculated effective areas of MXRH detection systems as a function of energy for normally incident photons.

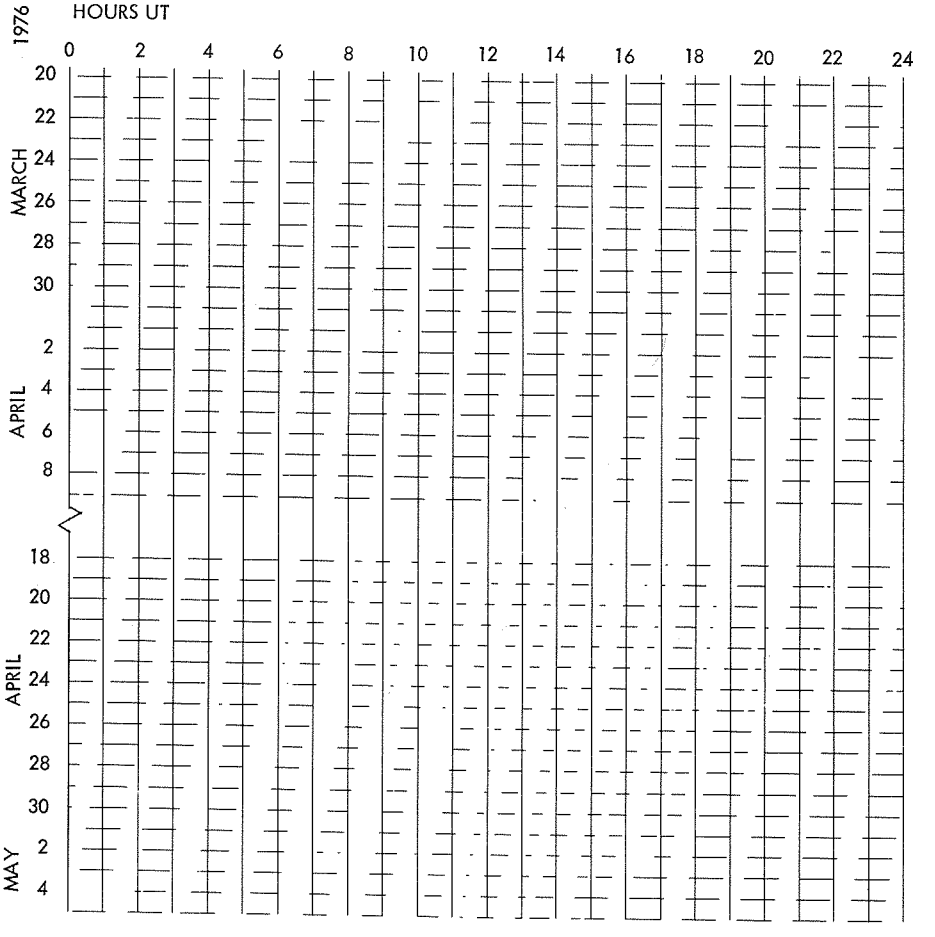

Fig. 2. A chart indicating the times of MXRH X-ray data during the intervals 20 May - 9 April and 18 April - 5 May 1976 when McMath Regions 14143 and 14179 were observable.

Specific Observations

A. 20 March

Type II radio bursts at the east limb were reported by Culgoora at 0205 and 2257 UT. A possible source was McMath 14143 which was approximately 54-43° behind the east limb. Figure 3 shows the X-ray sun for both of these times and shows no X-ray emission at the east limb for either time. A modest X-ray emitting region (McMath 14127) is located at approximately N07 W15

To observe the temporal behavior of a particular region, a spatial Area Segment from a system in which the emitting X-ray region is not confused by other regions is selected and the count rate versus time is plotted. Light curves such as these for McMath 14127 during the two periods of interest are shown in Figure 4 where the 18th Area Segment of the vertical system is used. During these time periods, McMath 14127 was undergoing moderate activity which to a full disk monitor might be mistakenly associated with the east limb radio events. However, during these intervals, no east limb activity was observed in excess of the background rate of 15-120 counts/s.

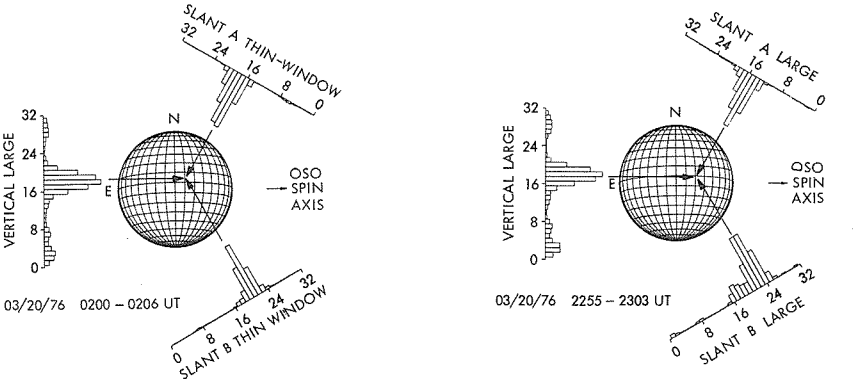

Fig. 3. The X-ray sun for the times when Type II radio bursts were observed at the east limb. Data are collected and displayed in terms of the 32 numbered Area Segments, 1.3 arc min in width. Each histogram is normalized to the peak intensity for that detection system. The arrows converge on the position of McMath 14127.

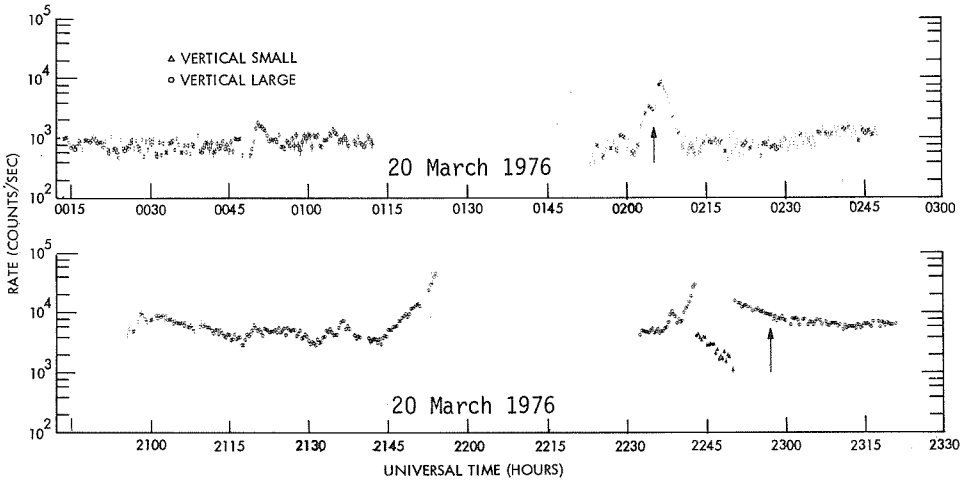

Fig. 4. Light curves of the X-ray emission from McMath 14127. The arrows at 0205 and 2257 UT mark the observations of the Type II radio events at the east limb. Automatic switching between the Vertical Large Detector and the less sensitive Small Detector occurs at 2241 and 2248 UT.

B. 23 March

The MONSEE Committee selected the period from 0840 to 1900 UT based on reported full disk X-ray enhancement, Hα loops at the east limb (1100 UT), and a Type IV radio burst at 0842 UT. McMath 14143, slightly behind the east limb, was judged the probable source. Although McMath 14127 continued to dominate the X-ray disk on the 22nd, significant X-ray emission from the east limb was observed by the MXRH instruemnt by mid-day; the map in Figure 5 is typical. A strong east limb X-ray burst occurred between 0404 and 0450 UT on the 23rd (a period missed due to orbit night and the South Atlantic Anomaly), making McMath 14143 the major source by 0450 UT. A spacecraft malfunction caused loss of data between 0601 and 0927 UT. By the time the malfunction was corrected, the region was in the decay phase of a large burst which peaked at about 0850 UT in the GOES-1 X-ray data. Figure 6 shows more than 10 hours of this smooth decay. Source characteristics determined by fitting the observed pulse height spectrum at 0950 UT to that expected from an isothermal plasma as described by Tucker and Koren [1971] were temperature = 10×10^6 K and emission measure = 2×10^{49} cm^{-3}. This implies a 1 - 8Å flux of 0.02 ergs/cm^{2}s and a 0.5 - 4Å flux of 0.002 ergs/cm^{2}s.

McMath 14127 was easily observable throughout this decay period but, although three optical flares were observed, it was never the dominant source. Its maximum contribution was at 1647 UT when it emitted 25% of the full disk X-ray flux. By 2115 UT, McMath 14127 and McMath 14143 had approximately equal intensities.

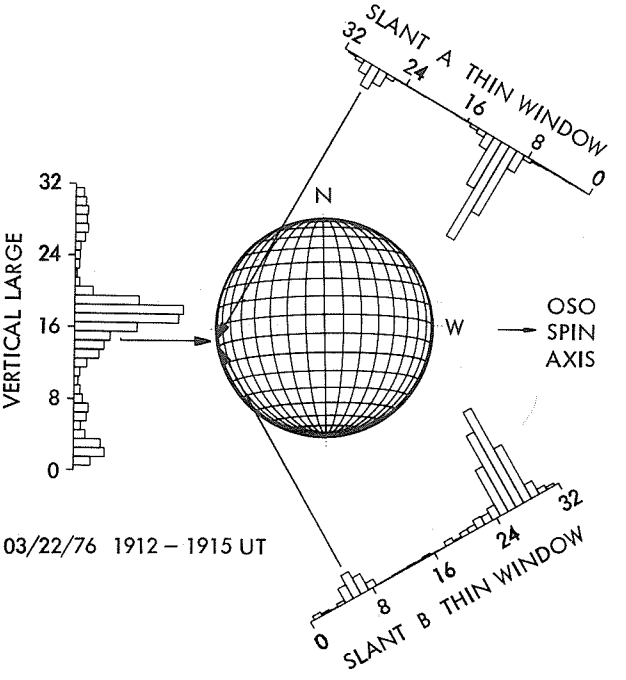

Fig. 5. The typical X-ray sun during the latter part of 22 March. Although McMath 14143 is about 20 degrees behind the east limb, the X-ray emitting plasma is high enough to produce a significant unocculted flux. The arrows indicate the position of this emission.

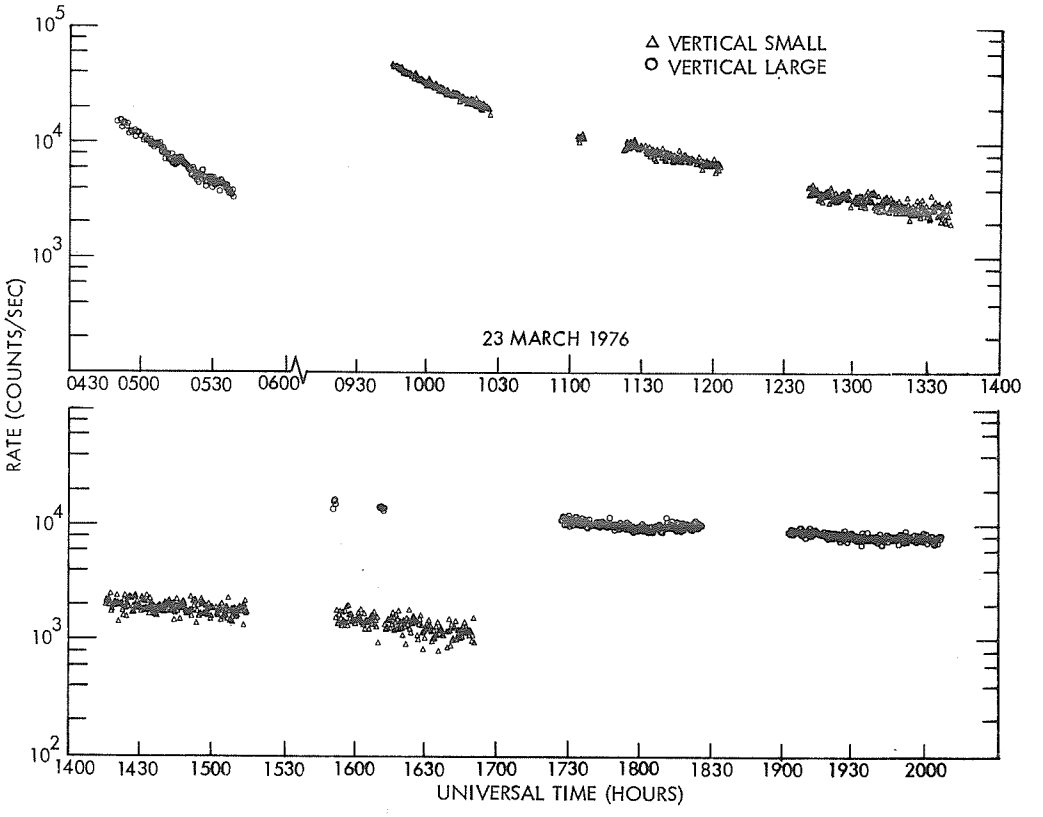

Fig. 6. X-ray light curve of McMath 14143 including 10 hours of the decay from an intense burst which occurred about 0900 UT on 23 March. The large data gap (0600 - 0930 UT) is a result of a spacecraft malfunction.

C. 28 March

Many Hα flares and radio bursts were reported from McMath 14143 between 1840 and 2400 UT. McMath 14127 had by then rotated behind the limb and was undetectable in X-rays while McMath 14146, McMath 14147, and McMath 14143 were on the disk and emitting detectable signals. McMath 14143 was dominant throughout this period. The intensity prior to the large event around 1840 UT was gradually decreasing with many superimposed enhancements (Figure 7). Several of these enhancements appear to be the sum of two or more bursts. For example, the event at 1840 UT seems to be the sum of a burst having a fast rise and a fast decay with a burst having a slow rise and a slow decay.

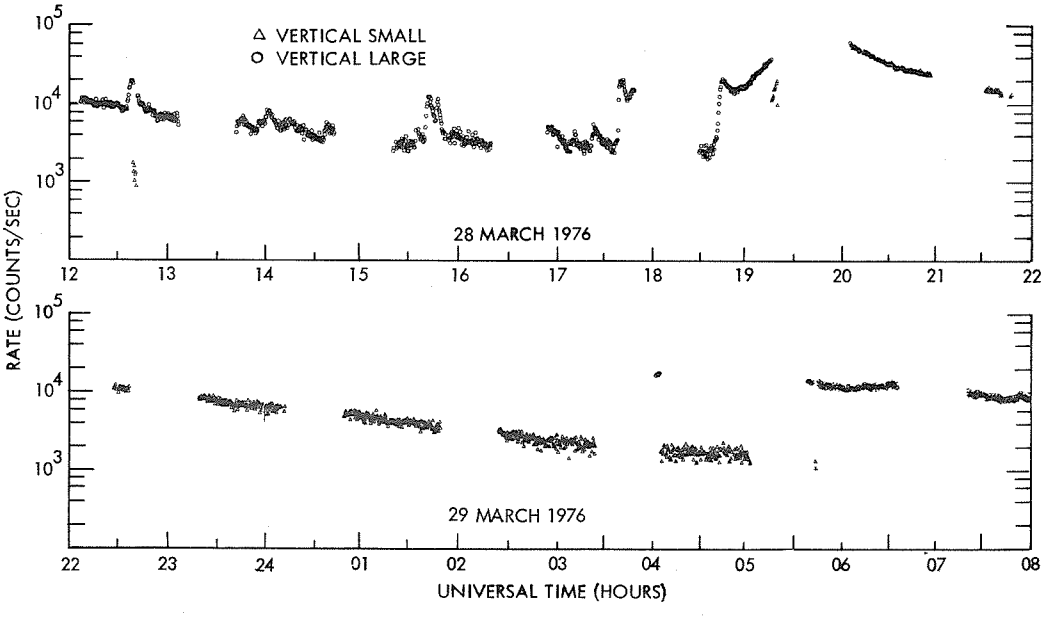

Fig. 7. The light curve for McMath 14143 on 28 and 29 March 1976.

D. 31 March

From 0730 to 1100 UT on 31 March, both McMath 14146 (on the west limb) and McMath 14143 (near disk center) were fairly stable and emitted nearly equal X-ray fluxes of about 500 counts/s in the Vertical Large Detector. The typical X-ray map for this period is shown in Figure 8. By the time the satellite came out of orbit eclipse at 1146 UT, McMath 14143 was more than 20 times as strong as McMath 14146 and continued to dominate the emission at least throughout the next day. Figure 9 shows the event which peaked around 1213 UT and then decayed for the next several hours. It should be noted that there was some additional enhancement during the orbit eclipse from 1248 to 1322 UT.

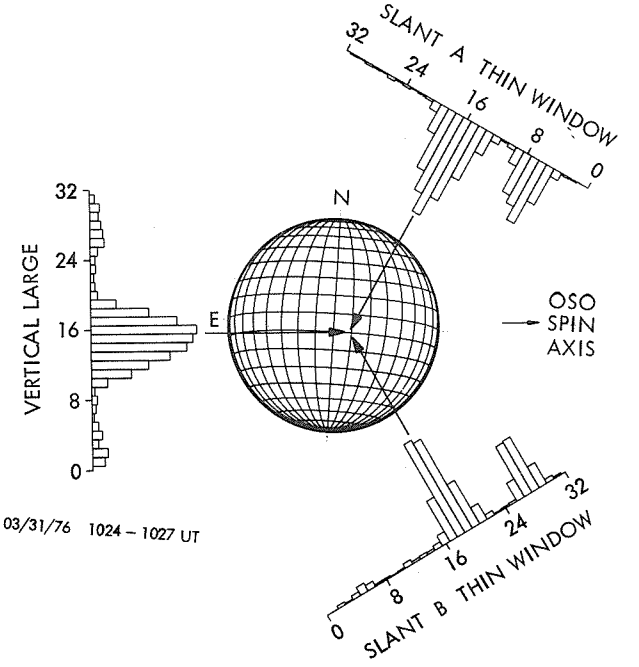

Fig. 8. The X-ray sun 90 min before the large enhancement of McMath 14143 near disk center.

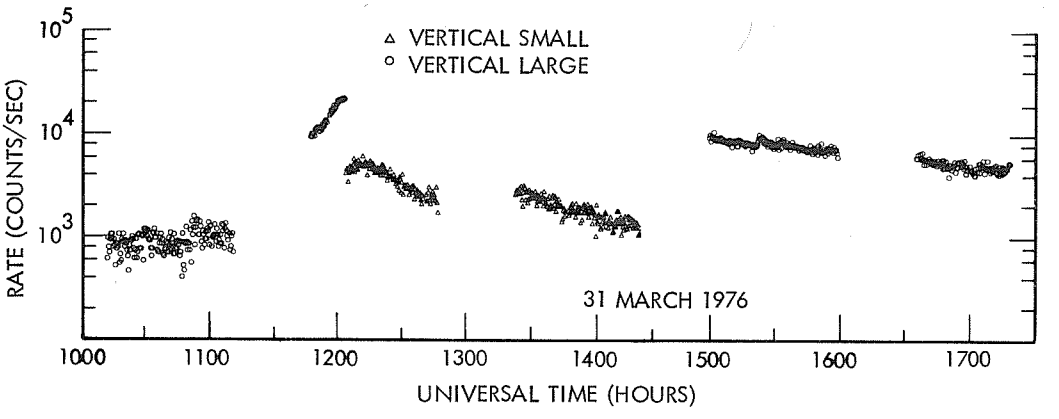

Fig. 9. The X-ray light curve for McMath 14143 on 31 March 1976. The peak emission was at approximately 1213 UT.

E. 30 April

As noted above, the region of interest, now on its third rotation, was redesignated McMath 14179. On 30 April many Hα, X-ray, and radio events were reported along with a ground level solar cosmic ray event. Although McMath 14185 (~ N03 E16) was producing a detectable flux, McMath 14179 (~ S08 W32) completely dominated the solar X-ray emission throughout this period. Figure 10 displays more than a 24-hour period for this region. The proton producing event appears to have maximized some time prior to the start of orbit day at 2121 UT. Plasma parameters which result from interpreting the data at 2122 UT as the

emission from an isothermal plasma are temperature = 15 x 10^6 K, emission measure = 2 x 10^{49} cm^{-3}, 1 - 8Å flux = 2 x 10^{-2} ergs/cm^2s, and 0.5 - 4Å flux = 4 x 10^{-3} ergs/cm^2s.

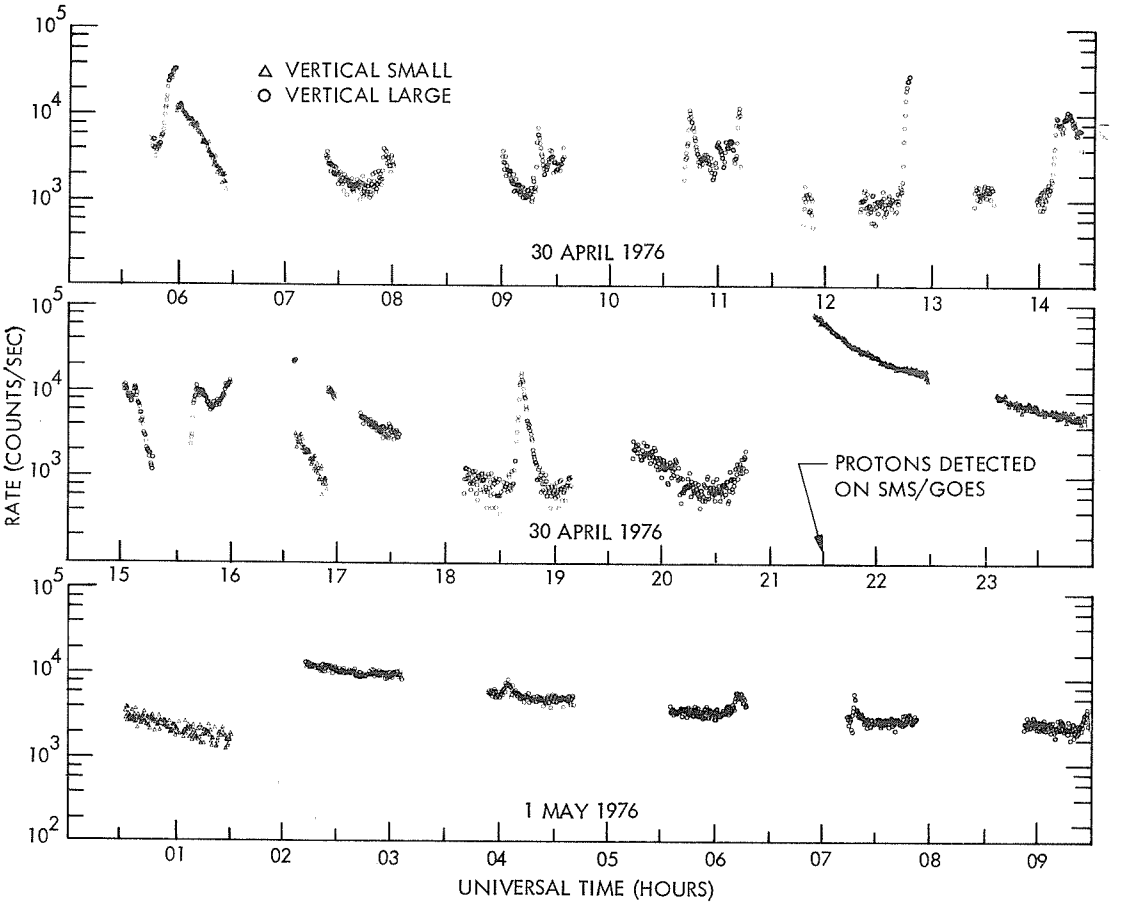

Fig. 10. The X-ray light curve for McMath 14179. The provisional time of the first 6 - 10 MeV proton detection is shown by the arrow at 2130 UT.

One immediately notes the large contrast in variability before and after this event. The visible impact is of course biased because the pre-event baseline is lower than the post-event baseline. However, examination of the counting rates establishes that bursts like these occurring during the 14 hours before the proton event would have registered well above the smooth post-event baseline after 0400 UT on 1 May.

Summary

We have presented six examples of the solar X-ray emission during STIP Interval II as observed with the Lockheed Mapping X-ray Heliometer instrument on the OSO-8 satellite. These data are representative of the data we have for the entire period. The major source of X-ray emission during STIP Interval II was a complex active region designated McMath 14143 on its second rotation and McMath 14179 on its third rotation. Other strong sources, however, were usually present also. The spatial resolution of the MXRH instrument enables one to separate clearly the emission from these different regions. Investigators desiring data not presented here, or a further reduction of these data, are encouraged to request it from the authors.

Acknowledgments

The authors wish to acknowledge the team that conceived, designed, and fabricated the MXRH instrument; especially Co-Investigators J. L. Culhane and R. C. Catura and Project Engineer, C. W. Gilbreth. Our thanks are extended to the personnel of GSFC who control OSO-8 and distribute the data. This work was supported by the National Aeronautics and Space Administration under contract NAS5-22411 and by the Lockheed Independent Research Program.

REFERENCES

BRADT, H., G. GARMIRE, M. ODA, G. SPADA, and B. V. SREEKANTAN — 1968 — The Modulation Collimator in X-ray Astronomy, *Space Science Reviews, 8*, 471.

ODA, M. — 1965 — High Resolution X-ray Collimator With Broad Field of View for Astronomical Use, *Applied Optics, 4*, 143.

TUCKER, W. H. and M. KOREN — 1971 — Radiation From a High-Temperature, Low-Density Plasma: The X-ray Spectrum of the Solar Corona, *The Astrophysical Journal, 168*, 283.

WOLFSON, C. J., L. W. ACTON, and C. W. GILBRETH — 1975 — Mapping X-ray Heliometer for Orbiting Solar Observatory-8, Final Report, *NASA-CR-144710*.

X-Ray Flux Measurements of Highly Ionized Silicon Lines in the Sun, 20 March - 5 May 1976

by

R. S. Wolff, H. L. Kestenbaum, K. S. Long, R. Novick, and M. C. Weisskopf
Columbia Astrophysics Laboratory, Departments of Astronomy and Physics,
Columbia University, New York, New York 10027 U.S.A.

The Columbia University solar X-ray spectrometer, mounted in the wheel section of the OSO-8 satellite, makes use of Bragg reflection to obtain high resolution solar X-ray spectra in the 1.5-6.7 Å range. A complete spectrum is obtained every 10 s, and the data are superposed to yield time-averaged fluxes. Particularly prominent emission lines found in these spectra include Si XII (5.82 Å), Si XIV (6.18 Å), and Si XIII (6.64 Å). Corrections for satellite orientation, instrument sensitivity, and exposure time are applied to the raw data to obtain absolute line fluxes in ergs/cm^{2}s. The results for these selected lines are reported as hourly averages in the Tables 2-4. The statistical accuracy of the measurements is generally very good because the background rate is low. At limiting sensitivity (10^{-8} ergs/cm^{-2}s), the statistical accuracy is 5%, comparable to uncertainties in the instrument parameters.

The spectrometer uses Bragg reflection from mosaic graphite crystals to disperse the incident X-ray flux, and proportional counters to detect the photons that satisfy the Bragg condition and that are reflected from the crystal panel. The properties of the crystals, the detectors, and other relevant parameters are listed in Table 1. Since the 0.8° rocking curve width of the crystal is greater than the solar angular diameter, specific regions of the Sun cannot be resolved. The spectra obtained are an average of the total solar emission. (In practice, one or two active regions on the disk usually dominate the X-ray emission in the wavelength range of the spectrometer.) The spectral scan of the instrument is accomplished by using the rotation of the spacecraft. The spectrometer entrance aperture is located in the perimeter of the satellite wheel which rotates uniformly at 6 rpm. The rotation axis is orthogonal to the Earth-Sun line, so that each rotation yields a complete X-ray spectrum. The spectrometer itself contains no moving parts. Masking collimators are included to avoid direct illumination of the detectors by the solar X-ray flux.

Table 1
Properties of the Columbia University OSO-8 Solar X-Ray Spectrometer

Parameter	Description
Field of view	Whole Sun, ±3° perpendicular to dispersion plane
Time resolution	One spectrum in 10 s
Crystal material	Pyrolytic graphite, grade ZYC (Union Carbide Corporation)
Crystal area	1221 cm^2
2d	6.7 Å
Rocking curve width	0.8°
Wavelength range	1.5-6.7 Å
Resolving power ($\lambda/\Delta\lambda$)	17 at 1.5 Å; 2500 at 6.7 Å
Detectors	Proportional counters
Windows	Beryllium, 0.002 inch
Gas filling	Argon (90%); carbon dioxide (10%)

The raw data for each revolution are encoded in azimuth bins, recorded, and telemetered each orbit. The 10-sec time resolution is maintained, but to improve statistical precision the data are superposed, and for the purposes of this report, ultimately presented as hourly averages. Conversion of the raw data as azimuth counts per revolution to line fluxes is accomplished by using the spacecraft aspect solution and the spectrometer response function. The azimuth code is translated to Bragg angle, and the data are binned in 0.16° intervals between 10° and 90°. The results for each revolution are then corrected for instrument response and combined to obtain the time-averaged spectrum. The fluxes in the particular lines are obtained by integrating to obtain the total intensity: line emission, continuum, and non-X-ray background. The continuum and non-X-ray background contributions are determined from adjacent regions of the spectrum where no known lines are found, and the net flux is then obtained by subtraction. The estimated systematic uncertainty in this procedure combined with uncertainties in the instrumental calibration is 5%.

When the solar X-ray emission is weak, the statistical error in an hourly average of data becomes comparable to the systematic error at an equivalent line intensity of 10^{-8} ergs/cm^{2}s. We use this as our limiting sensitivity, and flux measurements falling below this level are reported as "B" in Tables 2-4. Missing data, corresponding to hour long intervals when no relevant solar observations were made, are indicated by "M". The reported time are in GMT, and the interval corresponding to a particular hour "H" extends from H - 30^m to H + 30^m. The dynamic range of the spectrometer is approximately 10^5, and dead-time corrections at peak intensity can be reliably made for line fluxes equivalent to 10^{-3} ergs/cm^{2}s.

This work was supported by the National Aeronautics and Space Administration under contract NAS5-22408. This paper is Columbia Astrophysics Laboratory Contribution No. 132.

TABLE 2. COLUMBIA OSO-8 GRAPHITE CRYSTAL SPECTROMETER DATA
X-RAY EMISSION LINE FLUXES

SI12, 5.82A

YEAR= 1976
MARCH

-LOG(FLUX), ERGS/CM2-S, HOUR AVERAGES

DAY	DOY/HR	0	1	2	3	4	5	6	7	8	9	10	11	12	13	14	15	16	17	18	19	20	21	22	23
Mar. 23	83	M	M	M	M	M	M	M	M	M	M	M	5.16	5.47	4.94	5.05	5.03	5.03	5.01	5.08	5.11	5.15	5.15	5.14	5.01
	84	5.06	4.82	4.88	5.07	5.14	5.17	M	5.20	5.27	5.07	5.06	5.25	5.27	5.35	5.43	5.40	5.40	5.35	5.37	5.41	5.43	5.33	5.24	5.39
25	85	5.33	5.30	5.29	5.22	5.24	4.87	4.80	4.82	4.74	4.75	4.89	4.93	4.87	M	4.68	4.73	4.91	4.84	4.87	5.00	5.11	5.18	4.94	5.03
	86	M	M	M	M	M	M	M	M	M	M	M	M	M	M	M	M	M	M	M	M	M	M	M	M
	87	M	M	M	M	M	M	M	M	M	M	M	M	M	M	M	M	M	M	M	M	M	M	M	M
	88	5.21	5.30	5.40	5.48	5.44	5.47	5.29	5.37	5.44	5.44	5.19	4.91	5.16	5.18	5.33	5.43	5.41	5.44	5.39	5.32	M	M	M	5.36
	89	M	M	M	M	M	M	M	M	M	M	M	M	M	M	M	M	M	M	M	M	M	M	M	M
	90	M	M	M	M	M	M	M	M	M	M	M	M	M	M	M	M	M	M	M	M	M	M	M	M
31	91	5.94	5.56	5.82	5.86	5.76	5.58	5.54	5.57	5.70	M	M	M	M	M	M	M	M	M	M	M	M	M	5.71	5.94

APRIL

-LOG(FLUX), ERGS/CM2-S, HOUR AVERAGES

DAY	DOY/HR	0	1	2	3	4	5	6	7	8	9	10	11	12	13	14	15	16	17	18	19	20	21	22	23
Apr. 1	92	5.61	5.66	5.70	5.69	5.73	5.79	5.79	5.87	5.87	5.93	M	M	M	M	M	M	M	M	M	M	M	M	M	M
	93	M	M	M	M	M	M	M	M	M	6.32	M	M	M	M	M	M	M	M	M	M	M	M	M	M
	94	M	M	M	M	M	M	M	M	M	M	M	M	M	M	M	M	M	M	M	M	M	M	M	M
	95	M	M	M	M	M	M	6.43	6.43	M	6.47	M	M	M	M	M	M	M	M	M	M	M	M	M	M
5	96	M	M	M	M	M	M	M	6.57	M	M	M	M	M	M	M	M	M	M	M	M	M	M	M	M
	97	M	M	M	M	M	6.49	6.50	M	M	M	M	M	M	M	M	M	M	M	M	M	M	M	M	M
	98	M	M	M	M	6.18	6.35	6.28	M	M	M	M	M	M	M	M	M	M	M	M	M	M	M	M	M
	99	M	M	M	M	6.05	6.23	M	M	M	M	M	M	M	M	M	M	M	M	M	M	M	M	M	M
	100	M	M	M	M	M	M	M	M	M	M	M	M	M	M	M	M	M	M	M	M	M	M	M	M
10	101	6.57	6.16	7.20	6.32	6.15	6.41	6.58	6.85	6.43	6.09	6.50	6.31	6.49	6.12	6.81	M	6.21	6.33	M	6.66	5.95	5.76	6.50	4.42
	102	5.98	6.15	6.28	6.31	6.10	6.16	6.18	5.92	6.03	5.98	4.27	4.21	4.11	4.07	3.78	M	3.18	M	M	M	M	M	M	M
	103	M	M	M	M	M	M	M	M	M	7.09	M	6.77	6.36	M	6.06	6.05	6.21	6.93	M	6.54	6.16	6.11	M	5.95
	104	6.21	6.44	M	6.61	6.00	M	6.16	6.01	6.09	6.09	6.35	6.13	6.16	6.23	M	6.16	M	6.20	6.10	6.18	6.12	6.11	6.18	M
	105	M	M	M	M	M	M	M	M	M	M	M	M	M	M	M	M	M	M	M	M	M	M	M	6.15
15	106	6.26	6.23	6.24	6.24	6.07	6.19	6.24	6.28	6.34	6.23	6.30	6.24	6.35	6.29	6.41	6.28	6.15	6.21	6.11	5.90	5.89	6.08	6.29	6.06
	107	6.21	6.15	6.25	6.24	6.28	6.36	6.34	6.32	6.40	6.33	6.41	6.23	6.15	6.18	6.24	6.24	6.24	6.18	6.12	M	6.13	5.98	6.12	6.06
	108	6.01	6.10	6.11	6.18	6.17	6.13	6.30	6.13	6.22	6.27	6.23	6.26	6.20	6.16	6.07	6.19	6.20	6.25	6.15	6.04	6.11	6.24	6.24	6.24
	109	6.26	6.27	6.23	6.27	6.21	6.30	6.32	6.22	6.33	6.33	6.30	6.36	6.34	6.38	6.47	6.39	6.32	6.21	6.42	6.37	6.38	6.40	6.44	6.39
	110	6.38	6.30	6.35	6.33	6.31	6.30	6.33	6.33	6.38	6.30	6.33	6.20	6.21	5.71	6.03	6.29	M	6.40	6.32	6.37	6.33	6.32	6.35	6.39
20	111	6.34	6.37	6.27	5.79	6.15	6.31	6.27	6.31	6.36	6.37	6.33	6.42	6.36	6.16	6.31	6.34	6.35	6.31	5.75	5.15	5.26	5.73	5.82	5.91
	112	6.02	6.05	5.94	5.78	5.94	6.12	6.19	6.25	6.30	6.28	6.27	6.39	6.37	6.42	6.43	6.45	6.47	6.51	6.45	6.57	6.62	6.59	6.48	6.59
	113	6.56	6.53	6.56	6.49	6.53	6.56	6.59	6.52	6.59	6.55	6.46	6.38	6.43	6.55	6.50	6.54	6.03	6.04	6.28	6.57	6.64	6.70	6.64	6.71
	114	6.71	6.79	6.69	6.82	6.88	6.84	M	6.58	6.73	6.62	6.72	6.59	6.68	6.65	6.78	6.72	6.82	6.73	6.80	6.93	6.85	M	M	M
	115	M	6.70	6.76	6.70	M	M	M	M	M	M	6.77	6.74	6.78	6.48	6.75	6.76	6.68	6.72	6.48	6.50	6.48	6.52	6.63	6.66
25	116	6.65	6.68	6.57	6.38	6.49	6.31	6.60	6.63	6.77	M	6.74	6.78	6.73	6.53	M	6.66	6.59	M	6.44	6.13	6.11	6.29	5.94	6.34
	117	6.38	M	6.23	6.60	6.55	6.53	6.61	M	M	M	M	M	M	M	M	M	M	M	M	M	M	M	6.64	6.66
	118	6.69	6.52	6.48	6.22	M	6.55	6.54	6.53	6.61	6.60	6.59	6.55	M	6.50	6.58	6.50	6.52	M	6.61	6.61	M	6.60	6.61	6.68
	119	6.72	6.65	6.68	6.64	M	6.72	6.74	6.75	6.75	6.75	6.79	6.74	M	6.80	6.39	M	6.42	6.49	6.45	6.44	6.28	6.51	6.34	M
	120	5.85	5.50	5.65	5.82	5.78	5.83	5.84	M	6.01	6.06	6.09	6.14	6.11	6.14	6.02	M	6.02	5.87	5.71	5.81	5.26	5.35	5.52	M
30	121	5.58	5.85	M	5.57	5.76	5.79	5.00	5.60	5.67	5.67	5.64	5.59	5.88	5.87	5.75	M	5.42	5.33	M	5.89	M	M	M	M

MAY

-LOG(FLUX), ERGS/CM2-S, HOUR AVERAGES

DAY	DOY/HR	0	1	2	3	4	5	6	7	8	9	10	11	12	13	14	15	16	17	18	19	20	21	22	23
May 1	122	M	4.96	M	5.16	5.31	5.33	5.37	5.47	5.53	5.57	M	5.70	5.76	5.76	5.81	5.84	5.77	5.97	M	5.63	5.68	M	M	5.00
	123	5.16	5.48	M	5.73	5.84	M	5.98	M	6.02	5.98	5.95	5.90	6.08	6.13	5.61	5.94	6.03	6.04	6.07	6.07	6.13	M	6.23	6.11
	124	6.27	6.19	6.27	6.36	6.19	M	5.73	5.80	5.85	5.87	5.90	5.93	6.05	M	6.13	6.16	6.20	6.25	6.23	6.27	6.30	M	6.34	6.31
	125	M	6.36	6.44	6.42	6.33	6.32	6.35	6.29	M	6.32	5.84	5.87	5.81	5.92	5.95	6.19	M	6.29	6.27	6.32	6.26	6.26	6.31	6.27

TABLE 3. COLUMBIA OSO-8 GRAPHITE CRYSTAL SPECTROMETER DATA
X-RAY EMISSION LINE FLUXES

SI14, 6.18A

YEAR= 1976
MARCH

-LOG(FLUX), ERGS/CM2-S, HOUR AVERAGES

DAY	DOY/HR	0	1	2	3	4	5	6	7	8	9	10	11	12	13	14	15	16	17	18	19	20	21	22	23
Mar. 23	83	M	M	M	M	M	M	M	M	M	M	M	4.35	4.41	4.78	4.94	4.99	5.16	5.25	5.39	5.67	5.84	7.29	6.75	5.16
	84	5.87	4.97	7.14	M	M	6.09	M	5.77	7.58	4.95	6.14	B	M	7.40	M	7.33	7.29	7.34	M	7.57	M	6.98	6.37	M
25	85	6.40	5.53	5.86	7.24	6.53	5.33	5.12	5.12	5.33	5.56	5.66	5.22	4.75	M	5.18	5.29	5.55	5.13	5.70	7.27	5.25	7.16	4.92	4.95
	86	M	M	M	M	M	M	M	M	M	M	M	M	M	M	M	M	M	M	M	M	M	M	M	M
	87	M	M	M	M	M	M	M	M	M	M	M	M	M	M	M	M	M	M	M	M	M	M	M	M
	88	6.32	5.96	M	6.28	6.20	7.08	5.18	5.88	6.95	6.77	4.98	5.05	5.33	5.60	6.34	7.09	6.95	6.08	5.93	5.01	M	M	M	M
	89	M	M	M	M	M	M	M	M	M	M	M	M	M	M	M	M	M	M	M	M	M	M	M	M
	90	M	M	M	M	M	M	M	M	M	M	M	M	M	M	M	M	M	M	M	M	M	M	M	M
31	91	M	7.29	M	6.42	6.45	5.68	6.54	5.49	M	M	M	M	M	M	M	4.92	4.99	5.34	5.37	5.35	5.73	5.68	5.79	6.04

APRIL

-LOG(FLUX), ERGS/CM2-S, HOUR AVERAGES

	DOY/HR	0	1	2	3	4	5	6	7	8	9	10	11	12	13	14	15	16	17	18	19	20	21	22	23
Apr. 1	92	6.03	6.17	6.35	6.29	7.31	7.04	7.62	6.89	7.47	7.02	M	M	M	M	M	M	M	M	M	M	M	M	M	M
	93	M	M	M	M	M	M	M	M	M	6.44	M	M	M	M	M	M	M	M	M	M	M	M	M	M
	94	M	M	M	M	M	M	M	M	M	M	M	M	M	M	M	M	M	M	M	M	M	M	M	M
	95	M	M	M	M	M	M	M	M	M	7.75	M	M	M	M	M	M	M	M	M	M	M	M	M	M
5	96	M	M	M	M	M	M	M	7.55	M	M	M	M	M	M	M	M	M	M	M	M	M	M	M	M
	97	M	M	M	M	M	M	M	M	M	M	M	M	M	M	M	M	M	M	M	M	M	M	M	M
	98	M	M	M	M	7.15	M	M	M	M	M	M	M	M	M	M	M	M	M	M	M	M	M	M	M
	99	M	M	M	M	M	M	M	M	M	M	M	M	M	M	M	M	M	M	M	M	M	M	M	M
	100	M	M	M	M	M	M	M	M	M	M	M	M	M	M	M	M	M	M	M	M	M	M	M	M
10	101	7.75	M	B	7.74	8.00	M	7.53	M	B	7.55	M	7.31	M	M	M	M	M	M	M	6.81	6.88	7.02	7.02	M
	102	7.03	6.93	7.37	7.69	M	M	7.12	7.06	B	7.10	7.41	6.75	M	M	M	M	M	M	M	M	M	M	M	M
	103	M	M	M	M	M	M	M	M	M	B	M	7.81	M	M	M	6.64	M	M	M	M	6.97	M	M	M
	104	M	M	M	7.18	M	M	M	7.44	M	6.84	7.24	M	M	M	M	6.68	M	7.94	M	M	7.48	7.86	B	M
	105	M	M	M	M	M	M	M	M	M	M	M	M	M	M	M	M	M	M	M	M	M	M	M	M
15	106	7.26	M	M	M	7.69	M	M	B	M	B	M	M	M	M	M	M	M	M	7.31	6.04	6.07	M	7.34	M
	107	B	7.79	M	M	7.94	7.94	M	B	M	M	M	7.80	6.81	M	M	M	M	M	M	M	7.54	M	M	7.51
	108	6.63	M	7.39	M	M	M	M	M	7.90	M	M	M	M	M	M	7.45	M	M	M	M	M	M	M	M
	109	M	M	M	M	M	M	M	M	M	M	M	6.15	6.05	M	M	M	7.50	M	M	M	M	M	M	M
	110	M	7.17	M	M	M	M	M	B	M	M	7.87	M	M	5.50	M	M	M	M	7.25	M	B	M	B	7.28
20	111	B	7.44	B	6.22	6.99	7.87	M	M	M	M	B	7.23	7.55	6.50	B	7.37	M	7.04	6.01	5.37	5.71	6.52	6.82	6.80
	112	B	7.08	B	7.00	7.51	7.64	7.38	B	M	B	M	M	M	7.76	M	M	7.74	M	B	7.94	M	B	7.32	B
	113	M	7.55	7.59	M	B	7.99	7.12	M	B	7.63	M	M	M	M	M	M	6.72	7.14	M	7.93	7.94	7.11	7.59	7.85
	114	7.79	B	B	7.53	B	B	M	7.84	7.42	M	7.28	M	7.55	M	7.16	7.87	7.63	7.51	7.51	M	7.68	M	M	M
	115	M	6.92	7.78	7.16	M	M	M	M	M	M	B	M	7.77	B	7.07	M	7.34	7.73	M	7.41	M	7.48	7.66	7.72
25	116	7.43	M	B	B	6.32	7.28	B	7.94	7.49	M	B	B	M	7.76	M	6.15	7.82	M	5.90	7.37	6.56	6.57	7.03	7.43
	117	7.55	M	6.95	7.48	B	M	M	M	M	M	M	M	M	M	M	M	M	M	M	M	M	M	M	M
	118	M	M	7.32	6.79	M	7.27	M	M	7.47	M	B	B	M	7.90	7.87	M	M	M	B	M	M	B	7.68	M
	119	7.69	7.65	M	M	M	7.34	7.79	M	7.93	7.51	7.24	M	M	M	7.27	M	M	B	M	7.07	M	B	B	M
	120	7.14	6.01	M	6.87	6.81	6.69	7.16	M	B	M	M	7.99	M	M	7.07	M	M	M	6.52	6.68	5.41	5.49	6.78	M
30	121	6.29	7.23	M	6.52	6.69	M	5.21	M	6.31	B	6.13	5.88	M	5.38	5.74	M	5.18	M	M	5.57	M	M	M	M

MAY

-LOG(FLUX), ERGS/CM2-S, HOUR AVERAGES

	DOY/HR	0	1	2	3	4	5	6	7	8	9	10	11	12	13	14	15	16	17	18	19	20	21	22	23
May 1	122	M	5.07	M	5.20	5.63	5.70	5.68	5.86	5.90	5.95	M	6.51	7.67	M	7.42	M	6.68	M	M	5.74	6.06	M	M	5.13
	123	5.16	5.76	M	7.24	7.23	M	M	M	M	7.52	M	6.44	M	M	6.74	M	M	7.39	6.71	6.13	M	M	M	7.70
	124	M	M	M	M	M	M	6.32	7.19	M	M	M	M	M	M	M	M	M	M	M	M	M	M	M	M
	125	M	M	M	M	B	M	M	M	M	M	6.25	6.39	6.29	M	7.66	M	M	M	M	M	M	M	M	M

TABLE 4. COLUMBIA OSO-8 GRAPHITE CRYSTAL SPECTROMETER DATA
X-RAY EMISSION LINE FLUXES

SI13, 6.64A

YEAR= 1976
MARCH

-LOG(FLUX), ERGS/CM2-S, HOUR AVERAGES

DAY	DOY/HR	0	1	2	3	4	5	6	7	8	9	10	11	12	13	14	15	16	17	18	19	20	21	22	23
Mar. 23	83	M	M	M	M	M	M	M	M	M	M	M	4.19	4.13	4.18	4.24	4.29	4.32	4.34	4.41	4.46	4.49	4.50	4.52	4.49
	84	4.46	4.44	4.42	4.46	4.49	4.49	M	4.51	4.56	4.46	4.49	4.56	4.58	4.63	4.68	4.65	4.65	4.63	4.67	4.68	4.71	4.66	4.66	4.71
25	85	4.66	4.67	4.68	4.66	4.66	4.84	4.73	4.69	4.66	4.59	4.47	4.43	4.47	M	4.66	4.59	4.49	4.58	4.54	4.53	4.56	4.58	4.70	4.64
	86	M	M	M	M	M	M	M	M	M	M	M	M	M	M	M	M	M	M	M	M	M	M	M	M
	87	M	M	M	M	M	M	M	M	M	M	M	M	M	M	M	M	M	M	M	M	M	M	M	4.65
	88	4.67	4.68	4.73	4.75	4.69	4.72	4.66	4.66	4.70	4.68	4.67	4.77	4.64	4.63	4.64	4.70	4.69	4.72	4.72	4.73	M	M	M	M
	89	M	M	M	M	M	M	M	M	M	M	M	M	M	M	M	M	M	M	M	M	M	M	M	M
	90	M	M	M	M	M	M	M	M	M	M	M	M	M	M	M	M	M	M	M	M	M	M	4.90	5.18
31	91	5.20	4.75	5.04	5.07	4.95	4.72	4.77	4.87	5.07	M	M	M	M	M	M	4.44	4.47	4.73	4.86	4.83	4.80	M	M	M

APRIL

-LOG(FLUX), ERGS/CM2-S, HOUR AVERAGES

	DOY/HR	0	1	2	3	4	5	6	7	8	9	10	11	12	13	14	15	16	17	18	19	20	21	22	23
Apr. 1	92	M	M	M	M	M	M	M	M	M	M	M	M	M	M	M	M	M	M	M	M	M	M	M	M
	93	M	M	M	M	M	M	M	M	M	M	M	M	M	M	M	M	M	M	M	M	M	M	M	M
	94	M	M	M	M	M	M	M	M	M	M	M	M	M	M	M	M	M	M	M	M	M	M	M	M
	95	M	M	M	M	M	M	5.82	5.82	M	5.86	M	M	M	M	M	M	M	M	M	M	M	M	M	M
5	96	M	M	M	M	M	M	M	6.34	M	M	M	M	M	M	M	M	M	M	M	M	M	M	M	M
	97	M	M	M	M	M	6.20	6.21	M	M	M	M	M	M	M	M	M	M	M	M	M	M	M	M	M
	98	M	M	M	M	5.92	6.02	5.90	M	M	M	M	M	M	M	M	M	M	M	M	M	M	M	M	M
	99	M	M	M	M	5.84	5.97	M	M	M	M	M	M	M	M	M	M	M	M	M	M	M	M	M	M
	100	M	M	M	M	M	M	M	M	M	M	M	M	M	M	M	M	M	M	M	M	M	M	M	M
10	101	6.33	6.24	6.25	6.23	6.23	6.24	6.23	6.24	6.17	5.95	6.15	6.16	6.26	6.02	6.21	M	6.17	6.21	M	6.10	5.92	5.98	6.01	5.63
	102	5.88	6.00	6.06	6.06	6.04	6.06	5.90	5.97	5.87	5.83	5.84	5.64	4.14	5.00	M	M	M	M	M	M	M	M	M	M
	103	M	M	M	M	M	M	M	M	M	6.03	6.02	5.79	5.93	5.82	5.94	5.84	5.84	5.85	M	5.77	5.80	5.80	M	5.64
	104	5.74	5.80	M	5.66	5.80	M	5.70	5.77	5.81	5.80	5.87	5.81	5.89	5.78	M	5.64	M	5.67	5.77	5.77	5.72	5.71	5.76	M
	105	M	M	M	M	M	M	M	M	M	M	M	M	M	M	M	M	M	M	M	M	M	M	M	5.70
15	106	5.77	5.79	5.81	5.82	5.53	5.69	5.82	5.85	5.89	5.78	5.80	5.76	5.85	5.84	5.86	5.80	5.77	5.79	5.63	5.25	5.14	5.70	5.80	5.76
	107	5.76	5.70	5.82	5.82	5.87	5.90	5.90	5.89	5.91	5.87	5.83	5.74	5.55	5.68	5.69	5.73	5.72	5.77	5.63	M	5.71	5.52	5.70	5.57
	108	5.46	5.63	5.67	5.73	5.69	5.66	5.71	5.71	5.74	5.76	5.80	5.76	5.71	5.55	5.55	5.57	5.67	5.69	5.56	5.50	5.48	5.63	5.68	5.68
	109	5.67	5.68	5.64	5.67	5.58	5.70	5.74	5.61	5.72	5.76	5.75	5.72	5.67	5.75	5.85	5.79	5.61	5.53	5.77	5.77	5.77	5.75	5.76	5.78
	110	5.74	5.66	5.74	5.74	5.70	5.73	5.76	5.75	5.84	5.77	5.82	5.69	5.79	5.23	5.65	5.93	M	6.12	6.11	6.14	6.18	6.15	6.27	5.92
20	111	B	M	M	M	M	M	M	M	M	6.05	5.97	6.23	6.20	5.90	6.14	6.01	5.96	5.59	5.68	5.35	5.49	5.75	6.04	5.46
	112	6.68	6.02	M	M	M	M	M	6.80	6.10	6.21	6.18	6.57	6.30	6.62	6.49	6.32	6.39	6.54	6.43	6.65	6.59	6.37	6.19	6.46
	113	6.73	7.04	5.90	7.47	B	6.82	6.09	6.45	6.47	6.41	6.16	6.10	6.05	6.27	6.29	6.24	5.52	5.59	6.06	6.42	6.44	6.55	6.47	6.46
	114	6.55	6.60	6.46	6.77	6.29	6.45	M	7.31	M	M	M	M	M	M	M	M	M	M	M	M	M	M	M	M
	115	M	M	M	M	M	M	M	M	M	M	M	M	6.69	M	M	M	M	M	M	7.60	6.00	6.23	6.37	6.50
25	116	6.38	6.43	6.35	5.99	6.14	5.96	6.46	6.50	6.01	M	5.77	M	M	M	M	M	M	M	M	M	M	M	M	M
	117	M	M	M	M	M	M	M	M	M	M	M	M	M	M	M	M	M	M	M	M	M	M	M	M
	118	M	M	M	M	M	M	M	M	M	M	M	M	M	6.58	6.29	5.70	5.66	M	6.05	6.11	M	6.04	6.02	6.16
	119	5.94	6.21	5.97	6.03	M	6.29	6.28	6.28	6.33	6.44	6.40	6.35	M	6.42	5.80	M	5.97	6.03	6.10	5.96	5.89	6.17	5.92	M
	120	5.41	4.87	5.10	5.36	5.37	5.40	5.36	M	5.61	5.64	5.67	5.71	5.69	5.72	5.52	M	5.49	5.36	5.19	5.19	4.76	4.79	4.94	M
30	121	4.99	5.27	M	4.92	5.16	5.16	4.65	4.98	5.02	5.00	4.94	4.87	5.19	5.19	5.06	M	4.74	4.74	M	5.21	M	M	M	M

MAY

-LOG(FLUX), ERGS/CM2-S, HOUR AVERAGES

	DOY/HR	0	1	2	3	4	5	6	7	8	9	10	11	12	13	14	15	16	17	18	19	20	21	22	23
May 1	122	M	4.61	M	4.58	4.64	4.66	4.66	4.73	4.75	4.80	M	4.91	5.00	5.04	5.05	5.05	4.99	5.23	M	4.84	4.90	M	M	4.67
	123	4.66	4.74	M	4.94	5.07	M	5.21	M	5.32	5.16	5.11	5.10	5.33	5.37	4.83	5.19	5.28	5.23	5.23	5.26	5.32	M	5.46	5.32
	124	5.50	5.40	5.53	5.63	5.39	M	4.88	4.94	4.99	5.03	5.04	5.09	5.23	M	5.35	5.42	5.46	5.50	5.47	5.49	5.55	M	5.63	5.62
	125	M	5.63	5.69	5.66	5.63	5.61	5.64	5.55	M	5.59	4.97	4.98	4.97	5.05	5.13	5.42	M	5.57	5.55	5.56	5.50	5.47	5.47	5.48

5. COSMIC RAYS

Relativisitic Solar Cosmic Rays on 30 April, 1976

by

S. P. Duggal and M. A. Pomerantz
Bartol Research Foundation, University of Deleware
Newark, Del. 19711

Introduction

The ground level solar particle event (GLE) of 30 April 1976, is the twelfth and the last event of solar cycle 20. Thus, although maximum sunspot numbers were much lower in this cycle than in the previous one, the total number of events in the two cycles is comparable because only ten events were recorded in cycle 19 [Pomerantz and Duggal, 1974a]. The occurrence of this GLE during the minimum phase of cycle 20, near the beginning of cycle 21, again demonstrates that GLE can occur at any phase of the solar cycle [Pomerantz and Duggal, 1974a; Duggal, 1975].

Observations and Discussion

Several flares have been reported in McMath Region 14179 (presumably return of McMath Region 14143). Various observatories have assigned importance ratings ranging from sn to 2b for a flare on 30 April. However, despite this spread, the estimated onset times, about 2048 UT, are consistent. The solar particles that caused the ground level enhancement of 30 April, as well as the Forbush decrease on 2 May (Figure 1) were apparently associated with this flare. Its location (S08 W46) was close to the base of the nominal garden hose line that connects the Sun to the Earth.

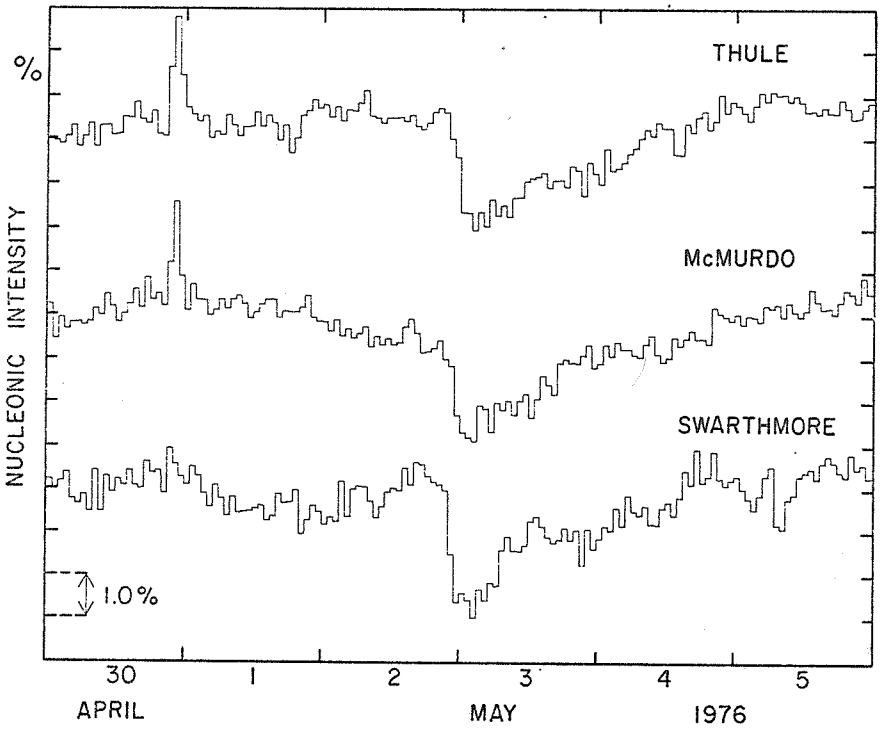

Fig. 1. Nucleonic intensity at two polar stations, Thule and McMurdo, and at the lower latitude station Swarthmore whose asymptotic cone of acceptance lies close to the equator. Both the GLE on 30 April and the Forbush decrease on 2 May can be associated with the same flare.

Figure 2 shows the profile of the solar particle increase at two polar stations, Thule and McMurdo. The maximum increase in hourly intervals is about 2.5%. The data recorded at Swarthmore are consistent with a small increase of roughly 0.5%. No significant increase was recorded by stations with geomagnetic cutoff $P_c > 3GV$, and the spectrum during a period in which the anisotropy was small is consistent with a power law exponent of ~ 5. Because of the effect of pre-event fluctuations upon the normalization, caution should be exercised in comparing hourly and short period data from different stations (Figures 2, 3, 4).

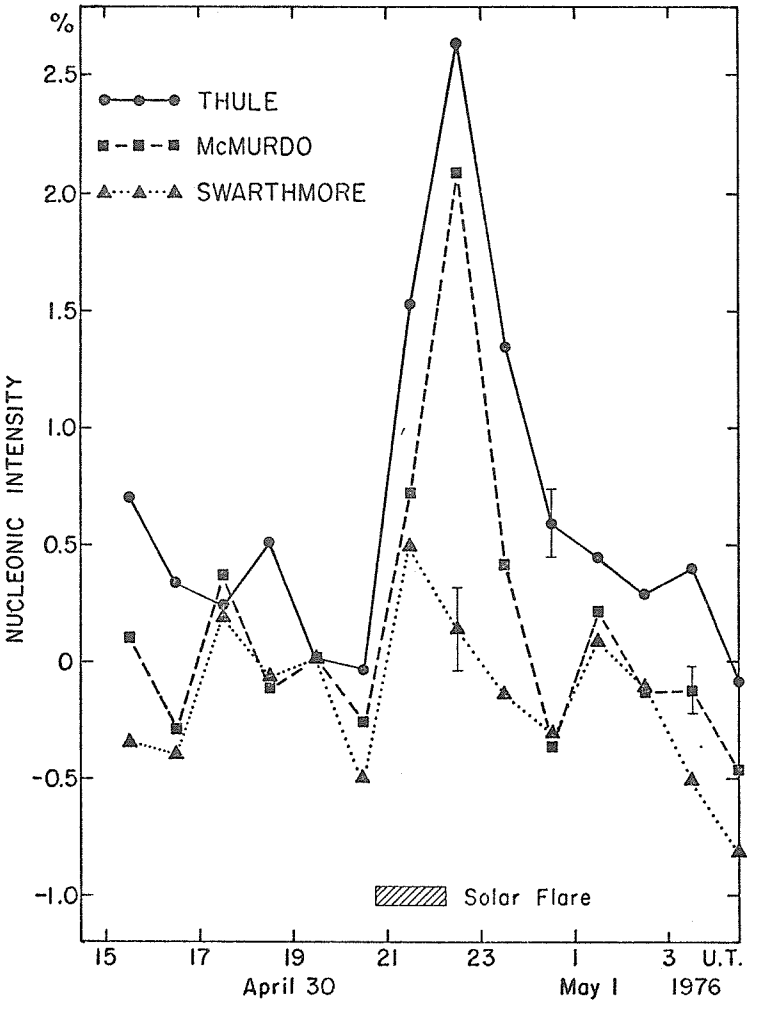

Fig. 2. Profile of the relativistic solar particle event in hourly intervals. The duration of the parent solar flare is also indicated. Note that because of the effect of pre-event fluctuations on the normalization, caution should be exercised in comparing the magnitude of the increase at different stations.

Pressure-corrected nucleonic intensity data recorded at Thule and McMurdo in 6-minute intervals are listed in Table 1 and plotted in Figure 3. In Figure 3a the onset of the event appears to be around 2133 UT. Analysis of 4-minute averages shows that the onset at Thule was at 2130±0002 UT, whereas it was later at McMurdo. This difference is presumably related to the anisotropy [Duggal *et al.*, 1971; Duggal and Pomerantz, 1971]. This indicates that, depending on the injection time of the relativistic particles, the interplanetary propagation time is likely to be ≤ 44 min.

Figure 4 shows the hourly average nucleonic intensity difference ΔI during 16 hours on 30 April - 1 May 1976. Here

$$\Delta I = (\Delta N/N_0)_T - (\Delta N/N_0)_M$$

where $(\Delta N/N_0)_i$ = the fractional intensity change at station i; T = Thule; and M = McMurdo.

The increase in ΔI during the GLE interval is symptomatic of the general anisotropy that is ascribed to the scattering of particles from the garden hose field direction [Duggal, *et al.*, 1971; Duggal and Pomerantz, 1972, 1973; Maurer *et al.*, 1973].

Analysis of data from several stations has revealed that there was a large anisotropy during the interval 2100-2200 UT which diminished significantly during the next hour. The axis of symmetry appears to be close to the classical direction, i.e., $\approx 50°$ west of the Sun-Earth line.

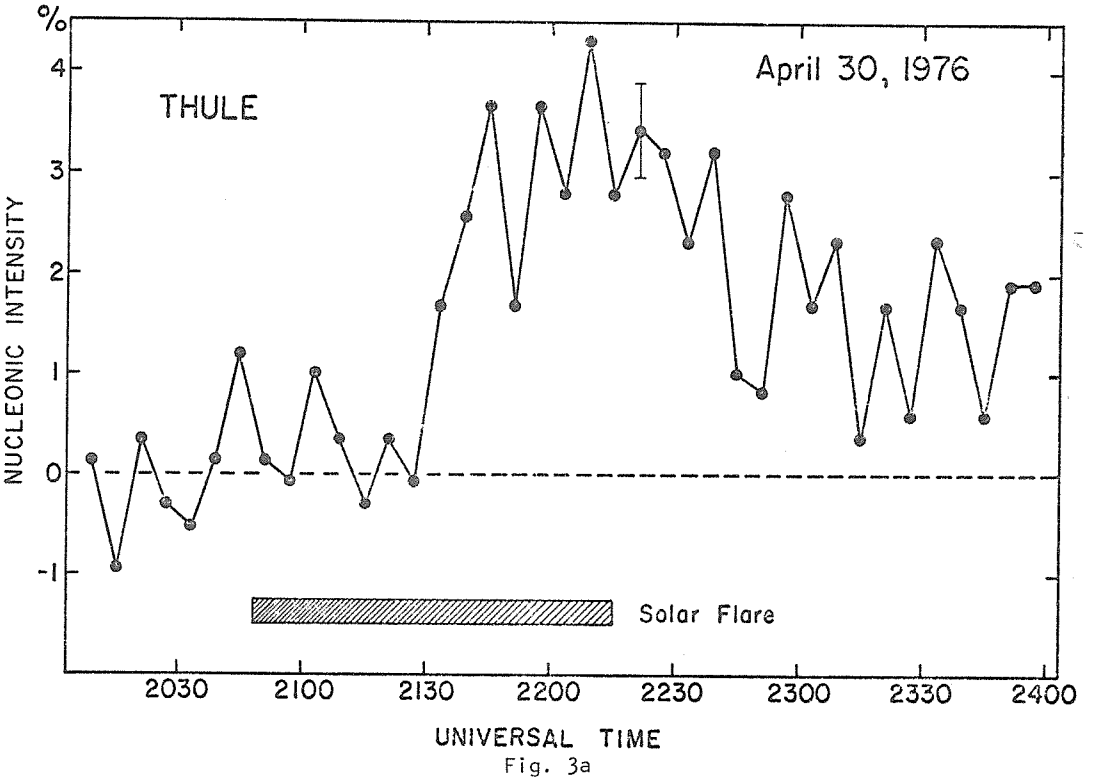

Fig. 3a

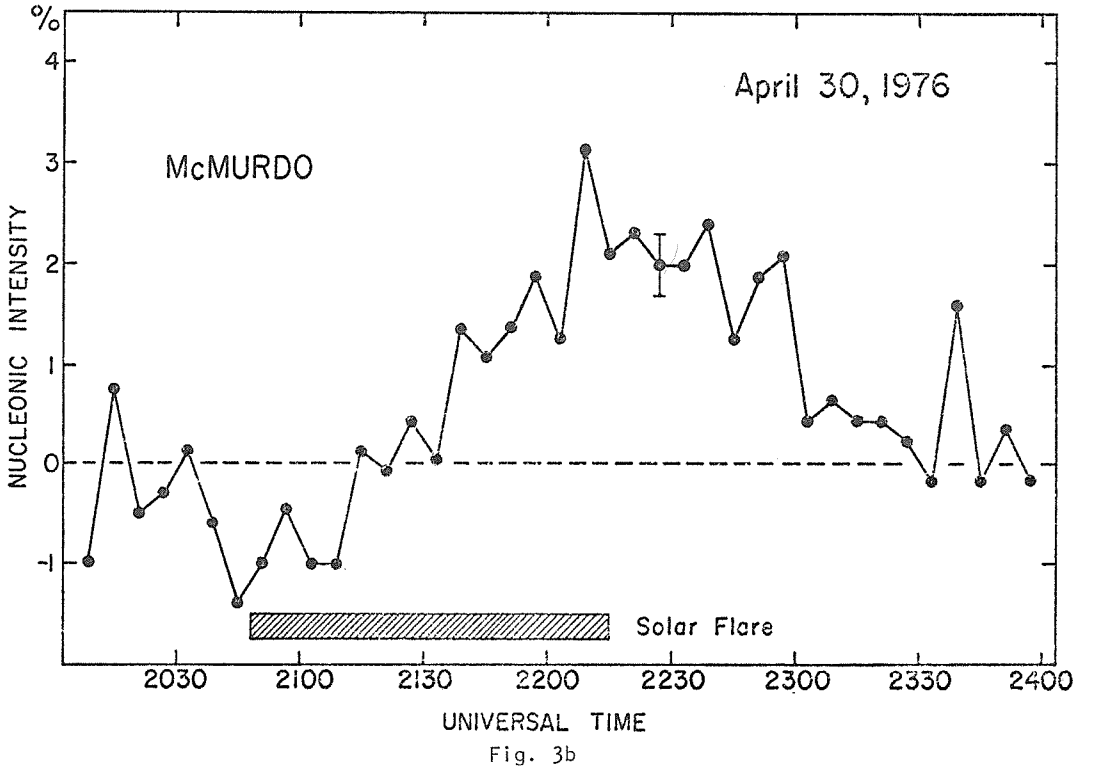

Fig. 3b

Fig. 3. Nucleonic intensity in 6-minute intervals at (a) Thule and (b) McMurdo on 30 April 1976.

Table 1

Nucleonic intensity data in 6-minute intervals recorded at Thule (N76.6 W68.8) and McMurdo (S77.9 E166.6). The listed time is at the center of the interval; the scaling factor for both stations is 100; and the readings are pressure-corrected.

30 April 1976

UT	THULE	McMURDO	UT	THULE	McMURDO
2003	450	968	2203	467	980
2009	455	958	2209	474	998
2015	450	975	2215	467	988
2021	456	963	2221	470	990
2027	453	965	2227	469	987
2033	452	969	2233	465	987
2039	455	962	2239	469	991
2045	460	954	2245	459	980
2051	455	958	2251	458	986
2057	454	963	2257	467	988
2103	459	958	2303	462	972
2109	456	958	2309	465	974
2115	453	969	2315	456	972
2121	456	967	2321	462	972
2127	454	972	2327	457	970
2133	462	968	2333	465	966
2139	466	981	2339	462	983
2145	471	978	2345	457	966
2151	462	981	2351	463	971
2157	471	986	2357	463	966

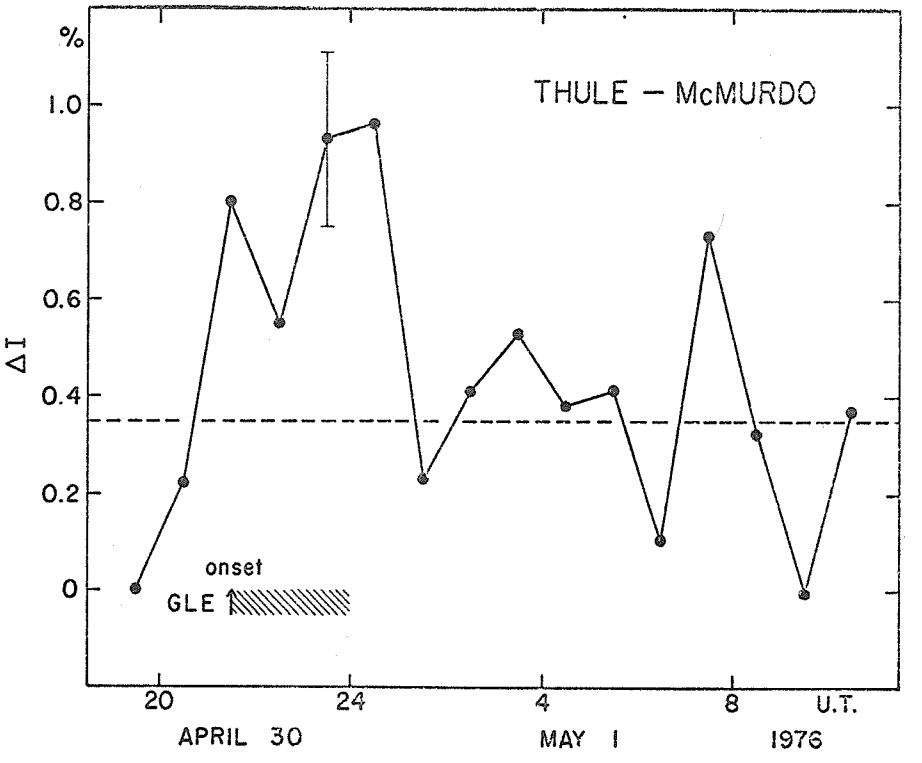

Fig. 4. North-south intensity difference in hourly intervals. Note that ΔI during the GLE arises from the general anisotropy with respect to the axis of symmetry, i.e., the direction of the apparent source.

Conclusion

Although the magnitude of this event is small, the absence of a pair of shock waves and the apparently normal characteristics of this GLE make it unnecessary to invoke an unusual process such as the acceleration of particles in interplanetary space [Pomerantz and Duggal, 1974b; Duggal, 1975; Levy, *et al.*, 1976]. The onset time with respect to that of the flare, as well as the spectrum and anisotropy during the GLE of 30 April 1976 are similar to other events associated with parent flares near the base of the garden hose field line. Analysis is in progress to determine the characteristics of particle propagation during this GLE.

Acknowledgment

This research was sponsored by the National Research Foundation.

REFERENCES

DUGGAL, S. P. 1975 Relativistic Solar Protons, *Reviews of Geophys. and Space Physics, 13,* 1084.

DUGGAL, S. P., I. GUIDI and M. A. POMERANTZ 1971 The Unusual Anisotropic Solar Particle Event of November 18, 1968, *Solar Physics 19,* 234.

DUGGAL, S. P. and M. A. POMERANTZ 1971 The Propagation of Energetic Solar Particles During Highly Anisotropic Ground Level Events, *Proceedings 12th International Conference on Cosmic Rays, Hobart, 2,* 533.

DUGGAL, S. P. and M. A. POMERANTZ 1972 Sectorial Anistropy of Solar Cosmic Rays, *Solar Physics, 27,* 227.

DUGGAL, S. P. and M. A. POMERANTZ 1973 Anisotropies in Relativistic Cosmic Rays from the Invisible Disk of the Sun, *J. Geophys. Res., 78,* 7205.

LEVY, E. H., S. P. DUGGAL and M. A. POMERANTZ 1976 Adiabatic Fermi Acceleration of Energetic Particles between Converging Interplanetary Shock Waves, *J. Geophys. Res., 81,* 51.

MAURER, R. H., S. P. DUGGAL and M. A. POMERANTZ 1973 Pitch Angle Distribution of Solar Flare Particles in Interplanetary Space, *J. Geophys. Res., 78,* 29.

POMERANTZ, M. A. and S. P. DUGGAL 1974a The Sun and Cosmic Rays, *Reviews of Geophys. and Space Physics, 12,* 343.

POMERANTZ, M. A. and S. P. DUGGAL 1974b Interplanetary Acceleration of Solar Cosmic Rays to Relativistic Energy, *J. Geophys. Res., 79,* 913.

The Results of Cosmic Ray Measurements in the Stratosphere in March-May 1976

by

A. N. Charakhchyan, G. A. Bazilevskaya, Yu. I. Stozhkov
P. N. Lebedev Physical Institute, Academy of Sciences of USSR
and
T. N. Charakhchyan
Nuclear Research Institute, Moscow State University, USSR

The measurements of cosmic ray charged particles with stratospheric radiosondes are regularly taken over Mirny, Antarctica (S66.57 E92.92); Murmansk Region (N68.95 E33.05); Moscow Region (N55.93 E37.52); and Alma-Ata (N43.25 E76.92). The radiosonde detector consists of two G-M tubes arranged as a telescope, interlaid by a 7 mm thick aluminum plate. The wall thickness of G-M tubes is 0.05 g cm^{-2} of steel. The counting rate of a single counter and of the two-counter coincidences are recorded.

In Table 1 are the data for the period 20 March 1976 to 5 May 1976 of the total flux ($cm^{-2}sec^{-1}$) and vertical intensity ($cm^{-2}sec^{-1}ster^{-1}$) of cosmic ray charged particles in the transition maximum of pressure dependence (Pfotzer maximum). The measurements in the transition maximum are taken over 10-15 min and have an accuracy of 1-2%. The mean time of the measurement is also indicated. For the period in question the transition maximum corresponds with following pressure (g cm^{-2}):

	Single Counter	Telescope
Mirny	20 - 40	35 - 70
Murmansk Region	20 - 70	35 - 70
Moscow Region	40 - 60	50 - 85
Alma-Ata	65 - 100	90 - 140

The main characteristics of the time dependence of cosmic ray intensity for the period in question are the following:

1. The gradual increase in agreement with the 11-year solar cycle.
2. On 26 March 1976, the onset of a Forbush-effect took place, producing the lowest intensity decrease since August 1972. This Forbush-effect initiated a 27-day cosmic ray variation that lasted for at least 6 solar rotations. This modulation appears in the Murmansk and Mirny data presented in Figure 1.

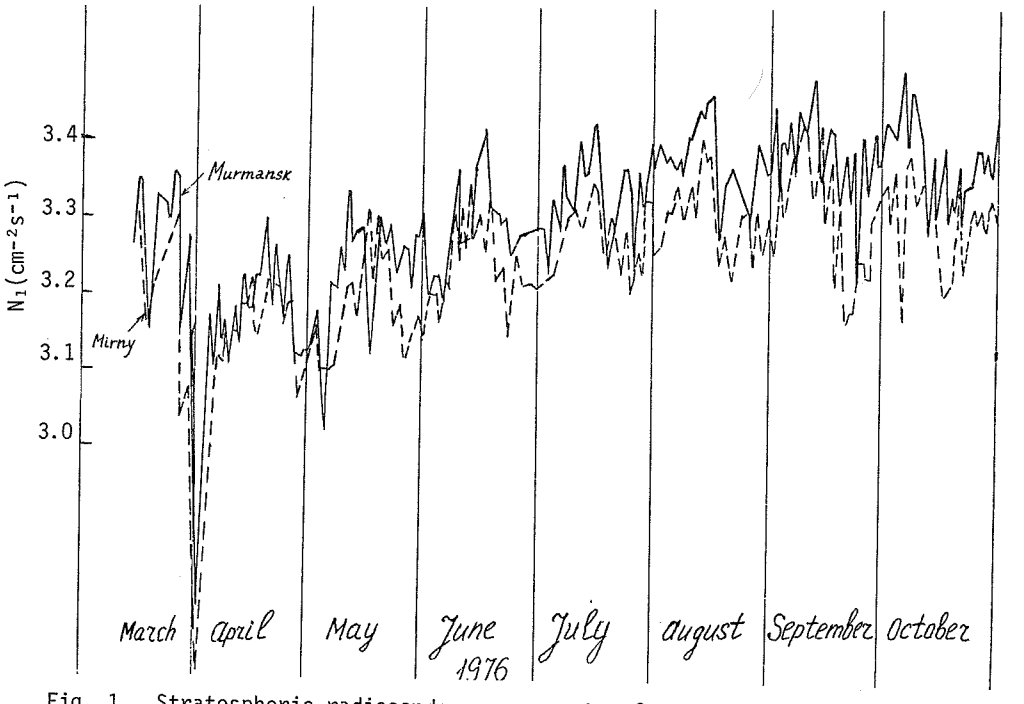

Fig. 1. Stratospheric radiosonde measurements of cosmic ray total flux over Mirny, Antarctica, and the Murmansk Region during the period March - October 1976. The solid line denotes the Murmansk flux; the dashed line Mirny.

Table 1. N_1-data of the single counter ($cm^{-2}s^{-1}$), N_2-data of the telescope ($cm^{-2}s^{-1}sr^{-1}$)

Date	Mirny				Murmansk Region				Moscow Region				Alma-Ata			
1976	UT	N_1	UT	N_2	UT	N_1	UT	N_2	UT	N_1	UT	N_2	UT	N_1	UT	N_2
March 20					0807	3.325	0752	0.464					0743	1.645	0743	0.248
					1307	3.277	1257	0.445								
21	0814	3.218	0806	0.434	0804	3.321	0759	0.458								
22			0755	0.470	1305	3.373	0802	0.478					0746	1.610	0740	0.246
							1304	0.460								
23	0816	3.238	0806	0.456	0806	3.311	0803	0.469	0637	2.792	0628	0.381	0746	1.614	0739	0.221
					1307	3.396	1301	0.473								
24	0819	3.277	0805	0.463	0805	3.281	0759	0.465	0632	2.792	0628	0.382	0739	1.552		
25	0825	3.288	0812	0.470	0812	3.359	0804	0.476								
					1310	3.254	1208	0.438								
26	0820	3.296	0809	0.456	0801	3.341	0802	0.457					0743	1.628	0736	0.221
					1303	3.231	1259	0.453								
27	0817	3.032	0815	0.442	0807	3.145	0801	0.438					0742	1.589	0734	0.231
28	0816	3.072	0808	0.434	0813	3.218	0805	0.438								
29	0813	3.063	0805	0.428	0815	3.269	0805	0.460	0623	2.701	0626	0.360	0745	1.625	0740	0.235
					1313	3.259	1312	0.435								
30	0814	2.892	0809	0.397	0813	2.909	0801	0.428	0628	2.808	0633	0.366	0744	1.602	0737	0.239
31	0807	2.814	0804	0.431	1306	2.981	1258	0.419	0632	2.690	0629	0.374	0818	1.581	0738	0.219
April 01	0807	2.700	0759	0.445	0805	2.774	0650	0.378	0631	2.681	0633	0.360	0745	1.602	0739	0.227
					1305	2.865	1251	0.390	1238	2.674	1236	0.385				
02	0811	2.825	0802	0.406	0803	2.919	0759	0.418	0640	2.501	0642	0.331	0741	1.610	0737	0.236
					1310	2.893	1306	0.417	1233	2.517	1233	0.338				
03					0818	3.090	0808	0.401					0756	1.554	0746	0.238
					1256	2.887	1254	0.404								
04	0807	2.957			0809	3.166	0800	0.426								
05	0822	3.052	0802	0.441	0812	3.084	0804	0.421	0629	2.646			0743	1.561	0733	0.228
					1247	3.136	1250	0.429								
06	0819	3.109	0756	0.448	0810	3.204	0800	0.428	0624	2.566	0621	0.370	0745	1.589	0735	0.245
					1308	3.186	1255	0.432								
07	0829	3.102	0821	0.444	0810	3.131	0752	0.421	0638	2.731	0636	0.359	0750	1.604	0746	0.245
					1310	3.119										
08	0822	3.136	0810	0.448	0812	3.161			0638	2.650	0632	0.359	0746	1.589	0742	0.241
					1308	3.172	1300	0.431								
09	0819	3.135	0811	0.448	0810	3.094	0758	0.433	0622	2.750	0625	0.377	1016	1.568	1013	0.232
					1312	3.027	1259	0.426	1225	2.707	1231	0.361				
10	0808	3.143	0800	0.463	0802	3.176	0753	0.432					0742	1.600	0739	0.224
					1304	3.068	1253	0.436								
11	0832	3.140	0813	0.446	0805	3.162	0759	0.433								
12	0811	3.156	0802	0.452	0804	3.124	0802	0.447	0638	2.645	0629	0.362	0758	1.639	0743	0.250
13	1004	3.172	0948	0.461	0810	3.226	0759	0.430	0634	2.738	0633	0.381	0820	1.638	0803	0.248
					1309	3.152	1256	0.443								

Table 1 (cont.) N_1-data of the single counter ($cm^{-2}s^{-1}$), N_2-data of the telescope ($cm^{-2}s^{-1}sr^{-1}$)

Date	Mirny				Murmansk Region				Moscow Region				Alma-Ata			
1976	UT	N_1	UT	N_2	UT	N_1	UT	N_2	UT	N_1	UT	N_2	UT	N_1	UT	N_2
April 14	0835	3.186	0722	0.452	0812	3.174	0759	0.412	1246	2.642	1245	0.345	0754	1.585	0745	0.239
					1320	3.144	1301	0.418								
15	0810	3.214	0801	0.454	0812	3.176	0804	0.442	0637	2.667	0634	0.369	0942	1.652	0932	0.228
					1309	3.166	1300	0.432	1235	2.668	1231	0.388				
16	0818	3.144	0804	0.466	0808	3.214	0756	0.431	0634	2.635	0623	0.391	0801	1.669	0746	0.236
					1313	3.208	1304	0.458	1246	2.644	1234	0.364				
17	0811	3.133	0759	0.455	0839	3.220	0827	0.465					0746	1.605	0740	0.233
					1308	3.204	1253	0.422								
18	0820	3.172	0814	0.464	0814	3.212	0806	0.458								
19	0815	3.215	0800	0.474	0815	3.293	0804	0.447	0651	2.722	0635	0.390	0751	1.599		
					1316	3.236	1308	0.437								
20	0813	3.216	0803	0.474	0812	3.185	0804	0.433	0636	2.680	0632	0.387	0748	1.582	0750	0.242
					1308	3.137	1257	0.437								
21			0838	0.453	0806	3.261	0800	0.449	0637	2.706	0632	0.385	0749	1.648	0745	0.234
					1302	3.209	1250	0.451								
22	0807	3.188	0800	0.450	1305	3.227	1303	0.456	0639	2.777	0628	0.404	0742	1.601	0738	0.239
23	0819	3.157	0809	0.459	0807	3.131			0635	2.722	0632	0.370	0958	1.662	0953	0.245
					1311	3.216	1304	0.448	1240	2.685	1231	0.378				
24	0811	3.175	0802	0.455	0815	3.247	0801	0.431					0804	1.663	0757	0.239
					1307	3.286	1307	0.454								
25	0807	3.178	0804	0.466	0808	3.191	0758	0.465								
26	0809	3.136	0801	0.464	0812	3.150	0826	0.461	0643	2.704	0627	0.386	0808	1.592	0750	0.241
					1303	3.120	1300	0.440								
27	0813	3.053	0802	0.436			1259	0.451	0639	2.695	0637	0.381	0807	1.623	0755	0.246
28	0807	3.060	0807	0.455	1312	3.113	1301	0.407					1021	1.623	1012	0.240
					0811	3.151	0805	0.448								
29			0809	0.454	0805	3.105	0758	0.436	0629	2.694	0624	0.377	0802	1.596	0750	0.239
					1310	3.121	1256	0.425	1230	2.718	1227	0.384				
30					0803	3.127	0757	0.443	0633	2.684	0625	0.390	0732	1.584	0735	0.248
May 01	1104	3.145	0754	0.482												
			1059	0.473												
02	0338	3.098	0421	0.446	0809	3.180	0802	0.444								
	0814	3.100	0759	0.447												
03					0834	3.045	0815	0.437	0632	2.657	0624	0.392	0847	1.624	0831	0.245
					1314	2.995	1258	0.430								
04					0818	3.070	0805	0.440	0632	2.687	0629	0.387	0749	1.611	0741	0.233
					1307	3.128	1301	0.436								
05	0821	3.094	0806	0.453	0825	3.215	0808	0.450	0639	2.669	0631	0.400	0738	1.597	0733	0.232
					1307	3.189	1300	0.451								

3. The burst of solar cosmic protons with energies more than 100 Mev took place on 1 May 1976. It was recorded in the daily radiosonde flight over Mirny. The energy spectrum found from the atmospheric absorption of solar protons corrected for nuclear interaction is presented in Figure 2. The repeated launches of radiosondes (see Table 1) did not give solar proton results because of the insufficient altitude of the flights.

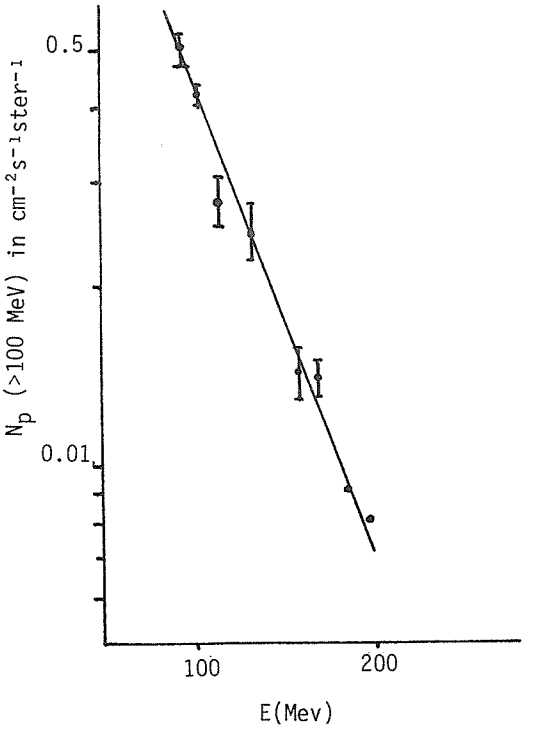

Fig. 2. Energy spectrum of solar cosmic ray protons recorded by radiosonde over Mirny on 1 May 1976 between 0805 and 0840 UT.

The Altitudinal Distribution of the Common Component Intensity of Cosmic Rays in the Stratosphere Over Tixie Bay in March 1976

by

A. M. Novikov
Institute of Cosmophysical Research and Aeronomy, Yakutsk Branch
Siberian Department of the USSR Academy of Sciences
Yakutsk, USSR

During 10 days of March 1976 at the Polar Geocosmophysical Observatory, Tixie Bay, the measurements of cosmic ray background in the stratosphere were carried out using Geiger counters and balloons. The characteristics of Tixie Bay are the following: a threshold rigidity of 0.52 GV and geographical coordinates N71.6 E129.0. The characteristics of the radiation detectors include a 106 cm^2 geometrical factor for the CTC-6 type Geiger counter and a 3.6 cm^2 factor for the two-coincidence telescope. There was a 5.5 mm thick aluminium plate between the telescope counters.

Curve 1 in Figure 1 is the result of cosmic ray background measurements in the stratosphere by a single counter. Curve 2 shows the same results measured by the two-coincidence telescope. Detector response in counts/min and the atmospheric depth in gm/cm^2 are shown along the Y and X axes, respectively.

In Table 1 the average daily sum of the 3-hourly K index, characterizing the magnetic activity during the cosmic ray background measurements in the stratosphere over Tixie Bay, are given.

Table 1. Average Daily Sum of 3-Hourly K Index

Date March 1976	Daily Sum K Index	Date March 1976	Daily Sum K Index
2	45	17	42
3	49	18	32
4	31	19	31
9	48	23	19
12	47	25	--

The results of cosmic ray background measurements in the stratosphere define an average during the period of strong solar activity occurring in the minimum of solar cycle 20. The contribution from the radiation belts and from solar cosmic rays to the constant background cosmic ray flux will be a minimum during this period. The estimate of this contribution for the time of minimum of the previous solar activity cycle was 2-4% (N.G. Skryabin, private communication).

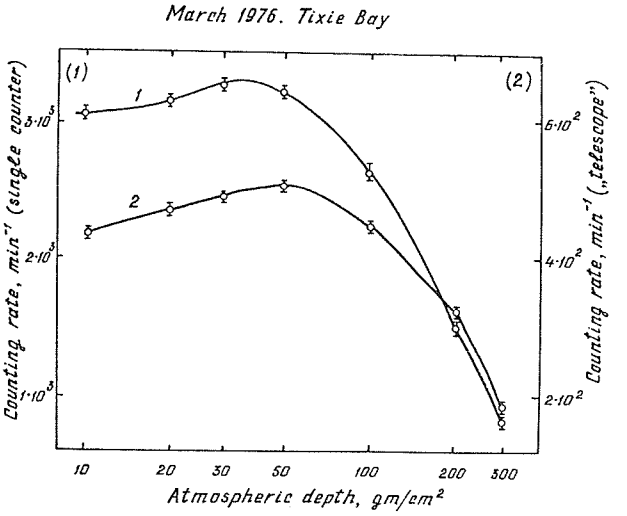

Fig.1. Curve 1 is from the cosmic ray background measurements in the stratosphere with a single Geiger counter. Curve 2 is similar, using the two-coincidence "telescope".

Solar Cosmic Ray Increase on 30 April 1976

by

N. P. Chirkov, A. M. Novikov, A. T. Filippov, A. I. Kuzmin
Institute of Cosmophysical Research and Aeronomy, Yakutsk Branch,
Siberian Department of the USSR Academy of Sciences, Yakutsk, USSR

A. V. Sergeyev, V. P. Karpov
Siberian Institute of Terrestrial Magnetism, Ionosphere and Radio Wave Propagation, Siberian Department of the USSR Academy of Sciences, Irkutsk, USSR

A. M. Okara
Institute of Geophysics and Tectonic, Far-East Scientific Center of the USSR Academy of Sciences, Khabarovsk, USSR

V. L. Borisov
Institute of Geology and Geophysics, Siberian Department of the USSR Academy of Sciences, Novosibitsk, USSR

T. T. Sokolova
North-East Complex Research Institute, Far-East Scientific Center of the USSR Academy of Sciences, Magadan, USSR

On 30 April 1976 a cosmic ray increase was recorded by the Siberian network of neutron supermonitors. Characteristics of the stations are given in Table 1 where ρ is the threshold rigidity, τ is the mean dead time of the radio trace, ϕ and λ are the geographical latitude and longitude of the station, respectively, and σ is an the hourly statistical error.

Table 1

Station	P (GV)	τ (μs)	Geographic Coordinates Lat.(ϕ)	E. Long.(λ)	σ (%)
Tixie Bay	0.52	20	71.6°	129.0°	0.17
Norilsk	0.60	1200	69.3	88.0	0.17
Yakutsk	1.86	20	62.0	129.7	0.18
Magadan	2.16	200	60.1	151.0	0.14
Novosibirsk	2.85	200	54.8	83.0	0.25
Irkutsk	3.74	10	52.5	104.0	0.18
Khabarovsk	5.55	200	48.5	135.2	0.31

As seen from Figure 1, the increase was observed at Tixie Bay, Norilsk, Yakutsk, and Magadan, but it was not observed at Novosibirsk, Irkutsk, and Khabarovsk. Thus, the largest energies of accelerated particles in this flare were ~2.5 GeV.

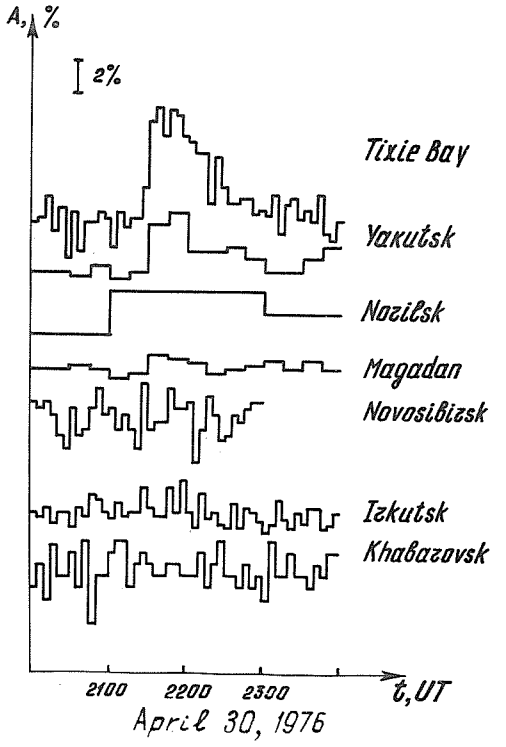

Fig.1. Cosmic Ray Variations on 30 April 1976 at Tixie Bay, Yakutsk, Norilsk, Magadan, Novosibirsk, Irkutsk and Khabarovsk.

The cosmic ray increase, according to observations at Tixie Bay, started on 30 April 1976 at 2130 UT and in 10 min reached a maximum of 7.4 ± 0.6% above the background counting rate. Using the methods suggested by Krymsky [1966] and Burlaga [1967], we found that the particle generation on the Sun began at 2110 UT, that the flare longitude was W45, and that the diffusion coefficient was 2.8×10^{22} cm^2/s.

Calculations confirm the observations of chromospheric flares. Thus, according to Chistyakov [1976], a chromospheric flare with coordinates S08 W40 was observed on the Sun on 30 April during 2108-2125 UT. The energy spectrum of the cosmic ray increase at 2200-2300 UT had the form

$$A(P) \sim P^{-\gamma},$$

where $\gamma = 2.64$ for rigidities $P > 1.3$ GV. Comparing data of the Siberian stations with that of the Apatity supermonitor (ϕ=N67, λ=E33), we showed that the cosmic ray increase had shock zones, and that therefore the beginning of the increase was anisotropic. The anisotropy burst at the beginning of the flare reached ~ 60%. These results affirm that the flare on 30 April 1976 was a solar cosmic ray source.

REFERENCES

BURLAGA, L. F. 1967 Amisotropic Diffusion of Solar Cosmic Rays, *J. Geophys. Res., 72,* 4449-4466.

CHISTYAKOV, V. F. 1976 Private communication.

KRYMSKY, G. F. 1966 Issledovaniya po Geomagnetizmy i Aeronomii, *izd-vo AN SSSR, M.,* 143.

Neutron Monitor Data of Jungfraujoch for the Period 20 March - 10 April 1976

by

E. Born, H. Debrunner and E. Flückiger
Physikalisches Institut, University of Berne
3012 Berne, Switzerland

The recordings of the IGY neutron monitor Jungfraujoch (geographic coordinates: N46.5 E8.0; altitude: 3550 m; effective vertical cutoff rigidity: 4.48 GV [Shea, 1972]) have been analyzed for the period 20 March - 5 May 1976. Unusual fluctuations of the cosmic ray intensity occurred between 25 March and 6 April 1976, as seen in Figure 1. The pressure-corrected hourly data for this particular period are listed in Table 1.

Table 1.

Pressure-Corrected Hourly Data of the Neutron Monitor Jungfraujoch for the Period 20 March - 10 April 1976. (Standard Pressure = 482 mm Hg; Scaling Factor = 100)

Y	M	D	UT= 1	2	3	4	5	6	7	8	9	10	11	12
1976	3	20	6008.9	6017.1	5993.6	6011.0	6020.1	6028.8	6038.0	6050.4	6098.8	6106.0	6077.2	6089.2
1976	3	21	6046.0	6026.3	6046.0	6049.9	6051.5	6072.8	6053.5	6075.6	6091.6	6114.7	6095.7	6073.3
1976	3	22	6079.6	6055.3	6034.9	6063.8	6054.3	6086.8	6113.5	6090.9	6086.9	6091.8	6084.9	6109.5
1976	3	23	6079.3	6076.4	6100.8	6096.9	6085.2	6098.8	6081.3	6089.1	6084.2	6099.8	6113.4	6093.1
1976	3	24	6075.2	6068.4	6077.2	6061.6	6066.5	6088.9	6073.0	6070.8	6038.7	6063.0	6058.5	6050.2
1976	3	25	6042.7	6044.3	6022.8	6013.3	6012.0	6019.4	6036.7	6038.7	6043.3	6028.0	6033.9	6022.2
1976	3	26	5962.7	5995.0	6015.2	6051.4	6112.1	6147.6	6147.7	6232.5	6260.2	6254.9	6248.9	6245.8
1976	3	27	6009.3	5959.3	5941.8	5983.1	5994.6	6005.3	6004.6	6010.5	5991.5	5972.6	6006.8	5989.8
1976	3	28	5980.1	5973.2	6000.7	5997.2	5991.5	5984.7	5962.7	5982.3	5990.3	5997.2	5997.2	6016.8
1976	3	29	5991.6	5991.6	5950.2-	5983.5	5969.8	5927.5-	5942.3	5946.9	5954.9	5944.6	5951.4	5976.5
1976	3	30	5838.1	5819.1	5826.6	5797.8	5795.5	5792.1	5789.9	5781.1	5769.0	5770.2	5809.8	5865.9
1976	3	31	5803.6	5782.8	5775.1	5791.5	5788.2	5796.1	5769.9	5793.1	5769.1	5792.3	5805.5	5802.2
1976	4	1	5801.4	5815.8	5819.1	5801.3	5877.7	5862.3	5844.8	5807.0	5845.0	5983.4	5970.0	5981.3
1976	4	2	5832.0	5849.5	5863.3	5856.3	5851.6	5884.4	5861.5	5849.5	5890.1	5887.7	5894.7	5878.2
1976	4	3	5902.0	5922.0	5934.4	5940.3	5919.5	5965.7	5944.6	5914.7	5948.8	5958.0	5949.4	5935.3
1976	4	4	5949.2	5932.1	5923.9	5938.3	5953.2	5951.1	5961.1	5953.6	5902.6	6030.5	6018.1	6007.7
1976	4	5	6069.3	6018.9	6011.3	5998.0	6017.4	6021.4	6021.1	6035.9	6041.4	6030.9	0.0	6029.7
1976	4	6	6045.5	6052.9	6062.1	6062.5	6083.9	6081.4	6041.0	6065.7	6079.9	6068.6	6093.6	6085.2
1976	4	7	6057.0	6060.1	6039.0	6046.2	6061.7	6058.6	6065.3	6075.1	6073.4	6091.1	6087.7	6078.5
1976	4	8	6054.1	6056.0	6048.6	6081.2	6067.6	6048.9	6053.9	6041.9	6056.9	6048.1	6049.9	6057.5
1976	4	9	6051.0	6075.8	6079.9	6087.9	6094.2	6056.1	6078.5	6058.6	6050.8	6068.8	6042.4	6037.0
1976	4	10	6080.9	6085.0	6093.6	6094.6	6080.9	6089.5	6069.2	6075.4	6065.5	6063.6	6092.4	6111.8

Y	M	D	UT=13	14	15	16	17	18	19	20	21	22	23	24
1976	3	20	6093.3	6101.6	6094.7	6063.1	6070.3	6058.0	6051.4	6075.8	6066.5	6077.9	6066.9	6058.3
1976	3	21	6091.8	6112.4	6099.6	6058.9	6062.4-	6039.2	6033.6-	6035.4	6018.8-	6037.1	6058.8	6052.4
1976	3	22	6076.3	6094.9	6071.4	6087.1	6104.7	6090.0	6092.0	6056.7	6053.9	6076.3	6070.4	6074.4
1976	3	23	6112.4	6104.6	6104.7	6097.9	6107.6	6108.6	6135.0	6108.6	6078.2	6087.9	6085.0	6072.2
1976	3	24	6068.6	6065.0	6088.6	6096.8	6120.3	6103.8	6103.4	6079.6	6045.8	6061.1	6045.0	6046.3
1976	3	25	6025.1	6025.5	6019.3	6026.6	6003.0	6012.7	5985.7	5974.3	5956.4	5916.6	5922.6	5920.7
1976	3	26	6197.9	6314.1	6397.8	6384.9	6370.2	6307.7	6278.3	6223.4	6137.2	6050.9	6011.0	6016.3
1976	3	27	6025.1	6027.5	6002.6	5970.8	5994.7	6020.0	5981.2	5989.2	5973.2	5961.7	6006.4	5972.0
1976	3	28	6021.5	6000.6	6031.9	6019.2	6009.9	6028.4	6024.9	5995.9	6033.1	6000.7	5998.4	6005.4
1976	3	29	5978.6	5971.6	5986.1	5985.9	5965.4	5988.9	5992.3	5960.7	5949.3	5940.1	5909.8	5867.2
1976	3	30	5893.1	5921.7	5942.6	5928.1	5929.0	5900.7	5847.7	5831.2	5796.2	5848.9	5795.1	5770.9
1976	3	31	5823.2	5790.1	5776.9	5769.2	5781.3	5794.6	5840.1	5818.1	5814.7	5812.5	5809.2	5834.8
1976	4	1	5978.0	6032.5	5935.1	5950.5-	5934.6-	5902.0	5869.9	5858.9	5842.2	5858.8	5831.0	5837.6
1976	4	2	5836.0	5870.0	5876.2	5895.0	5869.4	5816.0	5838.0	5794.2	5928.4	5880.6	5873.9	5892.5
1976	4	3	5935.8	5926.9	5968.9	5999.5	6003.8	5996.3	5966.4	5939.2	5958.1	5983.0	5959.2	5945.2
1976	4	4	6012.7	6021.9	6036.5	6036.5	6018.7	6015.5	6003.4	6003.5	6040.1	6021.8	6021.4	6039.1
1976	4	5	6052.2	6065.7	6075.6	6060.6	6087.2	6094.2	6105.2	6100.0	6083.3	6030.5	6027.2	6048.8
1976	4	6	6100.6	6135.5	6131.3	6146.5	6121.3	6139.0	6133.1	6120.2	6098.9	6095.2	6092.0	6067.6
1976	4	7	6065.8	6074.8	6066.2	6047.4	6049.1	6038.5	6051.8	6036.8	6037.4	6049.5	6054.1	6059.4
1976	4	8	6052.2	6040.4	6050.6	6059.3	6057.3	6066.2	6053.3	6070.0	6045.1	6059.1	6070.8	6057.5
1976	4	9	6106.9	6087.8	6096.4	6099.2	6114.8	6117.3	6129.3	6107.7	6076.5	6085.4	6097.1	6090.5
1976	4	10	6109.9	6068.0-	6081.9	6070.9	6056.3	6100.1	6076.5	6087.1	6084.0	6079.4	6070.8	6080.2

/ BEHIND VALUE = ONLY A PART OF MONITOR OPERATING

- BEHIND VALUE = MONITOR OPERATING ONLY A PART OF THE INTERVAL

Uncorrected and corrected 6-min data are available on special request for the whole Retrospective World Interval, 20 March - 5 May 1976.

This work has been supported by the Swiss National Science Foundation, Grant 2.269.74.

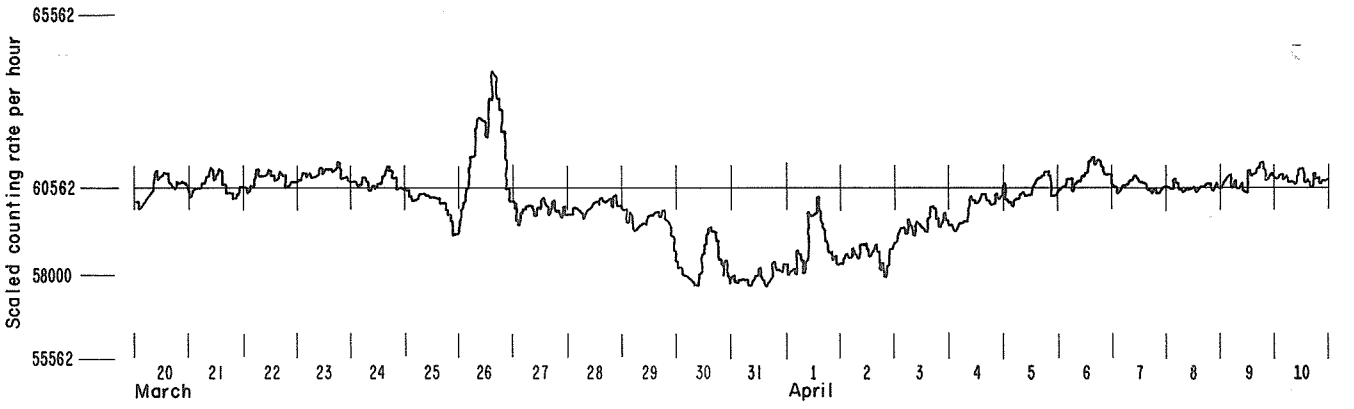

Fig. 1. Pressure-corrected hourly data of the neutron monitor Jungfraujoch for the period 20 March - 10 April 1976. Standard Pressure = 482 mm Hg; Scaling Factor = 10.

REFERENCE

SHEA, M. A. 1972 Ground-Based Cosmic-Ray Instrumentation Catalog, *Air Force Cambridge Research Laboratories, AFCRL-72-0411.*

Cosmic Ray Variations During the Retrospective World Interval 20 March - 5 May 1976 at Morioka, Japan

by

Hachiro Takahashi and Toshimi Chiba
Department of Physics
Iwate University
Morioka, Japan

In this communication continuous observation of cosmic ray neutron intensity during the Retrospective World Interval 20 March - 5 May 1976 at Morioka is reported together with a brief explanation and interpretation of the data.

The Monitor

The Simpson's type neutron monitor consisting of six BF_3 counters is used. The continuous observation of the neutron intensity by the monitor has been carried out since August 1970 at Morioka [Takahashi *et al.*, 1971; Chiba *et al.*, 1975; Chiba, 1976]. Its location is given in Table 1, together with the counting rate and the barometric coefficient.

Table 1

Station	Geographic Longitude	Geographic Latitude	Altitude	Cut-off Rigidity	Counting Rate	Barometric Coefficient
Morioka	141° 08'E	39° 42'N	135.0 m	10.13 GV	8620/h	-0.689%/h

Results and Interpretation

Figure 1 shows the time variations of the hourly values of the neutron intensities observed during the period 7 March - 26 May 1976 (Rot. Nos. 1950-1952) in which the Retrospective World Interval is included. The digital data for this period and an explanation of these observations are given in Table 2.

Although the plotted values in Figure 1 fluctuate considerably because of the low counting rate (see Table 1), the following features are found:

(1) The intensity increases which are regarded as the storm-time increase of cosmic rays are on 26 March, associated with the SSC storm (Ap=138) occurring at 0233 UT on 26 March; on 1 April, associated with the SSC storm (Ap=107) occurring at 0255 UT on 1 April; and on 2-3 May, associated with the geomagnetic storm (Ap=58 on 2 May and 94 on 3 May) on 2-3 May.

(2) The intensity decrease during the period from 26 March to ~ 5 April is composed of three consecutive Forbush decreases. The first one began on 26 March and was associated with the SSC storm of Ap=138; the second one began on 29 March and was associated with the solar flare (Type IV radio burst) on 28 March; and the third one began on 1 April and was associated with the solar flare (Type IV radio burst) on 31 March.

(3) The intensity decrease starting from ~11 April may have a relationship with the solar wind velocity enhancements observed by Pioneer 10 on 9 April 1976.

These features agree with those appearing in the time variations of the neutron intensities observed at Tokyo-Itabashi [private communication from Dr. Wada].

The data of geomagnetic storms, solar flares (Type IV radio bursts), and solar wind velocity enhancements used in this paper were taken from the "Preliminary List of Significant Solar-Terrestrial Phenomena (20 March - 2 May 1976)" compiled by the MONSEE Steering Committee Secretary M. A. Shea.

Table 2. Hourly neutron data for the period 7 March - 26 May 1976 at Morioka, Japan (N39.70 E141.13; 135.0 m; 6-IGY neutron monitor with 10.16 GV vertical cutoff rigidity). Tabulated values are 1000&n (counts/8/1000) in units of 0.1% corrected for the barometric effect to the standard pressure of 998.1 mbar. The barometric coefficient = -0.689%/mbar; the counting rate = 8620/hour; and 999 stands for "no observation."

Y	M	D	360	1	2	3	4	5	6	7	8	9	10	11	12	13	14	15	16	17	18	19	20	21	22	23	24	SUM	N	MEAN	D
76	3	7	67	87	115	104	97	113	107	122	125	110	97	89	109	88	77	95	85	102	74	101	110	99	95	97	97	2389	24	99.5	7
76	3	8	68	85	87	80	109	106	106	105	104	109	110	89	101	102	89	97	109	105	90	78	111	77	69	100	96	2314	24	96.4	8
76	3	9	69	113	91	95	92	69	85	98	92	86	86	79	88	94	94	82	114	97	87	95	126	114	85	104	89	2248	24	93.7	9
76	3	10	70	85	135	90	125	94	105	87	99	110	89	89	96	96	81	95	106	110	76	94	96	99	95	79	107	2332	24	97.2	10
76	3	11	71	94	92	96	99	106	90	127	111	94	90	66	101	102	84	70	76	98	96	96	115	105	95	84	85	2270	24	94.6	11
76	3	12	72	58	109	99	95	81	110	63	99	86	115	102	97	85	95	100	90	107	91	75	74	107	115	115	110	2276	24	94.8	12
76	3	13	73	95	105	105	98	81	108	111	107	106	107	118	71	89	94	118	86	91	97	87	115	75	85	97	98	2340	24	97.5	13
76	3	14	74	123	86	90	120	119	111	86	116	74	112	105	88	72	99	99	91	72	104	88	88	79	96	87	98	2296	24	95.7	14
76	3	15	75	104	105	120	61	119	85	114	97	81	95	84	106	64	88	95	111	96	105	101	102	74	84	108	106	2303	24	96.0	15
76	3	16	76	101	118	115	106	95	116	107	118	118	80	92	65	85	72	94	90	86	72	50	98	77	100	71	85	2207	24	92.0	16
76	3	17	77	84	101	89	72	102	86	81	90	89	88	106	107	75	65	116	85	114	83	72	79	93	59	70	85	2089	24	87.0	17
76	3	18	78	116	85	95	117	95	101	67	92	100	64	58	82	75	85	69	77	80	72	95	97	95	88	95	90	2084	24	86.8	18
76	3	19	79	95	99	120	101	80	84	71	78	80	97	88	98	71	81	84	87	110	100	91	91	85	88	71	85	2153	24	88.9	19
76	3	20	80	109	95	74	120	111	75	80	77	89	82	81	109	72	92	92	100	85	126	75	96	94	97	117	67	2211	24	92.1	20
76	3	21	81	78	79	99	78	86	85	82	90	69	75	72	112	60	98	77	86	69	85	96	92	108	89	71	103	2037	24	84.9	21
76	3	22	82	69	84	96	81	80	92	90	92	86	59	69	108	78	86	78	96	106	99	95	69	70	86	97	88	2010	24	83.8	22
76	3	23	83	90	100	107	121	112	109	96	77	85	105	91	75	86	91	93	85	71	93	105	100	69	81	88	56	2164	24	90.2	23
76	3	24	84	88	76	81	107	72	105	114	97	82	99	119	93	122	67	109	85	78	128	105	76	86	69	58	115	2225	24	92.7	24
76	3	25	85	86	125	87	84	105	102	82	104	127	116	87	76	91	117	79	88	79	101	95	105	76	109	110	95	2326	24	96.9	25
76	3	26	86	102	98	74	114	119	126	118	115	121	124	126	125	98	102	95	101	92	105	78	95	81	98	87	65	2453	24	102.2	26
76	3	27	87	88	99	112	85	109	104	92	98	84	93	70	64	78	75	93	85	86	96	93	92	84	89	115	79	2161	24	90.0	27
76	3	28	88	99	101	78	86	73	93	111	85	91	84	96	86	71	73	76	79	99	71	90	86	87	87	87	77	2064	24	86.0	28
76	3	29	89	82	74	82	85	79	78	86	73	70	61	74	78	68	77	95	98	67	55	66	61	77	69	49	64	1765	24	73.5	29
76	3	30	90	65	88	61	102	89	74	70	59	67	61	77	76	64	74	60	80	61	54	70	72	66	41	52	62	1645	24	68.5	30
76	3	31	91	68	55	70	67	73	93	89	60	78	70	85	57	50	65	47	61	100	57	46	85	57	61	50	79	1597	24	66.5	31
76	4	1	92	100	95	96	85	92	67	87	67	96	82	67	57	93	94	85	89	92	86	48	67	93	92	60	62	1950	24	81.3	1
76	4	2	93	86	82	58	65	87	61	42	69	70	80	54	79	99	91	61	69	116	79	80	86	97	57	62	69	1799	24	75.0	2
76	4	3	94	62	58	64	74	82	85	94	84	71	64	71	79	76	85	93	77	65	60	66	95	105	116	98	92	1912	24	79.7	3
76	4	4	95	90	54	91	108	86	106	80	78	65	99	111	82	80	102	92	90	77	92	80	92	90	68	62	74	2069	24	86.2	4
76	4	5	96	62	101	81	102	91	97	125	105	57	88	56	94	119	78	105	98	98	87	65	106	92	79	93	102	2177	24	90.7	5
76	4	6	97	70	80	81	86	94	81	114	115	82	96	92	101	74	89	100	101	125	94	68	93	89	74	101	83	2179	24	90.8	6
76	4	7	98	123	115	88	100	84	94	79	94	95	100	110	75	80	64	75	98	79	99	74	108	117	90	107	94	2248	24	93.7	7
76	4	8	99	86	111	90	106	98	122	91	75	92	85	84	84	95	93	94	94	92	78	110	90	107	98	98	101	2270	24	94.6	8
76	4	9	100	92	71	88	98	102	106	95	110	84	93	96	85	84	78	96	97	85	102	91	89	83	92	101	79	2197	24	91.5	9
76	4	10	101	101	76	80	115	92	111	85	106	107	72	70	115	100	100	94	101	89	93	105	110	86	97	92	108	2305	24	96.0	10
76	4	11	102	98	999	999	999	999	999	999	999	999	999	70	120	127	105	101	86	75	110	69	101	90	81	80	125	1436	15	95.7	11
76	4	12	103	125	99	79	101	95	100	86	88	87	83	85	86	93	85	89	98	76	90	92	105	86	68	93	96	2185	24	91.0	12
76	4	13	104	87	74	79	90	70	61	74	69	100	99	99	98	76	87	80	78	80	86	95	70	90	107	81	52	1982	24	82.6	13
76	4	14	105	85	58	72	75	109	91	77	71	77	49	70	74	61	67	49	56	80	60	64	72	67	102	80	95	1761	24	73.4	14
76	4	15	106	100	90	96	101	94	110	70	71	49	85	76	68	71	95	87	86	93	84	60	89	68	86	80	71	1968	24	82.0	15
76	4	16	107	87	95	87	68	62	81	87	82	64	71	66	82	79	68	74	77	65	82	90	85	75	61	96	87	1869	24	77.9	16
76	4	17	108	76	64	99	98	90	74	69	85	77	75	86	59	82	74	93	59	72	75	78	85	76	86	95	82	1905	24	79.4	17
76	4	18	109	106	97	75	109	86	79	80	76	99	58	85	67	82	71	93	82	94	76	82	84	77	91	90	102	2039	24	85.0	18
76	4	19	110	77	91	93	75	81	80	80	99	105	82	86	79	78	85	92	104	97	96	84	82	89	105	90	76	2104	24	87.7	19
76	4	20	111	85	75	64	79	89	59	66	75	76	75	66	55	82	87	75	92	96	65	44	95	81	101	86	65	1825	24	76.0	20
76	4	21	112	91	90	84	74	93	103	65	74	101	77	85	102	82	74	77	87	86	64	92	89	97	90	79	88	2044	24	85.2	21
76	4	22	113	88	84	80	92	54	87	49	105	89	87	93	91	114	92	85	62	105	90	80	89	87	50	94	98	2041	24	85.0	22
76	4	23	114	80	83	62	87	81	81	95	82	83	104	77	107	70	93	55	59	91	70	85	84	82	80	75	55	1919	24	80.0	23
76	4	24	115	65	54	89	78	66	61	54	89	64	97	74	95	65	90	63	65	90	88	67	69	87	62	56	78	1766	24	73.6	24
76	4	25	116	87	93	68	78	84	97	72	69	91	100	76	78	76	75	70	50	64	87	106	68	81	92	104	64	1930	24	80.4	25
76	4	26	117	60	85	98	92	109	105	78	81	45	91	57	68	96	100	100	71	93	66	66	64	68	74	85	85	1935	24	80.6	26
76	4	27	118	74	89	89	81	97	85	64	55	93	89	92	84	85	81	56	60	78	70	57	71	55	76	68	85	1832	24	76.3	27
76	4	28	119	78	89	84	100	81	91	62	90	80	82	91	67	81	69	58	98	65	84	51	88	88	64	69	82	1892	24	78.8	28
76	4	29	120	94	79	67	79	74	77	76	99	84	55	56	74	72	60	93	81	84	72	68	86	70	85	70	84	1855	24	76.5	29
76	4	30	121	79	98	108	80	101	72	66	75	67	63	76	58	69	68	84	85	81	64	76	89	72	111	106	82	1928	24	80.3	30
76	5	1	122	68	101	91	84	82	80	61	68	79	72	96	60	85	67	68	67	60	76	85	64	75	84	71	61	1797	24	74.9	1
76	5	2	123	105	107	88	85	54	96	68	96	91	69	64	90	76	74	71	58	88	87	95	79	94	86	99	78	1996	24	83.2	2
76	5	3	124	88	106	84	95	66	91	109	61	82	68	90	69	117	75	94	86	91	98	74	106	69	71	74	101	2063	24	86.0	3
76	5	4	125	61	105	51	66	79	95	65	97	75	75	87	78	88	71	79	89	84	62	64	66	87	93	77	85	1873	24	78.0	4
76	5	5	126	92	88	85	88	60	96	104	89	78	57	86	79	85	81	89	107	103	89	74	97	88	86	81	93	2073	24	86.4	5
76	5	6	127	71	97	86	85	84	106	77	81	95	101	98	87	87	90	92	59	89	111	73	95	51	74	93	99	2081	24	86.7	6
76	5	7	128	86	105	98	98	70	90	90	89	68	81	81	78	81	102	78	90	76	94	81	84	79	81	109	91	2089	24	87.0	7
76	5	8	129	94	101	106	114	115	74	80	101	82	72	110	97	95	82	80	85	67	75	86	102	103	80	91	80	2164	24	90.2	8
76	5	9	130	91	99	88	76	94	87	81	84	99	116	97	96	87	101	77	61	95	89	106	85	69	69	92	89	2127	24	88.6	9
76	5	10	131	72	86	68	85	85	77	93	101	96	82	115	85	75	86	85	65	95	106	105	97	100	99	77	99	2126	24	88.6	10
76	5	11	132	71	85	98	115	100	111	88	112	70	77	47	97	64	98	93	80	79	76	70	75	93	85	91	75	2331	24	97.1	11
76	5	13	134	102	76	97	67	72	78	79	56	81	91	89	72	81	85	66	95	88	85	105	98	89	72	92	96	2046	24	85.3	12
76	5	14	135	74	62	55	110	93	87	64	99	76	79	78	67	89	65	97	100	65	76	95	89	87	100	86	72	2010	24	83.8	13
76	5	15	136	113	93	95	60	101	81	81	120	101	54	78	85	69	84	96	53	74	79	104	87	65	65	80	91	1959	24	81.6	14
76	5	16	137	90	97	90	85	102	89	75	80	76	75	59	77	80	68	65	92	79	91	81	87	87	75	77	66	2005	24	83.5	15
76	5	17	138	79	92	106	100	104	75	108	80	79	92	69	88	102	74	78	97	76	95	65	50	86	63	79	95	1897	24	79.0	16
76	5	18	139	98	81	60	109	90	115	83	81	95	80	80	84	64	81	90	91	96	75	92	76	87	97	76	88	2010	24	83.8	17
76	5	19	140	90	75	92	90	87	91	87	59	62	87	79	93	73	87	88	90	70	75	70	104	77	72	71	77	2065	24	86.0	18
76	5	20	141	87	73	104	84	96	122	104	110	77	99	101	96	105	99	82	71	66	77	80	72	76	57	104	76	1944	24	81.0	19
76	5	21	142	55	75	74	102	55	90	55	90	71	70	64	65	67	75	73	85	86	69	77	65	94	59	61	76	2118	24	88.3	20
76	5	22	143	88	92	84	95	95	77	110	97	85	80	91	82	98	97	82	90	96	106	105	77	82	100	104	85	2193	24	91.4	22
76	5	23	144	88	84	81	71	90	84	64	76	81	96	88	88	89	80	79	63	61	95	76	91	56	85	71	85	1922	24	80.1	23
76	5	24	145	78	70	72	85	88	89	79	85	82	85	55	69	70	72	75	73	100	69	77	77	85	74	95	85	1885	24	78.5	24
76	5	25	146	87	57	99	90	97	56	68	80	80	69	71	60	73	67	88	76	94	106	76	56	91	91	71	81	1862	24	77.6	25
76	5	26	147	62	55	96	103	79	80	81	55	59	76	98	91	88	74	62	67	69	81	70	77	70	70	71	85	1775	24	74.0	26

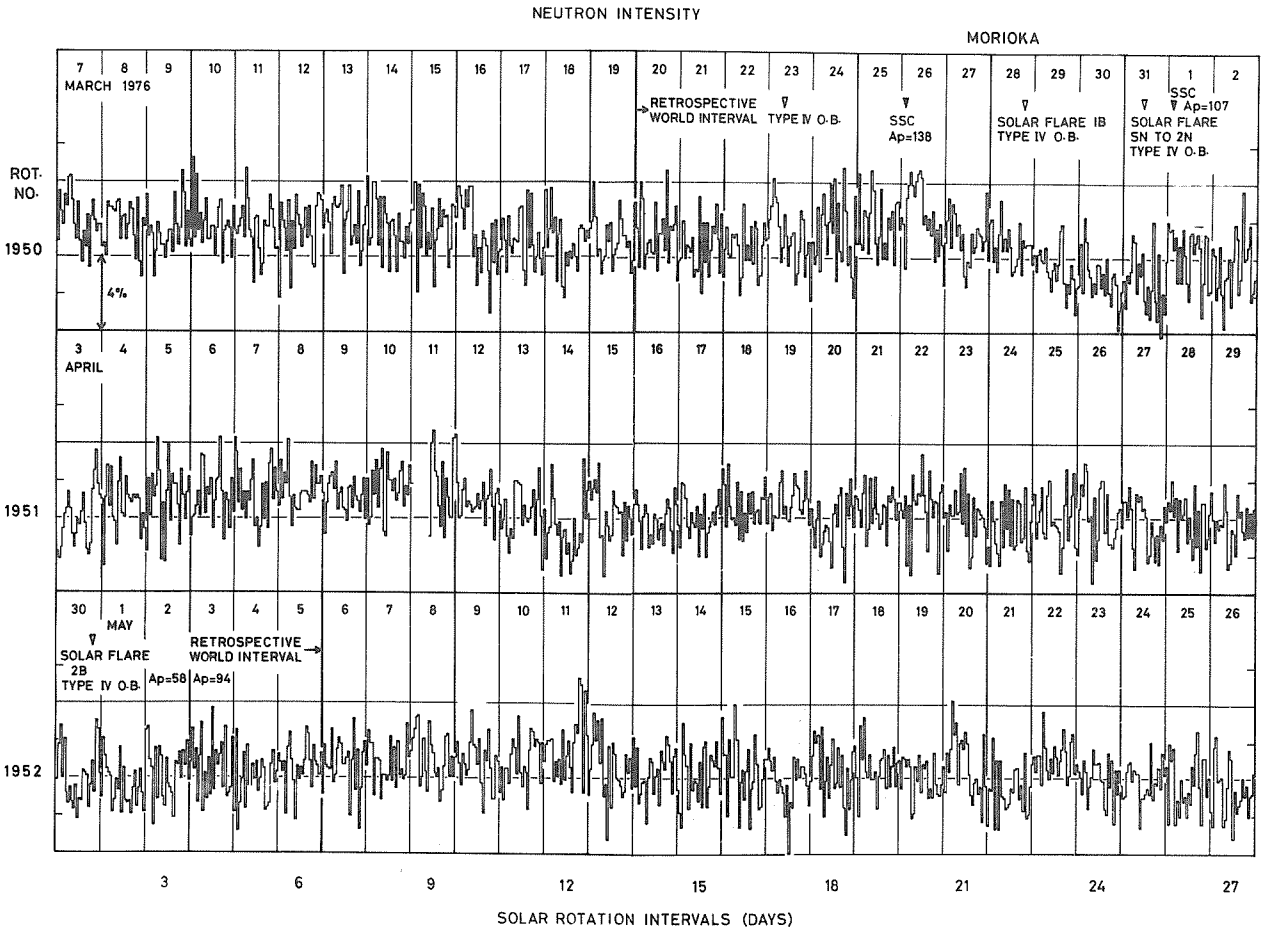

Fig. 1. Time variations of the hourly neutron intensities in percent as a function of solar rotation intervals in days observed during the period 7 March-26 May 1976 at Morioka, Japan.

REFERENCES

CHIBA, T. 1976 Time Variation of the Barometric Coefficient of Cosmic Ray Neutron Component at Morioka, Tokyo and Mt. Norikura during the period 1970-1973, *Annu. Rep. Fac. Educ. Univ. Iwate, 36,* 23-30.

CHIBA, T., TAKAHASHI, H., and KODAMA, M. 1975 Observation of Cosmic Ray Neutron Intensity at Morioka, Part III, Cosmic Ray Neutron Intensities Observed during August 1970 - January 1975, *Annu. Rep. Fac. Educ. Univ. Iwate, 35,* 25-45.

TAKAHASHI, H., CHIBA, T., and YAHAGI, N. 1971 Observation of Cosmic Ray Neutron Intensity at Morioka, Part I. The Neutron Monitor, *Annu. Rep. Fac. Educ. Univ. Iwate, 31,* 15-24.

WADA, M. 1977 Cosmic Ray Laboratory, Institute of Physical and Chemical Research, Kaga-1, Itabashi, Tokyo, Japan.

The Storm-Time Increases of Cosmic Rays

by

Masami Wada
The Institute of Physical and Chemical Research
7-13, Kaga-1, Itabashi, Tokyo, 173, Japan

The cosmic ray neutron counting rates observed at a middle latitude station are corrected for the storm-time increase effect and compared with those at a high latitude station. The storm-time increase in cosmic ray intensity found by Yoshida and Wada [1959] during the IGY period was interpreted by Kondo *et al.* [1960] as a geomagnetic effect on the cutoff rigidity. It is an effect clearly seen at middle latitude stations during a period of large Dst field depression.

In the period of STIP Interval II, 20 March - 5 May 1976, there were two magnetic storms in which the Dst field changed by more than 200 gammas [*SGD*, 1976]. Neutron monitor counting rates at Tokyo were corrected by applying a coefficient equal to 0.8%/100 gammas [Kondo *et al.*, 1960] for Dst variation. In Figure 1 both corrected and uncorrected data are plotted for Tokyo; for Kiel, the data need not be corrected for the Dst variation. When compared with the Dst field, the corrected Tokyo time profile improves on 26 March and 1 April. Among cosmic ray stations given in [*SGD*, 1976], both Climax (2.2%/100 gammas) and Tokyo are affected by the storm-time increase. At midday on 26 April, each of the stations displayed a clear increase -- one that cannot be attributed to some local time effect or to any variation outside the geomagnetic field. As with the Tokyo data in Figure 1, these increases can be removed completely by correcting for storm-time increases.

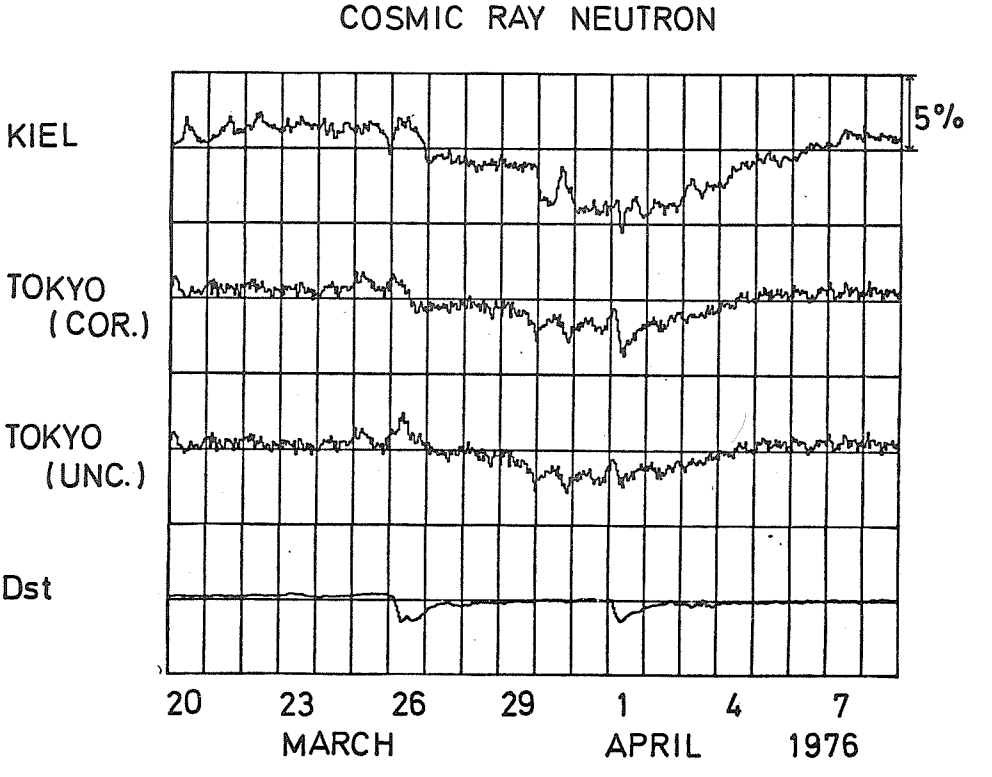

Fig. 1. Cosmic ray neutron intensities and magnetic Dst values for the period 20 March - 8 April 1976. COR. and UCOR. denote corrected for and uncorrected for Dst variation. The Dst scale has been converted to correction values; for this curve the horizontal line lies slightly below Dst=0.

Since there are enhanced diurnal variations in the period under study, the effectiveness of the correction may not be easily recognized unless a three-dimensional analysis of the Forbush decrease is performed with the middle latitude cosmic ray data. In this report, however, we point out only that storm-time increases should be taken into account in the study of Forbush decreases whenever the Dst field changes greatly.

We are indebted to Dr. O. Binder for supplying his Kiel neutron monitor data in digital form.

REFERENCES

KONDO, I., K. NAGASHIMA, S. YOSHIDA, and M. WADA 1960 On Worldwide Cosmic-Ray Intensity Increases Associated with Cosmic-Ray Storms, *Proc. Cosmic Ray Conf., Moscow 1959, 4,* 208-215.

SGD 1976 *Solar-Geophysical Data, 381 Part I,* 123, May 1976; *382 Part I,* 102-105, 110, June 1976, U.S. Department of Commerce, (Boulder, Colorado, U.S.A. 80302).

YOSHIDA, S. and M. WADA 1959 Storm-Time Increase of Cosmic-Ray Intensity, *Nature, 183,* 381-383.

Ring Current Effects on Cosmic Rays on 26 March and 1 April 1976

by

P. R. Hurly
Magnetic Observatory, Hermanus, South Africa

and

P. H. Stoker and P. J. König
Potchefstroom University for C.H.E., Potchefstroom, South Africa

The first two of the three geomagnetic storms which occurred during the 20 March - 5 May 1976 interval were characterized by large ring currents. Neutron monitors at mid-latitude stations registered increases associated with these ring currents.

Figure 1 shows the count rates for various neutron monitors for 23 March - 6 April. The count rates have been normalized to 100% on 23 March. Provisional equatorial Dst is also shown. Details of the neutron monitor stations are given in Table 1.

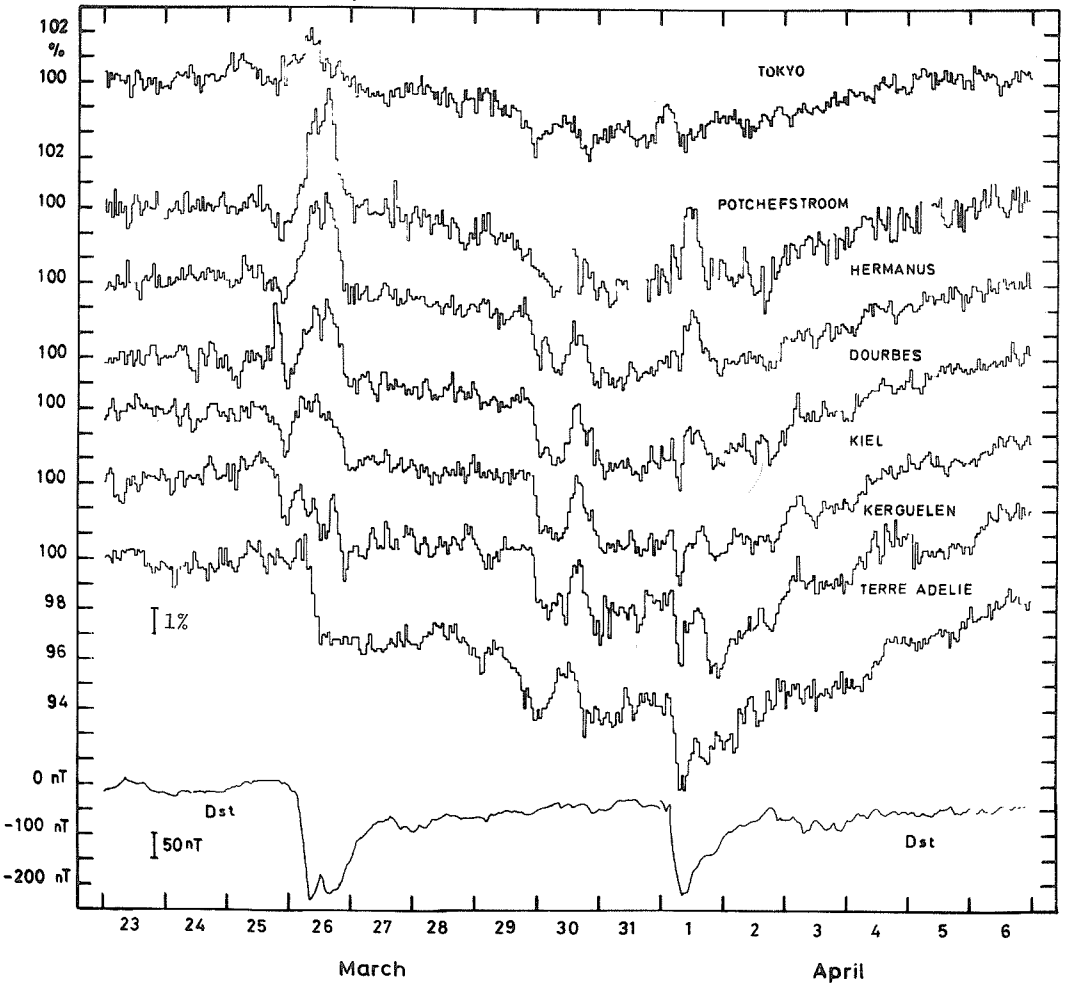

Fig. 1. Count rates for selected neutron monitors and provisional equatorial Dst for 23 March - 6 April 1976. Count rates are normalized to 100% on 23 March.

Table 1

Neutron Monitor Stations

Station	Lat.	Long.	Cutoff (GV)	Altitude (m)
Tokyo (Itabashi)	36°N	140°E	11.61	20
Potchefstroom	27°S	27°E	7.30	1351
Hermanus	35°S	19°E	4.90	26
Dourbes	50°N	5°E	3.24	225
Kiel	54°N	10°E	2.29	54
Kerguelen	49°S	70°E	1.19	0
Terre Adelie	67°S	140°E	0.01	45

The intensity increases of 26 March and 1 April are clearly associated with the ring currents occurring on those days, whereas the intensity peak of 30 March is not associated with a ring current. None of the stations used in Figure 1 is at mountain altitude. However, the Pic du Midi (2860 m, 5.36 GV) and Jungfraujoch (3550 m, 4.48 GV) data (not illustrated here) follow closely the pattern of the Hermanus data. During the geomagnetic storm of 2-3 May there was no clearly defined ring current growth and decay and no definite increases in the neutron monitor counting rates [see *Solar-Geophysical Data*, 1976].

Increases such as those of 26 March and 1 April have been ascribed to the lowering of the cosmic ray cutoff rigidity of the neutron monitor stations by the magnetic field of the ring current. The effect has been described by Kondo *et al.*, [1960] and by Yoshida *et al.*, [1968]. Kondo *et al.* found that the magnitude of the increase is strongly dependent on cutoff rigidity, the increase being negligible for stations with cutoff less than about 1 GV. Usually the increase is small compared with the Forbush decrease during which it occurs. This is the case for the 1 April increase. Increases such as the 26 March one, where the count rate increases to well above the pre-storm value, are rare with a frequency of perhaps one per year.

Figures 2 and 3 show the correspondence between the Hermanus neutron monitor count rate increases and the magnetic field decreases for 25-27 March and 31 March-2 April. The neutron monitor count rate has been roughly compensated for the effect of the Forbush decrease by subtracting the Hermanus and Terre Adelie graphs of Figure 1 and plotting the difference together with (minus) the provisional equatorial Dst and (minus) the H component of the magnetic field at Hermanus (Sq variation not removed). It should be noted that the Terre Adelie station is 120° east of Hermanus and that the magnitudes of normal Forbush decreases at polar stations and mid-latitude stations are not necessarily similar even for stations at the same longitude.

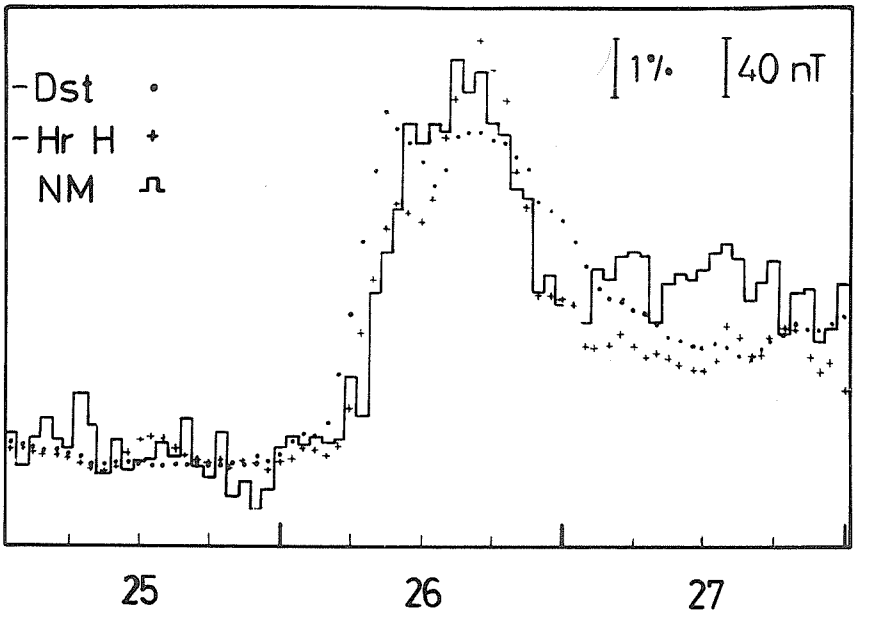

Fig. 2. Neutron monitor count rate difference (Hermanus minus Terre Adelie), provisional equatorial Dst (ordinate scale inverted), and Hermanus H component (ordinate scale inverted) for 25-27 March 1976.

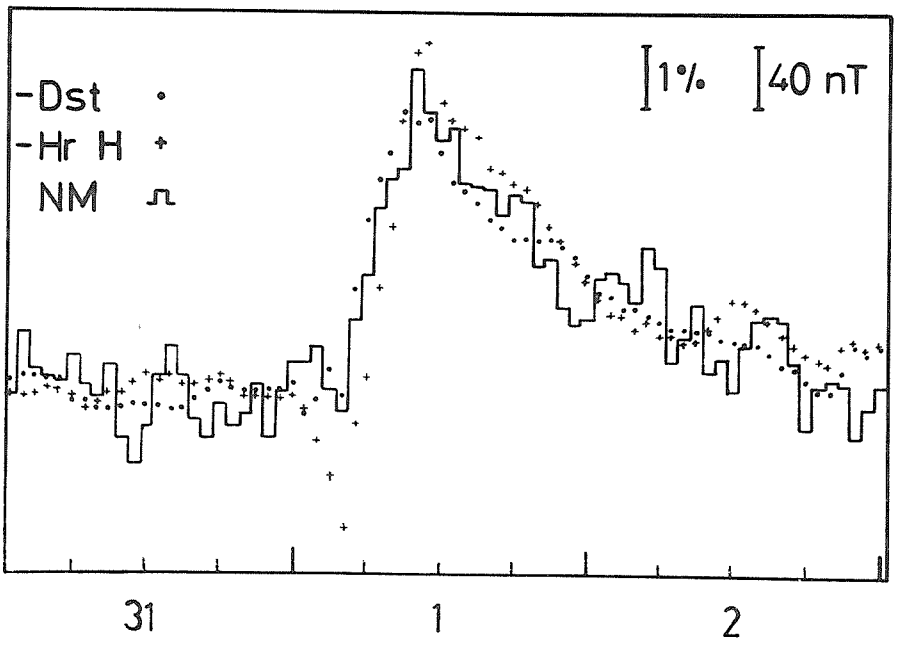

Fig. 3. Neutron monitor count rate difference (Hermanus minus Terre Adelie), provisional equatorial Dst (ordinate scale inverted), and Hermanus H component (ordinate scale inverted) for 31 March - 2 April 1976.

The resulting increases at Hermanus, after correction for the Forbush decrease as recorded at Terre Adelie, are 6% and 4.5% respectively for the 26 March and 1 April events (see Figures 2 and 3). According to the results obtained by Kondo *et al.*, [1960], the recorded decreases in Dst should give rise to sea level neutron monitor increases at the cutoff rigidity of Hermanus of about 3.5% and 3%, respectively, suggesting an overcompensation for the effect of the Forbush decrease as recorded at Terre Adelie. These increases, as calculated from Dst, could be explained by decreases in cutoff rigidity of 0.8 GV and 0.7 GV, respectively.

Figures 2 and 3 show clearly the connection between the changes in the neutron monitor count rates and those in the magnetic field. We have drawn a similar figure (not shown) for the 2-3 May storm and no connection is evident for this period.

We thank our colleagues at the various neutron monitor stations for the regular exchange of data which facilitates studies of this nature.

REFERENCES

SOLAR-GEOPHYSICAL DATA 1976 — *Solar-Geophysical Data, 383 Part 1,* July 1976; Department of Commerce, Boulder, Colorado U.S.A.

KONDO, I., K. NAGASHIMA, S. YOSHIDA and M. WADA 1960 — On Worldwide Cosmic-Ray Intensity Increases Associated with Cosmic Ray Storms. *Proc. Moscow Conf. Cosmic Rays 4,* 208.

YOSHIDA, S., S.-I. AKASOFU, and P.C. KENDALL 1968 — Ring Current Effects on Cosmic Rays, *J. Geophys. Res. 73,* 3377.

The Effect of Cosmic Ray Geomagnetic Cutoff Rigidity Variation Recorded by Spectrograph at Irkutsk During a Magnetic Storm on 26 March 1976

by

Yu. Ya. Krestyannikov, A. V. Sergeev, V. I. Tergoev, L. A. Shapovalova
Siberian Institute of Terrestrial Magnetism, Ionosphere
and Radio Wave Propagation, Siberian Division,
Academy of Sciences of the USSR, Irkutsk

The cosmic ray intensity variation spectrograph at Irkutsk (R_C = 3.81 GV) consists of three stations located at the heights of 435 m, 2000 m and 3000 m above sea level. All the stations comprise standard neutron supermonitors NM-64 to record the neutron component of cosmic rays with a statistical accuracy of ± 0.1% (for the 2-hour interval of measurements). In addition, at the 433-meter level the vertical μ-meson hard component is recorded by a telescope on Geiger counters with a statistical accuracy of ± 0.14%.

The experimental data for the neutron and μ-meson hard components recorded by spectrograph from 25 to 28 March 1976 are shown in Figure 1a. The diagrams show that on 26 March an increase in cosmic ray intensity is observed whose amplitude $(\Delta I/I)^{exper}$ in the neutron component at 433 m reaches 3.8% and 6% at 3000 m, while the hard μ-meson component reaches 0.3%.

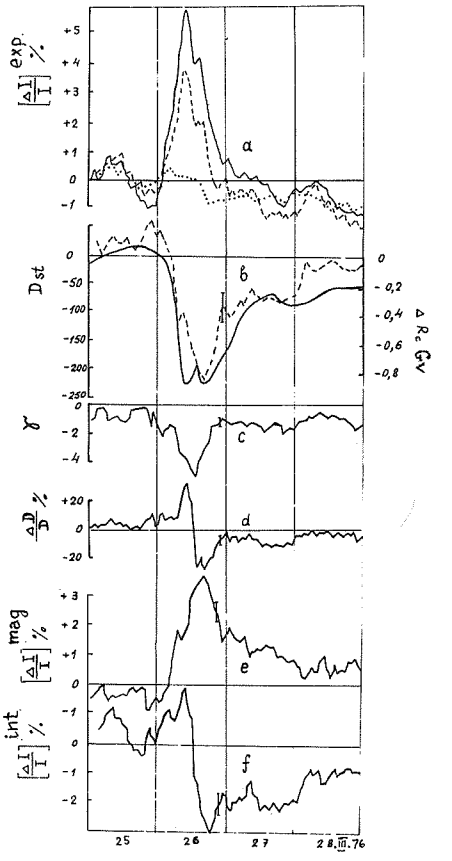

Fig. 1. Results of measuring cosmic ray intensity variations by spectrograph at Irkutsk (R_C = 3.81 GV) in March 1976: (a) data of the neutron (dashed) and μ-meson (dotted) hard components for the 433-meter level and data of the neutron component (solid line) at the 3000-meter level; (b) variation of the geomagnetic rigidity cutoff ΔR_C (dashed) and Dst variation data of the geomagnetic field (solid curve); (c) variation of the spectral index γ where variations in the primary spectrum have the assumed form $\Delta D/D \approx B \cdot R^{-\gamma}$; (d) variation of the primary spectrum for particles with a rigidity R = 4 GV; and (e and f) variation in the 433-meter level neutron component of magnetospheric and interplanetary origin.

Such regularity in solar cosmic rays is usually observed during their arrival at Earth. An analysis of the spectrograph's experimental data (Figure 1), however, reveals that the real cause of the increase in cosmic ray intensity is a variation in geomagnetic cutoff rigidity.

The spectrographic method is based on the construction and solution of a set of simultaneous equations of variations for different observing conditions or for various components of secondary cosmic rays measurable at one geographic point [Sergeev, 1973]. The result of determining the variation of the geomagnetic cutoff rigidity (ΔR_c) is given in Figure 1b. The ΔR_c amplitude is as large as -0.9 GV with the value of the geomagnetic cutoff threshold R_c = 3.81 GV. This Figure also presents the magnetic data of Dst variations that we borrowed from *Solar-Geophysical Data* [1976]. According to these data a magnetic storm with a field depression in the main phase of about 225 gammas was recorded on 26 March 1976. Although good agreement is found by comparing the behavior of ΔR_c and Dst, this feature cannot serve as direct evidence for the reality of the variation in the geomagnetic cutoff rigidity recorded by spectrograph at Irkutsk.

To prove the reality of this effect, experimental data of the neutron component have been considered for several worldwide network stations. The data are expressed as percentages (with respect to the period assumed as quiet) and appear in Figure 2 in the order of increasing R_c: Tixie R_c = 0.53 GV, Norilsk R_c = 0.63 GV, Yakutsk R_c = 1.0 GV, Novosibirsk R_c = 2.91 GV, Irkutsk R_c = 3.81 GV, Khabarovsk R_c = 5.54 GV, and Tokyo R_c = 11.61 GV. Analysis of the diagram has shown that a clear increase in intensity of $(\Delta I/I)^{exper}$ is observed at mid- and low-latitude stations while it is hardly in evidence at polar stations.

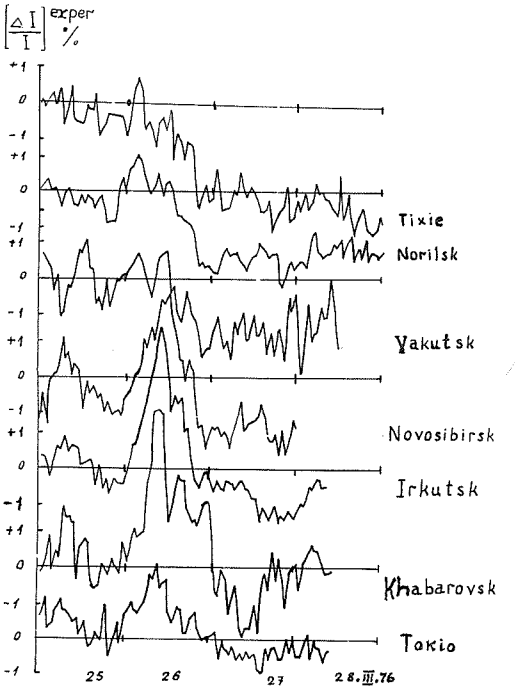

Fig. 2. Neutron component variations at several worldwide network stations for the period 24-28 March 1976.

It is of interest to determine the value of ΔR_c for each station. For this purpose we also have used the variations of the primary spectrum of $(\Delta D/D)$ obtained by spectrograph (Figures 1c and d) as well as the coefficients of coupling between the primary and secondary variation of the neutron component. In Figure 3 the final results of the calculations are plotted. These show the effect of the decrease in geomagnetic rigidity cutoff over the worldwide network of stations, since the value of ΔR_c depends on the geomagnetic cutoff rigidity R_c, i.e., on the geomagnetic latitude of a site. The dependence $\Delta R_c \sim f(R_c)$ is clearly seen in Figure 4 - a result obtained by averaging the data from Figure 3 for the observation interval 0900-2000 UT on 26 March 1976.

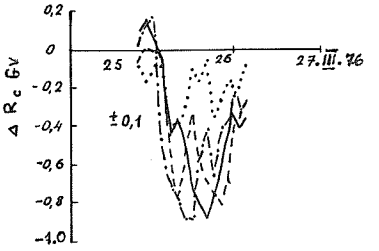

Fig. 3. Variation of rigidity of geomagnetic cutoff ΔR_c at several stations of the worldwide network: Novosibirsk (dash-dot line); Irkutsk (dashed line); Khabarovsk (solid line); and Tokyo (dotted line).

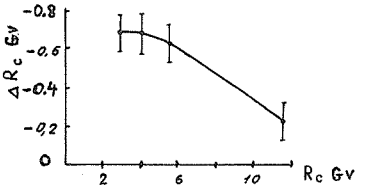

Fig. 4. ΔR_c as function of rigidity of geomagnetic cutoff R_c.

Thus, during the magnetic storm of 26 March 1976, a decrease in geomagnetic cutoff rigidity was ascertained by using two independent sources of data: the experimental spectrographic observations and the cosmic ray station network; ΔR_c was found to be a function of geomagnetic latitude. The presence of a maximum in the profile of $\Delta R_c \sim f(R_c)$ and of curve fragments with negative slope indicate the geomagnetic latitude extent of the westward drift current system in the magnetosphere responsible for the main phase of a magnetic storm.

In conclusion, note the difference in variations of the neutron component in the initial experimental data (see Figure 1a) and the variations of interplanetary origin $(\Delta I/I)^{int}$ (Figure 1f). In the latter case disturbances in the Earth's magnetic field have no effect on cosmic rays.

We thank all our colleagues for kindly sending us their observational data that we have used in this paper.

REFERENCES

SERGEEV, A. V. 1973 Thesis NIIYAF Moscow State University.

SGD 1976 *Solar-Geophysical Data, 381 Part I,* May 1976, U.S. Department of Commerce, (Boulder, Colorado, U.S.A. 80302).

The Corotative Model of Forbush Decreases Applied to the Events Associated With the Long-Lived McMath Region 14143 from 20 March to 8 June 1976

by

N. Iucci
Istituto di Fisica - Università
Piazzale delle Scienze, 5 - 00185 Roma, Italy

and

M. Parisi, M. Storini, G. Villoresi, N. L. Zangrilli, A. Felici
Laboratorio Plasma Spazio - C.N.R.
Istituto di Fisica - Università
Piazzale delle Scienze, 5 - 00185 Roma, Italy

ABSTRACT

The Forbush decreases occurring in the analyzed period are produced by Type IV solar flares, all stemming from the same active region. The interpretation of these events is based on the corotative model of Forbush decreases.

Introduction

The galactic cosmic ray (c.r.) intensity perturbation occurring between 20 March and 8 June 1976 is is interpreted in light of the corotative model of Forbush decreases (Fds) recently developed by our group. This model is derived from high-latitude neutron monitor data between 1957 and 1969. [Iucci *et al.*, 1973; 1975; 1977].

Whenever an energetic Type IV solar flare (emission over micrometric to metric wavelengths) occurs, new matter is emitted from the Sun in the form of a large, corotating magnetic tongue which expands into interplanetary space. This plasma cloud is surrounded by a shock region in which the magnetic field is compressed and in which the c.r. intensity is reduced. Inside the tongue the c.r. flux tends to recover toward the unperturbed level with a time constant $\tau \simeq 11$ days. Although the longitude extent of the modulated region varies from case to case, on the average it is $\sim 130°$ wide. Furthermore, it contains a zone of maximum depression (core) in its interior 70° wide. This core region itself lies shifted toward the magnetic tongue's leading edge.

Thus the corotative model implies that the time behavior of a Fd observed at Earth will depend upon the central meridian distance of the flaring region. For later Forbush decreases produced by Type IV solar flares from the same region, the time behavior of the last c.r. recovery will be tied to the central meridian distance of the last flare. Moreover, Fds produced by flares occurring on the Sun's backside can be observed at Earth after a proper corotation time. Their reduced amplitudes and long recovery times resemble Fds from flares near the east limb.

Analysis

In the period under study all the Type IV flares were produced by the same active region. A list of the events and their associated Fds are given in Table 1 [*SGD*, 1976]. The Fd amplitudes are determined from the daily intensities of the Deep River neutron monitor [*SGD*, 1976]. For events occurring during the recovery phase of earlier Fds, a tentative correction has been made. Hourly intensities for Deep River and Rome are plotted in Figures 1 and 2.

First rotation (20 March - 15 April 1976). The Fd of 26 March was associated with a Type IV flare that occurred 3 days earlier at the east limb. That the extension of the modulated region was very large ($\sim 160°$) can be deduced from the $\sim$72-hour delay between the flare and the onset of the Fd. In the Rome data the geomagnetic storm of 26 March ($\sim 250\ \gamma$) caused a large c.r. increase because of the change in rigidity threshold.

The series of Type IV flares between 25 and 31 March depressed the c.r. intensity inside the same corotating region in succeeding steps. A tentative association between flares and Fds is reported in Table 1. In the Rome data the event of 1 April is not visible because of the occurrence of a geomagnetic storm ($\sim 200\ \gamma$). The recovery after the last Fd agrees with the corotative model [Iucci *et al.*, 1977]. The 5 April flare near the west limb probably occurred within McMath Region 14143. No Fd was observed because corotation carried the modulated region ahead of the Earth.

Second rotation (16 April - 12 May 1976). The Fd of 26 April indicated that the Earth had reentered region 14179's magnetic bottle. At the time the active region lay about 10° east of the central meridian. Assuming a solar wind velocity between $\sim$400 and 500 km/s, the modulated c.r. region was estimated to extend 110° to 130° in longtitude. The recovery was very slow, as expected, having a time

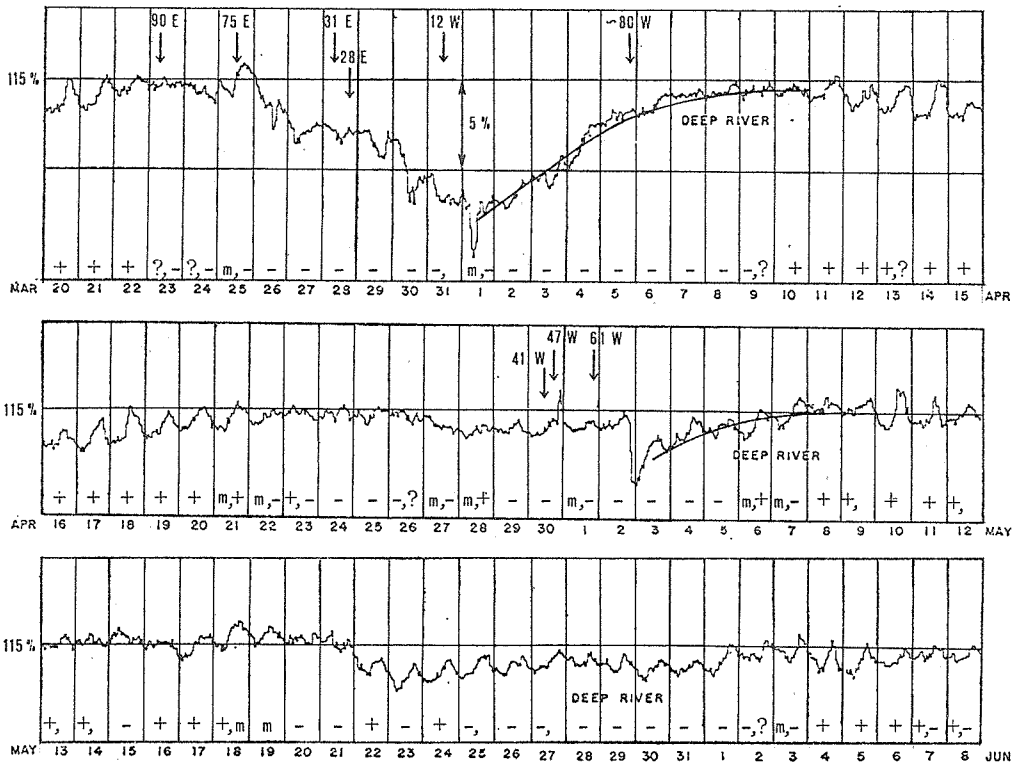

Fig. 1. Deep River neutron monitor intensity for the period 20 March - 8 June 1976. The arrows indicate the occurrence of Type IV solar flares at the reported heliolongitude. The inferred interplanetary magnetic field polarities [*SGD*, 1976] are reported; m indicates mixed polarity.

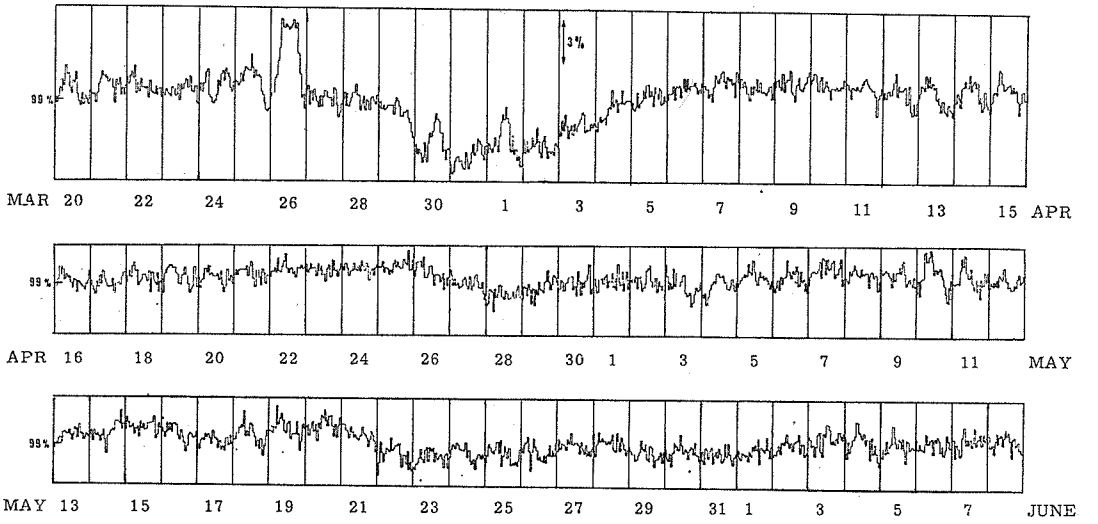

Fig. 2. Rome neutron monitor intensity for the period 20 March - 8 June 1976.

constant $\tau \simeq 10$ days.

The Fd of 2 May was produced by the 30 April and 1 May flares. The observed amplitude was presumably smaller than that existing inside the "core" because the Earth lay near the modulated region's trailing edge. In the Rome data only a small Fd was observed because of the onset of a geomagnetic disturbance ($\sim 100\ \gamma$) at the end of the day. Again, the recovery agreed with the corotative model.

Third rotation (13 May - 8 June 1976). The Fd of 21 May was probably due to the Earth re-entering the same modulated region when the active zone lay about 30° east of the central meridian. The c.r. intensity inside this region was still largely depressed ($\sim$ 2%) - probably by flares that occurred as the active region traversed the Sun's backside. The duration of the Fd and the heliolongitude of the active region at the time of the Fd onset implied a modulated region $\sim$150° in extent.

During McMath Region 14143's rotations, the polarity of the interplanetary magnetic field was negative inside the modulated zone. This suggests that the negative polarity of the active region lay nearer the Sun's equator than the positive portion, and that the magnetic bottle's closed lines of force lay on surfaces quasi-perpendicular to the ecliptic plane.

The small recurrent c.r. decrease observed inside the positive sector was probably produced by a fast stream coming from an M-region. This hypothesis remains to be tested with the solar wind data.

Table 1. Tentative Association Between Flares and Fds.

Forbush Decrease		Type IV Solar Flare			
Date 1976	ΔI/I (%)	Date 1976	Active Region	Position	Start UT
March 26	2.5	March 23	14143	S05 E90	0837
28	~1.0	25	14143	S06 E75	< 1203
30	~3.0	28	14143	S08 E31 S07 E28	< 0922 < 1905
April 1	~1.5	31	14143	S07 W12	1144
		April 5		(W80)	(2150)
26	1.0				
May 2	2.0	30	14179	S06 W41 S09 W47	1243 2048
		May 1	14179	S08 W61	2155
21	2.0				

REFERENCES

IUCCI, N., M. PARISI, M. STORINI and G. VILLORESI — 1977 — A Study of the Forbush Decrease Effect: The Origin and Development in Interplanetary Space, pre-print, to be submitted to *Solar Physics*.

IUCCI, N., M. PARISI, M. STORINI and G. VILLORESI — 1973 — The Heliolongitude of the Active Region and the Time Behavior of the Associated Forbush Decreases, *Proc. Inter. Conf. Cosmic Rays, Denver, 2*, 1261.

IUCCI, N., M. PARISI, M. STORINI, G. VILLORESI and N. L. ZANGRILLI — 1975 — The Corotation of the Magnetic Structure Associated with Forbush Decreases, *Proc. Inter. Conf. Cosmic Rays, Munich, 3*, 1064.

SGD — 1976 — *Solar-Geophysical Data, 380-384 Part I*, April - August 1976, U. S. Department of Commerce, (Boulder, Colorado, U.S.A. 80302).

Forbush-Effect Data of the Cosmic Ray Station Sverdlovsk during the Period from March to May 1976

by

E. Ya. Gidalevitch, S. F. Nossov, V. I. Utkin
Institute of Geophysics, Urals Scientific Center,
USSR Academy of Sciences, Pervmayskaya Str. 91
Sverdlovsk, 620169

Ground-based recordings of the neutron component of cosmic rays during the retrospective period from 20 March to 5 May 1976 were carried out by the three-section neutron supermonitor at the cosmic ray station Sverdlovsk (λ = 60°38'; ϕ = 56°48'; 300 m above sea level; geomagnetic limits 2.3 GeV). The statistical error of the recordings was less than 0.2% per hour. The Sverdlovsk station is equipped with an additional impulse counting recorder. This equipment permits the recording of 5-minute and hourly interval data simultaneously.

From the Sverdlovsk station data during the retrospective period, two clear Forbush decreases of cosmic ray intensity were observed: from 25 March to 7 April, and from 24 April to 5 May. The depth of the first decrease was about 10%, that of the second decrease about 7%. Although the time interval between the two decreases was of the order of the Sun's rotation period, the amplitudes of both events were much larger than the usual 27-day variation. A comparison with the solar activity events was not done, but taking into account the decreased profiles, they are the typical Forbush effects with complete intensity recovery. The recorded data corrected for atmospheric pressure are shown in Figure 1.

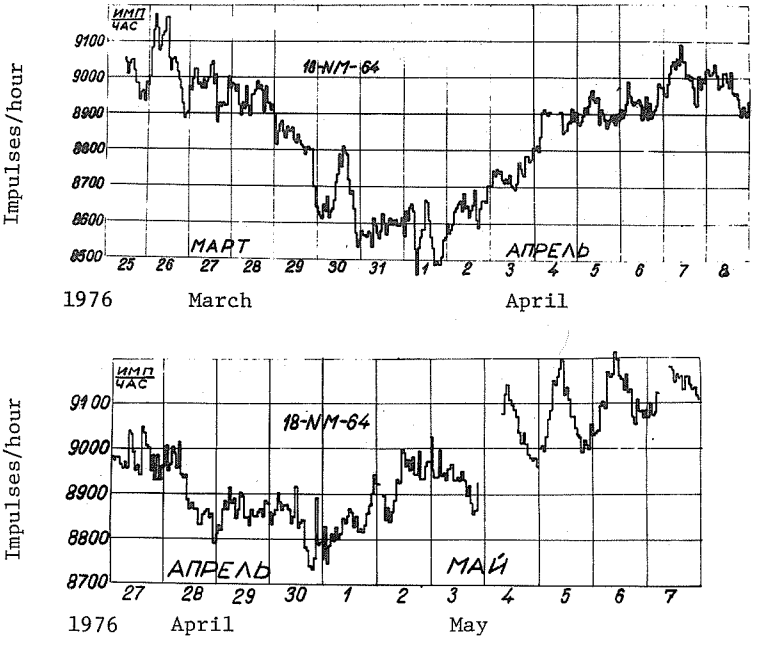

Fig. 1. Corrected cosmic ray neutron monitor data from Sverdlovsk for the periods 25 March - 8 April and 27 April - 7 May 1976.

6. IONOSPHERE

Ionospheric Variations at Taiwan Associated with Geomagnetic Storms of 26 March, 1 April, and 2 May 1976

by

Yinn-Nien Huang
Telecommunication Laboratories, M.O.C.
Chung-Li P.O. Box 71, Taiwan
Republic of China

The Telecommunication Laboratories, Ministry of Communications carries out a number of observations of upper atmospheric parameters. These include observations of geomagnetic field, ionospheric total electron content, and ionospheric scintillation at Lunping Observatory (N25.00 E121.17 geographic; N13.8 E189.5 geomagnetic); vertical ionospheric sounding at Chung-Li Ionosphere Station (N24.95 E121.23); and VLF phase recording at Kao-Jorng (N24.95 E121.15). The Ruska normal run magnetograph is used for the routine recording of the H, D and Z components of the geomagnetic field. The ionospheric total electron content (TEC) and ionospheric scintillation were observed from January to August 1976 by measuring the Faraday rotation and signal intensity of the 136.44 MHz beacon signal transmitted from the geostationary satellite INTELSAT 2F3 with an Air Force Cambridge Research Laboratory (AFCRL) polarimeter. The phase variations of the transequatorial VLF propagation are measured by receiving the NWC 22.3 kHz VLF signal transmitted from North West Cape, Australia. The great circle, passing through the transmitting and receiving stations, runs almost parallel with the meridional line and spans a distance of 5262 km.

The H and D components of the magnetic field, ionospheric scintillation index, ionospheric total electron content, critical frequency of the F2 layer (foF2), and VLF phase data obtained during the geomagnetic storms of 26 March, 1 April, and 2 May 1976 are presented in this report. The results are shown in Figures 1, 2 and 3, respectively. The H and D components plotted in Figures 1-3 were contructed from their respective magnetogram traces by using a Hewlett-Packard digitizer and plotter. The VLF phase variations were plotted by taking a reading every 5 min from the original paper records; missing curves were due to the unavailability of phase data. The ionospheric scintillation index (SI) was determined at 15-minute intervals from the amplitude recordings of the AFCRL polarimeter. The scintillation index is defined by the following equation:

$$SI = P_{max} - P_{min},$$

where P_{max} = the third highest peak in dB determined from the amplitude recording and P_{min} = the lowest null in dB determined from the amplitude recording. Adjacent data points were connected by straight lines. The plots were not made during those time intervals in which equipment malfunction or interference made the determination of the SI impossible. The ionospheric total electron content was plotted by readings made every 15 min from the Faraday rotation recordings of the AFCRL polarimeter. The foF2 data were reproduced from f-plots made every 15 min.

26 March 1976

A sudden commencement of the type SC(-) was observed at about 2339 UT on 25 March 1976. Large decreases of foF2 and total electron content were observed during the daytime of the second storm day (27 March); at nighttime there was a slight increase of foF2 and TEC. The lowering of the height of the nighttime E layer, as indicated by the VLF phase variation, was observed at night on the first and second storm days, 26 and 27 March. There seems to be a slight increase in the scintillation index at night on the first storm day.

1 April 1976

A sudden commencement of the type SC(-+) was observed at about 0257 UT on 1 April 1976. Significant decreases in TEC and foF2 were observed during daytime of the second storm day, 3 April. Unusual increases in TEC and foF2 during the early part of the main phase were also observed. Significant lowering of the nighttime E layer and an increase in the scintillation index were observed during the first night after the SC.

2 May 1976

A sudden commencement of the type SC(+) was observed at about 1828 UT on 2 May 1976. For this moderate storm no significant variation of VLF phase and increase of scintillation index were observed. The diurnal curves of TEC and foF2, however, became rather irregular during the disturbed period. No significant increase or decrease of TEC and foF2 was observed.

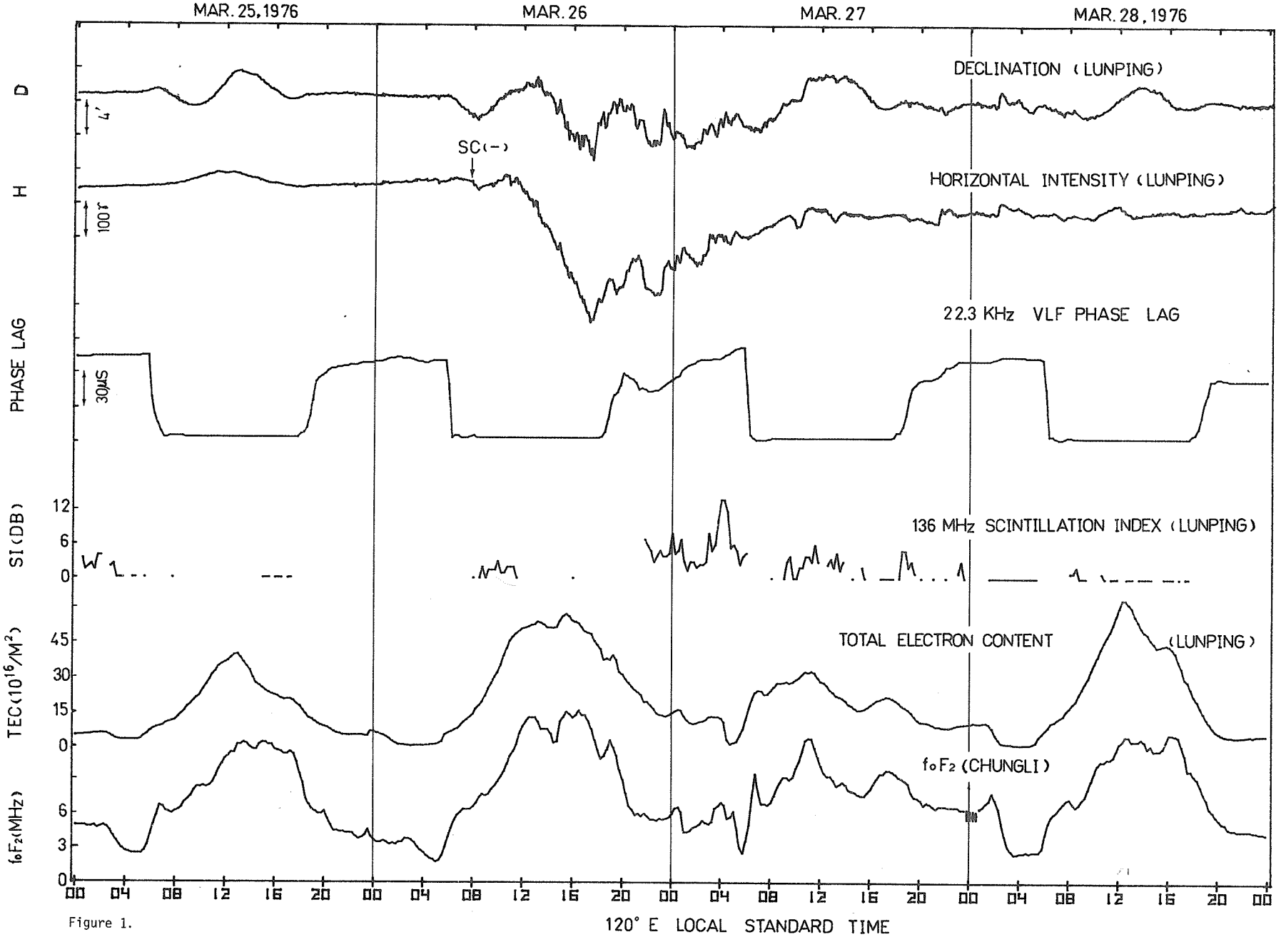
MAR. 25, 1976
MAR. 26
MAR. 27
MAR. 28, 1976
D
4'
DECLINATION (LUNPING)
SC(-)
H
100γ
HORIZONTAL INTENSITY (LUNPING)
PHASE LAG
30μS
22.3 KHz VLF PHASE LAG
SI(DB)
12
6
0
136 MHz SCINTILLATION INDEX (LUNPING)
TEC(10^{16}/M^2)
45
30
15
0
TOTAL ELECTRON CONTENT (LUNPING)
f_0F_2(MHz)
6
3
0
f_0F_2 (CHUNGLI)
00 04 08 12 16 20 00 04 08 12 16 20 00 04 08 12 16 20 00 04 08 12 16 20 00
120° E LOCAL STANDARD TIME

Figure 1.

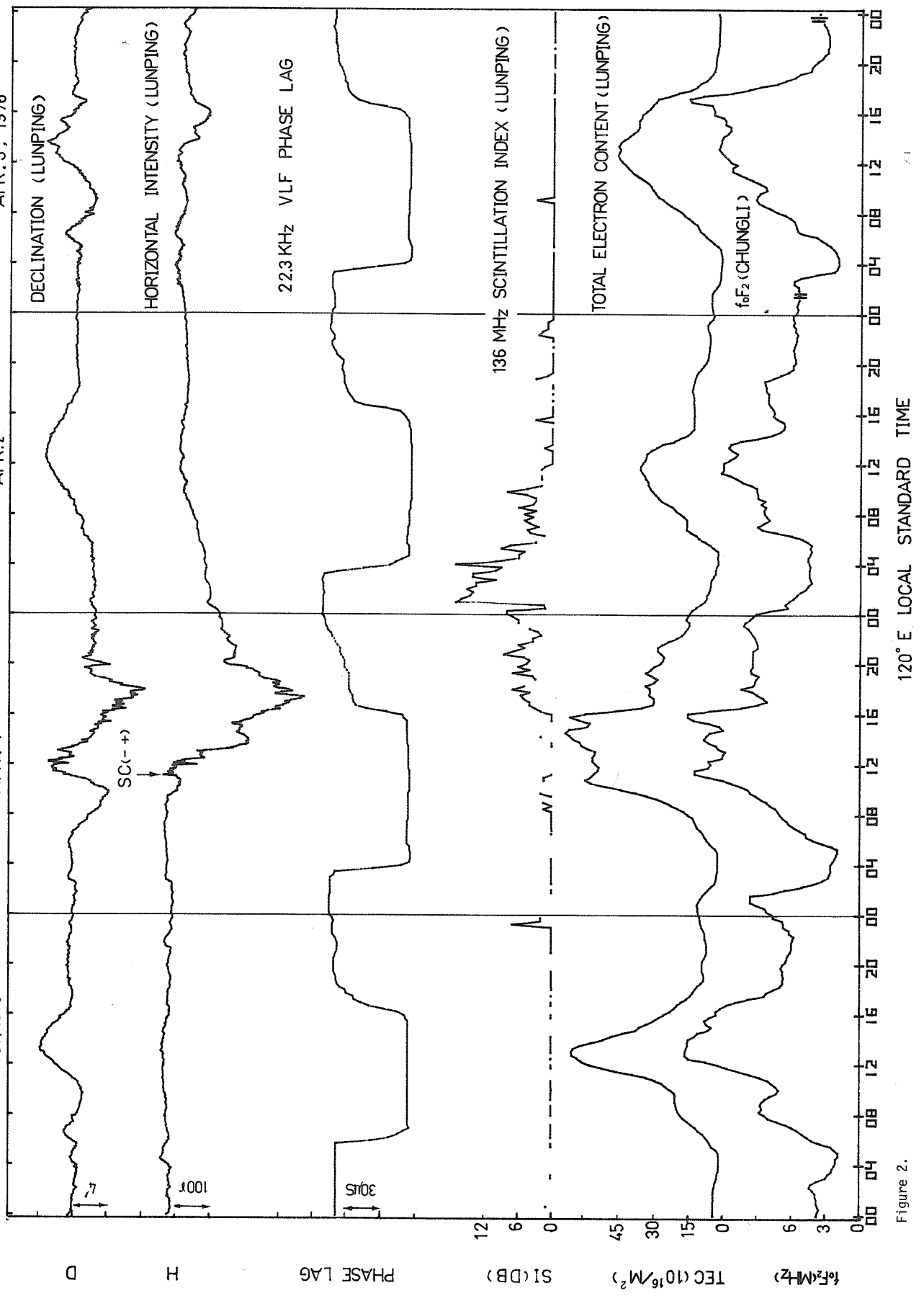
MAR. 31, 1976
APR. 1
APR. 2
APR. 3, 1976
DECLINATION (LUNPING)
HORIZONTAL INTENSITY (LUNPING)
22.3 KHz VLF PHASE LAG
136 MHz SCINTILLATION INDEX (LUNPING)
TOTAL ELECTRON CONTENT (LUNPING)
f_0F_2 (CHUNGLI)
SC(-+)
100γ
30μs
D
H
PHASE LAG
SI (DB)
TEC (10^{16}/M^2)
f_0F_2(MHz)
120° E LOCAL STANDARD TIME

Figure 2.

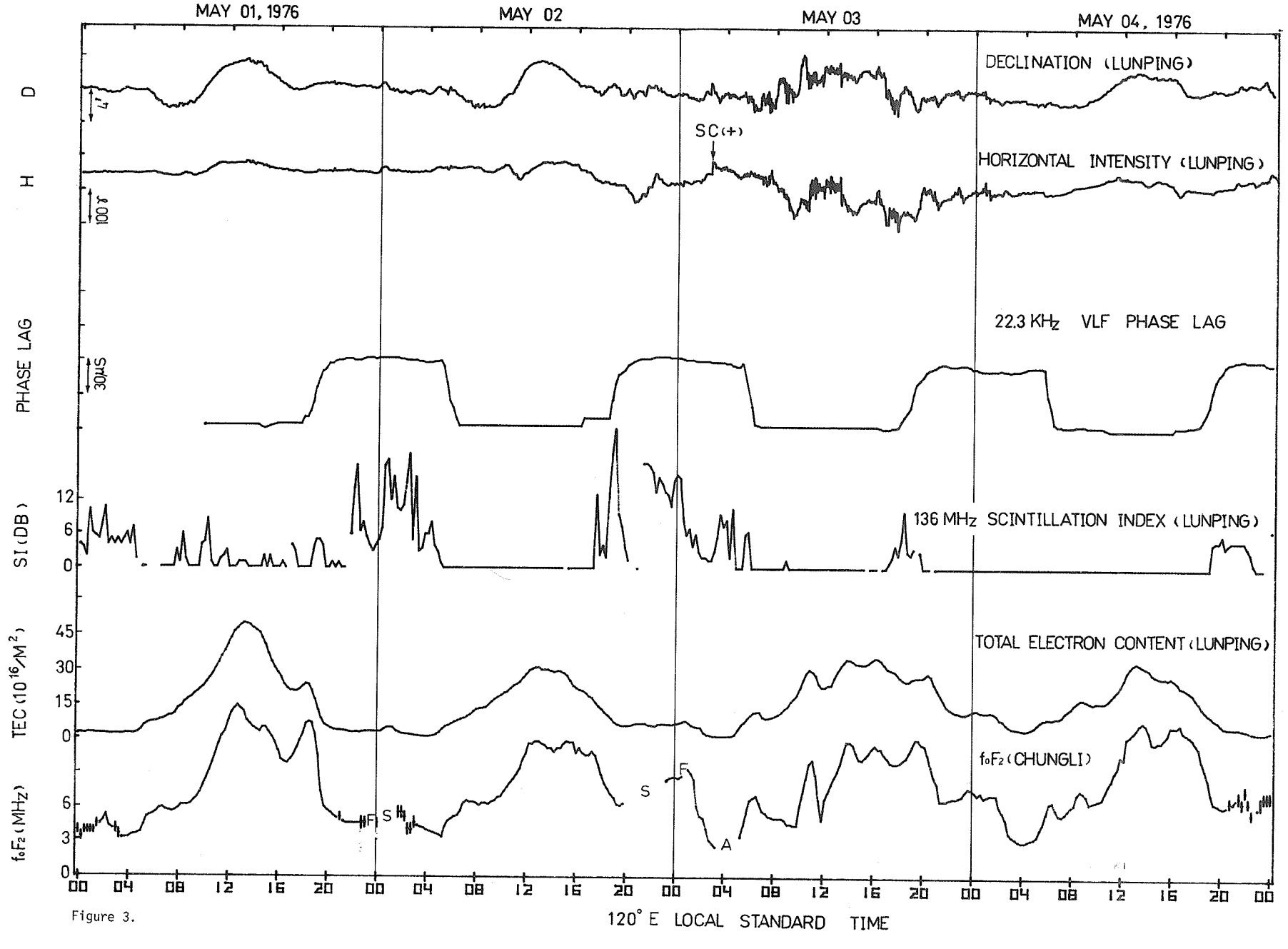
MAY 01, 1976
MAY 02
MAY 03
MAY 04, 1976
D
4'
DECLINATION (LUNPING)
SC(+)
H
100 γ
HORIZONTAL INTENSITY (LUNPING)
PHASE LAG
30μS
22.3 KHz VLF PHASE LAG
SI (DB)
12
6
0
136 MHz SCINTILLATION INDEX (LUNPING)
TEC (10^{16}/M^2)
45
30
15
0
TOTAL ELECTRON CONTENT (LUNPING)
f_0F_2 (MHz)
6
3
0
f_0F_2 (CHUNGLI)
F
S
S
F
A
00 04 08 12 16 20 00 04 08 12 16 20 00 04 08 12 16 20 00 04 08 12 16 20 00
120° E LOCAL STANDARD TIME

Figure 3.

Significant Events in TEC Measurements Between 20 March and 5 May, 1976

by

N. Jakowski
Academy of Sciences of GDR
Institute for Electronics
Neustrelitz, GDR

and

B. Lazo
Academy of Sciences of Republic of Cuba
Institute for Geophysics and Astronomy
Havana, Cuba

The following discussion is based on the determination of total ionospheric electron content (TEC) by means of Faraday rotation measurements. These observations are carried out at VHF telemetry frequencies of geostationary satellites in Havana, Cuba, (N23.1 W82.5) by recording the polarization angle Ω (given in all the figures) with a specially designed Two-Channel Polarimeter [Bettac *et al.*, 1975]. The Faraday angle Ω is proportional to the TEC and reflects the TEC variations. Unfortunately, our measurements did not cover the entire period from 20 March-5 May 1976, so we can present only data for three significant events during this period.

In Figures 1 and 2 are the recordings during the geomagnetic storms of 26 March and 2-3 May, respectively. The dashed line indicates the mean TEC behavior during the 6 preceding days; the solid line reflects the TEC variations during both geomagnetic and ionospheric storms.

In accordance with the results of other authors [Prölss *et al.*, 1974; Mendillo *et al.*, 1975], the geomagnetic storm effect in TEC (Figure 1) starts with a positive phase in the morning of 26 March and follows with a negative phase during the noon and afternoon hours. In the TEC variations there are slight indications of a wave-like structure, possibly generated in connection with the intense geomagnetic storm.

In the second example (Figure 2) indications of the geomagnetic storm effect appeared during 2 May 1976. On 3 May from 0000-0900 UT, the recording was heavily disturbed by an unknown origin. It would be very interesting to prove by comparison with other stations whether these short time fluctuations in the recording are of local origin only or are due to real large-scale density variations in the ionosphere. The discernible negative phase on 3 May probably shows an extraordinarily strong TEC reduction because of the long-lasting geomagnetic storm. The solar flare effect that caused a sudden increase in TEC by about 10% on 30 April represents the third significant event in our measurements. It is shown in Figure 3 in comparison with the mean TEC behavior of the 6 preceding days. This value is in general agreement with reported SID effects in TEC [Davies *et al.*, 1975; Soicher, 1975]. The TEC behavior on 29 and 30 April is accompanied by the typical geomagnetic storm effects as discussed in the previous cases.

REFERENCES

BETTAC, H. D. and A. WIENER, 1975. Zweikanal-Polarimeter zur Messung des ionosphärischen Faraday-Effektes auf 140 MHz (2 Channel Polarimeter) *Nachrichtent. Elektronik, 25,* 452.

DAVIES, K., R. B. FRITZ, R. N. GRUBB and J. E. JONES, 1975. The ATS-6 Radio Beacon Experiment: Technique and some early results, *Proc. on the Beacon Satellite Invest. of the Ionosp. Structure and ATS-6 Data,* November 1974, Vol II, Moscow, p. 93.

MENDILLO, M. and J. A. KLOBUCHAR, 1975. Investigations of the Ionospheric F Region Using Multi-station Total Electron Content Observations, *J. Geophys. Res., 80,* 643.

PRÖLSS, G. W. and K. NAJITA, 1974. Magnetic Storm associated changes in the electron content at low latitudes, *J. Atmos. Terr. Phys, 37,* 635.

SOICHER, H. 1975. ATS-6 Radio Beacon Experiment, *Nature, 253,* 252.

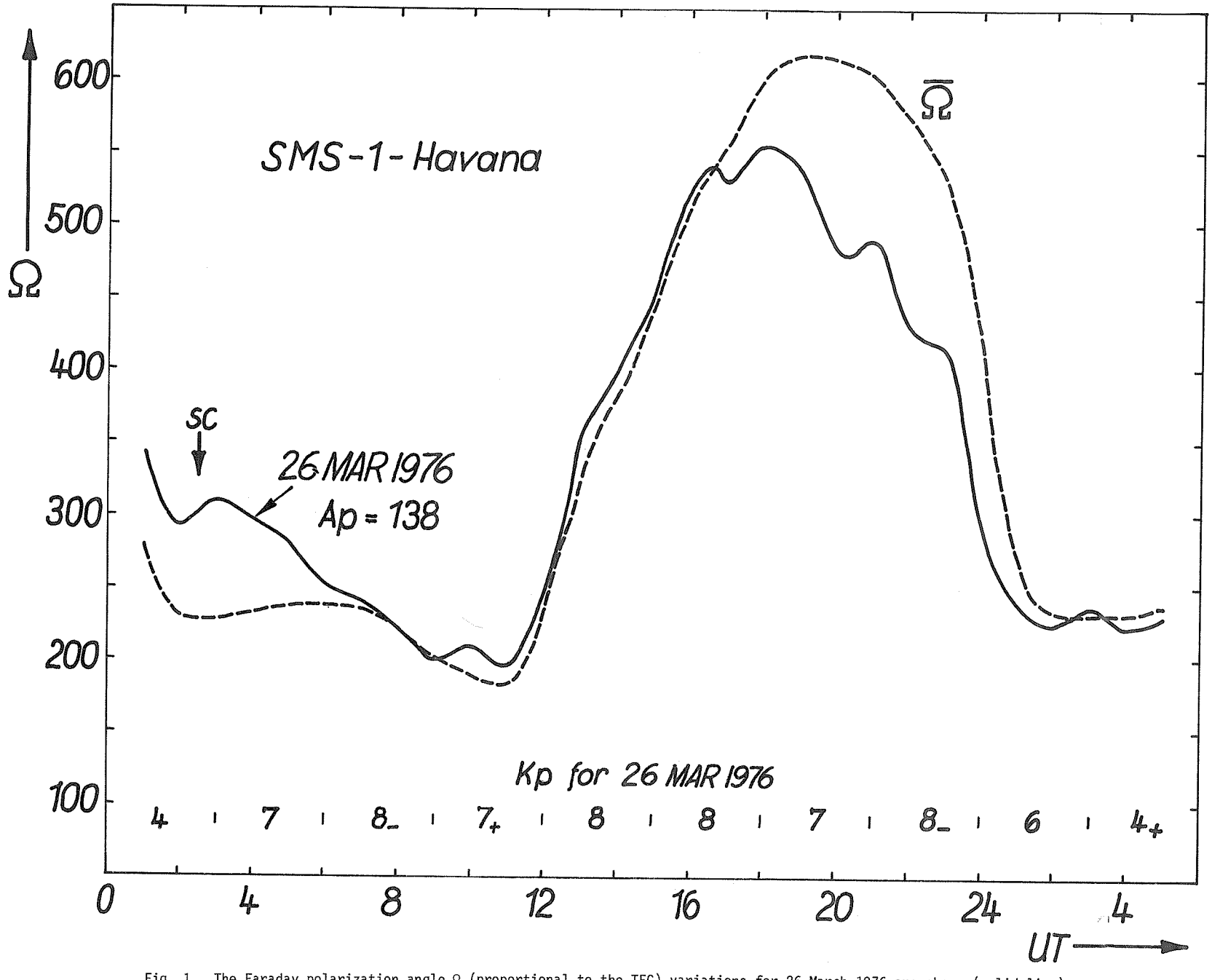

Fig. 1. The Faraday polarization angle Ω (proportional to the TEC) variations for 26 March 1976 are shown (solid line). Dashed line is the mean TEC behavior during the 6 preceding days.

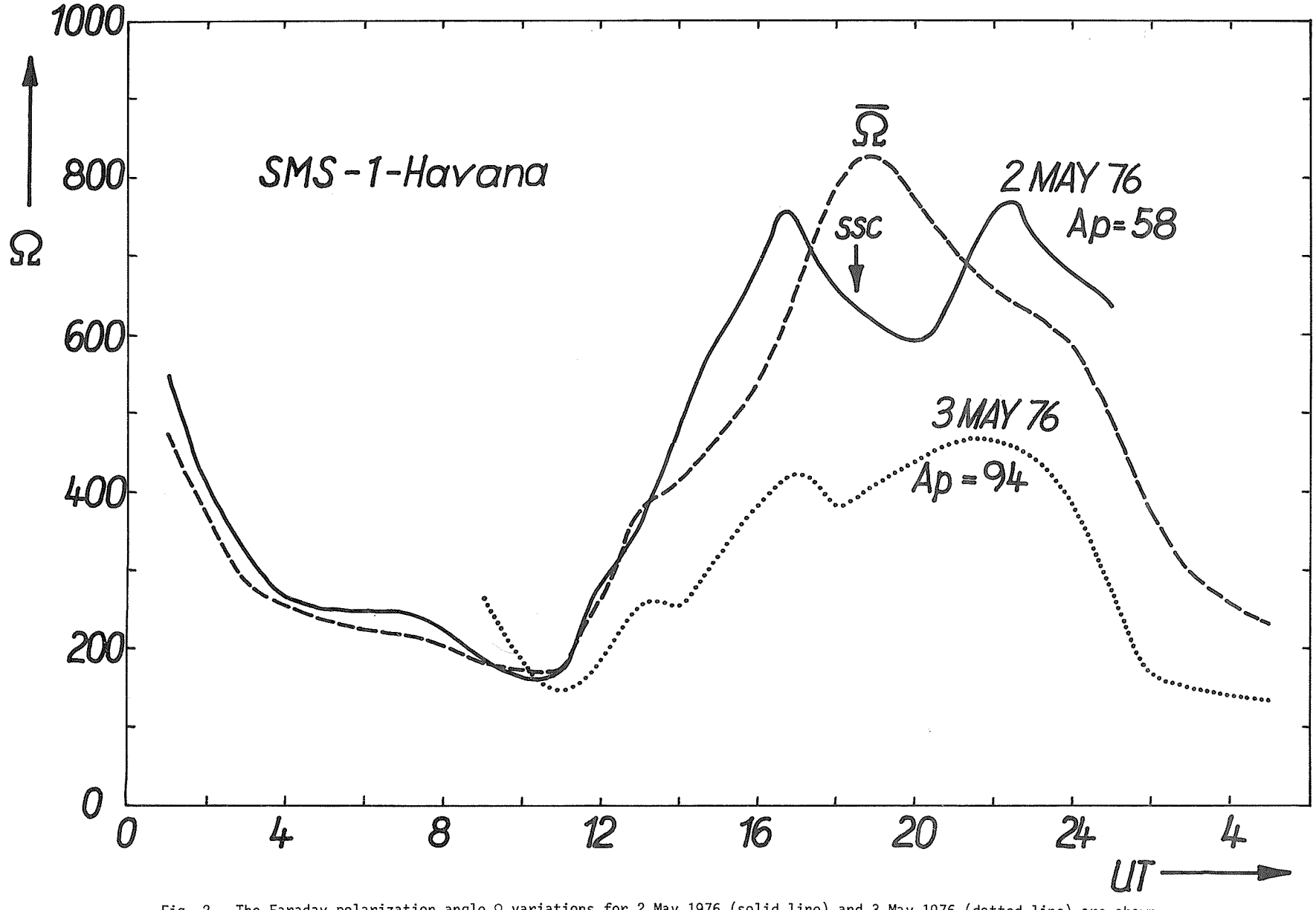

Fig. 2. The Faraday polarization angle Ω variations for 2 May 1976 (solid line) and 3 May 1976 (dotted line) are shown. The dashed line is the mean TEC behavior during the 6 preceding days.

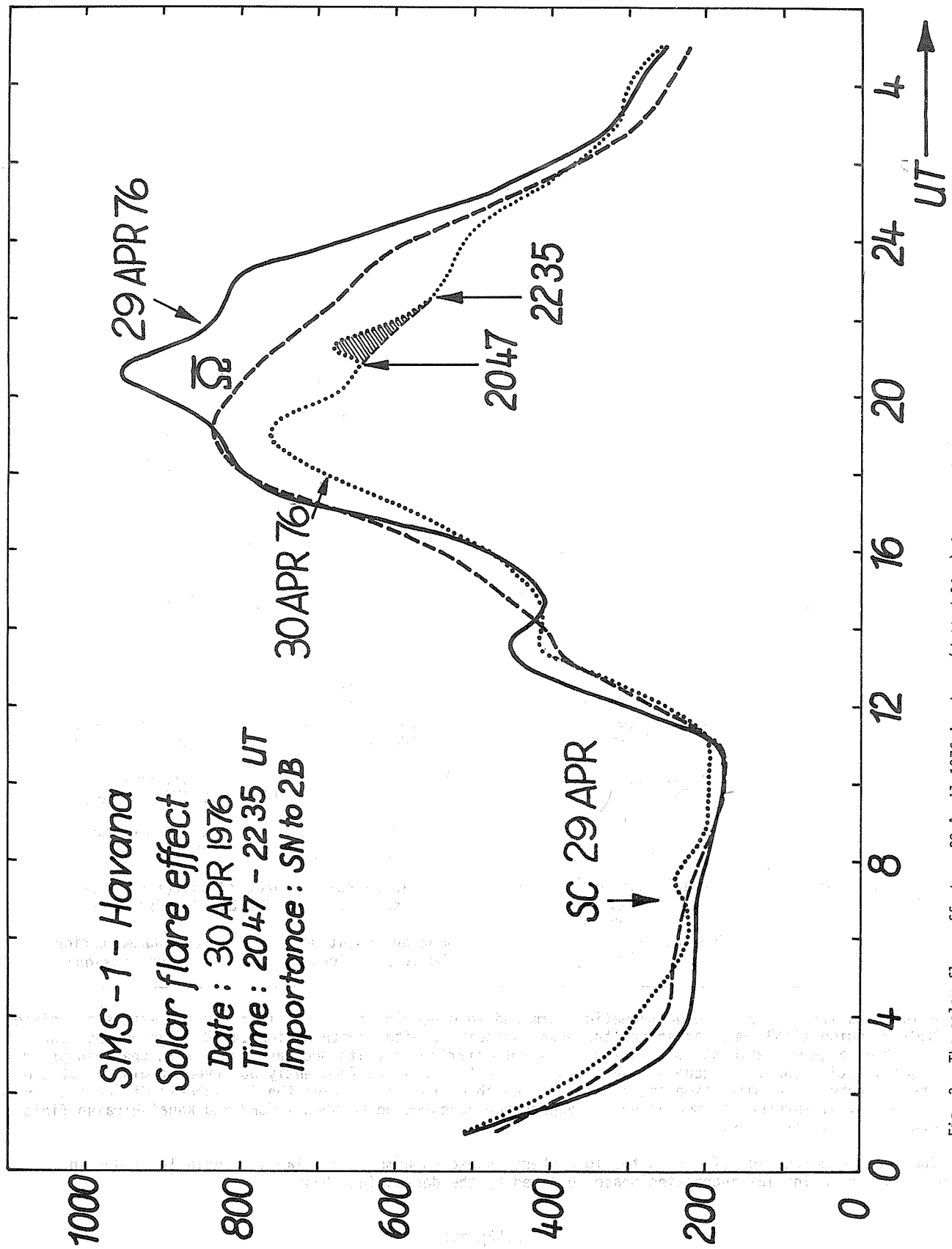

Fig. 3. The solar flare effect on 30 April 1976 is shown (dotted line) in comparison with the mean TEC behavior of the 6 preceding days (dashed line). Also shown is the TEC behavior on 29 April 1976 (solid line).

Ionospheric Storms Associated with Activities of McMath Region 14143 during March - April, 1976

by

Rikio Maeda
and
Kazuo Yoshikawa
Radio Research Laboratories
4-2-1, Nukui-Kita, Koganei, Tokyo 184, Japan

Three principal geomagnetic storms occurred in STIP Interval II (15 March-15 May 1976). These geomagnetic storms mediated between solar flares and ionospheric disturbances, effectively. The March and April events associated with McMath Region 14143 had distinctive effects on the ionosphere, but the May event associated with McMath Region 14179 did not.

This report briefly describes some detailed observational results of the ionospheric disturbances. Changes in the critical frequency of the F layer over Kokubunji and the received field strength of Kauai (WWVH) at Hiraiso showed typical patterns of ionospheric and propagation storms in winter middle latitudes. Figure 1 illustrates the March and April ionospheric storms detected by foF2 variations observed at Kokubunji, where the time used is JST (UT + 9h). The disturbed curve and the monthly median curve are denoted by solid lines connecting fifteen-minute values and hourly ones, respectively. The dashed lines connecting hourly values represent the median curves of the last month when the middle day of the disturbance fell on the 1st-10th of the month or the next month when the middle day of the disturbance fell on the 21st-31st of the month. The geomagnetic-ionospheric relations observed in Japan are compiled in Table 1.

Table 1. Geomagnetic-Ionospheric Relations in STIP II Interval

Solar Radio Burst (Hiraiso) DATE 1976	Geomagnetic Storm (Kakioka)	Ionospheric Storm (Kokubunji)	Propagation Storm (Hiraiso)
March 23 0824UT	3/25 13.3UT(start)	3/26 14.0JST(increase)	3/26 14.0JST(increase)
	3/26 03.1UT(main phase)	3/27 02.0JST(decrease)	3/27 05.0JST(decrease)
	3/27 24.0UT(end)	5MHz(augmentation)	50dB(augmentation)
	319γ(range)	-1MHz(depression)	-38dB(depression)
March 31 (1153UT)	4/01 0254UT(start)	4/01 14.0JST(increase)	4/01 14.5JST(increase)
	4/01 04.1UT(main phase)	4/01 23.0JST(decrease)	4/02 06.0JST(decrease)
	4/02 02.0UT(end)	5MHz(augmentation)	25dB(augmentation)
	243γ(range)	-1MHz(depression)	-26dB(depression)
April 30 2101UT	5/02 1828UT(start)	5/02 23.0JST(increase)	5/02 23.0JST(increase)
	5/02 21.5UT(main phase)	5/03 23.0JST(decrease)	5/03 23.0JST(decrease)
	5/03 22.0UT(end)	0MHz(augmentation)	0dB(augmentation)
	152γ(range)	-1MHz(depression)	-0dB(depression)

Relation shifts between the geomagnetic storm and ionospheric storm are clear for the events associated with McMath Region 14143, but not so for the event associated with McMath Region 14179. One or two hours after onset of a geomagnetic storm an increase of foF2 started, and its decrease began with the main phase of the geomagnetic storm. In general, such disturbance features are frequently observed at middle latitudes in winter. There was a small time lag of field strength disturbance behind the ionospheric disturbance in this case. That is, disturbance augmentation and depression appeared on Kokubunji foF2 and Kauai-Hiraiso field strength nearly simultaneously.

The three geomagnetic effects on the ionosphere showed phenomena familiar at middle latitudes in winter, that is an initial increasing phase followed by the decreasing phase.

REFERENCE

MAEDA, R. 1976 Ionospheric Storms, *Radio and Space Data*, *Vol. 3*, Part 4.

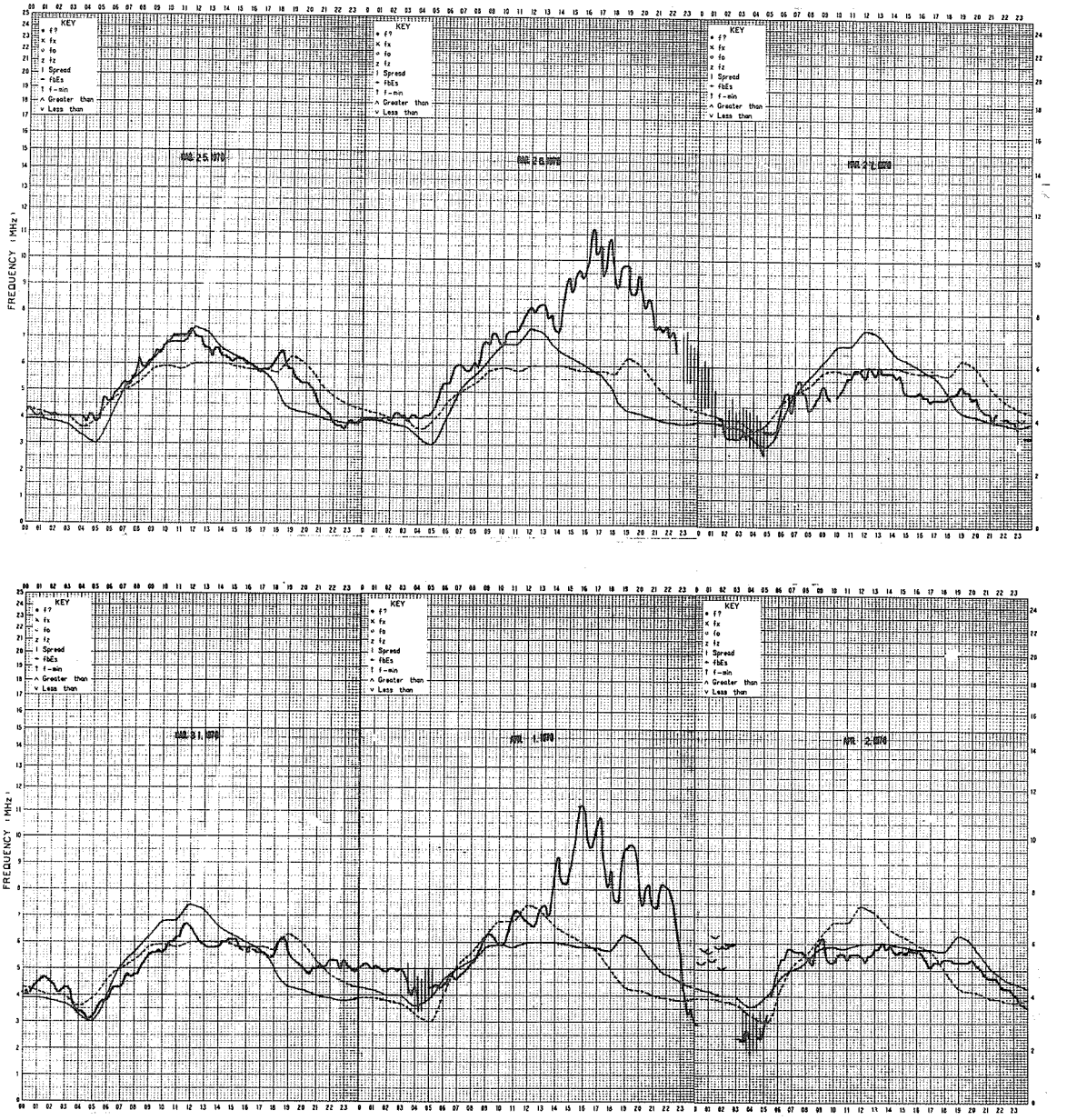

Fig. 1. foF2 changes during ionospheric storms observed at Kokubunji.

Anomalies in the Daytime Ionosphere at Medium Latitudes During the Period 20 March - 5 May 1976

by

G. T. Nestorov
Geophysical Institute
Bulgarian Academy of Sciences
Sofia, Bulgaria

Absorption and phase-height measurements on 12 paths at long, medium and short wavelengths were made by the A3 method at the ionospheric observatories of Sofia (N42.6 E23.3) and Roburent (N44.3 E7.9) during the period 20 March - 5 May 1976, as shown in Table 1. Significant ionospheric anomalies were observed on almost all paths. These disturbances in the daytime lower ionosphere were connected, in most cases, with X-ray flux enhancements, and in the high ionosphere, with an increase in geomagnetic activity as well.

Table 1

No.	Path	Freq. f(kHz)	Dist. d(km)	f.cos(i) $=f_i$ (kHz)	Reflection Point Coordinates	
					N	E
1	Allouis - Sofia	164	1720	25	45.5	13.2
2	Brašov - Roburent	155	1450	29	45.4	16.7
3	Ankara - Sofia	182	850	35	41.4	28.0
4	Donebach - Roburent	151	580	45	47.0	08.7
5	Kiev - Sofia	209	1000	45	46.7	26.8
6	Brašov - Sofia	155	370	75	42.7	23.4
7	Monte Carlo - Roburent	218	75	200	44.0	07.5
8	Berrombnster - Roburent	527	300	280	45.8	08.1
9	Priština - Sofia	1412	170	1100	42.7	22.3
10	Nice - Roburent	1554	80	1500	44.0	07.5
11	Bern - Roburent	3985	280	2300	45.7	07.7
12	Wien - Sofia	6155	800	2800	45.7	19.9

1. X-ray Enhancement (GOES-1) of 23 March 1976

Phase-height measurements were made along paths No. 3, 4 and 5 (see Table 1). The required minimum electron concentration for reflection (N_{min}) may by obtained according to Nestorov [1965] as follows:

$$N_{min} = \pi 10^{-10} \cos(i) \, [(\omega + \omega_L')^2 + \nu^2]/(1 + \omega_L'/\omega),$$

where i is the angle of incidence of the wave on the reflection region; $\omega = 2\pi f$ is the working frequency; $\omega_L' = 2\pi f_L'$ is the effective gyrofrequency of the plasma; and ν is the collision frequency. For the above indicated paths in a normal ionosphere, N_{min} varies within the limits of 500 - 1000 electrons cm^{-3}. Variations in the solar zenith angle χ, at which the concentration N_{min} is reached at two different heights (h_1' = 88 km and h_2' = 84.5 km) in the period under investigation, are seen in Figure 1 for path No. 4. The peak on 23 March 1976 is obvious, and this indicates a significantly more powerful flux of X-radiation I_R than that occurring on the control days. Besides, the variations of h_2' are much greater, and therefore the I_R flux intensified more at the harder end of the spectrum than at the softer X-ray wavelengths.

Absorption measurements along paths No. 1 and 2 were made at tangential wave incidence (long paths). These results are presented in Figure 2, where the mean values are given for typically daytime conditions (0900 to 1400 UT). On 21 March, and particularly on 23 March 1976, the absorption reached a maximum that was connected with the enhanced hard X-radiation I_R ($\leq$5Å) that occurred during these days.

The ionization influence of the hard X-radiation is further confirmed by Figure 3. It presents data from paths No. 6 (short path) and No. 7 (extremely short path; a quasivertical wave incidence). Three absorption peaks are seen on 21, 23 and 25 March 1976, which coincide with the excessive X-radiation measured by GOES-1 on the same dates [*SGD*, 1976]. The data of L_{155} refer to $\cos(\chi) = 0.1 = \text{const}$ (because of technical difficulties in measuring absorption for small zenith angles), and those of L_{218} represent mean values over the period 0900 to 1400 UT.

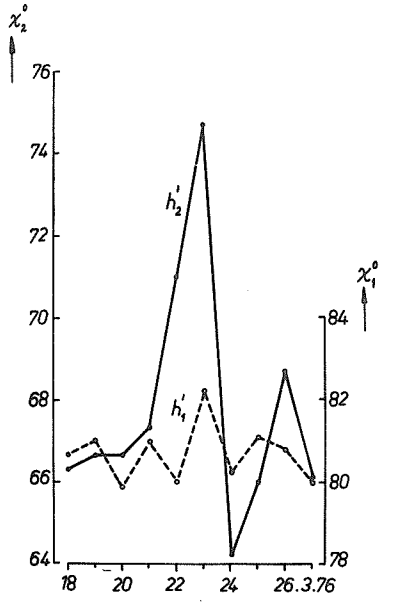

26 March 1976

Fig. 1. Average daily variation of the solar zenith angle at two different heights: $h_1' = 88$ km and $h_2' = 84.5$ km for $N_{min} = 800$ cm^{-3}.

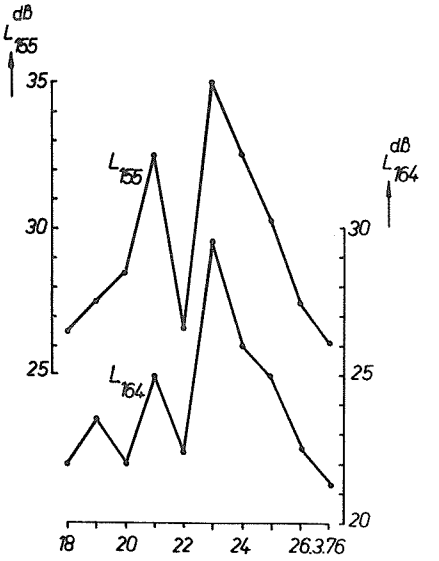

26 March 1976

Fig. 2. Average daily variation of absorption L_{155} and L_{164} (paths Nos. 1 and 2).

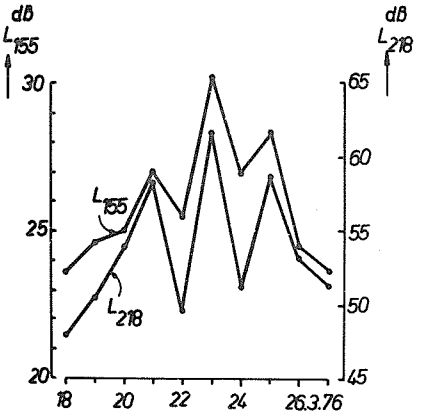

26 March 1976

Fig. 3. Average daily variation of absorption L_{155} and L_{218} (paths No. 6 and 7).

Observations of the absorption at medium wavelengths were carried out along paths No. 8, 9 and 10 (Figure 4). The results show the influence of the X-radiation flux I_R (≤ 8Å). The data also refer to typically daytime conditions, and in general, confirm the observations at long wavelengths. These measurements describe the ionization state of the lower ionosphere up to 85 km on path No. 8, and up to 95 km on path No. 10.

The absorption at short wavelengths (paths No. 11 and 12) is determined not only by the ionization of the D region but by the E and F layers as well. At lower frequencies, for example path No. 11, the D region takes a more active part in the absorption: the absorption peak in Figure 5 on 23 March 1976 is stronger at 3985 kHz than at 6155 kHz. Although the above results establish empirically the significant ionization role of the hard solar X-radiation, more concrete information is obtained by juxtaposing the field variation and the X-radiation data I_R (≤ 8Å) in ergs cm^{-2}s^{-1} from the satellite GOES-1. As an example see Figure 6.

On 23 March 1976, after the powerful solar flare which began at 0838 UT, the absorption was total to 1300 UT. Unfortunately, we do not have data on I_R during the next period in order to estimate what values of I_R caused the absorption to decrease to a normal value. One such critical flux level, however, is available from the 25 March 1976 record, where a flux of 6.3×10^{-3} ergs cm^{-2}s^{-1} again causes total absorption. Since at this time $\cos \chi = 0.61$ for the reflection point of the signal, the actual flux responsible for the total absorption was $I_{R(\chi)} = 3.9 \times 10^{-3}$ ergs cm^{-2}s^{-1}. This result is also confirmed by the next record of 26 March 1976, where at $I_{R(\chi)} = 3.7 \times 10^{-3}$ ergs cm^{-2}s^{-1} the absorption was total and where at $I_{R(\chi)} = 1.9 \times 10^{-3}$ ergs cm^{-2}s^{-1} it began to decrease. Hence, it follows that a flux $I_{R(\chi)} = 2 \times 10^{-3}$ ergs cm^{-2}s^{-1} causes basic absorption in the D region up to 95 km (equivalent frequency $f_i = f\cos(i) = 1.5$ MHz) for typical daytime conditions, and that this attenuation is determined by the X-radiation I_R (≤ 8Å).

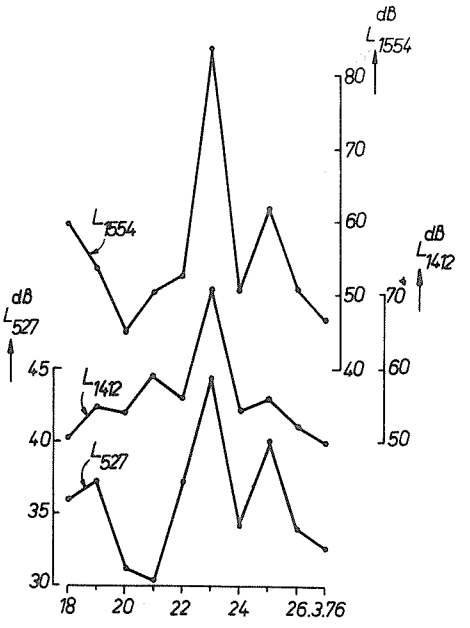

26 March 1976

Fig. 4. Average daily variation of absorption L_{527}, L_{1412} and L_{1554} (paths Nos. 8, 9 and 10).

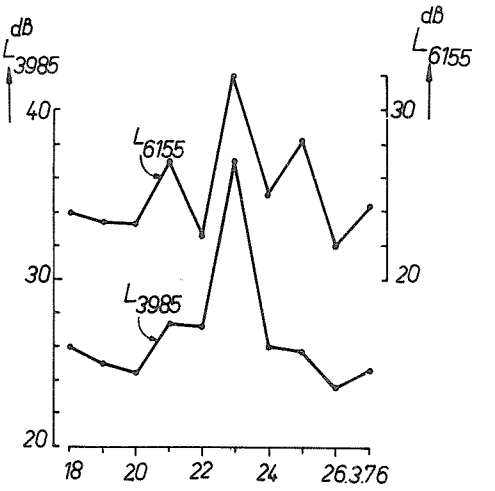

26 March 1976

Fig. 5. Average daily variation of absorption L_{3985} and L_{6155} (paths No. 11 and 12).

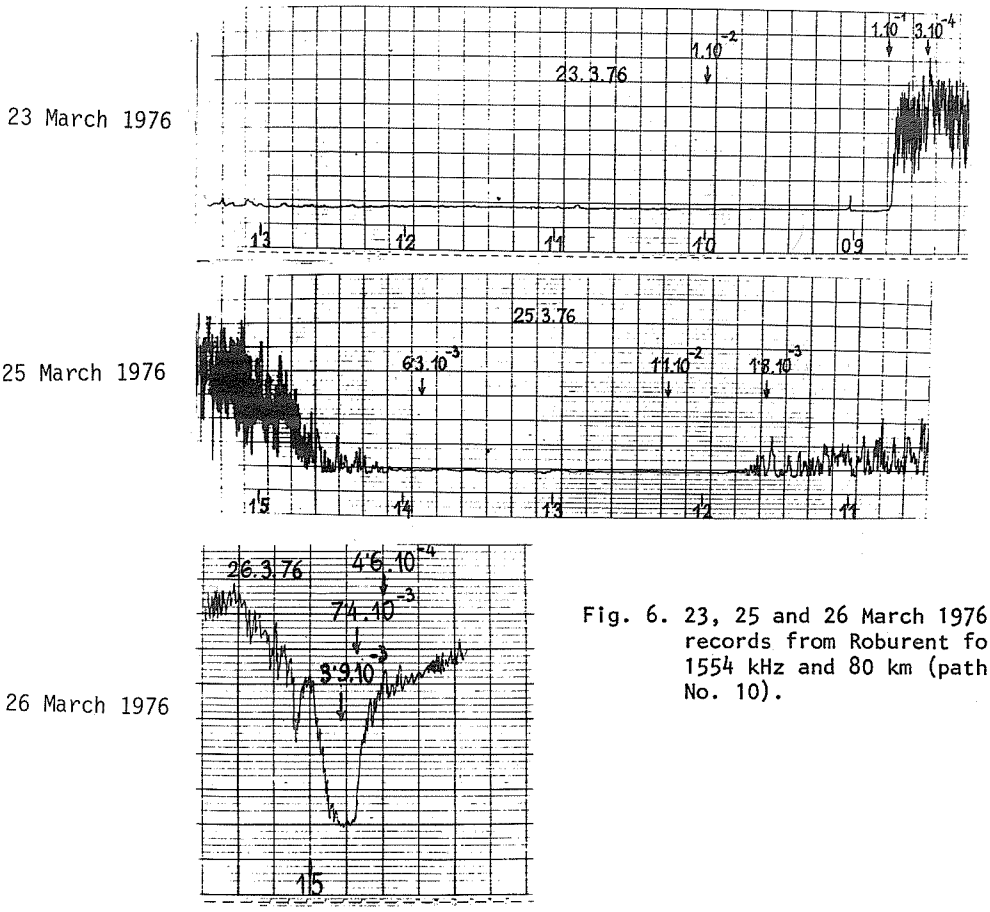

Fig. 6. 23, 25 and 26 March 1976 records from Roburent for 1554 kHz and 80 km (path No. 10).

2. X-ray Enhancement of 31 March 1976

Here we give only a few examples in order to avoid repeating the already known behavior of the D region during solar flares discussed in section 1. Figures 7a and 7b present the L_{218} behavior, and include a maximum on 31 March 1976 from the excessive X-radiation and a probable aftereffect of the 1 April SSC on 4 April 1976. The behavior of L_{527} absorption is similar, and a high peak is seen on L_{1554} on 31 March 1976 that is connected with the supplementary solar X-radiation. On the whole, path No. 10 turned out to be a sensitive indicator of the variations in I_R (≤ 8Å) -- a result seen from other investigations as well [Nestorov, 1975]. Concrete examples of records along path No. 10 are presented in Figure 8. On 28 March 1976, between 1000 and 1100 UT, the mean hourly value of I_R (≤ 8Å) = 3×10^{-4}, while the absorption was almost total; between 1100 and 1200 UT it equaled 2×10^{-4} ergs $cm^{-2}s^{-1}$; before 1000 UT I_R (≤ 8Å) = 1×10^{-4} ergs $cm^{-2}s^{-1}$. On 31 March 1976 around 1300 UT, $I_R < 2.9 \times 10^{-3}$ ergs $cm^{-2}s^{-1}$, while again the absorption was total.

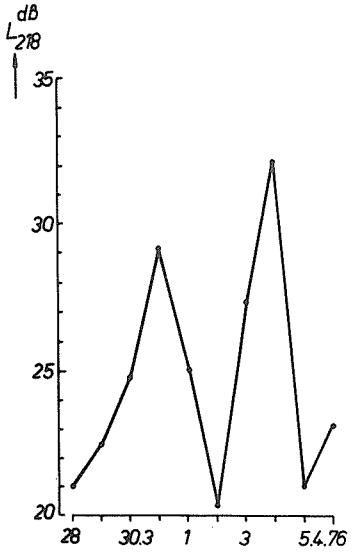

30 March 1976

Fig. 7a. Average daily variation of absorption L_{218} (path No. 7).

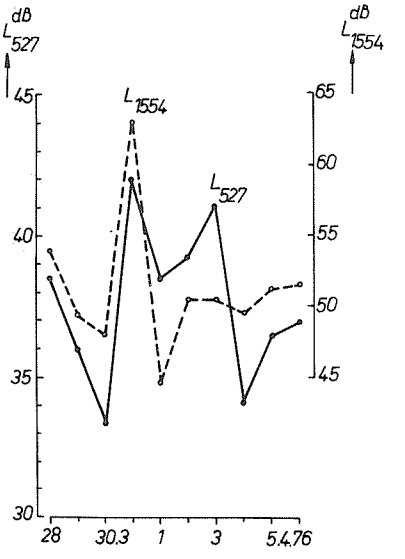

5 April 1976

Fig. 7b. Average daily variation of absorption L_{527} and L_{1554} (paths No. 8 and 10).

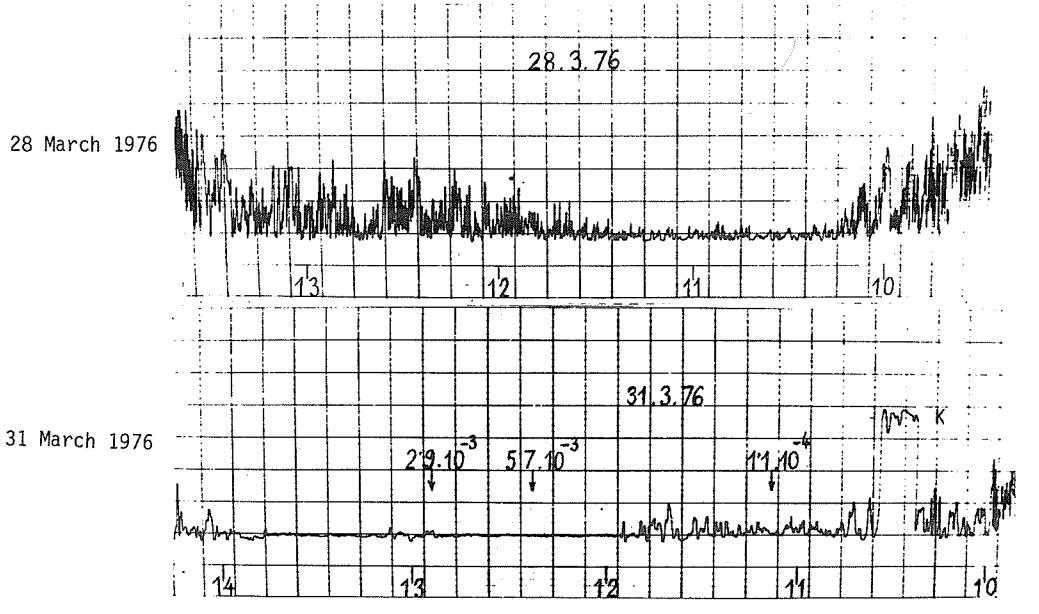

Fig. 8. 28 and 31 March 1976 records from Roburent for 1554 kHz and 80 km (path No. 10).

3. SSC of 1 April 1976

The geomagnetic storm that began with a sudden commencement at 0255 UT on 1 April 1976 was connected with energetic particle precipitation in the high atmosphere; the daytime ionospheric anomalies provide indirect evidence of these effects.

As seeen in Figure 7a, an aftereffect along path No. 7 appears with a high absorption on 4 April 1976, 3 days after the SSC. At medium wavelengths (path No. 8) the excessive absorption appears on the second day after the SSC (Figure 7b) -- a result known from another study by the author [1972].

The absorption effects at short wavelengths are illustrated in Figure 9 (path No. 11). On the day of the storm the absorption maximizes with an aftereffect occurring on 4 April 1976. Here the following question may be asked: Why on 1 April 1976 (A_p = 107) does the SSC have a strong absorption effect, and none on 26 March 1976 (A_p = 138)? Figure 10, displaying foF2 and h'F2 data from the Sofia ionosonde, contains the answer. The geomagnetic storm of 26 March 1976 is not connected with a negative foF2 effect, though h'F2 is slightly increased. On the contrary, the storm of 1 April 1976 has a strong negative effect in foF2 and a large increase in h'F2. Both parameters have, as a consequence, lead to a strong increase in absorption for frequencies near foF2. The plotted points are the means for each day from 0600 to 1500 UT; the upper part of Figure 10 gives the Ap variation during the period under investigation.

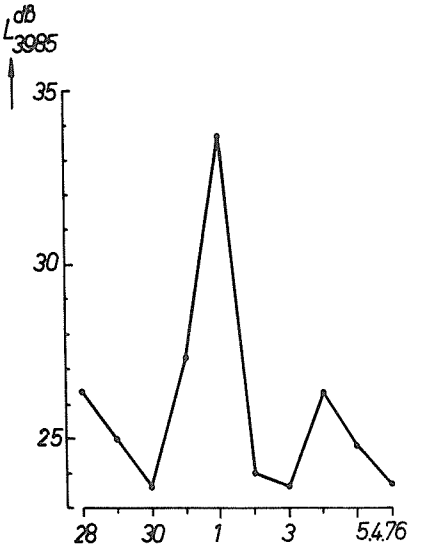

5 April 1976

Fig. 9. Average daily variation of absorption L_{3985} (path No. 11).

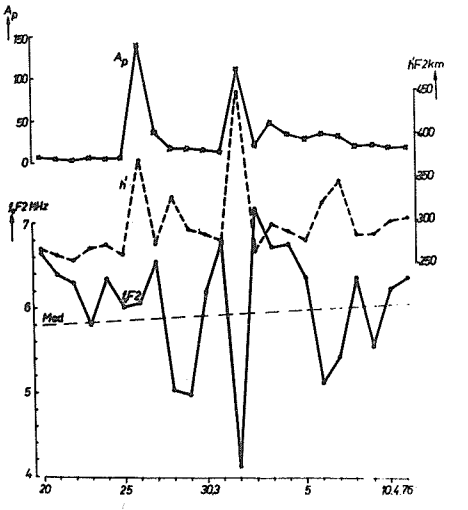

10 April 1976

Fig. 10. Average daily variation of the foF2 and h'F2 at Sofia and the A_p index.

It is of interest to compare the absorption behavior at very low frequencies with the response of the cosmic ray intensity (CR) during the Forbush effect at the end of March and the beginning of April. Figure 11 gives the trends in 3-day running means of the L_{155} and L_{164} absorption and the Kiel CR. It is evident that some relationship with a phase difference of a few days exists between the VLF ionospheric absorption and the CR. Velinov *et al.* [1969] have identified the geomagnetic field as the source of the absorption behavior, and Nestorov [1977] has established the reality of the connection between the VLF absorption and the CR.

4. 30 April to 3 May 1976 Events

Significant ionospheric effects at medium and short wavelengths were observed in this period. Figure 12 presents the L_{527} results (path No. 8) for $\cos(\chi)$ = 0.1 = const. A weak maximum is seen on 1 May 1976 and a strong L effect on 3 and 4 May 1976. For path No. 10 the L effect is weaker. The SID effect on path No. 10 on 30 April 1976 (Figure 13) confirms statements of section 1: the event appears at a zenith angle of 36° yielding an effective flux of $I_{R(\chi)}$ ($\leq 8\text{Å}$) = 2.4×10^{-3} ergs $cm^{-2}s^{-1}$ and the signal absorption is too high. In other words this solar X-ray flux determines the D region ionization under a height of 95 km.

Although weaker, some absorption effects are observed at short wavelengths as well (Figure 14). Here L_{6155} results are presented with a maximum absorption on 4 May 1976 and a weaker aftereffect peak on 6 May 1976.

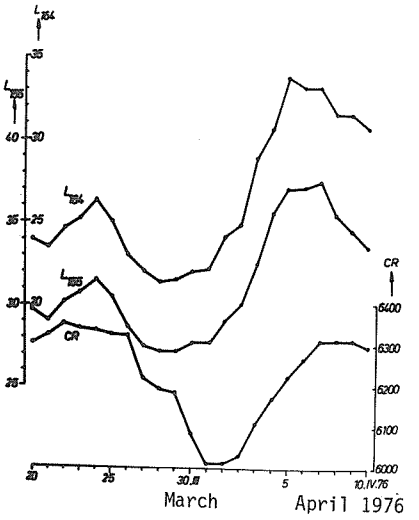

Fig. 11. Three-day running mean values of absorption L_{155} and L_{164} (paths Nos. 1 and 2) and cosmic ray intensity at Kiel.

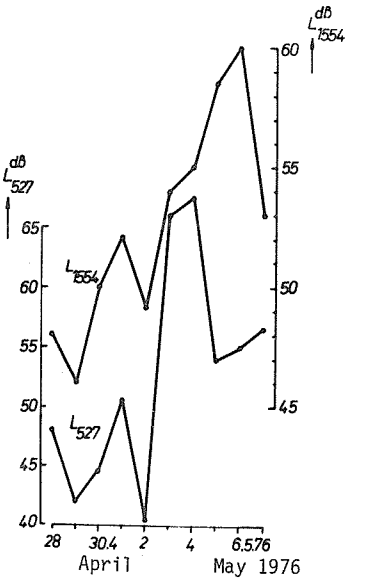

Fig. 12. Average daily variation of absorption L_{527} and L_{1554} (paths No. 8 and 10).

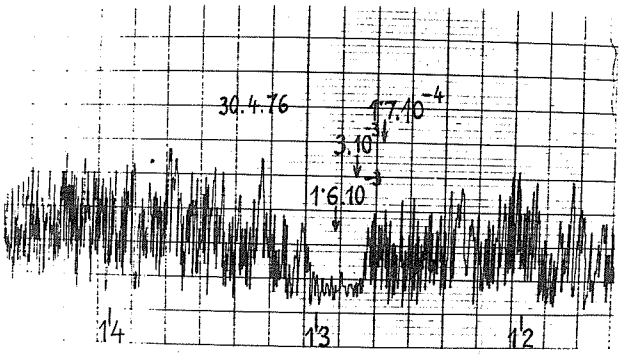

Fig. 13. 30 April 1976 record from Roburent for 1554 kHz and 80 km (path No. 10).

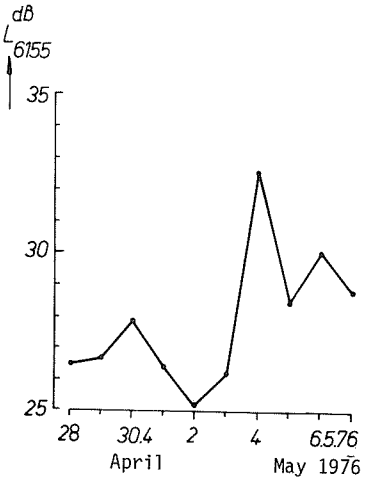

Fig. 14. Average daily variation of absorption L_{6155} (path No. 12).

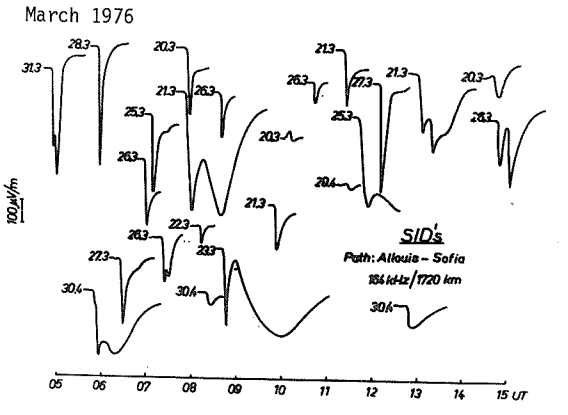

Fig. 15. SID records from Sofia for 164 kHz and 1720 km (path No. 1). On the left is the amplitude scale: 0.5 cm = 100 μV/m.

5. SIDs at Low Frequency for the Whole Period

In the whole Retrospective World Interval 25 SID effects at long wavelengths were recorded along paths No. 1 - 5. The most representative effects were those along path No. 1. These are drawn in Figure 15 where the amplitude scale is at left: 0.5 cm = 100 μV/m. Again the great sensitivity of this path as an indicator of heliophysical processes [Letfus and Nestorov, 1973] was confirmed. Table 2 was compiled for SIDs of importance 2 or greater. It illustrates the decrease in height (Δh) of the reflection region at the maximum of the SID effect. This tabulation was prepared from phase-height measurements on paths No. 3, 4 and 5. The electron concentration N_{min} in the reflection region varied within the boundaries 500 to 1500 cm^{-3}, depending on the frequency and the decrease Δh.

Table 2. SIDs of Importance 2 or Greater

Date 1976	Start UT	Max. UT	Dur. min	Imp.	Δh km
March 20	0750	0755	20	2	3.7
21	0755	0815	90	3+	9.5
21	1115	1118	18	2	3.9
21	1248	1306	72	2	3.8
23	0839	0856	130	3+	11.6
25	1136	1200	140	3+	10.0
26	0720	0724	20	3	5.8
26	1441	1449	35	2	4.0
27	0627	0631	40	2	3.6
27	1202	1212	30	3	6.2
28	0554	0601	20	3	7.5
April 30	0550	0607	90	2	3.5

REFERENCES

LETFUS, V. and G. NESTOROV 1973 Representability of the SID-Effects Observed by Different Methods, *Bull. Astron. Inst. Czech.*, *24*, 191.

NESTOROV, G. 1965 Mindestnotwendige Elektronendichte für die Reflexion von der ionosphärische D-Region, *C.R. Ac. Bulg. Sc.*, *18*, 631.

NESTOROV, G. 1972 Absorption in the Nighttime Lower Ionosphere as an Indicator for the Ionization Processes under Normal Conditions and Disturbances, *Geom. and Aeron.*, *12*, 33.

NESTOROV, G. 1975 Contribution of Solar X-Rays to Ionization of D-Region, *Compt. rend. Acad. Bulg. Sci.*, *28*, 1609.

NESTOROV, G. 1977 Signal Variations of LF-Radio Waves in Sunspot Cycle, *J. Atm. Terr. Phys.*, in press.

SGD 1976 *Solar-Geophysical Data, 380 Part I*, p. 28, April 1976, U.S. Department of Commerce, (Boulder, Colorado, U.S.A. 80302).

VELINOV, P., L. DORMAN and G. NESTOROV 1969 Influence of Forbush-Effects on Cosmic Ray-Layer in the Lower Ionosphere, *Geom. and Aeron.*, *9*, 813.

HF Doppler Observations Associated With McMath Regions 14143 and 14179

by

T. Ichinose
Department of Electronics
Doshisha University
Kyoto, Japan

and

T. Ogawa
Ionosphere Research Laboratory
Kyoto University
Kyoto, Japan

Figures 1-4 show SFDs observed on the 5 and 10 MHz signals of the standard frequency transmissions by the oblique HF Doppler technique. Propagation paths between the transmitters at JJY, WWVH, and BPV and the receiver at Doshisha University were used.

Figures 1 and 2 show SFDs correlated with a sudden commencement geomagnetic storm. In Figure 1, ionospheric disturbances have been observed on the 10 MHz wave reflected by the F layer. The trace of the SFD primarily shows a positive deviation followed by a negative peak and a slow recovery. The 5 MHz wave reflected by the E layer shows the influence of the storm sudden commencement. The SFD in Figure 2 shows only a gradual negative deviation.

Figures 3 and 4 show SFDs correlated with X-ray enhancement. In Figure 3, an SFD has been observed before sunset on the 5 MHz signal reflected by the E layer. The SFD data of Figure 4 show the condition of the ionosphere to be comparatively disturbed on both signals. In these data, particularly, SFDs caused by the solar flare have started at about 2103 UT; on the 5 MHz signal the weak absorption in the vicinity of 2115 UT may have been caused by the enhanced ionization in the D layer. The notation A, B and C shows the start, positive peak, and negative peak times of the Doppler shifts.

Table 1 gives the amplitude and the start and peak times of the SFDs shown in Figures 1-4.

Table 1. SFDs Observed at Kyoto

Date (1976)	Start(A) (UT)	Peak(B) (Positive) (UT)	Peak(C) (Negative) (UT)	Amplitude (Positive peak) (Hz)	Frequency (MHz)
March 23	0840.4	0841.0	0842.3	0.2	5
March 26	-	-	0232.5	-	10
April 1	0255.5	-	0257.8	1.0	10
April 30	2103.2	2103.5	2104.9	0.3	5

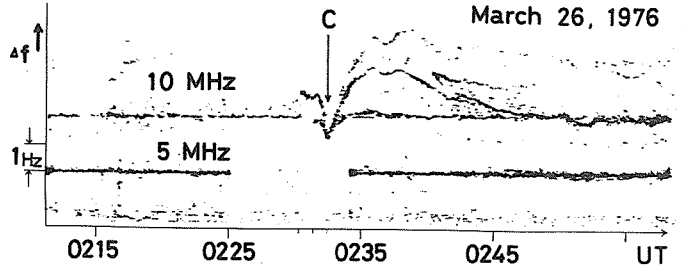

Fig. 1. SFDs associated with the geomagnetic storm beginning at 0231 UT. C marks the negative peak time.

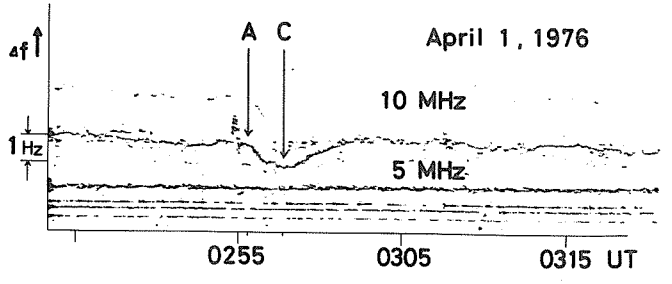

Fig. 2. SFDs associated with the geomagnetic storm beginning at 0254 UT. A and C mark the start and negative peak times.

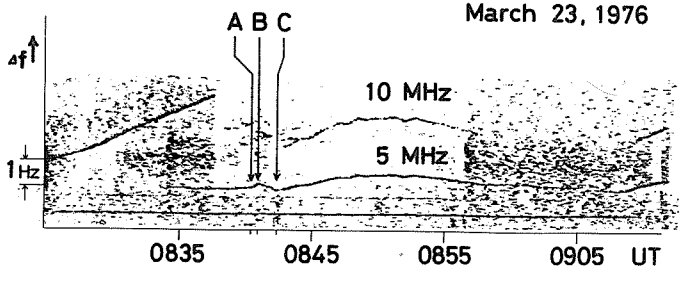

Fig. 3. SFDs associated with the SB flare at 0837 UT. A, B, and C mark the start, positive peak, and negative peak times.

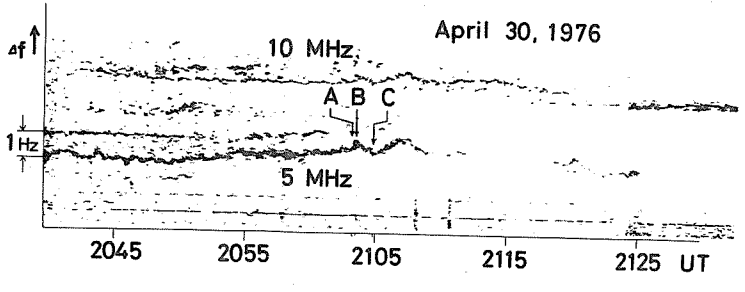

Fig. 4. SFDs associated with the 1B flare at 2047 UT. A, B, and C mark the start, positive peak, and negative peak times.

Solar Energy Particles During April - May 1976

by

A. I. Gusev and L. A. Eskova
Cosmophysical Observatory of the North-East Complex
Research Institute, Schmidt Cape, Magadan Region, USSR

Figure 1 of this paper presents hourly values for the variation of the minimum frequencies of reflection from the ionosphere (fmin) in MHz and also a diagram showing variations of cosmic radio noise absorption intensity at the frequency of 32 and 40 MHz (in dB) counted for the first minute of the hour.

The geographic and geomagnetic coordinates for Cape Schmidt are: ϕ = 68°55', λ = 179°29'W, ϕ_M = 62.70°, λ_M = 227.11°. Data are plotted against Universal Time. The antenna for the 40 MHz riometer is directed towards the north geographic pole, while the antenna for the 32 MHz riometer is directed towards the zenith.

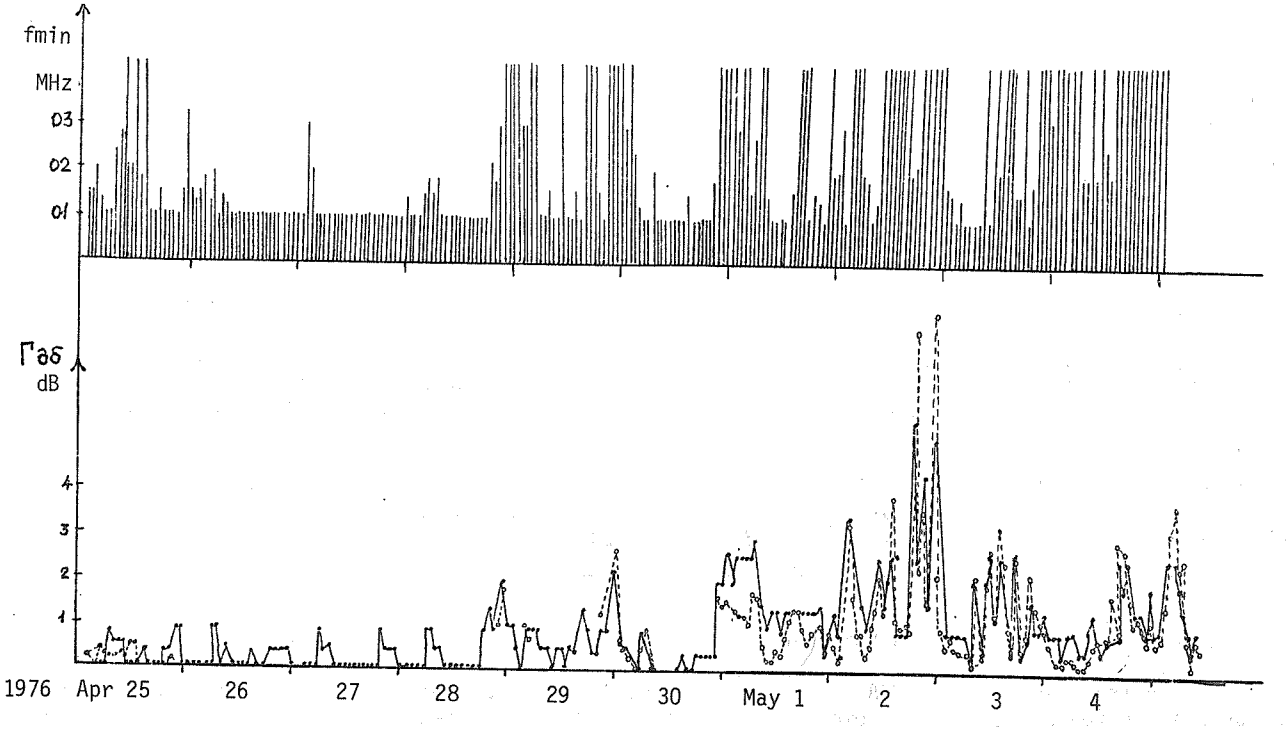

Fig. 1. Cape Schmidt hourly fmin values in MHz and cosmic radio noise absorption in dB for 40 MHz (solid line) and 32 MHz (dashed line) for the period 25 April to 4 May 1976.

Polar Cap Absorption Event of 30 April - 3 May 1976 by the Riometer Data at the Soviet Arctic and Antarctic Stations

by

V. M. Driatsky, V. A. Ulyev, A. V. Shirochkov
The Arctic and Antarctic Research Institute
Leningrad USSR

The present study is a preliminary analysis of the PCA event which occurred on 30 April - 3 May 1976 and was recorded by riometers at the Soviet Arctic and Antarctic stations. This analysis interprets some absorption variation effects during the PCA event. The PCA variations observed at the North Pole-22 drifting station, Heiss Island, Dixon Island, Cape Zhelaniya, Amderma, Molodezhnaya and Mirny stations are given in Figure 1. This figure also includes fmin variations for two stations where no absorption data are available (Salekhard and Vostok stations), and geomagnetic Kp index changes over the period considered. In addition Figure 1 shows the time of the SSC impulse and the solar flare believed responsible for the analyzed PCA event. Some data necessary for the analysis are summarized in Table 1.

Table 1. Soviet Arctic and Antarctic Station Information.

Station	Geographic Position Latitude	Long. East	Corrected Geomag. Lat.	Solar Zenith Angle at Flare Time	PCA Data Time (UT) Onset	Max	End	Max Value (dB)
North Pole 22	83°40'N	218°41'	81.2°	79°	30 Apr 2200	30 Apr 2300	3 May 0500	5.0
Heiss Island	80 37	58 03	73.8	85	30 Apr 2130	30 Apr 2330	3 May 0500	5.8
Cape Zhelaniya	76 57	68 35	70.3	88	30 Apr 2125	30 Apr 2330	2-3 May	4.8
Dixon Island	73 30	80 24	67.2	88	30 Apr 2125	30 Apr 2330	2-3 May	5.3
Amderma	69 46	61 41	63.9	105	30 Apr 2125	30 Apr 2330	2-3 May	3.0
Salekhard	66 32	66 32	61.0	108				
Molodezhnaya	67°46'S	45°51'	67.6°	128°	1 May 0400	1 May 0700	2 May	2.4
Mirny	66 33	93 01	76.8	120	1 May 0400	1 May 0700	2 May	2.4
Vostok	78 28	106 48	84.3	109				

The General Character of the PCA Variation

As seen from Figure 1 the PCA profile (at the stations of the Northern Hemisphere) has the following characteristic features: sudden commencement, rapid increase to the maximum value, well-defined maximum and gradual exponential decrease. On the whole such variation is typical of the PCA attributed to flares occurring on the western side of the solar disk. It reflects the diffusive character of the solar cosmic rays propagation in space.

It is rather unusual for the amplitude variations of the PCA of this kind to have a very sharp peak; it appears to be similar to the absorption burst induced by the flare shockwave protons. But this burst is probably different because no characteristics of a shockwave onset are observed, such as a SSC impulse, geomagnetic Kp value increase, or Forbush effect in cosmic rays variations. Thus, this absorption burst probably is caused by electrons ejected at the time of the flare.

The Sudden Cosmic Noise Absorption Effect (SCNA)

The SCNA effect is evident before the onset of a PCA event if 1) the flare occurs on the visible part of the solar disk and 2) the sun's zenith angle at the time of the flare at the observation site is less than 90°.

In the analyzed PCA event the first condition is fulfilled because this PCA is attributed to the flare occurring on the visible side of the solar disk ($\lambda = 47°$). The second condition according to the calculation of zenith angles (cf. Table 1), is observed only for the NP-22, Heiss Island, Cape Zhelaniya and Dixon Island stations. The analysis of these records indicates that only the Heiss Island and Dixon Island riometers measured SCNA effects on 30 April.

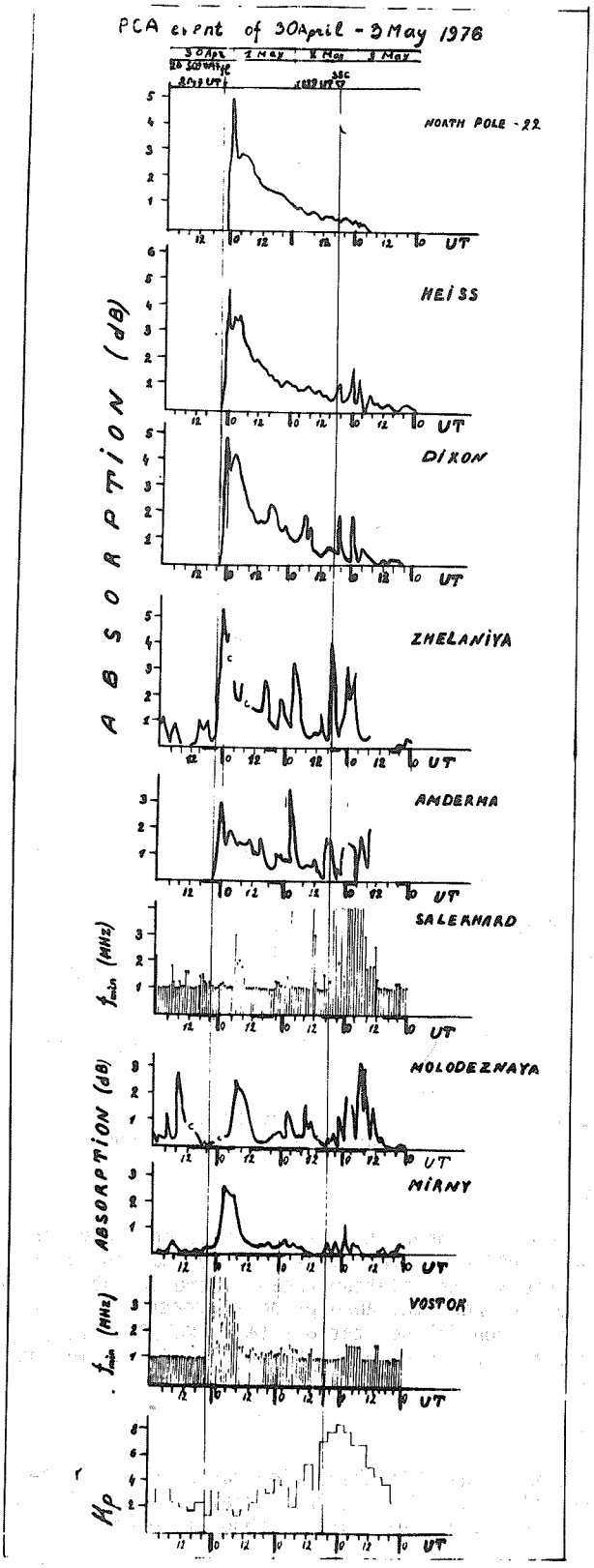

Fig. 1. Variations in the PCA, fmin, and geomagnetic index Kp during the period 30 April - 3 May 1976.

The Day/Night Variation Effect

The shaded areas on the time axis in Figure 1 indicate periods when the sun's zenith angle for the corresponding site exceeded 90°. At the stations of the Northern Hemisphere (Dixon Island, Amderma), where the dark period continued for a shorter interval, the day/night variation effect was weak (Figure 1). This effect is responsible for a small absorption decrease in the PCA variations at both stations on 1 May at about 1800 UT. This effect on 2 May could be obscured by the auroral absorption significantly exceeding the PCA residual absorption value.

At the stations of the Southern Hemisphere (Molodezhnaya, Mirny) the day/night effect was more evident, first because they registered the PCA 3 to 4 hours after onset when the sun was above the horizon, and second because on 1 May absorption during the last 12 hours of the day was found to be significantly lower than it should be when there is no day/night variation effect. This effect on other days is doubtful because of small PCA and large auroral absorption values.

On the basis of the given absorption variations at the stations of the Southern Hemisphere (Molodezhnaya, Mirny) two quantitative characteristics of this effect were calculated: the ratio of the daytime absorption to that of the nighttime (K = A day/A night) and the duration difference of the absorption increase and decrease periods (ΔT = T increase - T decrease). The obtained K and ΔT values are within the normal range [Driatsky, 1974].

The Midday Recovery Effect

The analysis of the absorption variations at the auroral zone stations (Dixon Island, Amderma, Molodezhnaya) where the midday recovery effect might be observed shows no midday recovery effect recorded in the analyzed PCA event. This agrees with the data given in Ulyev [1977], where it is shown that the midday recovery effects normally are not observed in the PCA events attributed to flares on the western side of the solar disk.

The Sudden Commencement Absorption Effect (SCA)

According to our data (cf. Figure 1) the effect was evident in the analyzed PCA event. Actually soon after the SSC impulse a short-time absorption enhancement was recorded at all stations. As is usually observed, its amplitude increased with decreasing latitude of the observation site.

The Effect of the PCA Region Expansion During the Main Phase of the Magnetic Storm

Absorption variations of Figure 1 do not allow us to reveal the effect in the considered PCA event. On the one hand we do not have data on absorption variations at the more southern stations (such as Salekhard) where this effect is most pronounced. On the other hand the auroral absorption bursts occurring after the onset of magnetic storm (after the impulse) obscure any possible PCA increase at other stations in the auroral zone (Dixon Island, Amderma).

One can draw some conclusions on the basis of the temporal variations at Salekhard. Prior to the magnetic storm onset all fmin values were within the normal range, that is, proton fluxes of solar cosmic rays did not reach the latitude of Salekhard station. After the magnetic storm onset the fmin values sharply increased. This is probably associated with the appearance of protons over Salekhard, but one should not exclude the possibility that this increase might be caused by auroral electrons.

The PCA Latitudinal Structure

The comparatively small number of observation sites gives only a general idea of the latitudinal PCA structure. Judging from the absorption maximum values at the stations of the Northern Hemisphere, this structure is composed of two regions: the plateau region where the absorption is approximately equal ($A \approx 5.3$dB) and the decrease region where the absorption decreases with the decreasing latitude. The NP-22, Heiss Island, Cape Zhelaniya and Dixon Island stations (ϕ' = N67.2 -N81.2) are within the plateau region. The decrease region begins at latitudes between the Dixon Island and Amderma stations and ends approximately at the Salekhard station latitude (ϕ' = N61.0 -N67.2).

The Asymmetry Absorption Effect

To verify this effect from the available absorption variations recorded at the stations in the center of the Polar Cap (NP-22, Heiss Island and Mirny), the variations at NP-22 station (ϕ' = N81.2) and Mirny station (ϕ' = S76.8) were selected because the auroral absorption at these stations was less pronounced than at Heiss Island.

Compare the absorption values at these stations on 1 May over the period 0400 - 0800 UT. Only during this period did the ionosphere over both sites have similar light conditions (daytime) and sufficiently large absorption values ($A \geq 2$ dB).

The comparison shows the absorption at NP-22 and Mirny stations to be nearly equal during the period considered, that is, the asymmetry effect was not present. The absence of this effect is probably associated with the proton fluxes in space being isotropic - a normal condition during the declining phase of a PCA event.

Conclusions

The analysis of the absorption variations at a number of high-latitude riometer stations during the PCA event of 30 April - 3 May 1976 shows the following:

1) The general character of absorption variations is typical of the PCA events attributed to solar cosmic ray fluxes which propagate diffusively in space.

2) Such effects as day/night variation, Sudden Cosmic Noise Absorption (SCNA), Sudden Commencement Absorption (SCA), polar plateau in latitudinal structure were evident in the absorption variations; morphological features of these effects for the analyzed PCA event are similar to those for other PCA events.

3) The asymmetry absorption and midday recovery effects were not observed in the analyzed PCA event.

4) It is possible that during the analyzed PCA event the effect of PCA equatorial boundary expansion during the main phase of magnetic storm was present, but to identify this effect additional data are needed.

REFERENCES

DRIATSKY, V. M. 1974 Nature of Anomalous Absorption of Cosmic Radio Emission in Lower Ionosphere of High Latitudes, *Gidrometeoizdat*, 224.

ULYEV, V. A. 1977 Relation of Midday Recovery Effect Onset During PCA to Flare Solar Longitude, *Trudy AANII, 350*, in press.

Riometer, Magnetometer, and VLF Ionosonde Data From the Polar Cap 21 March - 8 May 1976

by

J. P. Turtle, J. E. Rasmussen, E. A. Lewis
VLF/ULF Techniques Branch
Electromagnetic Sciences Division
Deputy for Electronic Technology
Rome Air Development Center
Hanscom AFB, MA 01731

Introduction

To study the reflectivity of the polar ionosphere to very low frequency radio waves, the U. S. Air Force is operating a high resolution VLF/LF pulse ionosonde [Lewis *et al.*, 1973; Kossey *et al.*, 1974] at Thule AFB in northern Greenland. Data from this ionosonde are being used as part of a program to determine the reliability and accuracy of low frequency communication, navigation, and detection systems in the Arctic. This program has operated continuously at Thule since late 1974. For interpretation a 30 MHz riometer, a 3-axis fluxgate magnetometer, and long path VLF receivers are also operated. Information from these instruments for the period 21 March (day 81) - 8 May (day 129) 1976, the "Retrospective World Interval", is shown in Figures 1 - 8. Data similar to those presented here have already been published [Rasmussen *et al.*, 1977] and are available from RADC/ETEE.

PCA Event

A discussion of the entire period is given in the last section, but since the most significant event during the period was the PCA disturbance of 30 April (day 121), it will be discussed first. Figure 1, parts A - F, show the data for 7 days, starting about 1 day before the PCA event. The curve shown in part A of this figure gives 30 MHz riometer data, normalized for the quiet day curve. The scale shows departures from the quiet day curve in dB. The negative spike at the beginning of the event (about 2100 UT) indicates a strong solar radio burst. The absorption which followed immediately reached a peak of about 2.8 dB and then slowly recovered over a period of about 3 days. Part B presents the magnitude of the horizontal component of the geomagnetic field, showing variations beginning about 1200 UT on 2 May that indicate a magnetic storm. The phase and amplitude of long path signals from the 18.6 kHz station, NLK (Jim Creek, Washington), are shown in parts C and D, respectively. While the phase shows no large change, there was an amplitude decrease from the normal diurnal pattern when the riometer absorption increased. The data shown in parts A, B, C and D are 10-min averages of data sampled every 30 seconds.

The transmissions from the VLF/LF short pulse ionosonde at Thule AFB are received 106 km north at Qanaq, Greenland. A "3-dimensional" presentation of the received waveforms is shown in Figure 1, part E, for the PCA period and for an undisturbed reference period. The large pulse along the left sides of these plots is the ground wave signal, while the ionospherically reflected (sky wave) signal is the weaker, time-delayed, pulse to the right. Coincident with the increase in riometer absorption, the apparent VLF reflection height dropped nearly 20 km (from about 75 km to 57 km) and then slowly recovered, resuming the normal diurnal pattern after about 4 days. Since the solar zenith angle (part F) was less than 90° during the period, the ionosphere was sunlit 24 hours per day.

Records for the Entire Period

Figures 2 - 8 present data derived from these measurements for the entire period, week by week. Part A of each figure shows the 30 MHz riometer signal, uncorrected for the quiet day curve, with a decrease in the dB scale corresponding to an increase in ionospheric absorption. Parts B, C and D show the magnetometer and long path VLF data on the same scales as in Figure 1. The ionosonde waveforms are given in part G, and basic parameters derived from these data are shown in parts E and F. Part E shows the apparent reflection height curve for 16 kHz and an "undisturbed" reference profile for comparison. Part F gives the 16 kHz $_{\parallel}R_{\parallel}$ reflection coefficient [Lewis *et al.*, 1973] along with its reference curve. Part H shows the solar zenith angle curve for the indicated midweek period.

Except for the PCA period previously described, neither the VLF propagation data nor the riometer data showed any significant effects of enhanced ionospheric absorption. There was, however, a noticeable increase in magnetic activity on 26 March lasting about 2 weeks.

REFERENCES

KOSSEY, P. A., J. E. RASMUSSEN and E. A. LEWIS — 1974 — VLF Pulse Ionosonder Measurements of the Reflection Properties of the Lower Ionosphere, *Akademie Verlag*, COSPAR, July.

LEWIS, E. A., J. E. RASMUSSEN and P. A. KOSSEY — 1973 — Measurements of Ionospheric Reflectivity from 6 to 35 kHz, *J. Geophys. Res.*, *78*, 19.

RASMUSSEN, J. E., J. P. TURTLE, R. P. PAGLIARULO and W. I. KLEMETTI — 1977 — VLF/LF Reflectivity of the Polar Ionosphere, 4 January - 3 July 1976, RADC TR-77-68.

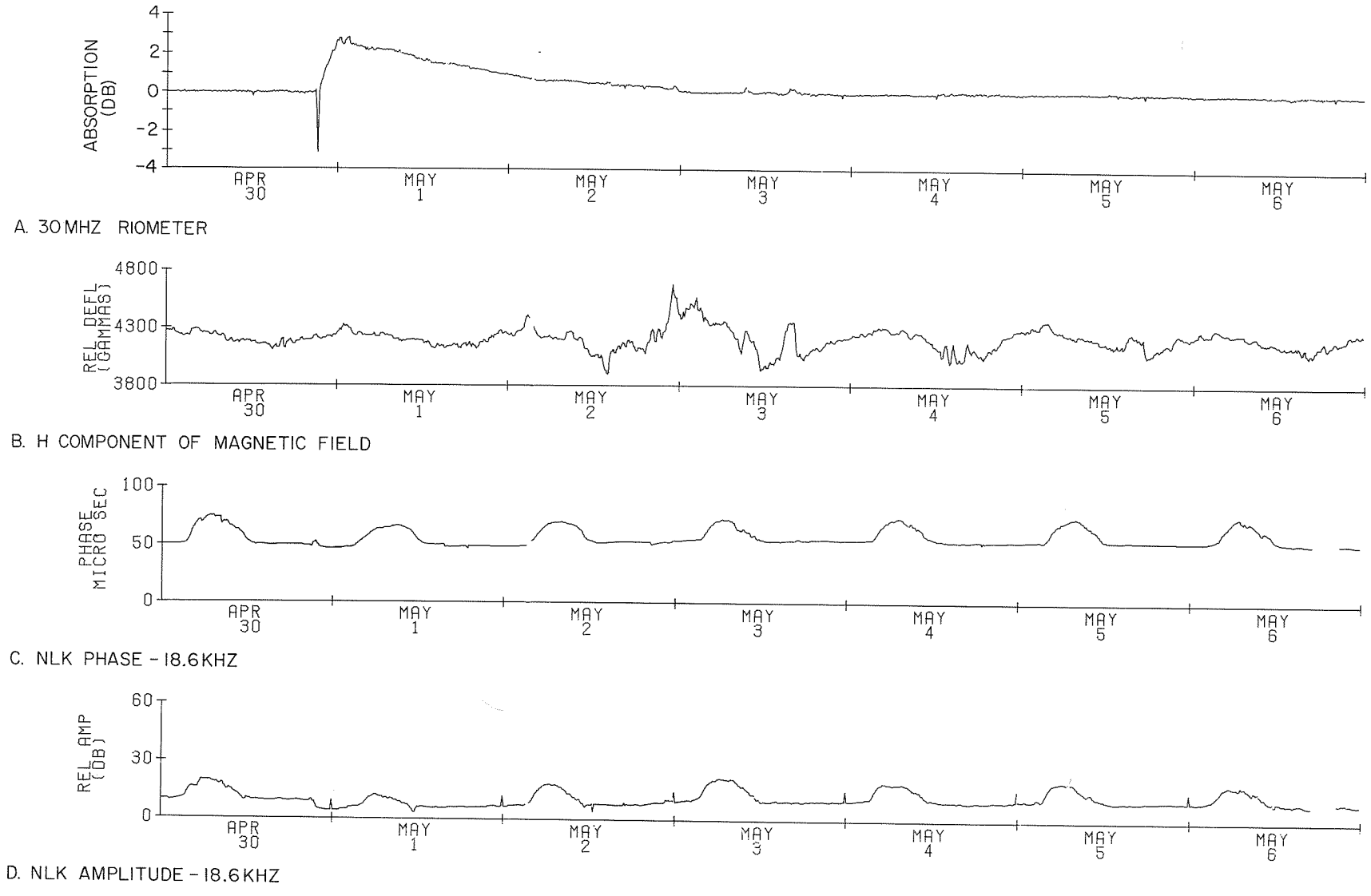

Fig. 1. Observations made during the 30 April 1976 PCA event: (A) Thule 30 MHz riometer trace normalized for the quiet day curve and presented as departures from it in dB, (B) horizontal component of the geomagnetic field, (C) and (D) phase and amplitude of the 18.6 kHz station, NLK, in Jim Creek, Washington.

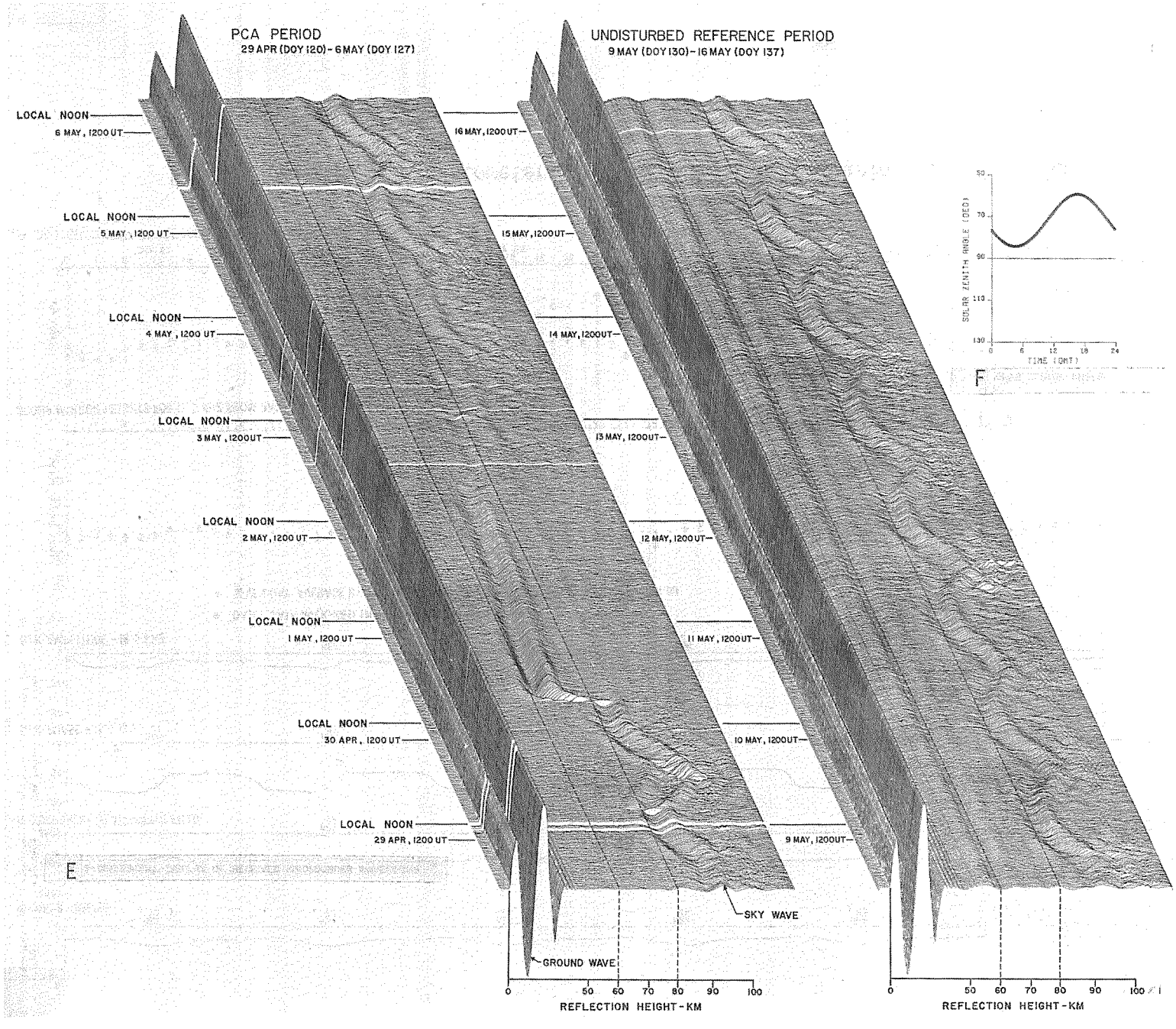

Fig. 1. (Continued). (E) Three-dimensional display of received ionosonde waveforms during the PCA period and an undisturbed reference period and (F) solar zenith angle.

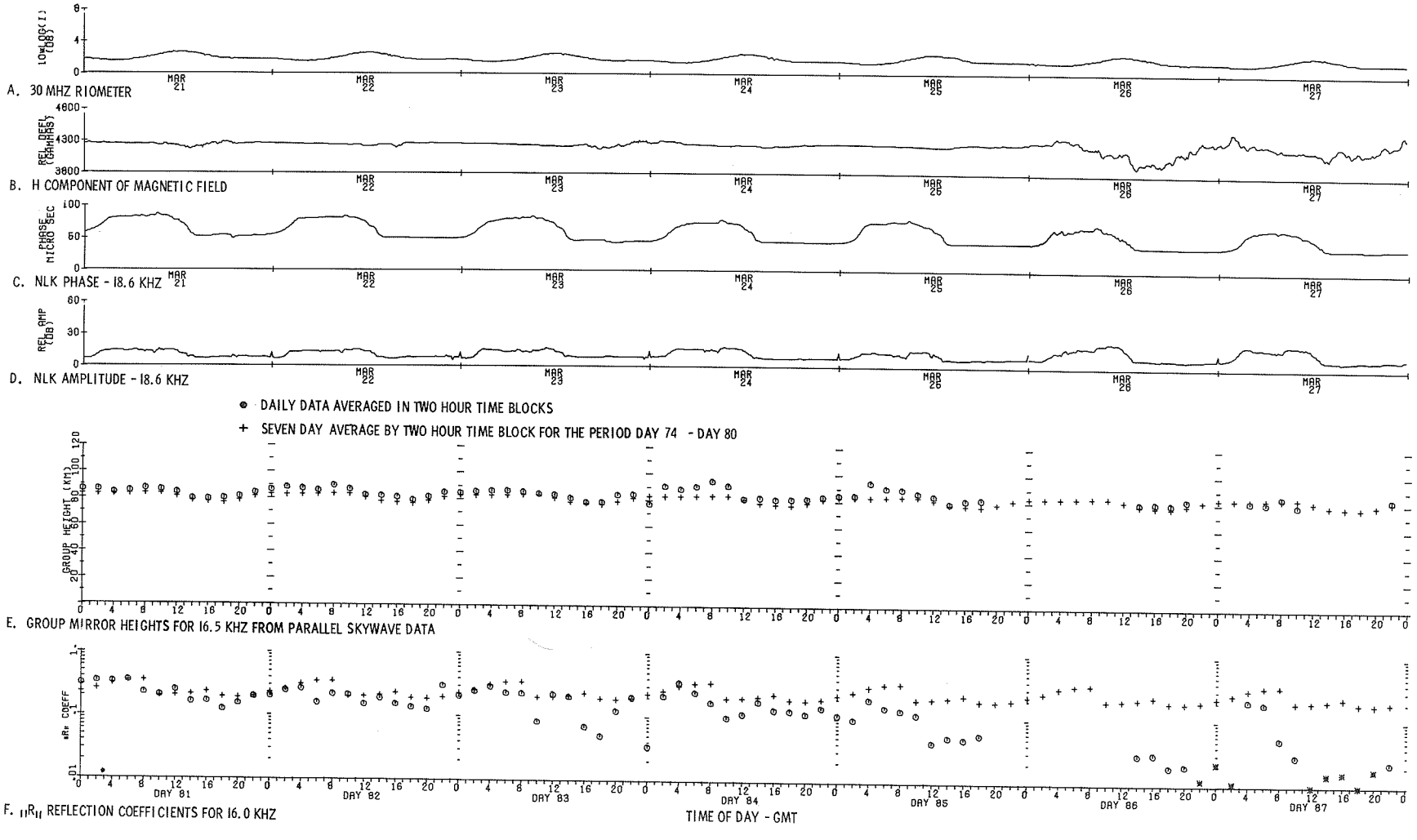

Fig. 2. Riometer, magnetometer, and VLF data for the period 21 - 27 March 1976.

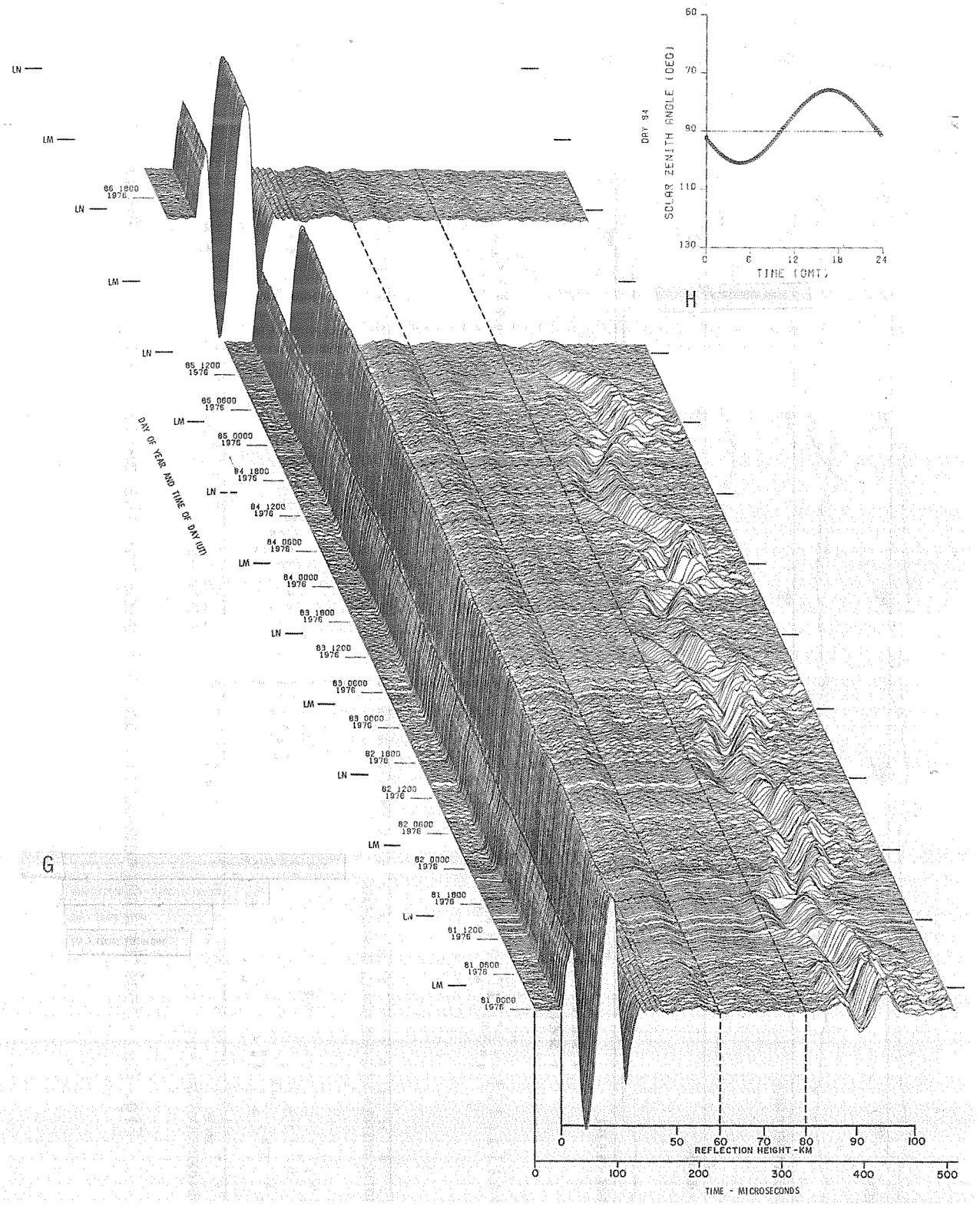

Fig. 2. (Continued). Three-dimensional display of received ionosonde waveforms during the period 21 (day 81) - 27 (day 87) March 1976 and solar zenith angle for 24 (day 84) March 1976. LN = Local Noon; LM = Local Midnight.

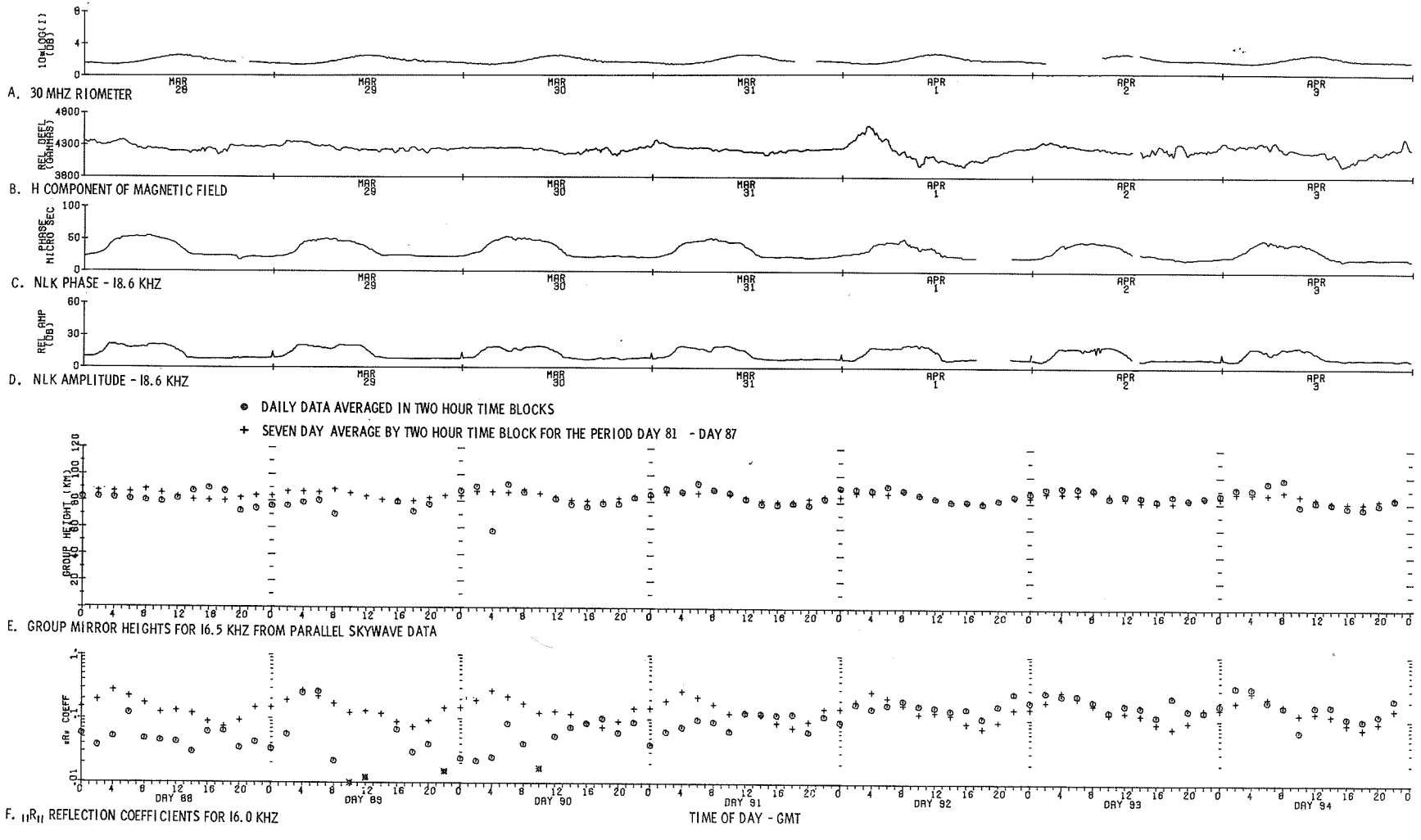

Fig. 3. Riometer, magnetometer, and VLF data for the period 28 March - 3 April 1976.

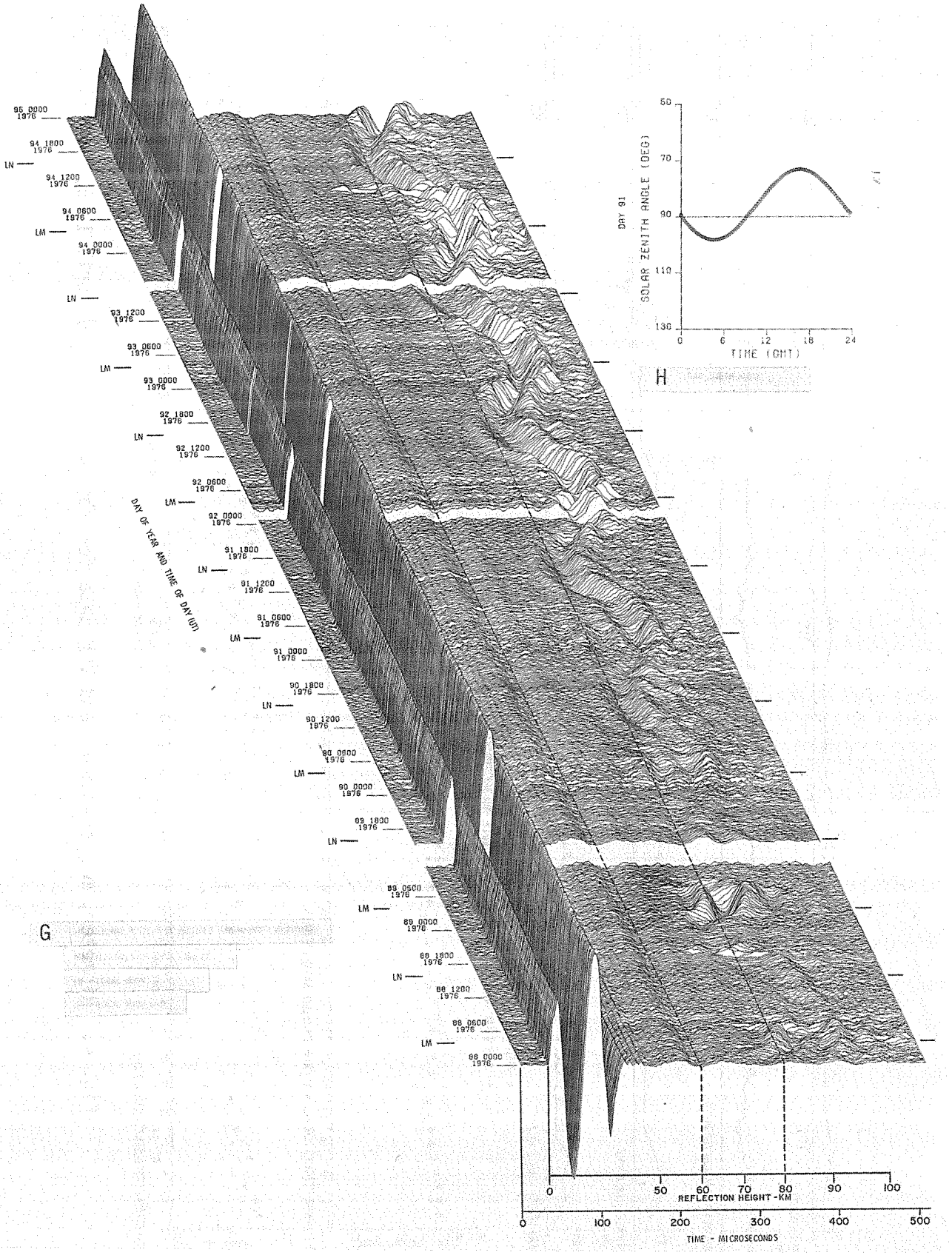

Fig. 3. (Continued). Three-dimensional display of received ionosonde waveforms during the period 28 (day 88) March - 3 (day 94) April 1976 and solar zenith angle for 31 (day 91) March 1976. LN = Local Noon; LM = Local Midnight.

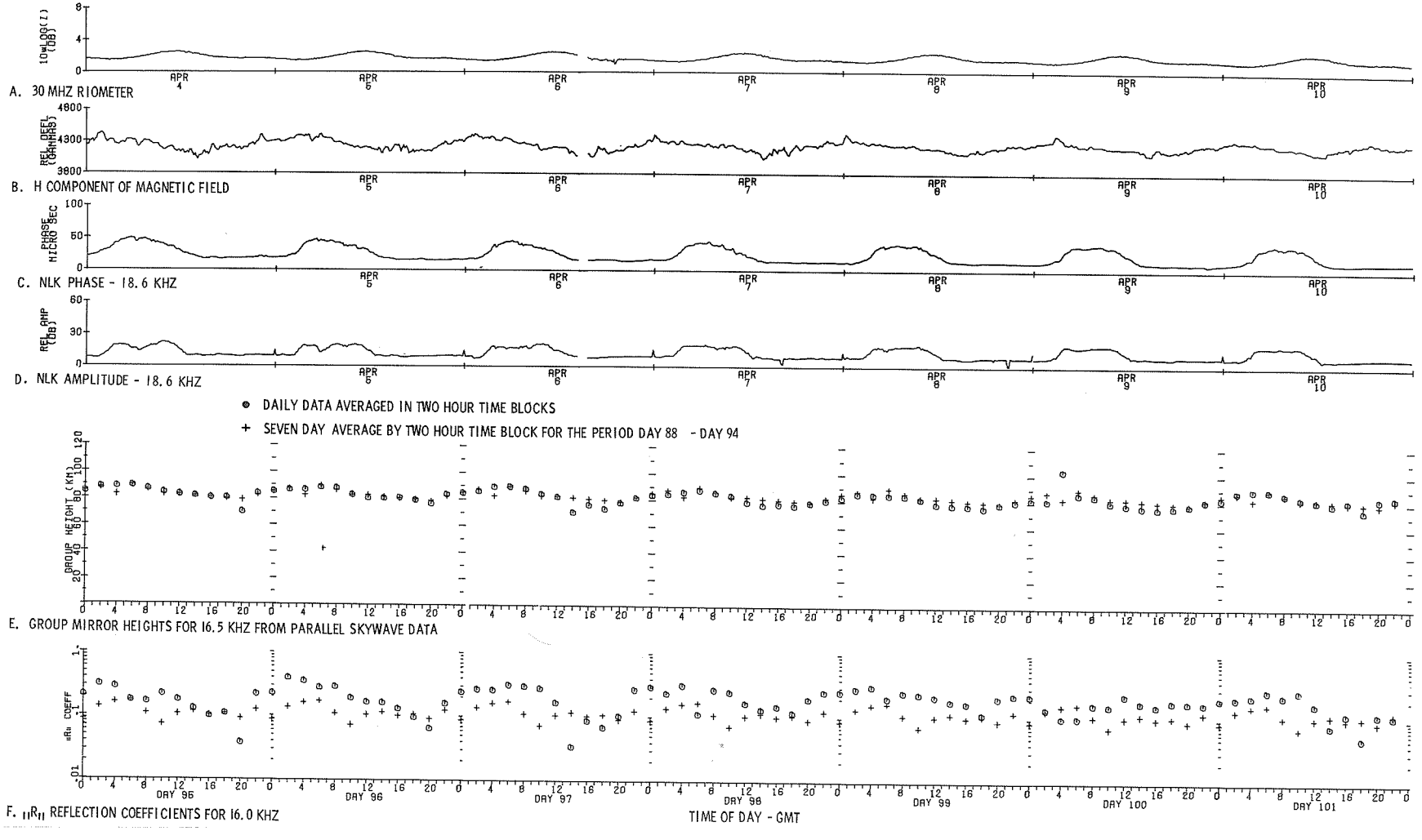

Fig. 4. Riometer, magnetometer, and VLF data for the period 4 - 10 April 1976.

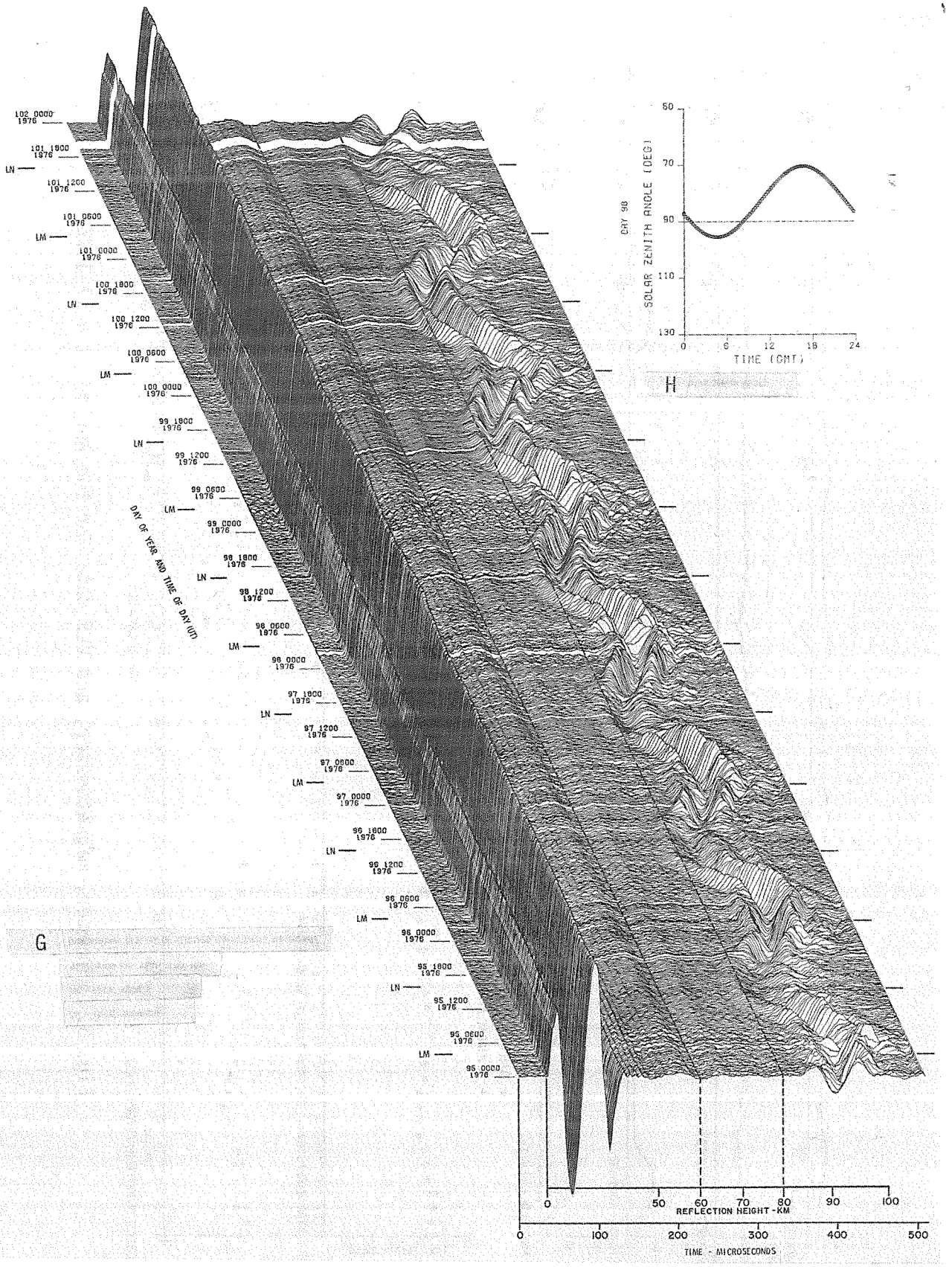

Fig. 4. (Continued). Three-dimensional display of received ionosonde waveforms during the period 4 (day 95) - 10 (day 101) April 1976 and solar zenith angle for 7 (day 98) April 1976. LN = Local Noon; LM = Local Midnight.

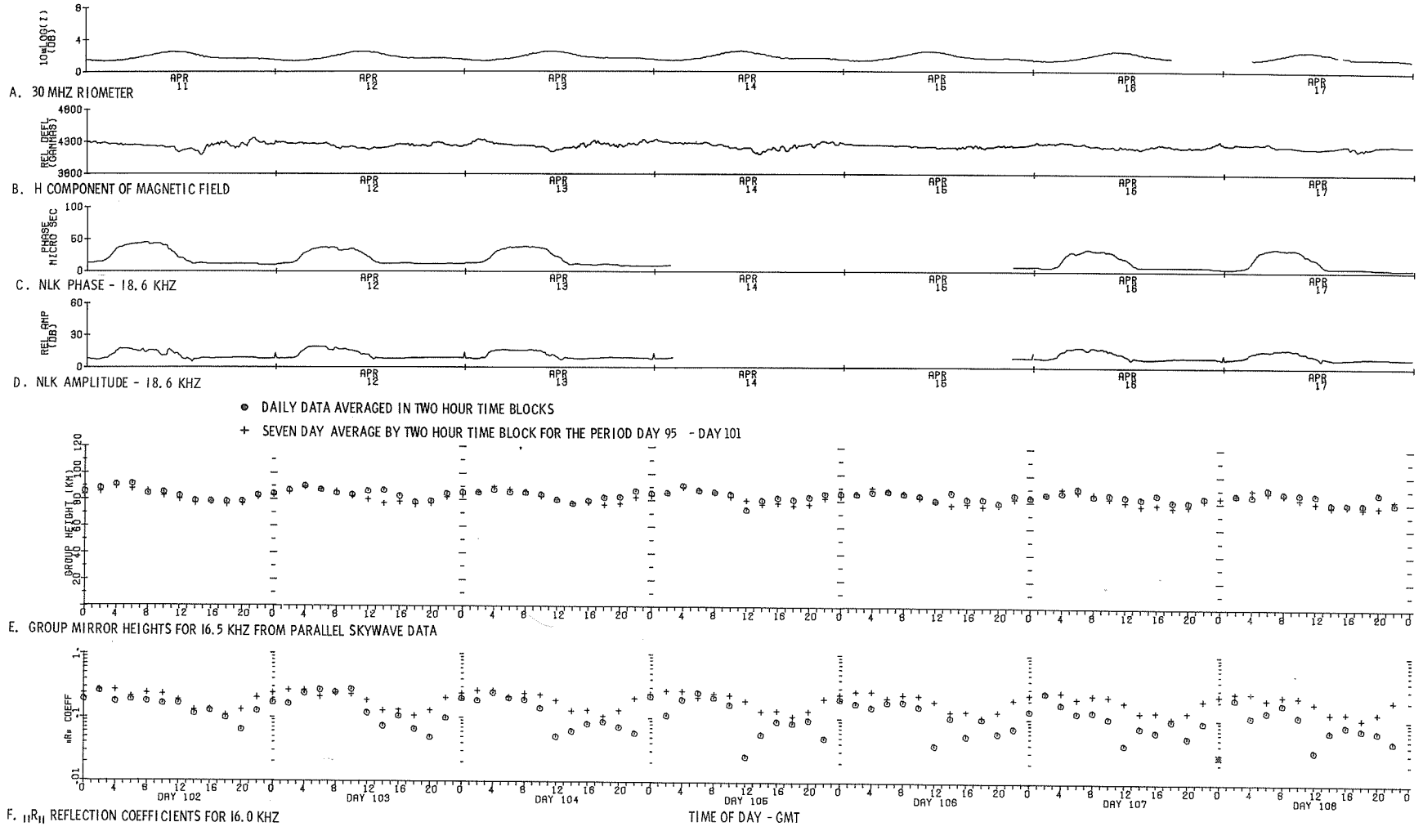

Fig. 5. Riometer, magnetometer, and VLF data for the period 11 - 17 1976.

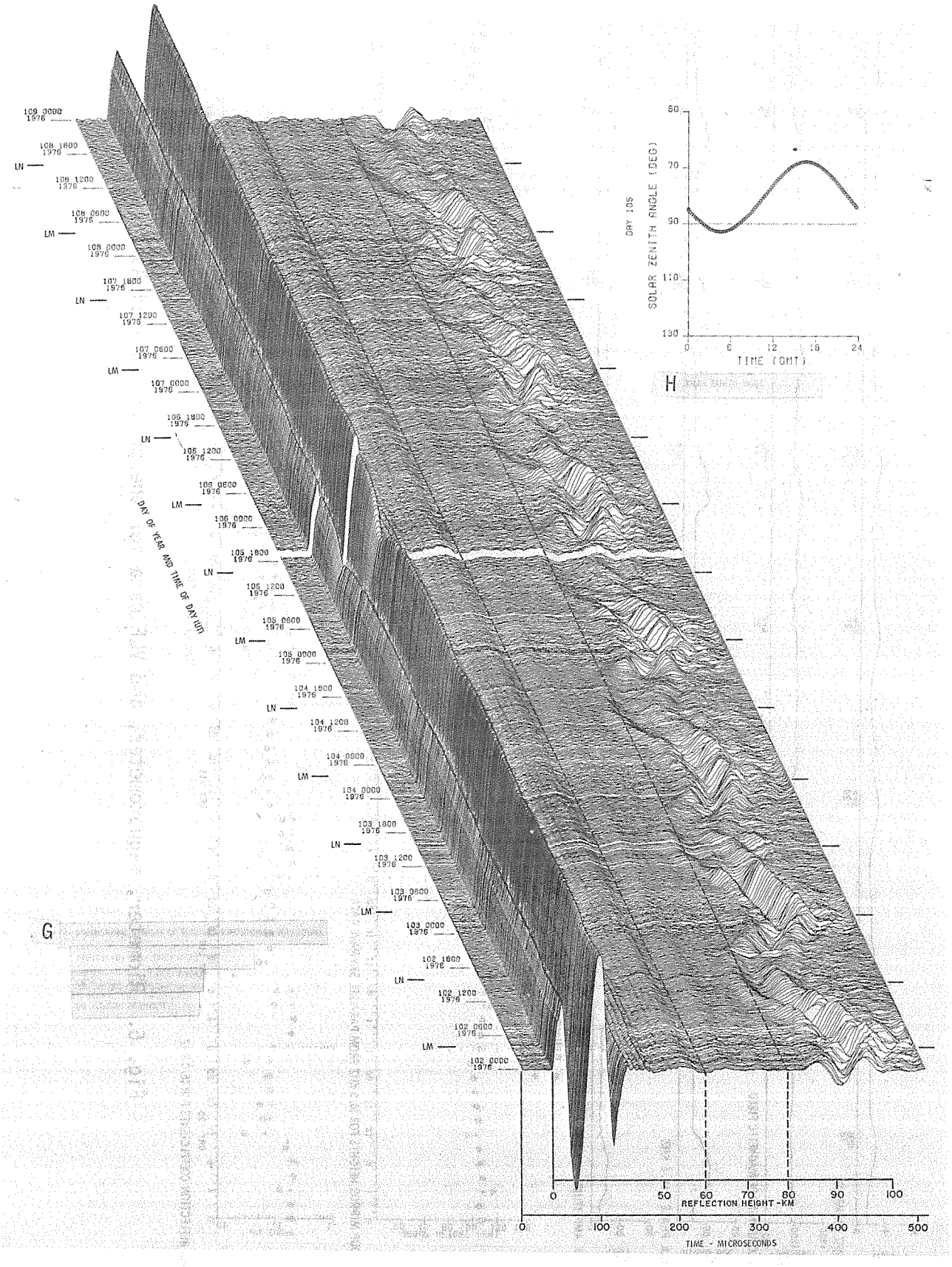

Fig. 5. (Continued). Three-dimensional display of received ionosonde waveforms during the period 11 (day 102) - 17 (day 108) April 1976 and solar zenith angle for 14 (day 105) April 1976. LN = Local Noon; LM = Local Midnight.

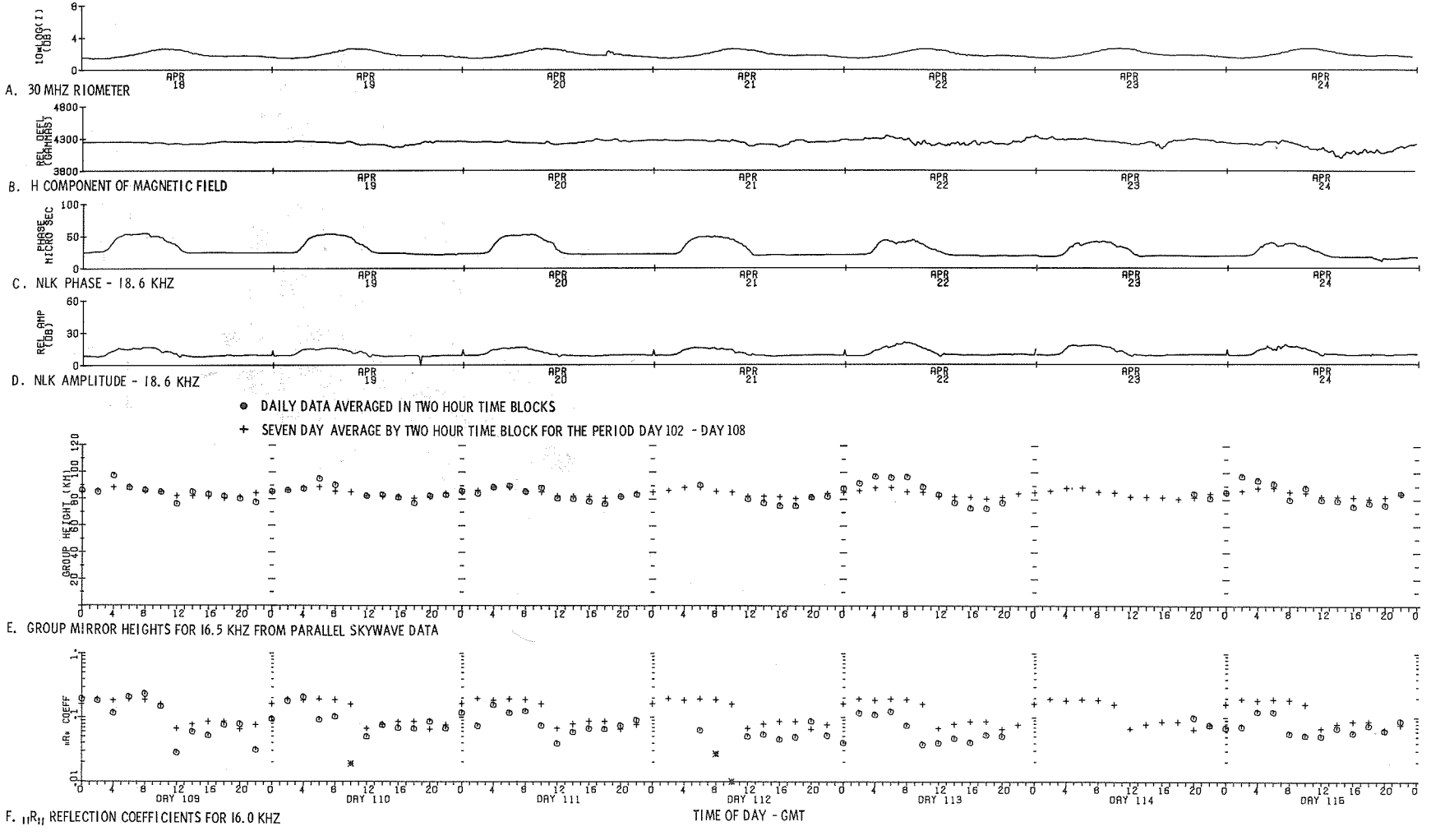

Fig. 6. Riometer, magnetometer, and VLF data for the period 18 - 24 April 1976.

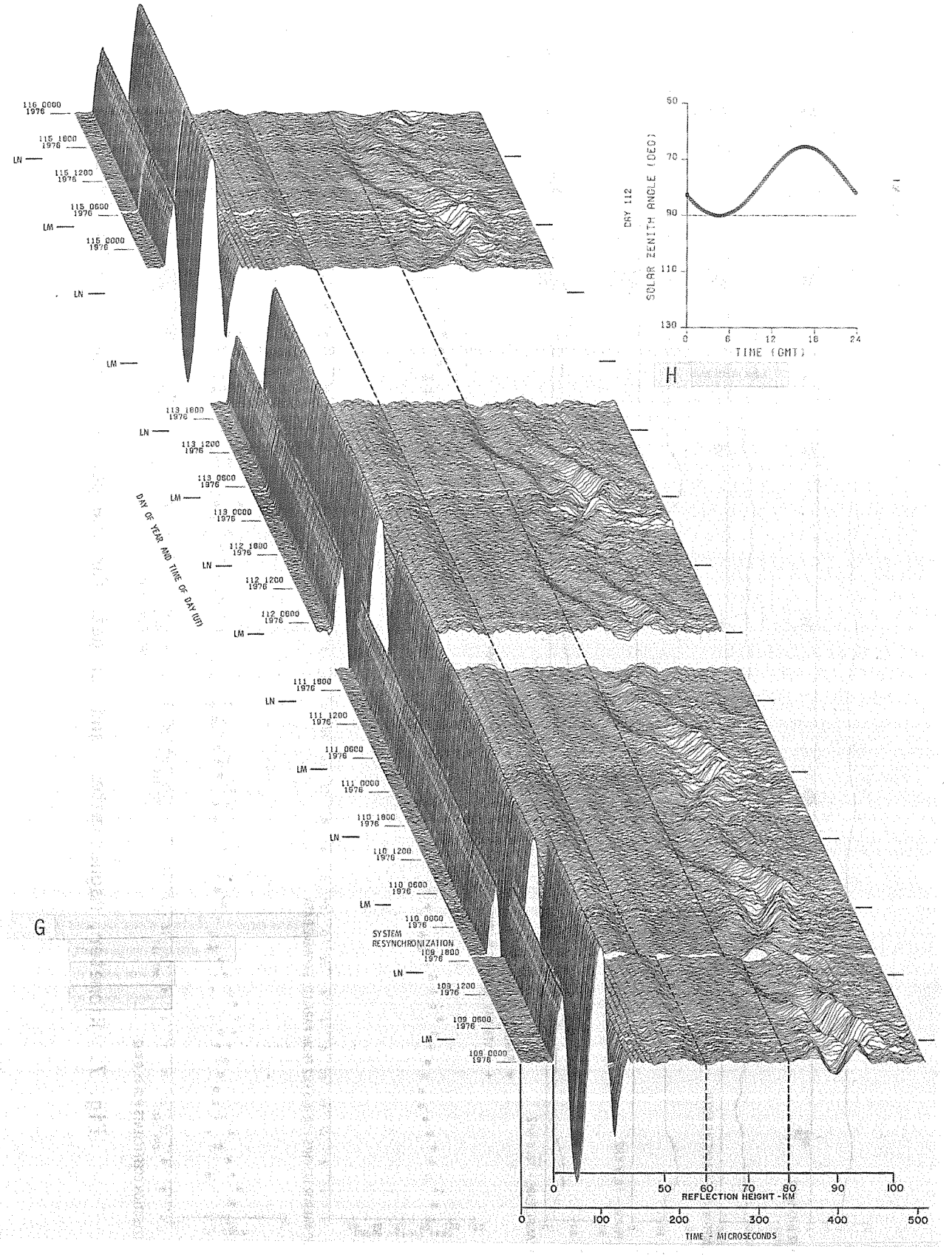

Fig. 6. (Continued). Three-dimensional display of received ionosonde waveforms during the period 18 (day 109) - 24 (day 115) April 1976 and solar zenith angle for 21 (day 112) April 1976. LN = Local Noon; LM = Local Midnight.

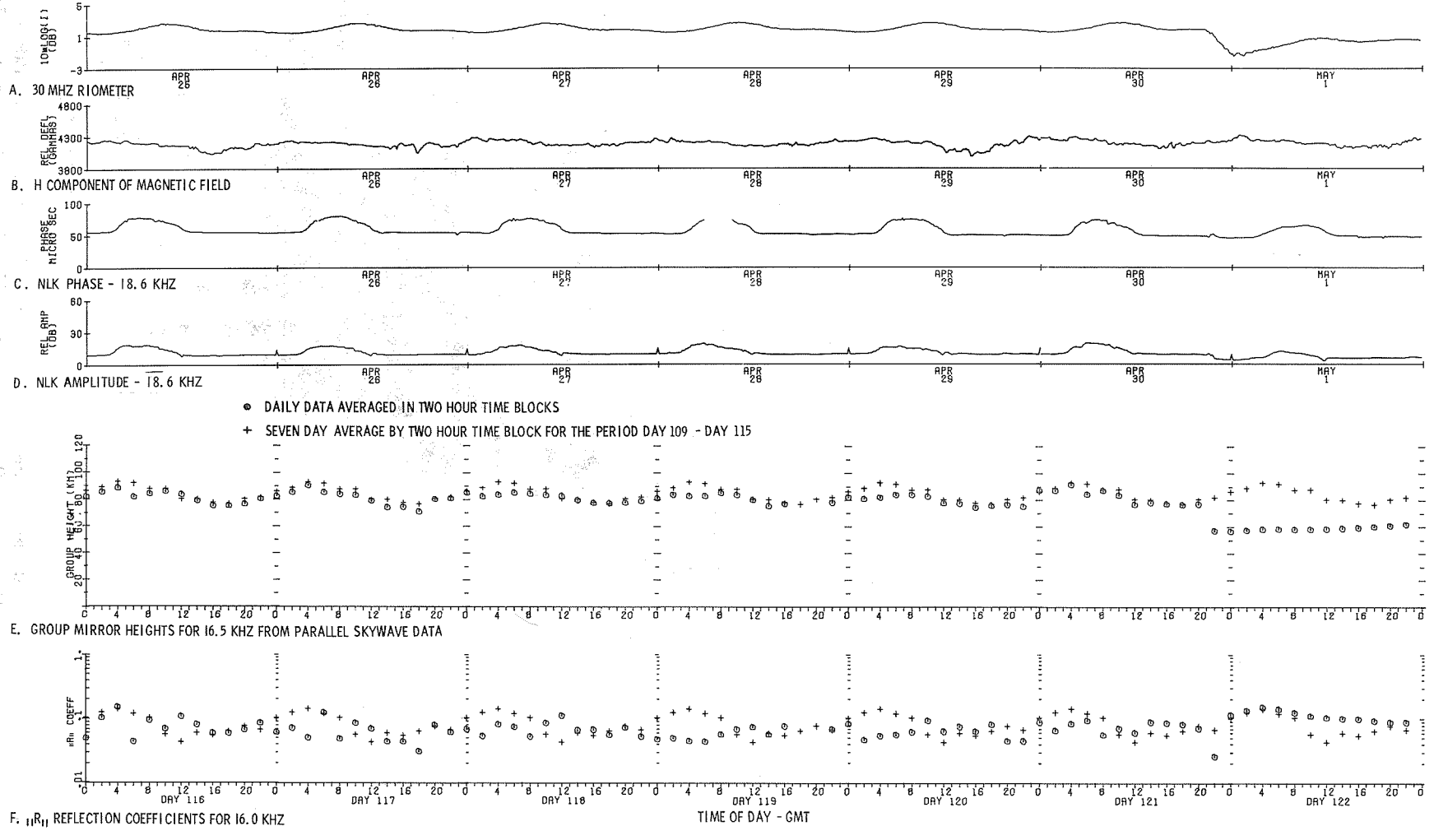

Fig. 7. Riometer, magnetometer, and VLF data for the period 25 April - 1 May 1976.

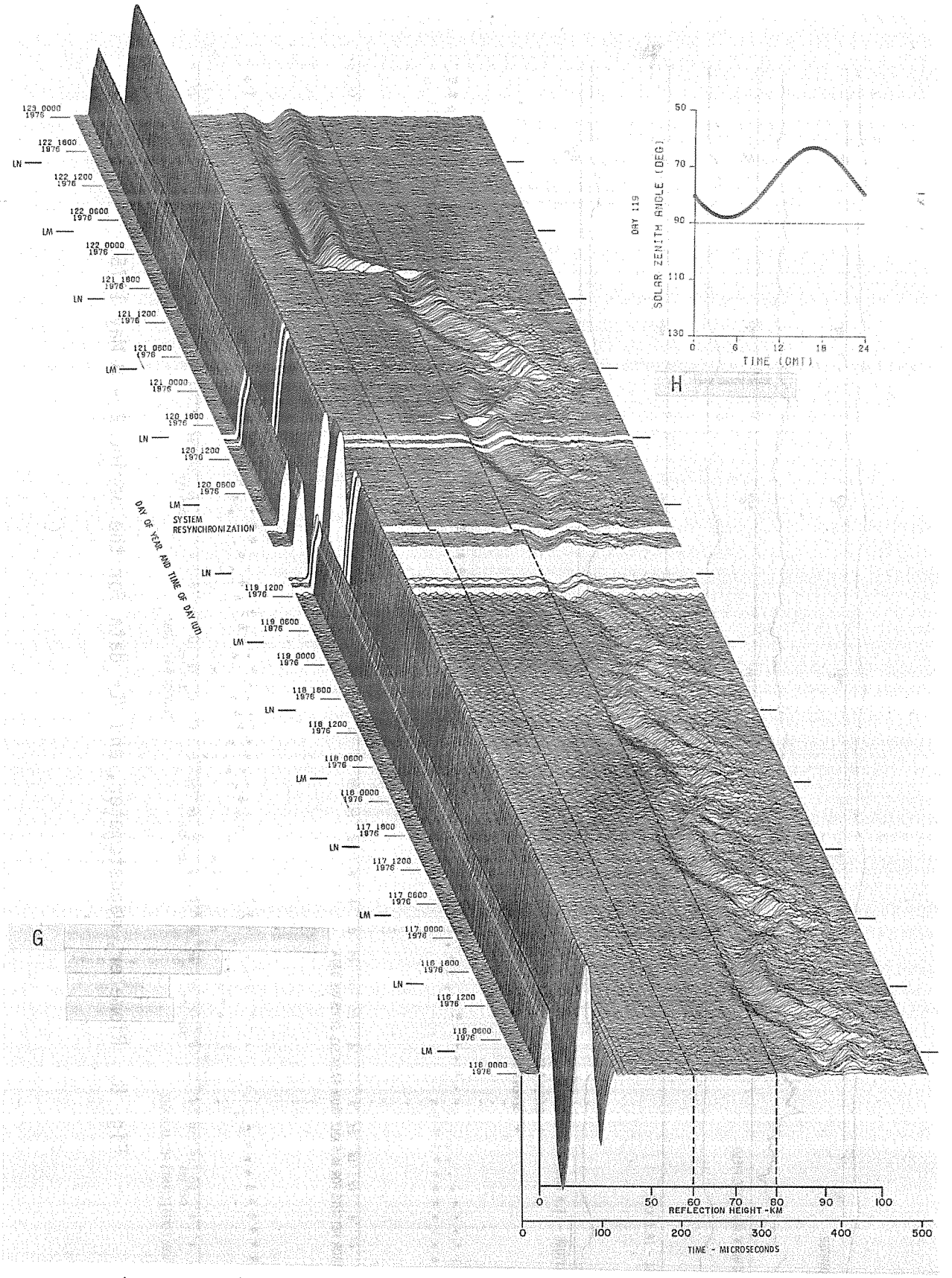

Fig. 7. (Continued). Three-dimensional display of received ionosonde waveforms during the period 25 (day 116) April - 1 (day 122) May 1976 and solar zenith angle for 28 (day 119) April 1976. LN = Local Noon; LM = Local Midnight.

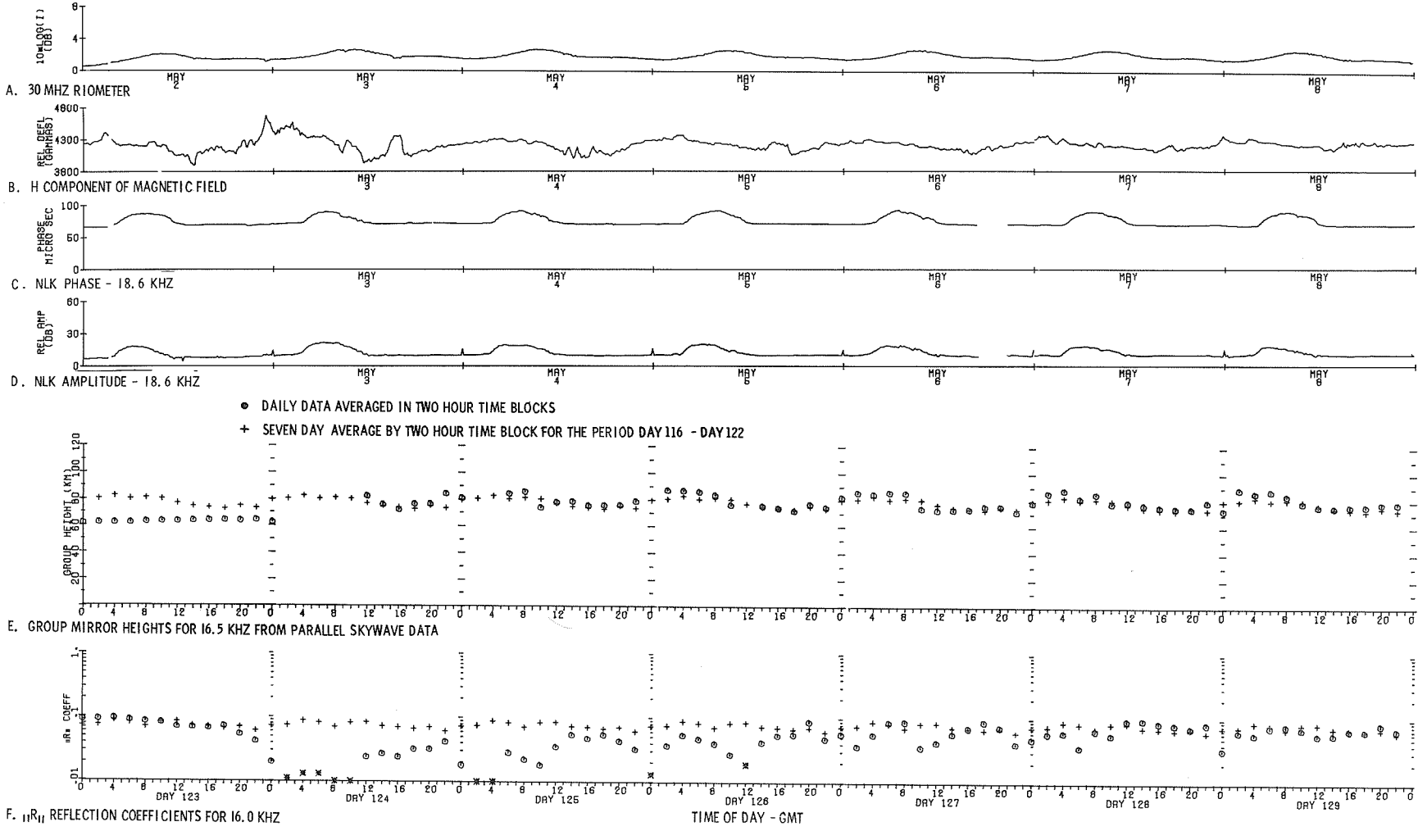

Fig. 8. Riometer, magnetometer, and VLF data for the period 2 - 8 May 1976.

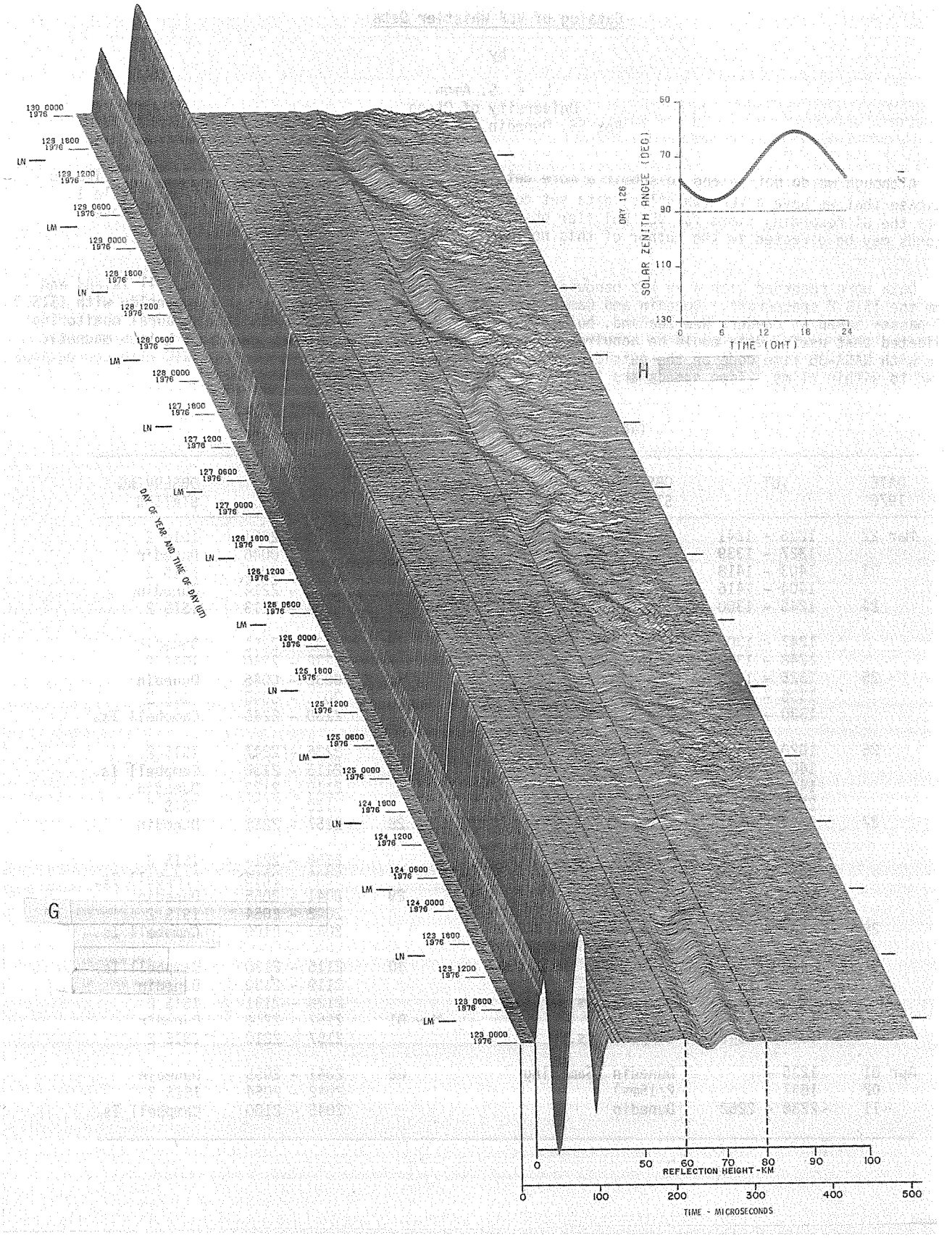

Fig. 8. (Continued). Three-dimensional display of received ionosonde waveforms during the period 2 (day 123) - 8 (day 129) May 1976 and solar zenith angle for 5 (day 126) May 1976. LN = Local Noon; LM = Local Midnight.

Catalog of VLF Whistler Data

by

L. E. S. Amon
University of Otago
Box 56, Dunedin, New Zealand

Although we do not intend to submit a more detailed contribution to this report, we would like to indicate that we have a VLF (Whistler) data set covering the 20 March - 5 May 1976 period. Table 1 lists the UT recording times for VLF Whistler observations in New Zealand. Inquiries about these records may be directed to the author of this note.

Data were recorded with a 16 kHz bandwidth (25 kHz from ISIS 2) at Dunedin and Campbell Island and from the ISIS 2 spacecraft. Dunedin and Campbell Island recordings were scheduled to coincide with ISIS 2 VLF passes taken at Lauder, New Zealand, but extra recordings were made at Dunedin when aural monitoring indicated that useful data could be acquired. Data are recorded on 2-channel, 4-track, ¼ inch magnetic tape with NASA-36 time code on the outside channel. Timing should be within ±5 ms of UTC with corrections known to within ±1 ms. Tape speeds are 3 and 3/4 and 7½ ips.

Table 1. VLF Whistler Observations

DATE 1976	UT	OBSERVING STATION	DATE 1976	UT	OBSERVING STATION
Mar 22	1226 - 1241	Dunedin	Apr 11	2239 - 2251	ISIS 2
	1327 - 1339	ISIS 2	12	0032 - 0046	Dunedin
23	1403 - 1418	Dunedin		0033 - 0045	ISIS 2
	1404 - 1416	ISIS 2	13	2200 - 2214	Dunedin
24	1245 - 1300	Campbell Is.		2201 - 2213	ISIS 2
	1247 - 1302	Dunedin	14	2237 - 2251	Dunedin
	1248 - 1300	ISIS 2		2238 - 2250	ISIS 2
25	1325 - 1340	Dunedin	15	0032 - 0046	Dunedin
	1326 - 1338	ISIS 2		0033 - 0045	ISIS 2
	1330 - 1345	Campbell Is.	26	2230 - 2245	Campbell Is.
26	1020 - 1405	Dunedin		2236 - 2247	ISIS 2
	1400 - 1415	Campbell Is.	27	2115 - 2130	Campbell Is.
	1402 - 1413	ISIS 2		2119 - 2133	Dunedin
	2230 - 0214	Dunedin		2120 - 2131	ISIS 2
27	0217 - 0602	Dunedin	28	2157 - 2211	Dunedin
	0602 - 0947	Dunedin		2158 - 221-	ISIS 2
	0948 - 1333	Dunedin		2200 - 2215	Campbell Is.
	1245 - 1300	Campbell Is.	29	2041 - 2055	Dunedin
	1248 - 1300	ISIS 2		2042 - 2054	ISIS 2
28	0003 - 0348	Dunedin		2045 - 2100	Campbell Is.
	0348 - 0733	Dunedin	30	2115 - 2130	Campbell Is.
	0735 - 1120	Dunedin		2119 - 2130	Dunedin
	0800 - 0815	Campbell Is.		2120 - 2131	ISIS 2
	1325 - 1337	ISIS 2	May 01	2157 - 2211	Dunedin
	1330 - 1345	Campbell Is.		2157 - 2210	ISIS 2
Apr 01	1235 -	Dunedin (Sampling	02	2041 - 2055	Dunedin
02	1637	2/15ms)		2042 - 2054	ISIS 2
11	2238 - 2252	Dunedin		2045 - 2100	Campbell Is.

7. GEOMAGNETISM

Provisional Dst, 7 March - 10 May 1976

by

M. Sugiura
Goddard Space Flight Center
Greenbelt, MD 20771

and

D. J. Poros
Computer Sciences Corporation
Silver Spring, MD 20910

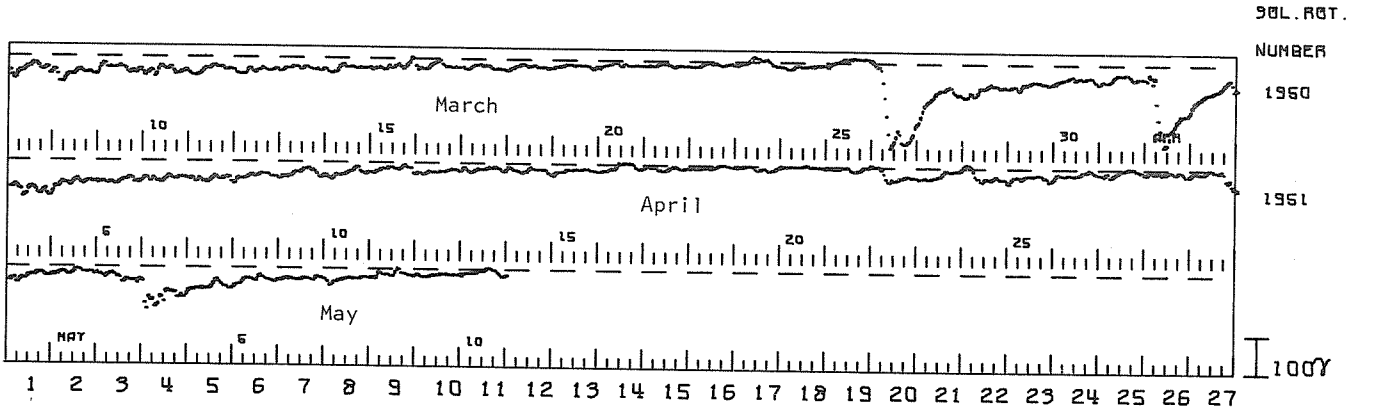

Forecasts of Geomagnetic Activity

by

B. Bednářová-Nováková, J. Halenka, M. Pavluchová and J. Pýcha
Geophysical Inst. Czechoslovak Acad. Sci., Prague, Czechoslovakia

Due to the scarcity of solar observations only a few forecasts could be made. In an attempt to cover as long periods as possible on the basis of isolated observations, data from all solar regions on the eastern hemisphere together with east limb observations had to be used. Thus the resulting forecasts were mostly of a lower degree of reliability. The forecasts were included in Praha Ursigrams under key words ADMAG PRAHA. The messages were as follows:

No. 1. (the second part only): 11(date) 11(hour) geomagnetic disturbance expected on 17 and 18 March (Kpmax around 4 or 5).
No. 2. 1211 geomagnetic disturbance expected on 18 and 19 March (Kpmax around 4).
No. 3. 2910 magnetic disturbance expected on 30 March. Magcalm expected on 31 March. Disturbances expected from 1 to 3 April (Kpmax around 4 or 5).
No. 4. 0108 magnetic disturbance expected from 2 April to 8 April (Kpmax around 4 or 5).
No. 5. 0209 recurr. magn. disturbance is expected to continue on 9 April (Kpmax around 4 or 3).
No. 6. 1413 on 16 April low geomagnetic activity is expected.
No. 7. 1511 after possible enhancement on 17 low activity (Kpmax about 3 or 2) from 18 to 20 expected.
No. 8. 2011 magcalm expected on 20 and 21 April. Magnetic disturbances expected from 21 to 27 April with possible ssc on 22 April.
No. 9. 2707 magcalm possible on 28 and 29 April. From 30 April to 4 May expected disturbances (Kpmax around 4 or 5).
No. 10. 2910 magnetic disturbances expected on 29 and 30 April (Kpmax around 4) and on 5 and 6 May (Kpmax around 3).
No. 11. 0209 geomagnetic disturbances expected from 2 to 9 May.
No. 12. 0508 in the period from 6 May to 10 May fluctuating geomagnetic activity (Kpmax around 4 or 3) expected. Short intervals of magcalm on 5 and 6 May possible.

The forecasts and their evaluation are schematically shown in Table 1. The day of solar observation (coinciding with the day the forecast is issued) and the days covered by the forecast are marked by open and filled circles, respectively. The content of the forecasts is indicated in the rectangular boxes. The nearest upper and lower rows contain maximum and minimum values of Kp indices, attained during individual days, and their frequencies, where needed, on days covered by forecasts. Symbols like n/ or /n serve for distinguishing values for the first and second part of a day. Sometimes a particular event was regarded in a forecast as possible but not explicitly expected; in such instances a question mark is used. When the level of activity is not stated by Kp values, D stands for disturbance (Kp maximum about 4); D^S represents more than one disturbance; Q denotes magnetic calm (Kp minimum 0 or 1); and L (low) and E (enhanced), both relative to neighboring activity, lie quantitatively between the Q and D levels.

In the upper evaluation rows of Table 1 satisfactory agreement between forecast and actual activity is indicated by +, disagreement by -. In this connection, differences of one Kp unit, in the sense of higher actual values than expected ones, are regarded as quite tolerable. In addition, symbols (+) and (-) are used in some doubtful cases resulting from various reasons such as a great difference between forecast and actual value, a possible but not expected event, or an unspecified level of activity.

The degree of agreement between forecast and actual activity is shown in a quantitative way in the lower evaluation rows of Table 1, where the differences between observed and predicted values are presented. Here again some doubtful cases resulting from an unspecified level of activity are marked by question marks (D and D^S were approximated by Kp=4 in order not to overestimate the agreement). In this connection it should be stressed that the exact upper level of disturbance during a magnetic storm cannot be reliably predicted with the means at hand. When an event was possible but not explicitly expected, the appropriate difference is given in parentheses.

Table 1

McMath Region 14143 CMP

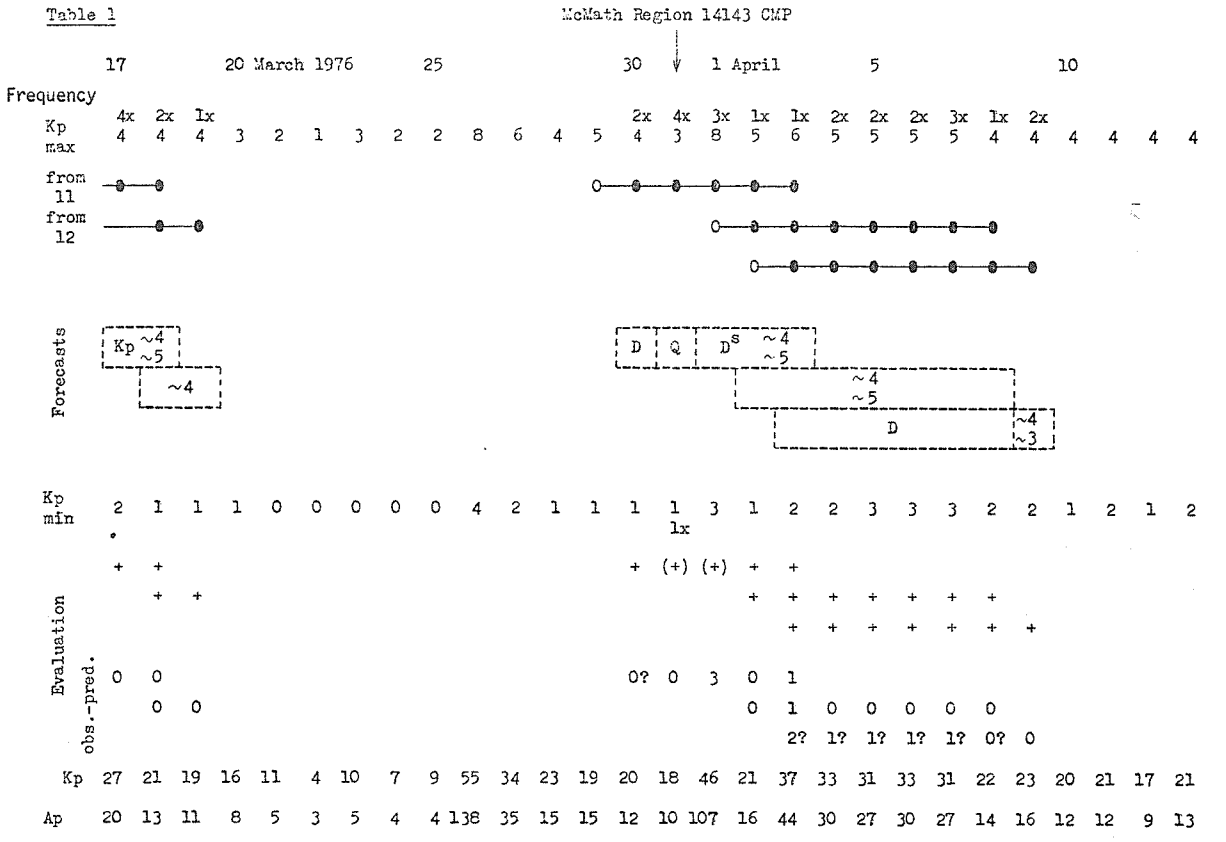

Table 1 continued

McMath Region 14179 CMP

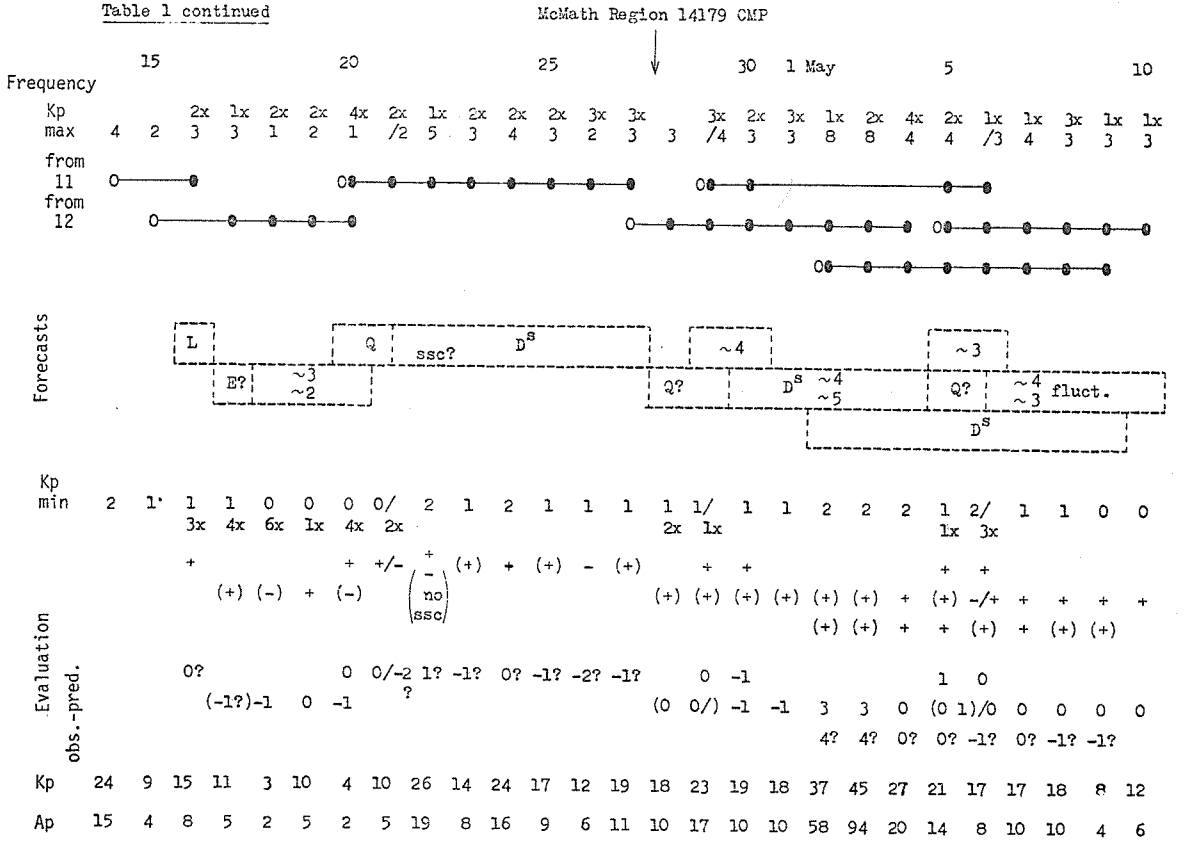

As can be seen from Table 2, the frequencies of cases marked by + or 0 are greatly enhanced. This means that the agreement between predicted and actual geomagnetic activity is quite satisfactory.

TABLE 2

			Kp Observed - Kp Predicted								
Certain Agreement	+	40									
Doubtful Agreement	(+)	18	Difference	-4	-3	-2	-1	0	1	2	3	4	Total
Doubtful Disagreement	(-)	3	All cases	0	0	2	12	34	9	1	3	2	63
Certain Disagreement	-	3	Clear cases	0	0	0	5	24	3	0	3	0	35
Total		64											

When the forecasts are compared to the time pattern of geomagnetic activity displayed in Kp diagrams (not reproduced here), then, according to shape, level and number of local maxima, the agreement can be classified as follows: "very good" for message Nos. 3 (with exception of level during storm and calm), 4, 5, 6, 8 (with exception of ssc); "good" for Nos. 1, 2, 10, 11, 12; and "fair" for Nos. 7 and 9.

For details on the method, limitations and reliability of forecasts we refer the reader to the papers given below.

REFERENCES

BEDNÁŘOVÁ-NOVÁKOVÁ, B. and J. HALENKA 1968 — New Method of Forecasting Geomagnetic Activity Using Features of the Solar Corona, *Nature, 220,* 250.

BEDNÁŘOVÁ-NOVÁKOVÁ, B. and J. HALENKA 1976 — Results of Investigating the Relations Between Solar and Geomagnetic Activity Obtained at the Geophysical Institute, CSAS, *Geofysikální sborník, XXII,* Travaux Inst. Géophys. Acad. Tchécosl. Sci. No. 424.

A Note on the Geomagnetic Activity Observed at Hyderabad During 20 March - 5 May 1976

by

B. J. Srivastava
National Geophysical Research Institute
Hyderabad-500007, India

Introduction

For the solar cycle 20 which began in October 1964, the monthly sunspot numbers steadily decreased toward a minimum in February 1976 (monthly R_Z=4.3). Then came a sudden and unexpected resurgence in solar activity during March and April 1976 (monthly R_Z=21.9 and 18.8 respectively), pushing the minimum in monthly numbers to July 1976 (monthly R_Z=1.9). On this basis the cycle has had a period of about 12 years. The solar activity associated with McMath Region 14143, which rotated onto the east limb of the sun on 24 March and returned as McMath Region 14179 at the east limb on 20 April, produced unusual global geomagnetic activity.

In this note, we discuss the major geomagnetic events and day-to-day activity as observed at the Hyderabad Magnetic Observatory (Geomag. Coords. N7.6 E149.2) - an ideal low-latitude station outside the influence of the equatorial electrojet and free from anomalous internal induction effects and coast effect - during the "Retrospective World Interval, 20 March - 5 May 1976". The microfilms of Hyderabad magnetograms (La Cour, normal-run) and the geomagnetic hourly values of D, H and Z components for the period are available to the entire geophysical community through the World Data Center A for Solar-Terrestrial Physics, NOAA, Boulder, CO USA.

The Data

Table 1 gives the data on the magnetic storms (large and small) recorded at Hyderabad. Table 2 presents the K and C indices of geomagnetic activity at Hyderabad for the period 20 March through 5 May 1976. Table 3 gives the rapid geomagnetic events (SFEs, SIs and bays) recorded in the Hyderabad magnetograms.

TABLE 1

Magnetic Storms Recorded at Hyderabad during 20 March - 5 May 1976

DATE	COMMENCEMENT			SC - AMPLITUDES			MAXIMUM 3 HOUR - INDEX K		RANGES			UT END	
1976	DAY	UT	TYPE	D(')	H(γ)	Z(γ)	DAY (3 HOUR PERIOD)	K	D(')	H(γ)	Z(γ)	DAY	HOUR
March	25	1300	..	..	..	..	26 (5)	9	7	390	34	27	20
April	01	0254	SC	-0.2	+37	-3	01 (2,3,4)	8	7	352	47	02	09
	02	1745	..	..	..	..	03 (6,7)	5	4	121	27	05	01
	07	0300	..	..	..	..	07 (5)	5	4	91	21	08	02
	21	1717	SC	-0.1	+ 8	-1	22 (2)	4	4	112	25	23	02
	29	0705	SC	-0.3	+10	-1	29 (6)	5	5	113	25	30	20
May	01	1200	..	..	..	..	02 (5)	6	7	97	22	02	17
	02	1828	SC	-0.3	+31	-2	03 (1,2,3)	6	7	181	32	03	22

Discussion

Following the solar flare activity in the vicinity of the large sunspot groups, three major magnetic storms were recorded during the period (see Table 1). The first storm of severe intensity began with a gradual commencement on 25 March 1976 around 1300 UT and showed a large range of 390 γ (nT) in H at Hyderabad. It became intense only on 26 March with a well developed main phase containing rapid fluctuations of only small amplitude. It yielded one K-index of value 9. The storm lasted more than 2 days. The second storm of severe intensity commenced suddenly on 1 April at 0254 UT, yielded three K-indices of value 8, and gave a range of 352 γ (nT) in H at Hyderabad. This storm again did not show large-amplitude rapid oscillations of the field. The third storm of moderately severe intensity began with a sudden commencement around local midnight on 2 May 1828 UT, yielded three K-indices of value 6, and a range of 181 γ (nT) in H. This storm was characterized by relatively large-amplitude rapid oscillations and pulsations throughout, similar to the August 1972 storms [Srivastava, 1973]. The day-to-day activity can be seen from Table 2.

Srivastava, *et al.* [1977] have also found a good correlation between the geomagnetic activity and the surface meteorological data observed at Hyderabad during March - May 1976.

TABLE 2

K and C Indices of Geomagnetic Activity at Hyderabad
20 March - 5 May 1976

Range for K 9=300γ

UT Day	March 1976 K-Indices		Sum	C
20	1122	3111	12	0
21	1112	2210	10	0
22	0111	1111	7	0
23	1112	2331	14	0
24	1110	1111	7	0
25	1111	2123	12	1
26	3788	9874	54	2
27	4322	4443	26	1
28	3321	2221	16	0
29	2231	1111	12	0
30	1122	3343	19	1
31	1222	2231	15	0
	April 1976			
01	5888	7653	50	2
02	3221	1334	19	1
03	2442	4553	29	1
04	3344	4433	28	1
05	2323	3242	21	1
06	3333	3341	23	1
07	2343	5234	26	1
08	2222	2133	17	1
09	1211	2332	15	1
10	1312	3211	14	0
11	1223	3233	19	1
12	1232	1121	13	0
13	1112	2232	14	0

UT Day	April 1976 K-Indices		Sum	C
14	1112	2323	15	1
15	1111	1111	8	0
16	1233	1112	14	0
17	1421	2230	15	1
18	0111	1111	7	0
19	1211	1321	12	0
20	1211	1111	9	0
21	1111	1313	12	1
22	3433	2331	22	1
23	1211	2322	14	0
24	2323	3232	20	1
25	1321	1111	11	0
26	1111	1211	9	0
27	3331	1233	19	1
28	2121	2232	15	0
29	0123	3543	21	1
30	2332	2221	17	0
	May 1976			
01	1211	1332	15	1
02	3335	6355	33	1
03	6665	5432	37	1
04	1233	3433	22	1
05	3233	2122	18	1

Scale values of Variometers in γ/mm:
D 3.5, H 4.6, Z 3.8

TABLE 3

Rapid Events (SFEs, SIs and Bays) Recorded at Hyderabad during 20 March - 5 May 1976

	Date		UT of beginning	UT of ending	Amplitudes D	H	Z	Type
					'	γ	γ	
SFEs	1976	March 23	08 44	09 30	-0.5	+5	+6	
		31	11 40	12 00	-0.2	+5	0	
SIs	1976	March 25	23 38	23 42	+0.2	-9	+1	
		26	02 32	02 34	+0.3	-11	+1	
		April 01	03 48	03 50	-0.1	-41	+5	
		19	05 00	05 08	0.0	-5	0	
		19	06 40	06 45	-0.1	+4	0	
		May 05	09 02	09 08	-0.3	+8	-2	
Bays	1976	March 23	18 10	19 10	-0.2	+16	+1	bp
		27	17 35	18 40	-0.6	+30	+3	b
		31	18 20	19 20	-0.3	+17	+1	bp
		April 03	18 28	20 25	-1.0	+39	+3	b
		04	10 35	12 00	-0.6	-36	-3	b
		04	15 55	16 55	-0.3	+23	+2	b
		05	18 00	19 40	-0.3	+33	+3	b
		06	18 45	20 15	-0.2	+23	+2	b
		09	17 15	19 00	-0.4	+23	+1	bs
		May 01	15 45	17 00	-0.2	+14	0	b
		04	15 10	16 15	-0.4	+23	+2	b
		04	17 35	19 15	±0.3	+31	+3	b

Acknowledgments

I am grateful to Dr. Hari Narain, Director, National Geophysical Research Institute, Hyderabad, India, for his kind permission to publish this note. I am also indebted to my colleagues at the Geomagnetic Observatory for assistance in compiling the data.

REFERENCES

SRIVASTAVA, B. J. 1973 Discussion of the geomagnetic data recorded at Hyderabad, India, during July 26 - August 14, 1972, WDC-A for Solar-Terrestrial Physics *Report UAG-28*, Part III, 754-761.

SRIVASTAVA, B. J., HABIBA ABBAS and SUBHASH SAXENA 1977 Solar-geomagnetic-climatic relationships at Bombay and Hyderabad, presented at "Space Sciences Symposium", Trivandrum, India, 18-21 January 1977, (Abstracts, 294-295).

Simosato Hydrographic Observatory Data During the Period 20 March to 5 May 1976

by

K. Sugiura

Hydrographic Department, Maritime Safety Agency
No. 3-1, 5-chome, Tsukiji, Chuo-ku, Tokyo 104, Japan

The Simosato Hydrographic Observatory is located geographically at N33.57, E135.93. Particulars of the magnetic storms and magnetic solar flare effects (sfe) observed at Simosato are tabulated below. In addition to these data, copies of the following items may be requested from the WDC-A for Solar-Terrestrial Physics:

1) Normal magnetograms for 23-28 and 31 March and 1, 2 and 30 April 1976.

2) Normal magnetograms (ink recorder) for 2-3 May 1976.

3) Induction magnetogram sensitivity for 23-24, 26-28 and 31 March; 1-2 and 30 April; and 2-3 May 1976.

4) Three-hour range indices (K) and character figures (C).

5) Observed baseline values and respective adopted values (adopted scale values).

Magnetic Storms

Simosato (U.T.)

Date	Time (U.T.)		Sudden Commencement				(2) C-figure degree of activity	Maximal activity on K-scale 0 to 9			Ranges		
	Beginning	Ending	Type	Amplitudes (1)				Day	3-hour period	K-index	D	H	Z
				D	H	Z							
1976	h m	d h		'/min.	γ/min.	γ/min.							
Mar. 25	13.3	29 11.0	...	−	−	−	ms	26	3	7	13.5	352	146
Apr. 1	02 54.3	2 04.3	SSC*	+0.6/0.1	− 2/1.0* +14/0.2	trace/1.0* +25/0.2	ms	1	2 3 4	7 7 7	12.9	286	186
2	14.9	—	...	−	−	−	−	−	−	−	8.1	95	56
May 2	18 28.3	3 21	SSC	−	+	+	record	missing	after	SSC			

Remarks

(1) Signs of amplitudes
- D: Positive when directed eastward.
- H: Positive when directed northward.
- Z: Positive when directed downward.

(2) Degree of activity
- ms: moderately severe (when maximum K=6 or 7)

(3) ... : Gradually commenced storm.

Magnetic Solar Flare Effect sfe

Simosato (U.T.)

Date	U.T. of beginning	Dur.	Q	Maximum or Minimum						K-index	Solar or Ionos. conf.	
				H		D		Z				
				U.T. of occur.	Amp.	U.T. of occur.	Amp.	U.T. of occur.	Amp.			
1976	h m			h m	γ	h m	γ	h m	γ			
Mar. 23	08 42	24	C	−	−	08 52	− 3	08 51	+ 3	1		0
24	00 14	8	C	00 18	+ 2	00 15	− 3	00 17	+ 3	1		0

Dur.: Duration Q: Quality occur: occurrence Amp.: Amplitude conf.: confirmation Ionos.: Ionospheric

Three Geomagnetic Storms Observed at Tevris and Arty Stations

by

N. A. Ivanov, L. N. Ivanova, B. L. Shirman
Institute of Geophysics, Urals Scientific Center
USSR Academy of Sciences, Pervomaiskaya Str. 91
Sverdlovsk, USSR

Figure 1 shows the standard-run H component magnetic records at Tevris (N57.5 E72.4) and Arty (Sverdlovsk) (N56.8 E60.7) stations. Figures 2 and 3 show the rapid run H, D and Z component magnetic records of the geomagnetic storms' sudden commencements at the Arty station.

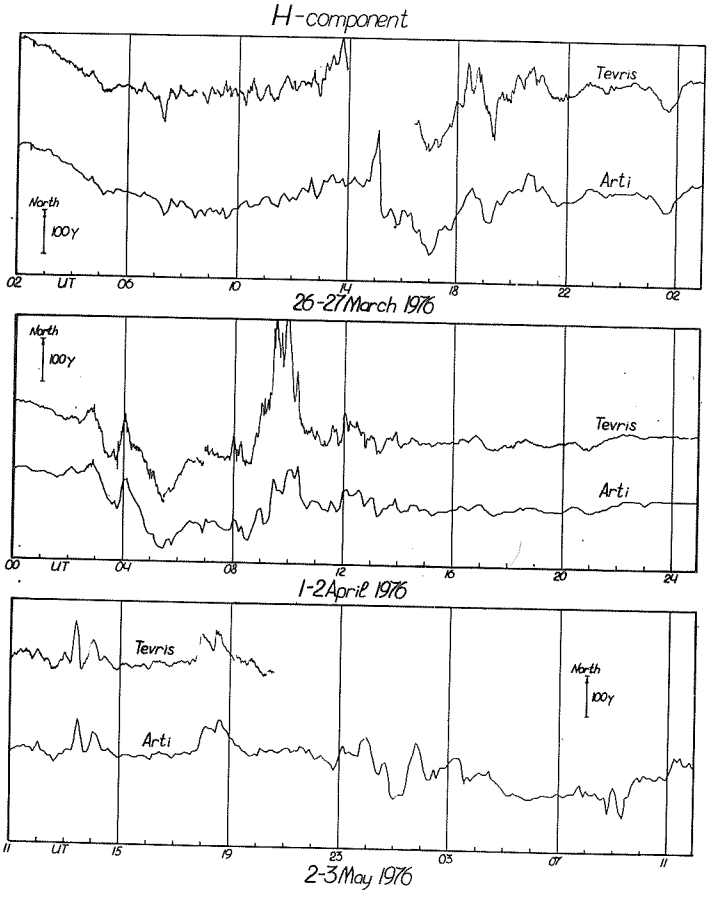

Fig. 1. H component magnetic records at Tevris and Arty for the periods 26-27 March, 1-2 April and 2-3 May 1976.

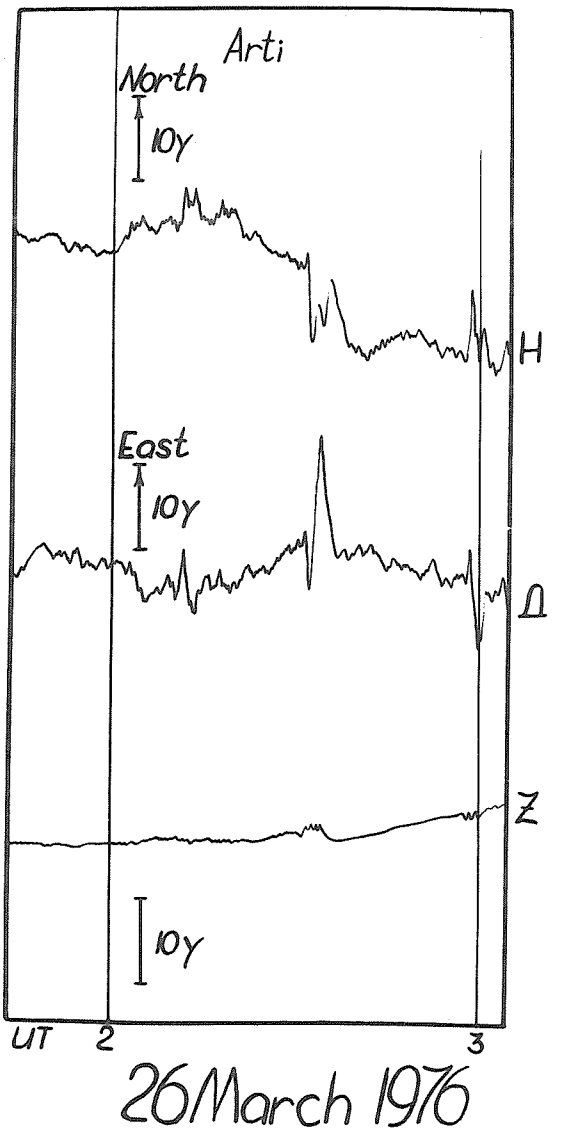

Fig. 2. Rapid run H, D and Z components at Arty for 26 March 1976.

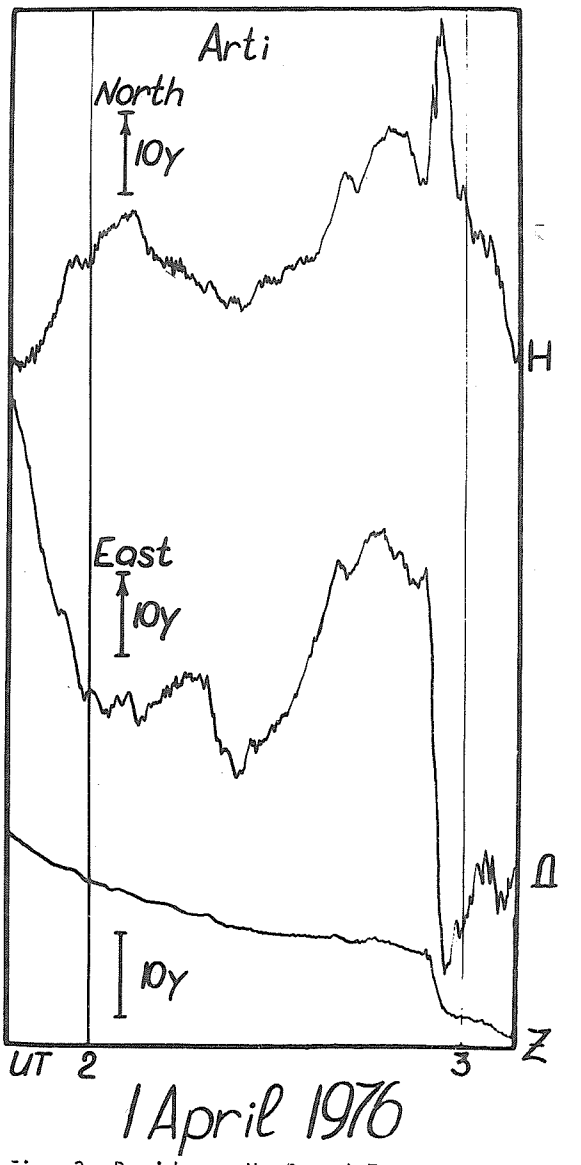

Fig. 3. Rapid run H, D and Z components at Arty for 1 April 1976.

Comparison of Low Latitude Magnetograms of Storms during 20 March - 3 May 1976

by

Victor L. Badillo
Manila Observatory
P.O. Box 1231, Manila

A study is made of the three SC-magnetic storms recorded by the Askania variometer located at the low latitude station in Davao City, Philippines. The coordinates of the 85-meter elevation station are N7.08 E125.58 geographic and S4.00 E194.97 geomagnetic. The study is limited to the H component of the geomagnetic field. Figure 1 shows selected portions of the storms, that is, the initial phase and early main phase. The Sq curve is almost symmetrical with local noon.

1. 25 March 1976

After a week of quiet magnetic conditions there occurred a major storm preceded by two SCs: the first on 25 March at 2339 UT and the second on 26 March at 0230 UT with rise times of 3 and 6 min, respectively. The magnitude of the first was -23.9 gammas; that of the second was -47.8 gammas. Both had positive initial phases. These could also be considered inverse SCs or SIs. Fluctuations of the main phase ceased by 0700 UT on 27 March. Before the storm the difference between maximum and minimum daily values was about 68 gammas; after the storm it was about 120 gammas. The daily mean value after the storm was lower than that before it. The source of the particles was probably on the east limb. If the solar disturbance began with the 23 March Type IV radio burst at 0842 UT, then the delay times to the two SCs were 62 hours 57 min and 65 hours 48 min, respectively.

2. 01 April 1976

This storm was a textbook example. A large amplitude (78 gammas) daytime SC, which was followed by a positive initial phase, preceded a severe main phase. Start time and rise time of the SC were 0252.5 UT and 3.6 min, respectively. The fluctuations in the main phase died out in a short time (by 1200 UT of the same day). The delay time to the SC was either 15 or 79 hours, depending on whether the solar disturbance began with the W09 Type IV radio burst at about 1200 UT on 31 March or with the E28 Type II burst at about 1921 UT on 28 March.

3. 02 May 1976

This storm was associated with a GLE and PCA. Its morphology was quite different from the two preceding disturbances. There was a small (20.5 gammas) nighttime SC at 1827 UT on 2 May with a rise time of 3.3 min. The initial phase was small and the main phase was not well developed. By daytime the main phase was characterized by many impulsive, large amplitude oscillations. In the original magnetograms only the turning points of the trace are discernible. If the solar disturbance is considered to have started with the maximum of the radio burst at 2109 UT on 30 April near W47, then the delay to the SC is about 45 hours. What appears to be unusual is the pre-SC bay starting at about 1200 UT on 2 May. This feature is usually a peculiarity of auroral zone magnetograms.

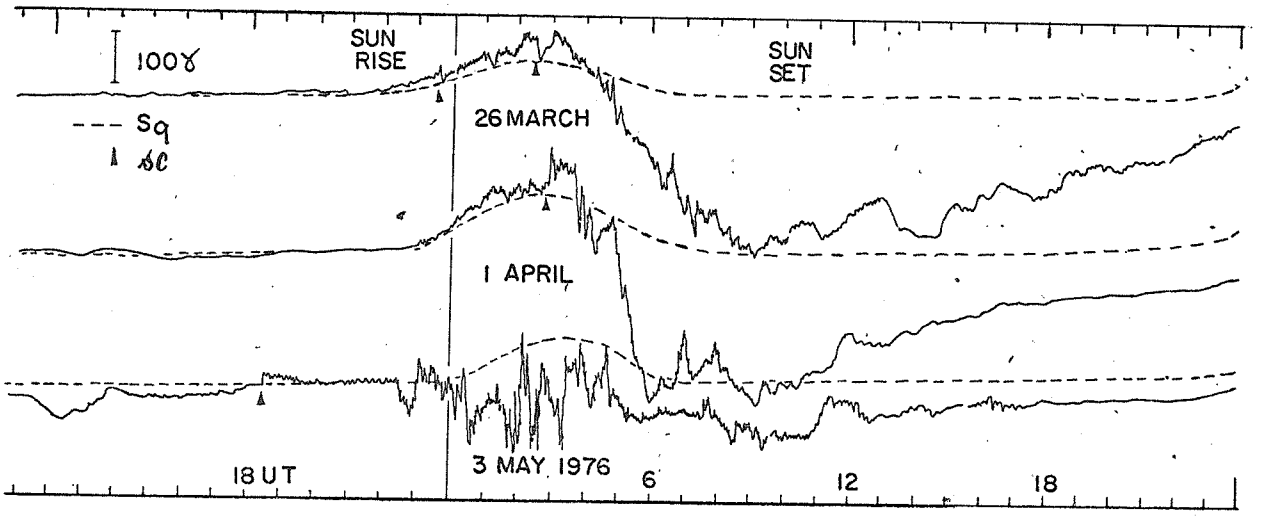

Fig. 1. H-component magnetograms of storms at Davao during 20 March - 3 May 1976.

Some Aspects of the Magnetic Storms of 26 March, 1 April and 3 May 1976, and of Two Prior Solar Flare Effects

by

A. M. van Wijk
Magnetic Observatory of the CSIR
Hermanus, Republic of South Africa

The data used in this report are derived from five of the six geomagnetic recording stations maintained by the Hermanus Magnetic Observatory. The stations are distributed as follows:

Station	Geographic Coordinates S Lat.		E Long.	
Tsumeb	19°	12'	17°	35'
Hartebeesthoek	25	53	27	42
Grahamstown	33	19	26	30
Hermanus	34	25	19	14
Marion Island	46	53	37	51

The only two geomagnetic solar flare effects recorded at these stations during the retrospective interval were those of 21 March (Figure 1) and 23 March (Figure 2). The SFEs in question were associated with sudden ionospheric disturbances of importance 3 and with optical flares in McMath Regions 14127 and 14143, respectively [Leighton and Lincoln, 1976]. The uncertainty in the onset times given in the captions to these figures is 1-2 minutes. (McMath Region 14127 is not one of the regions selected for special study). The event of 23 March is noteworthy in that the deflections at some of the stations are in the opposite sense to that of the prevailing diurnal departures. This suggests a generating mechanism other than the normal Sq current system.

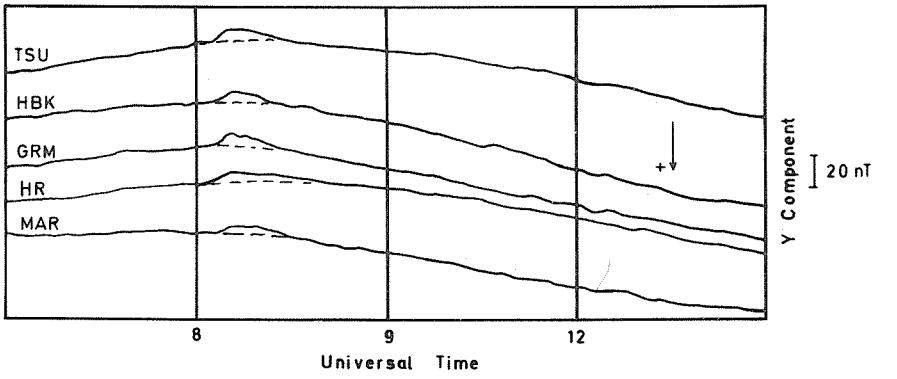

Fig. 1. Solar flare effect 0802 UT 21 March 1976

Figure 3 shows an analog record (computer plot) of the horizontal intensity at Hermanus for the period 21 March to 19 May, and of the difference between H at Hermanus and Tsumeb for the same period. The upper frame of Figure 3 illustrates some of the outstanding differences between the storms of 26 March, 1 April and 3 May. The first two storms show strong Dst ("ring current") effects but their initial phases are markedly different. The appearance of the 3 May storm on the other hand, suggests a combination of ring current and polar effects. The "difference curves" in the lower frame of Figure 3 show that the ring current effects are of about the same magnitude at Hermanus and Tsumeb. In these curves the difference between Sq at the two stations shows as a bump. The regularity of this bump is striking. "Difference curves" for pairs of stations in roughly the same longitude (e.g., Hermanus and Tsumeb) or in roughly the same latitude (e.g., Hermanus and Grahamstown) may be useful in studying the relative contributions of the various current systems to the magnetic field variations.

In Figure 4 the H variations at Hermanus during the three storms are presented in a novel way. The notation is that used by Sugiura [1964]. The hourly Dst values plotted in the upper portion of each frame were obtained from the regular monthly tabulations. The approximate "Dst + DS" data for Hermanus were obtained by subtracting the mean hourly values of H for the five quietest days in April from the corresponding hourly values in each of the three disturbed periods. The 'DS' curves for Hermanus (lower frames) were derived directly from the curves in the upper frames. Space does not permit a detailed discussion of the interesting features evident in Figure 4. However, the magnitude of the Hermanus DS is remarkable in view of the fact that Hermanus is one of the four observatories whose data are used in determining Dst.

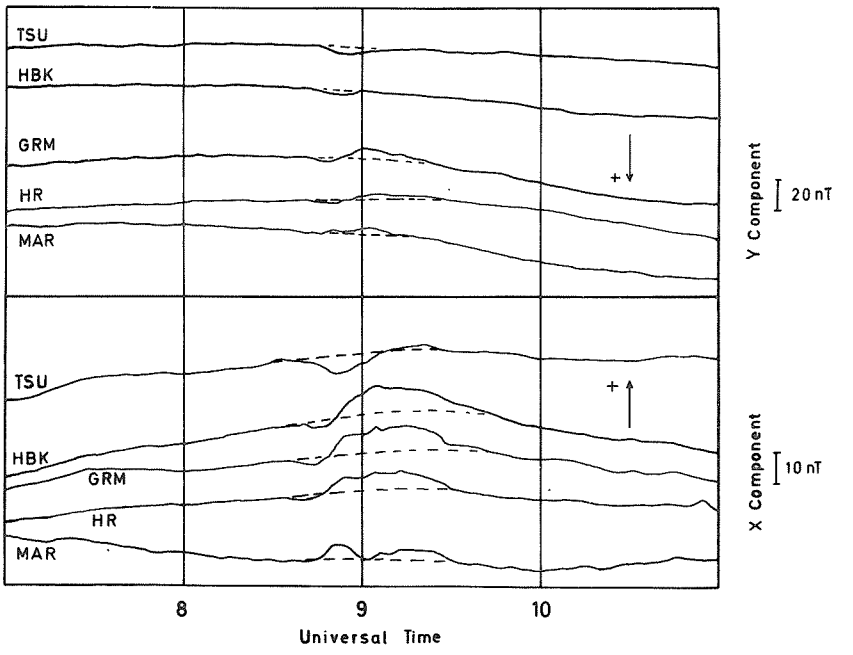

Fig. 2. Suspected solar flare effect 0836 UT 23 March 1976

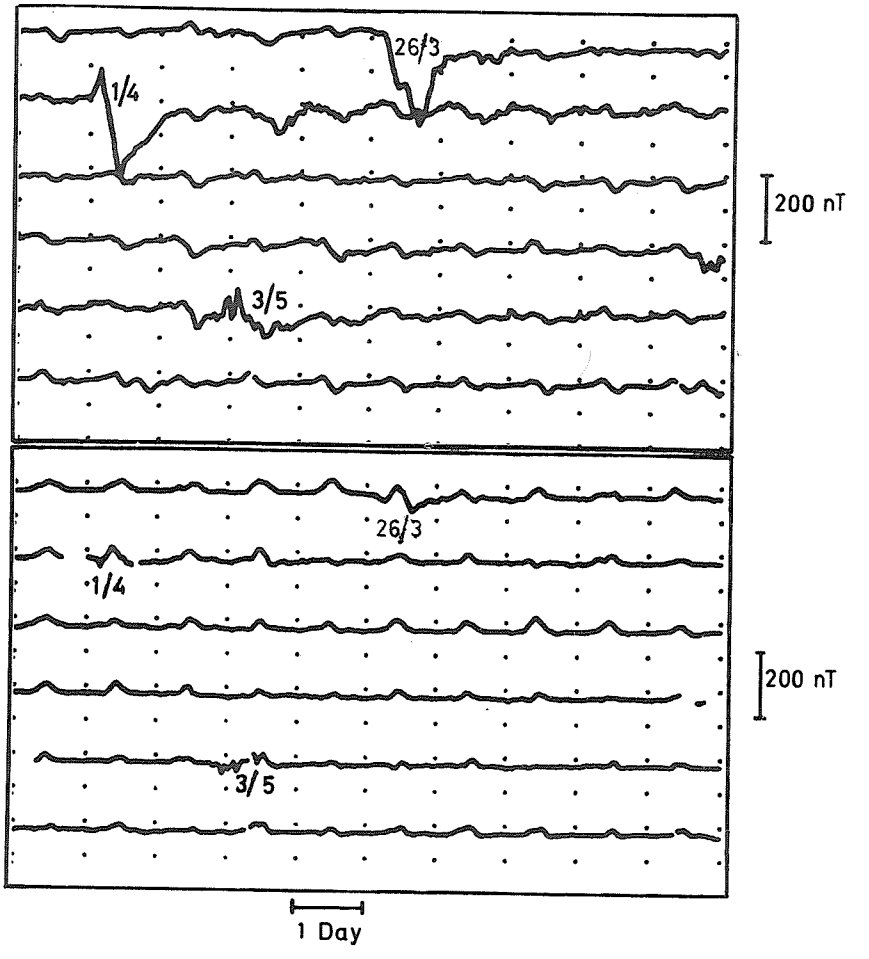

Fig. 3. Computer plot of horizontal intensity (H) at Hermanus for interval 21 March to 19 May (upper frame) and difference between H at Hermanus and Tsumeb for same interval (lower frame).

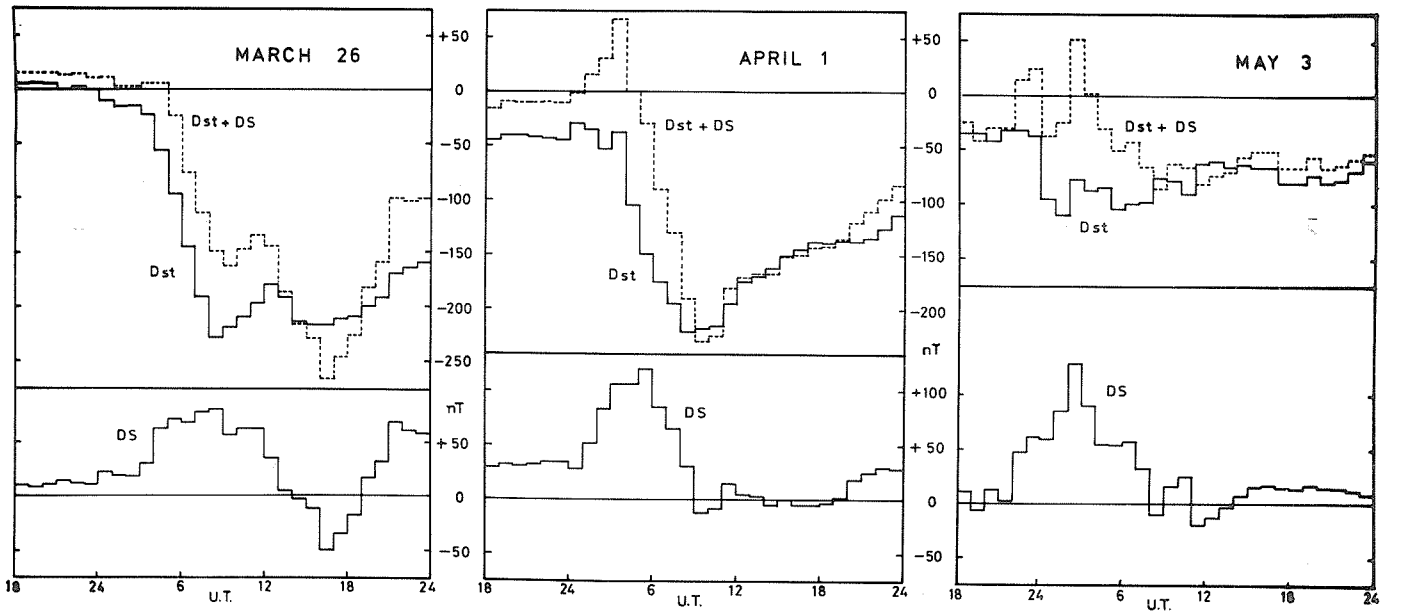

Fig. 4. Dst and Hermanus DS for the magnetic storms of 26 March, 1 April and 3 May 1976.

REFERENCES

LEIGHTON, H. I. (Ed.) and LINCOLN, J. V. 1976 *Solar-Geophysical Data*, U.S. Department of Commerce, (Boulder, CO, USA 80302) *381*, Part 1, 98.

SUGIURA, M. 1964 *Annals of the IGY, 35*, 9.

Measurement of the Electromagnetic Parameters of the Upper Atmosphere at Khabarovsk, USSR, from 20 March to 5 May 1976

by

G. G. Butvin, M. G. Savin,
A. I. Okara and M. A. Afroskin
Institute of Geophysics and Tectonics
Far East Scientific Center of the USSR Academy of Sciences
Khabarovsk, USSR

Data are presented from the observatory "Khabarovsk" located at N37 E200 in geomagnetic coordinates. This brief report includes the following kinds of observations: slow variations and micropulsations of the geomagnetic field, vertical soundings of the ionosphere, and counting rates of a neutron supermonitor.

Main Geomagnetic Disturbances

Three geomagnetic storms occurred in the period under review. Table 1 summarizes each of these events.

Table 1. Characteristics of the March - April 1976 Geomagnetic Storms.

N	commencement					main phase				
	type	time	amplitude			start	end	amplitude		
			D	H	Z			D	H	Z
1	SSC	25.03 20^{h}53^m	3.36 (1)	10γ	4γ	26.03 04^{h}47^m	26.03 18^{h}00^m	31.92 (1)	>230γ	68
	SSC	25.03 23 39	2.94	12	4.5					
	SSC	26.03 02 33	1.26	10	—					
2	SSC	1.04 02 55	2.94	20	4.5	1.04 04 51	1.04 09 17	33.18	>170	74
3	SSC	2.05 18 27	2.52	32	4.5	2.05 23 00	3.05 09 26	26.24	116	45

The first storm began with three SSCs in which 2.5 hours separated the first two, and 3 hours separated the third from the second. All three SSCs displayed a sharp negative break in H (see Figure 1). During the storm's initial phase, we observed small bays on which irregular oscillations with a 2 to 3-min period were superposed. The main phase began with a positive impulse at 0447 UT on 26 March. Moreover, as recorded on the horizontal component, it developed in two stages; the first occurred between 0447 and 0918 UT, the second between 0918 and 1800 UT on 26 March.

The SSC of the second storm resembled a delta function. After a shorter (by 2 hours) and more unstable initial phase than the storm mentioned above, the main phase began with a positive impulse. On 1 April H decreased 120γ by 0530 UT; H then partially recovered, only to be followed by a 130-gamma main phase decrease, beginning at 0706 UT and ending at 0917 UT.

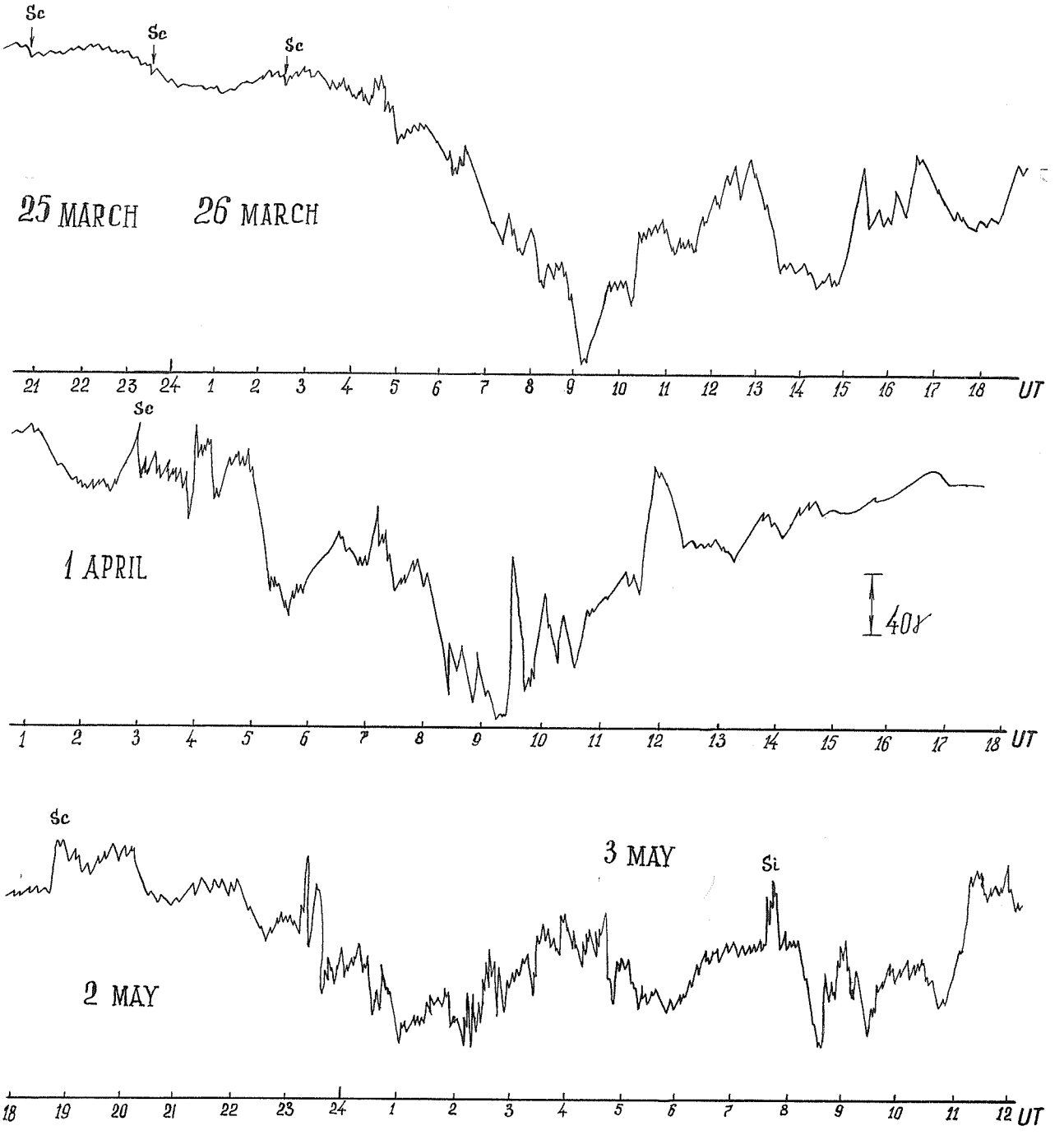

Fig. 1. Geomagnetic storms as observed on the horizontal component at "Khabarovsk" Observatory from 20 March - 5 May 1976.

The SSC of the third storm resembled an ordinary step function increase in H. Irregular oscillations with a 2 to 3-min period developed at the end of the initial phase and increased their amplitude during the main phase to 40γ. After a sudden impulse (SI) at 0748 UT on 3 May, the main decrease in H of 58γ was observed. This sharp decline was in turn followed by a sequence of highly irregular oscillations.

The appearance of the different types of geomagnetic micropulsations between 0.011 and 0.3 Hz during the 20 - 31 March 1976 period is shown in Table 2.

Table 2. Types of Geomagnetic Micropulsations Observed during the 20 - 31 March 1976 Period.

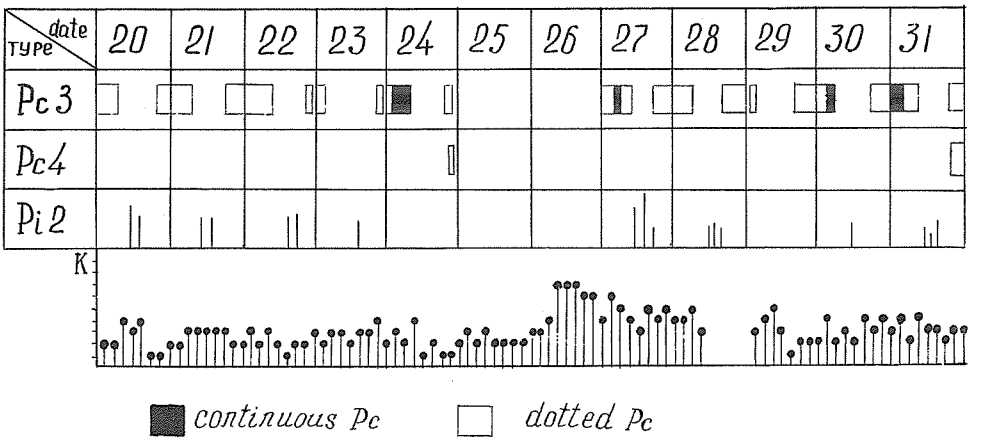

Between 0000 and 2200 UT on 25 March pulsations were completely absent. From 2200 UT, the beginning of the geomagnetic storm on 25 March, to 0300 UT on the 26th, irregular pulsations with relatively long periods were observed. For the next 17 hours the geomagnetic field pulsations vividly portrayed chaos, making it extremely difficult to isolate definite types of pulsations.

Vertical Ionospheric Soundings

Variations in foF2 and fmin for the period 20 March - 5 May are shown in Figure 2.

Cosmic Rays

Figure 3 illustrates that the changes in intensity of the cosmic ray neutron component did not lie beyond the limits of average daily variations. In Figure 4 the 5-min values of neutron intensity on 30 April 1976 indicate the absence of an increase in particles with energies $\geq$ 5.55 BeV during this period.

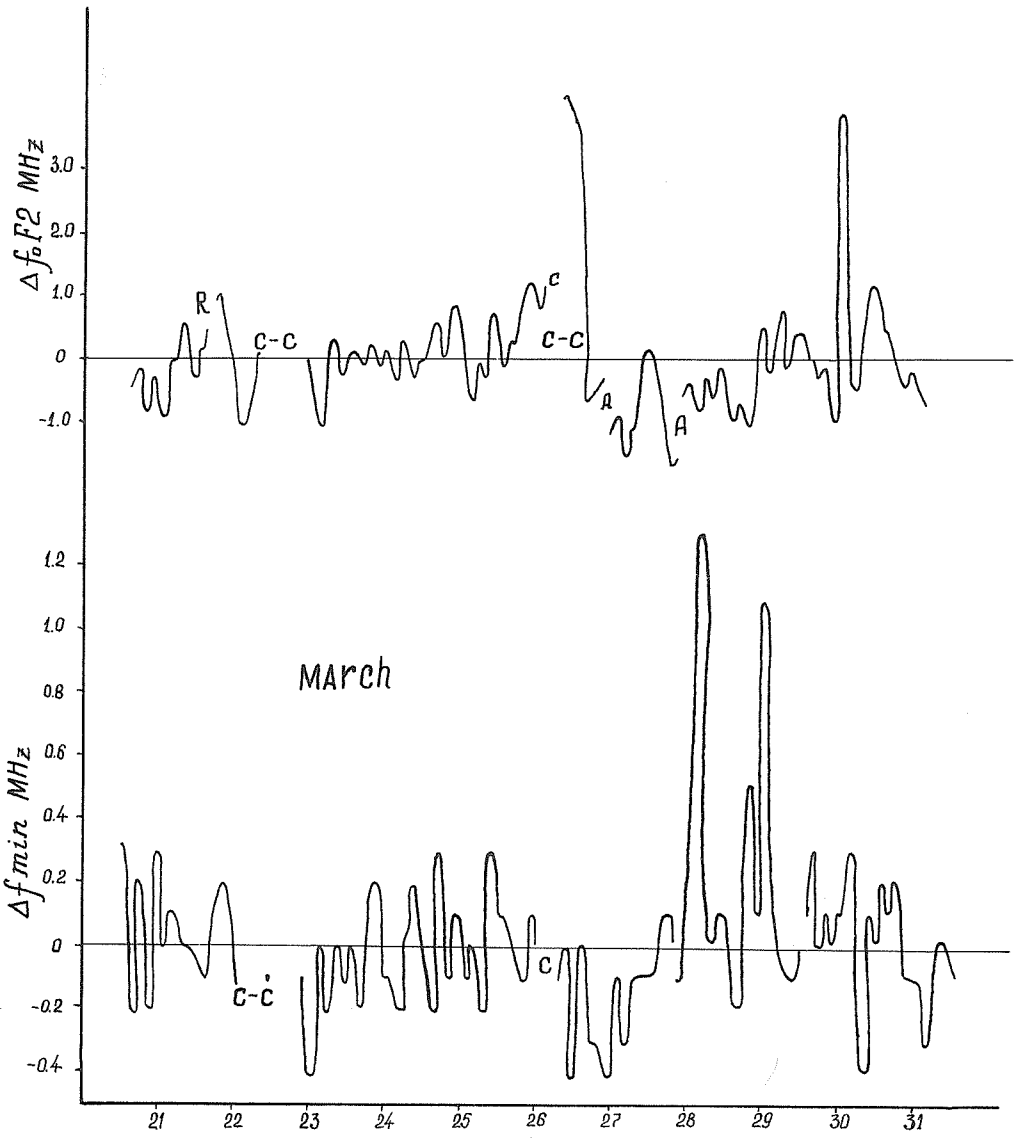

Fig. 2. Variations in the critical frequencies foF2 and fmin for the period from 20 March - 5 May 1976.

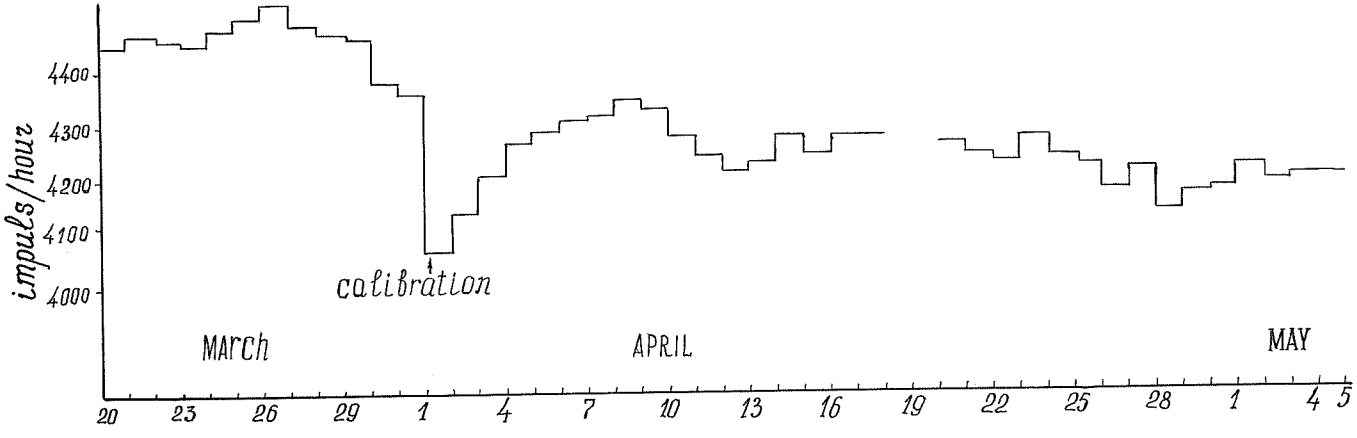

Fig. 3. Neutron component of the cosmic rays observed at "Khabarovsk" from 20 March - 5 May 1976.

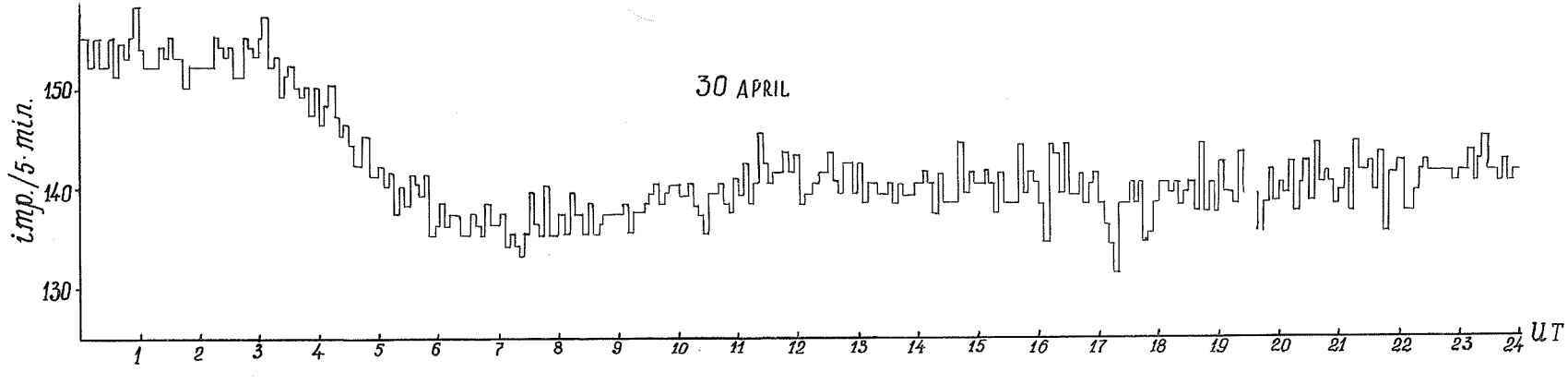

Fig. 4. Five-min values of the neutron component intensity on 30 April 1976.

Observation of Storm-Associated Geomagnetic Pulsations in Auroral Latitudes, March/April 1976

by

O. Hillebrand and U. Wedeken
Institut für Geophysik der Universität
3400 Göttingen, F.R.G.

Introduction

The Geophysical Institute of the University of Göttingen is participating in the IMS (International Magnetospheric Study) by making ground-based observations of geomagnetic pulsations. Generally six pulsation stations are set up on a profile along a geomagnetic meridian in northern Scandinavia. They operate during limited time periods during the IMS in order to study some characteristics of geomagnetic pulsations at auroral latitudes.

In the time interval from 9 March to 5 April 1976, geomagnetic pulsations have been recorded at three locations on a north-south profile in northern Sweden. These recordings were made in connection with the 'Porcupine' rocket program at Kiruna-Esrange (Sweden).

Instrumentation and Recording Sites

The sensors for the three components H, D and Z of the geomagnetic pulsations are Grenet-type induction variometers. The period range of the instruments extends from 2 s to approximately 600 s. In the period range around 20 s the maximum resolution is 0.05 nT. The sensitivity decreases toward larger and shorter periods. All three stations used in Sweden in March and April 1976 are equipped with digital tape recorders. The data rate is 1 sample/s for each component. A crystal clock insures a time accuracy of approximately 0.1 s. The location of the stations is listed in Table 1.

Table 1. Pulsation Recording Sites in Northern Sweden March/April 1976

Station	Abbr.	Geographic Coordinates Lat. N	Long. E	Distance from ESR	L-value
KEINOVUOPIO	KEI	68°53'	21°02'	+ 111 km	5.9
ESRANGE	ESR	67°53'	21°06'	0 km	5.4
HAKKAS	HAK	66°55'	21°35'	- 107 km	5.1

Observation of Geomagnetic Pulsations during Two Storms

Only the recorded data of two storms shall be treated here, i.e., data from 26 March and 1 April 1976. Figure 1 shows the data of ESR from 0000 UT to 1200 UT 26 March. The first ssc at 2339 UT 25 March is not displayed in Figure 1 because it is only accompanied by very slight pulsation activity. The ssc at 0233 UT 26 March is accompanied by a pse (pulsation single effect) with a main period of approximately 120 s. At about 0300 UT the real pulsation activity starts, comprising various frequencies and amplitudes. Maximum pulsation amplitudes appear shortly after 0400, 0500 and 0900 UT.

The second storm on 1 April contains much greater amplitudes. During two particular intervals, due to overcharging, parts of the records are unusable. These intervals begin just after 0255 UT (time of ssc) at KEI and after 0330 UT at KEI and ESR and last several minutes each. In the top section of Figure 2 only a small part of the recorded data of the second storm is represented.

In contrast with the data analysis, the frequency responses have not been taken into account for the data plots.

Preliminary Data Analysis

All the data of both storms were treated by dynamic spectrum analysis. In Figure 2 an example is taken from the second storm. Below the data recordings, the time-frequency contour maps of the H component of the geomagnetic pulsations in the same time interval 0542 - 0559 UT 1 April 1976 are shown for the three pulsation stations. The amplitude contour lines indicate the double amplitude envelope in nT. It can be seen that maximum amplitudes occur at the southern station HAK at 0547 UT in the period range about 150 s. In the analyzed period interval from 15 to 200 s the amplitude maximum of the northern station KEI is only half of HAK. This is in contrast to moderately disturbed times where maximum amplitudes are found

at the northern station. In the example the short period pulsations in the ranges around 70 s and 40 s are also dominant in the south.

An extract from the dynamic spectra in the complete time interval from 2300 UT 25 March to 1200 UT 26 March is summarized in Figure 3. The analyzed period range was subdivided into three bands which correspond approximately to the usual pulsation classification: 5 - 40 s ('pi1'), 40 - 150 s (pi2) and 150 - 300 s ('pi3'). Every four minutes the maximum double amplitude value of the subsequent four-minute interval is plotted corresponding to each station and to each period range and to the H and D components. The amplitude scale in the 'pi1' range differs from the other period ranges.

At all stations the pulsation activity starts shortly before 0000 UT. In the first interval of the storm in all period ranges the amplitudes of the H component increase to the north. On the average it is the same for the D component. The amplitude peaks in the 'pi1' range at 0130 UT are caused by the automatic calibration. The ssc at 0233 UT is visible only in the pi2 and 'pi3' range, especially in the H component of KEI and ESR. In all frequency bands the amplitudes rise to a maximum between 0300 and 0500 UT. During this time large differences in the amplitude distribution can be found between the three stations. While in the first hour of this interval the H component still rises to the north, in the second hour of this interval the amplitudes are distributed in an opposite sense, i.e., they rise to the south. At the same time the Kiruna magnetogram, which corresponds closely to the station ESR, shows a reversal of the Z component from negative to positive values and a minimum H, indicating a movement of the auroral electrojet to the south. According to Olson and Rostoker [1975] maximum pi2 amplitudes are found at the instantaneous location of the electrojet.

From 0500 to 0900 UT the amplitudes in the 'pi3' range are mostly moderate, especially at the northern stations. On the other hand the pi1 activity of the H component still rises; the station HAK shows maximum amplitudes in this period range around 0700 UT.

The amplitude distribution of the H and D component reverses again around 0900 UT, especially the pi2 and 'pi3' ranges which have increasing amplitudes to the north. Between 0900 and 1000 UT the Z component of the Kiruna magnetogram also reverses from positive to negative values.

It is generally remarkable that the amplitude pattern of the H and D component does not always coincide. An example is the prominent peaks in the D component between 0300 and 0500 UT in the 'pi1' range - peaks that can hardly be detected in the H records.

Acknowledgments

We are grateful to the helpful assistance of the researchers at Esrange during our participation in the 'Porcupine' project and to the Kiruna Geophysical Observatory. This work was supported by the Deutsche Forschungsgemeinschaft.

REFERENCE

OLSON, J. V. and G. ROSTOKER 1975 Pi2 Pulsations and the Auroral Electrojet. *Planet. Space Sci.*, *23*, 1129-1139.

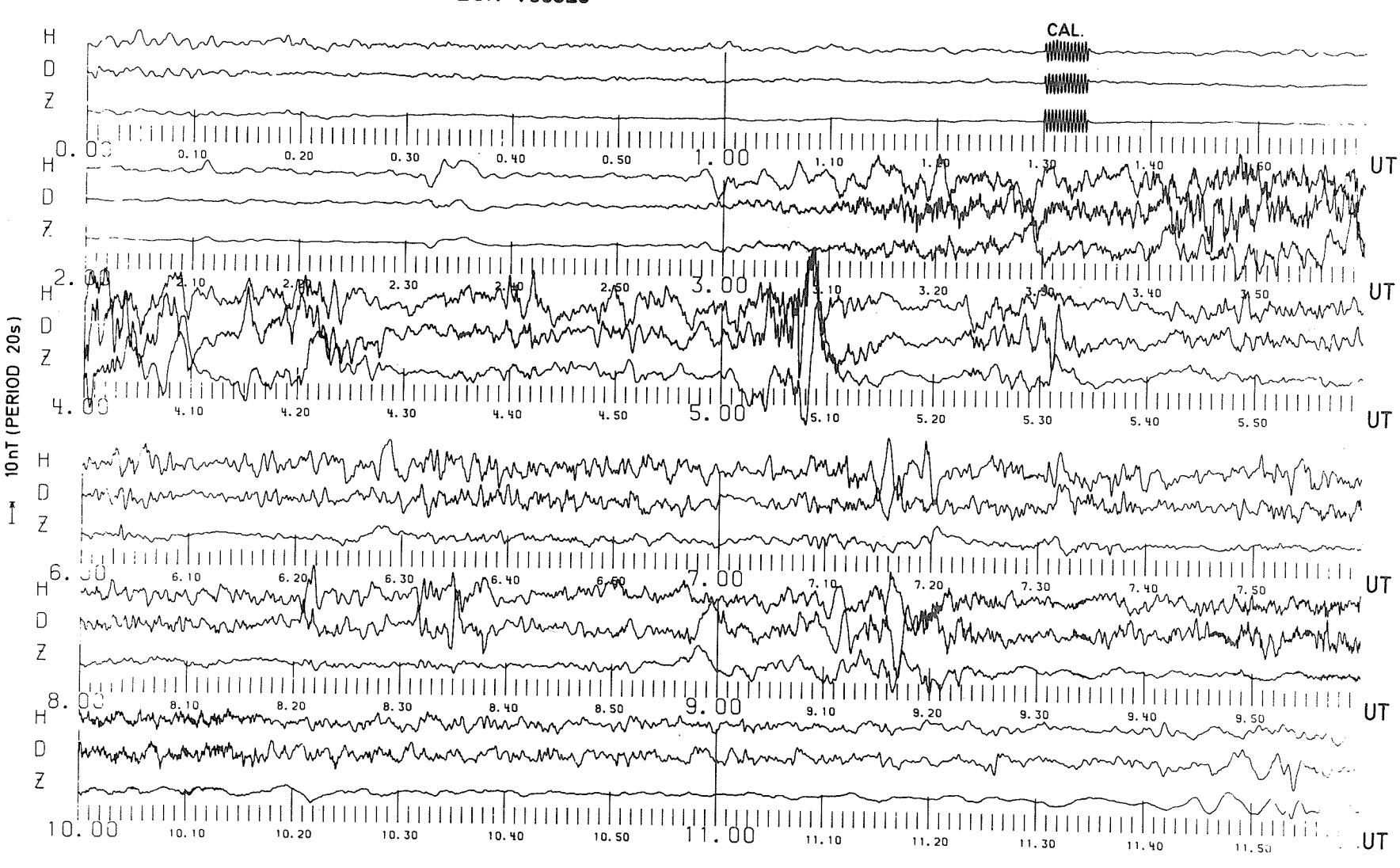

Fig. 1. Geomagnetic pulsations recorded at ESR, 0000 - 1200 UT 26 March 1976.

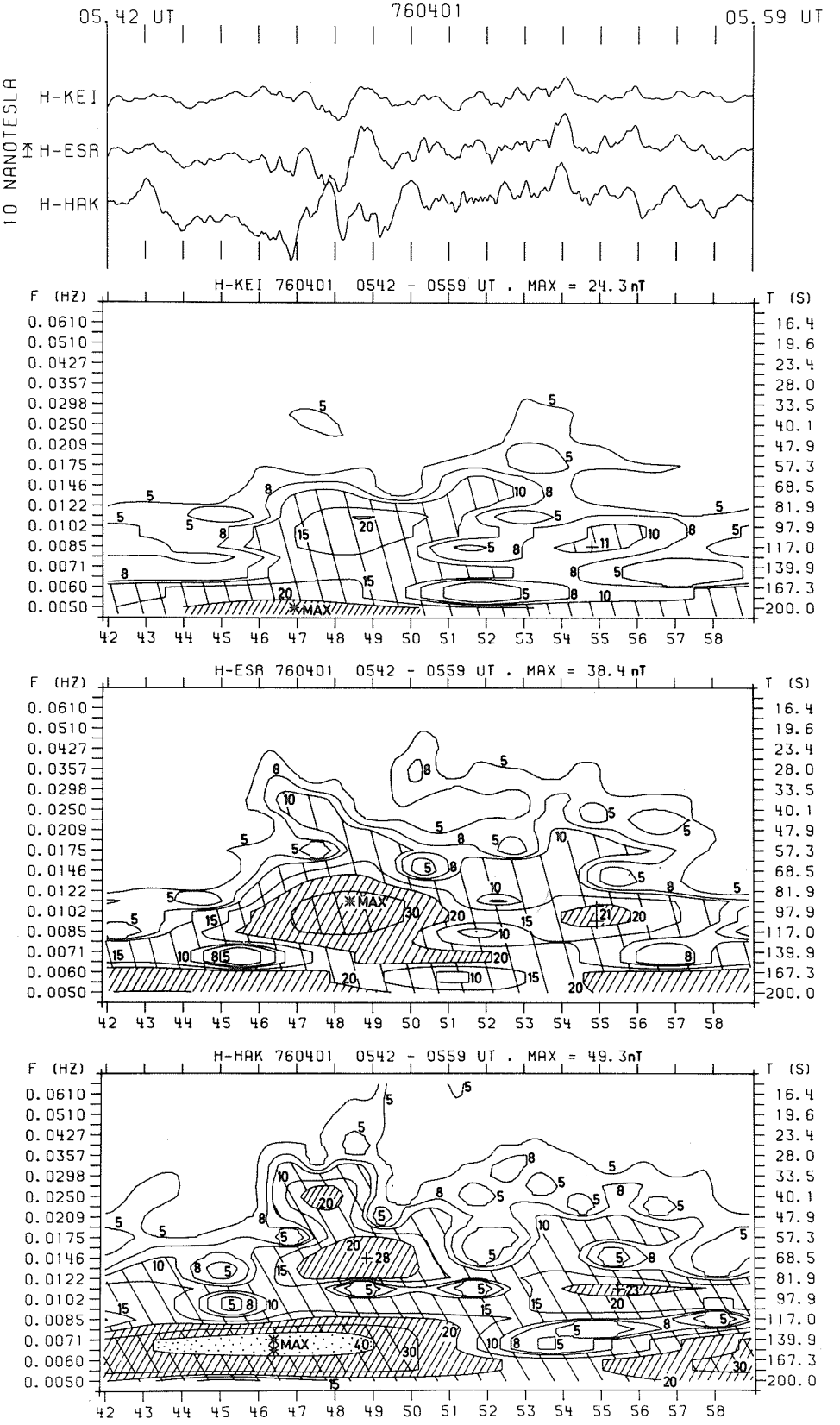

Fig. 2. Recordings and time-frequency displays of the H component of the three stations KEI, ESR and HAK for the time interval 0542 - 0559 UT 1 April 1976. The contour lines indicate the double amplitude envelope in nT.

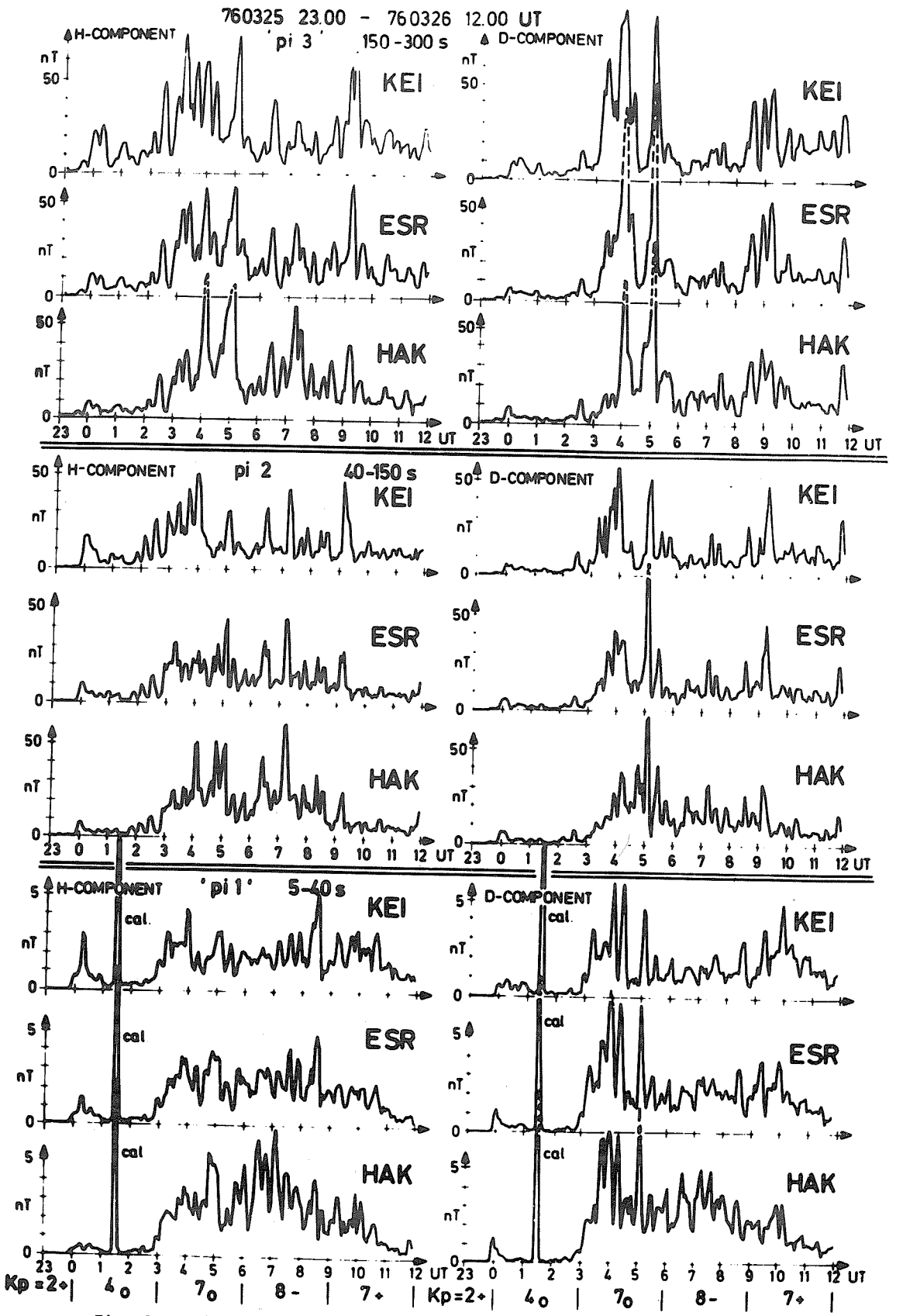

Fig. 3. Maximum double amplitudes of the H and D component for the three stations KEI, ESR and HAK and three frequency-bands; the analyzed time interval begins at 2300 UT 25 March and ends at 1200 UT 26 March 1976.

Geomagnetic Pulsations of the Pc3 Type Observed at Borok from 20 March to 5 May 1976

by

O. V. Bolshakova, V. K. Veretennikova and A. V. Gul'elmi
Geophysical Observatory Borok
Institute of Physics of the Earth, Moscow, USSR

ABSTRACT

This report presents the data on the frequency and amplitude of the Pc3 geomagnetic pulsations obtained at the Borok Observatory (ϕ = 53°). These data were used for calculation of the B and N indices.

The Pc3 type of geomagnetic pulsations is very useful for qualitatively estimating inhomogeneities in the solar wind for the following reasons. First, the Pc3 pulsations are excited permanently on the dayside of the Earth [Gul'elmi *et al.*, 1973b]. This permits one to build a continuous set of the indices for a long time interval. Second, the properties of Pc3 depend strongly on the parameters of the interplanetary magnetic field [Gul'elmi *et al.*, 1973a, 1973b; Bolshakova *et al.*, 1968]. This dependence is explained by the theory of extramagnetospheric origin of Pc3 [Gul'elmi, 1974]. Therefore, the possibility exists of deriving qualitative diagnostics of the interplanetary magnetic field inhomogeneities that are sampled by the Earth.

Here we present the Pc3 data obtained at the Borok Observatory (ϕ = 53°). The diurnal average values of the carried frequency (f in MHz) and amplitude (A in γ) are shown in Figures 1a and 1b.

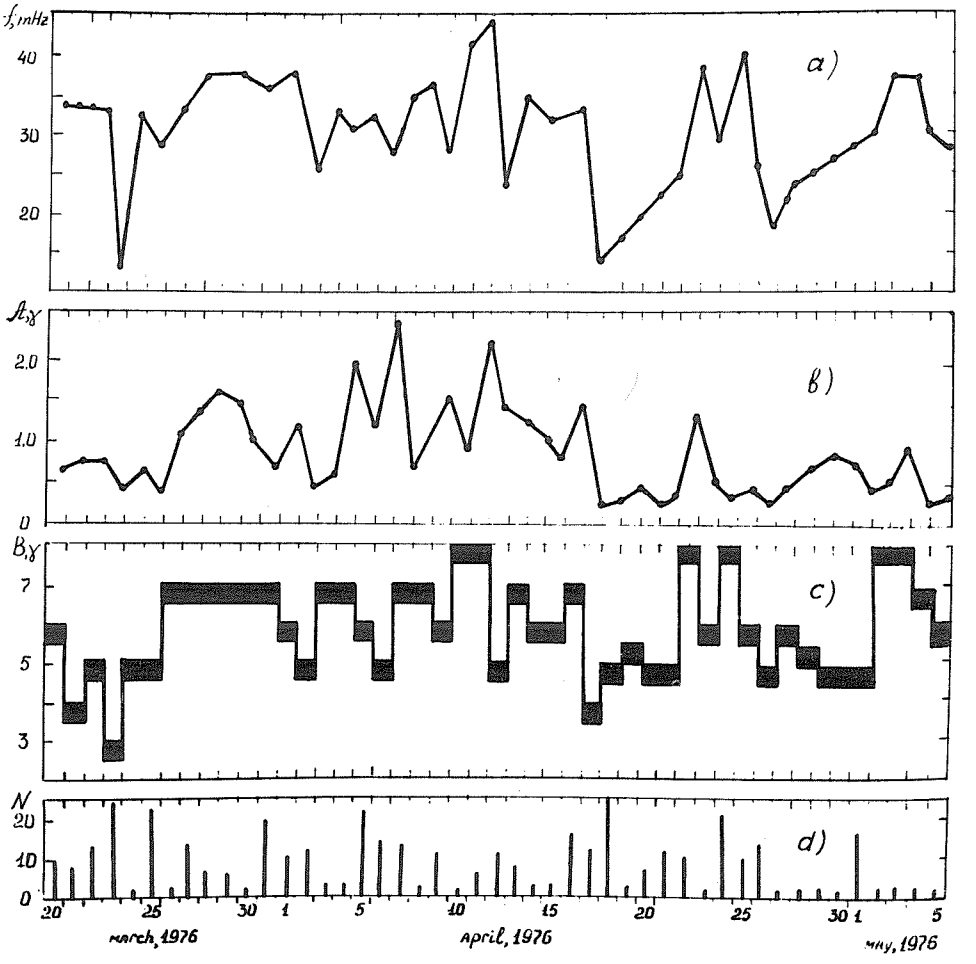

Fig. 1. Variations in the frequency (f) and amplitude (A) of the Pc3 pulsations observed during the period 20 March to 5 May 1976. Also shown are the B and N indices.

The values of the frequency (f) and the Kp index were used to calculate the B index, which characterizes the intensity of the interplanetary magnetic field before the bow shock (Figure 1c). The method of calculation of the B index is described by Gul'elmi *et al.* [1973a].

In Figure 1d the N index, which is approximately equal to the number of small scale ($\ell \sim 10^{11}$ cm) inhomogeneities in the interplanetary magnetic field, is shown. The index was built using the short-time ($\Delta t \sim 2 \times 10^3$ s) modulation of the Pc3 amplitude. The N index increases when the B index decreases.

REFERENCES

BOLSHAKOVA, O. V. and V. A. TROITSKAYA 1968 The connection between the direction of the interplanetary magnetic field and the geomagnetic pulsations, *Dokl. Akad. Nauk SSSR, 180,* 343.

GUL'ELMI, A. V. 1974 Diagnostics of the magnetosphere and interplanetary medium by means of pulsations, *Space Sci. Rev., 16,* 331.

GUL'ELMI A. V. and O. V. BOLSHAKOVA 1973a Diagnostics of interplanetary magnetic field on the data of period Pc2-4 pulsations, *Geom. Aeron., 13,* 535.

GUL'ELMI, A. V. and V. A. TROITSKAYA 1973b Geomagnetic pulsations and diagnostics of the magnetosphere, Moscow, *Nauka.*

Geomagnetic, Riometer, Ionosonde, and Micropulsation Observations at Kola Peninsula Stations

by

B.E. Brunelli, G.A. Loginov, G.A. Petrova,
N.V. Shulgina and L.T. Afanasieva

Polar Geophysical Institute.
Academy of Sciences of the USSR
Apatity, Murmansk Region, USSR

The observations carried out at stations Loparskaya (geomagnetism), Murmansk (ionosonde), and Lovosero (micropulsations) give the following picture of the development of geophysical disturbances near the end of March and the beginning of May 1976: days before 25 March were predominantly calm; on 25 March only, unusual ionospheric variation was observed; and between 26 and 28 March four periods of high auroral activity occurred, the last of which contained a PCA event that continued throughout the 29th. The next 2 days were quiet, but on 1 April a magnetic storm began with a sc. An intense magnetic storm followed another PCA event on 1 - 2 May.

Before 25 March, nevertheless, the general activity was low during each night that auroral arc or glow was observed near the northern horizon of Loparskaya. On these days long-lasting pulsations occurred, and often several types appeared simultaneously; at other times one variety of pulsation evolved into another. Even Pc-1 pulsations with increased or decreased periods appeared.

On 25 March, during the first half of the day, there arose IPDP-pulsations with periods 1-3 s followed by Pc-1 and Pc-4. As indicated in Figure 1, the second half of the day included an unusually high value of foF2 - one exceeding the median value by up to 80%. An foF2 increase of this magnitude often precedes major geomagnetic disturbances and may be considered as a precursor.

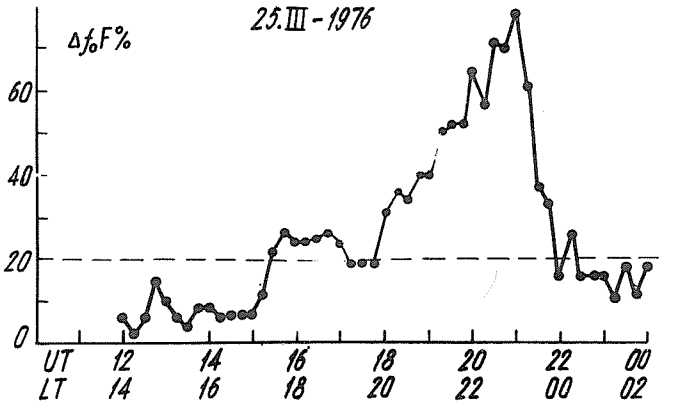

Fig. 1. The variation of foF2 excess over the median value on 25 March 1976.

Quiet geomagnetic variation was interrupted near 2330 UT on 25 March by a small disturbance. The next day, between 0000 and 0100 UT, a small absorption bay arose which was followed by a blackout and an auroral burst. The variation in the ratio ($\Delta Z/\Delta H$) during this disturbance confirms the existence of an ionospheric current flowing to the north of Loparskaya. Immediately after the sudden commencement at 0233 UT on 26 March, a negative bay arose, and the ionospheric current began to shift toward the equator, as is typical in the initial phase of a substorm (see Figure 2). The equatorward movement of the precipitation zone was also evident in the change in the absorption ratio of Loparskaya to that of Apatity. Figure 2 illustrates the unusual association of Pc-1 pulsations with a storm sudden commencement. The substorm and sc may be considered independent because of the Pi-2 pulsations apparent several minutes before the sc on the Lovosero magnetogram (see Figure 2b).

Figure 3 shows that the substorm continued for nearly 3 hours. The ionospheric disturbance extended several hours beyond 0600 UT, as the ionosonde recorded increased values of foF2. A second disturbed period began with a positive bay and blackout near 1100 UT. The disturbance, however, changed its character near 1300 UT: the positive bay became negative; the negative bay was not accompanied by the Pi-1 pulsations as is usual; and the ionosonde began to receive reflections and an absorption increase. This sequence of events suggests that the auroral oval dimensions increased, placing our stations inside the polar cap.

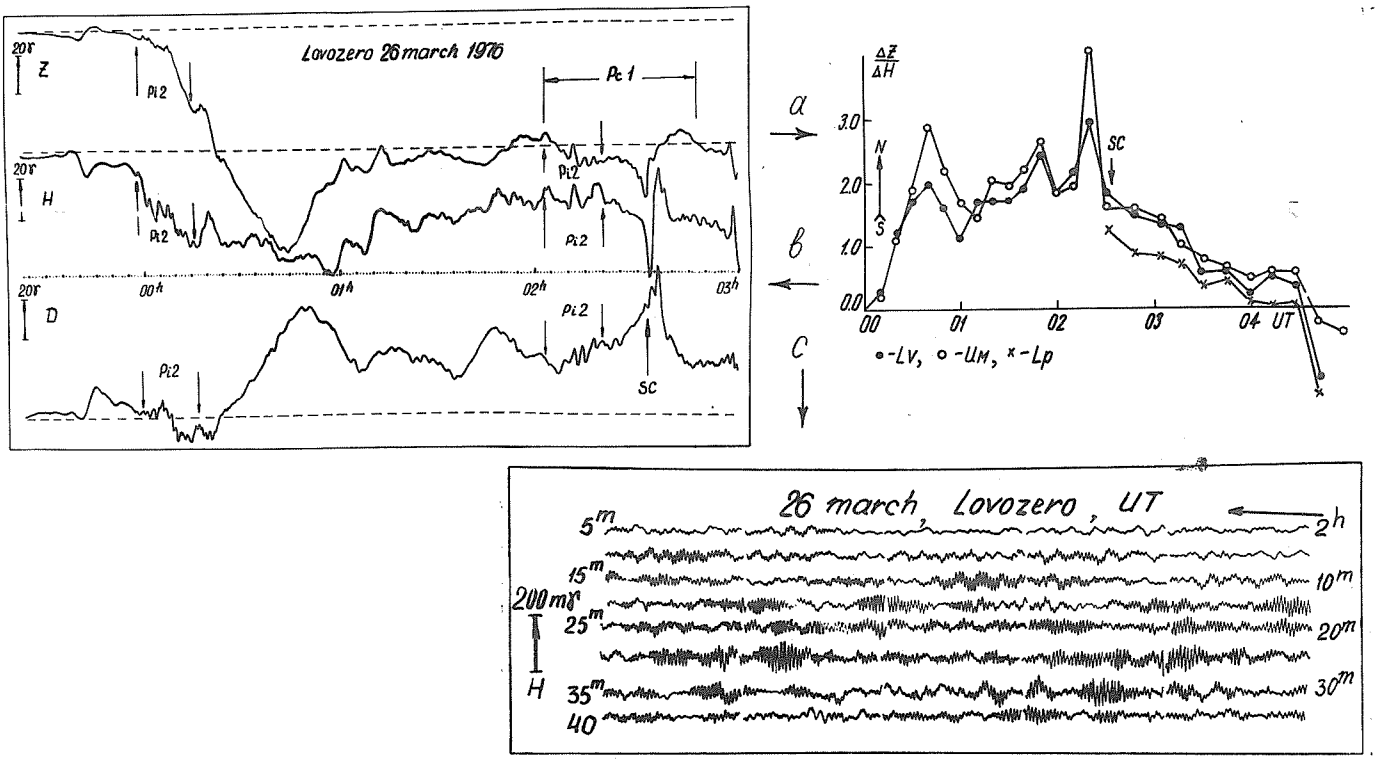

Fig. 2. Geomagnetic variations near the 0233 UT sc of 25 March 1976: (a) the ratio ($\Delta Z/\Delta H$), (b) Z, H, and D component traces from Lovosero Station, and (c) Pc-1 pulsations from Lovosero Station.

Intense disturbances with all the features of an auroral substorm were observed over the Kola Peninsula during the next several nights. At the end of the day on 28 March, absorption began to increase gradually. After a sharp change in absorption and magnetic field strength near 0130 UT on 29 March, the intense disturbance began. Near 0700 UT its character changed: the absorption remained intense, but its variations became smooth, and it failed to disappear in the afternoon and was not accompanied by magnetic bays. Whether or not this PCA event began after the last substorm or simultaneously with it remains unclear. Although the next 2 days, 30 and 31 March, were quiet, Pc-3 pulsations were observed for 12 hours on the 30th; near noon IPDP-pulsations arose.

On 1 April a severe magnetic storm with sc began. As in the 26 March event, the sudden commencement was preceded by a substorm. The change in the ($\Delta Z/\Delta H$) ratio of Figure 5 shows that the ionospheric current shifted slowly equatorward before the active phase began and poleward with higher velocity after it.

The next disturbance connected with a PCA event occurred in early May. During the nighttime hours of 28 - 30 April, weak substorms were recorded by magnetometer and riometer; during the morning hours, absorption increased up to 3 dB under quiet geomagnetic field conditons. On 30 April, after 5 hours of a calm geomagnetic field, the absorption began to increase gradually. Maximum signal attenuation occurred near 0130 on 1 May followed by a recovery to quiet-day absorption levels that spanned much of the remainder of the day. Daily variations of PCA due to the diurnal change in ionospheric illumination were absent. In the morning hours of 2 May, the PCA event had substorm activity superposed on it. A particularly intense substorm began with sharp changes in the H component of the geomagnetic field and in riometer absorption near 2000 UT on 2 May.

The authors wish to thank G. F. Totunova and V. G. Vorobiev for the auroral information.

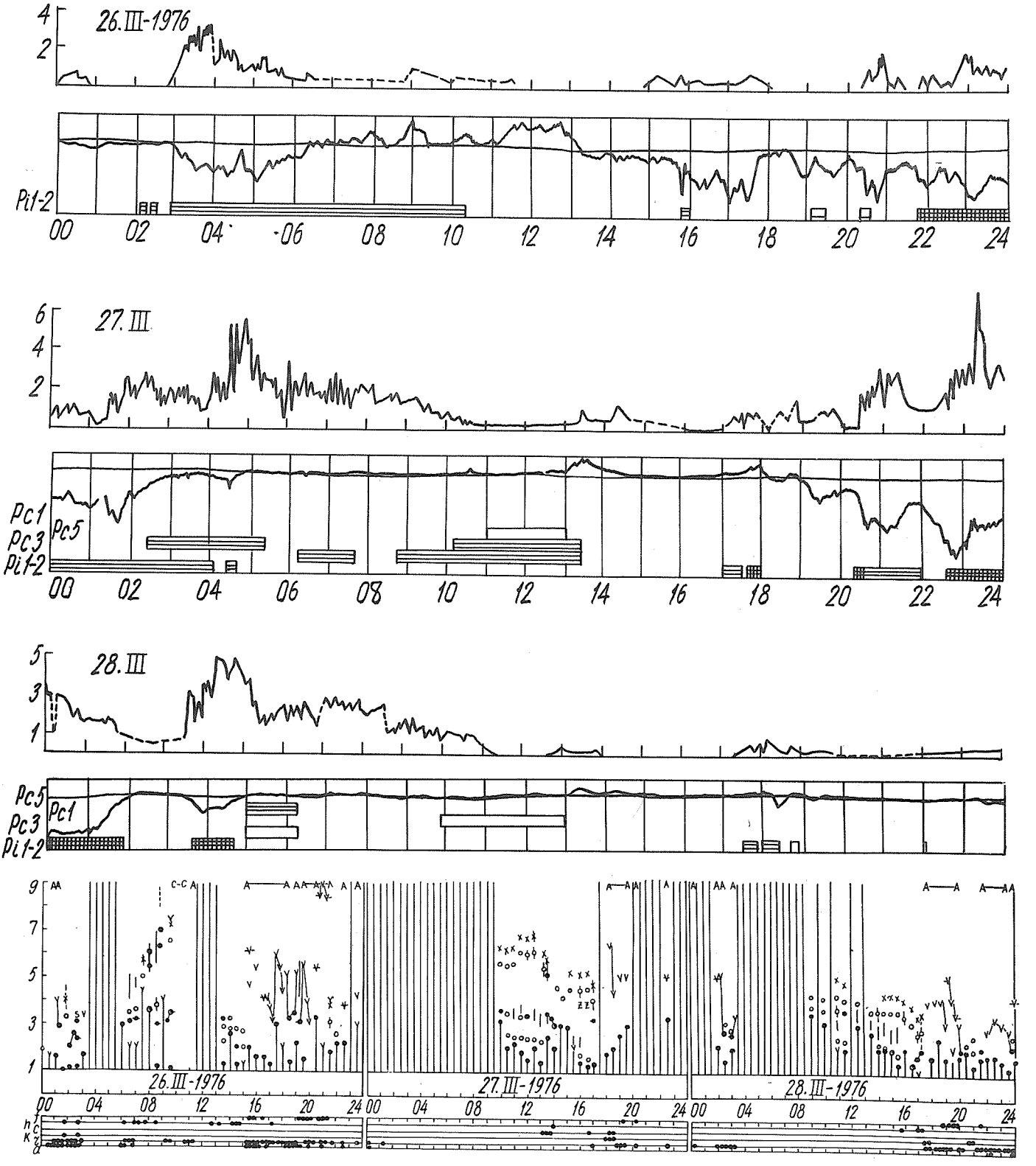

Fig. 3. Ground-based data for the period 26 - 28 March 1976. Upper graph for each day displays the 32 MHz riometer records of Loparskaya Station in dB. The lower graph illustrates the Loparskaya magnetogram and the pulsations observed at Lovosero: unmarked rectangles denote presence of pulsations; rectangles with two horizontal lines mark moderate intensity pulsations; and rectangles containing horizontal and vertical lines signify intense pulsations. Bottom panel shows frequency vs. time (f-plots) for the Murmansk ionosonde.

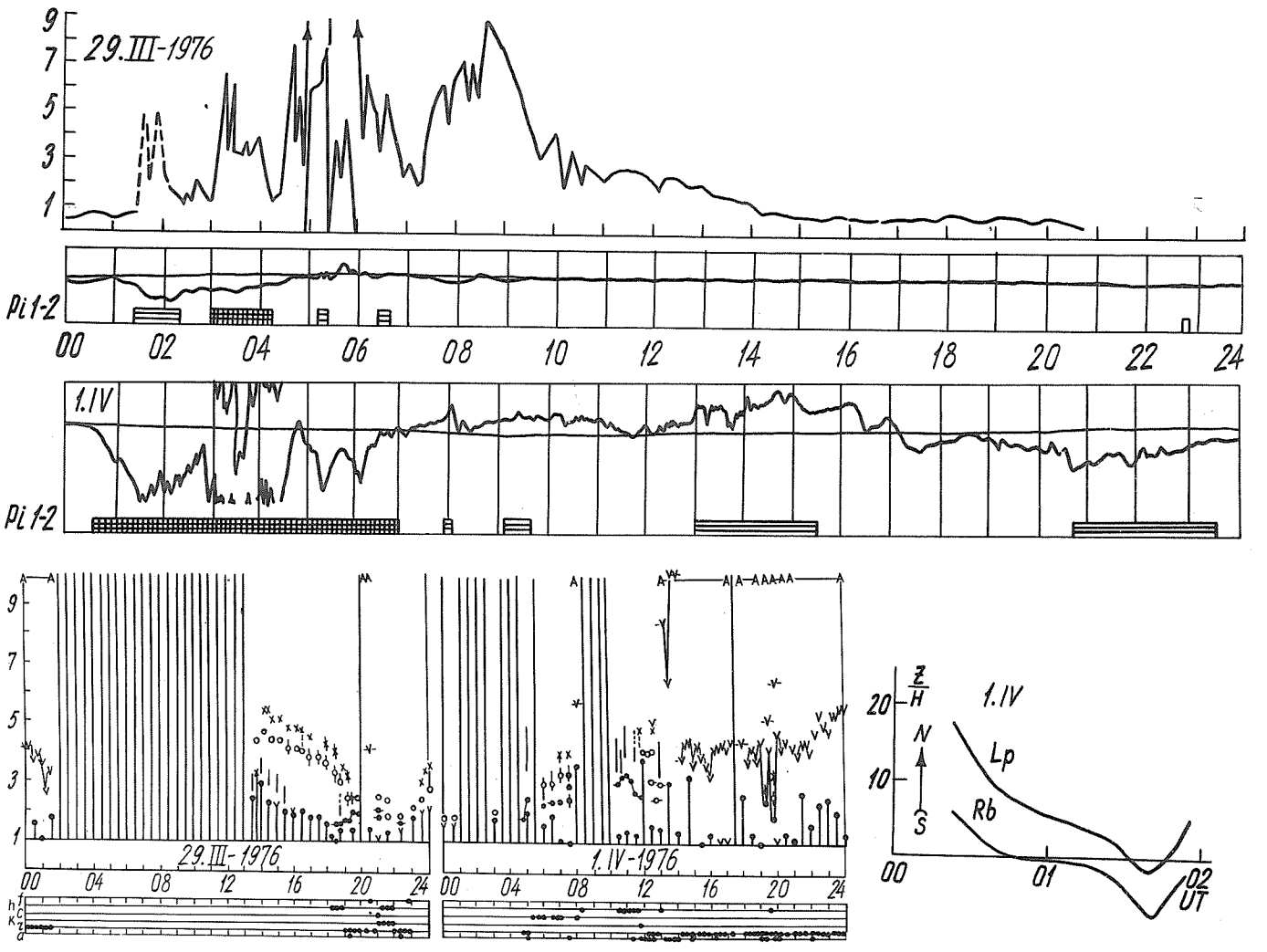

Fig. 4. Ground-based data for the period 29 March - 1 April 1976. Top graph displays the 32 MHz riometer records of Loparskaya Station in dB. The second and third graphs illustrate the Loparskaya magnetogram and the pulsations observed at Lovosero: rectangles with two horizontal lines mark moderate intensity pulsations and rectangles containing horizontal and vertical lines signify intense pulsations. Bottom graph shows frequency vs. time (f-plots) for the Murmansk ionosonde.

Fig. 5. Temporal variations of the ($\Delta Z/\Delta H$) ratio for the stations Lovosero and Ribachy during the first hours of the 1 April 1976 geomagnetic disturbance.

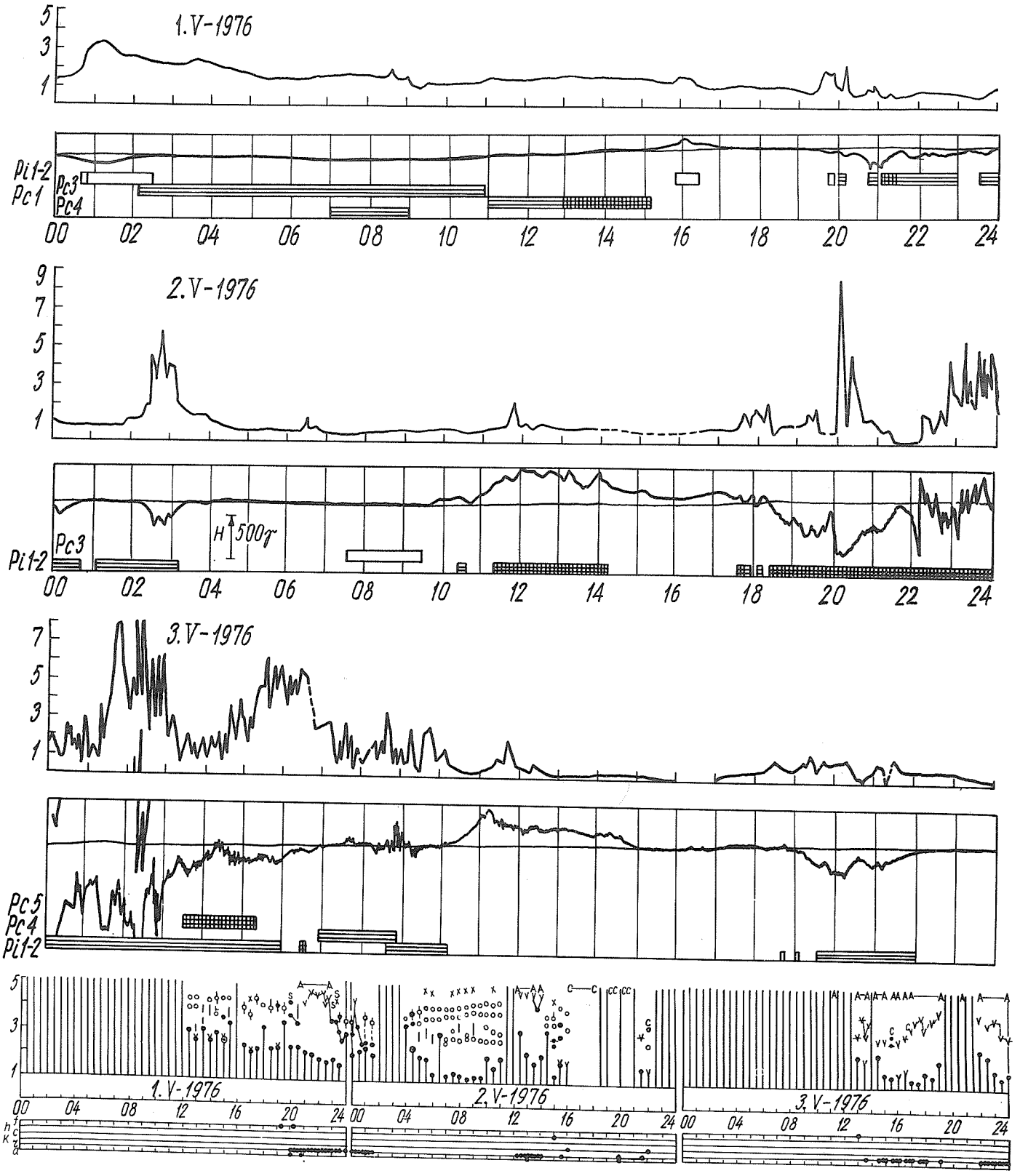

Fig. 6. Ground-based data for the period 1 - 3 May 1976. Upper graph for each day displays the 32 MHz riometer records of Loparskaya Station in dB. The lower graph illustrates the Loparskaya magnetogram and the pulsations observed at Lovosero: unmarked rectangles denote presence of pulsations; rectangles with two horizontal lines mark moderate intensity pulsations; and rectangles containing horizontal and vertical lines signify intense pulsations. Bottom panel shows frequency vs. time (f-plots) for the Murmansk ionosonde.

8. AIRGLOW AND AURORA

Night Airglow Intensities in Japan 20 March - 5 May 1976

by

Atsushi Takechi
Tokyo Astronomical Observatory
Mitaka, Tokyo, Japan

and

Bun-ichi Saito
Niigata Airglow Observatory
Niigata, Japan

Photoelectric observations of the night airglow in Japan for 20 March - 5 May 1976 were made at both the Dodaira Station (N36.0 E139.2; geomag. N25.7 E205.1) of the Tokyo Astronomical Observatory and the Niigata Station (N37.7 E138.8; geomag. N27.4 E204.6) of the Niigata University.

Figure 1 plots the mean zenith intensities and ranges of variation of the 5577Å emission line for each night measured at both stations and the 6300Å line measured at the Dodaira Station.

The dashed lines indicate the zenith intensities at midnight averaged over 5 years', (1968-1972) observations at the Dodaira Station. Compared with the averaged data, the intensities of both lines on 27 March were much higher; that of 5577Å in April was lower than the averaged values.

The lack of data between 8 and 25 April is due to the lunar and weather conditions.

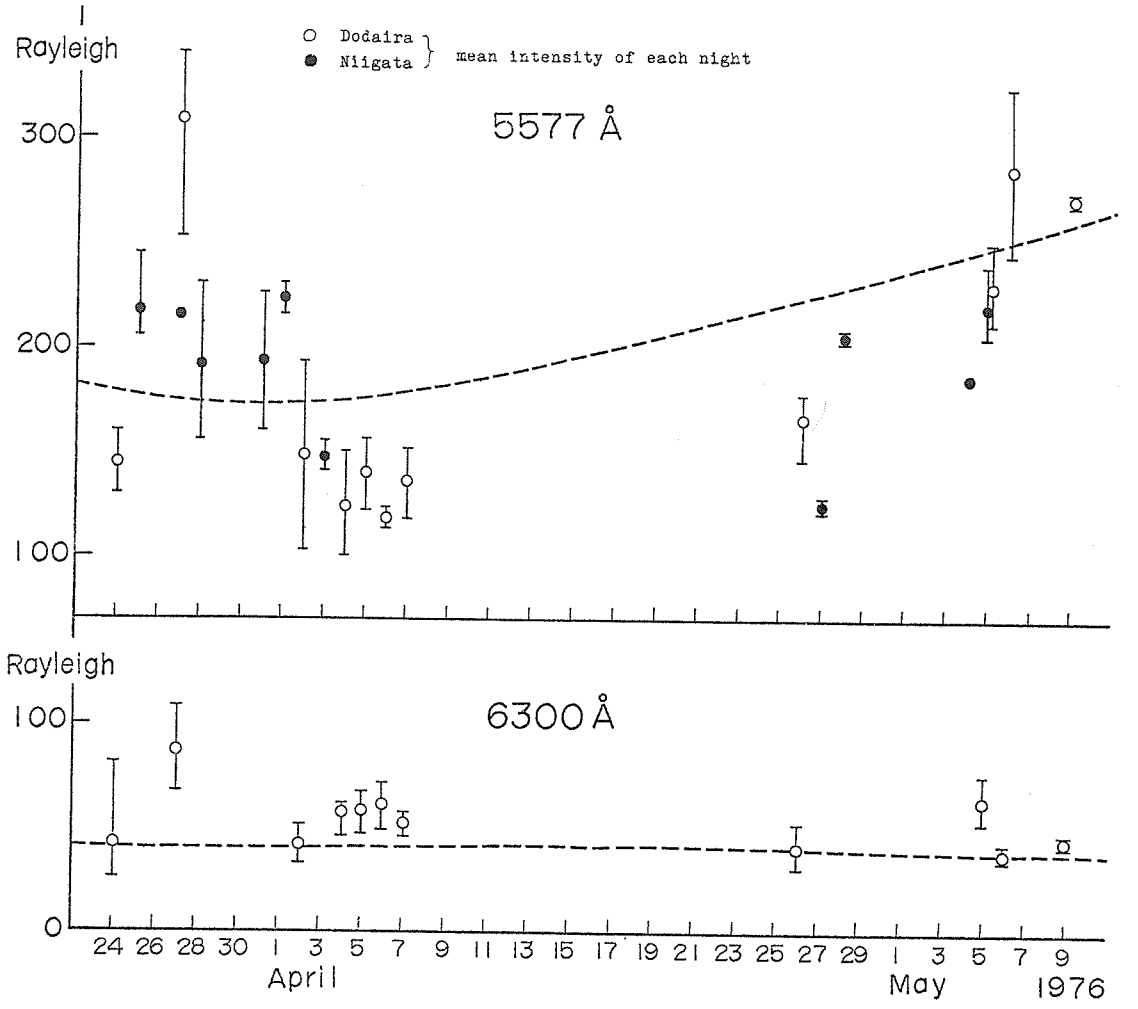

Fig. 1. The zenith intensities of night airglow for Dodaira and Niigata. The vertical bar is the range of variation in each night; the dashed line is the average midnight value for 5 years (1968-1972) from Dodaira Station observations.

Visual Auroral Display Observed in Bedford, Massachusetts on 26 March 1976

by

Paul F. Fougere
Space Physics Division
Air Force Geophysics Laboratory (AFSC)
Hanscom Air Force Base, MA 01731 USA

At midnight, local time* (LT), 26 March 1976, I observed the beginning of an auroral display as faint white bands in the northern sky near the horizon. For perhaps an hour, activity was quite faint and relatively quiescent. By about 0100 LT the brightness and extent increased steadily to the point where the entire northern quadrant of the celestial sphere - from the northern horizon to the zenith and from due east to due west - was brightly illuminated. At this time, from about 0130 to 0230 LT, the aurora was quite active and vibrant; its color was white; and it reached slightly beyond the zenith to the southern sky. After 0230 - 0330 LT, the display gradually faded, disappearing by about 0400 LT.

* Local Time = Eastern Standard Time = UT minus 5 hours.

Equatorward Boundary of the Northern Hemisphere Auroral Oval For 20 March Through 5 May 1976

by

H. W. Kroehl and M. A. Henning
National Geophysical and Solar-Terrestrial Data Center
Environmental Data Service
NOAA, Boulder, CO 80302 USA

Introduction

Simultaneous measurements of optical auroras and precipitating electrons by the DMSP and ISIS satellites allow comparisons of auroral features with the electron characteristics at 800 and 1400 km, respectively. From ISIS data reported by Kamide and Winningham [1977, in press], the authors identified an increase in the differential electron energy flux in the 50 - 150 eV channels over background to $\sim 10^7$ electrons/cm^{2}s sr keV as the equatorward boundary of electron precipitation during quiet conditions. From DMSP data an increase over background in the differential electron energy flux to $\sim 5 \times 10^7$ electrons/cm^{2}s sr keV at 200 eV emerged as a good discriminator of the equatorward boundary of the eveningside diffuse aurora.

In this data report we have combined the two results mentioned above: first by selecting times when the 200 eV sensor exceeded 10^7 electrons/cm^{2}s sr keV for more than 2 seconds (13.16 km at the Earth's surface) and secondly by requiring at least one value (recorded each second) to exceed 5×10^7 electrons/cm^{2}s sr keV. We then identified the equatorward boundary as the minimum corrected geomagnetic latitude of the interval. (For a description of the data see "Low-Energy Precipitating Electrons Over the Polar Caps Recorded by Instruments on DMSP Satellites", page 171 in this volume.)

Data

The precipitating electron data from instruments on DMSP 9532 and 10533 were used. Both satellites are in a dawn-to-dusk orbit over the Northern Hemisphere, crossing the equatorward boundary of the auroral oval every 102 min and sometime between 1800 and 2200 magnetic local time.

Plotted in Figure 1 are the corrected geomagnetic latitudes, CGL, of the boundary for all available orbits between 20 March and 5 May 1976. The dashed line at 70.7° CGL represents a nominal "quiet" auroral boundary. The minimum latitude, 53.2° CGL, of the equatorward boundary was recorded at 1436 UT on 26 March. Values below 60.0° CGL occurred at 1436, 1617, 1758, 1942, and 2124 UT on 26 March; 1751 UT on 2 April; 0725 UT on 3 April; 1330 and 2344 UT on 2 May; and 0448, 0628, 0809, and 1132 UT on 3 May. No data exist for 24 March or 24 April.

Satellite observations used to construct Figure 1 are available from the National Geophysical and Solar-Terrestrial Data Center, Boulder, CO 80302, USA.

Acknowledgments

The DMSP satellites are operated by the Air Weather Service. The authors thank Ms. Peggy Yotka and Mr. Charles Shanks for their assistance and Mr. Joe Allen and Mr. Alan Shapley for their support.

REFERENCES

KAMIDE, Y. and J. D. WINNINGHAM 1977 A Statistical Study of the Nightside Auroral Oval: The Equatorward Boundary of Electron Precipitation as Observed by ISIS 1 and 2, submitted to *J. Geophys. Res.*

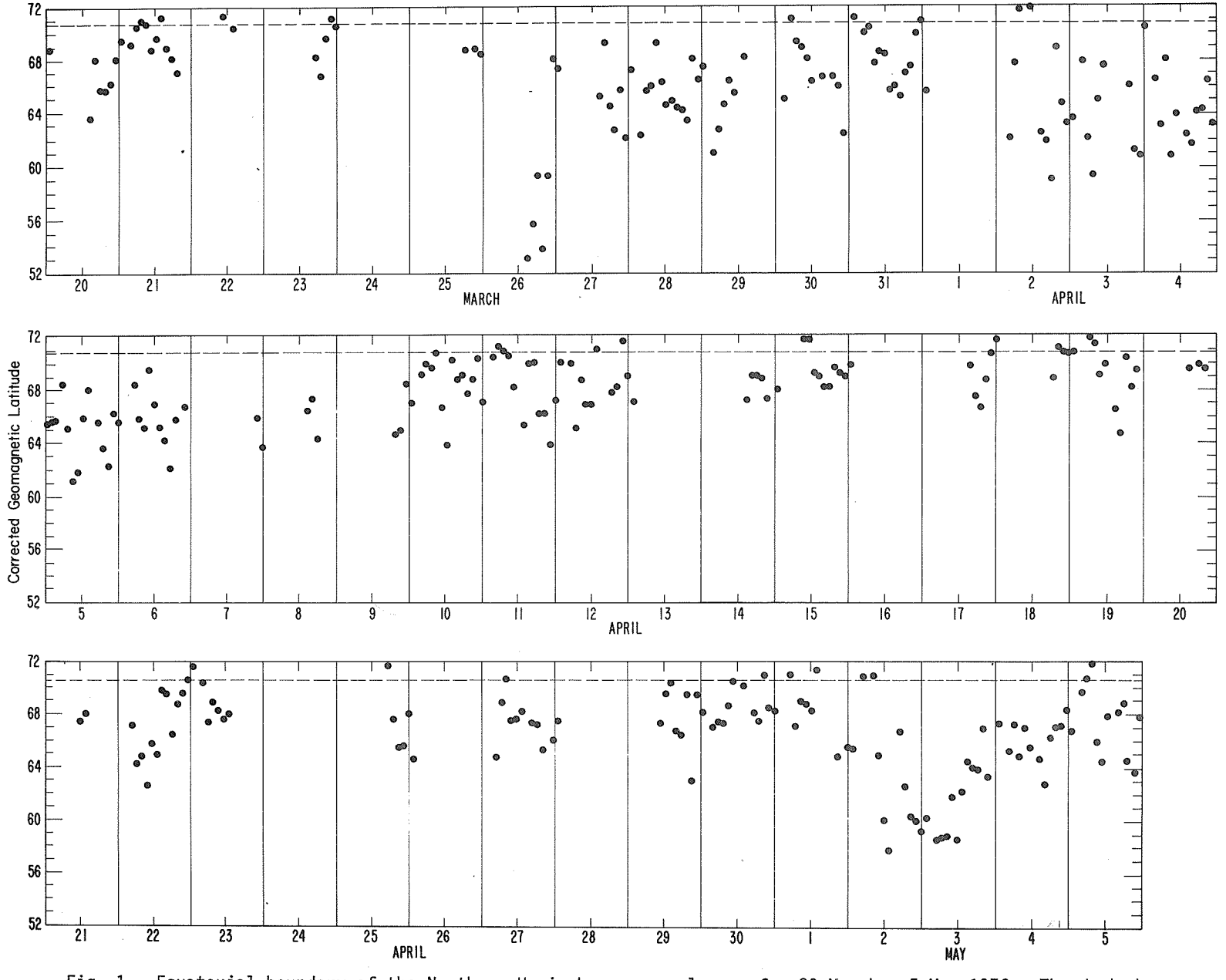

Fig. 1. Equatorial boundary of the Northern Hemisphere auroral zone for 20 March - 5 May 1976. The dashed line at 70.7° CGL represents the approximate "quiet" auroral boundary.

APPENDIX A. Special Data Sets Available from WDC-A for the STIP Interval II

Routine data published in *Solar-Geophysical Data* (SGD) include Common-scale Magnetograms for 1-3 May 1976 in SGD, 393 Part II, pages 48-49, May 1977 issue. In addition to the routine published data and other data routinely available from WDC-A (see catalogs), the following special data sets were either reduced at the data center from the original data or made available to us from the respective stations:

Ionosphere:
1) 30 MHz riometer 15-minute graphical values April 30 - May 2 from the stations: Thule, Ft. Yukon, College, Paxson, Sheep Mt., and Anchorage.
2) Wallops Island N(h) composite profiles for April and May at 1200 UT and individual profiles for April 30, May 1 and May 2 at 1200 UT; and corresponding tabulations April 30, May 1, and May 2.

Aurora:
1) DMSP precipitating electron data
2) DMSP auroral imagery film

Cosmic Rays:
1) Sulphur Mt. and Calgary 5-min graphical values April 30
2) Tabulations of cosmic ray neutron monitor data from the following stations:

Station	Cutoff Rigidity GV	Minutes Between Readings	Dates Available	Corrected Values	Uncorrected Values	Pressure
Alert	0.00	5	4/29-5/2	x	x	x
Apatity	0.61	15	4/25-5/5	x	x	x
Chacaltaya	12.64	5	4/25-5/5	x		x
Deep River	1.07	5	4/29-5/2	x	x	x
Durham	1.56	5	4/30	x	x	x
Goose Bay	0.59	5	4/29-5/2	x	x	x
Hafelekar	4.36	10	4/29-5/2	x		
Hermanus	4.68	10	4/30-5/1	x	x	x
Inuvik	0.17	5	4/29-5/2	x	x	x
Jungfraujoch	4.49	6	4/29-5/2	x	x	
Kerguelen	1.12	5	4/30-5/1	x		x
Kiel	2.30	5	4/25-5/5	x	x	x
Kiev	3.53	5	4/25-5/5	x		
McMurdo	0.00	6	4/30	x		
Mt. Washington	1.35	5	4/30	x	x	x
Oulu	0.84	5	4/29-5/2		x	x
Potchefstroom	7.04	10	4/30-5/1	x		
Predigtstuhl	4.28	60	4/25-5/5	x	x	x
Rome	6.20	15	4/25-5/5	x		
Sanae	0.94	10	4/30-5/1	x		
Tashkent	7.67	5	4/29	x		
Terre Adelie	0.01	15	4/30-5/1	x		x
Thule	0.00	6	4/30	x		
Tixie	0.49	5	4/30-5/1	x		
Tokyo	11.55	10	4/30-5/2	x	x	x
Utrecht	2.78	5	4/30-5/2	x	x	x

x = available

WDC-A has prepared a Multidisciplinary Event-Oriented Data Collection package for 30 April 1976. This package combines all published SGD data for the 30 April 1976 period, along with some special data sets for this period. Copies may be ordered by sending your request, along with your check or money order (payable in U.S. currency to Department of Commerce, NOAA/NGSDC) to World Data Center A for Solar-Terrestrial Physics, NOAA D63, Boulder, Colorado 80302, U.S.A. The package, in its present form, is priced at $50 U.S.

AUTHOR INDEX

UAG Series of Reports

Prepared by World Data Center A for Solar-Terrestrial Physics, NOAA, Boulder, Colorado, U.S.A.

These reports are for sale through the National Climatic Center, Federal Building, Asheville, NC 28801, Attn: Publications. Subscription price: $25.20 a year; $12.00 additional for foreign mailing; single copy price varies. These reports are issued on an irregular basis with 6 to 12 reports being issued each year. Therefore, in some years the single copy rate will be less than the subscription price, and in some years the single copy rate will be more than the subscription price. Make check or money order payable to: Department of Commerce, NOAA.

Some issues are now out of print and are available only on microfiche as indicated. Requests for microfiche should be sent to World Data Center A for Solar-Terrestrial Physics, NOAA, Boulder, CO 80302, with check or money order made payable to Department of Commerce, NOAA.

UAG-1 "IQSY Night Airglow Data", price $1.75.
UAG-2 "A Reevaluation of Solar Flares, 1964-1966", price 30 cents.
UAG-3 "Observations of Jupiter's Sporadic Radio Emission in the Range 7.6-41 MHz, 6 July 1966 through 8 September 1968", microfiche only, price 45 cents.
UAG-4 "Abbreviated Calendar Record 1966-1967", price $1.25.
UAG-5 "Data on Solar Event of May 23, 1967 and its Geophysical Effects", price 65 cents.

UAG-6 "International Geophysical Calendars 1957-1969", price 30 cents.
UAG-7 "Observations of the Solar Electron Corona: February 1964-January 1968", price 15 cents.
UAG-8 "Data on Solar-Geophysical Activity October 24-November 6, 1968", price (includes Parts 1 & 2) $1.75.
UAG-9 "Data on Cosmic Ray Event of November 18, 1968 and Associated Phenomena", price 55 cents.
UAG-10 "Atlas of Ionograms", price $1.50.

UAG-11 "Catalogue of Data on Solar-Terrestrial Physics" (now obsolete).
UAG-12 "Solar-Geophysical Activity Associated with the Major Geomagnetic Storm of March 8, 1970", price (includes Parts 1-3) $3.00.
UAG-13 "Data on the Solar Proton Event of November 2, 1969 through the Geomagnetic Storm of November 8-10, 1969, price 50 cents.
UAG-14 "An Experimental, Comprehensive Flare Index and Its Derivation for 'Major' Flares, 1955-1969", price 30 cents.
UAG-15 "Catalogue of Data on Solar-Terrestrial Physics" (now obsolete).

UAG-16 "Temporal Development of the Geographical Distribution of Auroral Absorption for 30 Substorm Events in each of IQSY (1964-65) and IASY (1969)", price 70 cents.
UAG-17 "Ionospheric Drift Velocity Measurements at Jicamarca, Peru (July 1967-March 1970)", microfiche only, price 45 cents.
UAG-18 "A Study of Polar Cap and Auroral Zone Magnetic Variations", price 20 cents.
UAG-19 "Reevaluation of Solar Flares 1967", price 15 cents.
UAG-20 "Catalogue of Data on Solar-Terrestrial Physics" (now obsolete).

UAG-21 "Preliminary Compilation of Data for Retrospective World Interval July 26 - August 14, 1972", price 70 cents.
UAG-22 "Auroral Electrojet Magnetic Activity Indices (AE) for 1970", price 75 cents.
UAG-23 "U.R.S.I. Handbook of Ionogram Interpretation and Reduction", price $1.75.
UAG-24 "Data on Solar-Geophysical Activity Associated with the Major Ground Level Cosmic Ray Events of 24 January and 1 September 1971", price (includes Parts 1 and 2) $2.00.
UAG-25 "Observations of Jupiter's Sporadic Radio Emission in the Range 7.6-41 MHz, 9 September 1968 through 9 December 1971", price 35 cents.

UAG-26 "Data Compilation for the Magnetospherically Quiet Periods February 19-23 and November 29 - December 3, 1970", price 70 cents.
UAG-27 "High Speed Streams in the Solar Wind", price 15 cents.
UAG-28 "Collected Data Reports on August 1972 Solar-Terrestrial Events", price (includes Parts 1-3) $4.50.
UAG-29 "Auroral Electrojet Magnetic Activity Indices AE (11) for 1968", price 75 cents.
UAG-30 "Catalogue of Data on Solar-Terrestrial Physics", price $1.75.

UAG-31 "Auroral Electrojet Magnetic Activity Indices AE (11) for 1969", price 75 cents.
UAG-32 "Synoptic Radio Maps of the Sun at 3.3 mm for the Years 1967-1969", price 35 cents.
UAG-33 "Auroral Electrojet Magnetic Activity Indices AE (10) for 1967", price 75 cents.
UAG-34 "Absorption Data for the IGY/IGC and IQSY", price $2.00.
UAG-35 "Catalogue of Digital Geomagnetic Variation Data at World Data Center A for Solar-Terrestrial Physics", price 20 cents.

UAG-36 "An Atlas of Extreme Ultraviolet Flashes of Solar Flares Observed Via Sudden Frequency Deviations During the ATM-SKYLAB Missions", price 55 cents.
UAG-37 "Auroral Electrojet Magnetic Activity Indices AE (10) for 1966", price 75 cents.
UAG-38 "Master Station List for Solar-Terrestrial Physics Data at WDC-A for Solar-Terrestrial Physics", price $1.60.
UAG-39 "Auroral Electrojet Magnetic Activity Indices AE (11) for 1971", by Joe Haskell Allen, Carl C. Abston and Leslie D. Morris, National Geophysical and Solar-Terrestrial Data Center, Environmental Data Service, February 1975, 144 pages, price $2.05.

UAG-40 "H-Alpha Synoptic Charts of Solar Activity For the Period of Skylab Observations, May, 1973-March, 1974", by Patrick S. McIntosh, NOAA Environmental Research Laboratories, February 1975, 32 pages, price 56 cents.

UAG-41 "H-Alpha Synoptic Charts of Solar Activity During the First Year of Solar Cycle 20, October, 1964 - August, 1965", by Patrick S. McIntosh, NOAA Environmental Research Laboratories, and Jerome T. Nolte, American Science and Engineering, Cambridge, Massachusetts, March 1975, 25 pages, price 48 cents.

UAG-42 "Observations of Jupiter's Sporadic Radio Emission in the Range 7.6-80 MHz 10 December 1971 through 21 March 1975", by James W. Warwick, George A. Dulk, and Anthony C. Riddle, Department of Astro-Geophysics, University of Colorado, Boulder, Colorado 80302, April 1975, 49 pages, price $1.15.

UAG-43 "Catalog of Observation Times of Ground-Based Skylab-Coordinated Solar Observing Programs", compiled by Helen E. Coffey, World Data Center A for Solar-Terrestrial Physics, May 1975, 159 pages, price $3.00.

UAG-44 "Synoptic Maps of Solar 9.1 cm Microwave Emission from June 1962 to August 1973", by Werner Graf and Ronald N. Bracewell, Radio Astronomy Institute, Stanford University, Stanford, California 94305, May 1975, 183 pages, price $2.55.

UAG-45 "Auroral Electrojet Magnetic Activity Indices AE (11) for 1972", by Joe Haskell Allen, Carl C. Abston and Leslie D. Morris, National Geophysical and Solar-Terrestrial Data Center, Environmental Data Service, May 1975, 144 pages, price $2.10.

UAG-46 "Interplanetary Magnetic Field Data 1963-1974", by Joseph H. King, National Space Science Data Center, NASA Goddard Space Flight Center, Greenbelt, Maryland 20771, June 1975, 382 pages, price $2.95.

UAG-47 "Auroral Electrojet Magnetic Activity Indices AE (11) for 1973", by Joe Haskell Allen, Carl C. Abston and Leslie D. Morris, National Geophysical and Solar-Terrestrial Data Center, Environmental Data Service, June 1975, 144 pages, price $2.10.

UAG-48A "Synoptic Observations of the Solar Corona during Carrington Rotations 1580-1596 (11 October 1971 - 15 January 1973)", [Reissue with quality images] by R. A. Howard, M. J. Koomen, D. J. Michels, R. Tousey, C. R. Detwiler, D. E. Roberts, R. T. Seal and J. D. Whitney, E. O. Hulbert Center for Space Research, NRL, Washington, D. C. 20375 and R. T. and S. F. Hansen, C. J. Garcia and E. Yasukawa, High Altitude Observatory, NCAR, Boulder, Colorado 80303, February 1976, 200 pages, price $4.27.

UAG-49 "Catalog of Standard Geomagnetic Variation Data", prepared by Environmental Data Service, NOAA, Boulder, Colorado, August 1975, 125 pages, price $1.85.

UAG-50 "High-Latitude Supplement to the URSI Handbook on Ionogram Interpretation and Reduction", by W. R. Piggott, British Antarctic Survey, c/o SRC, Appleton Laboratory, Ditton Park, Slough, England, October 1975, 292 pages, price $4.00.

UAG-51 "Synoptic Maps of Solar Coronal Hole Boundaries Derived from He II 304Å Spectroheliograms from the Manned Skylab Missions", by J. D. Bohlin and D. M. Rubenstein, E. O. Hulbert Center for Space Research, Naval Research Laboratory, Washington, D. C. 20375 U.S.A., November 1975, 30 pages, price 54 cents.

UAG-52 "Experimental Comprehensive Solar Flare Indices for Certain Flares, 1970-1974", compiled by Helen W. Dodson and E. Ruth Hedeman, McMath-Hulbert Observatory, The University of Michigan, 895 Lake Angelus Road North, Pontiac, Michigan 48055 U.S.A., November 1975, 27 pages, price 60 cents.

UAG-53 "Description and Catalog of Ionospheric F-Region Data, Jicamarca Radar Observatory (November 1966 - April 1969)", by W. L. Clark and T. E. Van Zandt, Aeronomy Laboratory, NOAA, Boulder, Colorado 80302 and J. P. McClure, University of Texas at Dallas, Dallas, Texas 75230, April 1976, 10 pages, price 33 cents.

UAG-54 "Catalog of Ionosphere Vertical Soundings Data", prepared by Environmental Data Service, NOAA, Boulder, Colorado 80302, April 1976, 130 pages, price $2.10.

UAG-55 "Equivalent Ionospheric Current Representations by a New Method, Illustrated for 8-9 November 1969 Magnetic Disturbances", by Y. Kamide, Cooperative Institute for Research in Environmental Sciences, University of Colorado, Boulder, Colorado 80302 and Geophysical Institute, University of Alaska, Fairbanks, Alaska 99701, H. W. Kroehl, Data Studies Division, NOAA/EDS/NGSDC, Boulder, Colorado 80302, M. Kanamitsu, Advanced Study Program, National Center for Atmospheric Research, Boulder, Colorado 80303, J. H. Allen, Data Studies Division, NOAA/EDS/NGSDC, Boulder, Colorado 80302, and S.-I. Akasofu, Geophysical Institute, University of Alaska, Fairbanks, Alaska 99701, April 1976, 91 pages, price $1.60.

UAG-56 "Iso-intensity Contours of Ground Magnetic H Perturbations for the December 16-18, 1971 Geomagnetic Storm", by Y. Kamide, Cooperative Institute for Research in Environmental Sciences, University of Colorado, Boulder, Colorado 80302 and Geophysical Institute, University of Alaska, Fairbanks, Alaska 99701 (currently Guest worker at Data Studies Division, NOAA/EDS/NGSDC, Boulder, Colorado 80302), April 1976, 37 pages, price $1.39.

UAG-57 "Manual on Ionospheric Absorption Measurements", edited by K. Rawer, Institut für Physikalische Weltraumforschung, Freiburg, G.F.R., June 1976, 202 pages, price $4.27.

UAG-58 "ATS6 Radio Beacon Electron Content Measurements at Boulder, July 1974 - May 1975", by R. B. Fritz, Space Environment Laboratory (currently with Wave Propagation Laboratory), NOAA, Boulder, Colorado 80302 USA, September 1976, 61 pages, price $1.04.

UAG-59 "Auroral Electrojet Magnetic Activity Indices AE(11) for 1974", by Joe Haskell Allen, Carl C. Abston and Leslie D. Morris, National Geophysical and Solar-Terrestrial Data Center, Environmental Data Service, December 1976, 144 pages, price $2.16.

UAG-60 "Geomagnetic Data for January 1976 (AE(7) Indices and Stacked Magnetograms)" by J. H. Allen, C. A. Abston and L. R. Morris, NGSDC/EDS/NOAA, July 1977, 57 pages, price $1.07.

USCOMM-NOAA-ASHEVILLE, NC--8-31-77--1800